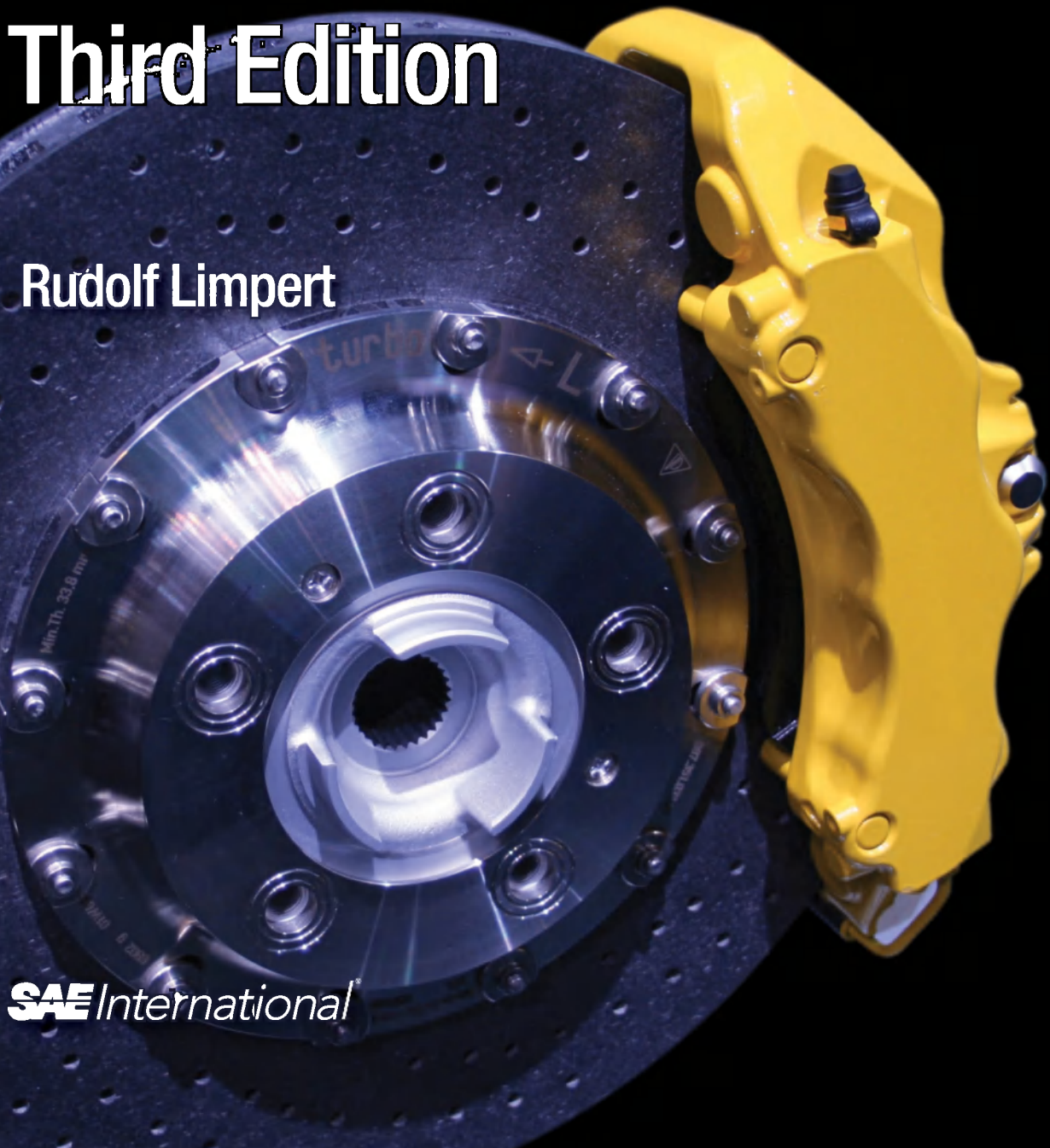


Brake Design and Safety

Third Edition

Rudolf Limpert



SAE International

Brake Design and Safety

Third Edition

Other related resources from SAE International:

Brake Technology Handbook

By Bert J. Breuer and Karlheinz Bill
(Product Code: R-375)

**Electric and Hybrid-Electric Vehicles -
Braking Systems and NVH Considerations**

By Ronald K. Jurgen
(Product Code: PT-143/4)

Disc Brake Squeal

By Frank Chen, Chin An Tan, and Ronald L. Quaglia
(Product Code: R-353)

Advanced Brake Technology

By Bert J. Breuer and Uwe Dausend
(Product Code: R-352)

For more information or to order a book, contact SAE International at

400 Commonwealth Drive, Warrendale, PA 15096-0001

E-mail: CustomerService@sae.org
Phone: 877-606-7323 (inside USA and Canada)
724-776-4970 (outside USA)
Fax: 724-776-0790
<http://books.sae.org>

Brake Design and Safety

Third Edition

By Rudolf Limpert

SAE International®

Warrendale, PA
USA



400 Commonwealth Drive
Warrendale, PA 15096-0001 USA

E-mail: CustomerService@sae.org
Phone: 877-606-7323 (inside USA and Canada)
724-776-4970 (outside USA)
Fax: 724-776-0790

Copyright © 2011 SAE International. All rights reserved.

No part of this publication may be reproduced, stored in a retrieval system, distributed, or transmitted, in any form or by any means without the prior written permission of SAE. For permission and licensing requests, contact SAE Permissions, 400 Commonwealth Drive, Warrendale, PA 15096-0001 USA; e-mail: copyright@sae.org; phone: 724-772-4028; fax: 724-772-9765.

ISBN 978-0-7680-3438-7

SAE Order No. R-398

DOI 10.4271/R-398

Library of Congress Cataloging-in-Publication Data

Limpert, Rudolf.
Brake design and safety / Rudolf Limpert. — 3rd ed.
p. cm.
Includes index.
ISBN 978-0-7680-3438-7
1. Automobiles—Brakes—Design and construction. I. Title.

TL269.L56 2011
629.2'46—dc22

2011011904

Information contained in this work has been obtained by SAE International from sources believed to be reliable. However, neither SAE International nor its authors guarantee the accuracy or completeness of any information published herein and neither SAE International nor its authors shall be responsible for any errors, omissions, or damages arising out of use of this information. This work is published with the understanding that SAE International and its authors are supplying information, but are not attempting to render engineering or other professional services. If such services are required, the assistance of an appropriate professional should be sought.

To purchase bulk quantities, please contact:

SAE Customer Service
E-mail: CustomerService@sae.org
Phone: 877-606-7323 (inside USA and Canada)
724-776-4970 (outside USA)
Fax: 724-776-0790

Visit the SAE Bookstore at
<http://books.sae.org>

Dedication

To Dr. Hans Strien,
at Alfred Teves, Co. in Frankfurt, Germany,
who took into his brake department a young engineering trainee.
16. April 1963.

Table of Contents



Chapter 1 Fundamentals of Braking Performance, Design, and Safety	1
1.1 The Functions of a Brake System	1
1.2 Vehicle Deceleration and Stopping Distance	2
1.3 Elements of Automotive Brake System Design.....	10
1.4 Pedal Force and Pedal Travel	17
1.5 Design Solution Selection Process.....	18
1.6 Braking System Involvement in Accidents.....	20
 Chapter 2 Design and Analysis of Friction Brakes.....	 27
2.1 Brake Torque	27
2.2 Brake Factor.....	27
2.3 Brake Factor of Drum Brakes	29
2.4 Disc Brakes	48
 Chapter 3 Thermal Analysis of Automotive Brakes	 65
3.1 Temperature Analysis.....	65
3.2 Thermal Stress Analysis	107
3.3 Thermal Design Measures	112
 Chapter 4 Analysis of Mechanical Brake Systems	 119
4.1 General Observations.....	119
4.2 Wheel Brakes.....	120
4.3 Driveshaft-Mounted Brakes	122
 Chapter 5 Analysis of Hydraulic Brake Systems	 125
5.1 Manual Hydraulic Brakes	125
5.2 Boost System Analysis.....	127
5.3 Brake Line Pressure Control Devices.....	141
5.4 Brake Fluid Volume Analysis	150
5.5 Dynamic Response of Hydraulic Brake Systems	175

Chapter 6 Analysis of Air Brake Systems	183
6.1 Basic Concepts	183
6.2 Foundation Brakes	184
6.3 Brake Torque	190
6.4 Vehicle Deceleration	194
6.5 ABS Modulating Valves	196
6.6 PC-BRAKE AIR Multi-Axle Software Application	199
6.7 Response Time of Air Brake Systems	200
6.8 Electronic Brake Control (Braking by Wire)	209
Chapter 7 Single Vehicle Braking Dynamics	213
7.1 Static Axle Loads	213
7.2 Dynamic Axle Loads	214
7.3 Optimum Braking Forces	216
7.4 Actual Braking Forces Developed by Brakes	224
7.5 Comparison of Optimum and Actual Braking Forces	225
7.6 Tire-Road Friction Utilization	228
7.7 Braking Efficiency	230
7.8 Fixed Brake Force Distribution Analysis	232
7.9 Variable Brake Force Distribution Analysis	238
7.10 Braking Dynamics of Two-Axle Truck Equipped with Air Brakes	249
7.11 Three-Axle Straight Truck – Air Brakes	253
7.12 Vehicle Stability Analysis	258
7.13 Braking Dynamics While Turning	267
Chapter 8 Braking Dynamics of Combination Vehicles	275
8.1 Tow Vehicle-Trailer Combination	275
8.2 Electronic Stability Control and Trailer Swing	278
8.3 Braking of Tractor-Trailer Combinations	279
8.4 Braking of 2-S1 Combination	281
8.5 2-S1 Tractor-Trailer Combination – PC-BRAKE AIR Software	302
8.6 Braking of 3-S2 Tractor-Semitrailer Combination	312
8.7 2-S1-2 Combination: Two-Axle Tractor, Single-Axle Semitrailer, and Double-Axle Trailer	318
8.8 2-S2 Tractor-Semitrailer	320
8.9 2-S3 Tractor-Semitrailer – Triple-Axle Trailer with Leaf Springs	321
8.10 Test Results	325

Chapter 9 Automatic Brake Control	327
9.1 Basic Considerations	327
9.2 Wheel-Lockup Analysis	328
9.3 Basic Performance Requirements of ABS Systems.....	343
9.4 Hydraulic ABS Systems.....	353
9.5 ABS System Components	360
9.6 Drivetrain Influence on ABS	364
9.7 ABS Systems for Air Brakes.....	364
Chapter 10 Analysis of Brake Failure	373
10.1 Basic Considerations	373
10.2 Development of Brake Failure.....	374
10.3 Analysis of Partial Brake Failure.....	376
10.4 Comparison of Dual Brake Systems.....	389
10.5 Vacuum Assist Failure	391
10.6 Full Power Brake Failure.....	392
10.7 Degraded Braking Due to Air Inclusion.....	393
10.8 Brake Fluid Considerations in Design and Failure Analysis.....	394
10.9 Seal and Rubber Materials	396
10.10 Data Collection in Brake System Failures.....	396
10.11 Failure of Air Brake Systems.....	403
Index	405
About the Author	415

Preface to the Third Edition



While writing the third edition, I have carefully considered the comments received from readers all over the world. One engineer remarked that whenever he has new trainees in his brake department, they must read Limpert's brake book. Following that mandate I have added explanations and examples to the theoretical analysis of braking and brake temperature while retaining the practical aspects of brake system design.

Electronic system controls have significantly increased the potential of braking systems. Notwithstanding the advances made in applying brakes by mechanical, hydraulic, or electrical means, vehicles are slowed and stopped by friction between pad and rotor. Only when the underlying brake system is properly engineered will automatic controls perform effectively and vehicles brake safely under all foreseeable operating conditions.

The third edition provides the fundamental tools necessary to design efficient braking systems that will comply with safety standards, minimize consumer complaints, and perform safely and efficiently long before and while electronic brake controls become active. New to the readers is the brake design software, developed by the author as an effective companion tool to this edition. The efficient design of automotive brake systems, including trucks and trailers, with PC-BRAKE software is demonstrated with detailed examples. Automotive engineering students, brake engineers, and forensic experts will benefit greatly from the third edition in conjunction with the computer programs and brake design workshop available from the author's website www.pcbrakeinc.com.

Rudy Limpert

Preface to the Second Edition



The Second Edition continues to provide a systems approach to designing safer brakes. Consulting experts will find it a single reference in determining the involvement of brakes in accident causation.

Brake system technology has attained a high standard of quality over the last two decades. Nearly all automobiles are now equipped with antilock brakes. Federal braking standards require commercial vehicles to use antilock brakes. Revolutionary innovative brake designs are not expected. Improvements in brake systems will only be achieved through basic research, the application of sound engineering concepts, and testing, resulting in small, yet important, design changes.

The objective of the Second Edition is to assist the brake engineer in accomplishing his task to design safer brakes that can be operated and maintained safely. The brake expert will find all the analytical tools to study and determine the potential causes of brake failures. The Second Edition is expanded to cover all essential subjects, including the mechanical and thermal analysis of disk brakes. Mistakes found in the First Edition were corrected.

I thank all those who have made valuable suggestions and comments and helped me to understand brakes better, in particular the many individuals who attended my Brake Design and Safety seminars.

Preface to the First Edition



The purpose of this book is to provide a systems approach to designing safer brakes. Much of the material presented was developed during my work as a brake design engineer, conducting automotive research, consulting as a brake expert, and teaching brake design.

The book is written for automotive engineers, technical consultants, accident reconstruction experts, and lawyers involved with the design of brake systems, the analysis of braking performance, and product liability issues. Junior engineers will benefit from the book by finding in one single source all essential concepts, guidelines, and design checks required for designing safer brakes.

Chapter 1 reviews basic stopping distance performance, design rules, and product liability factors.

In Chapter 2, drum and disc brakes are discussed. Brake torque computations are shown for different drum and disc brake designs.

Temperature and thermal stresses are analyzed in Chapter 3. Practical temperature equations are shown whenever possible.

Chapter 4 briefly reviews basic concepts involved in analyzing mechanical brake systems.

The operation and design of hydraulic brakes are discussed in Chapter 5.

Air brake systems and their components are discussed and analyzed in Chapter 6.

Brake force distribution, braking efficiency, optimum brake force distribution, and vehicle stability during braking for the single vehicle are analyzed in Chapter 7.

Car-trailer and commercial truck-trailer braking is discussed in Chapter 8.

Important elements of antilock braking performance and design are introduced in Chapter 9.

Brake failures are discussed in Chapter 10.

Chapter 1



Fundamentals of Braking Performance, Design, and Safety

1.1 The Functions of a Brake System

A vehicle is connected to the roadway by the normal and traction forces produced by the tires. Braking, steering, or accelerating forces must be generated by the small tire tread area contacting the ground. Only forces equal to or less than the product of tire normal force and tire-road coefficient of friction can be transmitted between vehicle and ground. Even the ideal braking and stability control system cannot utilize more traction than provided by the tires and road.

The safe operation of a motor vehicle requires continuous adjustment of its speed to changing traffic conditions. The brakes and tires along with the steering system are the most safety-critical accident avoidance components of a motor vehicle. Brakes must perform safely under all reasonably foreseeable operating conditions, including slippery, wet, and dry roads; with a lightly or fully laden vehicle; when braking straight or while turning; with new or worn brakes; when applied by the novice or experienced driver; on smooth or rough roads; or when pulling a trailer.

The basic functions of a brake system must be provided under foreseeable circumstances, at reasonable cost and brake wear life, while providing directional stability and acceptable tire-road friction utilization.

The braking system must comply with all applicable safety standards. Under most conditions, safety standards are considered minimum performance requirements.

1.1.1 Slowing and/or Stopping

Decelerating a vehicle to a lower speed or to a complete stop is the function most often performed by the service brakes of a vehicle. Safety standards and industry practices place stringent requirements on effectiveness of stops including repeated braking under a variety of operating conditions. Critical design parameters include proper brake balance front-to-rear to ensure directional stability while braking at, or near, the limit of tire-road friction,

and optimum brake rotor geometry to minimize brake temperature rise and thermal stresses. Statistically speaking, most domestic drivers rarely exceed 0.1 to 0.2 g braking severity, and may approach dry-road brake lockup or antilock braking system (ABS) modulation only twice a year. Consequently, optimizing brake designs with respect to maximum-effectiveness braking may not yield optimum braking performance in terms of brake wear life for low-level braking effectiveness or continued braking. Large values of thermal conductivity, specific heat, and density for brake rotors yield lower swept surface temperatures.

1.1.2 Maintaining Speed on a Downgrade

In most downgrade driving situations, service brake systems perform adequately when properly used by the driver. During constant-speed downgrade operation, the potential energy is converted into thermal energy by the brakes, resulting in increased brake temperature. As long as the operating conditions in terms of the potential energy rate (weight, slope, and speed) are such that the steady-state brake temperature reached is less than a brake-specific critical temperature, the vehicle will be able to safely descend the downgrade. Important design parameters are that each brake produces an optimum share of the overall low-level braking force over an extended time, which is often different from the share required for maximum-effectiveness braking; that the convective cooling is optimized through effective ambient airflow and large cooling areas; and that, in the case of interstate buses and similar vehicles, cooling airflow obstructions are eliminated or minimized.

1.1.3 Holding Stationary on a Downgrade

Holding a vehicle stationary is primarily a function of the force transmission or mechanical gain between the application lever and braked tires. Safety standards generally require a specified hill-holding capacity. However, because a parking brake may be used in an emergency situation when the service brake has failed, both thermal and vehicle dynamic factors must be considered by the brake engineer. In addition, in such an emergency, human factors may be of critical importance in terms of parking brake control location, hand or foot application, and apply modulation.

1.2 Vehicle Deceleration and Stopping Distance

1.2.1 Basic Measures of Motion

The motion of a decelerating vehicle can be described by four measures of physics, namely distance, time, velocity, and deceleration. Distance and time are fundamental measures; that is, they cannot be broken down into submeasures. Velocity and deceleration are measures derived from distance and time; i.e., they can be broken down into fundamental measures.

The velocity V of a vehicle is computed by the ratio of distance S and time t :

$$V=S/t \quad , \quad \text{m/s (ft/s)} \quad (1-1)$$

where S = distance, m (ft)

t = time, s

The term “speed,” often used to describe velocity, only refers to the magnitude of the velocity, and does not indicate angular orientation and direction of the moving vehicle.

The deceleration, a , of a vehicle is computed by dividing the velocity decrease by the time interval during which the velocity change has occurred:

$$a = \frac{\Delta V}{\Delta t} = \frac{V_2 - V_1}{t_2 - t_1} \quad , \quad \text{m/s}^2 (\text{ft/s}^2) \quad (1-2)$$

where t_1 = time at start of deceleration, s

t_2 = time at end of deceleration, s

V_1 = velocity at start of deceleration, m/s (ft/s)

V_2 = velocity at end of deceleration, m/s (ft/s)

With the basic motion parameters defined, we can now compute the stopping distance and other related factors of a moving vehicle.

1.2.2 Simplified Stopping Distance Analysis

The motion of a vehicle as it changes over time can be shown graphically in the *velocity-time diagram* (V-t diagram) (Refs. 1.1, 1.2). In the case of constant velocity, the velocity curve is a straight line, as illustrated in Fig. 1-1. The rectangular area under the V-line is given by the product of height and length, or velocity multiplied by time. Inspection of Eq. (1-1) reveals that the distance S traveled is also equal to velocity multiplied by time, i.e., equal to the area under the V-curve.

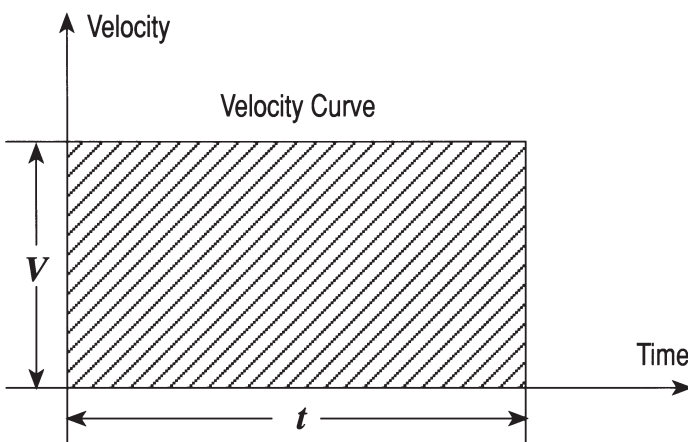


Figure 1-1. Constant velocity-time diagram.

This observation can be expressed as

The distance traveled by a vehicle is equal to the area under the velocity-time curve.

In a simple analysis, the vehicle motion for an emergency braking maneuver with constant deceleration can be approximated as shown in Fig. 1-2. After the driver's reaction time t_r and the brakes are applied, the vehicle begins to slow at constant deceleration from its travel speed V_{tr} , and the vehicle stops after the braking time t_s .

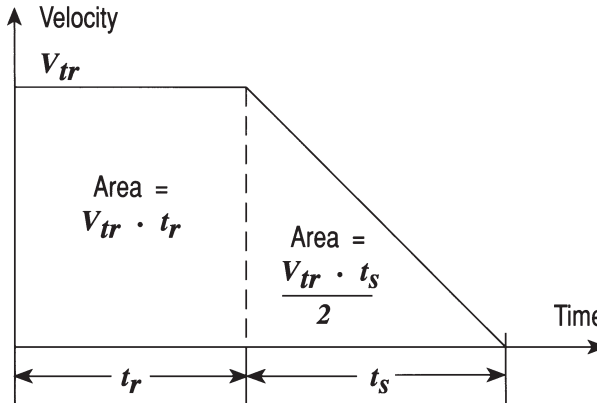


Figure 1-2. Velocity-time diagram for stopping process.

The V-t diagram shown in Fig. 1-2 consists of a rectangle under the constant speed portion, and a triangle under the decreasing speed portion of the maneuver. The total distance S_{total} is equal to the area of the rectangle plus the area of the triangle, or

$$S_{total} = V_{tr} t_r + V_{tr} t_s / 2 \quad , \quad \text{m(ft)} \quad (1-3)$$

The last term of Eq. (1-3) can be rewritten using $t_2 - t_1 = t_s$ or $t_s = V_{tr} / a$ from Eq. (1-2) as

$$S_{total} = V_{tr} t_r + V_{tr}^2 / 2a \quad , \quad \text{m(ft)} \quad (1-4)$$

Eq. (1-4) is the basic equation used for simple speed and stopping distance calculations in accident reconstruction.

1.2.3 Expanded Stopping Distance Analysis

In braking maneuvers where the maximum sustained vehicle deceleration is not achieved quickly and the deceleration rise cannot be ignored, a more detailed stopping distance analysis must be carried out.

Consider the basic braking parameters illustrated in Fig. 1-3. The idealized pedal force as a function of time is shown in Fig. 1-3a. At time zero (0) the driver recognizes the danger. After the reaction time t_r has elapsed, the driver begins to apply pedal force. After the brake system application time t_a has

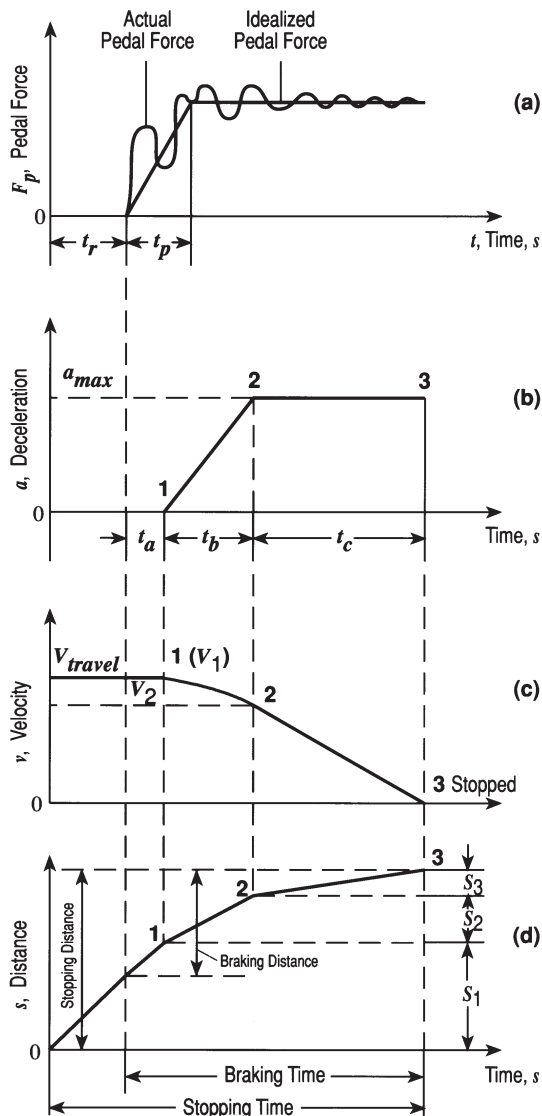


Figure 1-3. Stopping distance analysis.

passed, the brake shoes contact the drums and vehicle deceleration begins. The linear rise of pedal force is an approximation and occurs over the time t_p . In critical emergency situations, unskilled drivers tend to reduce their pedal forces somewhat after 0.1 to 0.2 s of brake initiation in an attempt to modulate the braking process (Ref. 1.3). When the obstacle comes closer, pedal forces rise again. Skilled drivers generally have pedal forces that more closely resemble the idealization. At higher speeds the pedal force rise characteristics that are actually present may be of lesser importance because their influence on overall stopping distance is small. Special designs such as the brake assist compensate for driver factors by rapidly and forcefully applying brake line pressure automatically to minimize response time.

The idealized deceleration is shown in Fig. 1-3b. The deceleration begins to rise linearly at point 1 when brake torque development starts, and stops at point 2, either because the pedal force is constant or all brakes are locked or brakes ABS modulate and no further increase in tire-road braking forces is possible.

The velocity change as a function of time is shown in Fig. 1-3c. Prior to any deceleration, the travel velocity remains constant. Deceleration forces other than those produced by the wheel brakes themselves may slow the vehicle before the brake pedal is applied. Depending on the vehicle and braking process involved, these retarding forces may come from engine drag, retarders, aerodynamic drag, or gravity when braking on an incline. If they are significant relative to the decrease in travel speed prior to brake application, then they must be included by using a bilinear deceleration rise characteristic. In most emergency situations with rapid pedal force applications, the single linear deceleration rise idealization provides excellent correlation with actual stopping distance tests. The stopping distances predicted with a linear deceleration rise generally are only 0.5 to 1% longer than those obtained with bilinear rise.

In the velocity diagram shown in Fig. 1-3c, the velocity is a curved line between points 1 and 2. The deceleration remains constant when it has reached its maximum value. The velocity line between points 2 and 3 is straight. The vehicle stops at point 3.

The total stopping distance is the summation of the individual distances associated with the different time intervals, i.e., beginning of reaction until deceleration begins to rise, deceleration rise time, and when the deceleration is constant until the vehicle stops.

a. Distance S_1 traveled during reaction and application time, t_r and t_a , respectively:

$$S_1 = V_1(t_r + t_a) , \text{ m(ft)} \quad (1-5)$$

where V_1 =velocity at point 1, m/s (ft/s)

b. Distance S_2 traveled during deceleration rise time t_b : The deceleration is given by the ratio of maximum deceleration and rise time, or

$$a(t) = a_{\max} t / t_b , \text{ m/s}^2(\text{ft/s}^2) \quad (1-6)$$

where a_{\max} = maximum deceleration, $\text{m/s}^2(\text{ft/s}^2)$

$a(t)$ = deceleration as function of time, $\text{m/s}^2(\text{ft/s}^2)$

t = time, s

t_b = deceleration rise time, s

The velocity as a function of time during the deceleration rise is equal to the initial velocity minus the change in velocity, or

$$V(t) = V_1 - \int a_{\max} t / t_b dt = V_1 - a_{\max} t^2 / 2t_b , \text{ m/s (ft/s)} \quad (1-7)$$

The distance S_2 traveled during the deceleration rise time t_b is computed by integrating Eq. (1-7) between time zero and t_b , or

$$S_2 = \int_0^{t_b} V dt = V_1 t_b - a_{\max} t_b^2 / 6 , \text{ m(ft)} \quad (1-8)$$

where V = velocity as function of time, m/s (ft/s)

c. *Distance S_3 traveled during constant deceleration time interval t_c : With the deceleration a_{\max} constant, the velocity as a function of time is computed by*

$$V(t) = V_2 - a_{\max} \int dt = V_2 - a_{\max} t , \text{ m/s (ft/s)} \quad (1-9)$$

where V_2 = velocity at point 2, m/s (ft/s)

The velocity at point 2 is computed by Eq. (1-7):

$$V_2 = V_1 - a_{\max} t_b / 2 , \text{ m/s (ft/s)} \quad (1-10)$$

The time required for the vehicle to stop, or for velocity $V(t)$ to be equal to zero, is computed by setting $V(t) = 0$ in Eq. (1-9), solving for V_2 and substituting into Eq. (1-10), and solving for time t_c :

$$t_c = V_2 / a_{\max} = V_1 / a_{\max} - t_b / 2 , \text{ s} \quad (1-11)$$

The distance S_3 traveled during the constant deceleration interval is computed by

$$S_3 = \int_0^{t_c} V dt = V_2 t_c - a_{\max} t_c^2 = V_2^2 / 2a_{\max} , \text{ m(ft)} \quad (1-12)$$

$$S_3 = 1/2a_{\max} (V_1^2 + a_{\max}^2 t_b^2 / 4 - V_1 a_{\max} t_b) , \text{ m (ft)}$$

The total stopping distance S_t is computed by the sum of all individual distances, or

$$S_t = S_1 + S_2 + S_3 = V_1 (t_r + t_a + t_b / 2) + V_1^2 / 2a_{\max} - a_{\max} t_b^2 / 24 , \text{ m (ft)} \quad (1-13)$$

In most cases the third term in Eq. (1-13) is small for short deceleration rise times t_b as compared to the other terms and, consequently, is neglected, yielding for the total stopping distance S_t :

$$S_t = V_1 (t_r + t_a + t_b / 2) + V_1^2 / 2a_{\max} , \text{ m (ft)} \quad (1-14)$$

The total time t_t from the driver reaction to vehicle stopping is given by

$$t_t = t_r + t_a + t_b / 2 + V_1 / 2a_{\max} , \text{ s} \quad (1-15)$$

The following example illustrates the influence of the different factors on stopping distance. A vehicle travels at a speed of 96 km/h or 26.7 m/s (88 ft/s), when the driver recognizes a hazard. After one second reaction time ($t_r = 1$ s), 0.25 s brake system application time ($t_a = 0.25$ s), and 0.3 s deceleration rise time ($t_b = 0.3$ s), the vehicle slows at a constant deceleration of 0.6 g or 5.9 m/s^2 (19.3 ft/s^2)

Substitution into Eq. (1-13) yields

$$\begin{aligned} S_t &= (26.7)(1.55) + (26.7)^2/2(5.9) - (5.9)(0.3)^2/24 \\ &= 41.3 + 60.3 - 0.02 = 10,158 \text{ m} \end{aligned}$$

$$\left[\begin{aligned} S_t &= (87.5)(1.55) + (87.5)^2/2(19.3) - (19.3)(0.3)^2/24 \\ &= 135.6 + 198.3 - 0.07 = 333.8 \text{ ft} \end{aligned} \right]$$

The total time is computed by Eq. (1-15) as

$$t_t = 1 + 0.55 + 0.3/2 + 26.7/5.9 = 5.93 \text{ s}$$

Inspection of the numerical values reveals the third term with 0.02 m (0.07 ft) to be insignificant compared to the others.

1.2.4 Driver Reaction Time in Emergency Braking

Emergency braking may be caused by a partial or complete service brake system failure, or by an exterior event such as a person stepping into the path of a vehicle. In the first case drivers may or may not respond correctly. Most drivers will not use the emergency or parking brake because a partial or complete service brake failure is an unexpected and sudden event in terms of excessive brake pedal travel and expected deceleration, and average drivers have not “practiced” a proper response action. In the second case the driver most likely will apply full pedal force and the brake system responds as designed and/or maintained.

In the discussion that follows, an emergency caused by an exterior event is assumed. The overall stopping distance is strongly affected by driver reaction time. Driver reaction times used in accident reconstruction generally cover a time period from the perception of the hazard until some or all brakes are locked or the ABS modulation begins.

Driver reaction consists of four phases: perception, judgment, reaction initiation, and reaction execution (Ref. 1.4). In certain cases such as a panic-type brake application, the judgment time may be at a minimum. Results of a large number of reaction time tests measured in simulated emergency braking maneuvers show that typical values of 0.75 to 1.5 s are generally acceptable (Refs. 1.5, 1.6). Statistical analyses of a large body of test data suggest that differences may exist for reaction times used in accident reconstruction. A brief review of the findings is presented next.

In general, an object or hazard will first appear in the driver's peripheral vision.

Only after the driver has focused the eyes on the object can an intended and planned human reaction begin. It is important to recognize that the first appearance of an object in the driver's peripheral vision, such as a pedestrian stepping off the curb on the left side of the highway, is not the beginning of the driver's reaction time. Experimental psychology has also determined that human reaction times are shorter for an expected signal than for less-observed unexpected ones. Drivers use *distributive* attention as they drive to scan the entire scene around them for signal gathering and possible conflicts. Only after they change to *concentrative* attention and focus on the hazard can a controlled reaction begin.

Prior to focusing the eyes, the head may have to be moved to bring the object into direct vision. Test results show that between 0.32 and 0.55 s will elapse from the time an object has entered a driver's peripheral vision to when the eyes are focused on the object.

The basic reaction time follows and runs from the moment the eyes are focused until the driver begins to lift the foot off the gas pedal. Test results show a basic reaction time range of 0.22 to 0.58 s. It is noted again that no general judgment time or actual accident threats were associated with the tests.

The pedal switchover time covers the period from the moment the right foot lifts off the gas pedal and begins to displace the brake pedal. Measurements show a range of 0.15 to 0.21 s.

For hydraulic brakes, a brake system response or application time of 0.03 to 0.06 s was measured, indicating that only a small amount of time is required to bring the shoes or pads in contact with the drums or discs.

The deceleration rise or buildup time is the time during which the wheel brake torque increases from zero to its maximum value until brakes are locked or ABS modulation begins. Measurements indicate a range of 0.14 to 0.18 s. These time values are a function of vehicle speed and tire/road friction levels. The total time from the moment the object entered the driver's peripheral vision until the brakes are locked ranges from 0.86 to 1.58 s.

In certain accident situations not requiring head movement, the driver may not claim the extended reaction time. For example, when a driver follows a truck too closely and is focusing on the tail lights of the truck, the hazard signal indicated by the brake lights coming on does not enter through the driver's peripheral vision. Under these circumstances a reaction time of only 0.54 to 1.03 s should be used.

1.2.5 Average and Maximum Sustained Deceleration

The maximum sustained deceleration existing between points 2 and 3 is illustrated in Fig. 1-3b. The resulting stopping distance as a function of time is illustrated in Fig. 1-3d. The average deceleration is defined as that fictitious constant deceleration existing between points 0 and 4 that would have resulted in the same stopping distance produced by the actual deceleration.

The average deceleration a_{av} is calculated by:

$$a_{av} = \frac{a_{max}}{1 + \frac{19.7a_{max}(t_a + \frac{t_b}{2})}{V}}, \text{ g-units} \quad (1-16)$$

where a_{max} = sustained maximum deceleration, g-units

t_a = brake application time, s

t_b = deceleration rise time, s

V = velocity at beginning of braking, m/s

In the imperial measuring system, replace 19.7 in Eq. (1-16) by 44 and use velocity V in mph.

1.2.6 Deceleration Measurement

All deceleration or acceleration measuring devices use the inertial displacement of a mass as velocity changes. Commercially available devices such as the Vericom VC4000 measure deceleration as a function of time every 0.01 s [Eq. (1-6)], and integrating twice yields velocity [Eq. (1-7)] and distance over time [Eq. (1-13)]. In a particular tractor-semitrailer braking test on a dry roadway, the following data were measured with a VC4000: peak or maximum deceleration 0.603 g; average deceleration 0.438 g; initial velocity 46.8 km/h (29.1 mph); braking time 2.99 s; distance traveled 18.9 m (62 ft). Assuming that a brake application time $t_a = 0.25$ s and a deceleration buildup time $t_b = 0.4$ s existed during the test, Eq. (1-16) yields an average deceleration of 0.43 g.

1.3 Elements of Automotive Brake System Design

1.3.1 Basic Design Considerations

Design engineers satisfy human needs problems. Whether a device is a complicated machine consisting of many parts or a simple item such as a paper clip, it was planned and designed before it was manufactured.

Most design errors and malfunctioning of devices are caused by insufficient planning and lack of proper identification of requirements and constraints. To achieve a certain design objective, several alternative solutions are generally available. Automotive braking systems are no exception. The brake design engineer must be able to rate the significance of a host of influence factors including braking stability, stopping distance, response time, reliability, safety, cost, maintainability, wear, noise, or human factors. The engineer must decide whether to use disc or drum brakes, vacuum or hydro-boost, deceleration or load-sensitive proportioning valves, standard or antilocking brakes, parking brakes using in-hub or disc application, diagonal or front-to-rear dual split, wedge or S-cam brakes, and many more. In addition, proper sizing of component parts is essential for an effective and safe brake system operation.

The first design solution is generally not the best one. Alternative designs must be considered and evaluated by a rational process frequently employing a design selection table, resulting in a prototype final design. Only when the designer has found the best compromise among the different constraints will the design be judged as best. The prototype final design is then optimized relative to several critical and important influence factors. With the prototype final design completed in most respects, a prototype braking system is tested and evaluated. Questions answered include: Does it work and function properly? Are all critical design and operational objectives met? Are safety standards and industry practices satisfied? How is it affected by in-use factors? Will it last? Is the customer happy with it?

The prototype is followed by the production model. This is the brake system sold to the customer. Future design improvements are made based on simplifications, cost reductions, and hopefully, infrequent customer complaints and safety recalls. Modifications may be introduced based on different applications and markets. Standardization; limitations to certain models, sizes, or performance levels; and different materials or manufacturing methods may be considered as running production changes to optimize cost-benefit ratios.

1.3.2 Product Design and Development Guides

For an engineer to accomplish the design task, he or she must consider a number of engineering design concepts, guides, standards, and practices. In the search for the “best” brake system design, the basic design and product development rules that follow must be considered:

1. Reliability takes precedence over such considerations as efficiency or cost. An unreliable brake system will create safety hazards, and possibly costly recalls. Reliability is achieved through proper design based on sound engineering principles, use of proven machine elements, testing, and other factors.
2. System-Based Design Methods will ensure that a safe functioning of the brake system is obtained. Guard against making singular changes that accomplish a specific objective but cause system performance to suffer. For example, increasing the brake drum diameter on the rear axle to improve lining life without an appropriate change on the front brakes will shift brake balance to the rear, thus increasing the potential for premature rear brake lockup.
3. Safety and Product Liability requires that the brake system absolutely does not exhibit any unreasonable safety hazards or develop any during the operation of the vehicle. The design engineer must know basic human ergonomics, not only based on what a driver can do in a laboratory experiment, but also based on what typical drivers will do during an emergency. During foreseeable operations the vehicle should remain stable and controllable by the driver. Any unexpected vehicle behavior, especially when uncontrollable, will create critical situations and may cause accidents.

4. Material Selection is based on cost-efficiency with respect to strength, weight, wear life, and performance.
5. Surface Finish should be the least expensive one in terms of machining or surface treatment required to ensure proper and safe functioning of components and subsystems.
6. Economics is considered by including prefabricated materials or subcomponents and proven in-house parts.
7. Production Methods are based on a consideration of all possible methods such as machining, casting, welding, forging, or gluing, in connection with the number of pieces to be produced.
8. Assembly is considered during the design in terms of cost-effective manufacturing, maintenance, repair, and inspection. Brakes that are difficult to maintain tend to be unsafe.
9. Warnings are part of the responsibility of the designer when he or she knows of an inherent design hazard but is unable to design the hazard out or otherwise guard against it.
10. New-Versus-Used conditions must be considered by the design engineer. For example, new brakes tend to produce lining friction different from that of broken-in or burnished linings.
11. Failure Analyses show the effect of critical component failure on performance, reduced safety, and potential for driver error including design-induced driver errors.
12. Safety Standards for global, federal, state, and industry level are satisfied and/or exceeded.
13. Accelerated Testing is used to reveal any in-use conditions that may show problems.
14. Inspection and Maintenance procedures are established which ensure a safe and efficient operation of the brakes.
15. Advertisement Guidelines are provided which guard against misleading claims.
16. Production Approval is given only after the design is reviewed by persons experienced in the use, inspection, repair, maintenance, safety, and manufacturing of the brake system.
17. Packaging, Labeling, and Shipping may be of lesser importance than other considerations. However, labels must clearly identify parts and state use limitations such as shelf life, etc.
18. Customer Complaints and Accident Data are analyzed relative to potential input data for design modifications. Accident databases such as National Automotive Sampling System (NASS) or Fatal Accident Reporting System (FARS) contain valuable information for brake engineers when properly queried (see Chapter 1.6).

The design engineer considers most if not all of the points mentioned when designing a braking system or evaluating alternative design solutions. Frequently, additional specific factors are included that have a direct bearing on the particular design analyzed.

1.3.3 Basic Brake System Design Considerations

The brake engineer has the following data available when designing the brakes of a vehicle. In some cases, certain data such as maximum weight may change as an entirely new vehicle is developed. The design of a braking system must always be based on a systems approach. A small change in one area may adversely affect the overall performance of the braking system in a safety-critical area.

1. Empty and loaded vehicle weight.
2. Static weight distribution lightly and fully laden.
3. Wheelbase.
4. Center of gravity height lightly and fully laden.
5. Intended vehicle function.
6. Tire and rim size.
7. Maximum speed.
8. Global braking standards.
9. Trailer use, if any.

1.3.4 Specific Steps for Hydraulic Brake System Design

The design of a hydraulic brake system must include the ten steps discussed next. Generally, the design follows the sequence as shown, but an iterative process will evolve. The design steps are based upon engineering concepts and mathematical formulation. Certain input data such as lining/rotor coefficient of friction or brake factor, or convective heat transfer cooling coefficients may have to be obtained from laboratory testing. It is important to recognize that in general, it is more cost-efficient to utilize a well-known pad or lining material with established performance characteristics, and to design the brake system hardware around it, rather than to develop a new pad material to “fit” with a particular caliper size. The result may be costly running of production changes to adjust the brake hardware at a later time. The use of the ten steps results in a properly engineered brake design. Design input data obtained under laboratory conditions may not respond to actual in-use conditions of the vehicle brake system.

Step 1: Brake Balance Front-to-Rear: Proper balance ensures directional stability while braking for lightly and fully laden operating conditions, optimum tire-road friction utilization, and hence, minimum stopping distances. For a single vehicle without trailer, optimum brake balance is determined by wheel base, weight (empty and laden), weight distribution, center-of-gravity height, and deceleration range. For

brake systems utilizing ABS brakes, the underlying brake system must perform safely with ABS brakes disabled.

- Step 2: Wheel Brakes and Brake Torques: With the proper brake balance established, the individual brake torques among axles can be formulated in terms of component dimensions such as wheel cylinder or caliper sizes, rotor diameter, and brake factors (type of brake and lining friction material).
- Step 3: Brake Line Pressure, Valves, and Dual Split: With the wheel/foundation brake sizes established, the brake line pressure required for a design deceleration as well as any modulating valves and diagonal or front-to-rear hydraulic split can be determined.
- Step 4: Master Cylinder and Brake Fluid Volume: The master cylinder diameter (cross-sectional area) is determined for a specified pedal force and deceleration when the booster (if any) has failed. The travel of the individual master cylinder pistons for each hydraulic split circuit is determined based upon zero-pressure volume needs such as pad/rotor play and air inclusions, and pressurized volume needs such as elastic caliper deformation and brake hose expansion. For the case of a partial hydraulic brake failure, pedal travel, pedal force, and associated deceleration are analyzed.
- Step 5: Brake Pedal Force and Booster: For a specified pedal force and pedal travel, the vacuum booster or hydro-boost size is determined based on safety standards and human factors limitations. An adjustable brake pedal may have to be considered to accommodate small and large drivers.
- Step 6: Specific Design and Wear Measures: The sizes of brake pads or width of brake linings are “checked” against a number of specific design measures to ensure acceptable pad wear and rotor life, as well as brake fade performance.
- Step 7: Brake Temperature and Cooling: With brake balance and brake sizes established, brake temperatures are determined for maximum braking and loading conditions and checked against limit values.
- Step 8: Parking Brake System: With the wheel brakes established, the parking brake is designed in terms of location (front, rear, or drive shaft) and hill-holding capacity, as well as deceleration capability. Human factors are considered in terms of location and modulation.
- Step 9: Braking-in-a-Turn: With the entire brake system established, the braking performance while turning is analyzed in terms of tire-road friction utilization for a specified lateral acceleration. In particular, the brake pedal force or deceleration at which the brake of the first inner wheel will lock is determined.

Step 10: Safety Standards: The braking performance of the vehicle is evaluated with respect to any applicable safety standard, industry practice, global compliance and certification, and customer expectations.

1.3.5 Brake System Design/Testing Checkpoints

The brake engineer and manufacturer must recognize that safety standards in general are minimum standards, and compliance with the requirements does not automatically produce a safe brake system in all respects. The reader is reminded of Federal Motor Vehicle Safety Standard 105 (FMVSS 105) which, since its inception in 1968, did not have a requirement for braking on wet or slippery road surfaces. Ignoring brake design factors applicable to low-friction wet roads resulted in unsafe braking systems, especially when rear drum brakes with large brake factors were used. Moisture sensitivity resulted in loss of directional stability while braking (Ref. 1.7).

The design and testing of the braking system must include the following design checkpoints:

1.3.5.1 Braking Effectiveness

- a. Maximum straight-line wheels-unlocked/ABS modulation deceleration.
- b. Braking effectiveness, that is, brake-line pressure-deceleration characteristic.
- c. Pedal force-deceleration characteristic.
- d. If appropriate, vacuum-assist characteristic.
- e. If appropriate, full-power characteristic.
- f. If appropriate, retarder characteristic.

1.3.5.2 Braking Efficiency

- a. Maximum straight-line wheels-unlocked/ABS modulation deceleration for low and high roadway friction coefficient, both lightly and fully laden.
- b. Maximum curved-line wheels-unlocked/ABS modulation deceleration for low and high roadway coefficient of friction, both lightly and fully laden.

1.3.5.3 Stopping Distance, Lightly and Fully Laden

- a. Minimum stopping distance without wheel-lockup/ABS modulation.
- b. Minimum stopping distance without loss of directional control with wheel-lockup/ABS modulation, for wet and dry brakes, and for “cold” and heated brakes.
- c. Minimum stopping distance without wheel-lockup/ABS modulation while turning.
- d. Ensure directional stability in the event of ABS failure.

1.3.5.4 Response Time

- a. For air brakes, application and release time lags.
- b. For hydraulic brakes, pedal force-boost lag.
- c. No brake delay with ABS modulation when operating on rough roadways or ice.

1.3.5.5 Partial Brake System Failure

- a. Braking effectiveness with service-system circuit failure.
- b. Braking effectiveness with partial or complete loss of power assist.
- c. Braking effectiveness with brakes in thermal fade condition.
- d. Directional stability with diagonal split failure or front-circuit failure.
- e. Increased pedal travel with service-system circuit failure.
- f. Increased pedal force with service-system circuit failure.

1.3.5.6 Brake Fluid Volume Analysis

- a. Master cylinder bore and piston travel for each brake circuit.
- b. Wheel-cylinder piston travel available with full pedal travel.
- c. Proper return of pad after brake release to minimize brake pedal travel and pad/rotor drag.

1.3.5.7 Thermal Analysis

- a. Heat-transfer coefficient for drum or rotor.
- b. Brake temperature during continued and repeated braking, and maximum effectiveness stop.
- c. Reduced braking effectiveness during faded conditions.
- d. Thermal stresses to avoid rotor cracking and heat checking.
- e. Brake fluid temperatures in wheel cylinders or calipers to avoid brake fluid vaporization (may be critical in diagonal hydraulic circuit split with brake dragging on one axle).
- f. Temperature analysis with in-use factors affecting cooling such as rotor vane corrosion, brake shrouding, off-road conditions such as mud, etc.

1.3.5.8 Emergency or Parking Brake

- a. Maximum deceleration by application of emergency brake lever on level and sloped roadway.
- b. Ability by driver to apply/modulate in the event of an emergency caused by a service brake system failure.
- c. Optimum location of warning light and/or buzzer when driving with parking brake inadvertently applied. In case of diagonal dual brake circuit, entire service brake may fail due to brake fluid vaporization on brakes on one axle.
- d. Maximum grade-holding capacity.
- e. Determination under what conditions an automatic emergency brake application should occur.

1.3.5.9 Specific Design Measures

- a. Heat flux into drum or rotor surface.
- b. Horsepower absorbed by brake lining or pad.
- c. Wear measure in form of product of lining friction coefficient and mechanical pressure.
- d. Design brake temperature.

1.3.5.10 In-Use Factors

- a. Determination of whether certain maintenance practices or lack of maintenance by particular user groups may require redesign to ensure

- adequate component performance and life.
- b. Determination of whether the operating environment is adverse to parts of the brake system (corrosion, dust, mud, water, ABS-delayed braking when operating on rough roadways).
 - c. Determination of whether wear or use affects brake force distribution and, hence, braking stability due to premature rear brake lockup (“green” versus burnished or wet versus dry brakes).

1.3.5.11 Component Sizing

- a. Based on fatigue loading.
- b. Based on overload.
- c. Based on wear life, temperature, heat checking, etc.

1.3.5.12 Safety Regulations

- a. Federal standards and global certification.
- b. Industry standards.
- c. Consumer expectations and limitations.

1.4 Pedal Force and Pedal Travel

Safety standards provide for certain limitations on pedal force. Ergonomic considerations and driver acceptance limit pedal force and pedal travel to a particular range established over the years. The maximum force exerted with the right foot for the 5th percentile female is approximately 445 N (100 lb); for the male approximately 823 N (185 lb) (Ref. 1.4). Both pedal force and pedal travel are important parameters for the human operator to safely modulate braking effectiveness. Brake systems without sufficient pedal travel feedback, particularly on slippery roads, may cause loss of vehicle control due to inadvertent brake lockup.

The pedal apply speed of skilled drivers is approximately 1 m/s (3 to 3.5 ft/s); of normal drivers it is approximately 0.5 ft/s. For a pedal travel of 100 mm, pedal apply times are between 100 and 200 ms. A “soft” pedal does not only cause unsafe driver response but also increased stopping distances.

1.4.1 Manual or Standard Brakes

For brakes without a booster, the brake system should be designed so that for a maximum pedal force of 445 to 489 N (100 to 110 lb), a theoretical deceleration of 1 g is achieved when the vehicle is loaded at GVW (Gross Vehicle Weight; maximum allowable weight designated by the manufacturer). Maximum pedal travel between fully released and the point where the master cylinder piston bottoms out should not exceed 150 mm (6 in.). Drivers generally have rated pedal force/deceleration ratios of 267 to 445 N/g (60 to 100 lb/g) as very good, and 445 to 668 N/g (100 to 150 lb/g) as good. An adjustable brake pedal may have to be considered.

1.4.2 Brake Systems with Booster

A maximum pedal force of approximately 223 to 334 N (50 to 75 lb) should provide a deceleration of 0.9 to 1 g. The associated pedal travel should not

exceed 75 to 90 mm (3 to 3.5 in.) for “cold” (less than 366 K or 200°F) brakes. The booster characteristic should increase linearly with pedal force and pedal travel. The booster run-out point should be reached for decelerations greater than 0.9 to 1 g. In order to ensure proper brake force modulation, a pedal force not greater than 13 to 22 N (3 to 5 lb) should be required to start boost assist. The boost ratio or gain should not be greater than approximately 4 to 6 to ensure safe vehicle deceleration in the event of a boost failure. Hydraulic brake line pressure rise time delays of 100 ms for single, and up to 180 ms for double diaphragm boosters must be considered.

1.4.3 Partial Failure Performance

Federal Motor Vehicle Safety Standard (FMVSS) 105 and 135 provide certain limits on pedal force and stopping distances in the event of a partial brake failure. These are considered minimum requirements. In general, brake systems can achieve higher braking effectiveness at lower pedal forces than those required by the safety standard.

A maximum pedal force of approximately 445 N (100 lb) should achieve a deceleration of approximately 0.3 g for the vehicle loaded at GVW in the event of a booster failure.

In the case of a hydraulic circuit failure, a maximum pedal force of approximately 445 N (100 lb) should slow the vehicle laden at GVW at a deceleration of approximately 0.3 g.

In the event of repeated or continued braking with increased brake temperatures, a pedal travel of approximately 115 to 130 mm (4.5 to 5 in.) out of 150 mm (6 in.) available should not be exceeded for a maximum pedal force of approximately 445 N (100 lb).

1.4.4 Parking Brake

The parking brake should hold the vehicle stationary when laden at GVW on a 30% slope (16.7 degrees) with a hand force of not more than 356 N (80 lb) or a foot force of less than 445 N (100 lb). With the apply force limitations stated, the parking brake should be able to slow a vehicle laden at GVW at approximately 0.3 g.

1.5 Design Solution Selection Process

For the design of mechanical devices, including a brake system, the following rules should be considered:

1. A reasonable best compromise among all constraints yields the best design.
2. Needs and requirements must be determined clearly.
3. One sound and basic design thought implementation is better than running production changes.
4. The first solution may not be the best one.
5. Use a systems approach when optimizing.

6. Clearly evaluate different design concepts and alternative solutions.
7. Practice concept variation (example: pad application mechanisms in air disc brakes).
8. For equivalent designs minimize material cost to lower manufacturing expenses.
9. Standardize for global use.
10. Valid complaints yield valuable design input data.
11. Monitor accident databases with respect to critical brake causation data.
12. In the design solution selection process, ranking points are assigned to each different solution relative to the various influence factors or constraints (Ref. 1.8). A point spread of zero to five has worked well, with the ideal solution receiving five points. It should be recognized that design experience and personal inclinations may affect certain rankings. Because the final result, however, is based on many rank entries, reasonable objectivity is ensured. The ranking matrix or design selection table has the different design solutions written across the top, and the influence factors or constraints in the left-hand column. Frequently, cost and safety are ranked individually to assign more weight to their respective contribution in the ranking process and, hence, final design.

For the example of a parking brake design, some of the factors that influence design concept evaluation and/or alternative solutions are listed:

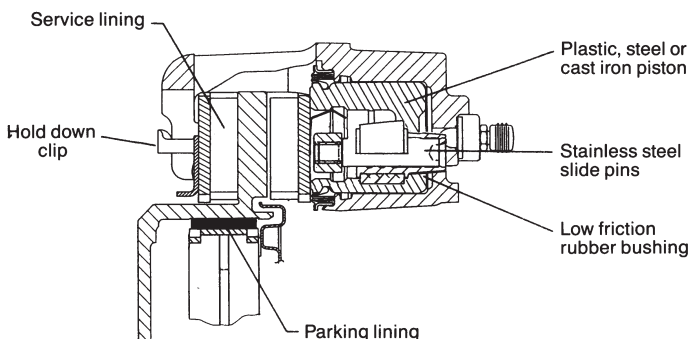


Figure 1-4. Floating caliper with drum-in-hat parking brake.

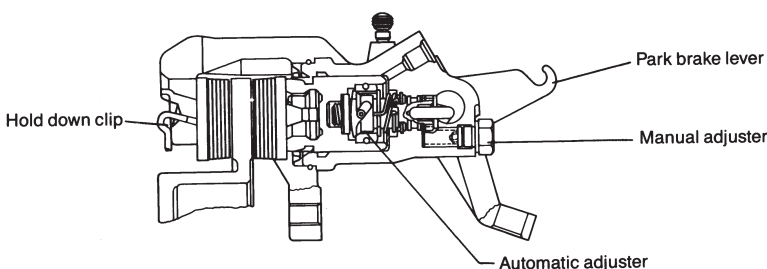


Figure 1-5. Floating caliper with integral parking brake.

1. Disc Service Brake: Drum-in-hat (Fig. 1-4) or pad-apply integral (Fig. 1-5).
2. Drum brake: Leading-trailing (LT) shoe brake.
3. Automatic pad wear adjustment.
4. Electric or mechanical apply.
5. Deceleration and/or hill holding/safety standards.
6. Front axle, rear axle, drive shaft.
7. Hand or foot application, electric button, control location.
8. Driver modulation in case of service brake failure.
9. Automatic apply in case of service brake failure.
10. Manufacturing cost, reliability, complexity.
11. Inspection, maintenance and repair ability.
12. Effectiveness and efficiency.
13. Left-to-right braking imbalance.
14. Wear, corrosion, water, road debris interactions, off-road factors.
15. Warning light and/or audible when inadvertent apply.
16. Diagonal versus front-to-rear split.
17. OEM versus after market practices.
18. Proven product, shelf item – little or no research required.

For many of the individual influence factors listed, subsections must be considered. For example, when designing a pad-apply disc parking brake, factors relating to the apply mechanism such as screw, cam, lever or electric system, automatic adjustment, corrosion, deformation when a large service brake pedal force is applied while applying the parking brake, etc. must be carefully evaluated.

1.6 Braking System Involvement in Accidents

1.6.1 Basic Safety Considerations

The safety of a braking system is affected by many factors. Brake component and vehicle manufacturers are responsible for the inherently sound design, manufacture, and reliability of the brakes. Users are responsible for continued safety of their brakes by ensuring proper maintenance and repair. Governmental agencies are responsible for meaningful and safety-oriented standards and regulations.

1.6.1.1 Reliability

Reliability is an important safety consideration for a design engineer. It is defined as the probability that a component or subassembly will not fail within a specified time period. The change of failure probability with time, or failure

rate, is the probability that a given component will fail after a specified period of time. Failures occurring early in the life of a vehicle are generally caused by manufacturing defects, whereas late failures are caused by aging and wear. Time-independent failures are caused by such events as accidental rock impact, improper repairs, or misuse. We must also recognize that the relationship between failure probability and accident probability cannot be established easily.

1.6.1.2 Danger, Hazard, and Risk

Product liability analyses frequently involve terms such as “danger,” “hazard,” “risk,” “unreasonably defective,” and many more. It appears helpful to define these terms for the limited scope of this book. According to Webster’s Dictionary, risk is the chance of injury, damage, or loss; a hazard exists when a risky or a dangerous condition is present; and danger is the likelihood of injury, or a thing that may cause injury.

For our purposes we will define the terms as follows: *Hazard* is the potential for causing injury or loss; *danger* is the likelihood that a hazard will be involved in causing injury; *risk* is a person’s planned or inadvertent operation of a vehicle in such a manner that injury or harm may occur; and *safety* is a measure of the probability that a hazard or danger does not exist. We should be aware that the terms are often used interchangeably in the literature and by attorneys.

An example may help to illustrate the use of the terms. Consider an empty pickup without antilock brakes whose rear brakes may lock first when sufficient pedal force is applied. Because locking of the rear brakes first may cause directional instability and loss of control and, consequently, is a potential for causing an accident and injury, it is a hazard. How dangerous is the vehicle in the empty condition with this brake system? Obviously it depends on how often the pickup truck is operated in the empty or driver-only condition relative to the loaded one, and how often brakes are locked. Other factors of importance are road conditions, speed, and general usage of the pickup truck. For example, on a wet or slippery road surface it is more likely for wheels to lock, while vehicle miles driven on wet and slippery roads are fewer.

The dangerous nature associated with a particular design may be expressed as the product of hazard consequences and frequency of hazard occurrence (Refs. 1.9, 1.10), or

$$\text{Danger} = \text{Hazard Consequences} \times \text{Hazard Frequency}$$

We see that products, including braking systems, will have a high degree of danger, which is often expressed as being unreasonably dangerous and, hence, defectively designed, when there is a great level of hazard consequence associated with the use, and when the hazardous condition has a high likelihood of occurring. For example, heavy commercial vehicles are extremely hazardous when their S-cam manual slack adjusters are at a critical adjustment level that may render the vehicle virtually without brakes under certain operating conditions. The fact that manual S-cam air brakes frequently are not adjusted near their optimum level is well known, resulting in a high degree

of hazard occurrence. Consequently, the danger associated with manually adjusted air brakes is high, because the product of hazard consequences and hazard frequency is high. Since 1993, FMVSS 121 requires air brake systems to be equipped with automatic slack adjusters (ASA). Problems may exist when mechanics manually adjust ASA, potentially over-adjusting the push rod travel and causing shoes to drag (brake fade), or rendering the ASA ineffective.

An example of a low danger level and, hence, safe braking system notwithstanding a high hazard is that associated with the safety analysis of brake fluid vaporization of diagonal-split dual-brake systems. When the brake temperatures of both front brakes reach a critical level sufficient to boil and vaporize brake fluid, the entire service or foot brake will fail because no brake line pressure can be produced in either brake circuit. There is no question that this is a very hazardous condition with a high potential for doing harm. However, the likelihood for brakes to reach temperatures sufficiently high for brake fluid to vaporize is extremely low. Under normally foreseeable conditions with proper brake maintenance, this may never occur. Therefore, the danger given by the product of hazard consequences and frequency is low relative to diagonal-split brake systems and brake fluid vaporization. We should, however, recognize that under abnormal yet somewhat foreseeable conditions, diagonal split systems may fail due to brake fluid vaporization. These abnormalities may result from improper parking brake release for both drum and disc brakes, dragging brake pads due to defective caliper design or maintenance, excessive braking on extended down grades, and lowering of the brake-fluid boiling-point temperature through a high water content. Changing brake fluid every one to two years will minimize brake fluid boil.

Accident statistics show that slightly less than 2% of all highway crashes involve brake malfunctioning as a contributing accident causation factor (Ref. 1.4). Of these, nearly 90% are related to braking system defects caused by improper maintenance, whereas the remaining 10% involve directional braking instability. The 10% figure is expected to decrease as more vehicles are equipped with electronic stability control (ESC) systems as required by FMVSS 126 (Ref. 1.11).

1.6.2 National Accident Databases – Braking Accident Causation

The national accident databases discussed next contain statistical data that may be used to compare vehicle component/system performance, including braking systems, prior to and after a design change was implemented. For example, a brake engineer may decide to compare the crash involvement of a specific model vehicle before and after an ABS brake system was installed. In order for the data analyst to properly filter the databases, specific information such as road conditions, precrash driver braking and steering maneuver, roadway geometry, or stopped traffic ahead must be provided by the brake engineer.

1.6.2.1 National Accident Statistical Sampling - NASS

NASS is composed of two systems - the Crashworthiness Data System (CDS) and the General Estimates System (GES). Both systems are based on approximately 5000 cases selected yearly from a sample of police crash reports

and investigated in depth. NASS collects detailed data on representative, random samples of minor, serious, and fatal crashes involving passenger cars, pickup trucks, vans, large trucks, motorcycles, and pedestrians (Ref. 1.12). The following are variables that are brake related:

1. Antilock.
2. Skidding longitudinally.
3. Skidding laterally – clockwise.
4. Skidding laterally – counterclockwise.
5. Mechanical failure, such as brakes, steering, tires, or other vehicle problems.
6. Vehicle Contributing Factors: Brake System.
7. Braking (no lockup).
8. Braking (lockup).
9. Braking (lockup unknown).
10. Releasing brakes.
11. Braking and steering left.
12. Braking and steering right.
13. Braked/slowed.

On vehicles equipped with Air Bag Event Data Recorders, the precrash brake status is shown. Examples of defects not considered safety related are ordinary wear of equipment that has to be inspected, maintained, and replaced periodically such as shock absorbers, batteries, brake pads and shoes, and exhaust systems.

In a particular application NASS was queried to look at certain model-year pickup trucks equipped with vacuum (gasoline engine) or hydro-boost (diesel engine) power brake systems. The hydro-boost system used a single steering pump for both braking and steering assist, and in the case of combined braking-and-steering maneuvers with brake pedal forces greater than 450 to 500 N (100 to 110 lb), the braking system overrides (starves) the steering assist. For the vacuum power brake, the steering pump is used only for steering assist. The NASS data, when filtered with respect to combined braking right-turn maneuvers in an attempt to avoid the crash, showed 85.1% were diesel engine trucks compared to 14.9% gasoline trucks. In combined braking left-turn maneuvers, the percentages were 38.9% and 61.1%, respectively.

In another case a fatal accident had occurred. The road was wet and an earlier accident caused all traffic to stop. The driver of a 1999 Plymouth Voyager approached the vehicles in front, not realizing quickly enough that they were stopped. He steered to the right, avoiding the stopped traffic, only to crash into a guardrail. His vehicle slid along the guardrail and collided with the trailer of a tractor-trailer. The driver side A-pillar smashed into the right rear corner

of the trailer, killing the driver. Inspection of the mechanical condition of the Voyager revealed no brake or steering system defects. The subject Voyager was equipped with standard brakes, although ABS was available as an option. NASS was accessed to look for 1995-2001 Plymouth Voyagers with and without ABS brakes that were involved in accidents in which the critical precrash event was a stopped vehicle in the lane on wet roads. The numerical codes in NASS identify the following brake system equipment:

1. ABS not available
2. Four-wheel ABS, standard
3. Rear ABS-only, standard
4. ABS standard, wheel location unknown
5. Four-wheel ABS, optional
6. Rear ABS-only, optional
7. ABS optional, wheel location unknown
8. (not used)
9. Unknown

Only codes 1 and 2 need to be considered. The data showed that there were 84.8% non-ABS-Voyagers versus only 4.9% ABS-Voyagers involved in all accidents on wet roads; however, none involved a stopped vehicle ahead. Readers are cautioned that without a proper accident reconstruction NASS data may be misleading. The most difficult issues in the Voyager case were related to the driver's pedal force application, because no front brakes locked in the accident (the driver was able to steer his vehicle away from stopped traffic on a wet road) and, if the driver had applied the brakes, would ABS have made a difference in view of the reduced friction (wet road) and short distance in which to stop or lower the impact speed to mitigate injuries?

1.6.2.2 Fatality Analysis Reporting System – FARS

FARS is a nationwide census providing yearly data regarding fatal injuries suffered in motor vehicle crashes. FARS data are derived from a census of fatal traffic crashes in the U.S., the District of Columbia, and Puerto Rico. To be included in FARS, a crash must involve a motor vehicle traveling on a traffic way customarily open to the public and result in the death of a person (occupant of a vehicle or a non-motorist) within 30 days of the crash. FARS was conceived, designed, and developed by the National Center for Statistics and Analysis (NCSA) of NHTSA in 1975 to provide an overall measure of highway safety, to help identify traffic safety problems, to suggest solutions, and to help provide an objective basis to evaluate the effectiveness of motor vehicle safety standards and highway safety programs.

The following are brake-related variables:

Codes “01–19” — These are preexisting conditions not caused by damage in the crash. It refers to the condition of vehicle components as indicated in the police accident report (PAR). The report may indicate that a component, such as the braking system, is inadequate, inoperative, faulty, damaged, or defective. The condition may be due to owner/user neglect, poor maintenance, tampering, or defective manufacturing. The vehicle condition(s) noted only indicates the existence of the condition(s). They may or may not have played a role in the accident.

Chapter 1 References

- 1.1 Limpert, Rudy and Franco Gamero, "The Velocity-Time Diagram: Its Effective Use in Accident Reconstruction and Court Room Presentations," *The Accident Investigation Quarterly*, Issue 48, Fall 2007.
- 1.2 Strothers, Charles E., "Velocity Histories as An Accident Reconstruction Tool," SAE Paper No. 850249, SAE International, Warrendale, PA, 1985.
- 1.3 Burckhardt, Manfred, *Fahrwerkstechnik: Bremsdynamik und Pkw Bremsanlagen*, Vogel Verlag, Germany, 1991.
- 1.4 Limpert, Rudolf, *Motor Vehicle Accident Reconstruction and Cause Analysis*, Lexis-Nexis, 6th edition, 2009.
- 1.5 Burckhardt, Manfred, *Reaction Times in Emergency Braking Maueuvers*, Verlag TUV Rheinland, Germany, 1985.
- 1.6 Mitschke, Manfred, *Vehicle Dynamics*, Springer-Verlag, Germany, 1972.
- 1.7 Limpert, Rudolf, "A Critical Review of Federal Motor Vehicle Safety Standard 105(75) - Its Requirements, Test Procedures and Safety Benefits," SAE Paper No. 760217, SAE International, Warrendale, PA, 1976.
- 1.8 Nieman, G., *Machine Elements*, Vol. 1, Springer-Verlag, Germany, 1981.
- 1.9 Kuhlman, A., *Introduction into Safety Sciences*, Verlag TUV Rheinland, Germany, 1981.
- 1.10 Kuhlman, A., et al., *Prognose der Gefahr*, Verlag TUV Rheinland, Germany, 1969.
- 1.11 Forkenbrock, Garrick J. , et al., "NHTSA's Light Vehicle Handling and ESC Effectiveness Research Program," Paper No. 05-0221, NHTSA and Transportation Research Center, 2005.
- 1.12 www.nhtsa.gov/DOT/NHTSA/NCSA/Content/PDF/NASSbrochure.pdf

Chapter 2



Design and Analysis of Friction Brakes

2.1 Brake Torque

A torque or moment exists when two parallel and opposite forces of equal magnitude, separated by a distance, act on a body. In the case of a disc brake, the two parallel forces are the drag forces between pads and rotor, and the bearing force. The distance is the effective rotor radius measured from the center of the bearing spindle to the rotor drag force. The brake torque is computed by taking the product of total drag force acting on the drum or rotor and the drum radius or effective rotor radius. The brake torque is reacted upon by the road torque which produces the braking force between tire and roadway.

2.2 Brake Factor

2.2.1 Definition of Brake Factor

The brake factor is defined as the ratio of total drum or rotor drag F_d to the application force F_a against one shoe or pad:

$$BF = F_d/F_a \quad (2-1)$$

For a standard (non-self-energizing) caliper disc brake with two brake pads producing drag forces on the in- and out-board sides of the rotor, the brake factor is

$$BF = 2F_d/F_a = (2\mu_L F_a)/F_a = 2\mu_L \quad (2-2)$$

where μ_L = lining or pad coefficient of friction.

Brake factor sensitivity S_{BF} of a brake is a measure of how much the brake factor changes for a given pad-rotor coefficient-of-friction change, or how steep the brake factor curve is. The slope of the curve is obtained by taking the derivative of the brake factor with respect to the friction coefficient. For a disc brake [(Eq. (2-2)], the sensitivity is

$$S_{BF} = d(2\mu_L)/d(\mu_L) = 2$$

A comparison of the brake factors for different brakes is shown in Fig. 2-1.

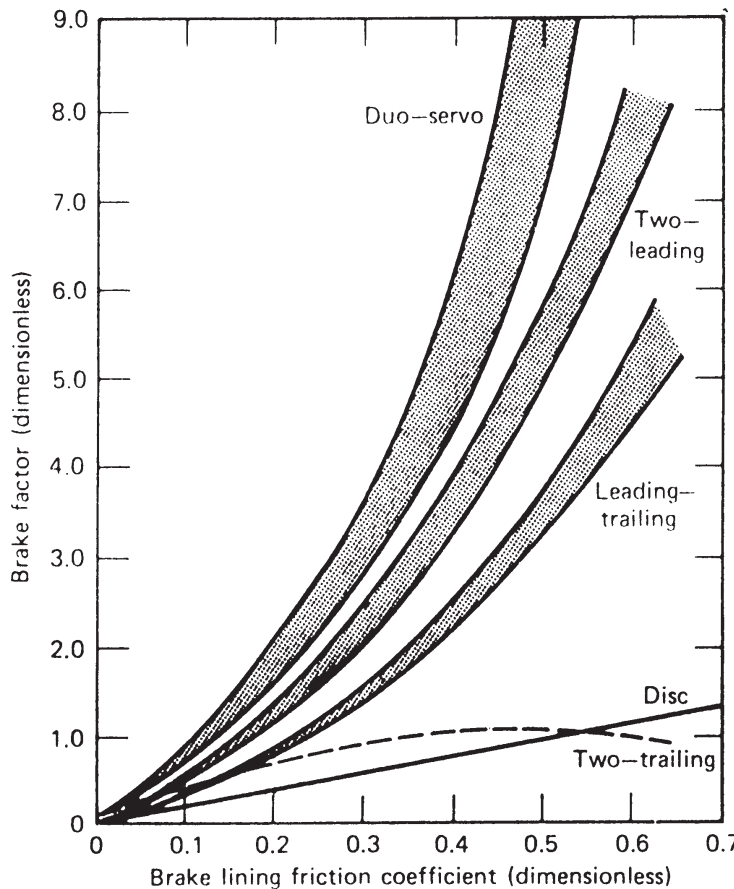


Figure 2-1. Brake factor comparison.

2.2.2 Importance of the Brake Factor to Brake System Design

The brake factor is of critical importance to the proper design and effectiveness of a braking system. The brake factor represents the connection or gain between the hydraulic brake line pressure entering the wheel cylinder or caliper, and the brake torque or braking forces between tires and ground, and hence, deceleration of the vehicle. The brake design engineer must select a design brake factor that ensures proper braking effectiveness, as well as a friction pad/rotor material combination that maintains the design brake factor for all reasonably foreseeable operating conditions. Because the pad/rotor coefficient of friction is a function of many variables, it is better to choose a well-known pad or lining material with established performance and wear characteristics and to design the mechanical brake components “around it,” rather than to develop a new brake material to fit into existing hardware. The development of a new pad or lining material is solely based upon empirical science, that is, costly testing, while the mechanical hardware design and brake component selection are based upon fundamental physical laws (Refs. 2.1, 2.2, 2.3). Brake maintenance must ensure that only properly tested brake linings and pads are used to maintain the manufacturer's design braking performance.

2.3 Brake Factor of Drum Brakes

2.3.1 Brake Factor Analysis of Drum Brakes

One distinguishing characteristic of drum brakes is their higher brake factor when compared with disc brakes. The higher brake factor results from self-energizing within the brake. No one brake design can be rated superior to others in all respects.

2.3.2 Lining Pressure Distribution and Wear

With the assumption that the brake drum and brake shoes are rigid and all deformation occurs within the lining material, the compression of the lining as a result of the shoe displacement against the drum, measured by the angle rotated by the shoe about its pivot, is related to the strain and the original lining thickness d_{Lo} by

$$\varepsilon = d_L/d_{Lo} \quad (2-3)$$

where d_L = lining compression, mm (in.)

d_{Lo} = original lining thickness, mm (in.)

ε = strain of lining material

Tests have shown that the pressure p is approximately proportional to strain; i.e., Hooke's Law is valid provided excessive mean pressures are avoided. The actual pressure distribution between lining and drum is bound by functional relationships of the form

$$p = E\varepsilon = E(a\varphi/d_{Lo}) \sin \alpha, \text{ N/m}^2(\text{psi}) \quad (2-4)$$

and

$$p = c(e^{ka\varphi \sin \alpha / d_{Lo}} - 1), \text{ N/m}^2(\text{psi}) \quad (2-5)$$

where a = brake dimension, mm (in.)

c = constant for determining pressure distribution between lining and drum, N/m^2 (psi)

E = elastic modulus, N/m^2 (psi)

k = constant for determining pressure distribution between lining and drum

ε = strain of lining material

α = lining angle, deg

φ = shoe rotation, rad

The results obtained for several lining materials with different elastic behaviors are presented in Fig. 2-2, where the pressure distribution over the lining angle is shown (Ref. 2.4). Inspection of Fig. 2-2 reveals that the constant c varies between 0.2 and $5 \times 10^5 \text{ N/m}^2$ (2.94 and 73.5 psi) for the linings tested. The information contained in Fig. 2-2 may be used to compute the approximate strain values. At a lining angle of 50 deg, the strain ε of the soft lining is

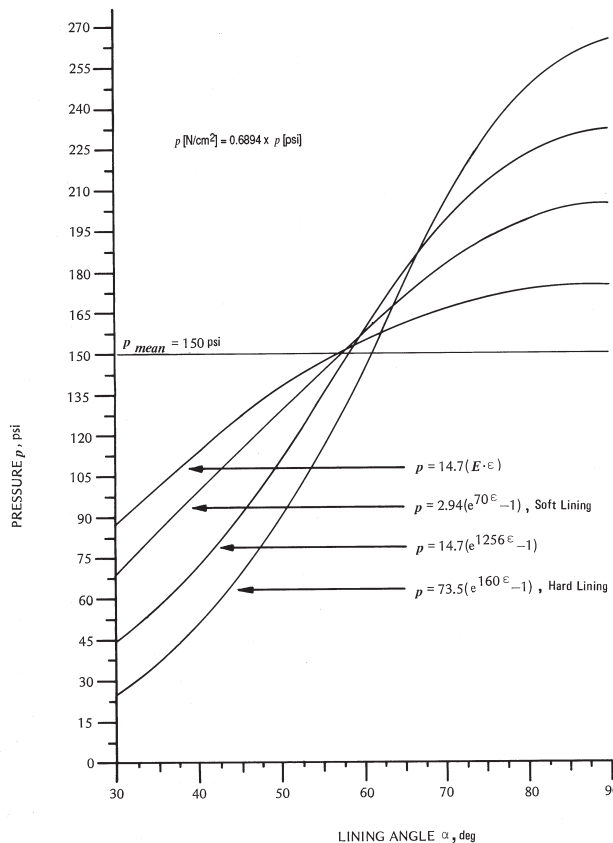


Figure 2-2. Measured pressure distribution over lining angle for different linings.

approximately 0.05, that of the hard lining 0.005. The corresponding values of the elastic modulus are 165 to 1200×10^5 N/m 2 (2400 to 17,500 psi) for the soft and hard lining, respectively.

When the wear behavior of the lining material is known, the pressure distribution along the lining arc can be determined. A detailed analysis is complicated. Only some basic observations are presented.

For a pivoted leading shoe, a wear relationship of the form

$$w_1 = k_1 \mu_L p v_1 \quad , \quad m^3 (\text{in.}^3) \quad (2-6)$$

is assumed, where

k_1 = wear constant, s m 4 /N (s in. 4 /lb)

p = pressure, N/m 2 (psi)

v_1 = sliding speed, m/s (in./s)

w_1 = lining wear, m 3 (in. 3)

μ_L = lining drum friction coefficient

With Eq. (2-6), a sinusoidal pressure distribution may be found to exist along the brake lining. The pressure distribution obtained analytically after successive brake applications and, thus, wear are presented in Fig. 2-3. Inspection of Fig. 2-3 reveals that a sinusoidal distribution of $p = 9.1 \times 10^5 \sqrt{\sin \alpha}$, N/m^2 ($p = 132.2 \sqrt{\sin \alpha}$, psi) is developed after 11 brake applications.

For a wear relationship of the form

$$w = k_2 \mu_L p^2 v_1^2, \text{ m}^3 (\text{in.}^3) \quad (2-7)$$

where k_2 = wear constant, $\text{s}^2 \text{m}^5/\text{N}^2$ ($\text{s}^2 \text{in.}^5/\text{lb}^2$)

w = lining wear, m^3 (in.^3)

v_1 = sliding speed, m/s (ft/s)

a pressure distribution of the form $p = \text{constant} \times \sin \alpha$ is obtained. This pressure distribution is shown in Fig. 2-3.

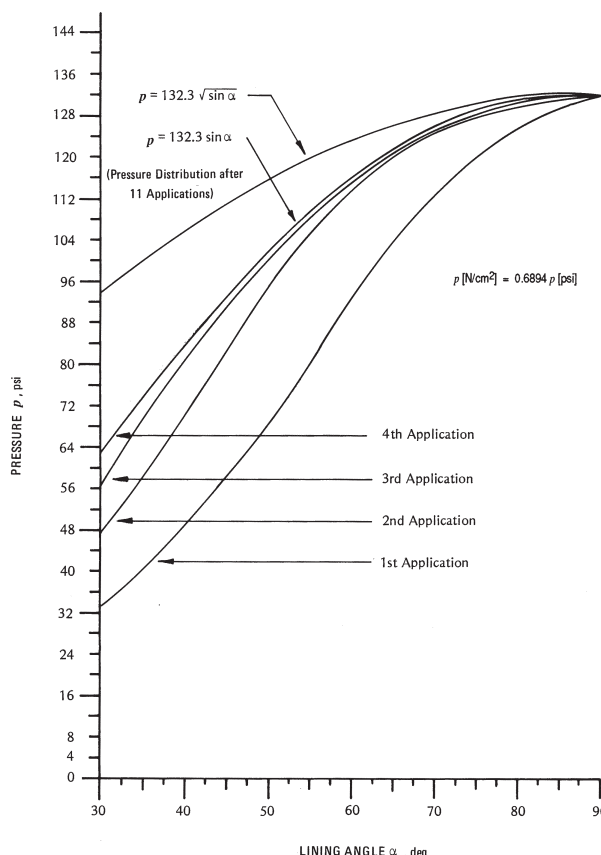


Figure 2-3. Computed pressure distributions as a function of wear after successive brake applications.

Inspection of the curves in Fig. 2-3 reveals that new brakes will have a different pressure distribution than brakes in service. For an exact prediction of pressure distribution, hence brake torque, knowledge of both the wear relationship and the elastic behavior of the lining material is essential. It is an established fact that the pressure distribution changes during the run-in periods. Burnishing procedures subject the vehicle brake system to a series of brake applications during which the pressure distribution along the lining tends to approach run-in conditions.

New or unburnished—sometimes called green—brakes can have a drastic effect on vehicle braking stability, particularly in connection with rear duo-servo drum brakes for which variations in pressure distribution with wear may increase brake torque and, hence, the potential for premature rear-brake lockup. Green or not fully burnished drum brakes often exhibit higher brake torque than those in the burnished condition. Finite element analysis (FEA) models have been developed that include linear and nonlinear behavior of the drum and shoe in predicting brake factor of truck brakes (Ref. 2.5).

2.3.3 Self-Energizing and Self-Locking

A brake shoe with a single brake block is illustrated in Fig. 2-4. Only the leading shoe is shown. The application force F_a against the tip of the shoe pushes the brake block against the drum. The counterclockwise rotation of the drum produces a drag force F_d as shown.

Moment balance around the shoe pivot point (A) yields

$$-F_a h - F_d c + F_d b / \mu_L = 0$$

where b = brake dimension, mm (in.)

c = brake dimension, mm (in.)

h = brake dimension, mm (in.)

μ_L = friction coefficient block/drum

Solving for the ratio of drum drag F_d to application force F_a yields the brake factor BF of the leading shoe as

$$BF_l = F_d / F_a = \mu_L h / (b - \mu_L c) \quad (2-8)$$

Inspection of Fig. 2-4 reveals that the drum drag rotates the brake shoe such that it will increase the normal force of the block pushing against the drum. This increased normal force causing an additional increase in drum drag is the self-energizing effect of the brake. The self-energizing shoe is called the leading shoe.

The ratio of drum drag to application force as expressed by Eq. (2-8) will increase for smaller denominators, and will be infinite when the denominator, $b - \mu_L c$, is zero.

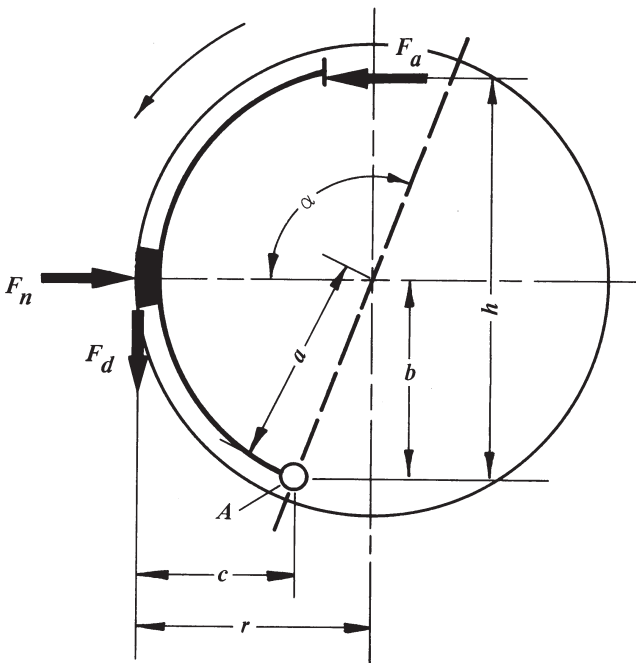


Figure 2-4. Self-energizing shoe of a drum brake.

The lining friction coefficient at which the denominator will be zero for the brake geometry given is b/c , designated as $\mu_{L\infty}$. If the actual lining friction coefficient were equal to $\mu_{L\infty}$, then a brake application would cause ever-increasing self-energizing until the brake locked. Even releasing the application force would not disengage the brake block from the drum. Although self-locking generally is not a problem because $b > c$, brake engineers must guard against it by ensuring that neither friction levels nor brake geometries are such that self-locking may occur. If it does occur, then it would most likely occur only in high-brake-factor duo-servo brakes used as in-hub parking brakes for which adverse conditions such as moisture have significantly increased lining/drum friction coefficients.

For reversed or clockwise rotation of the drum, the leading shoe shown in Fig. 2-4 turns into a trailing shoe. The drum drag force would be directed upward attempting to "lift" the brake block off the drum, thus reducing the effect of the application force. The brake factor of the trailing shoe is given by Eq. (2-8) except that the minus sign in the denominator is replaced by a plus sign. The plus sign indicates the decrease in brake factor with increasing lining friction coefficients, i.e., non-self-energizing of the trailing shoe. The brake factor curve of a two-trailing shoe brake is illustrated in Fig. 2-1.

The total brake factor of the leading-trailing-type block brake is given by adding the brake factors of each shoe, resulting in

$$BF = \frac{2\mu_L h/b}{1 - (\mu_T c/b)^2} \quad (2-9)$$

The self-locking coefficient of friction at which the brake factor of the entire brake, i.e., the leading and the trailing shoe, becomes infinite is the same as for the leading shoe alone, namely $\mu_{L\infty} = b/c$. This is expected because the trailing shoe does not contribute to self-energizing.

The sensitivity S of the block brake is given by the derivative of the brake factor relative to the friction coefficient in Eq. (2-9), or

$$S = \frac{d(BF)}{d(\mu_L)} = \frac{2h/b \left[1 + (\mu_L c/b)^2 \right]}{\left[1 - (\mu_L c/b)^2 \right]^2} \quad (2-10)$$

For $h = 200$ mm (8 in.), $b = 100$ mm (4 in.), and $c = 75$ mm (3 in.), the brake factor curve for the block brake is illustrated in Fig. 2-5. Self-energizing of the leading shoe is clearly evident as shown by the increasing steepness of the curve.

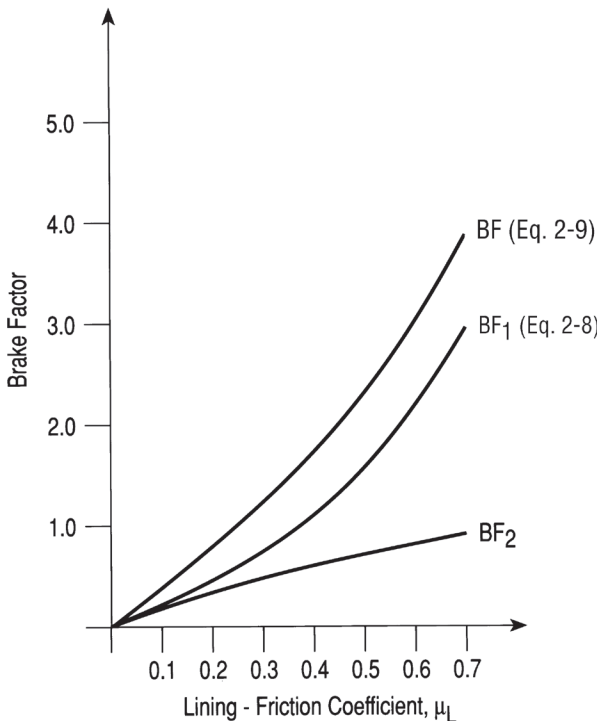


Figure 2-5. Brake factor for block brake.

For the example shown, self-locking will occur when the lining friction coefficient equals $100/75 = 1.33$. The brake factor curve will have an infinite slope; that is, it becomes vertical (Fig. 2-5).

2.3.4 Brake Factor of Drum Brakes

The brake factor calculations for actual drum brake designs use lining pressure distributions as discussed earlier. No elastic shoe or drum deformations are included. All brake factor calculations shown are based upon the work done

by Dr. Hans Strien (Ref. 2.4). PC-BRAKE FACTOR computer software is available for all brake factor calculations discussed in Section 2.3.4 (Ref. 2.6). Based upon specific drum brake designs and lining materials used, brake factor calculations may vary from test results.

2.3.4.1 Brake Factor of Leading-Trailing Shoe Brake with Pivot on Each Shoe

The schematic of one shoe is illustrated in Fig. 2-6. The total brake factor is the summation of the individual brake factors of the leading shoe BF_1 and of the trailing shoe BF_2 :

$$BF = BF_1 + BF_2 = F_{d1}/F_a + F_{d2}/F_a \quad (2-11)$$

where F_{d1} = drag force on leading shoe, N (lb)

F_{d2} = drag force on trailing shoe, N (lb)

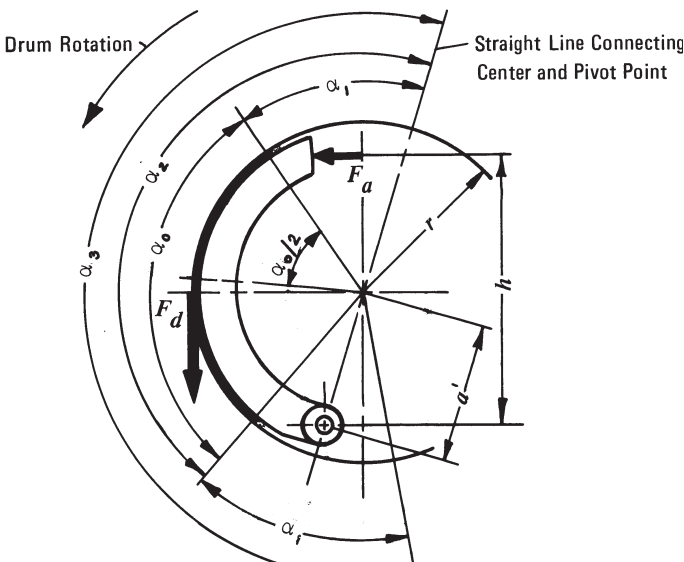


Figure 2-6. Leading shoe with pivot.

The brake factor of the leading shoe is given by the following expression, using the minus sign in the denominator:

$$BF_1 = F_{d1}/F_a = \frac{\mu_L h/r}{(a'/r) \left[\frac{(\hat{\alpha}_0) - \sin \alpha_0 \cos \alpha_3}{4 \sin(\alpha_0/2) \sin(\alpha_3/2)} \right] \pm \mu_L [1 + (a'/r) \cos(\alpha_0/2)(\alpha_3/2)]} \quad (2-12)$$

where a' = brake dimension, mm (in.)

$\hat{\alpha}_0$ = arc of the angle α_0 , rad

α_1 = angle between beginning of lining and straight line connecting center and pivot point, deg

$\alpha_2 = \alpha_1 + \text{arc angle}$, deg

$\alpha_3 = \alpha_1 + \alpha_2$, deg (as defined in Fig. 2-6)

The brake factor of the trailing shoe is determined by using the plus sign in the denominator of Eq. (2-12).

2.3.4.2 Brake Factor of Two-Leading Shoe Brake with Pivot on Each Shoe

For this case, the brake factor can simply be determined from

$$BF = 2(BF_1) = 2(F_{d1}/F_a) \quad (2-13)$$

with F_{d1}/F_a determined from Eq. (2-12) using the minus sign in the denominator. The minus sign is used because both shoes are self-energizing.

2.3.4.3 Brake Factor of Leading-Trailing Shoe Brake with Parallel Sliding Abutment

The schematic of one shoe is illustrated in Fig. 2-7. The brake factor BF is determined by Eq. (2-11). The individual brake factors are:

For the leading shoe:

$$BF_1 = F_{d1}/F_a = \left[(\mu_L D_B + \mu_L^2 E_B) / (F_B - \mu_L G_B + \mu_L^2 H_B) \right]_1 \quad (2-14)$$

For the trailing shoe:

$$BF_2 = F_{d2}/F_a = \left[(\mu_L D_B - \mu_L^2 E_B) / (F_B + \mu_L G_B + \mu_L^2 H_B) \right]_2 \quad (2-15)$$

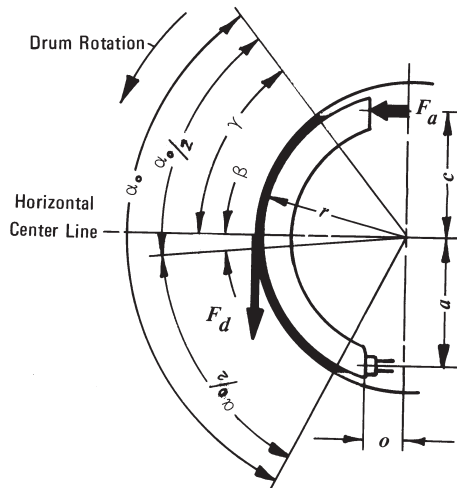


Figure 2-7. Leading shoe with parallel sliding abutment.

$$\text{where } D_B = [c/r + a/r + \mu_s(o/r)] \cos \beta + \mu_s(c/r) \sin \beta$$

$$E_B = \mu_s(c/r) \cos \beta - [c/r + a/r + \mu_s(o/r)] \sin \beta$$

$$F_B = \frac{\hat{\alpha}_0 + \sin \alpha_0}{4 \sin(\alpha_0/2)} [a/r + \mu_s(o/r)]$$

$$G_B = \cos \beta + \mu_s \sin \beta$$

$$H_B = F_B - (\mu_s \cos \beta - \sin \beta)$$

o = brake dimension, mm (in.)

r = drum radius, mm (in.)

α_0 = arc angle of lining, deg

β = angle between center of arc angle and horizontal center line, deg

γ = angle between beginning of lining and horizontal center line, deg

μ_s = friction coefficient at shoe tip and abutment

The value of μ_s is associated with the sliding friction between the tip of the shoe and the abutment. For steel on steel, $\mu_s \approx 0.2$ to 0.3 . The angle β is positive when $\gamma > \alpha_0/2$, and negative when $\gamma < \alpha_0/2$.

An application of the brake factor analysis and the use of PC-BRAKE FACTOR software to an actual case are described next. A vehicle crash was caused by improper brake maintenance, resulting in a left front wheel bearing play of 1.25 mm (0.050 in.) and excessive pad knock-back. The front circuit piston of the master cylinder bottomed out at maximum hydraulic brake line pressure of approximately 280 N/cm^2 (407 psi). As the driver applied the brake pedal to avoid a loose tire in his lane, the rear brakes locked, causing the vehicle to lose directional stability and roll over (Ref. 2.7).

As part of the brake system design analysis, the brake factor of the right rear leading-trailing shoe drum brake of the SUV involved in the accident had to be calculated. The brake shoes were supported by parallel sliding abutment.



Figure 2-8. Field measurements of LT-shoe brake.

Eqs. (2-14) and (2-15) apply. The author's field notes are shown in Fig. 2-8. All dimensions and angles required as shown in Fig. 2-7 were measured directly at the subject brake and/or obtained from the scale photograph. The input data and brake factor calculation are shown in Fig. 2-9. Based upon a lining-drum coefficient of friction range of 0.35 to 0.40 for both linings, a brake factor range of 2.2 to 2.7 should be used.

1.4 Brake Factor of a Leading-Trailing Shoe Brake with Parallel Sliding Abutment.

Leading-trailing shoe brake.
Leading shoe with parallel sliding abutment.
For Trailing shoe use mirror image.

Project ID: Figure 2-9 Rear LT-shoe brake

Input the following data, based on Figure 2-7:

LEADING SHOE		TRAILING SHOE	
μ_L =	0.40	μ_L =	0.40
μ_s =	0.20	μ_s =	0.20
a =	3.87	a =	3.87
c =	4.55	c =	4.55
o =	1.09	o =	1.09
r =	5.82	r =	5.82
α_0 =	108.00	α_0 =	108.00
β =	0.00	β =	0.00
γ =	54.00	γ =	54.00

Data calculated based on the above data and on Figure 2-7:

$\text{Arc}\alpha_0$ =	1.88	$\text{Arc}\alpha_0$ =	1.88
D_B =	1.48	D_B =	1.48
E_B =	0.16	E_B =	0.16
F_B =	0.62	F_B =	0.62
G_B =	1.00	G_B =	1.00
H_B =	0.42	H_B =	0.42
BF_L =	2.19	BF_T =	0.53

Brake Factor of the Leading shoe and Trailing shoe dimensionless

Total Brake Factor (*)

BF_{LT} = 2.72

See: [Table 1.4](#)

* Note: The '***' indicates that the μ_L used is too high. This will cause BF to approach infinity (∞).

Figure 2-9. PC-BRAKE Factor LT-shoe data printout.

2.3.4.4 Brake Factor of Two-Leading Shoe Brake with Parallel Sliding Abutment

The brake factor can be determined from the general expression for two-leading shoe brakes, Eq. (2-11), with the brake factor of one shoe determined by Eq. (2-14).

2.3.4.5 Brake Factor of Leading-Trailing Shoe Brake with Inclined Abutment

A schematic of a typical shoe is illustrated in Fig. 2-10. The total brake factor may be determined from Eqs. (2-11), (2-14), and (2-15) with the abutment friction coefficient μ_s replaced by $(\mu_s + \tan\Psi)$, where Ψ is the inclination angle of the abutment in degrees.

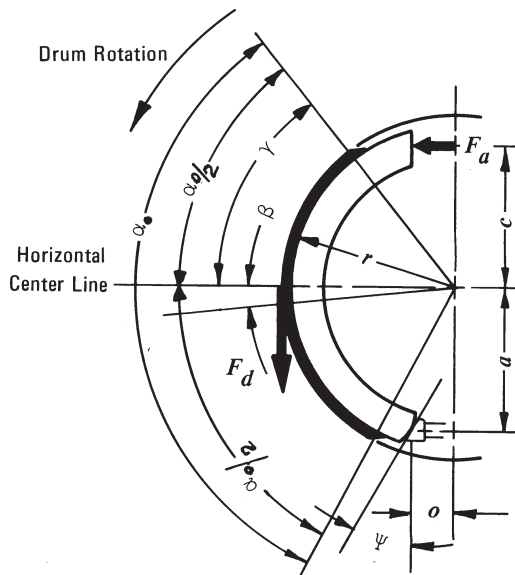


Figure 2-10. Leading shoe with inclined abutment.

2.3.4.6 Brake Factor of Two-Leading Shoe Brake with Inclined Abutment

The total brake factor may be determined from Eqs. (2-13) and (2-14), with μ_s replaced by $(\mu_s + \tan \Psi)$, where Ψ is the inclination angle of the abutment.

2.3.4.7 Brake Factor of Duo-Servo Brake with Sliding Abutment

The schematic is illustrated in Fig. 2-11. The relationships shown earlier can be used to determine the brake factor. In this case, however, the internal application force F_{ax} of the primary shoe, designated by 1, becomes the actuation force of the secondary shoe, designated by 2.

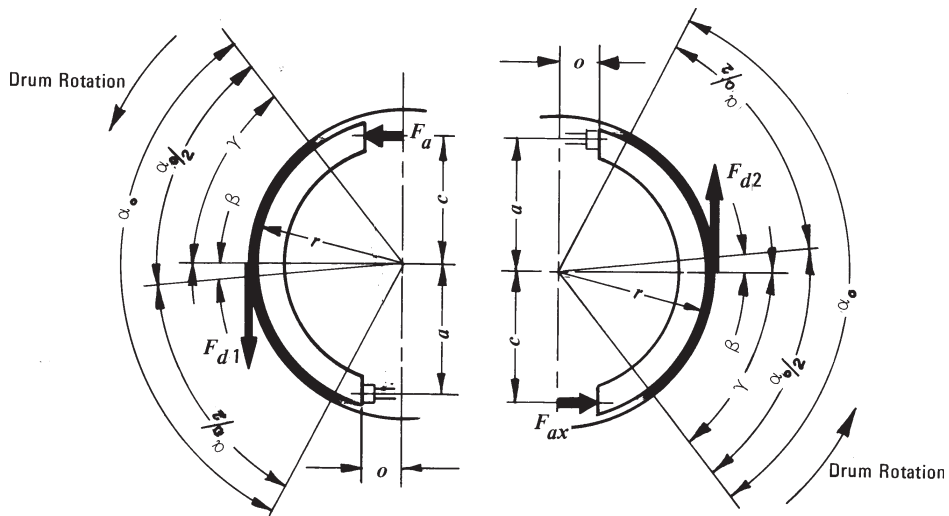


Figure 2-11. Duo-servo brake with sliding abutment.

The total brake factor BF is determined by

$$\begin{aligned} BF &= BF_1 + BF_2 = F_{d1}/F_a + F_{d2}/F_a \\ &= F_{d1}/F_a + (F_{d2}/F_{ax})(F_{ax}/F_a) \end{aligned} \quad (2-16)$$

$$F_{d1}/F_a = (\mu_L D_B + \mu_L^2 E_B)/(F_B - \mu_L G_B + \mu_L^2 H_B)$$

$$F_{d2}/F_{ax} = (\mu_L D_B + \mu_L^2 E_B)/(F_B - \mu_L G_B + \mu_L^2 H_B)$$

The relative support force F_{ax}/F_a is determined from a moment balance about the center of the brake, and can be expressed as

$$F_{ax}/F_a = c/a + (F_{d1}/F_a)(r/a) \quad (2-17)$$

2.3.4.8 Brake Factor of Duo-Servo Brake with Pivot Abutment

A schematic is shown in Fig. 2-12. The total brake factor can be determined from Eqs. (2-16) and (2-17) with the brake factor BF_1 of the primary shoe given by Eq. (2-14) and the brake factor BF_2 of the secondary shoe given by Eq. (2-12); the minus sign is used in the denominator.

Example 2-1: Duo-Servo Drum Brake

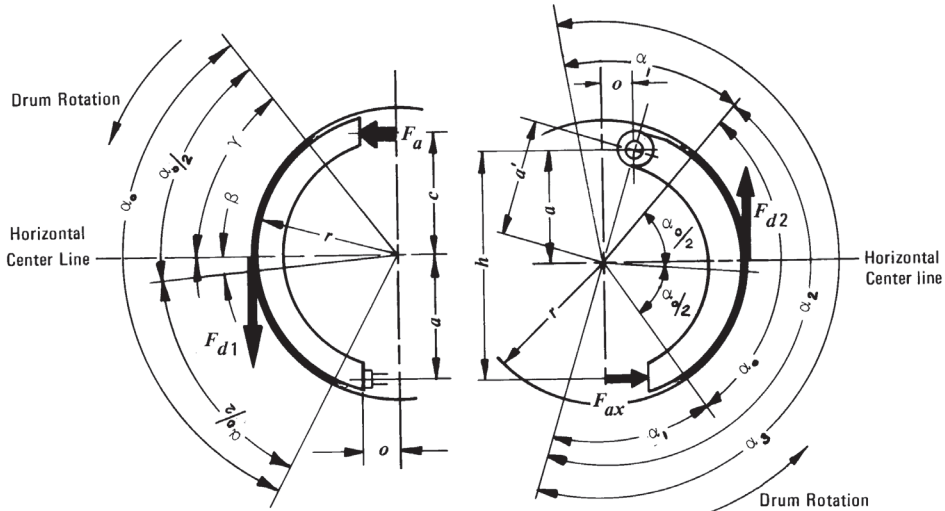


Figure 2-12. Duo-servo brake with pivot of secondary shoe.

Primary Shoe	Secondary Shoe
$a = 102 \text{ mm (4 in.)}$	$a = 102 \text{ mm (4 in.)}$
$c = 102 \text{ mm (4 in.)}$	$h = 203 \text{ mm (8 in.)}$
$o = 38 \text{ mm (1.5 in.)}$	$o = 0 \text{ mm}$
$r = 127 \text{ mm (5 in.)}$	$r = 127 \text{ mm (5 in.)}$
$\alpha_0 = 126 \text{ deg}$	$\alpha_0 = 126 \text{ deg}$
$\hat{\alpha}_0 = 2.2 \text{ rad}$	$\hat{\alpha}_0 = 2.2 \text{ rad}$
$\beta = 3 \text{ deg}$	$\alpha_1 = 24 \text{ deg}$
$\mu_s = 0.2 \text{ (steel on steel)}$	$\alpha_2 = 150 \text{ deg}$

The total brake factor BF may be computed by Eqs. (2-12), (2-14), and (2-16) with the brake factor BF_1 of the primary shoe given by Eq. (2-14) and the brake factor BF_2 of the secondary shoe given by Eq. (2-12).

Substitution of the appropriate data of the primary shoe into Eq. (2-14) yields

$$BF_1 = F_{d1}/F_a = \frac{\mu_L(1.67) + \mu_L^2(0.073)}{0.726 - \mu_L(1.01) + \mu_L^2(0.579)} \quad (2-18)$$

where F_a = brake shoe application force, N (lb)

F_{d1} = drag force due to primary shoe, N (lb)

μ_L = friction coefficient between lining and drum

Eq. (2-18) presents the variation of the brake factor of the primary shoe with lining friction coefficient μ_L . Eq. (2-14) is used to derive Eq. (2-18) because the primary shoe of the brake to be analyzed is supported by a parallel sliding abutment.

Eq. (2-18) may be evaluated for different values of μ_L , giving the values listed in Table 2-1.

TABLE 2-1

BF_1 vs. μ_L

μ_L	0.1	0.2	0.3	0.4	0.5	0.6
$BF_1 = F_{d1}/F_a$	0.266	0.616	1.068	1.639	2.332	3.131

The secondary shoe is actuated by the support force between the primary and secondary shoe. Because the brake factor is defined by the ratio of drum drag to application force produced by the wheel cylinder, the brake factor of the secondary shoe must be computed in two steps. First, the brake factor is determined by Eq. (2-12) with the support force of the primary shoe used as the actuation force of the secondary shoe. Then the brake factor is modified using

Eq. (2-16) to yield the brake factor of the secondary shoe. Substitution of the appropriate data into Eq. (2-12) with $\alpha_3 = \alpha_1 + \alpha_2 = 174$ deg yields

$$F_{d2}/F_{ax} = \mu_L (1.6) / [0.67535 - \mu_L (1.019)] \quad (2-19)$$

where F_{ax} = application force of secondary shoe, N (lb)

F_{d2} = drag force due to secondary shoe, N (lb)

The minus sign is used to determine the brake factor of the secondary (or leading) shoe. Eq. (2-19) may be evaluated for different values of μ_L , yielding the values given in Table 2-2.

TABLE 2-2

F_{d2}/F_{ax} vs. μ_L						
μ_L	0.1	0.2	0.3	0.4	0.5	0.6
F_{d2}/F_{ax}	0.279	0.679	1.299	2.390	4.824	15.012

Because the brake factor is defined as the ratio of total drum drag to the application force F_a at the wheel cylinder, the shoe factor of the secondary shoe must be modified [Eq. (2-16)]:

$$BF_2 = (F_{d2}/F_{ax})(F_{ax}/F_a) \quad (2-20)$$

The ratio F_{ax}/F_a is determined by Eq. (2-17):

$$\begin{aligned} F_{ax}/F_a &= (c/a) + (F_{d1}/F_a)(r/a) \\ &= 1.0 + (F_{d1}/F_a)(1.25) \end{aligned} \quad (2-21)$$

where a = brake dimension, mm (in.)

c = brake dimension, mm (in.)

The ratio F_{ax}/F_a assumes different values for various values of μ_L . Using the values F_{d1}/F_a from Table 2-1 in Eq. (2-21) gives the values of F_{ax}/F_a listed in Table 2-3.

TABLE 2-3

F_{ax}/F_a vs. μ_L						
μ_L	0.1	0.2	0.3	0.4	0.5	0.6
F_{ax}/F_a	1.333	1.770	2.335	3.049	3.915	4.914

The brake factor BF_2 of the secondary shoe can now be determined by Eq. (2-20). Values of BF_2 for various values of μ_L are given in Table 2-4.

TABLE 2-4 **BF_2 vs. μ_L**

μ_L	0.1	0.2	0.3	0.4	0.5	0.6
$BF_2 = (F_{d2}/F_{ax})(F_{ax}/F_a)$	0.372	1.202	3.036	7.287	18.870	73.579

The total brake factor BF is obtained by adding the individual shoe brake factors, yielding the data in Table 2-5. Using the input data in PC-BRAKE Factor yields the same results as shown in Fig. 2-13 for a lining friction coefficient of 0.3.

1.9: Brake Factor of a Duo-Servo Brake with Pivot Support. PC BRAKE

Duo-Servo Brake (ITT-Teves)
Duo-Servo Brake with pivot.

Project ID: Figure 2-13. Duo-servo brake of Example 2-1.

Input the following data, based on Figure 2-12:

PRIMARY $\mu_L =$ <input type="text" value="0.30"/> Lining-drum friction coefficient, dimensionless $\mu_s =$ <input type="text" value="0.20"/> Shoe-abutment $a =$ <input type="text" value="4.00"/> Brake dimension, mm $c =$ <input type="text" value="4.00"/> Brake dimension, mm $o =$ <input type="text" value="1.50"/> Brake dimension, mm $r =$ <input type="text" value="5.00"/> Drum radius, mm $\alpha_0 =$ <input type="text" value="126.00"/> Lining angle, degrees $\beta =$ <input type="text" value="3.00"/> Angle between center of angle α_0 and horizontal center line, degrees $\gamma =$ <input type="text" value="38.00"/> Angle between beginning of lining and horizontal center line, degrees	SECONDARY $\mu_L =$ <input type="text" value="0.30"/> Lining-drum friction coefficient, dimensionless (Positive Numbers only) $a' =$ <input type="text" value="4.00"/> Brake dimension, mm $h =$ <input type="text" value="8.00"/> Brake dimension, mm $r =$ <input type="text" value="5.00"/> Drum radius, mm $\alpha_0 =$ <input type="text" value="126.00"/> Lining angle, degrees $\alpha_1 =$ <input type="text" value="24.00"/> Angle between beginning of lining and line connecting center of pivot, degrees
---	--

Data calculated based on the above data and on Figure 2-12:

$\text{Arc}\alpha_0 =$ <input type="text" value="2.20"/> Arc of lining angle, radians $D_B =$ <input type="text" value="1.67"/> $E_B =$ <input type="text" value="0.07"/> $F_B =$ <input type="text" value="0.73"/> $G_B =$ <input type="text" value="1.01"/> $H_B =$ <input type="text" value="0.58"/> $BF_P =$ <input type="text" value="1.07"/>	$\text{Arc}\alpha_0 =$ <input type="text" value="2.20"/> Arc of lining angle, radians $\alpha_2 =$ <input center;"="" text"="" text-align:="" type="text" value="174.00/> <math>(\alpha_1 + \alpha_2)</math>, degrees </td> </tr> </table> <p style="/> Total Brake Factor (*) See: Table 1.9 <p style="text-align: center;">$BF_{PS} =$ <input type="text" value="4.10"/></p> <p>*Note: The '*' indicates that the μ_L used is too high. This will cause BF to approach infinity (∞).</p>
--	---

Figure 2-13. PC-BRAKE Factor output for 0.3.**TABLE 2-5** **BF vs. μ_L**

μ_L	0.1	0.2	0.3	0.4	0.5	0.6
BF	0.638	1.818	4.103	8.926	21.202	76.890

The brake factor is illustrated in Fig. 2-14. Inspection of the brake factor curves of the individual shoes reveals that both shoes are self-energizing, but that the secondary shoe contributes the most to the total brake factor.

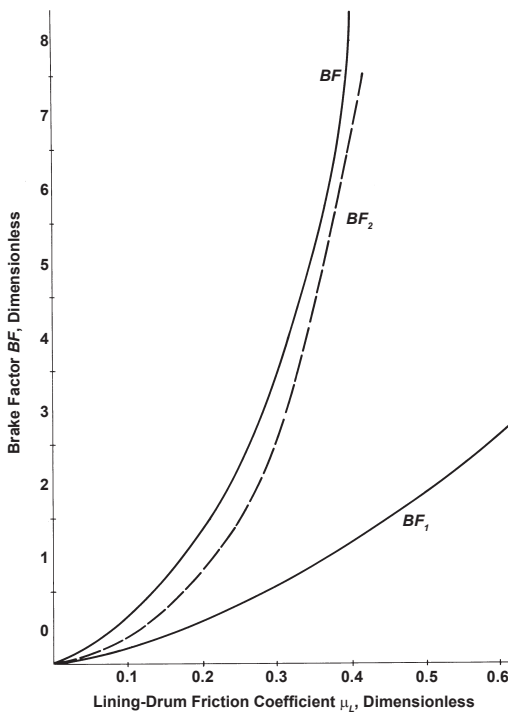


Figure 2-14. Brake factor characteristic of a duo-servo drum brake.

Research in duo-servo brakes for parking brake application to analyze brake factor sensitivity has been published (Ref. 2.8). Attempts at designing high-brake-factor drum brakes have been made (Ref. 2.9). Although increases in brake torque of over 50% have been realized, they must not be accompanied by high brake factor sensitivity when used as foundation brakes in the service brake systems.

2.3.4.9 Brake Factor of S-Cam Brake

The basic S-cam brake configuration is a leading-trailing shoe design as discussed in Section 2.3.4.1. Resulting from the fixed actuation of the cams, the reaction forces between cam and rollers are oriented such that the effectiveness of the leading shoe is decreased, while that of the trailing shoe is increased. The average brake factor of the S-cam brake can be expressed as (Ref. 2.10)

$$BF = \frac{4(BF_1)(BF_2)}{BF_1 + BF_2} \quad (2-22)$$

where BF_1 = brake factor of leading shoe determined by Eq. (2-12), using the minus sign in the denominator

BF_2 = brake factor of trailing shoe determined by Eq. (2-12), using the plus sign in the denominator

For example, for $BF_1 = 1.6$ and $BF_2 = 0.5$, the S-cam brake factor is 1.52, and not 2.1 as would be the case for a hydraulic wheel cylinder or floating actuation

against the shoe. The individual brake factors of Eq. (2-22) are based upon calculations, while the correlation factor 4 is based upon curve fitting of experimental data (Ref. 2.10). Dynamometer test data were used by the author to determine the accuracy of Eq. (2-22) (Refs. 2.11, 2.12). The S-cam brake was tested at an equivalent speed of 40 mph in the burnish test, resulting in a brake torque of 5719 lbft at an average brake line pressure of 64 psi and a final brake drum temperature of 389°F. The calculated brake factor was 1.33. After 290 stops, the brake torque was 5728 lbft at an average brake line pressure of 58 psi and a final drum temperature of 552°F. A brake factor $BF = 1.5$ based on the test data was calculated. In Fig. 2-15, the PC-BRAKE Factor data output show $BF = 1.64$ for a lining friction coefficient of 0.35, indicating acceptable agreement with the measurements. The edge code of the linings used in the dynamometer tests was FF, indicating a lining friction coefficient range of 0.35 to 0.45 for cold (366 K or 200°F) as well as hot brake (588K or 600°F), according to SAE J661.

When compliance of the S-cam brake components was included in the theoretical analysis (Ref. 2.5), a brake factor of 1.5 to 1.7 was obtained for a lining friction coefficient of 0.35, as compared with the brake factor of 1.64 obtained by PC-BRAKE FACTOR.

The mechanical efficiency of the S-cam brake is approximately 65 to 70%, indicating that as much as one third of the brake chamber pushrod force is used to overcome friction in the apply mechanism (Refs. 2.13, 2.14).

1.10: Brake Factor of Air S-Cam Brake.

PC BRAKE

Leading shoe with pivot.
For trailing shoe, use mirror image.

Project ID: **Figure 2-15. PC-BRAKE Factor S-cam brake data output.**

Input the following data, based on Figure 2-6:

LEADING SHOE <div style="border: 1px solid black; padding: 5px; margin-bottom: 5px;"> $\mu_L =$ 0.35 </div> <div style="border: 1px solid black; padding: 5px; margin-bottom: 5px;"> $a' =$ 6.5 </div> <div style="border: 1px solid black; padding: 5px; margin-bottom: 5px;"> $h =$ 13 </div> <div style="border: 1px solid black; padding: 5px; margin-bottom: 5px;"> $r =$ 8.5 </div> <div style="border: 1px solid black; padding: 5px; margin-bottom: 5px;"> $\alpha_0 =$ 120 </div> <div style="border: 1px solid black; padding: 5px; margin-bottom: 5px;"> $\alpha_1 =$ 30 </div>	TRAILING SHOE <div style="border: 1px solid black; padding: 5px; margin-bottom: 5px;"> $\mu_L =$ 0.35 </div> <div style="border: 1px solid black; padding: 5px; margin-bottom: 5px;"> $a' =$ 6.5 </div> <div style="border: 1px solid black; padding: 5px; margin-bottom: 5px;"> $h =$ 13 </div> <div style="border: 1px solid black; padding: 5px; margin-bottom: 5px;"> $r =$ 8.5 </div> <div style="border: 1px solid black; padding: 5px; margin-bottom: 5px;"> $\alpha_0 =$ 120 </div> <div style="border: 1px solid black; padding: 5px; margin-bottom: 5px;"> $\alpha_1 =$ 30 </div>		
Lining-drum friction coefficient, dimensionless (Positive Numbers only) Brake dimension, mm Brake dimension, mm Drum radius, mm Lining angle, degrees Angle between beginning of lining and straight line connecting center of pivot, degree			
Data calculated based on the above data and on Figure 2-6:			
<div style="border: 1px solid black; padding: 5px; margin-bottom: 5px;"> $\alpha_2 =$ 150 </div> <div style="border: 1px solid black; padding: 5px; margin-bottom: 5px;"> $\alpha_3 =$ 180 </div> <div style="border: 1px solid black; padding: 5px; margin-bottom: 5px;"> $\text{Arcc}\alpha_0 =$ 2.09 </div> <div style="border: 1px solid black; padding: 5px; margin-bottom: 5px;"> $BF_L =$ 1.76 </div>	$(\alpha_0 + \alpha_1)$, degrees $(\alpha_1 + \alpha_2)$, degrees Arc of lining angle, radians Total Brake Factor (*) $BF_{LT} =$ 1.64	<div style="border: 1px solid black; padding: 5px; margin-bottom: 5px;"> $\alpha_2 =$ 150 </div> <div style="border: 1px solid black; padding: 5px; margin-bottom: 5px;"> $\alpha_3 =$ 180 </div> <div style="border: 1px solid black; padding: 5px; margin-bottom: 5px;"> $\text{Arcc}\alpha_0 =$ 2.09 </div> <div style="border: 1px solid black; padding: 5px; margin-bottom: 5px;"> $BF_T =$ 0.53 </div>	
See: Table1.10			

* Note: The ** indicates that the μ_L used is too high. This will cause BF to approach infinity (∞).

Figure 2-15. PC-BRAKE Factor for S-cam brake.

2.3.4.10 Brake Factor of Wedge Brake

Brake factors of single-chamber wedge brakes are computed by the regular leading-trailing shoe brake equation. For pivot support on each shoe, use Section 2.3.4.1, for parallel abutment, use Section 2.3.4.3. The brake factor of

a dual-chamber or two-leading shoe brake is computed by the relationships presented in Section 2.3.4.2 or 2.3.4.4. The mechanical efficiency of wedge brakes is approximately 90 to 95% (Ref. 2.13). The apply mechanism is designed with an integrated automatic adjustment.

Dynamometer tests for dual-chamber wedge brakes indicate typical brake factors of 3.5 to 4.5. Due to their two-leading-shoe design, they are more affected by lining friction coefficient changes.

2.3.5 Effects of Brake Wear on Brake Factor

The brake factor calculations in previous sections are based upon rigid drum-shoe geometry, with all deformation occurring in the lining. Any lining wear that changes the pressure distribution between lining and drum will affect the brake factor. Large self-energizing shoe designs, such as the duo-servo brake, will be more affected by lining wear than less self-energizing brakes such as the LT-shoe design. As lining wear develops, the pressure distribution between lining and drum changes, resulting in different drag forces and changes in the respective lever arms relative to the shoe support point. The corresponding brake factor change may be studied by changing the input data in the brake factor calculations. For example, reducing the lining angle of the secondary shoe in Example 2-1 from 126 to 50 degrees increases the brake factor from 4.1 to 7.6. Wear across the lining width due to drum bell-mouthing will also affect the pressure distribution between lining and drum, and hence, the brake factor.

Improper maintenance of brakes may also affect the brake factor of a drum brake. Mismatching drum and shoe circle diameters will affect the pressure distribution between lining and drum. The brake factor will approach the performance of a block brake, as illustrated in Figs. 2-4 and 2-5.

2.3.6 Effects of Temperature on Brake Factor

The temperature increase of the drum during braking will enlarge the drum diameter due to thermal expansion, resulting in change in pressure distribution between lining and drum. The higher temperature will affect the effective lining/drum coefficient of friction, with significant friction decreases at elevated temperatures (brake fade).

2.3.7 Effects of Humidity on Brake Factor

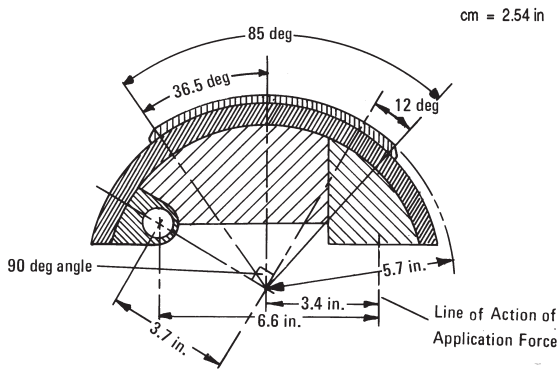
Humidity increases the effective lining/drum coefficient of friction, and hence, brake factor (Ref. 2.15). Duo-servo brakes with a steep brake factor curve may experience a brake factor increase of 30% over its dry value. The humidity in the brakes may be caused by parking a vehicle in a high-humidity environment, by driving in wet/rainy weather, or in a car wash. Flooding the brakes may cause the opposite, namely a drastic reduction of the brake factor due to a significant drop in lining friction coefficient. FMVSS 105 places some performance requirements on brakes while wet.

2.3.8 Effects of Shoe and Drum Stiffness on Brake Factor

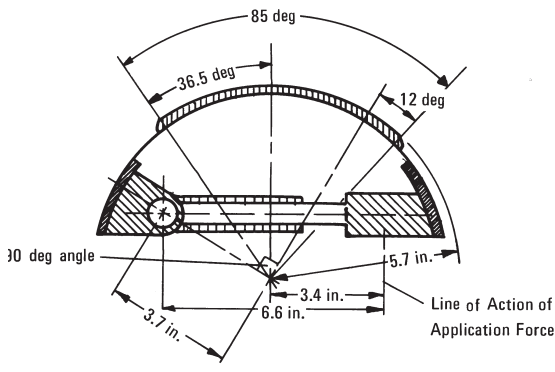
The derivation of the brake factor in the previous paragraphs was based on a rigid shoe and drum. All elastic deformation and wear was assumed to occur in the lining material. Test results show a significant effect of brake shoe elasticity on brake torque. Experimental data obtained for the "rigid" and "elastic" brake shoe geometries shown in Fig. 2-16 are presented in Fig. 2-17 (Ref. 2.16). Although both shoes have identical dimensions as far as brake factor calculations are concerned, their actual brake force production is different. Reasons for this difference are found in the change in pressure distribution between lining and drum in the case of the elastic brake shoe. As indicated by Eq. (2-4), in the case of a rigid shoe, the pressure distribution is approximated by $p = E \alpha \sin \alpha / d_{L_o}$. An elastic shoe produces a pressure distribution that has higher pressure concentrations at or near the ends of the linings. The pressure distribution may be approximated by

$$p = (a \varphi E / d_{L_o})(2 \sin \alpha + \cos 2\alpha), \text{ N/m}^2 (\text{psi}) \quad (2-23)$$

Application of this pressure distribution to the brake factor analysis under consideration for an elastic shoe yields fairly complicated equations for



Rigid Brake Shoe



Elastic Brake Shoe

Figure 2-16. Brake shoes of different stiffness.

predicting brake torque. The analysis is made difficult by the complicated designs found in many brake shoes, which prevent establishment of a simple equation for the elastic deformation.

The effect of the difference in pressure distribution may be analyzed by increasing angle β (Fig. 2-7) from a typical value of 3 deg to 30 or 40 deg. This change would effectively alter the pressure distribution and concentrate pressure near the end of the lining. Application of this

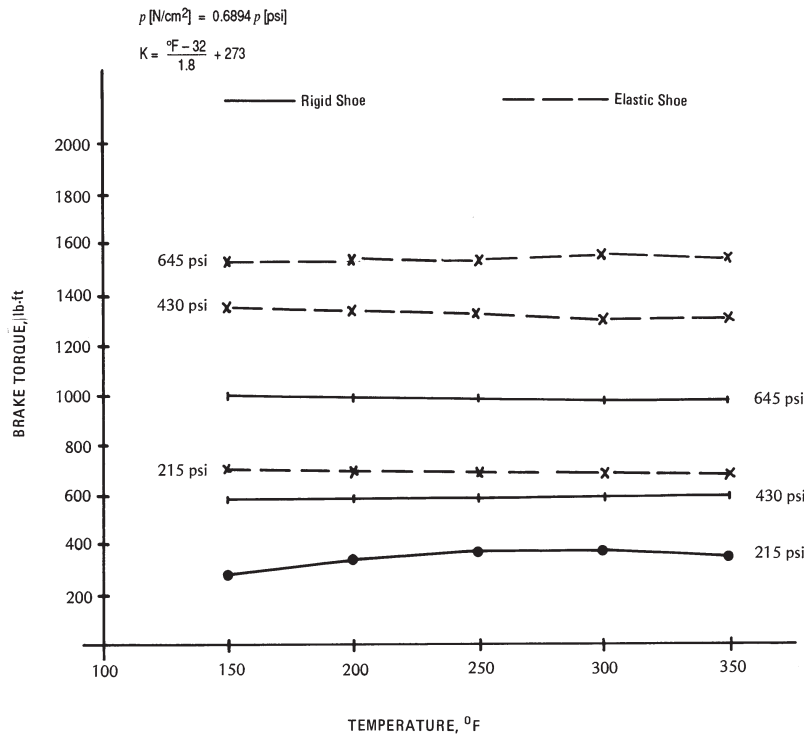


Figure 2-17. Brake torque vs. temperature for different brake line pressures.

change to the brake factor equations yields significantly higher brake factors at moderate values of lining friction coefficients. The undesirable side effect is increased lining wear.

2.4 Disc Brakes

2.4.1 Basic Caliper Design Considerations

Disc brakes generally do not use self-energizing designs in their pad-apply mechanisms. A *fixed-caliper* design is illustrated in Fig. 2-18. The caliper, bolted solidly to the flange, has either two or four pistons which push the pads out. Fixed-caliper disc brakes have more balanced inner and outer pad wear with less pad taper than floating-caliper designs. They require no anchor or integral knuckle for shoe support. They attach with standard fasteners; have no sleeves, grommets, or hold-down springs; and require fewer service parts.

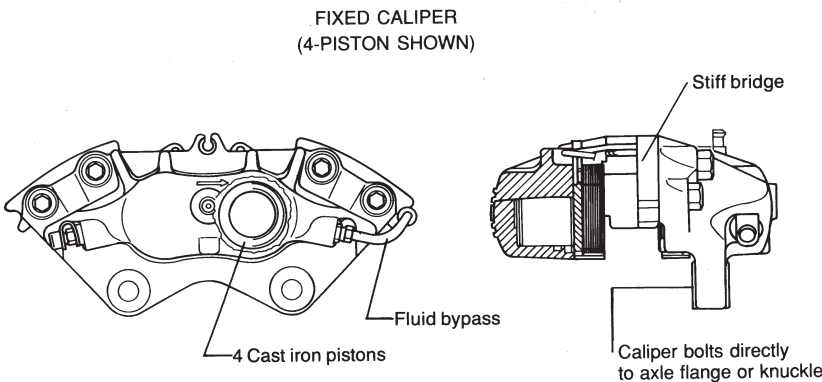


Figure 2-18. Fixed-caliper disc brake (Continental Teves).

A typical *floating-caliper* disc brake is shown in Fig. 2-19. One or two pistons are used on the inboard side only. The hydraulic pressure forcing the piston and pad toward the rotor also forces the piston housing (wheel cylinder) in the opposite direction to apply the outboard pad against the rotor.

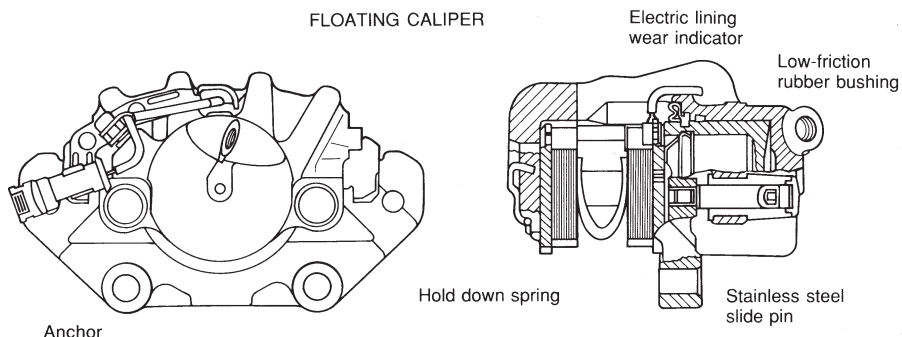


Figure 2-19. Floating-caliper disc brake (Continental Teves).

Floating-caliper brakes offer a number of advantages over fixed-caliper designs. They are easier to package in the wheel because they do not have a piston on the outboard or wheel side. They have a lower brake fluid operating temperature than the fixed caliper and, hence, lower potential for brake fluid vaporization. They also have fewer leak points, and are easier to bleed in service.

Hydraulic disc brake adjustment is accomplished automatically by the caliper piston seal. The seal is designed so that in the event of a piston displacement, it distorts elastically for approximately 0.152 mm (0.006 in.). Provided no pad wear has occurred, the piston seal pulls the piston back when brake line pressure is released, as shown in Fig. 2-20. If the clearance between pad and rotor becomes greater due to wear, the piston travels greater than 0.152 mm (0.006 in.), and the piston seal preload is overcome, forcing the piston closer to the rotor. The return movement of the piston is determined by how much the seal can deflect during application. In the floating-caliper design, one seal must return the pad on the piston side as well as the outboard caliper pad. Low-drag

Brake Design and Safety

caliper designs use a special chamfer to increase seal deflection. Because the resulting pad clearance is greater than normal, special quick take-up master cylinders may be used to provide the extra brake fluid to bring the pads against the rotor.

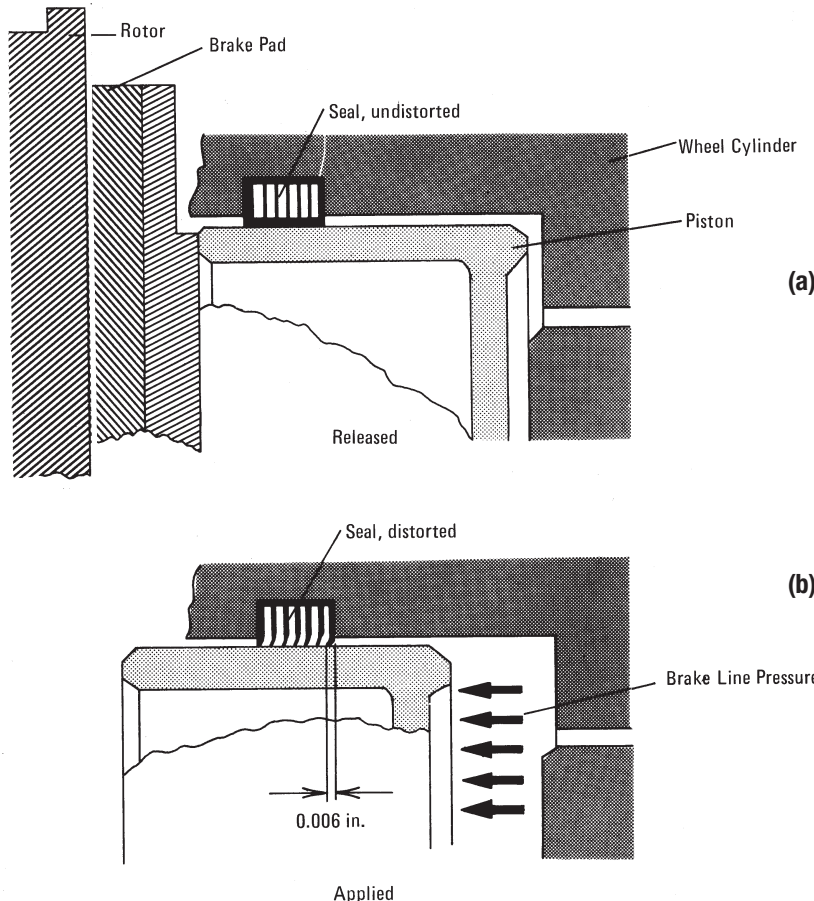


Figure 2-20. Disc brake adjustment. (a) Released brakes. (b) Applied brakes.

In some disc brake designs with integral parking brakes, the rear brake pads are automatically adjusted when the parking brake is applied. Because some drivers rarely use the parking brake, safety problems have arisen when rear disc brakes were found to be severely out of adjustment or corroded.

Adjustment of air disc brakes generally is accomplished by a regular automatic slack adjuster.

A major disadvantage of floating-caliper disc brakes is the potential for pad dragging due to insufficient pad return because one piston seal return force must provide the clearance for both pads. Increased potential also exists for squeal due to a larger number of degrees of freedom when compared with the fixed-caliper designs. Some earlier designs experience reduced effectiveness due to

corrosion of sliding surfaces. Modern calipers all have sealed-lubricated sliding pins as guiding members. The problems mentioned tend to be more pronounced for floating-caliper disc brakes with wheel cylinder sizes greater than 2 to 2.25 inches in diameter. Medium-weight trucks in the U.S. generally use disc brakes on all four wheels in connection with a full-hydraulic pressurized system.

The brake factor of standard non-energizing disc brakes is computed by Eq. (2-2). For multiple- disc brakes the brake factor is multiplied by the number of discs. While this design will increase the brake factor, and hence, the internal gain of the brake, it will not increase the overall system gain because more brake fluid volume must be available to overcome the increased pad clearance travels required. The larger brake fluid volume would require a larger-diameter master cylinder, resulting in a lower hydraulic gain between master- and wheel cylinder(s). See Eq. (5-20) for details.

2.4.2 Pad Pressure and Wear in Disc Brakes

One of the major requirements of the disc brake caliper is to press the pads against the rotor as uniformly as possible. Uniform pressure between pad and rotor results in uniform pad wear and brake temperatures, and more stable pad/rotor friction coefficients. Non-uniform pressure distribution wears the brake pads unevenly, particularly during severe brake applications from high speeds (Ref. 2.17). Pad wear increases rapidly for brake temperatures greater than approximately 573 to 623 K (600°F), resulting in tapered pad wear when ineffective caliper designs are used. Uniform pad wear is a major indicator of a quality caliper design.

Worn disc brake pads may show significantly more wear on the leading end (rotor entrance) as compared to the trailing end (rotor exit). This non-uniform wear is caused by higher pressure between pad and rotor at the leading end compared to that at the trailing end. The non-uniform pressure distribution is caused by the lever arm between pad drag force and abutment force. For a symmetrical wheel cylinder piston and pad design, the drag/abutment force moment results in pad pressures at the leading end that are approximately one-third greater than the average pressure. The corresponding pressure at the trailing end is approximately two-thirds of the average pad pressure.

Solutions to minimize or eliminate tapered pad wear involve an off-center pad application force produced by an asymmetrical caliper piston contact edge, effectively moving the piston force more in the direction of the trailing end of the pad, which creates a counter moment balancing the pad friction moment.

Other solutions locate the piston closer to the trailing end of the pad, again producing a counter moment.

A design patented by Continental-Teves, called “hammerhead” because of its shape, is illustrated in Fig. 2-21. In this particular caliper/pad design, the pad is pulled by the drag force rather than pushed. This design solution has proven to be reliable for both fixed and floating-caliper disc brakes. Other advantages of this pad anchor system include lack of pad vibrations and, hence, low potential

for brake noise or brake judder; less weight, because the reaction load is carried by each end of the pad; minimum deflection; and uniform pad temperatures.

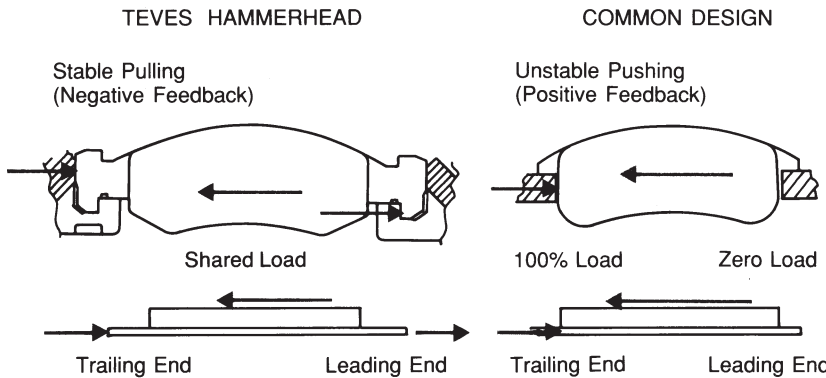


Figure 2-21. Continental-Teves “hammerhead” pad design.

Expensive designs minimizing tapered pad wear use four pistons per caliper. The pads are pushed with two pistons of different diameter, with the smaller piston located at the leading end of the pad.

Some basic design analyses to minimize non-uniform pad wear are presented next. The basic formulations of the pad pressure distribution can be used with fixed or floating calipers. The assumption is made that the caliper is rigidly mounted relative to the rotor. If the caliper is mounted in elastic slider bushings, the motion of the caliper relative to the rotor will adversely affect pressure distribution and pad wear (Refs. 2.18, 2.19).

2.4.2.1 Non-Uniform Pad Pressure Distribution

The non-uniform pressure distribution with a linear pressure change is illustrated in Fig. 2-22. The average force pressing the pad against the rotor is indicated by F_{av} . The pressure change at the leading and trailing edge of the pad is indicated by ΔF . Using a linear pressure change over the length of the pad yields a triangular pressure distribution as shown in Fig. 2-22. The resultant force of the pressure triangle is located $2/3 \ell_p$ from the tip of the triangle.

Application of moment balance about point A yields

$$F_{av}\mu_p t_p + F_{av}\mu_p\mu_f \frac{\ell_p}{2} = \frac{\Delta F \ell_p}{6}$$

Solving for pressure change ΔF results in

$$\Delta F = \frac{F_{av} 6}{\ell_p} \left(\mu_p t_p + \mu_p \mu_f \frac{\ell_p}{2} \right)$$

With $F_{max} = F_{av} + \Delta F$, the maximum pad pressure is

$$F_{max} = F_{av} \left[1 + \frac{6}{\ell_p} \left(\mu_p t_p + \mu_p \mu_f \frac{\ell_p}{2} \right) \right], \text{ N (lb)} \quad (2-24)$$

where ℓ_p = pad length, mm (in.)

t_p = pad thickness/support distance, mm (in.)

μ_f = pad support friction coefficient

μ_p = pad/rotor friction coefficient

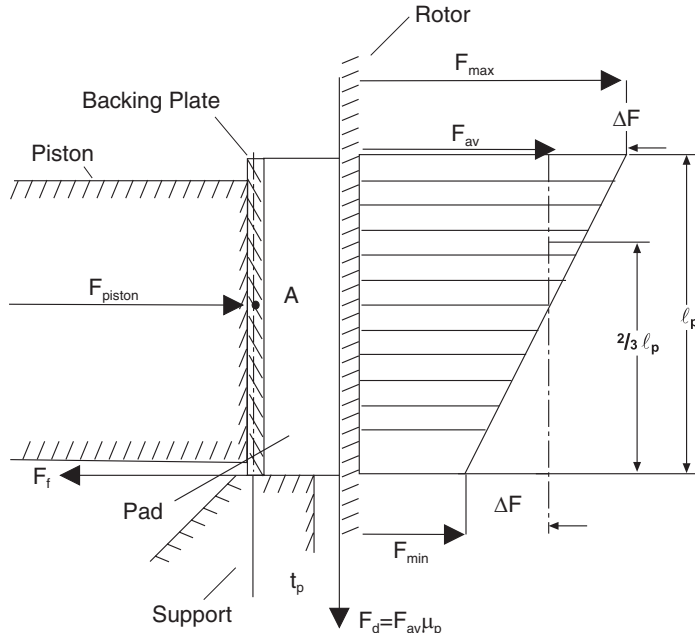


Figure 2-22. Non-uniform pad pressure in standard caliper design.

Substitution of typical values for a disc brake yields $F_{\max} = 1.33 F_{\text{av}}$, indicating that pressure at the rotor entrance will be as much as one-third greater than the average pressure, and at the rotor exit will be only two-thirds the average.

2.4.2.2 Offset Piston Design

The basic layout and dimensions are illustrated in Fig. 2-23. The offset distance is designated by c . If the distance c is computed properly, the pressure distribution will be uniform over the length of the pad.

F_d is the friction drag force between rotor and pad. F_{av} is the piston application force. F_f is the friction force at the pad backing plate support.

Moment balance about point A yields

$$F_{\text{av}}c = F_d t_p + F_f \frac{\ell_p}{2}$$

Force balance yields

$$F_{\text{av}} = F_p + F_p \mu_p \mu_f$$

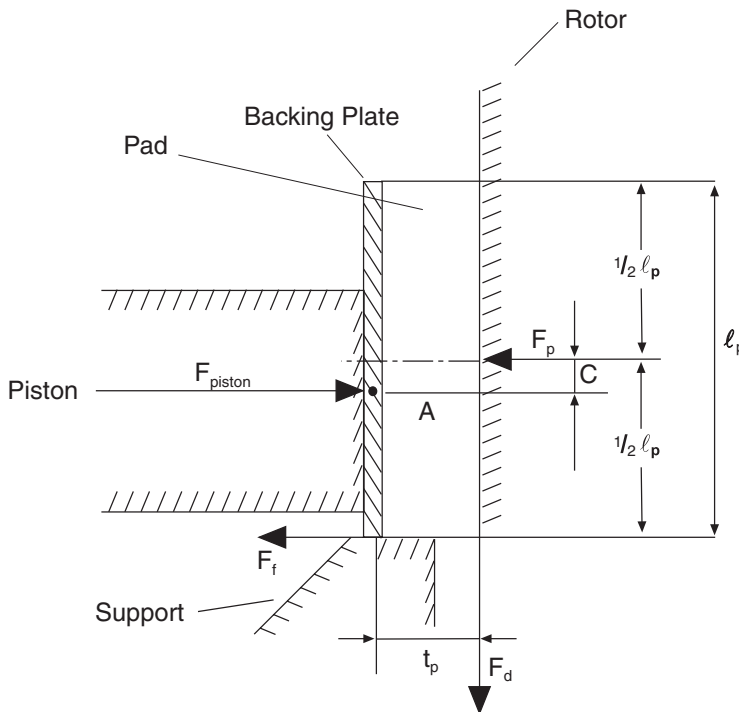


Figure 2-23. Uniform pad pressure with offset piston.

Combining both equations and solving for offset c results in

$$c = \frac{\mu_p t_p + \mu_p \mu_f \frac{\ell_p}{2}}{1 + \mu_p \mu_f}, \text{ mm (in.)} \quad (2-25)$$

The offset computed by Eq. (2-25) produces a uniform pressure distribution for the data used. As the pad thickness decreases, uneven pad wear will result. A somewhat smaller distance t_p may be used to adjust for pad wear with use of the vehicle. Manufacturing costs due to non-symmetry may be excessive, particularly for smaller production numbers.

2.4.2.3 Pulled or “Hammerhead” Pad Design

The basic schematic of the pad design is illustrated in Fig. 2-24.

Moment balance about point A yields

$$F_{av} \mu_p t_p - F_f b = \Delta F \frac{\ell_p}{6}$$

Solving for pressure change ΔF results in

$$\Delta F = F_{av} \frac{6}{\ell_p} (\mu_p t_p - \mu_p \mu_f b)$$

where b = distance from piston center to pad support, mm (in.)

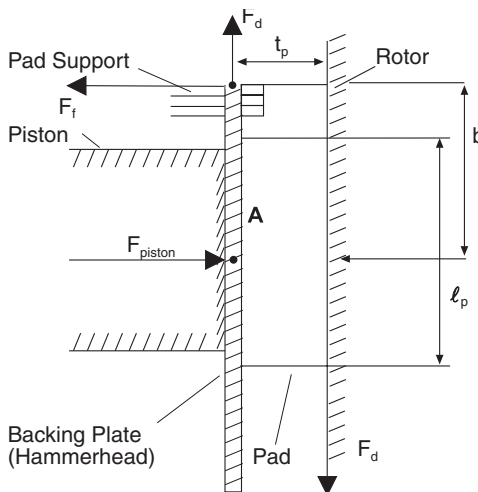


Figure 2-24. Pulled or hammerhead pad design.

With $F_{\max} = F_{av} + \Delta F$ the maximum pressure becomes

$$F_{\max} = F_{av} \left[1 + \frac{6}{l_p} (\mu_p t_p - \mu_p \mu_f b) \right], \text{ N(lb)} \quad (2-26)$$

Substitution of typical data yields a maximum pressure of $F_{\max} = 1.033 F_{av}$. The result shows a significant improvement with the pulled pads versus the pushed pads by providing a nearly uniform pressure distribution. Pulled pads can carry heavier specific loadings and are used increasingly in high-performance vehicles.

2.4.2.4 Four-Piston Fixed-Caliper Design

A more expensive solution to achieve uniform pad wear is the four-piston caliper design as illustrated in Fig. 2-25. The pads are pushed together by two opposing pistons of different diameters.

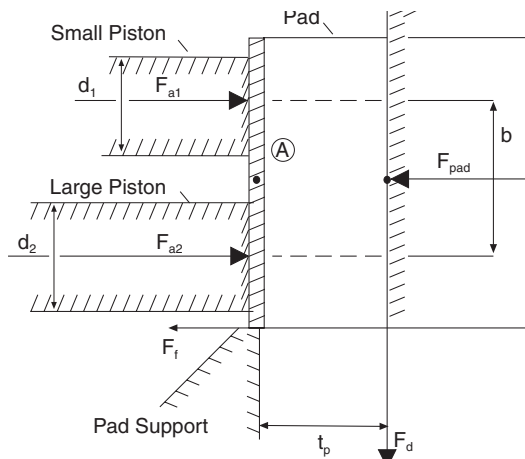


Figure 2-25. Four-piston fixed-caliper design.

Uniform pad pressure distribution is achieved when all moments balance about point A. Hence

$$F_d t_p + F_f \frac{\ell}{2} + F_{a1} \frac{b}{2} - F_{a2} \frac{b}{2} = 0$$

where F_{a1} = force of piston 1, N (lb)

F_{a2} = force of piston 2, N (lb)

With $F_d = \mu_p F_{\text{pad}}$ and $F_f = F_d \mu_f = F_{\text{pad}} \mu_p \mu_f$ and $F_{\text{pad}} = F_{a1} + F_{a2} - F_f$ we have

$$F_{a1} = F_{\text{pad}} \left(\frac{1}{2} - \frac{\mu_p t_p}{b} - \frac{\mu_p \mu_f \ell}{2b} + \frac{\mu_p \mu_f}{2} \right)$$

$$F_{a2} = F_{\text{pad}} \left(\frac{1}{2} + \frac{\mu_p t_p}{b} + \frac{\mu_p \mu_f \ell}{2b} + \frac{\mu_p \mu_f}{2} \right)$$

Finally, the piston application force, and hence diameter, ratio is

$$\frac{F_{a1}}{F_{a2}} = \frac{\frac{1}{2} - \frac{\mu_p t_p}{b} - \frac{\mu_p \mu_f \ell}{2b} + \frac{\mu_p \mu_f}{2}}{\frac{1}{2} + \frac{\mu_p t_p}{b} + \frac{\mu_p \mu_f \ell}{2b} + \frac{\mu_p \mu_f}{2}}$$

where d_1 = diameter of piston 1, mm (in.)

d_2 = diameter of piston 2, mm (in.)

The individual diameters are obtained from the fictitious single wheel-cylinder diameter d_3 by

$$d_3^2 = d_1^2 + d_2^2$$

The single diameter d_3 is obtained from a brake balance analysis employed for a single piston caliper. Solving for the individual diameters results in

$$d_1 = \sqrt{\frac{d_3^2}{1 + \frac{F_{a1}}{F_{a2}}}} , \text{ mm (in.)} \quad (2-27a)$$

$$d_2 = \frac{d_1}{\sqrt{F_{a1}/F_{a2}}} , \text{ mm (in.)} \quad (2-27b)$$

Typical brake data and $d_3 = 57$ mm used in Eq. 2-27 may result in $d_1 = 36$ mm and $d_2 = 44$ mm. For vehicles not requiring extreme braking performance, a smaller diameter difference such as 38 and 42 mm may be used to account for the fact that increased pad wear reduces t_p . High-performance sports and race cars would use a 36/44 diameter ratio because generally pads are not worn to minimum levels. All previous uniform pad wear analyses apply fully only to fixed-caliper designs. For floating calipers limitations exist, including play tolerances and deformations. Design solutions involving two pistons per pad, piston offset, and others have not proven fully successful in practical applications. Only pulled pad solutions are advantageous for floating-caliper disc brakes.

2.4.3 Disc Brake Caliper Installation

Most calipers are installed so that the mounting bolts are located vertically above each other, with the caliper either located in front (nine o'clock) or aft (three o'clock) of the rotor. This installation ensures that the air bleeding valve is located at the highest point of the caliper, an important detail for proper brake maintenance.

The front or aft location has a significant effect on the hub bearing forces sustained during severe braking. With the aft location, the bearing force will increase to more than twice its normal static value for a deceleration of 1 g. The front location may increase bearing forces to a value equal to four times the static level. For front- and four-wheel-drive vehicles using press fit hub and shaft connections, the bearing force may be too high, possibly resulting in fatigue hub failure and wheel separation during braking. In addition, significant shaft bending during severe braking may cause undesirable vibrations and noise.

Two opposing calipers will increase the bearing force only by approximately 170% of its normal value.

2.4.4 Disc and Drum Brake Comparison

The major advantage of the disc brake is its ability to operate with little fade at high temperatures of up to 1073 to 1173 K (1500 to 1600°F). Heating of the brake rotor increases its thickness, thereby causing no loss in brake fluid volume, i.e., no increased pedal travel or soft pedal feel. In the case of air disc and drum brakes, and when considering lower legal speed limits for trucks such as in Germany (80 km/h or 50 mph), researchers have concluded that the drum brake is equal to the disc brake in terms of performance (Ref. 2.20). However, when considering the U.S. truck speed limits of 75 mph, disc brakes are superior to drum brakes in most respects, assuming that no in-use factors (rust, dirt) affect the cooling capacity of the disc brake.

An additional important benefit of disc brakes is their linear relationship between brake torque and pad/rotor friction coefficient. For example, a 10% increase in pad friction coefficient increases the brake torque by 10%. For a typical duo-servo brake, a similar friction rise increases brake torque by as much as 30 to 35%.

Drum brakes are highly temperature sensitive. A maximum temperature of 673 to 700 K (750 to 800°F) should not be exceeded. Not only are the friction coefficients affected, but the drum diameter increases with increasing temperatures. At 648 K (700°F), typical passenger drum brake diameters may increase by 1 to 1.5 mm (0.05 to 0.06 in.), with a correspondingly longer wheel cylinder piston travel sufficient to increase pedal travel by 30 to 40% of its normal value when the brakes are cold. In addition, the larger drum diameter causes improper contact between lining and drum, which results in lining/drum pressure peaks and thus higher local lining temperatures, and a variation in brake torque output. Brake drums for S-cam brakes have increased pushrod travels of 12 mm (0.5 in.) for a temperature increase of 590 K (600°F) over the cold pushrod travel value.

The specific brake torque or brake factor, defined as the ratio of drum drag to application force of one shoe [Eq. (2-1)], is a general indicator of the ability of a brake to produce torque for different lining/drum friction coefficients. More details are presented in Section 2.3. A brake factor comparison of different drum brake designs with the disc brake is shown in Fig. 2-1. Inspection of this figure reveals that the duo-servo brake has the highest brake factor for any given friction coefficient. Although this characteristic is desirable for parking brake design, it has proven unsafe when used as a rear brake for the service brake. Duo-servo brakes should not be used on front brakes due to the severe left-to-right brake unbalance potential. The straight brake factor line for the disc brake reveals its linear relationship to the friction coefficient. The two-trailing shoe drum brake has a brake factor curve similar to that of the disc brake. Although no applications are envisioned, future designs may make use of this design by providing a stable service rear brake, and a higher brake factor parking brake.

2.4.5 Lining/Pad Friction and Classification

All linings begin to disintegrate at the friction surface due to high temperatures developed from the heat-generation process. Due to non-uniform pressure distributions between lining and drum or pad and rotor, and other surface irregularities, pad friction surface temperatures will not be uniform over the pad contact area. Areas of higher temperature will have lower friction levels than those with lower temperatures. An exact analytical prediction of the pad/rotor friction coefficient is not possible at the present time. However, close estimates based on test data can be made.

The basic brake system design layout is based on the brake torque performance achieved with “cold” brakes. A brake is considered cold when its temperature is less than 366 K (200°F). Most lining friction coefficients will increase as brake temperatures rise to approximately 423 to 473 K (300 to 400°F). At elevated temperatures near 523 to 588 K (500 to 600°F) and above, linings tend to exhibit fade; i.e., their friction coefficient decreases below its cold value. Good linings will recover to their intended design levels after cooling. At extremely low temperatures, friction coefficients tend to decrease below the cold value. Because brake systems have to perform safely under all

foreseeable operating conditions, the proper selection of a lining material can be a challenge, particularly for drum brakes, and even more so for duo-servo brake designs.

Test procedures have been developed to measure lining friction at different temperatures and to classify ranges. SAE J661 procedure is used to determine the cold (366 K or 200°F) and hot (588 K or 600°F) friction levels of lining material samples, one inch square in size, when used with a drum made of a particular material to a particular set of dimensions. Two letters are used to mark cold and hot friction coefficients. The first letter represents an average value of the normal (cold) friction, the second hot friction. The higher the letter, the higher the coefficient of friction, so that

- C refers to friction coefficients less than 0.15
- D 0.15 to 0.25
- E 0.25 to 0.35
- F 0.35 to 0.45
- G 0.45 to 0.55
- H over 0.55
- Z unclassified

For example, a lining edge code FE indicates that the normal (cold) coefficient of friction is between 0.35 and 0.45, say, 0.38, and when heated to 588 K (600°F) between 0.25 and 0.35, say, 0.34.

It is important to recognize that the SAE J661 lining classifications using fairly broad ranges of friction coefficients may cause errors when used in the design analysis of an existing braking system. Calculations determining brake lockup sequence require reasonably accurate brake factor computations and, hence, lining friction coefficients. Simply using any value within the specified letter range will not be acceptable. As a minimum, the actually measured average friction coefficients used to establish the friction range should be considered in the design analysis. Because only a lining sample area of 25.4 by 25.4 mm (one inch by one inch) is actually tested, additional differences may exist between the classification friction coefficient and the effective lining friction coefficient actually experienced by the drum brake.

Albin Burkman of General Motors used a laboratory test method to determine that moisture may have a significant effect on lining friction coefficient (Ref. 2.15). He concluded that the friction coefficients are higher during periods of high humidity than under dry operating conditions, and lower when the brakes are flooded by water.

Brake torque and brake factor can be measured directly with special torque hubs, or indirectly from vehicle deceleration tests. If such data are available, they should be used as a basis for the brake system design analysis.

2.4.6 Self-Energizing Disc Brake

Self-energizing disc brakes are not used in typical automotive applications. Their basic operational principles involve a wedge effect provided by a ball-and-ramp type design, as illustrated in Fig. 2-26 for a fully covered disc brake design. The actuating force is the force directly pressing against the disc. This force is increased by the friction force, which causes an additional relative rotation. This leads to pushing the circular brake pads apart and increased normal force by means of the ball-and-ramp mechanism, thus introducing self-energizing.

With the notation shown in Fig. 2-26, the friction force of one circular brake pad is given by the relationship (Ref. 2.4):

$$F_d = \mu_L [F_a + F_d (r_m / r_k)] \cot \delta, N \text{ (lb)}$$

or solved for the plate brake factor as

$$\frac{F_d}{F_a} = \frac{\mu_L (r_k / r_m)}{(\tan \delta)(r_k / r_m) - \mu_L} \quad (2-28)$$

where r_k = disc brake dimension, mm (in.)

r_m = disc brake dimension, mm (in.)

δ = disc brake ramp angle, deg

μ_L = pad friction coefficient

Because two friction surfaces are involved, the total brake factor is

$$BF = 2(r_k / r_m) \frac{\mu_L / \mu_{L\infty}}{1 - \mu_L / \mu_{L\infty}} \quad (2-29)$$

where $\mu_{L\infty}$ = self-locking pad friction coefficient

and the self-locking limits (see Section 2.3.3 for self-locking limit details) for the pad friction coefficient are given by

$$\mu_{L\infty} = (\tan \delta)(r_k / r_m)$$

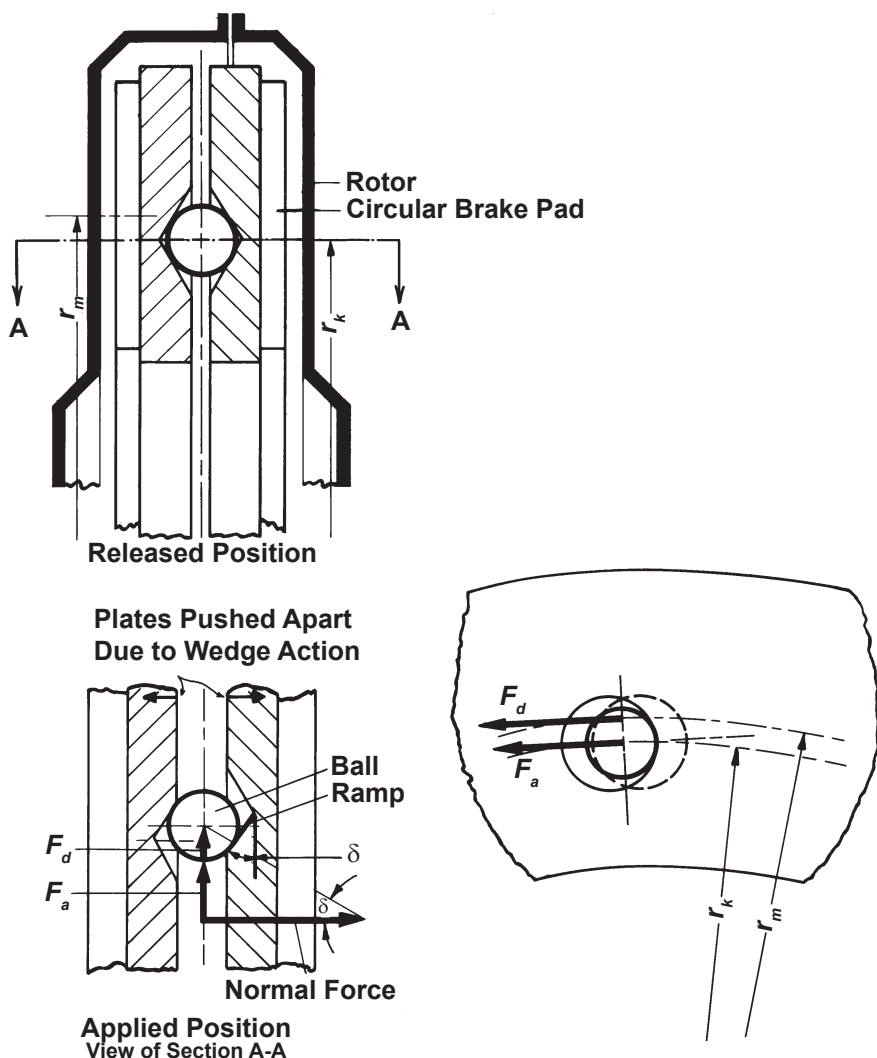


Figure 2-26. Schematic of self-energizing fully covered disc brake.

The sensitivity of the brake S_B is expressed by

$$S_B = \frac{2 \cot \delta}{(1 - \mu_L / \mu_{L_\infty})^2} \quad (2-30)$$

Chapter 2 References

- 2.1 Breuer, Bert and Bill, and H. Karlheinz, *Brake Technology Handbook*, SAE International, Warrendale, PA, 2008.
- 2.2 Ostermeyer, George P. and M. Mueller, "New Insights into the Tribology of Brake Systems," Proc. IMechE. Vol. 222, Part D: *Journal of Automobile Engineering*.
- 2.3 Chao, Min Hyung, et al., "The Role of Raw Material Ingredients of Brake Linings on the Formation of Transfer Film and Friction Characteristics," SAE Paper No. 2001-01-3130, SAE International, Warrendale, PA, 2001.
- 2.4 Dr. Strien, Hans, "Calculation and Testing of Automotive Friction Brakes," Ph.D. Dissertation, Technical University, Braunschweig, 1949.
- 2.5 Shih, Shan, et al., "Improved Drum Brake Shoe Factor Prediction with the Consideration of System Compliance," SAE Paper No. 2000-01-3417, SAE International, Warrendale, PA, 2000.
- 2.6 PCBRAKE FACTOR at www.pcbrakeinc.com.
- 2.7 Limpert, Rudy, et al., "Brake System Analysis in Pre-Crash Accident Reconstruction," Short Paper PCB 9-2006, e-Publishing, www.pcbrakeinc.com, 2006.
- 2.8 Elvenkemper, Andreas, "Investigation of Torque Output Variation in a Duo-Servo Park Brake System Using Six Sigma Tools and FE-Analysis," SAE Paper No. 2006-01-3199, SAE International, Warrendale, PA, 2006.
- 2.9 Raajha, M.P. and V. Lakshmi Narayanan, "High Performance Drum Brake Assembly for Automotive Braking Applications," SAE Paper No. 2003-01-3306, SAE International, Warrendale, PA, 2003.
- 2.10 *Automotive Handbook*, Robert Bosch, 7th edition, SAE International, Warrendale, PA, 2007.
- 2.11 Agudelo, Carlos E. and Eduard Ferro, "Technical Overview of Brake Performance Testing for Original Equipment and Aftermarket Industries in the US and European Markets," Link Technical Report FEV205-01.
- 2.12 LINK Engineering, Brake Dynamometer Test Report, 16.5×7 inches S-Cam Drum Brake.
- 2.13 Buckman, Leonard, Commercial Vehicle Braking System, Volume 1, Seminars, SAE International, Warrendale, PA.

- 2.14 MacAdams, C. and T. Gillespie, Determining the Sensitivity of S-Cam Brakes, Report No. UMTRI-98-6, February 1998.
- 2.15 Burkman, Albin J., "A Laboratory Method for Testing Moisture Sensitivity of Brake Lining Materials," SAE Paper No. 620128, SAE International, Warrendale, PA, 1962.
- 2.16 Mueller, W., "Contribution to the Analysis and Testing of Motor Vehicle Drum Brakes," Deutsche Kraftfahrtforschung und Strassenverkehrstechnik, No. 207, 1971.
- 2.17 Zhang, Shaoyang, Weiping Chen, and Yuanyuan Li, "Wear of Friction Materials during Vehicle Braking," SAE Paper No. 2009-011032, SAE International, Warrendale, PA, 2009.
- 2.18 Tumbrink, H.J., "Measurement of Load Distribution on Disc Brake Pads and Optimizing of Disc Brakes Using the Ball Pressure Methods," SAE Paper No. 890863, SAE International, Warrendale, PA, 1989.
- 2.19 Wang, Nui, "The Evolution of the Pad Guided Disc Brake Caliper," SAE Paper No. 940332, SAE International, Warrendale, PA, 1994.
- 2.20 Gohring, Ernst and Egon-Christian von Glasner, "Performance Comparison of Drum and Disc Brakes for Heavy Duty Commercial Vehicles," SAE Paper No. 902206, SAE International, Warrendale, PA, 1990.

Chapter 3



Thermal Analysis of Automotive Brakes

3.1 Temperature Analysis

3.1.1 General Considerations

Brakes convert the kinetic and potential energy of the vehicle into heat at the friction surface by the heat generation process. Heat generation, and hence, brake temperature, is the product of rubbing velocity between pad and rotor, mechanical pad pressure, and pad/rotor coefficient of friction (Ref. 3.1). Brakes must be designed such that operating temperatures are kept below a certain level to ensure safe operation of brake components including pads or linings, rotors or drums, wheel cylinders or calipers, brake fluid, wheel bearings, axle and bearing seals, and lubricating oils or greases. Sound engineering analysis, and component and vehicle testing must be carried out to ensure safe and efficient brake system operation under foreseeable conditions.

Brake engineers are cautioned not to make single design changes without considering their effects on system performance. Design changes may appear not to have any effects on surrounding components while in actuality they do. Replacing drum by disc brakes may not always result in lower brake temperatures when installation and in-use factors are considered. For example, a 7-in.-wide drum brake may be more effectively cooled by airflow than a 2.5-in.-wide ventilated disc brake rotor when installed on the third rear axle of a bus.

In the early 1990s, the front disc brake calipers of a particular heavy-duty pickup truck were equipped with phenolic pistons. In some vehicles, to save material cost, the piston material was changed to aluminum. The higher thermal conductivity of the aluminum piston caused more heat to be conducted through the piston into the hydraulic brake fluid. During severe braking, the brake fluid of the front brakes vaporized, resulting in partial brake failure. Before design changes were made, a field fix was done by inserting a thin, flat piece made of Nomax material between pad and piston to minimize thermal conductivity. A proper engineering analysis of the effects of the design changes on critical brake system components would have avoided the recall action.

3.1.2 Braking Energy and Braking Power

For a vehicle decelerating on a level surface from a higher velocity V_1 to a lower velocity V_2 , the braking energy E_b is

$$E_b = (m/2)(V_1^2 - V_2^2) + (I/2)(\omega_1^2 - \omega_2^2) , \text{ Nm (lbft)} \quad (3-1)$$

where I = mass moment of inertia of rotating parts, kgm^2 (lbft^2)

m = vehicle mass, kg (lbs^2/ft)

V_1 = velocity at beginning of braking, m/s (ft/s)

V_2 = velocity at end of braking, m/s (ft/s)

ω_1 = angular velocity of rotating parts at beginning of braking, $1/\text{s}$

ω_2 = angular velocity of rotating parts at end of braking, $1/\text{s}$

If the vehicle comes to a complete stop, then $V_2 = \omega_2 = 0$ and Eq. (3-1) becomes

$$E_b = mV_1^2 / 2 + I\omega_1^2 / 2 , \text{ Nm (lbft)} \quad (3-2)$$

When all rotating parts are expressed relative to the revolutions of the wheel, then with $V = R\omega$, Eq. (3-2) becomes

$$E_b = \frac{m}{2} \left(1 + \frac{I}{R^2 m} \right) V_1^2 \approx \frac{kmV_1^2}{2} , \text{ Nm (lbft)} \quad (3-3)$$

where k = correction factor for rotating masses [$k \approx 1 + I/(R^2 m)$]

R = tire radius, m (ft)

Typical values of k for passenger cars range from 1.05 to 1.15 in high gear to 1.3 to 1.5 in low gear. Corresponding values for trucks are 1.03 to 1.06 for high gear and 1.25 to 1.6 for low gear.

Braking power P_b is equal to braking energy divided by the time t during which braking occurs, or

$$P_b = d(E_b) / dt , \text{ Nm/s (lbft/s)} \quad (3-4)$$

If the deceleration a is constant, then the velocity $V(t)$ is given by

$$V(t) = V_1 - at , \text{ m/s (ft/s)} \quad (3-5)$$

where a = deceleration, m/s^2 (ft/s^2)

t = time, s

Eqs. (3-3) through (3-5) yield the brake power as

$$P_b = kma(V_1 - at) , \text{ Nm/s (lbft/s)} \quad (3-6)$$

Inspection of Eq. (3-6) shows that braking power is not constant during the braking process. At the beginning of braking ($t = 0$), brake power is a maximum, decreasing to zero when the vehicle stops.

The time t_s for the vehicle to come to a stop is

$$t_s = V_1 / a \quad , \quad \text{s} \quad (3-7)$$

The average braking power P_{bav} , excluding tire slip and engine braking, over the braking time t_s for a vehicle coming to a stop is

$$P_{\text{bav}} = kmaV_1 / 2 \quad , \quad \text{Nm/s (lbft/s)} \quad (3-8)$$

Example 3-1: A vehicle weighing 22,240 N (5000 lb) decelerates to a stop from a speed of 30.5 m/s (100 ft/s) at 7.6 m/s² (25 ft/s²). Use $k = 1$.

With Eq. (3-3), the braking energy is

$$E_b = \frac{(1)(22,240)(30.5)^2}{(2)(9.81)} = 1,054,473 \text{ Nm}$$

$$\left[E_b = \frac{(1)(5000)(100)^2}{(2)(32.2)} = 776,398 \text{ lbft} \right]$$

The average braking power is

$$P_{\text{bav}} = \frac{(1)(22,240)(7.6)(30.5)}{(2)(9.81)} = 262,754 \text{ Nm/s} = 262.7 \text{ kW}$$

$$\left[P_{\text{bav}} = \frac{(1)(5000)(25)(100)}{(2)(32.2)} = 194,099 \text{ lbft/s} = 353 \text{ hp} \right]$$

The braking time is $t_s = 30.5 / 7.6 = 4 \text{ s}$. Consequently, the average braking power of 262.7 kW (353 hp) is produced during the relatively short time period of 4 s. The maximum power at the onset of braking is 525.4 kW (706 hp).

For a vehicle traveling downhill while decelerating, the brakes have to absorb kinetic and potential energy, as illustrated in Fig. 3-1. Using energy balance, the braking energy is

$$E_b = Wh + (km / 2)(V_1^2 - V_2^2) \quad , \quad \text{Nm (lbft)} \quad (3-9)$$

where h = vertical drop of vehicle mass, m (ft)

W = vehicle weight, N (lb)

For continued braking at constant speed, Eq. (3-9) becomes, with $V_1 = V_2$,

$$E_b = Wh \quad , \quad \text{Nm (lbft)} \quad (3-10)$$

Braking power during continued braking is obtained by differentiating energy with respect to time, or

$$P_b = d(E_b)/dt = [d(E_b)/dh](dh / dt) \quad , \quad \text{Nm/s (lbft/s)} \quad (3-11)$$

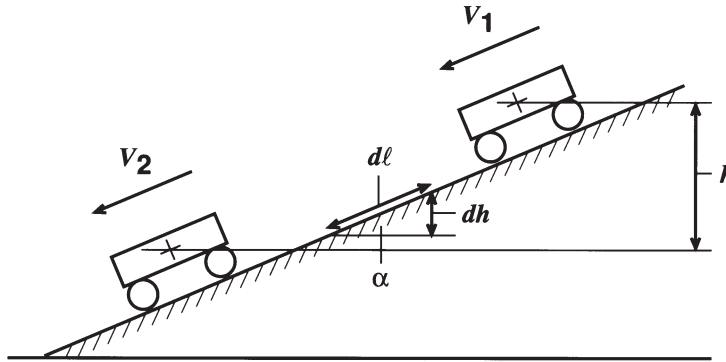


Figure 3-1. Kinetic and potential energy on grade.

With the grade expressed by angle α and the actual distance traveled on the highway expressed by ℓ (Fig. 3-1), the change in height and road distance are related to the slope by

$$\sin \alpha = dh / d \ell$$

and Eq. (3-11) may be rewritten as

$$P_b = WV \sin \alpha \quad , \quad \text{Nm/s (lbft/s)} \quad (3-12)$$

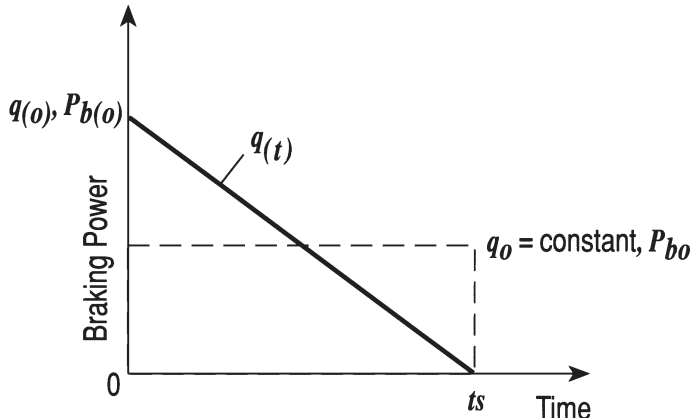


Figure 3-2. Braking power vs. time.

When using imperial units in the temperature analyses, it becomes convenient to express average braking power for a vehicle coming to a complete stop [Eq. (3-8)] in thermal units rather than foot-pounds per second as follows:

$$q_0 = \frac{k(1-s)V_1 a W(3600)}{2(778)} , \text{ BTU/h} \quad (3-13)$$

where a = deceleration in g-units

k = correction factor for rotating masses

q_0 = average braking power, BTU/h

s = tire slip, defined by the ratio of the difference between vehicle forward speed and circumferential speed to vehicle forward speed

V_1 = initial velocity of vehicle, m/s (ft/s)

W = vehicle weight, N (lb)

The tire slip accounts for the energy absorbed by the tire/roadway due to partial slipping of the tire. In the extreme, when the brake is locked, no energy will be absorbed by the brake; i.e., $s = 1.00$.

For the general case of decelerating on a downgrade, Eq. (3-13) may be modified by adding $\sin(\alpha)$ to deceleration a . For example, for a vehicle decelerating at 0.5 g on a downgrade of $\alpha = 10$ deg, the brakes "feel" an effective deceleration of $0.5 + \sin(10) = 0.674$. For uphill braking, the slope effect is subtracted from the actual deceleration because the brakes do not have to absorb all of the kinetic energy, namely that portion transformed into potential energy.

The maximum brake power $P_{b(0)}$ produced at the onset of braking is equal to (see Fig. 3-2)

$$P_{b(0)} = 2P_{bavg} , \text{ Nm/h} \quad (3-14)$$

$$[q_{(0)} = 2q_0 , \text{ BTU/h}]$$

where $q_{(0)}$ = braking power at beginning of braking ($t = 0$), BTU/h

During continued downhill brake application at constant speed, the power absorbed by the vehicle brakes, when expressed in imperial thermal units, is obtained from Eq. (3-12) as

$$q_0 = \frac{WV(G - R_r)3600}{778} , \text{ BTU/h} \quad (3-15)$$

where G = road gradient (percentage; for example 0.06 for 6% down grade)

R_r = tire rolling resistance coefficient

V = vehicle velocity, ft/s

W = vehicle weight, lb

3.1.3 Braking Power Absorbed by Lining and Drum

The analysis of brake temperatures requires an accurate determination of both the total energy absorbed by the brakes and how this energy is distributed between lining and drum or pad and disc.

The distribution of braking energy between lining and drum cannot be predicted readily. The braking or thermal energy distribution is related directly to the thermal resistance associated with both sides of the interface where the heat is generated. It is assumed that the heat transfer into the drum or rotor and lining or pad may be determined from the equivalent resistance network. For the steady-state conditions, this may be expressed as

$$q_R''/q_P'' = \sum R_p / \sum R_R \quad (3-16)$$

where q_P'' = heat flux into pad, Nm/hm² (BTU/hft²)

q_R'' = heat flux into rotor, Nm/hm² (BTU/hft²)

R_p = thermal resistance to conductive heat flow into pad, hK/Nm (h°F/BTU)

R_R = thermal resistance to conductive heat flow into rotor, hK/Nm (h°F/BTU)

For short brake application times, the lining and drum may be considered as semi-infinite solids. Under these conditions, no cooling of the brakes occurs because the temperature at the cooling surfaces has not increased. The requirement of identical temperatures at the interface and the fact that the total heat generation equals the heat absorbed by the lining and drum yields with Eq. (3-16)

$$\frac{q_R''}{q_P''} = \left(\frac{\rho_R c_R k_R}{\rho_p c_p k_p} \right)^{1/2} \quad (3-17)$$

where c_p = pad specific heat, Nm/kg K (BTU/lb_m °F)

c_R = rotor specific heat, Nm/kg K (BTU/lb_m °F)

k_p = pad thermal conductivity, Nm/mh K (BTU/hft °F)

k_R = rotor thermal conductivity, Nm/mh K (BTU/hft °F)

ρ_p = pad density, kg/m³ (lb_m/ft³)

ρ_R = rotor density, kg/m³ (lb_m/ft³)

It becomes convenient to express the portion of the total heat generation absorbed by the drum or rotor in terms of the material properties. The requirement that the total heat generated equals $q_R'' + q_P''$ and Eq. (3-17) yield the relative braking energy γ absorbed by the drum or rotor:

$$\gamma = \frac{q_R''}{q_R'' + q_P''} = \frac{1}{1 + \left(\frac{\rho_p c_p k_p}{\rho_R c_R k_R} \right)^{1/2}} \quad (3-18)$$

For continued braking or repeated braking, Eq. (3-18) assumes a more complicated form due to the convective heat transfer occurring as a result of higher brake temperatures. The schematic is illustrated in Fig. 3-3 for a disc brake. For steady-state conditions, no additional energy will be stored in the rotor. Consequently, the thermal resistance R_R associated with the rotor is given by

$$\Sigma R_R = 1 / (h_R A_R) , \text{ hK/Nm (h}^\circ\text{F/BTU}) \quad (3-19)$$

where A_R = area of cooling surface, m^2 (ft^2)

h_R = convective heat transfer coefficient, $\text{Nm}/\text{hm}^2\text{K}$ ($\text{BTU}/\text{h}^\circ\text{F ft}^2$)

The thermal resistance R_p associated with the pad is

$$\begin{aligned} \sum R_p &= 1 / (h_p A_p) + \delta_p / (k_p A_p) \\ &\quad + \delta_s / (k_s A_p) , \text{ hK/Nm (h}^\circ\text{F/BTU}) \end{aligned} \quad (3-20)$$

Where A_p = pad surface, m^2 (ft^2)

h_p = convective heat transfer coefficient of the pad, $\text{Nm}/\text{hm}^2\text{K}$ ($\text{BTU}/\text{h}^\circ\text{F ft}^2$)

k_p = thermal conductivity of pad material, Nm/hmK ($\text{BTU}/\text{h}^\circ\text{F ft}$)

k_s = thermal conductivity of pad support, Nm/hmK ($\text{BTU}/\text{h}^\circ\text{F ft}$)

δ_p = pad thickness, m (ft)

δ_s = pad support thickness, m (ft)

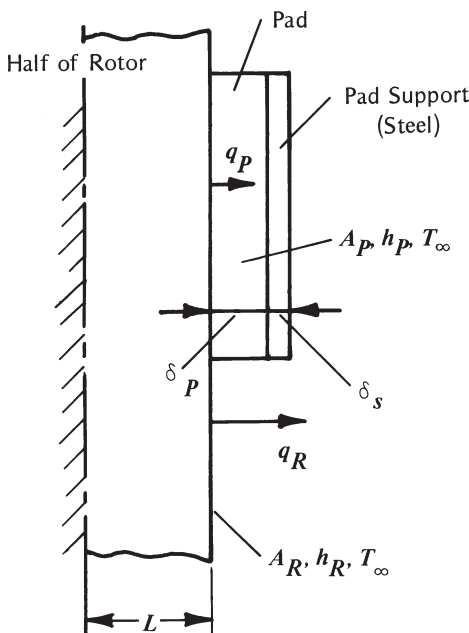


Figure 3-3. Heat distribution for continued braking

With the heat distribution factor defined in Eq. (3-18), Eqs. (3-19) and (3-20) yield

$$\gamma = \frac{q''_R}{q''_R + q''_P} = \frac{1}{1 + \frac{\sum R_R}{\sum R_P}}$$

and the heat distribution to the rotor is given by

$$\gamma = \left(1 + \frac{h_P k_P k_S A_P}{h_R A_R (k_P k_S + \delta_P h_P k_S + \delta_S h_P k_P)} \right)^{-1} \quad (3-21)$$

For brakes attaining high temperatures, thermal radiation may contribute substantially to cooling of the brakes. As is shown in Section 3.1.9, radiation heat transfer may be included by increasing the effective convective heat transfer coefficient.

3.1.4 Simplified Temperature Analysis in a Single Stop

In a single stop with high heat generation, i.e., high deceleration levels, the braking time may be less than the time required for the heat to penetrate through the drum or rotor material. Under these conditions no convective brake cooling occurs and all braking energy is assumed to be absorbed by the brake and lining.

For drum brakes, the heat penetration time t_b to reach the outer drum surface is given by (Ref. 3.2)

$$t_b = L^2 / 5a \quad , \quad h \quad (3-22)$$

where a = thermal diffusivity = $k / (\rho c)$, m^2/h (ft^2/h)

c = specific heat of drum or rotor material, Nm/kgK ($BTU/lb_m \text{ } ^\circ F$)

k = thermal conductivity of drum material, Nm/hmK ($BTU/hft \text{ } ^\circ F$)

L = drum thickness, m (ft)

t_b = time for heat to penetrate, h

ρ = drum density, kg/m^3 (lb_m / ft^3)

The heat flux penetration time expressed by Eq. (3-22) can also be used to determine the time until the heat flux has reached the midpoint in a solid disc brake. For that case, L would be half the rotor thickness. For a drum brake, Eq. (3-22) may be rewritten in terms of penetration time measured in seconds and typical drum material properties as

$$t_b = 0.0127(L_d)^2 \quad , \quad s \quad (3-23)$$

$$\left[t_b = 8.19(L_d)^2 \quad , \quad s \right]$$

where L_d = drum thickness expressed in mm (in).

For example, a truck drum brake having a thickness between the friction and cooling surface of 25 mm (1 in.) would only experience an increase in cooling surface temperature after 8.19 s of braking. In a typical maximum effectiveness stop involving heavy commercial vehicles with a deceleration of 0.5 g, the heat penetration time t_b to the outer cooling surface of the drum would only be exceeded for braking speeds of 144 km/h (90 mph) or higher.

For smaller drum brakes or ventilated disc brakes with smaller wall thicknesses, the heat penetration time will be shorter, thus raising the cooling surface temperature above its initial level. Notwithstanding, the convective cooling will be significantly lower than the heat stored in the rotor during the short duration of braking.

If a linearly decreasing braking power similar to Eq. (3-6) is assumed, the surface temperature as a function of time may be expressed as

$$T(L, t) - T_i = (5/4)^{1/2} (q''_{(0)}/k)(at)^{1/2} (1 - 2t/3t_s) , \text{ K (}^{\circ}\text{F}) \quad (3-24)$$

where a = thermal diffusivity, m^2/h (ft^2/h)

k = thermal conductivity, $\text{Nm}/\text{hm K}$ ($\text{BTU}/\text{hft}^{\circ}\text{F}$)

$q''_{(0)}$ = heat flux into drum or rotor surface existing immediately after beginning of braking, $\text{Nm}/\text{h m}^2$ (BTU/hft^2)

t = braking time, h

T_i = initial temperature, K ($^{\circ}\text{F}$)

t_s = time to stop vehicle, h

It should be noted that $q''_{(0)}$ is the braking power per unit area absorbed by the drum or rotor, i.e., only that portion conducted into the drum material and not the total amount of brake power generated by the brake.

Differentiation of Eq. (3-24) with respect to time indicates a maximum of the surface temperature at $t = t_s/2$. Thus, the maximum surface temperature $T_{\max,L}$ in a single stop without ambient cooling may be expressed as

$$T_{\max,L} - T_i = (5/18)^{1/2} \frac{q''_{(0)}(t_s)^{1/2}}{(\rho c k)^{1/2}} , \text{ K (}^{\circ}\text{F}) \quad (3-25)$$

where c = specific heat of drum or rotor material, Nm/kgK ($\text{BTU}/\text{lb}_m^{\circ}\text{F}$)

and $q''_{(0)}$ is determined by Eq. (3-14), however, divided by the swept area of the brake rotor.

Inspection of Eq. (3-25) reveals that for a specified heat flux $q''_{(0)}$ and braking time t_s , the maximum brake drum or rotor temperature will decrease for

increased values of density, specific heat, and thermal conductivity. Lowering the heat flux by increasing the swept area of the brake will also decrease the maximum surface temperature.

Typical material properties for drum or disc, and asbestos-based lining and pad material are listed in Table 3-1 below. Semi-metallic pad materials will have increased values for ρ , k and c .

TABLE 3-1A

Brake Design Values, SI Units				
	Lining	Pad	Drum or Disc	Units
ρ	2034	2595	7228	kg/m ³
c	1256	1465	419	Nm/kgK
k	4174	4362	174,465	Nm/hKm
a	0.00163	0.0011	0.0576	m ² /h

TABLE 3-1B

Brake Design Values, Imperial Units				
	Lining	Pad	Drum or Disc	Units
ρ	127	162	455	lb _m /ft
c	0.30	0.35	0.10	BTU/lb _m °F
k	0.67	0.7	28	BTU/h°F ft
a	0.0176	0.0124	0.615	ft ² /h

Example 3-2: Compute the maximum front disc brake temperature of a passenger car decelerating at 0.80 g from a speed of 128 km/h (80 mph) without brake lockup. Use the data that follow: $W = 20,003$ N (4500 lb), percent braking on front brakes 72%, heat distribution onto rotor 0.90, tire slip 8%, swept area of one rotor side 323 cm² (50 in.²), initial brake temperature 311 K (100°F).

Solution: The average braking power of the entire vehicle is computed from Eq. (3-8) [or Eq. (3-13) for imperial units]:

$$P_{\text{bavg}} = \frac{1(1-0.08)(20003)(0.8)(9.81)(35.6)}{2(9.81)} = 262,055 \text{ Nm/s}$$

$$\left[q_0 = \frac{1(1-0.08)(4500)(0.8)(117.3)(3600)}{2(778)} = 898,838 \text{ BTU/h} \right]$$

The stopping time is computed from Eq. (3-7)

$$t_b = 35.6/[0.8(9.81)] = 4.54 \text{ s} = 0.001261 \text{ h}$$

$$[t_b = 117.3/[0.8(32.2)] = 4.54 \text{ s}]$$

The average braking power absorbed per hour by one half or one side of one front brake is

$$P_{bav} = (262,055)(3600)(0.72)(0.5)(0.5)(0.90) = 1.528 \times 10^8 \text{ Nm/h}$$

$$[q_0 = (898,838)(0.72)(0.5)(0.5)(0.90) = 145,612 \text{ BTU/h}]$$

The braking power at the onset of braking is computed from Eq. (3-14) as

$$P_{b(0)} = 2(1.528 \times 10^8) = 3.056 \times 10^8 \text{ Nm/h}$$

$$[q_{(0)} = 2(145,612) = 291,224 \text{ BTU/h}]$$

The temperature calculation in Eq. (3-25) requires the heat flux into the swept surface area, i.e., the number of Nm (BTU) per hour and per unit area. Hence, the heat flux designated by $p''_{(0)}$ is

$$p''_{(0)} = (3.056 \times 10^8)/(323 \times 10^{-4}) = 9.461 \times 10^9 \text{ Nm/hm}^2$$

$$[p''_{(0)} = [291,224(144)]/50 = 838,725 \text{ BTU/hft}^2]$$

Substitution of the appropriate data into Eq. (3-25) yields the maximum swept surface temperature increase above the initial temperature as

$$T_{max,L} - T_i = \frac{(5/18)^{1/2}(9.461 \times 10^9)(0.00126)^{1/2}}{[7288(419)(174,465)]^{1/2}} = 242 \text{ K}$$

$$[T_{max,L} - T_i = \frac{(5/18)^{1/2}(838,725)(0.00126)^{1/2}}{[455(0.1)(28)]^{1/2}} = 439^\circ \text{F}]$$

The maximum temperature is $242 + 311 = 553 \text{ K}$ ($439 + 100 = 539^\circ \text{F}$). The maximum temperature at the friction surface is reached after $4.55/2 = 2.3 \text{ s}$ from beginning of braking.

Application of Eq. (3-25) to a fully laden commercial tractor-semitrailer vehicle yields a maximum brake surface temperature of approximately 300 to 400°C or 573 to 673 K (600 to 700°F), sufficiently high to produce in-stop fade. PC-BRAKE TEMPERATURE applies to the temperature analysis.

3.1.5 Complete Disc Temperature Analysis in a Single Stop

In the previous section, brake temperature was computed for one location on the rotor only, namely at the friction surface. Convective cooling was ignored. In this section brake temperatures will be computed for any location beneath the friction surface, and as a function of time. Convective cooling is included (Ref. 3.3).

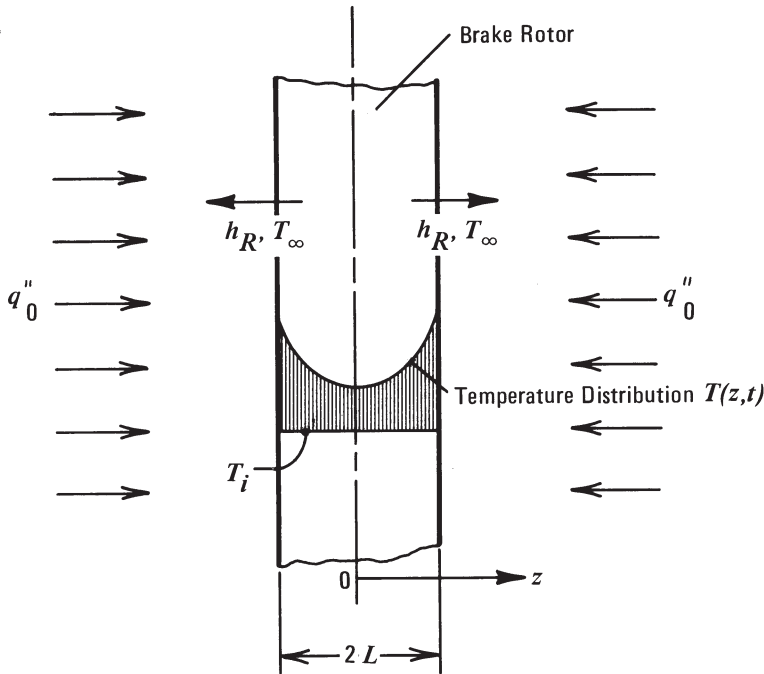


Figure 3-4. Physical system representing solid rotor.

The physical system to be analyzed is illustrated in Fig. 3-4. The temperature formulation results in the following set of equations in terms of the transformation $\theta = T - T_\infty$:

$$\text{Differential equation: } \frac{\partial \theta}{\partial t} = a \left(\frac{\partial^2 \theta}{\partial z^2} \right)$$

$$\text{Boundary conditions: } \frac{\partial \theta}{\partial z}(0,t) = 0; \frac{\partial \theta}{\partial z}(L,t) + (h/k)\theta(L,t) = q_0''/k$$

$$\text{Initial condition: } \theta(z,0) = \theta_i = T_i - T_\infty$$

Because the temperature reaches a finite value as time approaches infinity, the solution may be obtained by a superposition of the form: $\theta(z,t) = \psi(z,t) + \Phi(z)$. The function $\Phi(z)$ satisfies the following conditions:

$$\frac{\partial^2 \Phi(z)}{\partial z^2} = 0$$

$$\frac{\partial \Phi(L)}{\partial z} + (h/k)\Phi = q_0''/k$$

$$\frac{\partial \Phi(0)}{\partial z} = 0$$

The function $\psi(z,t)$ satisfies the following conditions:

$$\frac{\partial \psi}{\partial t} = a \left(\frac{\partial^2 \psi}{\partial z^2} \right)$$

$$\frac{\partial \psi(L,t)}{\partial z} + (h/k)\psi(L,t) = 0$$

$$\psi(z,0) = \theta_i - \Phi(z) \text{ at time } t = 0.$$

Solving the differential equations is accomplished by first deriving the temperature response due to a constant heat flux as observed during constant-speed downhill braking. The final temperature expression is obtained from the constant heat flux temperature and the application of Duhamel's theorem using a time-varying heat flux.

The solid non-ventilated rotor is illustrated in Fig. 3-4. Both sides of the rotor are heated by the heat flux $q''_{(0)}$, and are cooled by convection h_R . For the solid rotor, the conditions permit an analytical solution for a constant heat flux (Ref. 3.3).

$$\theta_0(z, t) = \frac{q''_0}{h_R} \left[2 \left(\frac{\theta_i h_R}{q''_0} - 1 \right) \sum_{n=1}^{\infty} \frac{\sin(\lambda_n L)}{\lambda_n L + \sin(\lambda_n L) \cos(\lambda_n L)} \times e^{-a_n \lambda_n^2 t} \cos(\lambda_n z) + 1 \right], \text{ K } (\text{°F}) \quad (3-26)$$

where $a_n = k_R / (\rho_R c_R) = \text{thermal diffusivity, m}^2/\text{h (ft}^2/\text{h)}$

$h_R = \text{convective heat transfer coefficient, Nm/h K m}^2 \text{ (BTU/h°F ft}^2)$

$L = \text{one-half rotor thickness, m (ft)}$

$n = \text{numerals 1, 2, 3, ...}$

$q''_0 = \text{average heat flux into rotor, Nm/h m}^2 \text{ (BTU/h ft}^2)$

$t = \text{time, h}$

$T_0(z, t) = \text{transient temperature distribution in rotor due to a constant heat flux, } \text{K (°F)}$

$T_i = \text{initial temperature, K (°F)}$

$T_\infty = \text{ambient temperature, K (°F)}$

$z = \text{horizontal distance measured from midplane of rotor, m (ft)}$

$\theta_0(z, t) = T_0(z, t) - T_\infty, \text{ relative temperature of brake resulting from constant heat flux}$

$\theta_i = T_i - T_\infty = \text{initial temperature difference between brake and ambient, K (°F)}$

$\lambda_n = n\pi / L, 1 / \text{m (1 / ft)}$

The value of $\lambda_n L$ is determined from the transcendental equation

$$(\lambda_n L) \tan(\lambda_n L) - h_R L / k = 0$$

Inherent in the derivation of Eq. (3-26) are the following assumptions

1. The temperature is only a function of the coordinate normal to the friction surface and time t .
2. The heat transfer coefficient h_R is constant.
3. The heat flux is in the direction normal to the friction surface.
4. The thermal properties of both friction partners are constant and evaluated at some mean temperature.
5. The ambient temperature T_∞ is constant.
6. Radiation heat transfer is included in terms of an equivalent radiation heat transfer coefficient (see Section 3.1.9).

A few solutions to the transcendental equation of practical importance for typical brakes are presented in Table 3-2. For different hL/k -values, the roots of the transcendental equation can easily be solved by trial and error. The use of Eq. (3-26) requires the calculation of a summation term (Σ). For braking

times greater than approximately 0.5 to 1 second, only the first two terms ($n = 1$ and 2) in the summation are required for an acceptable accuracy of the brake temperatures calculated.

Solid rotors are frequently used on rear axles of cars and pickup trucks as well as in drive shaft-mounted parking brakes of heavy construction vehicles.

Example 3-3: Pickup Truck Brake Temperature - Solid Rotor – Constant Heat Flux

Calculate the brake temperatures at the mid plane and swept surface at the end of the braking process for the following data: Vehicle weight 40,034 N (9000 lb), deceleration 0.9 g, speed 128 km/h (80 mph), tire slip 10%, rotating mass factor $k = 1$, brake force distribution $\Phi = 0.40$, solid rotor rear disc 25.4 mm (1 in.) thick, outer diameter 355.6 mm (14 in.), convective heat transfer coefficient $h_R = 278,038 \text{ Nm/hKm}^2$ (13.4 BTU/h°Fft²), ambient temperature 278 K (40°F), initial brake temperature 311 K (100°F), heat distribution into rotor $\gamma = 0.95$, swept rotor surface area of one rear rotor side 0.0645 m^2 (100 in²), rotor material thermal diffusivity $a_t = 0.058 \text{ m}^2/\text{h}$ [0.62 ft²/h], thermal conductivity $k = 174,465 \text{ Nm/(hKm)}$ [28 BTU/(h°Fft)].

Equation (3-26) applies, however limited to only one term of the summation, that is, λ_1 only. As is shown in Ref. 3.3, one term only is sufficient for acceptable accuracy for the solid rotor case. We will carry out the calculation to demonstrate the somewhat complicated mathematics involved. We first must calculate the temperature response achieved by a constant heat flux braking power equal to the braking power of the time-varying heat flux, as illustrated in Fig. 3-2.

With the data given, Eq. (3-8) [or Eq. (3-13) with imperial units] yields an average braking power for the entire vehicle $q_0 = 2.07 \times 10^9 \text{ Nm/h}$ (1,978,082 BTU/h). The average heat flux into one rear rotor side equals $q_0'' = 3.21 \times 10^9 \text{ Nm/(hm}^2)$ [284,848 BTU/(hft²)].

Next, we calculate $h_R L/k$ to obtain the value for the $\lambda_1 L$ term given in Table 3-2. For the data specified, we have $(278,038)(0.0127)/(174,465) = 0.0202$ [(13.4)(0.5/12)/28 = 0.0199] or 0.02. Consequently, Table 3-2 yields $\lambda_1 L = 0.1410$.

However, if, for example, the heat transfer coefficient had been 373,484 Nm/(hKm²) [18 BTU/(h°Fft²)], then $h_R L/k = 0.02678$. The roots of the transcendental equation are solved by trial-and-error. Inspection of Table 3-2 reveals the value to be $0.141 < \lambda_1 L < 0.1987$. After several tries, using 0.1629 yields: $(0.1629)\tan(0.1629)(57.29) = 0.026771$, which is close enough to $\lambda_1 L = 0.02678$.

In Equation (3-26) the arguments for sine and cosine must be entered as angles in degrees, resulting in $0.141 \times 57.3 = 8.08$ degrees.

TABLE 3-2

Roots of Transcendental Equation $(\lambda_n L) \tan(\lambda_n L) = h_R L/k$			
$h_R L/k$	$\lambda_1 L$	$\lambda_2 L$	$\lambda_3 L$
0.008	0.0893	3.1441	6.2845
0.01	0.0998	3.1448	6.2848
0.02	0.1410	3.1479	6.2864
0.04	0.1987	3.1543	6.2895
0.06	0.2425	3.1606	6.2927
0.08	0.2791	3.1668	6.2959
0.10	0.3111	3.1731	6.2991

In Eq. (3-26) the exponent of e , λ_1 must be used. It is calculated from one-half rotor thickness L as

$$\lambda_1 = \lambda_1 L/L = (0.141)/(0.0127) = 11.1 \text{ m}^{-1} [(0.141)(12)/(0.5) = 3.384 \text{ ft}^{-1}]$$

The stopping time is $35.7/(0.9 \times 9.81) = 4.05 \text{ s}$ [$117.28/(0.9 \times 32.2) = 4.05 \text{ s}$] or 0.00114 h . The temperatures to be calculated are located at $z = 0 \text{ ft}$ (mid plane), and $z = 0.00127 \text{ m}$ [0.0417 ft] (swept surface).

Substituting into Equation (3-26) for $z = 0.00127 \text{ m}$ [0.0417 ft] yields for $n = 1$ using the imperial system:

$$\begin{aligned} \Theta_0(L, 4 \text{ s}) &= T_0 - T_\infty \\ &= (284,848/13.4) \{2[(100 - 40)(13.4)/(142,422) - 1] \\ &\quad \times [\sin 8.08/(0.141 + \sin 8.08 \cos 8.08)] \\ &\quad \times (e^{-0.62(3.384)^2(0.0011)}) \cos[(3.384)(0.0417)(57.3)] + 1\} = 368^\circ\text{F} \end{aligned}$$

The swept surface temperature increase over the ambient temperature is 460K [368°F] when only one λ_1 value is used. The summation term for $n = 1$ equals 0.49274. For $n = 2$, the summation term equals $0.49274 + 0.0000339 = 0.49277$. Consequently, in this particular example $n = 1$ is sufficient.

To calculate the temperature at the mid plane, only $\cos(\lambda_1 z)$ changes to $\cos(0) = 1$. The term 0.49274 changes to 0.49768, and the temperature increase at the mid plane is 343 K [158 °F] at the moment the vehicle comes to a complete stop. The results indicate that after four seconds of braking, the temperature difference between swept surface and mid plane is 372 K [210°F].

For very large braking times, the exponential term in Equation (3-26) approaches zero, and the theoretical maximum swept surface temperature is

determined by the ratio of q''_0/h . No automotive brake system would be able to withstand the extremely large brake temperature obtained for very long braking times with input data of Example 3.3.

Eq. (3-26) computes the temperature response resulting from a constant heat flux at the rotor surface. When the vehicle decelerates, the heat flux varies with time. In most cases a linearly decreasing heat flux is assumed. The temperature response of the brake rotor for the time-dependent heat flux may be obtained directly from the temperature solution shown by Eq. (3-26) associated with the constant heat flux q''_0 by application of Duhamel's theorem or superposition integral. The temperature response from a time-varying heat flux is (Ref. 3.4):

$$\theta(z, t) = \frac{q''_{(0)}}{q''_0} \theta_0(z, t) + \frac{1}{q''_0} \int_0^t \frac{dq''(\tau)}{d(\tau)} \theta_0(z, t - \tau) d\tau, \quad K (\text{°F}) \quad (3-27)$$

where d = differential operator

q''_0 = time-varying heat flux into rotor at time $t = 0$, Nm/hm^2 ($\text{BTU}/\text{h ft}^2$)

$q''(\tau)$ = time-varying heat flux, Nm/hm^2 ($\text{BTU}/\text{h ft}^2$)

t = time, h

$\theta(z, t) = T(z, t) - T_\infty$ = relative temperature response resulting from time-varying heat flux, $K (\text{°F})$

$\theta_0(z, t) = T_0(z, t) - T_\infty$ = relative temperature of brake resulting from constant heat flux, $K (\text{°F})$

$T_0(z, t)$ = transient temperature distribution in rotor due to a constant heat flux, $K (\text{°F})$

τ = time, h

If a time-varying heat flux [Eq. (3-5)]

$$q''(t) = q''_{(0)}(1 - t/t_s) \quad \text{Nm}/\text{hm}^2 (\text{BTU}/\text{h ft}^2) \quad (3-28)$$

is assumed, where t = time, h, and t_s = braking time to a stop, h, then integration of Eq. (3-27) with Eq. (3-26) and $\theta_i = 0$ yields the temperature response in a solid disc brake resulting from a time-varying heat flux:

$$\begin{aligned} \theta(z, t) = & \frac{q''_{(0)}}{q''_0} \theta_0(z, t) \\ & - \frac{q''_{(0)}}{t_s h_R} \left[t - 2 \sum_{n=1}^{\infty} \frac{\sin(\lambda_n L)}{\lambda_n L + \sin(\lambda_n L) \cos(\lambda_n L)} \right. \\ & \left. \times \left(\frac{1 - e^{-a_t \lambda_n^2 t}}{a_t \lambda_n^2} \right) \cos(\lambda_n z) \right], \quad K (\text{°F}) \end{aligned} \quad (3-29)$$

where $q''_{(0)}$ = time-varying heat flux into the rotor at time $t = 0$, Nm/hm^2 ($\text{BTU}/\text{h ft}^2$)

q''_0 = average heat flux into rotor = $q''_{(0)}/2$, Nm/hm^2 ($\text{BTU}/\text{h ft}^2$)

t_s = braking time to a stop, h

$\theta_0(z, t)$ = relative temperature of brake resulting from constant heat flux, $K (\text{°F})$, obtained from Eq. (3-26).

Example 3-4: Linearly decreasing heat flux for Example 3-3.

For the data of Example 3-3, compute the temperature response at the swept surface. Inspection of Eq. (3-29) indicates that the brake temperature for the braking process with decreasing velocity, that is linearly decreasing heat flux, uses the constant heat flux case modified by the negative term of Eq. (3-29). The instantaneous heat flux at the beginning of braking is $q_0'' = 6.42 \times 10^9 \text{ Nm/h}$ [569,696 BTU/(hft²)] [Eq. (3-14)]. The temperature at the end of the braking process after 4 s of braking existing at the swept surface ($z = L$) with imperial units becomes [Eq. (3-29)]:

$$\begin{aligned}\Theta(L, 4 \text{ s}) &= T - T_{in} \\ &= (569,696)(368)/(284,848) - 569,696/[(0.01124)(13.4)]\{(0.00112 \\ &\quad - 2[\sin 8.08/(0.141 + \sin 8.08 \cos 8.08)] x \\ &\quad (1 - e^{0.62(3.384^2)(0.0011)})/[0.62(3.384^2)] \cos 8.08\} \\ &= 443^\circ\text{F}.\end{aligned}$$

The temperature increase at the swept surface ($z = L$) is 501K (443 °F) at the end of the braking process when the vehicle is stationary.

Eq. (3-29) was evaluated for a particular test vehicle with a solid disc brake having an outer diameter of 317.5 mm (12.5 in.) and a rotor thickness of 12.7 mm (0.5 in.). The heat flux into one rotor side at the onset of braking is $q_0'' = 5.56 \times 10^9 \text{ Nm/hm}^2$ (489,500 BTU/hft²). The convective heat transfer coefficient is 255,553 Nm/hKm² (12.5 BTU/h°Fft²).

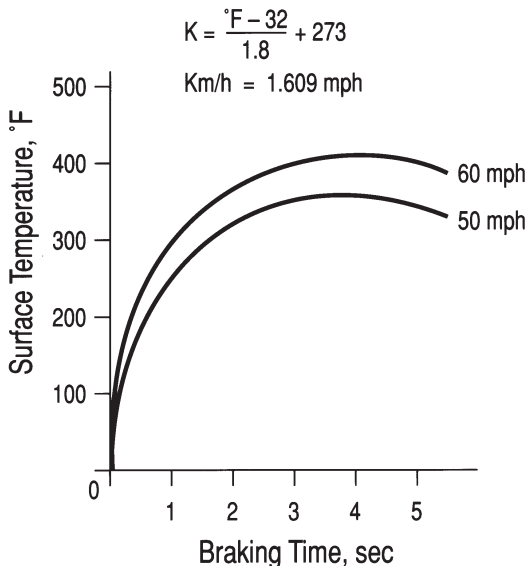


Figure 3-5. Surface temperature computed from Eq. (3-29).

The surface-temperature response computed from Eq. (3-29) is shown in Fig. 3-5, using a vehicle deceleration of 0.46 g and speeds of 80 and 97 km/h (50 and 60 mph). The braking times are approximately 5 and 6 s, respectively.

With the same input parameters, the temperature distribution in the rotor computed for a stop from 97 km/h (60 mph) is illustrated in Fig. 3-6. Inspection of Fig. 3-6 reveals that the temperature is nearly uniformly distributed across the width of the rotor after 5 seconds of braking. The temperature gradient existing at the surface after 1.0 s is approximately 45 K/mm (1580°F/in.).

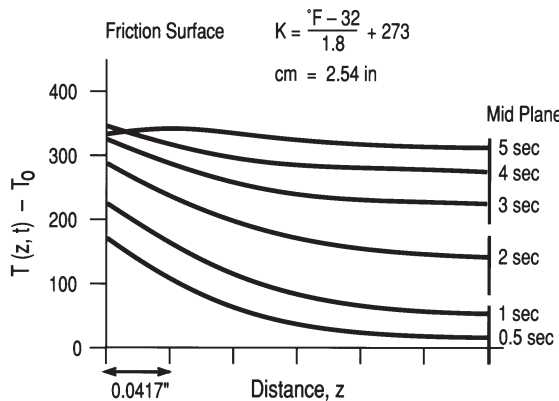


Figure 3-6. Temperature distribution in the rotor – 97 km/h (60 mph) stop.

Equations (3-26) and (3-29) apply to a solid rotor, that is, extremely simple geometry. Later the finite difference temperature formulation will be used to analyze the temperature response of complex brake geometries as well as randomly varying heat flux.

3.1.6 Temperature Analysis for Repeated Braking

During repeated brake applications, the vehicle is decelerated at a given deceleration from, e.g., 97 km/h (60 mph) to a lower or zero speed, after which the vehicle is accelerated again to test speed and the next braking cycle is carried out. Repeated braking tests are required by safety standards. Brake pumping involves repeated brake application from one single speed until the vehicle stops. Brake temperatures attained during brake pumping will be less than those achieved during repeated braking because the braking power is lower.

The brake temperatures attained during repeated braking may be computed from simple analytical solutions, provided the braking power, cooling intervals, and braking times remain unchanged during the braking process as in brake burnishing. Under these conditions, the equations for computing the temperature increase during repeated brake applications may be expressed in a simple form. Assumptions are that the drum or disc can be treated as a lumped system, and that the heat transfer coefficient and thermal properties are constant. In the lumped analysis, the temperature is assumed to be uniformly distributed throughout the drum or rotor, making it a function of time only and not of space (Ref. 3.5). This assumption means that the temperature of the friction surface equals the cooling surface temperature.

If the braking time is considerably less than the cooling time, then the cooling during braking may be neglected. In this case the drum or disc temperature will increase uniformly by

$$\Delta T = \frac{q_0 t_s}{\rho_R c_R V_R} , \text{ K } (\text{°F}) \quad (3-30)$$

where c_R = specific heat, Nm/kg K (BTU/lb_m F)

q_0 = braking power absorbed by the rotor, Nm/h (BTU/h)

t_s = braking time to a stop, h

V_R = rotor volume, m³ (ft³)

ρ_R = rotor density, kg/m³ (lb_m/ft³)

The lumped formulation results in a differential equation describing the cooling of the brake after a brake application:

$$\rho_R c_R V_R dT/dt = -h_R A_R (T - T_\infty) , \text{ Nm/h(BTU/h)} \quad (3-31)$$

where A_R = rotor surface, m² (ft²)

h_R = heat transfer coefficient Nm/hKm² (BTU/h°F ft²)

T = temperature at time t , K (°F)

T_∞ = ambient temperature, K (°F)

With an initial temperature of T_i , integration of Eq. (3-31) yields a cooling temperature response

$$\frac{T(t) - T_i}{T_i - T_\infty} = e^{(-h_R A_R t) / (\rho_R c_R V_R)} \quad (3-32)$$

An analysis combining heating by means of Eq. (3-30) and cooling by means of Eq. (3-32) may be developed to derive the temperatures of a brake after the first, second, third, or n th brake application. The relative brake temperature before the n th brake application is

$$[T(t) - T_\infty]_b = \frac{\{1 - e^{[-(n_a - 1)h_R A_R t_c] / [\rho_R c_R V_R]}\} e^{(-h_R A_R t_c) / (\rho_R c_R V_R)} \{\Delta T\}}{1 - e^{-(h_R A_R t_c) / (\rho_R c_R V_R)}}, \text{ K } (\text{°F}) \quad (3-33)$$

where n_a = number of brake applications

t_c = cooling time cycle time, h

The relative brake temperature after the n th application is

$$[T(t) - T_\infty]_a = \frac{\left[1 - e^{(-n_a h_R A_R t_c) / (\rho_R c_R V_R)}\right] [\Delta T]}{1 - e^{(-h_R A_R t_c) / (\rho_R c_R V_R)}}, \text{ K } (\text{°F}) \quad (3-34)$$

The limit values of the temperature before and after braking for a large number of cycles ($n_a \rightarrow \infty$) may be obtained from Eqs. (3-33) and (3-34) by dropping the term involving the factor n_a .

Example 3-5: Federal Motor Vehicle Safety Standards 105 and 135 require burnishing of the brakes at GVW from a speed of 64 km/h (40 mph) at a deceleration of 3.66 m/s^2 (12 ft/s^2) for 200 stops. The cycle distance is 1.61 km (1 mile). The approximate cooling cycle time is 88 s.

Compute the average rear brake temperature after the fifth, tenth, and 200th stop. Use the data that follow: 15% of total brake power absorbed by one rear brake, brake drum volume $V_R = 0.00057 \text{ m}^3$ (0.02 ft^3), brake cooling area $A_R = 0.051 \text{ m}^2$ (0.55 ft^2), convective heat transfer coefficient $h = 367,992 \text{ Nm/hKm}^2$ ($18 \text{ BTU/h}^\circ\text{F ft}^2$), vehicle weight $W = 16,458 \text{ N}$ (3700 lb).

Solution: The average braking power per rear brake is computed by Eq. (3-8). [Eq. (3-13) is used for imperial units ∞]:

$$P_{\text{bav}} = \frac{1(16,458)(3.66)(17.78)(3600)(0.15)}{2(9.81)} = 2.94 \times 10^7 \text{ Nm/h}$$

$$\left[q_0 = \frac{1(58.6)(12)(3700)(3600)(0.15)}{2(778)(32.2)} = 28,061 \text{ BTU/h} \right]$$

The brake application time is computed as $t_s = V/a = 60/(3.6 \times 3.65) = 4.9 \text{ s}$ or 0.00136 h ($58.6/12 = 4.9 \text{ s}$).

The average temperature increase per stop is computed by Eq. (3-30) as

$$\Delta T = \frac{(2.94 \times 10^7)(0.00136)}{(7288)(419)(0.00057)} = 23 \text{ K}$$

$$\left[\Delta T = \frac{(28,061)(0.00136)}{(455)(0.1)(0.02)} = 41.9^\circ\text{F} \right]$$

The temperature increase for each stop is 23 K (also 23°C) or 41.9°F . The reader is reminded that the $\Delta T = 1\text{K} = 1^\circ\text{C} = 1.8^\circ\text{F}$.

The brake temperature increase after the 5th brake application is computed from Eq. (3-34) as

$$T_5 - T_\infty = (23) \times \frac{1 - e^{-[5(367,992)(0.051)(88)]/[7288(419)(0.00057)(3600)]}}{1 - e^{-[367,992(0.051)(88)]/[7288(419)(0.00057)(3600)]}} = 72.7 \text{ K}$$

$$\left[T_5 - T_\infty = (41.9) \times \frac{1 - e^{-[5(18)(0.55)(88)]/[455(0.1)(0.02)(3600)]}}{1 - e^{-[18(0.55)(88)]/[455(0.61)(0.02)(3600)]}} = 131.8^\circ\text{F} \right]$$

Adding the ambient temperature of 299 K (80°F) yields the brake temperature of 372 K (212°F) after the 5th brake application. The corresponding brake temperatures for the 10th and 200th stop are 392 K and 399 K (246°F and 259°F), respectively. Inspection of the results reveals that the final brake temperature level is reached within the first few brake applications. PC-BRAKE TEMPERATURE applies.

3.1.7 Temperature Analysis for Continued Braking

3.1.7.1 Lumped Formulation

When the brakes are applied during a downhill descent at constant velocity, cooling while braking must be considered. Similar to the lumped temperature formulation of Section 3.1.6, the temperature is assumed to be the same throughout the brake drum and varies only as a function of time. The response of a drum or disc during continued braking is computed by (Ref. 3.6)

$$T(t) = [T_i - T_\infty - q_0 / h_R A_R] e^{(-h_R A_R t) / (\rho_R c_R v_R)} + T_\infty + q_0 / h_R A_R, \quad K \text{ (°F)} \quad (3-35)$$

where q_0 = braking power absorbed by the rotor, Nm/h (BTU/h)

t = time during which brakes are applied, h

Example 3-6: Compute the average brake temperature of a tractor-semitrailer descending a 7% grade at a constant speed of 32.2 km/h (20 mph). Neglect any engine retardation. Compute the brake temperatures after 1.6, 3.2, and 8 km (1, 2, and 5 miles) of operation. Use the data that follow: Vehicle weight $W = 355,840$ N (80,000 lb), tire rolling resistance coefficient 0.01, brake drum volume 0.00793 m^3 (0.28 ft³), cooling area 0.372 m^2 (4 ft²), convective heat transfer coefficient $265,772 \text{ Nm/hKm}^2$ (13 BTU/(h°F ft²)), relative braking power per one tractor rear brake 0.11, initial brake temperature 338 K (150°F), ambient temperature 283 K (50°F).

Solution: The braking power that must be absorbed continuously by one rear brake is computed by Eq. (3-12) [Eq. (3-15)] as

$$P_b = (355,840)(0.11)(0.07 - 0.01)(32.2)(1000) = 7.56 \times 10^7 \text{ Nm/h}$$

$$q_0 = [(80,000)(0.11)(0.07 - 0.01)(3600)(20)(1.466)] / 778$$

$$= 71,648 \text{ BTU/h}$$

The brake application time at 32.2 km/h (20 mph) for one mile is 0.05 h. Substitution of the appropriate data into Eq. (3-35) yields the brake temperature after 1.61 km (1 mile) of braking as

$$T_t = [338 - 283 - 7.56 \times 10^7 / (0.372)(265,772)]$$

$$\times e^{[-265,772(0.372)(0.05)] / [7288(419)(0.00793)]}$$

$$+ 283 + 7.56 \times 10^7 / (0.372)(265,772) = 469 \text{ K}$$

$$\left[\begin{aligned} T_t &= [150 - 50 - 71,648 / (4)(13)] \\ &\times e^{-[(13)(4)(0.05)] / [(455)(0.11)(0.28)]} \\ &+ 50 + 71648 / (4)(13) = 386^{\circ}\text{F} \end{aligned} \right]$$

For the 3.22-km (2-mile) and 8-km (5-mile) brake temperature calculations, only the brake application times change to 0.1 h and 0.25 h, respectively. When those changes are made in Eq. (3-35), the brake temperature after 3.2 km (2 miles) is 576 K (578°F); after 8 km (5 miles), 792 K (967°F). Brake temperatures exceeding 588 K (600°F) generally involve significant brake fade. The PC-BRAKE TEMPERATURE printout is shown in Fig. 3-7.

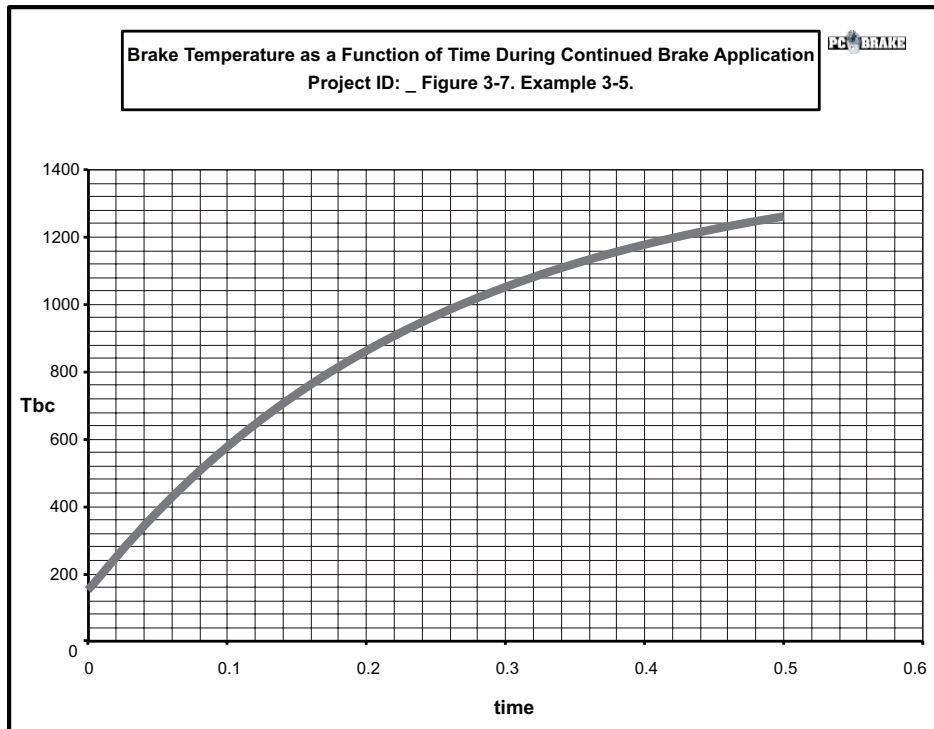


Figure 3-7. PC-BRAKE Temperature output - Example 3-6.

Continuous braking temperature data were measured and analyzed with theoretical predictions for disc brake systems of three different vehicles. A simple, however effective, finite difference model of the rotor-caliper system was used to study brake fluid vaporization (Ref. 3.7).

3.1.7.2 Distributed Formulation

The temperature response of a brake drum is derived similarly to that of a disc in Section 3.1.5. The major difference is that convective cooling occurs at the outer surface and not at the heat-generation surface as is the case for a

solid disc brake. Continued braking involving a solid rotor disc brake can be analyzed by Eq. (3-26).

The temperature attained by a brake drum when subjected to a constant heat flux is given by (Ref. 3.2):

$$\theta_0(z, t) = \frac{q_0'' L}{k} \left\{ 1 - \frac{z}{L} + \frac{k}{h_R L} - 2 \sum_{n=1}^{\infty} \frac{e^{-a_t \lambda_n^2 t} \cos(\lambda_n z)}{\lambda_n L [\lambda_n L + \sin(\lambda_n L) \cos(\lambda_n L)]} \right\} \quad K \text{ (°F)} \quad (3-36)$$

where k = thermal conductivity of drum, Nm/hKm (BTU/h°F ft)

L = drum thickness, m (ft)

z = distance measured from friction surface, m (ft)

The roots $\lambda_n L$ are determined from the transcendental equation $\lambda_n L \tan(\lambda_n L) = h/(kL)$. Thermal diffusivity is designated by a_t .

Example 3-7. Heavy Truck Brake Temperature. Use the data that follow: $W = 355,856$ lb (80,000 lb), constant velocity $V = 16.1$ km/h (10 mph), down grade 5%, tire-rolling resistance coefficient 0.01, brake force distribution of one rear brake 11%, swept surface area of rear drum $A_s = 0.232$ m² (2.5 ft²). The drum thickness is 0.00774 m (1 in.), $h = 306,660$ Nm/hKm² (15 BTU/h°Fft²), $k = 174,465$ Nm/hKm (28 BTU/h°Fft), $a_t = 0.058$ m²/h (0.62 ft²/h). The braking time is $t_s = 0.2$ h; that is, a travel distance of 6.44 km (4 miles). Initial and ambient temperatures are 0°F in the example. Determine the temperature rise at the friction and cooling surface when the vehicle has traveled 6.44 km or 4 miles.

The braking power is computed by Eq. (3-12) [Eq. (3-15)] as

$$P_b = (355,856)(4.47)(\sin 2.86 - 0.01)(0.11)(3600) \\ = 2.513 \times 10^7 \text{ Nm/h for one rear brake.}$$

$$[q_0 = [(80,000)(14.66)(0.05 - 0.01)(3600)(0.11)]/778 = 23,878 \text{ BTU/h}]$$

The heat flux into the swept drum surface is equal to $2.513 \times 10^7 / (0.232) = 1.083 \times 10^8 \text{ Nm/(hm}^2\text{)}$ [$q_0'' = (23,878)/(2.5) = 9,551 \text{ BTU/(hft}^2\text{)}$]. Solving the transcendental equation by trial and error yields $\lambda_1 L = 0.20967$ and $\lambda_1 = 0.20967 / 0.0833 = 2.517 \text{ ft}^2$ or 0.0254 m^2 . Substitution into Eq. (3-36) for $z = 0$ (friction surface) and $n = 1$ using imperial system yields a temperature increase of

$$\theta_0(0, t_s) = (9,551)(0.0833)/(28) \{ 1 - 0 + (28) / ((15)(0.0833)) \\ - (2)(0.45585) / (0.08666) \} \\ = 366 \text{ °F or } 203 \text{ K.}$$

The temperature at $z = L = 0.0254 \text{ m (0.0833 ft)}$ is affected by the $(-z/L = -1)$ and $\cos(\lambda_1 z)$ terms as $\cos(2.571)(57.29)(0.0833) = \cos(12.01) = 0.9781$. Multiplying 0.45585 by 0.9781 yields 0.44587 and a cooling surface temperature of 344°F or 446 K. The temperature difference between friction and cooling surface is 22°F or 40 K. For very long braking times, the summation term (Σ) approaches zero, and the friction surface temperature increase would be $\theta_0(0, \infty) = q_0'' L/k (1 + k/(hL)) = 665 \text{ °F or } 369 \text{ K}$. The cooling surface temperature

increase would be $\theta_0(L, \infty) = q_0''/h = 637^\circ\text{F}$ or 352 K. When this steady-state temperature condition exists, the heat generated at the friction surface equals the heat cooled from the drum surface by convection (and radiation at higher temperatures). The temperature gradient at the friction surface is determined by taking the derivative of temperature with respect to distance at the friction surface, or $d\theta/dz = (q_0''(L/k)(-1/L) = -q_0''/k = -1.08 \times 10^8/(174,465) = -619 \text{ K/m} [-9551]/(28) = -341^\circ\text{F/ft}$.

Using PC-BRAKE TEMPERATURE for continued braking yields a lumped brake temperature of 349°F after 0.2 h of braking, compared with a friction surface and cooling surface temperature of 366 and 344°F, respectively, obtained with the distributed formulation of Example 3-7. Consequently, the lumped formulation computes brake temperatures that are approximately 5% lower than the actual friction surface temperature for a braking time of 0.2 h or 12 minutes.

For very long braking times, the lumped formulation temperature is 637°F, that is, identical to the distributed formulation. At steady-state conditions the temperature distribution does not change with more braking, with 665°F existing at the friction surface and 637°F at the cooling surface.

Analysis of heavy-duty vehicle drum brake temperature data has revealed that mathematical prediction and test results show acceptable correlation and may be used as a design tool in the development stage of the vehicle (Ref. 3.8).

3.1.8 Convective Cooling of Brakes

3.1.8.1 Fundamentals of Convective Cooling

The computation of brake temperature requires information on the convective heat transfer coefficient, which varies with vehicle speed. In many cases it is sufficient to evaluate the heat transfer coefficient at some mean speed. In addition to convection, brakes are cooled by conduction and radiation. However, conduction only redistributes heat, and thus, temperature, and may affect other critical components in an unsafe manner such as bearings, lubricants, or seals.

Textbooks on heat transfer provide a large number of empirical equations for predicting the convective heat transfer coefficient for a variety of test conditions and geometries. These equations generally apply to discs or drums not obstructed by tire and rim or disc caliper.

At the outset it should be stated that any relationship expressing the convective heat transfer coefficient will yield only approximate results. A difference between predicted and measured temperature levels of 10 to 30% may be considered normal. Often “excellent” correlation is obtained by adjusting the convective heat transfer coefficient until agreement between prediction and measurement is achieved. In addition, brake temperature data obtained under controlled field or laboratory conditions with “new” components may not always represent the actual use of the same

components. Attempts at designing optimum rotor cooling geometry for a particular application show that it may not be rated superior in all respects (Refs. 3.9, 3.10, 3.11, 3.12, 3.13, 3.14, 3.15, 3.16).

It has been shown that experimental results of a cooling analysis can be represented by the product of dimensionless numbers raised to some power (Refs. 3.3, 3.17); i.e.,

$$Nu = C Re^m Pr^n \quad (3-37)$$

where C = heat transfer constant

c_a = specific heat of air, Nm/kg K (BTU/lb_m °F)

h_R = convective heat transfer coefficient, Nm/hKm² (BTU/h°F ft²)

k_a = thermal conductivity of air, Nm/hKm (BTU/h°F ft)

L_c = characteristic length, m (ft)

m_a = mass flow rate of air, m³/s (ft³/s)

m = heat transfer parameter

n = heat transfer parameter

$Nu = h_R L_c / k_a$ = Nusselt number

$Pr = 3600 C_a m_a / k_a$ = Prandtl number

$Re = V \rho_a L_c / m_a$ = Reynolds number

V = vehicle speed, m/s (ft/s)

μ_a = viscosity of air, kg/m s (lb_m/ft s)

ρ_a = density of air, kg/m³ (lb_m/ft³)

The constant C in Eq. (3-37) is a function of the geometry of the brake and assumes different values for brake drums, solid rotors, and ventilated rotors. For ventilated rotors the value of C depends on the shape of the vanes used for ventilation.

The heat transfer parameter m is a function of the type of flow, i.e., turbulent, laminar, or transition flow. For most practical cases, m is a function of vehicle velocity and the associated brake rotor angular velocity. The heat transfer parameter n depends on the thermal properties of the surrounding air. Because these properties are a function of temperature, the Prandtl number effect is nearly constant for most cases and is often included in the constant C of Eq. (3-37). The characteristic length L_c is either a length or diameter depending on the definition of the Nusselt or Reynolds number.

3.1.8.2 Heat Transfer Coefficient for Drum Brakes

For a brake drum fully exposed to the air flow, the heat transfer coefficient h_R is (Ref. 3.17)

$$h_R = 0.1(k_a/D)Re^{2/3}, \text{ Nm/hKm}^2 (\text{BTU/h}^{\circ}\text{Fft}^2) \quad (3-38)$$

where D = drum diameter, m (ft)

k_a = thermal conductivity of air, Nm/hKm (BTU/h F ft)

For example, a 381 mm or 0.381 m (15 in.) diameter drum moving through air at a speed of 97 km/h (60 mph) at an ambient temperature of 312 K (100°F) will have a convective heat transfer coefficient of approximately 183,996 Nm/hKm² (9 BTU/h°F ft²).

Road test data obtained from testing of heavy vehicles equipped with drum brakes indicate that the convective heat transfer coefficient may be expressed by functional relationship of the form (Ref. 3.16)

$$h_R = 18808 + 67073\beta Ve^{-0.01V}, \text{ Nm / hKm}^2 \quad (3-39)$$

$$[h_R = 0.92 + \beta Ve^{-V/328}, \text{ BTU / h}^{\circ}\text{Fft}^2]$$

where h_R = convective heat transfer coefficient, Nm/hKm² (BTU/h Fft²)

V = vehicle speed, m/s (ft/s)

β = 0.70 for front drum brake, Nm s/hKm³ (BTU s/h F ft³)

= 0.30 for rear drum brake Nm s/hKm³ (BTU s/h F ft³)

The corresponding values of β associated with the heat transfer from the brake shoes inside the brake assembly were found to be 0.15 and 0.06, respectively. When the vehicle is braked to a stop, the convective cooling capacity is reduced to that of natural convection indicated by 18,808 Nm/hKm (0.92 BTU/h°F ft) in Eq. (3-39).

Inspection of Eq. (3-39) shows that the front brake drums cool more efficiently than the rear drums ($\beta = 0.7$ versus $\beta = 0.3$) due to their frontal location on the truck. Under extreme repeated braking conditions, the lower rear brake cooling may lead to excessive brake temperatures, particularly for brakes on the tag axle of coaches with luggage compartments and air conditioning units obstructing cooling air flow.

3.1.8.3 Heat Transfer Coefficient for Solid Discs

For solid, non-ventilated disc brakes the convection heat transfer coefficient associated with laminar flow may be approximated by

$$h_R = 0.70(k_a/D)Re^{0.55}, \text{ Nm/hKm}^2 (\text{BTU/h}^{\circ}\text{F ft}^2) \quad (3-40)$$

where D = outer diameter, m (ft)

For $Re > 2.4 \times 10^5$, the flow characteristics will be turbulent and the heat transfer coefficient may be expressed as

$$h_R = 0.40(k_a/D)Re^{0.8}, \text{ Nm/hKm}^2 (\text{BTU/h}^{\circ}\text{Fft}^2) \quad (3-41)$$

Eqs. (3-40) and (3-41) were obtained from experimental data collected with a disc brake system of a light truck (Ref. 13). Using the data of the previous example, a 381 mm (15 in.) outer diameter rotor at 97 km/h (60 mph) will have a convective heat transfer coefficient of approximately $408,880 \text{ Nm/hKm}^2$ ($20 \text{ BTU/h}^{\circ}\text{F ft}^2$). For the example chosen, the transition from laminar to turbulent flow lies at about 38.4 km/h (24 mph). Consequently, the convective heat transfer coefficient at 32 km/h (20 mph) is computed by Eq. (3-40) to be approximately $143,108 \text{ Nm/hKm}^2$ ($7 \text{ BTU/h}^{\circ}\text{F ft}^2$).

A comparison of the computed heat transfer coefficients indicates clearly that a disc brake has a higher convective heat transfer coefficient than a drum brake, assuming that it is fully exposed to the cooling air flow.

It should be noted that Eqs. (3-40) and (3-41) were obtained from experiments with two calipers located horizontally 180 deg apart at the 3 and 9 o'clock positions. The particular location of the caliper relative to the air flow may have an effect on the cooling capacity of disc brakes.

3.1.8.4 Heat Transfer Coefficient of Ventilated Disc Brakes

Ventilated disc brakes generally exhibit convective heat transfer coefficients approximately twice as large as those associated with solid discs. The cooling effectiveness associated with the internal vanes tends to decrease somewhat for higher speeds due to the increased stagnation pressure of the air. In-use factors such as rust or mud may significantly reduce the heat transfer coefficient of ventilated rotors, as illustrated in Fig. 3-8.



Figure 3-8. Reduced cooling air flow due to rusted rotor vanes.

For estimating purposes the following relationship may be used to obtain the heat transfer coefficient inside the vanes of the brake rotor (Refs. 3.16, 3.18):

$$h_R = 0.023[1 + (d_h / \ell)^{0.67}] Re^{0.8} Pr^{0.33} \times (k_a / d_h), \text{ Nm/hKm}^2 (\text{BTU/h}^{\circ}\text{Fft}^2) \quad (3-42)$$

where d_h = hydraulic diameter, m (ft)

ℓ = length of cooling vane, m (ft)

$$Re = (\rho_a d_h / m_a) V_{\text{average}}$$

V_{average} = average velocity, m/s (ft/s)

Eq. (3-42) is valid for $Re > 10^4$, i.e., for turbulent flow. The hydraulic diameter is defined as the ratio of four times the cross-sectional flow area (wetted area) divided by the wetted perimeter, as illustrated in Fig. 3-9. For vanes with varying cross-sectional size, an average hydraulic diameter is determined from the dimensions of the inlet and outlet locations on the vane.

The velocity associated with the Reynolds number is the air flow velocity existing in the vanes, which is not identical to the forward speed of the vehicle.

For low values of velocity, laminar flow will exist in the vanes. For $Re < 10^4$, the convective heat transfer coefficient may be approximated by

$$h_R = 1.86(Re Pr)^{1/3} (d_h / \ell)^{0.33} \times (k_a / d_h), \text{ Nm/hKm}^2 (\text{BTU/h}^{\circ}\text{Fft}^2) \quad (3-43)$$

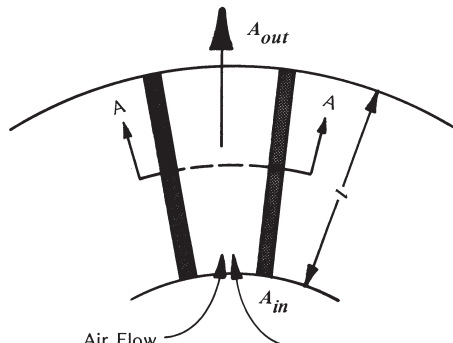
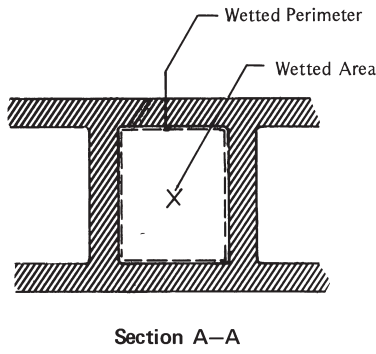


Figure 3-9. Ventilated brake rotor.

The average velocity through the cooling vanes can be computed by

$$V_{\text{average}} = (V_{\text{in}} + V_{\text{out}})/2 \quad , \quad \text{m/s (ft/s)} \quad (3-44)$$

where A_{in} = inlet area, m^2 (ft^2)

A_{out} = outlet area, m^2 (ft^2)

d = inner diameter, m (ft)

D = outer diameter, m (ft)

n_T = revolutions per minute, $1/\text{min}$ (rpm)

$V_{\text{in}} = 0.0158n_T(D^2 - d^2)^{1/2} \quad , \quad \text{m/s}$

$[V_{\text{in}} = 0.052n_T(D^2 - d^2)^{1/2} \quad , \quad \text{ft/s}]$

$V_{\text{out}} = V_{\text{in}}(A_{\text{in}} / A_{\text{out}}) \quad , \quad \text{m/s (ft/s)}$

The air flow rate m_a is determined by

$$m_a = 0.00147n_T[(D^2 - d^2)A_{\text{in}}]^{1/2} \quad , \quad \text{m}^3/\text{s} \quad (3-45)$$

$$\left[m_a = 0.052n_T[(D^2 - d^2)A_{\text{in}}]^{1/2} \quad , \quad \text{ft}^3/\text{s} \right]$$

If the ventilated rotor is exposed to air, i.e., the friction surfaces are not shielded, then the convective heat transfer coefficient is obtained by the summation of the heat transfer coefficients of Eqs. (3-41) and (3-42), or (3-40) and (3-43).

Example 3-8. Thermal analysis of ventilated disc brake for military vehicle.

The objective is the design check of a disc brake system for a heavy track vehicle to demonstrate the use of Eq. (3-42). The imperial unit system is used. The following vehicle data are specified:

1. Weight 66,000 lb
2. Maximum speed 45 mph
3. Maximum deceleration 0.6 g
4. Gear ratio between brake shaft and track drive sprocket 1:11
5. Track drive sprocket radius 16 in.
6. Track rolling resistance coefficient 0.045 for operation on smooth dirt road, 0.075 for operation on off road surface
7. Mass moment of inertia per track 1000 in.lbs²

The following disc brake data are specified:

1. Brake rotor weight 175 lb (ventilated rotor)
2. Outer brake rotor diameter 22.5 in.
3. Inner brake rotor diameter 12 in.
4. Maximum brake rotor revolutions, 4750 rpm at a vehicle speed of 45 mph
5. Brake rotor revolutions, 1825 rpm at 17 mph during continued down-hill operations

Brake Design and Safety

6. Effective brake rotor radius 8.5 in.
7. Number of wheel cylinders per rotor 2
8. Wheel cylinder diameter 2 in.
9. Brake factor 0.50
10. Number of rotors 2

Mechanical Analysis:

The maximum braking force $F_{x,\text{total}}$ may be obtained by

$$F_{x,\text{total}} = (66,000)(0.6) = 39,600 \text{ lb}$$

One track has to produce a braking force of 19,800 lb. Rolling resistance opposes vehicle motion. Under consideration of the rolling resistance, the braking force per track becomes

$$F_x = 19,800 - \frac{(0.045)(66,000)}{2} = 18,315 \text{ lb}$$

The brake torque T_B at the rotor may be obtained by

$$T_B = F_x R \eta / \rho$$

where F_x = braking force per track = 18,315 lb

R = track drive sprocket radius = 16 in.

η = mechanical efficiency = 0.95

ρ = gear ratio = 1:11

$$T_B = \frac{(18315)(16)(0.95)}{(11)(12)} = 2109 \text{ lb ft}$$

The kinetic energy E_T produced in the 45 mph effectiveness stop by both rotors may be obtained by

$$E_T = \left(\frac{W}{2g} \right) V^2 + \left(\frac{I}{2 \times 12} \right) \omega^2$$

where g = gravitational constant = 32.2 ft/s²

I = mass moment of inertia = 44.26 in. lb s²

V = velocity = 66 ft/s

W = weight = 66,000 lb

ω = angular velocity = $4750/(\pi 30) = 497 \text{ rad/s}$

$$\begin{aligned} E_T &= \frac{66,000}{(2)(32.2)} (66)^2 + \frac{(2)(44.26)}{(2)(12)} (497)^2 \\ &= 4,464,223 + 911,052 = 5,375,275 \text{ lb ft} \end{aligned}$$

In general, the equivalent mass moment of rotational inertia $I_{t,Rotor}$ at the brake rotor is obtained by

$$I_{TR} = I_R + \rho_t^2 I_d + \rho_t^2 \rho_d^2 I_e \text{ (in.lbs}^2\text{)}$$

where I_d = drive shaft mass moment of inertia, in.lbs²

I_e = engine mass moment of inertia, in.lbs²

I_R = wheel and shaft mass moment of inertia, in.lbs²

ρ_d = final drive ratio

ρ_t = transmission ratio

$$\begin{aligned} I_{t,Rotor} &= I_R + \frac{1000}{(11)^2} = 36 + 8.26 \\ &= 44.26 \text{ in. lbs}^2 \end{aligned}$$

The track mass moment of inertia of 1000 in.lbs² and the mass moment of inertia of the brake rotor of 36 in.lbs², estimated from rotor weight and inner and outer diameter, are used.

The kinetic energy absorbed by the rotor is equal to the kinetic energy of the vehicle minus the work due to rolling resistance. The total rolling resistance work is equal to the product of rolling resistance and stopping distance, giving 335,610 lb ft when a stopping distance of 113 ft is used. Consequently, the kinetic energy absorbed by one brake rotor becomes 2,519,832 lb ft.

Use the value of brake torque above in Eq. (5-2) (solved for brake line pressure) to determine brake line pressure required for an effective stop, without consideration of the pushout pressure, as

$$p_l - p_o = \frac{(2109)(12)}{(8.5)(0.5)(2)(3.14)(0.92)} = 1031 \text{ psi}$$

The “2” in the denominator indicates that two separate wheel cylinders are used in the caliper, each having a wheel cylinder area of 3.14 in.² A brake factor of 0.50 and a wheel cylinder efficiency of 0.92 are used.

The pad friction area may be obtained from Eq. (3-63). Eq. (3-63) requires the use of Eq. (3-13). The tire slip is replaced by the track slip, which is assumed to be zero. Eq. (3-13) yields a braking energy per rotor friction surface of 1,511,722 BTU/h. With $q_p'' = 2300 \text{ hp/ft}^2$ and $\phi_i = 1$, the minimum pad area A_p per rotor friction surface is 37 in.²

The requirement of the secondary brake system is to hold the vehicle on an 80% slope on off-road surfaces. The track rolling resistance coefficient is approximately 0.075.

The braking force per track F_x becomes

$$\begin{aligned} F_x &= (W / 2) \sin \alpha - (W / 2) (0.075) \\ &= (33,000)(0.625) - 2475 = 18,150 \text{ lb} \end{aligned}$$

where W = vehicle weight, lb

α = incline angle, deg

The brake torque per rotor T_B is

$$T_B = \frac{(18,150)(16)(0.95)}{(11)(12)} = 2090 \text{ lb ft}$$

The hydraulic pressure p_1 required to produce the brake torque is

$$p_1 = \frac{(2090)(12)}{(8.5)(0.60)(2)(3.14)(0.92)} = 851 \text{ psi}$$

For the secondary brake, a slightly larger brake factor was assumed. The reason for this is the larger static pad-rotor friction coefficient as compared to the smaller sliding value. The secondary system uses the same wheel cylinder and brake pads for the brake force production. The actuation mechanisms are different from those of the service brake.

Thermal Analysis:

The temperature response of the brake during a continued downhill brake operation must be determined for a vehicle speed of 17 mph, 10% slope, and travel distance of 6 miles. The thermal energy to be absorbed and dissipated by one brake rotor may be obtained by Eq. (3-15) as

$$\begin{aligned} q_0 &= \frac{(33,000)(24.9)(0.10 - 0.045)(3600)}{(778)} \\ &= 209,122 \text{ BTU/h} \end{aligned}$$

The time required for the continued braking process is 0.35 h or 1270.6 s.

The heat transfer coefficient of a ventilated rotor may be obtained by Eq. (3-42). The number of cooling vanes n_v may be determined by the approximate relationship

$$n_v = \frac{4\pi D_o}{D_o - D_i} \quad (3-46)$$

where D_i = inner rotor diameter, ft

D_o = outer rotor diameter, ft

Substitution of the rotor data yields 27 vanes. More cooling vanes reduce the cooling air flow and convective heat transfer coefficient, however increase the mass of the rotor. Increased rotor mass results in lower brake temperatures in single stops where convective cooling is of less importance.

The hydraulic diameter d_h is determined by the ratio of four times the cross-sectional flow area of one cooling passage divided by the wetted perimeter of one cooling passage (Fig. 3-10). By the use of a rotor width of 3.5 in., a flange thickness of 0.5 in., and a fin thickness of 0.5 in., d_h is determined as

$$d_h = \frac{(4)(3.768)}{8.014} = 1.88 \text{ in.}$$

The hydraulic diameter is based on the vane dimensions existing at the average rotor diameter, i.e., 17.25 in. The cross-sectional area is determined from the product of vane width and vane circumferential dimension. For the example, the area is given by $(3.5 - 1.0) \times [17.25 \times \pi/(27) - 0.5] = 3.768 \text{ in.}^2$. The wetted perimeter is determined from the sum of twice the vane width and twice the circumferential dimension; i.e., $(3.5 - 1.0) \times 2 + [17.25 \times \pi/(27) - 0.5] \times 2 = 8.014 \text{ in.}$

The Reynolds number for Eq. (3-42) can be determined from the hydraulic diameter, the density and viscosity of the cooling air, and the average velocity of the cooling air through the vanes. The average velocity may be determined by Eq. (3-44). The inlet velocity V_{in} is determined by the outer and inner rotor diameter, and the revolutions per minute of the rotor as [Eq. (3-44)]

$$\begin{aligned} V_{in} &= (0.052)(1825)[(1.875)^2 - (1)^2]^{1/2} \\ &= 150.5 \text{ ft/s} \end{aligned}$$

The outlet velocity V_{out} is determined by the inlet velocity and the inlet and outlet areas. By use of a ratio of inlet area to outlet area of 0.534, the outlet velocity is

$$V_{out} = (150.5)(0.534) = 80.38 \text{ ft/s}$$

The average velocity determined by Eq. (3-44) is 115.45 ft/s.

The convective heat transfer coefficient obtained by Eq. (3-42) is 24.9 BTU/h °F ft². The thermal properties of the air were evaluated at an assumed expected mean temperature of 500°F. The parameters used in Eq. (3-42) are $d_h = 1.88 \text{ in.}$, $\ell = 5.25 \text{ in.}$, $Re = 48,069$, $Pr = 0.683$, $k_a = 0.0231 \text{ BTU/h °F ft}$. The Reynolds number is computed for an air density of $0.0412 \text{ lb}_m/\text{ft}^3$, air viscosity of $1.89 \times 10^{-5} \text{ lb}_m/\text{ft s}$, hydraulic diameter of 0.191 ft, and an average velocity of 115.45 ft/s.

The rotor temperature may be obtained by Eq. (3-35). The rotor surface is

9.67 ft², the rotor volume is 0.385 ft³, the rotor density is 455 lb_m/ft³, the rotor specific heat is 0.10 BTU/lb_m °F, the ambient temperature is 50°F, the duration of the brake application is 0.35 h, and the initial temperature is 50°F. The rotor temperature T is determined as

$$T = \left[50 - \left(50 - \frac{209,122}{9.67 \times 24.9} \right) \right] \times \exp \left(-\frac{24.9 \times 9.67 \times 0.35}{455 \times 0.10 \times 0.385} \right) + 50 + \frac{209,122}{9.67 \times 24.9} = 925°F$$

Inspection of Fig. 3-10 reveals a heat transfer coefficient due to radiation of approximately 4 BTU/h °F ft² at a rotor temperature of 925°F. By the use of a total heat transfer coefficient of 28.9 BTU/h °F ft² in Eq. (3-36), a rotor temperature of 801°F is determined at the end of the downhill brake application. In this analysis, it was assumed that the entire surface area of the rotor contributed to convective and radiation cooling. To accomplish the cooling of the swept areas of the rotor, cooling air must be channeled against the rotor in addition to the self-ventilating effect of the rotor.

The maximum surface temperature of the rotor attained in an effectiveness stop from 45 mph at 0.6 g deceleration may be obtained by Eq. (3-25) as

$$T = \frac{(0.52)(1,530,086)(3.42 / 3600)^{1/2}}{[(455)(0.10)(28)]^{1/2}} + 50° \\ = 737°F$$

A stopping time of 3.42 s is determined by dividing vehicle speed by vehicle deceleration. The thermal conductivity of the rotor = 28 BTU/h °F ft.

The maximum brake power produced at the outset of braking at one friction surface of one rotor for zero slip is obtained by Eq. (3-13) and Eq. (3-14):

$$q_{(0)} = \frac{(66,000)(66)(0.6)(3600)}{(4)(778)} = 3,023,445 \text{ BTU/h}$$

The braking power per one swept rotor area is obtained from

$$q''_{(0)} = 3,023,445 / 1.976 = 1,530,086 \text{ BTU/hft}^2$$

where the swept area is determined by

$$A_s = (1.875^2 - 1^2) \frac{\pi}{4} = 1.976 \text{ ft}^2$$

If engine drag is considered in the braking analysis, with engine retarding torque computed by the empirical expression $M_e = 8 \times 10^{-5} p_m V_e$ (Ref. 1.4), braking power absorbed per rotor friction surface is decreased to approximately 2,437,233 BTU/h. An engine retarding moment $M_e = 546 \text{ lbft}$ is computed with an engine displacement $V_e = 1000 \text{ in.}^3$ and an average retarding pressure $p_m = 84 \text{ psi}$, resulting in a retarding force F_{ret} at the track of 7678 lb due to engine drag. The retarding force due to the brakes and the engine for a deceleration

of 0.6 g must be $(0.6) \times (66,000) = 39,600$ lb and, consequently, the brakes are required to produce only 31,922 lb. Hence, the engine retarding effect reduces the braking power absorbed by one rotor friction surface to approximately 2,437,233 BTU/h. Based on this reduced braking power, a brake rotor temperature of approximately 604°F is determined by Eq. (3-25).

3.1.9 Radiation Heat Transfer

At higher brake temperatures, the radiation cooling capacity of the brakes has to be considered. A radiation heat transfer coefficient $h_{R,rad}$ may be defined by (Refs. 3.6, 3.11):

$$h_{R,rad} = \frac{\sigma \varepsilon_R (T_R^4 - T_\infty^4)}{T_R - T_\infty} , \quad \text{Nm/hKm}^2 (\text{BTU/h}^\circ\text{Fft}^2) \quad (3-47)$$

where T_R = rotor surface temperature, K ($^\circ$ F)

T_∞ = ambient temperature, K ($^\circ$ F)

ε_R = rotor surface emissivity

$$\sigma = \text{Stefan-Boltzmann constant} = 3.56 \times 10^{-5} \text{ Nm/m}^2 \text{K}^4$$

$$= 0.1714 \times 10^{-8} \text{ BTU/h ft}^2 \text{ }^\circ\text{F}^4$$

$$\frac{\text{Nm}}{\text{hKm}^2} = 20444 \frac{\text{BTU}}{\text{h}^\circ\text{Fft}^2}$$

$$K = \frac{^\circ\text{F} - 32}{1.8} + 273$$

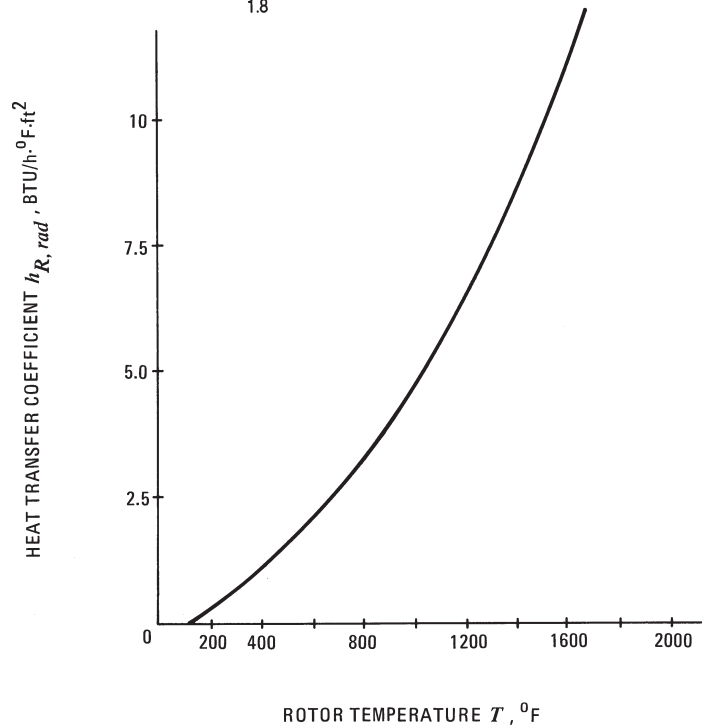


Figure 3-10. Radiation heat transfer coefficient as function of temperature.

Evaluation of Eq. (3-47) using $\epsilon_R = 0.55$, a value typical of machined cast iron surfaces of brake rotors, yields the radiation heat transfer characteristics illustrated in Fig. 3-10. It is apparent that significant radiation cooling does not occur until high brake temperatures are attained. However, for hot brakes with the vehicle traveling at low speed, radiation cooling may be the predominant cooling mechanism.

3.1.10 Computer-Based Brake Temperature Analysis

3.1.10.1 General Considerations

Only the basic elements of finite difference temperature computations are shown. The reader interested in transient two- or three-dimensional systems is referred to a standard text on heat transfer (Ref. 3.17). In the unsteady-state system, the initial temperature distribution is known; however, the variation of temperature with time must be determined. Because wheel brake systems represent many different geometries and can be used under a variety of operating conditions, the finite difference method for analyzing brake temperatures is the most efficient tool (Refs. 3.19, 3.20, 3.21, 3.22, 3.23, 3.24, 3.25, 3.26, 3.27, 3.28).

3.1.10.2 Finite Difference Method Formulation

The system, i.e., the drum or disc thickness, is divided into a number of discrete nodal points, as illustrated in Fig. 3-11, for a one-dimensional temperature analysis. In Fig. 3-11 the temperature is analyzed only as a function of distance x and time t . Application of the first law of thermodynamics, or energy balance, to each individual node results in a set of algebraic equations whose solution will yield individual nodal temperatures for each finite time interval. It is therefore necessary to calculate the temperature distribution at some future time from a given distribution at an earlier time, the earliest time being associated with the known initial temperature distribution existing at the onset of braking. The relationship expressing heat conduction between two nodes is known as Fourier's Conduction Law and may be expressed in the form of an exact integral

$$q_{ij} = \int_{\Delta y} -k(\partial T / \partial x) b dy, \text{ Nm/h (BTU/h)}$$

$$\approx -k(dT/dx)_{\text{average}} b \Delta y \approx -k(\Delta T / \Delta x)_{\text{av}} b \Delta y \quad (3-48)$$

where b = width of plate, m (ft)

q_{ij} = heat flow between nodal points i and j , Nm/h (BTU/h)

x = horizontal distance between two adjacent nodal points, m (ft)

y = vertical distance between two adjacent nodal points, m (ft)

$\partial T / \partial x$ = temperature gradient, K/m (F/ft)

The distances Δx , Δy , and b designate control volume size, and k the thermal conductivity of the material. Eq. (3-48) may be rewritten in the form of the temperature of the two nodal points

$$q_{ij} = -\frac{k(T_j - T_i)b\Delta y}{\Delta x} , \text{ Nm/h(BTU/h)} \quad (3-49)$$

where T_i = temperature of node i, K (F)

T_j = temperature of node j, K (F)

For two-dimensional temperature problems, where $T = f(x, y, t)$, for example, and a square grid size with $\Delta x = \Delta y$, the basic heat conduction between two nodal points becomes

$$q_{ij} = k(T_i - T_j)b , \text{ Nm/h(BTU/h)} \quad (3-50)$$

For one-dimensional systems such as a solid disc brake, the basic heat conduction equation with Δy equal to unity becomes

$$q_{ij} = \frac{k_R(T_i - T_j)b}{\Delta x} , \text{ Nm/h(BTU/h)} \quad (3-51)$$

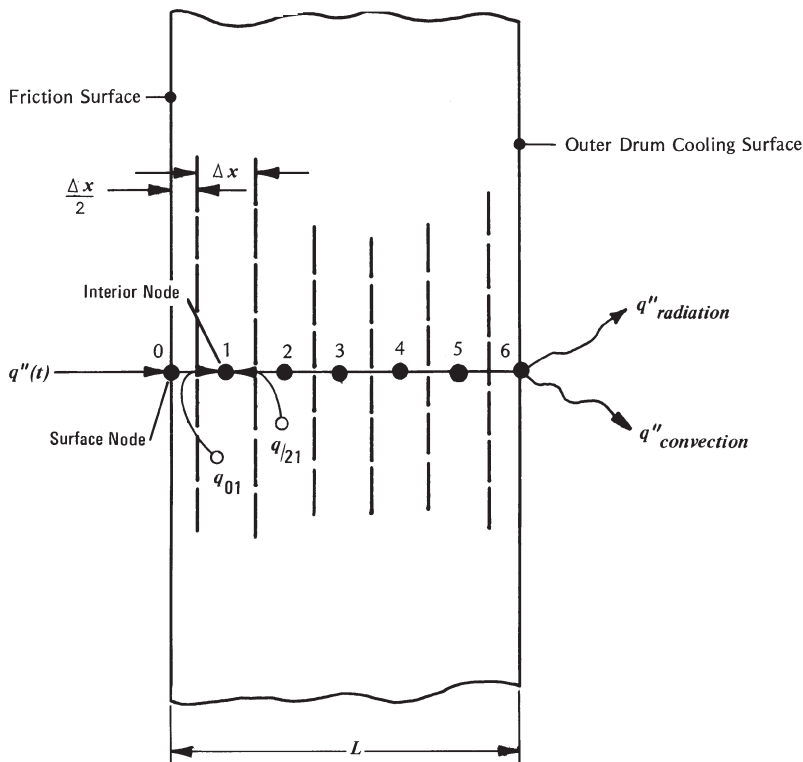


Figure 3-11. Thermal model for finite difference computation (drum brake shown).

With the mass contained in the control volume of thickness Δx , $d_m = r_R \Delta x b(1)$, and the change in enthalpy, $\Delta h = c_R \Delta T$, the first law of thermodynamics applied, e.g., to the interior node 2, results in the expression (Fig. 3-11)

$$\rho_R \Delta x b c_R [(T'_2 - T_2) / \Delta t] = k_R [(T_1 - T_2) / \Delta x] b + k_R [(T_3 - T_2) / \Delta x] b, \text{ Nm/h(BTU/h)}$$

where c_R = specific heat of rotor, Nm/kgK (BTU/lb_m °F)

k_R = thermal conductivity of rotor, Nm/hmK (BTU/hft°F)

T_1 = temperature at node 1, K (°F)

T_2 = temperature at node 2, K (°F)

T_3 = temperature at node 3, K (°F)

ρ_R = rotor density, kg/m³ (lb_m/ft³)

Here T'_2 represents the temperature attained by node 2 after the time interval Δt has elapsed. Solving for T'_2 yields

$$T'_2 = (1/M)(T_3 + T_1) + [1 - (2/M)]T_2, \text{ K (°F)} \quad (3-52)$$

where a_t = thermal diffusivity, m²/h (ft²/h)

$$M = (\Delta x)^2 / (a_t \Delta t)$$

t = time interval, h

Eq. (3-51) may be expressed for any arbitrary interior point n in the form

$$T'_n = (1/M)(T_{n+1} + T_{n-1}) + [1 - (2/M)]T_n, \text{ K (°F)} \quad (3-53)$$

Application of the first law of thermodynamics to a surface point yields (Fig. 3-12)

$$T'_0 = \left(1 - \frac{2N+2}{M}\right)T_0 + \frac{2NT_\infty}{M} + \frac{2T_1}{M} + \frac{2\Delta x q''_R}{k_R M} - \frac{2\Delta x q''_{rad}}{kM}, \text{ K (°F)} \quad (3-54)$$

where h_r = convective heat transfer coefficient, Nm/hm²K (BTU/hft² F)

k_R = thermal conductivity of rotor, Nm/hmK (BTU/hft F)

$$M = (\Delta x)^2 / (a_t \Delta t)$$

$$N = h_R \Delta x / k_R$$

q''_{rad} = radiation heat flux away from surface

$$= \varepsilon \sigma (T_0^4 - T_\infty^4), \text{ Nm/hm}^2 (\text{BTU/h ft}^2)$$

q''_R = heat flux absorbed by the rotor computed from Eq. (3-55), Nm/hm² (BTU/hft²)

T_∞ = ambient temperature, K (°R)

ε_R = emissivity ≈ 0.8 for black drum surface, 0.55 for metallic disc surface

σ = Stefan-Boltzmann constant, 3.56×10^{-5} Nm/m²K (0.174 $\times 10^{-8}$ BTU/hft² °R)

Mathematical stability conditions require that M be chosen

$$M \geq 2N + 2 \quad (3-55)$$

Otherwise the coefficient of T assumes negative values, resulting in an unstable temperature solution. The time step Δt and grid size may be chosen arbitrarily, provided the conditions in Eq. (3-55) are satisfied.

The instantaneous heat flux q''_R per rotor friction surface may be determined from

$$q''_R = \mu_L p_\ell A_{WC} \eta (1-s) V (r_i/R) [(3600\gamma)/A_j] , \quad \text{Nm/hm}^2 \quad (3-56)$$

$$\left[q''_R = \mu_L p_\ell A_{WC} \eta (1-s) V (r_i/R) [(3600\gamma)/(778A_j)] , \quad \text{BTU/hft}^2 \right]$$

where A_j = friction area of one rotor side, m^2 (ft^2)

A_{WC} = wheel cylinder area, cm^2 (in.^2)

p_ℓ = brake line pressure, N/cm^2 (psi)

r_i = distance of nodal point i from center of rotor, m (ft)

R = tire radius, m (ft)

s = tire slip

V = vehicle speed, m/s (ft/s)

γ = heat distribution to the rotor computed from Eq. (3-18) or (3-21)

η = wheel cylinder efficiency

μ_L = pad/rotor friction coefficient

The velocity in Eq. (3-56) may be determined by Eq. (3-5) with the deceleration either specified or computed from vehicle brake system parameters as discussed in Chapter 5 or 6.

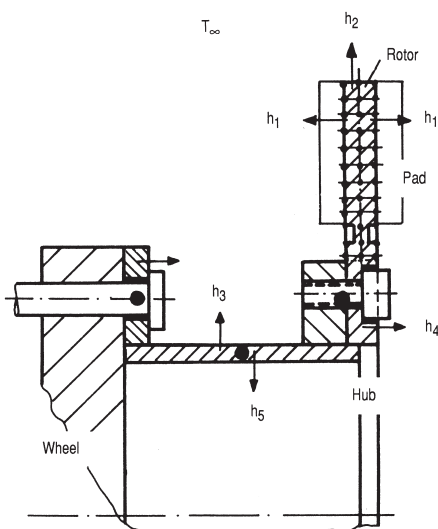


Figure 3-12. Two-dimensional finite difference model for solid rotor.

For the two-dimensional solid brake rotor illustrated in Fig. 3-12 and an initial temperature of 297 K (75°F), a vehicle speed of 97 km/h (60 mph), and a 324 mm (12.75 in.) outer diameter solid disc, the temperature response as a function of rotor radius r at 0.5 and 5 seconds after brake application is shown in Fig. 3-13. Note that the inner radius of the swept surface is approximately 102 mm (4 in.) from the center of the rotor. Inspection of the temperature curves reveals that, initially, the brake temperature is not, near the end of braking, only a slight function of the rotor radius. Underlying in the temperature calculations for this two-dimensional problem was a non-uniform pad pressure distribution with higher pressures at the inner radius, and lower pressures at the outer radius. This non-uniform pressure distribution between pad and rotor frequently results after burnishing or use of brakes. However, as discussed in Chapter 2, the particular design of the caliper may have a specific effect on pad pressure distribution and, hence, temperature distribution.

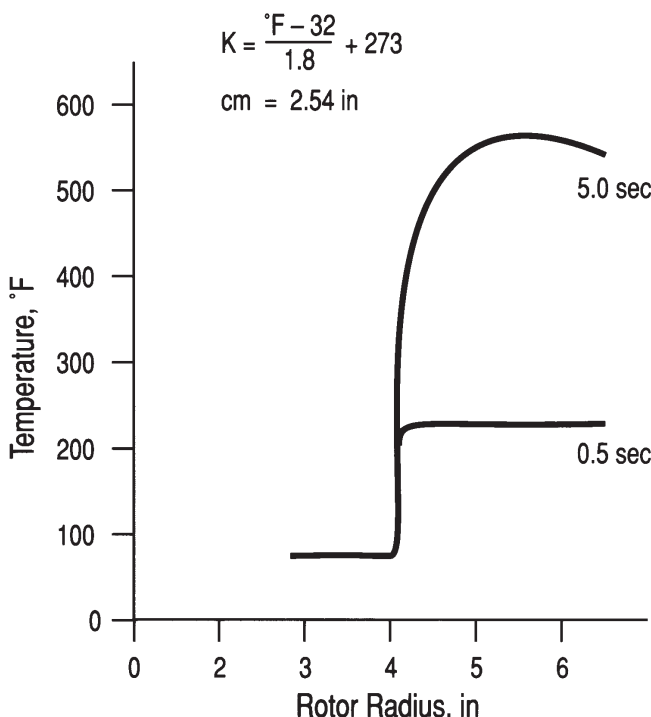


Figure 3-13. Computed radial temperature distribution; 60 mph; non-uniform pad pressure.

3.1.10.3 Temperature Analysis of Ventilated Disc

A finite difference temperature analysis was used that included the brake rotor, rotor hub, inner and outer bearing, spindle, and cooling oil. In addition, repeated braking snubs with varying cycle times and decelerations, including bearing heat generation had to be included. A working sketch of the geometry of the rotor to be analyzed is shown in Fig. 3-14. A total of 30 successive

braking and cooling cycles were formulated followed by a long period of traveling without brake application. The purpose of the study was to investigate the temperatures of bearings and lubricating oil and the cooling rates for brake and bearing components.

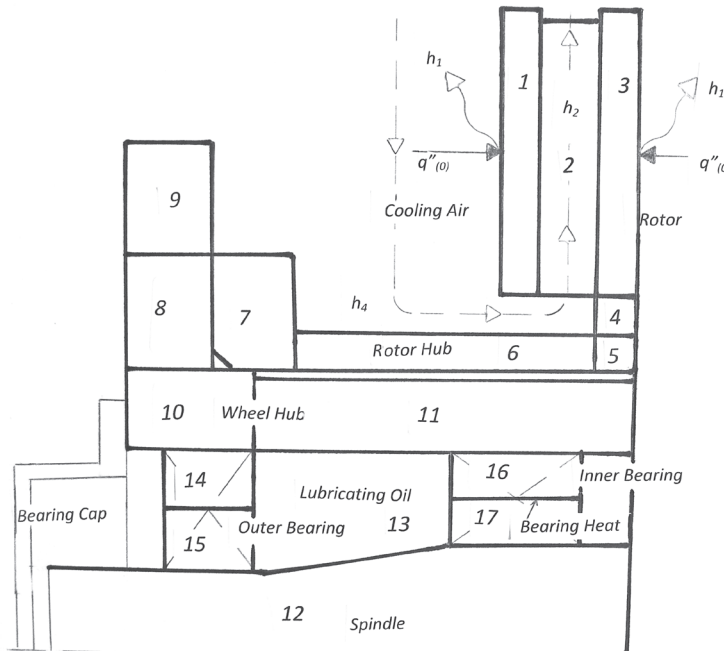


Figure 3-14. Finite difference model for ventilated rotor.

The individual nodes are identified in Fig. 3-14. The entire rotor, hub, and bearing system was divided into 17 nodes; for example, node 1 is the outboard plate, node 3 the inboard plate of the brake rotor. Nodes 16 and 17 represent the outer and inner race of the inboard axle bearing, with heat generation in between the races. In writing the thermal balance equation for each node, it is convenient to express the heat flows as if they were conducted from the contacting adjacent nodes into the node under consideration. For example, applying the first law of thermodynamics to node 3 (inboard rotor plate against which the pad rubs) yields the following expression:

$$\begin{aligned} \rho c V_3 (T'_3 - T_3) / \Delta t &= k A_{23} (T_2 - T_3) / \Delta x_{23} + q'' A_{S3} + h_3 A_{S3} (T_\infty - T_3) \\ &+ h_2 A_{23} (T_{\infty,2} - T_3) + k A_{43} (T_4 - T_3) / \Delta x_{43} \end{aligned} \quad (3-57)$$

Solving for the future time T'_3 after Δt has elapsed yields

$$\begin{aligned} T'_3 &= [(k A_{23} / (M_3 \Delta x_{23})) (T_2 - T_3) + q'' A_{S3} / M_3 + h_3 A_{S3} (T_\infty - T_3) / M_3 \\ &+ h_2 A_{S2} (T_{\infty,2} - T_3) / M_3 + k A_{43} (T_4 - T_3) / (M_3 \Delta x_{43})] + T_3 \end{aligned} \quad (3-58)$$

$$M_3 = \rho c V_3 / \Delta t \quad (3-59)$$

where

A_{23} = area between nodes 2 and 3, m^2 (ft^2)

A_{43} = area between node 4 and 3, m^2 (ft^2)

A_{S3} = cooling area of node 3 on inboard side of rotor, m^2 (ft^2)

A_{S2} = cooling area of node 3 on interior vane side, m^2 (ft^2)

c = specific heat of rotor material, Nm/kgK ($\text{BTU/lb}_m^{\circ}\text{F}$)

h_2 = heat transfer coefficient in vane, $\text{Nm/hm}^2\text{K}$ ($\text{BTU/h}^{\circ}\text{Fft}^2$)

h_3 = heat transfer coefficient on inboard side of node 3,
 $\text{Nm/hm}^2\text{K}$ ($\text{BTU/h}^{\circ}\text{Fft}^2$)

k = thermal conductivity of rotor material, Nm/hmK ($\text{BTU/hft}^{\circ}\text{F}$)

V_3 = volume of node 3, m^3 (ft^3)

T_2 = initial or last temperature of node 2, K ($^{\circ}\text{F}$)

T_3 = initial or last temperature of node 3, K ($^{\circ}\text{F}$)

T_4 = initial or last temperature of node 4, K ($^{\circ}\text{F}$)

T_{∞} = ambient temperature cooling inboard side of node 3, K ($^{\circ}\text{F}$)

$T_{\infty,2}$ = air temperature inside cooling vane of rotor, K ($^{\circ}\text{F}$)

q'' = time-varying heat flux, Nm/hm^2 , (BTU/hft^2)

Δt = time interval between temperature calculations, h

Δx_{23} = distance between centers of node 2 and node 3, m (ft)

Δx_{43} = distance between centers of node 4 and node 3, m (ft)

ρ = density of rotor material, kg/m^3 (lb_m/ft^3)

Similar equations were derived for each of the 17 nodes. Radiation heat transfer was included between the rotor hub (node 6) and the bearing hub (node 11). The proper braking power for each braking cycle was specified as time-varying heat flux q'' at nodes 1 and 3. Bearing heat generation input was 30 and 20 BTU/h for the inner and outer bearing, respectively (nodes 14 through 17). The vehicle was traveling at 70 mph and decelerated at 0.29 g. The cooling time between each braking cycle was approximately 100 seconds. Changes in braking severity and cooling time occurred after the 8th, 18th and 29th cycle, as inspection of the calculated temperature curves of Fig. 3-15 indicates. After the 30th braking cycle, the vehicle was driven at 70 mph for approximately 50 minutes without any brake application. After the brakes were released at the end of the 30th braking cycle, the only heat generation occurred at the two wheel bearings. The temperature response of the 17 nodes after 30 braking cycles and the cooling run is shown in Fig. 3-15.

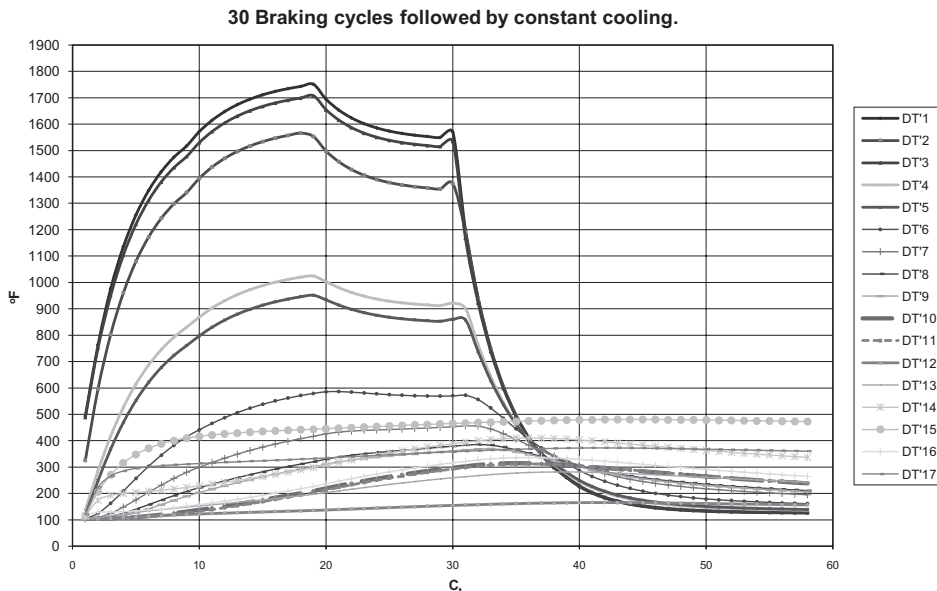


Figure 3-15. Brake temperature response for 30 braking cycles and cooling.

3.2 Thermal Stress Analysis

Thermal stresses result from non-uniform temperature distributions. In addition, mechanical stresses may arise from body deformations or body forces. In most practical thermal stress problems, it is permissible to separate the temperature problem from the stress problem and to solve both consecutively.

3.2.1 Thermal Stress in Disc Brake Rotors

The approximate compressive stress σ developed in the surface layer of an infinite flat plate as a result of a sudden temperature increase is (Refs. 3.3, 3.21)

$$\sigma = -\left(\frac{E}{1-\nu}\right)\alpha_T \Delta T \quad , \quad \text{N/m}^2(\text{psi}) \quad (3-60)$$

where E = elastic modulus, N/m^2 (psi)

ΔT = temperature difference, K ($^{\circ}\text{F}$)

α_T = thermal expansion coefficient, m/K m ($\text{in.}/^{\circ}\text{F}$ in.)

ν = Poisson's ratio

The solid rotor of a disc brake can be treated as a thin flat plate, as illustrated in Fig. 3-16. The thermal stress in the rotor can be analyzed based on the following limitations:

1. Surface traction is negligible.
2. Body forces are negligible.
3. Temperature is a function of thickness z and time t only.
4. Temperature distribution is symmetrical.

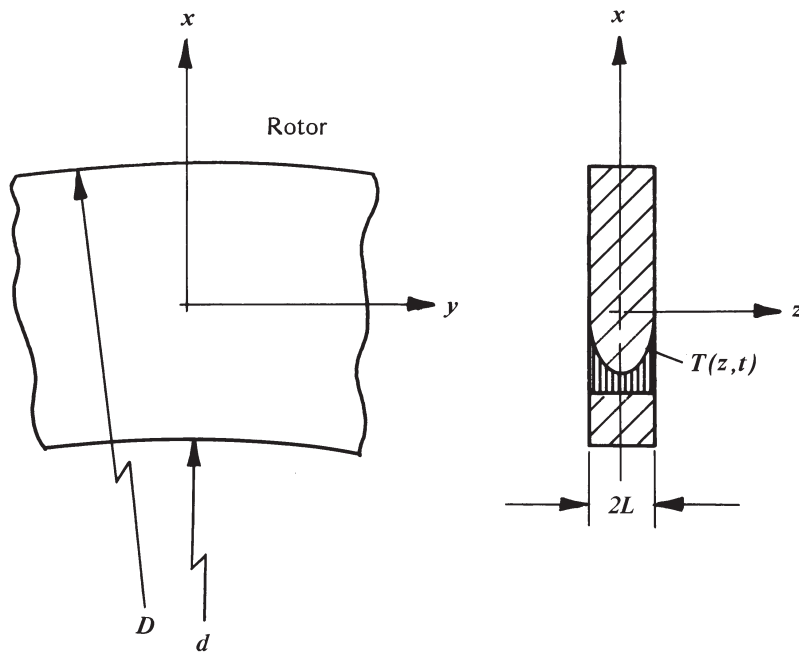


Figure 3-16. Flat plate representation of brake rotor.

The stress analysis of a free plate yields the expression for computing the thermal stresses in the rotor

$$\sigma_x = \sigma_y = \frac{\alpha_T E}{1-\nu} \left[-T(z) + \frac{1}{L} \int_0^L T(z) dz \right], \quad \text{N/m}^2 (\text{psi}) \quad (3-61)$$

where L = one-half rotor thickness, m (ft)

$T(z)$ = temperature distribution over z , K (F)

σ_x = stress in x -direction, N/m² (psi)

σ_y = stress in y -direction, N/m² (psi)

The thermal stresses $\sigma(z, t)$ produced by a linearly decreasing heat flux are determined from the temperature response given by Eq. (3-29) for a solid rotor and Eq. (3-61) as

$$\begin{aligned} \sigma(z, t) = & \frac{q''_{(0)}}{q''_0} \sigma_0(z, t) + \frac{2q''_{(0)} \alpha_T E}{t_s (1-\nu) h_R} \\ & \times \sum_{n=1}^{\infty} \left\{ \frac{\sin(\lambda_n L)}{\lambda_n L + \sin(\lambda_n L) \cos(\lambda_n L)} \times \frac{1 - e^{-a_t \lambda_n^2 t}}{a_t \lambda_n^2} \right. \\ & \left. \times \left[\frac{\sin(\lambda_n L)}{(\lambda_n L)} - \cos(\lambda_n z) \right] \right\}, \quad \text{N/m}^2 (\text{psi}) \quad (3-62) \end{aligned}$$

where L = one-half rotor thickness, m (ft)

t_s = stopping time, h

$\sigma_0(z, t)$ = stress produced by a constant heat flux, N/m^2 (psi)

The stress $\sigma_0(z, t)$ produced by a constant heat flux, required in Eq. (3-62), is computed from the constant heat flux temperature response and Eq. (3-61) as

$$\sigma_0(z, t) = \frac{2\alpha_T E q_0''}{(1-\nu) h_R} \sum_{n=1}^{\infty} \left\{ \frac{\sin(\lambda_n L) e^{-a_t \lambda_n^2 t}}{\lambda_n L + \sin(\lambda_n L) \cos(\lambda_n L)} \times \left[\frac{\sin(\lambda_n L)}{(\lambda_n L)} - \cos(\lambda_n z) \right] \right\}, \quad \text{N/m}^2 \text{ (psi)} \quad (3-63)$$

The theoretical thermal stresses at the surface of a solid rotor computed by Eq. (3-62) for stops from 97 and 128 km/h (60 and 80 mph) are illustrated in Fig. 3-17. Inspection of the curves reveals a maximum near a braking time of 1 s.

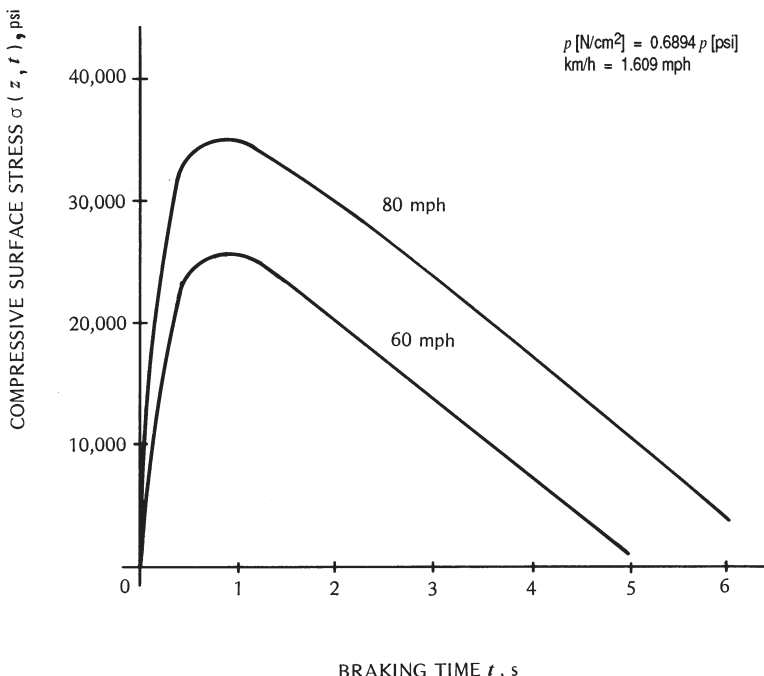


Figure 3-17. Thermal surface stresses; stops from 97 and 128 km/h (60 and 80 mph).

Because thermal shock and subsequent surface cracking are functions of the initial temperature gradient at the swept rotor surface, Eq. (3-62) also may be used to approximate the thermal stresses produced in a ventilated rotor. In this case L equals the flange thickness.

3.2.2 Thermal Stress in Brake Drums

The detailed equations for predicting thermal stresses in brake drums are very complicated. Approximate equations may be given for drums with the ratio of drum width to drum radius much less than unity. However, this approach would exclude a large number of brakes, especially those for heavy vehicles.

A rough estimate of the thermal stresses produced in a single stop may be obtained from Eq. (3-60).

3.2.3 Thermal Rotor Failure

Normal braking operation will cause fine, hairline cracks laterally across the swept surface of brake drums. This is a normal condition caused by constant low-energy heating and cooling of the braking surface.

Excessive heating and cooling may cause the drum to crack all the way through the entire drum wall from the swept surface to the cooling surface.

Heat-spotted drums show hard, slightly raised, dark-colored spots on the braking surface, with uneven wear. Heat (or hot) spots are caused by localized high-temperature-caused material changes of the structure.

Bluish, discolored swept braking surfaces are caused by excessive heat exceeding 533 to 588 K (500 to 600°F), possibly by constant low shoe drag or by overheating in severe fade.

Rotor surface cracking will occur when the stress exceeds the strength of the material. The occurrence of surface rupture is affected by thermal stress, number and frequency of braking cycles, surface condition due to machining, corrosion, and rotor geometry (Ref. 3.29).

For a given rotor material having a certain strength, the tendency of the surface to rupture will be decreased if, for a given heat flux, the temperature gradient at the surface is small, the cooling is not extremely rapid, the thermal expansion coefficient and the elastic modulus are decreased, and the rotor is designed so that thermal expansion is maximally unconstrained. Rotor deformation due to hub mouth widening should be minimized. The temperature gradient, again for a given heat flux, depends during the first few brake applications on the thermal properties of the rotor material.

For example, a high thermal conductivity results in a less marked temperature gradient. The rate of change of temperature at a given location in the rotor will be less pronounced for increased values of specific heat and material density. The rotor thickness has a twofold effect on the stress state: A thicker rotor produces higher temperature gradients and tends to be more rigid, thus producing more marked constraints on free thermal expansion. Consequently, thicker disc brake rotors have lower allowable heat flux values than thinner rotors [Eq. (3-61)].

In single brake applications wherein the rotor surface was not subjected to excessive temperature, surface cracks (if they occurred) developed generally in

a radial direction. Subsequent braking cycles with the brake operating below certain maximum temperatures produced a stress pattern that was mainly a further development of the original cracks caused by thermal shock.

The other failure mode appears to be associated with severe surface temperatures, resulting in partial surface melting and dislocation of particles at the surface. Those conditions might produce hot spots, resulting in randomly oriented localized stress patterns. Stress patterns of this type may also be caused by localized interference of heat transfer, resulting from subsurface porosities. The surface porosities may be produced by material tearing or opening of subsurface porosities, and localized geometry changes due to temperature-induced micro-structural changes of the base material.

Excessive heating alone generally is of no severe consequence to the rotor material. Maximum cooling rates may have significant effect on the performance of the rotor. This condition occurs when a vehicle is subjected to successive high effective stops and is then driven at high speeds to cool the brakes. With improper rotor materials, martensite is formed, causing surface thickness variations. Martensite occupies a larger volume than pearlite. The results are brake shudder and brake torque variations due to different friction coefficients between martensite, pearlite, and bainite. High-carbon-content cast iron up to 3 to 3.5% C generally yields favorable rotor performance.

In general, rotor surface rupture or cracking will be prevented in a sudden high-deceleration stop for the following condition:

$$[(5/18)^{0.5} \alpha E q_{(0)}'' (t_s)^{0.5}] / [(1 - v)(\rho c k)^{0.5} S_y] < 1 \quad (3-64)$$

where

c = specific heat, Nm/kgK (BTU/(lb_m °F))

E = elastic modulus, N/m² (psi)

k = thermal conductivity, Nm/hKm (BTU/h°Fft)

$q_{(0)}''$ = heat flux at beginning of braking, Nm/hm² (BTU/(hft²))

t_s = stopping time, h

α = thermal expansion coefficient, m/mK (in./(in. °F))

v = Poisson's ratio

ρ = density, kg/m³ (lb/ft³)

When the condition of Eq. (3-64) is fulfilled, compressive thermal stresses will be less than the yield strength of the rotor material. Eq. (3-64) assumes that the temperature rise at the friction surface is instantaneous.

3.3 Thermal Design Measures

Experience gained by engineers over the years in the design, testing, and use of automotive brakes has led to a number of design guides relative to the thermal performance of drum and disc brakes. These measures are generally based on commonly used materials for rotors and pads or linings. After brakes have been designed based on these guides, testing must always be done to ensure that the actual thermal performance falls within expected safety limits. PC-BRAKE HYDRAULIC applies.

3.3.1 Allowable Heat Flux into Drum or Rotor

3.3.1.1 Brake Drums

In general, thermal surface cracking of the drum friction surface has not been observed when the heat flux into the swept area of the drum is kept below a certain value as defined by Eq. (3-65):

$$q''_{D, \text{allowable}} = q_0 \phi_i / 3600 A_s < 170 \quad \text{Nm/cm}^2 \text{s} \\ [< 150 \quad , \quad \text{BTU/ft}^2 \text{s}] \quad (3-65)$$

where $q''_{D, \text{allowable}}$ = allowable heat flux into drum, $\text{Nm/cm}^2 \text{s}$ ($\text{BTU/ft}^2 \text{s}$)

A_s = swept area of rotor or drum, cm^2 (ft^2)

q_0 = braking power, Nm/h (BTU/h)

ϕ_i = brake force of i th brake divided by total brake force

In general, passenger-car drums showing crack widths of 0.7 mm (0.027 in.) and lengths of 50 mm (~2 in.) are still serviceable.

3.3.1.2 Brake Rotors

Rotor materials are cast iron such as GG-20 with a tensile strength of 150 – 250 MPa. The maximum allowable temperature is approximately 700°C. Carbon-based rotor materials allow temperatures as high as 1400°C (Ref 2.1). The design measures that follow are all based upon cast iron rotor materials.

In earlier discussions on thermal stress, it was indicated that the thickness of the disc brake rotor has an influence on rotor failure. A rotor material will have improved thermal performance with higher thermal endurance strength, higher thermal conductivity, decreased elastic modulus, and decreased thermal expansion coefficient. Thicker rotors tend to exhibit higher potential for thermal stress and, hence, rotor failure. Disc brake rotors generally have sufficient thermal endurance when the heat flux is limited to a value computed by (Ref. 1.3)

$$q''_{R, \text{allowable}} = 28.8(439 - 0.46T)/L \quad , \quad \text{Nm/cm}^2 \text{s} \\ [q''_{R, \text{allowable}} = (439 - 0.46T)/L \quad , \quad \text{BTU/ft}^2 \text{s}] \quad (3-66)$$

where T = brake temperature, °C (°F)

L = rotor thickness, mm (in.)

The actual heat generation between pad and swept rotor surface for a disc brake is not uniformly distributed. It is a function of how uniformly the entire pad surface is pressing against the rotor surface. The actual swept rotor surface involved in heat generation is not identical to the geometrical swept surface. For fixed-caliper disc brakes, the swept surface to be used is only 70 to 75%, for floating-caliper disc brakes, only 50 to 65% of the geometrical swept surface is used.

For example, for an average brake temperature of 623 K or 350°C (662°F) and a rotor thickness of 22 mm (0.85 in.), Eq. (3-66) yields an allowable heat flux of 364 Nm/cm²s (327 BTU/ft²s). The actual heat flux produced during a stop is computed by Eq. (3-65), however, with the swept area adjusted by the correction factor indicated above. The velocity and deceleration used for computing the heat flux produced should be the maximum speed and deceleration attainable. If the heat flux produced exceeds the heat flux allowable, then the disc brake rotor will exhibit a limited endurance relative to thermal cracking. High-performance vehicles equipped with ABS should be able to withstand a minimum of 100 high effectiveness stops without rotor surface failure.

Because most vehicles in public use are not subjected to repeated severe brake applications, a deceleration level of 0.7 g may be used relative to Eq. (3-66) in connection with the maximum speed attainable. With a disc size based on Eq. (3-66), thermal surface performance should generally be unlimited for vehicles in normal use.

The theoretical temperature increase of the swept surface mass of the rotor should not exceed certain limits. The mass is computed by the product of swept surface area, rotor thickness in the case of a solid rotor, and rotor material density. For ventilated rotors, three times the thickness of one rotor plate should be used as effective rotor thickness.

The braking energy is computed by Eq. (3-9), adjusted for one front (or rear) brake. The theoretical temperature increase is computed by an expression similar to Eq. (3-30), where density multiplied by rotor volume equals the swept surface rotor mass, and c is the specific heat of the rotor material.

For example, for one front brake on a level road, the theoretical temperature increase $T_{th,F}$ is

$$T_{th,F} = \frac{(1-\Phi)}{2} \left[\frac{W(V_1^2 - V_2^2)}{2g\rho_R c_R v_R} \right] , \text{ K (°F)} \quad (3-67)$$

where c_R = rotor specific heat, Nm/kgK (BTU/lb_m °F)

g = gravitational constant, 9.81 m/s² (32.2 ft/s²)

V_1 = initial velocity, m/s (ft/s)

V_2 = final velocity, m/s (ft/s)

v_R = rotor volume, m³ (ft³)

W = vehicle weight, N (lb)

ρ_R = rotor density, kg/m³ (lb_m/ft³)

The fraction of rear braking is designated by the Greek letter Φ . T_{th} is a theoretical temperature only because heat transfer to the brake pad and all other cooling mechanisms have been ignored. T_{th} , however, yields a good comparison measure for the evaluation of a brake system based on the temperature limits stated below (Ref. 1.3).

For T_{th} less than 500 K (440°F), the rotor dimensions are sufficient for most passenger cars.

For T_{th} between 500 and 600 K (440 and 621°F), high-performance passenger vehicles still have enough brake size.

A value of T_{th} greater than 600 K (621°F) must be avoided.

3.3.2 Horsepower into Lining or Pad

Brakes generally do not exhibit significant in-stop fade if the power q_p'' absorbed by the lining or pad is kept less than a certain value, as defined by Eq. (3-68):

$$q_p'' = \lambda \phi_i P_{bav} / A_p < 400 \text{ Nm / cm}^2 \text{ s (drum)} \\ < 2000 \text{ Nm / cm}^2 \text{ s (disc)} \quad (3-68)$$

$$\left[q_p'' = \lambda \phi_i P_{bav} / 555 A_p < 500 \text{ hp / ft}^2 \text{ s (drum)} \right. \\ \left. < 2500 \text{ hp / ft}^2 \text{ s (disc)} \right]$$

where A_p = lining or pad rubbing area of leading or secondary shoe or brake pad, cm² (ft²)

P_{bav} = braking power, Nm/s (lbft/s) from Eq. (3-8)

λ = relative portion of braking power absorbed by an individual brake shoe
 = 0.5 for two-leading shoe brake
 = 0.7 for leading-trailing shoe or duo-servo brake
 = 1.0 for disc brake

For a stop from maximum speed and fully laden vehicle and modern pad materials, total energy absorbed per one square inch of pad friction surface should be limited to a value of 20,000 Nm/cm².

3.3.3 Lining or Pad Wear

Excessive wear of the linings or pads in normal automotive operation generally has not been observed if the product of the mean pressure p_m between the lining and drum or disc and lining friction coefficient μ_L is kept below a certain value as defined by Eq. (3-69):

$$\begin{aligned} \mu_L p_m &= \lambda W a \phi_i (R / r) / A_{pp} < 65 \text{ N/cm}^2 (95 \text{ psi}) \text{ (drum)} \\ &< 241 \text{ N/cm}^2 (350 \text{ psi}) \text{ (disc)} \end{aligned} \quad (3-69)$$

where a = deceleration, g-units

A_{pp} = projected lining area of leading or secondary shoe

= $1.62ru$, cm^2 (in.^2)

r = effective drum or rotor radius, cm (in.)

R = effective tire radius, cm (in.)

u = effective width of brake drum swept area, cm (in.)

W = vehicle weight, N (lb)

μ_L = lining or pad friction coefficient

The maximum mechanical pressure for disc brake pads should be less than 1200 N/cm^2 (1750 psi).

3.3.4 Rotor Design Considerations

An important consideration in designing brake rotors is the expected thermal expansion and associated deformation of the entire rotor geometry. Minimizing thermal stresses results in increased thermal endurance strength and rotor life.

Thermal stress in the lateral or thickness direction of the rotor is mostly affected and controlled by material properties. Stress in the circumferential direction is a function of the deformation of the entire rotor, including hub. Minimum circumferential stresses are obtained when the actual brake rotor ring is bolted to the hat section. In this design the ring can expand via the bolts without forcing its geometry change onto the hat or hub. The design is relatively expensive and not used for normal passenger cars.

For conventional ventilated rotors it is advantageous to make the rotor plates of different thickness. The outboard plate should be thicker than the inboard facing plate. This design reduces the cone-shape deformation or opening of the hub and rotor structure as well as minimizes surface cracking sensitivity.

If ventilation holes are used, they must be located such that cooling air can circulate from the inboard side of the brake underneath the vehicle through the brake. In this regard, wheel rim, hub design, and hub covers (if any) must be optimized for maximum brake cooling.

Thermal rotor stresses are minimized when stress raisers are eliminated as much as possible. For example, the number of cooling vanes of a ventilated rotor should always be arranged symmetrically with respect to the attachment bolts.

Chapter 3 References

- 3.1 Thuresson, Daniel, "Thermo-mechanical Analysis of Friction Brakes," SAE Paper No. 2000-01-2775, SAE International, Warrendale, PA, 2000.
- 3.2 Arpacı, Vedat S., *Conduction Heat Transfer*, Addison-Wesley Publishing Company, 1966.
- 3.3 Limpert, R., "Temperature and Stress Analysis of Solid-Rotor Disc Brakes," Ph.D. Dissertation, University of Michigan, 1972.
- 3.4 Carlslaw, H. S. and J. C. Jaeger, *Conduction of Heat in Solids*, Oxford Science Publications, 2000.
- 3.5 Hasselgruber, H., *Temperature Calculations for Friction Clutches*, Friedrich Vieweg & Sohn Verlag, Braunschweig, 1956.
- 3.6 Limpert, R., "Cooling Analysis of Disc Brake Rotors," SAE Paper No. 751014, SAE International, Warrendale, PA, 1975.
- 3.7 Emery, A.F., "Measured and Predicted Temperatures of Automotive Brakes under Heavy or Continuous Braking," SAE Paper No. 2003-01-2712, SAE International, Warrendale, PA, 2003.
- 3.8 Wang, Xuanfeng, "Experimental Research on Heavy-Duty Tractor Heat Performance of Brake," SAE Paper No. 2009-01-3039, SAE International, Warrendale, PA, 2009.
- 3.9 Zhang, Jian J., "A High Aerodynamic Performance Brake Rotor Design Method for Improved Brake Cooling," SAE Paper No. 973016, SAE International, Warrendale, PA, 1997.
- 3.10 Daudi, Anwar R., "Hayes High Airflow Design Rotor for Improved Cooling and Coning," SAE Paper No. 982248, SAE International, Warrendale, PA, 1998.
- 3.11 Daudi, Anwar R., "72 Curved Fins and Air Director Idea Increases Airflow Through Brake Rotors," SAE Paper No. 1999-01-0140, SAE International, Warrendale, PA, 1999.
- 3.12 Daudi, Anwar R., "72 Curved Fin Rotor Design Reduces Maximum Rotor Temperature," SAE Paper No. 1999-01-3395, SAE International, Warrendale, PA, 1999.
- 3.13 Barigozzi, Giovanna and Antonio Perdichizzi, "Aero-Thermal Characteristics of an Automotive CCM Vented Brake Disc," SAE Paper No. 2005-01-3930, SAE International, Warrendale, PA, 2005.
- 3.14 Mishra, Rakesh, David Bryant, and John D. Fieldhouse, "Analysis of Air Flow and Heat Dissipation from High Performance GT Car Front Brake Disc," SAE Paper No. 2008-01-0820, SAE International, Warrendale, PA, 2008.

- 3.15 Nutwell, Brian and Thomas N. Ramsay, "Modeling the Cooling Characteristics of a Disc Brake on an Inertia Dynamometer, Using Combined Fluid Flow and Thermal Simulation," SAE Paper No. 2009-01-0861, SAE International, Warrendale, PA, 2009.
- 3.16 Limpert, R., *Engineering Design Handbook, Analysis and Design of Automotive Brake Systems*, US Army Material Development and Readiness Command, DARCOM-P-706-358, 1976.
- 3.17 Kreith, F., *Principles of Heat Transfer*, International Textbook Company, 1965.
- 3.18 Pyung Hwang, Wu Xuan Wu, and Jeon YoungBae, "Repeated Brake Temperature Analysis of Ventilated Brake Disc on Downhill Road," SAE Paper No. 2008-01-2571, SAE International, Warrendale, PA, 2008.
- 3.19 Parmigiani, John P. and Timothy C. Ovaert, "The Transient Temperature Distribution in a Heavy-Brake System During Fatigue Crack Testing," SAE Paper No. 2000-01-0441, SAE International, Warrendale, PA, 2000.
- 3.20 Liang Li, Song Jian, and Qi Xuele, "Study on Vehicle Braking Transient Thermal Based on Fast Finite Element Method Simulation," SAE Paper No. 2005-01-3945, SAE International, Warrendale, PA, 2005.
- 3.21 Apte, Amol A. and H. Ravi, "FE Prediction Thermal Performance and Stresses in a Disc Brake System," SAE Paper No. 2006-01-3558, SAE International, Warrendale, PA, 2006.
- 3.22 Hertel, Jim E., et al., "Finite Difference Heat Transfer Model of a Steel-clad Aluminum Brake Rotor," SAE Paper No. 2005-01-3943, SAE International, Warrendale, PA, 2005.
- 3.23 Schuetz, Thomas Christian, "Cooling Analysis of a Passenger Car Disc Brake," SAE Paper No. 2009-01-3049, SAE International, Warrendale, PA, 2009.
- 3.24 Mi-Ro Kim, et al., "Numerical Investigation of Thermal Behaviour in Brake Assembly Driving the ALPINE Braking Mode," SAE Paper No. 2007-01-1021, SAE International, Warrendale, PA, 2007.
- 3.25 Lozia, Zbigniew and Andrej Wolff, "Thermal State of Automotive Brakes After Braking on the Road and on the Roll-Stand," SAE Paper No. 971040, SAE International, Warrendale, PA, 1997.
- 3.26 Jerhamre, Anders and C. Bergstrom, "Numerical Study of Brake Disc Cooling Accounting for Both Aerodynamic Drag Force and Cooling Efficiency," SAE Paper No. 2001-01-0948, SAE International, Warrendale, PA, 2001.

- 3.27 Damodaran, Vijay, Radhika Cherukuru, and Ajith M. Jayssundera, CFD-Based Lumped Parameter Method to Predict the Thermal Performance of Brake Rotors in Vehicle," SAE Paper No. 2003-01-0601, SAE International, Warrendale, PA, 2003.
- 3.28 Eppler, Steffen, Thomas Klenk, and Jochen Wiedermann, "Thermal Simulation Within the Brake System Design Process," SAE Paper No. 2002-01-2587, SAE International, Warrendale, PA, 2002.
- 3.29 Limpert, R., "An Investigation of Thermal Conditions Leading to Surface Rupture of Cast Iron Rotors," SAE Paper No. 720447, SAE International, Warrendale, PA, 1972.

Chapter 4



Analysis of Mechanical Brake Systems

4.1 General Observations

Mechanical braking systems use mechanical devices such as cables, rods, levers, cams, spindles, or wedges to transmit force to the wheel brakes. In current design practice, mechanical brakes are used primarily for parking brakes or for service brakes of golf carts, small ATVs, etc. Their mechanical efficiency is low at approximately 65%. An efficiency of 65% indicates that 35% of the operator apply force is lost in terms of friction and is not available for vehicle braking. Mechanical brakes in poor condition, or designs with long, curved cable tubes, may have efficiencies below 65%. Frequent adjustment and lubrication are required for proper operation.

Time delays are relatively small, and are largely a function of the distance required to overcome shoe-to-drum clearance. The brake force build-up time, during which various load-carrying components deflect, is relatively short.

The actuation force of the parking brake may be manual as hand- or foot-apply force, electric motor, or compressed spring used in air brakes or hydraulic brakes for heavy equipment (Refs. 4.1, 4.2, 4.3). Self-adjusting parking brake systems have been introduced to save labor cost during manufacturing (Ref. 4.4). Inadvertent release of the parking brake has occurred when the pawl rested on or near the top of the next adjustment tooth of the gear sector. Antilock brakes have been designed for cable-actuated brakes (Ref. 4.5).

Air-actuated S-cam brakes use a number of mechanical devices between the brake chamber and the tip of the brake shoes, such as lever arm (slack adjuster), camshaft, cam, and rollers. Air-actuated wedge brakes use a wedge and rollers to apply the shoes against the drum. However, in current applications, full mechanical brakes are those systems in which the energy required for the brake shoe/drum pressing force is transmitted from the energy source to the shoes by mechanical means.

FMVSS 135 requires the vehicle loaded at GVW to be held stationary on a 20% grade with the transmission in neutral for five minutes with a hand or foot force of not more than 400 N (90 lb) or 500 N (112.4 lb), respectively. The

vehicle must be tested facing both uphill and downhill. FMVSS 105 has similar requirements for vehicles with hydraulic brakes and a GVW greater than 44,450 N (10,000 lb).

4.2 Wheel Brakes

A typical mechanical brake for parking brake purposes is illustrated in Fig. 4-1. The cable force F_c moves the lever ℓ_2 to the left such that both shoes are spread apart to apply the brake. The individual shoe tip forces are slightly different. However, if the average actuation force is used, then the mechanical gain ρ_B between the cable force into the brake and the average actuation force is given by

$$\rho_B = 1/2[(\ell_2 / \ell_1 \ell_5)(\ell_3 - \ell_1) + (\ell_3 / \ell_1 \ell_5)(\ell_2 - \ell_1)] \quad (4-1)$$

where ℓ_1 through ℓ_5 are brake dimensions identified in Fig. 4-1.

For a typical drum parking brake, the mechanical gain ranges between 2.75 and 3.

The total brake force F_x between tires and ground at the two wheels braked by the mechanical system may be computed by

$$F_x = (BF)(F_H \rho_H \eta_H - 2F_s) \rho_B \eta_B (r/R) , \quad N (lb) \quad (4-2)$$

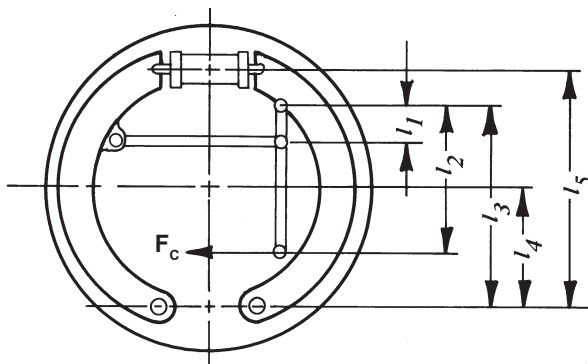


Figure 4-1. Schematic of parking brake.

where BF = brake factor

F_H = hand or foot force, N (lb)

F_s = return spring force, N (lb)

R = tire radius, m (in.)

r = effective rotor or drum radius, m (in.)

η_H = mechanical efficiency of parking brake from hand force to cable force

η_B = efficiency of actuation mechanism inside wheel brake

ρ_B = gain of mechanical brake [Eq. (4-1)]

ρ_H = displacement gain between hand force and cable force

The displacement gain ρ_H is equivalent to the pedal lever ratio of the foot-operated service brake. It is determined by the ratio of hand travel available (or foot travel in the case of a foot-operated parking brake) to the cable travel.

The average displacement d_H of the tip of each brake shoe is determined by

$$d_H = Y_H / \rho_B \rho_H \quad (4-3)$$

where Y_H = maximum available hand or foot travel for parking brake, mm (in.)

The displacement d_H of each shoe tip associated with the parking brake should exceed the corresponding value obtained for the hydraulic service brake system by approximately 10 to 15%. This is to ensure adequate emergency braking in the event of excessive brake wear resulting in service brake loss due to increased pedal travel.

The deceleration, a , achievable with the parking brake is determined by Newton's second law and Eq. (4-2) as

$$a = [(BF)(F_H \rho_H \eta_H - 2F_S) \rho_B \eta_B (r/R)]/W, \text{ g-units} \quad (4-4)$$

where BF = brake factor of wheel brake

W = vehicle weight, N (lb)

The slope angle α on which a vehicle can be held stationary for a given hand or foot force F_H is indirectly expressed by Eq. (4-4) because $\sin \alpha$ = deceleration a .

The coefficient of friction between tire and road surface must be equal to or greater than the values computed below to prevent wheel slipping.

Parking brake acting on front brakes (vehicle facing up hill):

$$\mu_F = \frac{\sin \alpha - f_{\text{roll}}}{(1-\psi) \cos \alpha - \chi \sin \alpha} \quad (4-5)$$

Parking brake acting on rear brakes (vehicle facing down hill):

$$\mu_R = \frac{\sin \alpha - f_{\text{roll}}}{\psi \cos \alpha - \chi \sin \alpha} \quad (4-6)$$

where f_{roll} = tire rolling resistance coefficient

α = slope in degrees

χ = center-of-gravity height divided by wheelbase

ψ = level-road static rear axle load divided by vehicle weight

Example 4-1: A small pickup truck with a GVW of 22,907 N (5150 lb) and a wheelbase of 3.2 m (126 in.) carries a slide-in camper. Determine if a rear brake factor $BF = 1.8$ is sufficient to hold the vehicle stationary on a 20% slope. Use the data that follow: GVW rear axle 11,565 N (2,600 lb), tire radius 0.3683 m (14.5 in.), rear drum radius 0.127 m (5 in.), center-of-gravity-height 0.91 m (36

in.), $l_1 = 0.0254$ m (1 in.), $l_2 = 0.102$ m (4 in.), $l_3 = 0.127$ m (5 in.), $l_5 = 0.1524$ m (6 in.), $F_s = 66.7$ N (15 lb), $\eta_B = 0.8$, $\eta_H = 0.65$.

A 20% slope is equal to a 11.3-degree slope. The braking force required on the rear wheels is equal to $22,907 \sin(11.3) = 4488.5$ N [$(5150) \sin(11.3) = 1009$ lb]. Substitution of the drum brake lever data into Eq. (4-1) yields $\rho_B = 2.58$. Using a maximum allowable foot apply force of $F_H = 500$ N (112.4 lb) in Eq. (4-4) yields a level roadway deceleration of $a = 0.17$ g or a braking force of $(0.17)(22,907) = 3,894$ N [$(0.17)(5150) = 876$ lb]. Consequently, a brake factor of 1.8 is not sufficient to produce a braking force of 4,488.5 N (1009 lb). BF = 2.1 would be required. With Eq. (4-6), a tire-road coefficient of friction $\mu_R = 0.39$ is obtained.

4.3 Driveshaft-Mounted Brakes

Current design practice generally does not use driveshaft-mounted brakes as parking brakes except in medium weight trucks with 4-wheel disc brakes. In the past they were installed on medium and heavy trucks using either hydraulic or air brakes. Since FMVSS 121 became effective for heavy trucks and trailers in 1975, air-brake-equipped trucks use spring-actuated parking brakes. Four-wheel disc-brake-equipped medium trucks use disc integrated parking brakes or drive shaft-mounted brakes.

The total braking force F_x at the wheels retarded by the driveshaft-mounted brake is determined by

$$F_x = \frac{F_H \rho_H \eta_m B F \rho_D r}{\eta_t R} , \quad \text{N (lb)} \quad (4-7)$$

where BF = brake factor

F_H = hand or foot force, N (lb)

r = drum or effective rotor radius, mm (in.)

η_m = mechanical efficiency between hand force and cable into brake

η_t = mechanical efficiency between vehicle transmission and driven wheels

ρ_D = final drive or rear axle ratio

ρ_H = isplacement gain between hand force and cable force

The deceleration, a , achieved with the driveshaft-mounted parking brake is determined by

$$a = F_x / W , \quad \text{g - units} \quad (4-8)$$

where W = vehicle weight, N (lb)

Bureau of Motor Carrier Safety regulations required that the shaft brake stop the vehicle laden at GVW from 32.2 km/h (20 mph) in a distance of 25.9 m

(85 ft) or less (average deceleration of 0.16 g). Under those conditions the theoretical brake temperature of the swept surface of the brake is approximately 477 K (400°F). If the braking speed were increased to a typical highway speed of 80.5 km/h (50 mph), then the parking brake temperature would exceed 1089 K (1500°F), clearly indicating that driveshaft-mounted parking brakes are not suitable as emergency brakes in the event the service brake has failed.

Eq. (4-7) may also be used to determine the slope on which the vehicle can be held stationary with the driveshaft-mounted parking brake for a given hand force by

$$\sin \alpha = F_x / W \quad (4-9)$$

where W = vehicle weight, N (lb)

α = slope angle, deg

Federal Motor Vehicle Safety Standard 105 requires for GVWs greater than 10,000 lb that the vehicle, when loaded at GVW, remain stationary for five minutes on a 20% slope with a lever apply force of not more than 556 N (125 lb) when foot-applied, or 400 N (90 lb) when hand-applied.

The driveshaft torque T_s developed by the weight of the vehicle parked on a slope is determined by

$$T_s = WR\eta_t \sin \alpha / \rho_D \quad , \quad \text{Nm (lb in.)} \quad (4-10)$$

For example, for $W = 222,400$ N (50,000 lb), a slope of 20% (11.3 deg), a tire radius of $R = 0.533$ m (21 in.), a rear axle ratio of 4.1 to 1, and an efficiency of $\eta_t = 0.90$, the maximum driveshaft torque that the parking brake has to react against is obtained by Eq. (4-10) as

$$T_s = 222,400(0.533)(0.9) \sin(11.3) / 4.1 = 5098.7 \text{ Nm}$$

$$[T_s = 50,000(21)(0.9) \sin(11.3) / 4.1 = 45,163 \text{ lb in.}]$$

The brake torque T_B produced by the parking brake is determined by

$$T_B = F_H \rho_H \eta_H B F_r \quad , \quad \text{Nm (lb in.)} \quad (4-11)$$

As long as the brake torque of the parking brake exceeds the torque developed by vehicle weight attempting to turn the driveshaft, the vehicle will remain stationary, assuming the tire-road friction coefficient is sufficiently large to prevent locked-wheel sliding [Eq. (4-6)].

Chapter 4 References

- 4.1 Cheon, Jae Seung and Jaewoo Jeon, "Investigation of the Main Control Design Factors to Improve Performance of Cable Puller Type and Caliper Integrated Type Electric Parking Brakes," SAE Paper No. 2009-01-3022, SAE International, Warrendale, PA, 2009.
- 4.2 Leiter, Ralf, "Design and Control of an Electric Park Brake," SAE Paper No. 2002-01-2583, SAE International, Warrendale, PA, 2002.
- 4.3 Huang, Chien-Tai, "Design and Testing of a New Electric Parking Brake Actuator," SAE Paper No. 2008-01-2555, SAE International, Warrendale, PA, 2008.
- 4.4 Barbosa, Manuel and Harry L. Worosz, "Aerostar Self-Adjusting Parking Brake System," SAE Paper No. 841696, SAE International, Warrendale, PA, 1984.
- 4.5 Winck, Ryder, Ngoo ChengShu, and Kenneth Marek, "Active Anti-Lock Brake System for Low Powered Vehicles Using Cable-Type Brakes," SAE Paper No. 2010-01-0076, SAE International, Warrendale, PA, 2010.

Chapter 5



Analysis of Hydraulic Brake Systems

5.1 Manual Hydraulic Brakes

PC-BRAKE HYDRAULIC software applies to the design of manual as well as vacuum-boosted hydraulic brake system. Their specific purpose is to facilitate lengthy mathematical calculations rather than to replace sound engineering understanding and judgement.

Manual or standard brakes use only the pedal effort by the driver to press the shoes against the drum, or pads against the rotors. No additional energy source is used. Manual brakes are only used on small and lightweight vehicles.

Application of the pedal force displaces the foot pedal, which in turn presses the pushrod into the master cylinder. The pedal linkage is designed to produce a mechanical force advantage or gain between the pedal and the master cylinder piston, resulting in a master cylinder piston travel which is less than the foot pedal travel.

The cross-sectional area of the master cylinder and the cross-sectional areas of the wheel cylinders are chosen to produce an increase of force transmitted between the master cylinder and the wheel cylinders. (NOTE: The term wheel cylinder refers to both drum and disc brakes, except where noted otherwise.) This force increase or gain is accomplished by having the total wheel cylinder cross-sectional areas greater than the master cylinder cross-sectional area. Because the master cylinder piston travel is limited by the pedal ratio and pedal travel, the gain ratio between master cylinder and wheel cylinders is limited, too. To keep the pedal force below a certain maximum value of approximately 445 N (100 lb), brake boosters in the form of vacuum assists or pump-pressured hydro-boosts are installed for heavier vehicles. See Eq. (5-18) for details.

The hydraulic brake line pressure p_ℓ produced by the pedal force F_p is determined by

$$p_\ell = F_p \ell_p \eta_p / A_{mc} \quad , \quad \text{N/cm}^2 \text{ (psi)} \quad (5-1)$$

where A_{mc} = master cylinder cross-sectional area, cm^2 (in.^2)

F_p = pedal force, N (lb)

ℓ_p = pedal lever ratio

η_p = pedal lever efficiency

A typical value for the pedal lever efficiency is 0.8, which includes the efficiency of the master cylinder and return springs.

The braking force F_x produced by one brake is obtained from the definition of the brake factor from Eq. (2-1). The rotor or drum drag force equals $F_d = [F_a]$ (BF) = $[(p_l - p_o)A_{wc}\eta_c](\text{BF})$. The brake torque equals $T_B = F_d r$. The braking force produced by the two brakes of one axle equals $F_x = 2T_B r/R$ or

$$F_x = 2(p_l - p_o)A_{wc}\eta_c\text{BF}(r / R) , \text{ N (lb)} \quad (5-2)$$

where A_{wc} = wheel cylinder area or caliper size (area), cm^2 (in.^2)

BF = brake factor

p_o = pushout pressure required to bring brake shoes or pads in contact with drum or rotor, N/cm^2 (psi)

r = drum or effective rotor radius, mm (in.)

R = tire radius, mm (in.)

η_c = wheel cylinder efficiency

Pushout pressures for disc brakes in good mechanical condition are small at 3.5 to 7 N/cm^2 (5 to 10 psi). Floating-caliper disc brakes with corroded slider surfaces may exhibit significantly larger pushout pressures. Pushout pressures for drum brakes are determined by the shoe return spring force and wheel cylinder area, and may assume values as high as 70 to 172 N/cm^2 (100 to 250 psi). The wheel cylinder efficiency is approximately 0.96 for drum and 0.98 for disc brakes.

The wheels-unlocked deceleration, a , of the vehicle is determined from the summation of the braking forces of all axles and Newton's second law, $a = \sum F_x/W$ or

$$a = (2 / WR)[(A_{wc}B\text{Fr}\eta_c)_F(p_l - p_o)_F + (A_{wc}B\text{Fr}\eta_c)_R(p_l - p_o)_R] , \text{ g-units} \quad (5-3)$$

where W = vehicle weight, N (lb)

The subscripts F and R indicate that the wheel brake parameters A_{wc} , BF , and r must be evaluated for the front and rear brakes, respectively. If more than two axles are braked, then the appropriate terms are added to Eq. (5-3).

For vehicles equipped with proportioning valves, the brake line pressures front and rear are not the same for pressures above the knee-point. See Eq. (5-11) for determining rear brake line pressures as a function of input or front brake line pressures.

5.2 Boost System Analysis

5.2.1 Overview and Requirements

Brake boost systems allow the driver to decelerate heavy vehicles with pedal force levels and pedal travels well within the acceptable range of the average driver. They contribute significantly to braking safety and driver comfort (Refs. 5.1, 5.2, 5.3, 5.4, 5.5, 5.6, 5.7). The boost assist or booster factor must be optimized relative to the vehicle involved. Safety considerations place certain requirements on booster design.

The following performance requirements should be observed in the design of a brake boost system:

1. The brake booster must be sensitive enough so that the operator can modulate braking effectiveness when low pedal forces are involved (low friction surfaces). Less than 13 to 22 N (3 to 5 lb) pedal force should initiate boost assist.
2. Pedal force/deceleration feedback must be provided so that the operator can gage the severity of braking through the level of pedal force feedback.
3. The booster response time should be less than 0.1 second to reach the saturation point in the event of a rapid brake application with pedal travel rates at 1 m/s (3 ft/s).
4. A smooth transition from boost to manual braking at the saturation point should be provided so that the operator will be able to continue to increase pedal force when the booster has failed.
5. Reliability should be high to minimize booster failure. Booster failure may contribute to operator confusion, including abandoning of brake application in an emergency. Some drivers think that the entire brake system has failed because the pedal feels hard without boost and the associated deceleration levels are lower than expected.
6. Small size and low weight to allow optimum design location within the engine compartment.
7. Boost ratios must not be excessive to provide sufficient braking effectiveness in case the boost assist has failed (racing engine, booster failure, engine running rough during cold-start).

5.2.2 Vacuum-Assisted Brake Booster

Vacuum-assisted hydraulic brakes, also called power brakes, use a vacuum booster as illustrated in Fig. 5-1 to assist the driver effort in pressing the shoes against the drums. The common system, sometimes called mastervac, is

mounted directly against the fire wall opposite the driver's foot. It is mounted between the foot pedal and the master cylinder. The assist force, acting on the pushrod which actuates the master cylinder piston, is produced by the difference in pressure across the booster piston or diaphragm, with the vacuum or low pressure on the master cylinder side, and the atmospheric or high pressure on the input side. The level of assist force for a given pedal force is controlled by the reaction disc shown in Fig. 5-2. The rubber-like material of the reaction disc acts like a hydraulic fluid, producing equal pressures against all surfaces it contacts. The result is a finely modulated atmospheric air pressure inlet valve with correspondingly modulated pushrod forces against the master cylinder pushrod piston. The vacuum developed in the intake manifold of gasoline engines is generally sufficient to fully actuate the booster, except when operating at high revolutions. Diesel engines require a separate vacuum pump due to their insufficient manifold vacuum, caused by the absence of a throttle. Vacuum pumps are of the vane-, diaphragm-, or piston-type design. Vane-type vacuum pumps require engine oil lubrication to seal and produce proper vacuum.

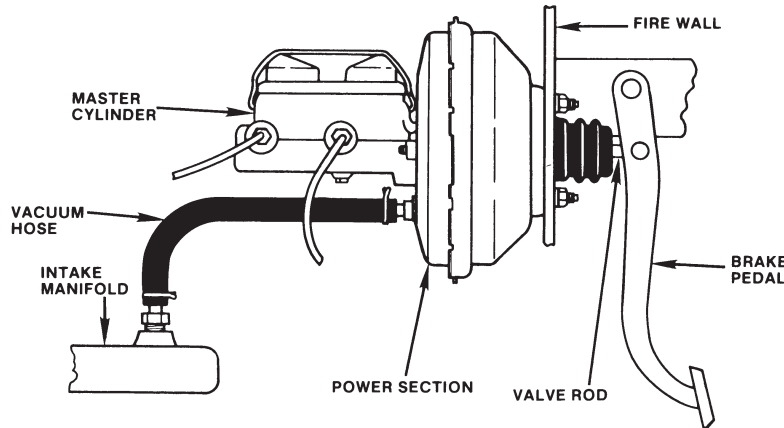


Figure 5-1. Vacuum-booster master cylinder (Bendix).

Due to their limited amount of assist, both in terms of booster pressure and booster size, vacuum-assisted boosters generally are used for master cylinder volumes of only up to 24.6 cm^3 (1.5 in.³).

Dual diaphragm or tandem vacuum boosters are used to increase boost force.

5.2.2.1 Vacuum Booster Analysis

The boost ratio B is defined as the ratio of the pushrod force against the master cylinder piston to the pedal effort input into the booster,

$$B = (F_p \ell_p + F_A) / F_p \ell_p \quad (5-4)$$

where F_A = booster force, N (lb)

F_p = pedal force, N (lb)

ℓ_p = pedal lever ratio

In the past vacuum boosters increased the pedal effort gain by as much as eight or nine to one for most heavy domestic passenger cars, and approximately three to four for smaller cars. A gain of eight means that the effect of the pedal force is increased eightfold. Although this high gain permits maximum braking effectiveness with small pedal forces, in the event of a booster failure the driver will most likely not be able to produce sufficient pedal force to decelerate the vehicle at an acceptable level (Ref. 5.1).

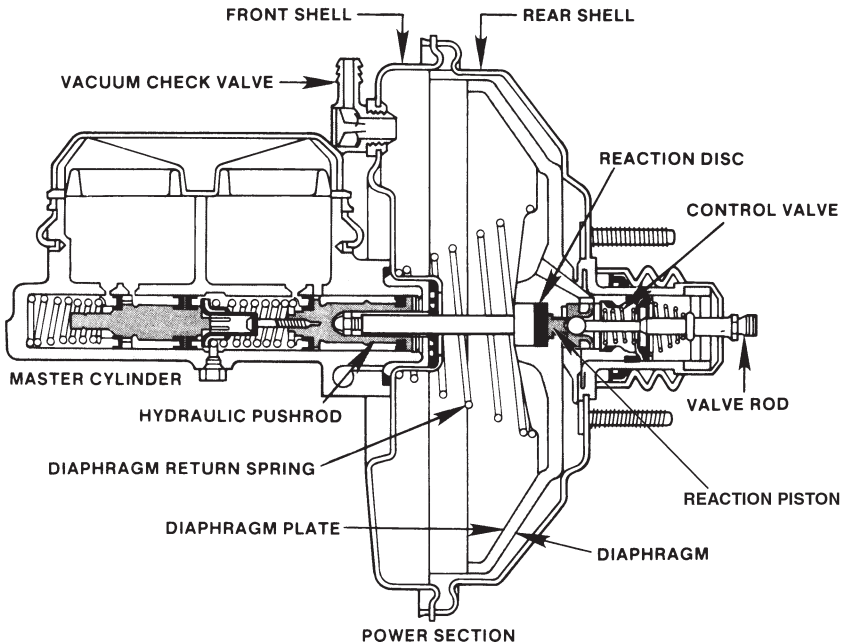


Figure 5-2. Bendix single-diaphragm mastervac.

The brake line pressure p_e is determined by an expression similar to Eq. (5-1); however, it is modified by the boost ratio B as

$$p_e = F_p \ell_p \eta_p B / A_{mc} \quad , \quad \text{N/cm}^2 \text{ (psi)} \quad (5-5)$$

The boost ratio can be computed from the basic dimensions and spring forces associated with a basic mastervac, as illustrated in Fig. 5-2. The outer diameter of the reaction disc is D_o . The diameter of the reaction piston is D_r . The computations that follow are carried out for a single-diaphragm mastervac with 203 mm (8 in.) diameter diaphragm. The diameter of the reaction disc and reaction piston are 30.7 and 18.5 mm (1.21 and 0.729 in.), respectively.

The pushrod force produced by the boost assist is computed first.

The effective booster area A_B is equal to the booster area minus the pushrod area,

$$A_B = 20.3^2 \pi / 4 - 0.838^2 \pi / 4 = 323 \text{ cm}^2$$

$$[A_B = 8^2 \pi / 4 - 0.33^2 \pi / 4 = 50.18 \text{ in.}^2]$$

where a pushrod diameter of 8.38 mm or 0.838 cm (0.33 in.) was assumed.

The booster force F'_B for an effective vacuum of 7.928 N/cm² (11.47 psi; 80% of maximum) and a mechanical efficiency of 0.95 is

$$F'_B = 323(7.928)(0.95) = 2432.7 \text{ N}$$

$$[F'_B = 50.18(11.47)(0.95) = 546.9 \text{ lb}]$$

The effective booster force F_B is smaller due to the diaphragm piston return spring force opposing the boost action. Hence,

$$F_B = 2432.7 - 155.7 = 2277 \text{ N}$$

$$[F_B = 546.9 - 35 = 511.9 \text{ lb}]$$

where a return spring force of 155.7 N (35 lb) was assumed. The computations thus far show that the booster portion produces a hydraulic pushrod force of 2277 N (511.9 lb).

The manually produced force against the hydraulic pushrod is computed next.

The rubber reaction disc acts similar to a pressurized hydraulic fluid. The pressure in the reaction disc p_r is equal to the effective booster force divided by the difference in cross-sectional area of the reaction disc A_2 and the reaction piston A_1 ,

$$p_r = \frac{2277(4)}{(3.07^2 - 1.85^2)\pi} = 483 \text{ N / cm}^2$$

$$\left[p_r = \frac{510.2(4)}{(1.21^2 - 0.729^2)\pi} = 696.5 \text{ psi} \right]$$

The control pressure p_r is acting against any surface in contact with the reaction disc. Because the reaction piston is pushing against a portion of the reaction disc, the reaction piston force F_r is equal to the reaction pressure multiplied by the reaction piston area A_1 , hence

$$F_r = p_r A_1 = 483(1.85)^2(\pi / 4) = 1298 \text{ N}$$

$$[F_r = p_r A_1 = 696.5(0.729)^2(\pi / 4) = 290.7 \text{ lb}]$$

The reaction piston force is opposed by the reaction piston return spring force. For a 203 mm (8 in.) diameter vacuum booster, the return spring force is approximately 66.7 N (15 lb). Consequently, the effort against the pushrod piston of the master cylinder produced by the foot pedal is 1298 + 66.1 = 1364 N (290.7 + 15 = 305.7 lb).

The total force on the master cylinder pushrod piston and, hence, the brake line pressure producing force is equal to the sum of the effective booster force and reaction piston force, or 2277 + 1298 = 3575 N (510.2 + 290.7 = 800.9 lb).

Finally, the vacuum boost ratio B is given by the ratio of pushrod force on the master cylinder piston to the reaction piston force

$$B = 3575 / 1298 = 2.75$$

$$[B = 800.9 / 290.7 = 2.75]$$

It is interesting to note that the booster factor B is also equal to the ratio of reaction disc area A_2 to reaction piston area A_1 , or

$$B = A_2/A_1 = 3.07^2/1.85^2 = 2.75$$

$$[B = A_2/A_1 = 1.21^2/0.729^2 = 2.75]$$

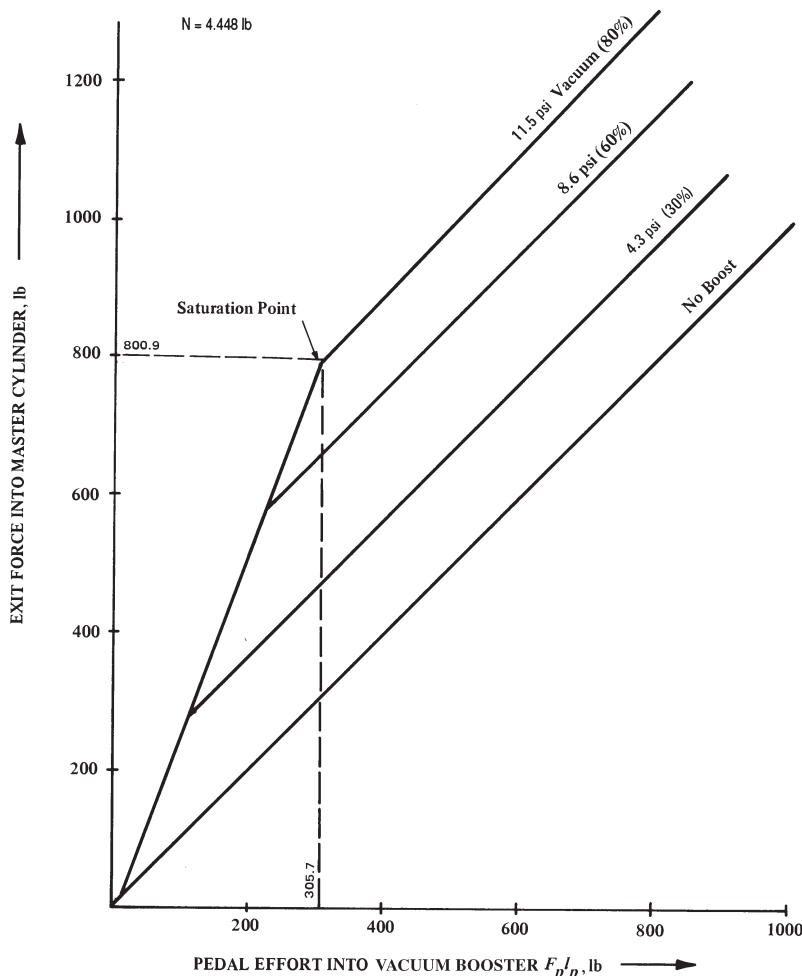


Figure 5-3. Vacuum booster characteristics.

The theoretical results may be used to construct a diagram illustrating the booster performance. In Fig. 5-3, the pushrod force on the master cylinder piston versus the pedal force multiplied by the pedal lever ratio is shown. As

can be seen, the booster has a maximum assist of approximately 3561 N (800.9 lb). For decelerations requiring higher brake line pressures and, hence, pushrod forces, the additional work input into the vacuum booster must come from the pedal effort, i.e., the driver. The booster saturation point should not be reached for decelerations less than 0.9 to 1 g.

Also shown in Fig. 5-3 are the different booster output forces as a function of different levels of vacuum. The vacuum booster analysis presented for a given booster size may be expanded to a general analysis relating the various parameters in graphical form as shown in Fig. 5-4. The use of the chart is as follows for a vehicle with the values presented here.

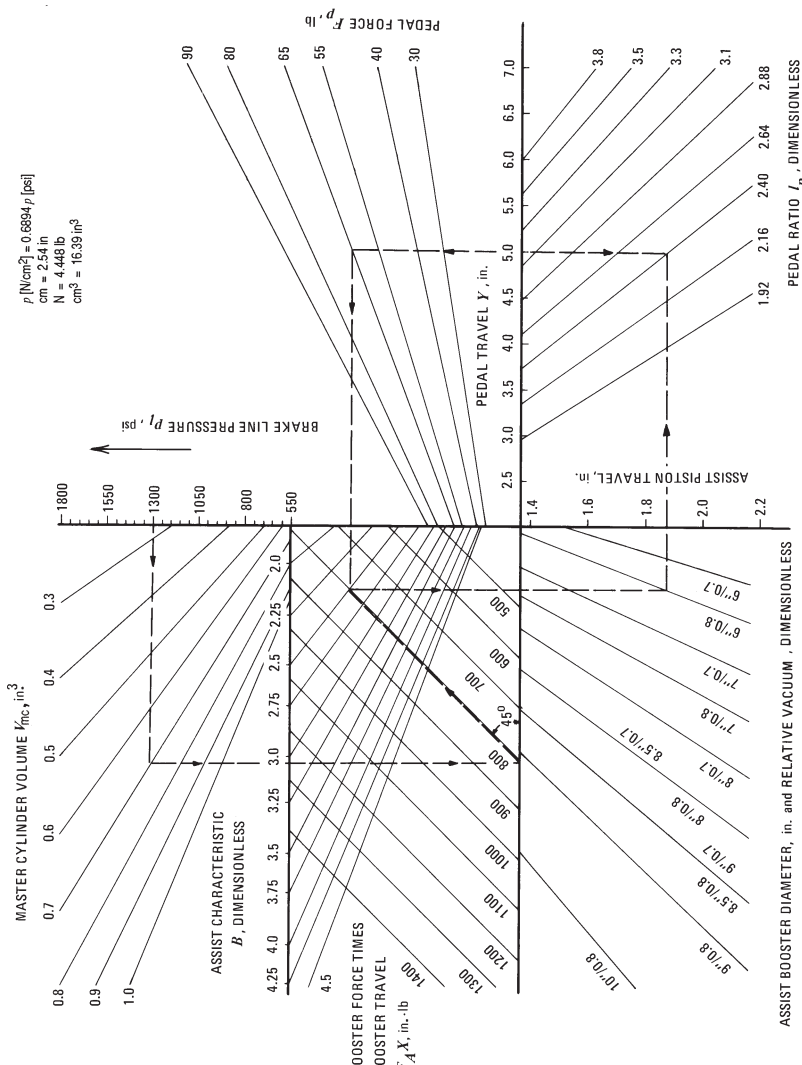


Figure 5-4. Vacuum booster design chart.

1. Given

- Pedal force $F_p = 289 \text{ N (65 lb)}$
- Pedal travel $Y = 127 \text{ mm (5.0 in.)}$
- Brake line pressure $p_\ell = 896 \text{ N/cm}^2 (1300 \text{ psi})$
- Master cylinder volume $V_{mc} = 11.5 \text{ cm}^3 (0.7 \text{ in.}^3)$

2. Find

- Booster work $F_A X$
- Boost ratio B
- Booster diameter
- Relative vacuum
- Booster piston travel
- Pedal lever ratio ℓ_p

The solution is illustrated by broken lines in the chart (Fig. 5-4).

3. Solution

a. Booster work $F_A X$:

- Draw a horizontal line from the brake line pressure $p_\ell = 896 \text{ N/cm}^2 (1300 \text{ psi})$ to the line representing $V_{mc} = 11.47 \text{ cm}^3 (0.7 \text{ in.}^3)$.
- From the point of intersection of the horizontal line with the line representing $V_{mc} = 11.47 \text{ cm}^3 (0.7 \text{ in.}^3)$, drop a vertical line to the second horizontal line on the chart.
- The intersection of the vertical line with the second horizontal line gives the booster work $F_A X$, which, in this case, is $90.4 \text{ Nm (800 lbin.)}$.

b. Boost ratio B:

- Draw a vertical line from the pedal travel $Y = 127 \text{ mm (5.0 in.)}$ to the line representing pedal force $F_p = 289 \text{ N (65 lb)}$.
- From the intersection of the vertical line with $F_p = 289 \text{ N (65 lb)}$, draw a horizontal line to the left.
- From the point representing booster work $F_A X = 90.4 \text{ Nm (800 lbin.)}$ draw a line extending upward at an angle of 45 deg .
- The intersection of the horizontal line with the one drawn at 45 deg gives a boost ratio of $B = 2.5$.

- c. Booster diameter and relative vacuum:
 - (1) Drop a vertical line from the point established in b(4).
 - (2) The intersection of this vertical line with one of the booster lines gives acceptable values of booster diameter and relative vacuum. In this case let the vertical line intersect the line representing booster diameter and relative vacuum of 152.4 mm/0.8 (6 in./0.8).
- d. Pedal ratio ℓ_p :
 - (1) Drop a vertical line from pedal travel $Y = 127$ mm (5.0 in.).
 - (2) Draw a horizontal line through the point established in c(2).
 - (3) The intersection of the vertical and horizontal lines gives the pedal ratio, in this case $\ell_p = 2.4$.
- e. Booster piston travel:
 - (1) The intersection of the horizontal line established in d(2) with the vertical axis determines the booster piston travel, in this case approximately 47.5 mm (1.87 in.).

If a different booster diameter and/or relative vacuum is chosen, then the pedal travel and booster piston travel change accordingly. For example, with a booster diameter of 178 mm (7 in.) and a relative vacuum of 0.7, the pedal ratio becomes 2.88 and the booster piston travel 39 mm (1.54 in.). If desired, a pedal ratio may be selected rather than the booster diameter and/or relative vacuum. The choice of booster diameter or pedal ratio is a function of the space available for the installation of the booster or foot pedal. In addition, the master cylinder volume must meet the requirements of the brake fluid volume analysis discussed in Section 5.4.

5.2.2.2 Hydrovac Analysis

In the mastervac the amount of assist force is controlled by a rubber-like reaction disc. In the hydrovac the application is controlled by the hydraulic fluid pressure produced by the operator. The hydrovac unit can be located anywhere on the vehicle, with the frame rails near the driver's cab being the preferred location. The design of a typical hydrovac is shown in Fig. 5-5, with the brakes in the applied position. The hydrovac consists of the vacuum cylinder (1) with piston (2), return spring (3), and pushrod (4). The control pipe (5) connects the left chamber of the vacuum cylinder with the lower chamber of the membrane (6) of the vacuum valve, while the right chamber of the vacuum cylinder is connected to the vacuum inlet (7) leading to the engine manifold. The right side of the vacuum cylinder is also connected to the upper side of the membrane (8). The hydraulic cylinder consists of the cylinder (9), the piston (10) equipped with a check valve (11), and the pushrod (4).

In the "off" position, piston (2) is held at the left side of the vacuum cylinder

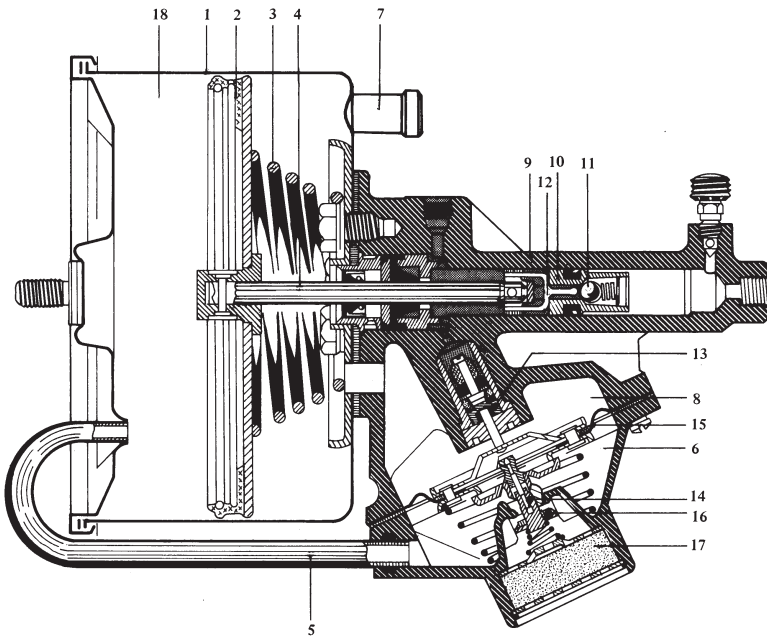


Figure 5-5. Hydrovac in “on” position.

by the return spring (3). In this position, the arm (12) of the piston (10) rests against the back plate, and the ball of the check valve (11) is lifted off the seat. The control piston (13) is located at its uppermost position, thus separating the control valve (14) from the seat of the membrane.

During application of the driver-operated master cylinder located at the fire wall, the line pressure is transmitted through the check valve into the brake system and to the wheel brakes. At the same time the hydraulic pressure in front of the control piston (13) begins to rise, moving the piston and membrane downward until the membrane contacts the control valve (14). At this moment the two chambers to the left and right of the vacuum piston (2) are separated. Any further motion of the membrane (15) downward will open the ambient valve (16).

The atmospheric air flows past the air filter (17) through the ambient valve (16) into the valve chamber (6) and through the control pipe (5) into the cylinder chamber (18), resulting in a rightward motion of the piston (2), pushrod (4), and piston (10). The check valve (11) will be closed as a result of the movement of the piston (10) to the right, allowing the line pressure to increase and to be transmitted to the wheel brakes. The vacuum difference across piston (2) is identical to the pressure difference across the membrane (15). The position of the membrane (15) is determined by the pressure in the pedal-master cylinder and the pressure differential across the membrane. Any change in pedal force will cause a corresponding change in vacuum application and, hence, pressure differential across the piston (2), allowing a sensitive control of the brake application.

Vacuum boosters have been installed on trailers to increase braking effectiveness (Ref. 5.8).

5.2.3 Hydraulic Brake Booster

In the hydraulic boost system, the energy source is pressurized fluid. In most cases the steering pump is used (Refs. 5.9, 5.10). The brake system remains totally conventional with only the booster and plumbing added. Because two incompatible fluids are used in the two different circuits, extreme care must be taken not to contaminate one circuit with the fluid of the other. If it does occur, all seals must be replaced. Its compact size and high pressure potential allow it to be used in virtually all applications from passenger cars to light- to medium-weight trucks. Although certain details vary between manufacturers, the hydraulic booster without accumulator is limited to master cylinder volumes of 33 to 41 cm³ (2 to 2.5 in.³). A schematic of a hydraulic boost system is shown in Fig. 5-6. The pressure line runs from the steering pump to the brake booster, and from there to the steering gear and back to the reservoir. A spool valve in the brake booster controls the fluid flow from the steering pump. Without any brake application, the fluid flow is not affected. During braking the fluid flow is restricted, resulting in a corresponding pressure rise in the fluid and pressure application to the booster piston. The spool valve is designed so that the brake and steering operations do not interfere during either apply or release operation.

A reserve pressure accumulator is provided which allows two to three brake applications with the pump failed or engine stalled. In the '70s, a spring-loaded accumulator was used, either integral with the booster, or separately mounted in the engine compartment. Later, a gas-charged accumulator was used for energy storage in the event of a pump failure.

For medium- to heavy-vehicle applications, an electrical pump is used as a reserve energy source. In the event that the normal fluid flow from the steering pump is interrupted, the integral flow switch inside the booster closes, which energizes a power relay and provides electric power to the pump. The reserve pump then circulates the fluid throughout the system and builds up pressure as demanded. Master cylinder volumes up to 107 to 115 cm³ (6.5 to 7 in.³) are accommodated by the electric reserve pump design booster.

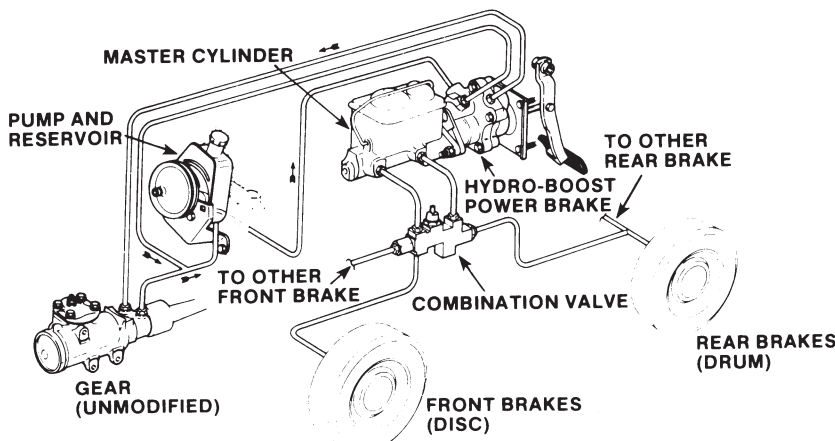


Figure 5-6. Hydroboost brake system (Bendix).

Because a single steering pump is used to assist power brakes and power steering, the pump must have sufficient flow rate to accommodate both systems in the event of a combined severe braking and steering maneuver to avoid lack of steering assist.

Modifications to the basic hydraulic booster system have been introduced where the steering pump charges a gas-charged accumulator, which, in turn, pressurizes brake fluid. As the driver applies pedal force, the regulated brake fluid pressure is transmitted to the wheel brakes. The advantages of this system include increased reserve capacity in the event of a pump failure, quicker brake torque response time because the brake line pressure does not have to be built up from zero, and sufficient energy source for ABS application and for combined braking and steering maneuvers.

The size of the accumulator is a function of vehicle weight and the number of stops required by one accumulator charge. The schematic of a hydraulic booster is shown in Fig. 5-7. The pressure p_B supplied by the accumulator to the booster in addition to the pedal effort by the driver acts on the master cylinder piston, which, in turn, produces the hydraulic brake line pressure to the wheel brakes.

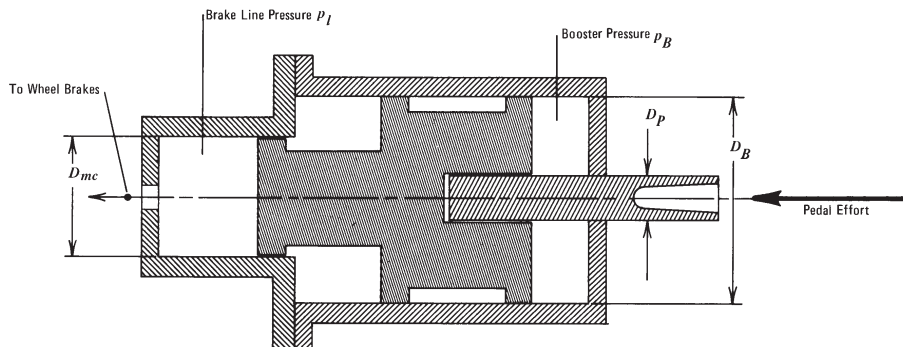


Figure 5-7. Schematic of hydraulic booster.

The effective input force to the booster is determined by the booster area and the pushrod cross-sectional area.

The booster input area ratio A_R is given by

$$A_R = (D_B / D_p)^2 \quad (5-6)$$

where D_B = booster piston diameter, cm (in.)

D_p = pushrod diameter, cm (in.)

The booster pressure ratio p_R is defined by the ratio of output pressure to input pressure and may be expressed in terms of the diameters as

$$p_R = (D_B / D_{mc})^2 \quad (5-7)$$

where D_{mc} = output to master cylinder diameter, cm (in.)

The brake line pressure may be determined for a given booster pressure (or accumulator pressure) once the booster pressure ratio has been computed. With the brake line pressure determined, vehicle deceleration is computed by Eq. (5-3).

The boost circuit fluid volume, i.e., size and operating pressure range of the accumulator, are a function of the maximum accumulator pressure p_A and the initial gas charge pressure p_G of the gas used for energy storage by the accumulator. The volume ratio V_R of the booster is defined by the ratio of the volume displaced at the booster side to the volume displaced at the output side and is determined by

$$V_R = (D_B^2 - D_p^2) / D_{mc}^2 \quad (5-8)$$

A typical booster characteristic is shown in Fig. 5-8, indicating both boosted and no-boost performance.

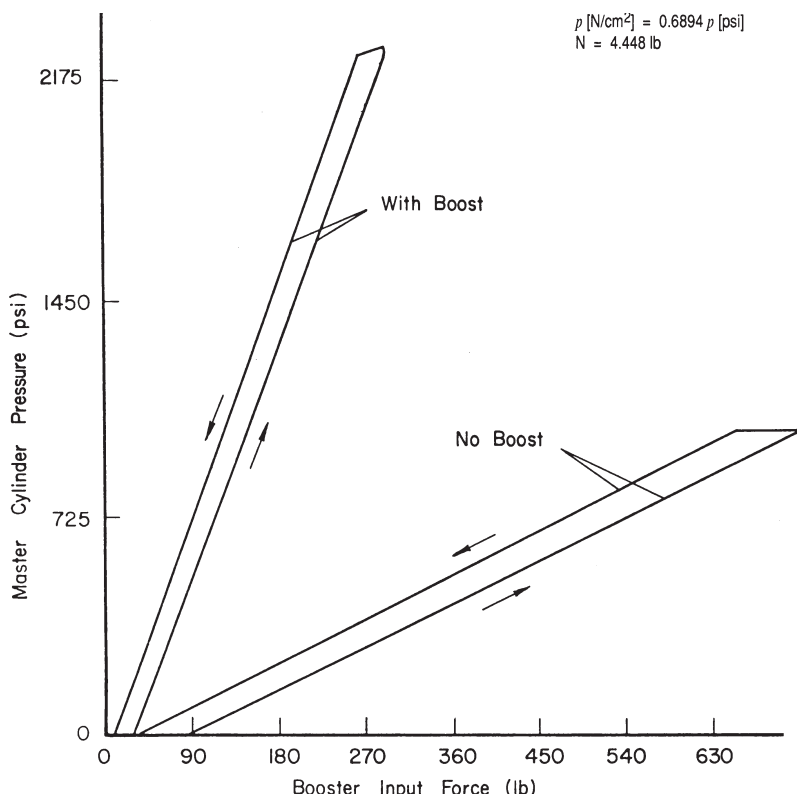


Figure 5-8. Master cylinder pressure vs. booster input force.

The minimum size of the accumulator required for a safe deceleration of a vehicle in successive stops may be obtained from the accumulator design chart shown in Fig. 5-9.

It is assumed for the preparation of the accumulator design chart that approximately 67% of the master cylinder volume is required for an emergency stop. The example illustrated in Fig. 5-9 indicates that a vehicle having a master

cylinder volume $V_{mc} = 49 \text{ cm}^3$ (3.0 in.³), five emergency stops, a volume ratio $V_R = 2.4$ computed by Eq. (5-8), and a pressure ratio $p_G/p_A = 0.35$ requires an accumulator size of approximately 623 cm^3 (38 in.³).

If the same energy had to be stored by a vacuum-assist unit, a volume approximately 40–50 times larger than that associated with a medium-pressure accumulator, or 100–130 times larger than that associated with a high-pressure accumulator would be required.

The energy stored in the accumulator is affected by the ambient temperature. The fluid volume available for braking at high pressures decreases with decreasing temperature. For example, an accumulator having a volume of 656 cm^3 (40 in.³) available between the pressure range of 1448 to 1792 N/cm^2 (2100 to 2600 psi) when operating at 353 K (176°F), provides only 246 cm^3 (15 in.³) when the temperature is 233 K (-40°F) (Ref. 5.2).

For vehicles that do not have a steering pump, and to avoid the potential problems associated with the use of two different fluids, an integral accumulator/pump system has been designed. It is operated with brake fluid only. Because brake fluid does not provide adequate lubrication for long periods of operation, an intermittently operating electrical pump is used to charge the accumulator only when needed. The compact design is advantageous for installation in the crowded engine compartment. The basic design has been expanded for application to ABS braking systems.

5.2.4 Full-Power Hydraulic Brakes

All hydraulic brake systems discussed in earlier sections had the ability for the driver to manually apply the brakes in the event of a power or energy source failure, however at extremely low braking effectiveness.

In the full-power hydraulic brake system, the pedal effort is only used to modulate and control the amount of assist demanded. The pedal force itself is not involved in pressing the brake shoes against the drum. Because no manual backup system exists except for the parking brake, the hydraulic system has many components in dual fashion. The brake system consists of one or two pumps, two accumulators, a dual circuit control valve, the hydraulic lines and hoses, and the wheel brakes. In the past, Rolls Royce used two pumps and accumulators for each individual circuit, and mineral oil as working fluid. Extreme care must be taken not to contaminate the mineral oil with regular brake fluid because mineral oil-resistant rubber components are made of neoprene and will be damaged if they come in contact with polyglycolether-based brake fluid. The pumps used are either vane or radial piston designs. Vane pumps are generally limited to a pressure of approximately 965 N/cm^2 (1400 psi); extreme pressure levels may go as high as 1379 N/cm^2 (2000 psi). Radial piston pumps may produce pressures up to 2068 N/cm^2 (3000 psi).

5.2.5 Comparison of Brake Boost Systems

A comparison of hydraulic and full-power boost systems with vacuum-assisted brakes indicates the latter to be the most economical power source, assuming

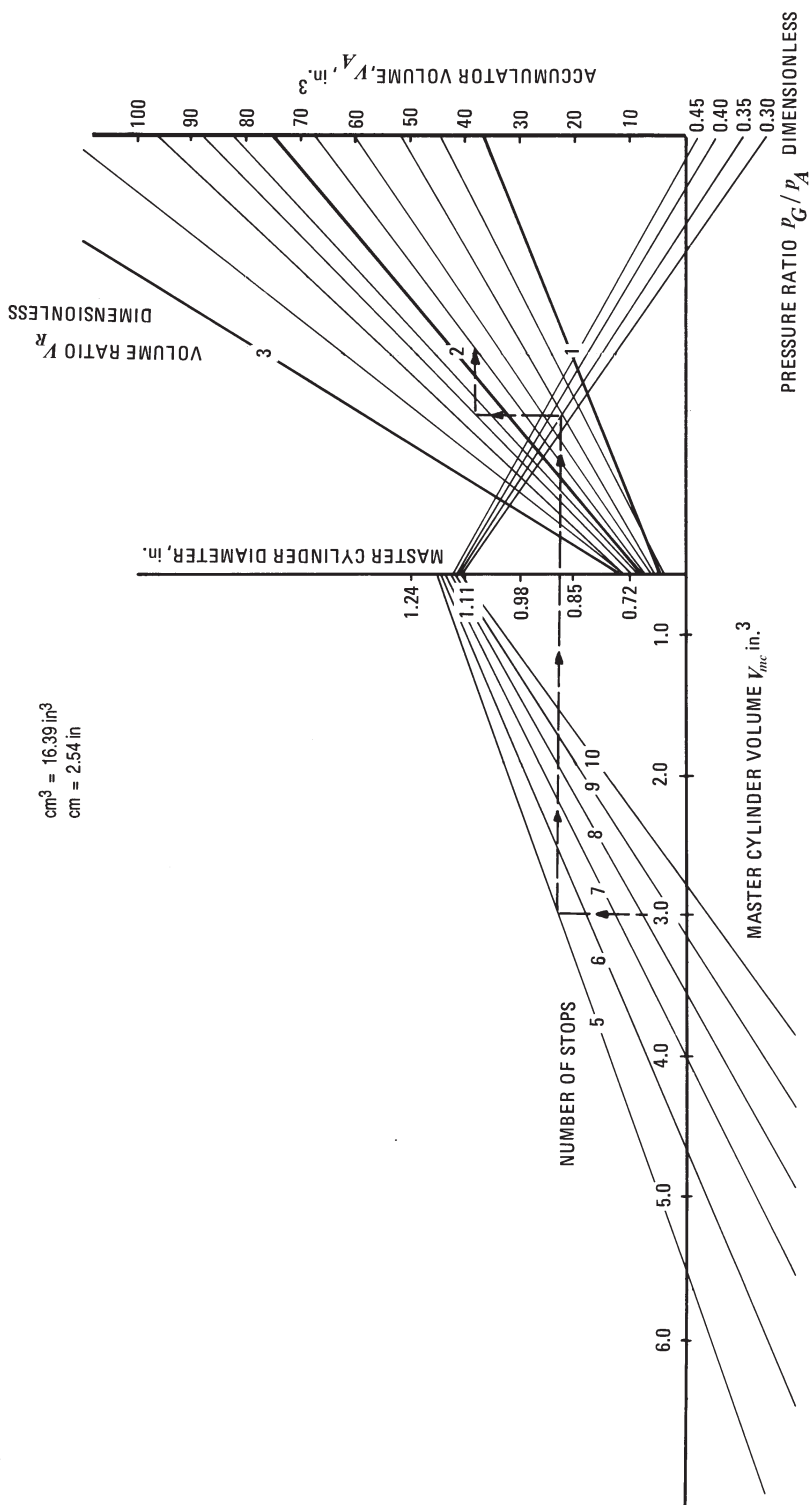


Figure 5-9. Accumulator design chart.

that a sufficient quantity of vacuum is available. However, exhaust emission regulations and fuel injection systems have greatly reduced the degree of vacuum available as energy source. In addition, diesel engine-powered vehicles require an additional vacuum pump. Consequently, more and more future designs will require a hydraulic energy source consisting of a pump and, if necessary, a gas-loaded accumulator. For light- to medium-weight trucks, the vacuum booster capacity is generally too small for an adequate brake boost system. Modern ABS and ESC systems require a pump to produce sufficient brake fluid volume at high pressures at minimum delay time.

5.3 Brake Line Pressure Control Devices

Because the rear axle normal force decreases as deceleration increases, relatively less brake line pressure is required on the rear brakes to keep the rear brakes from locking before the front brakes. In addition, differences in load distribution for the lightly and fully laden cases require different brake torque balance front to rear for the empty and laden vehicle. Different valve designs are used to affect brake force distribution front to rear (Ref. 5.11).

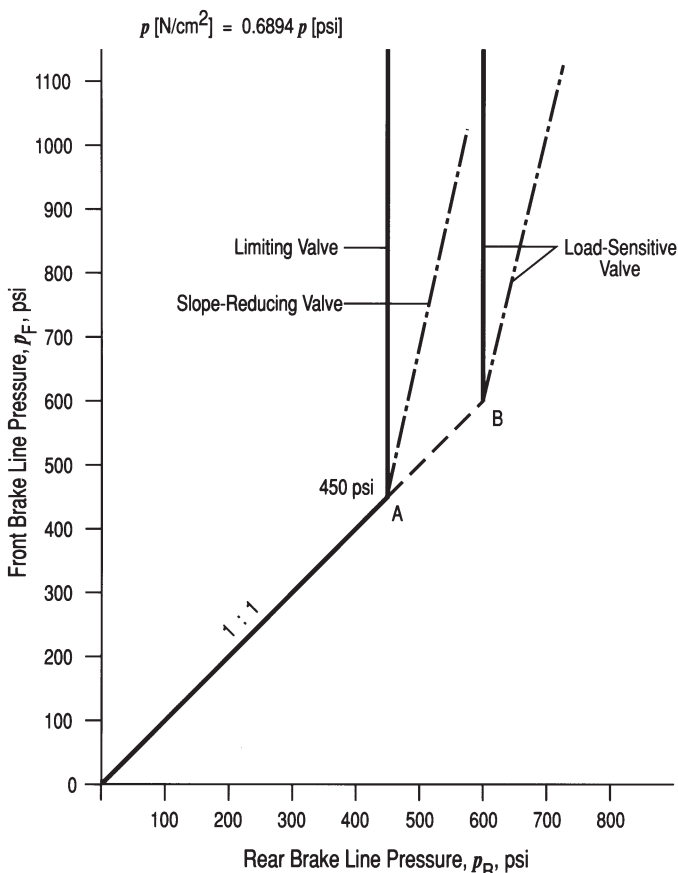


Figure 5-10. Rear brake-line pressure valve characteristics.

5.3.1 Brake Line Pressure Limiter Valve

A typical pressure curve of a limiter valve is shown in Fig. 5-10. Up to a brake line pressure of 310 N/cm^2 (450 psi) chosen in this example, both front and rear brakes receive equal pressures. For brake line pressures beyond 310 N/cm^2 (450 psi), the rear brake line pressure remains at a constant 310 N/cm^2 (450 psi), while the front brake line pressure increases. Consequently, for braking maneuvers with the front brakes locked, any further pedal force increase will not increase vehicle deceleration because the rear brake line pressure cannot be increased any further with the limiting valve.

A schematic of a limiter valve is shown in Fig. 5-11. The master cylinder pressure enters the limiter valve at A. Spring force (5) holds valve (2) open, and the master cylinder pressure can pass through the valve to the outlet B and to the rear brakes. As the pressure increases on top of the piston, the pressure force overcomes the spring force (5) and closes valve (2), at which point no further pressure increase occurs at outlet B, thus limiting the pressure in the rear circuit. If the brake fluid volume increases in the rear circuit due to lining wear or drum expansion, then the pressure at B decreases; valve (2) opens briefly to allow a slight pressure increase to the rear until valve (2) closes again.

When the pedal force is lowered or fully released, the pressure at B is greater than the pressure at A, and the valve seat (6) moves against the spring force (6), releasing the pressure, and valve (2) returns to its released position, permitting a free fluid flow from inlet A to outlet B.

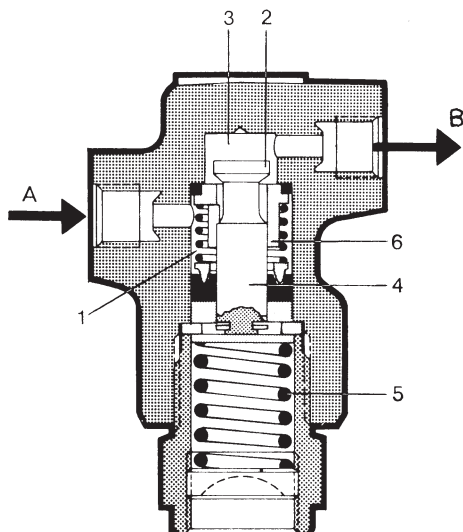


Figure 5-11. Limiter valve (Continental Teves).

As more weight is placed in the vehicle, more braking force can be utilized by the rear brakes before locking up. This increase in rear brake line pressure is accomplished by load-sensitive or suspension-height-sensitive valves. For a given valve geometry the spring force (5) determines the switch point from the 1:1 slope to the limited condition. In load-sensitive valve designs, the spring

force is increased through cam and lever action as the suspension deflects as more weight is placed into the vehicle. The increased spring force moves the knee-point from point A in Fig. 5-10 to point B. For the example chosen, the rear brake line pressure is now limited to 414 N/cm^2 (600 psi), that is, 103 N/cm^2 (150 psi) more than for the lightly loaded case.

5.3.2 Brake Line Pressure Reducer Valve

With the reducer valve, also called proportioning valve, the rear brake line pressure is identical to the front brake line pressure up to the knee-point pressure. For higher pressures the rear brake line pressure increases at lower amounts than that of the front brakes, as illustrated in Fig. 5-10. The advantages of the reducer over the limiter valve include increasing rear brake forces after the front brakes have locked, and front and rear brake line pressures that are closer to the optimum values (Chapter 7).

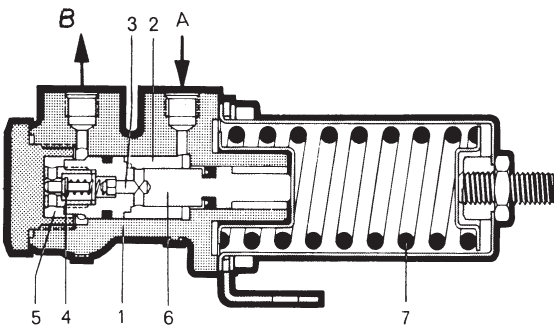


Figure 5-12. Brake line pressure reducer valve (Continental Teves).

A typical schematic of a reducer valve is shown in Fig. 5-12. The master cylinder brake line pressure enters at A and reaches the rear brakes spaces (2, 3, and 5) and through outlet B, because the spring force (7) has pushed the differential piston (6) to the left, which opens valve (4). The difference in pressurized surface area of piston (6) acts against the spring force (7). When the switch point pressure is reached, the piston moves to the right until valve (4) closes. With valve (4) closed, no further pressure increase develops in space B until the increased pressure on the right side of piston (6) pushes the piston slightly to the left so that valve (4) opens again, allowing the brake line pressure to increase again at B. The piston oscillates back and forth, allowing the pressure to increase to the rear brakes in direct relationship to the ratio of the ring area to full area of piston (6). When the brakes are released, the higher pressure at B opens valve (4) against the small valve spring, and piston (6) returns to its released position.

Brake systems with front-to-rear dual hydraulic split generally have a proportioning valve bypass feature if the front circuit fails. Under these conditions the rear brakes will receive full master cylinder pressure at all levels of brake line pressure because the reducer function of the valve is locked out.

When the spring force pushing against the differential piston is made a function of the weight carried by the vehicle, the switch or knee-point can be moved to

higher pressure levels. These variable knee-point valves are commonly known as load- or height-sensitive proportioning valves.

Height-sensitive proportioning valves (HSPV) were used on a number of cars, light trucks, and vans. Starting in the early '80s through the late '80s, most domestic manufacturers used HSPVs on pickup trucks and vans. In many light trucks the HSPV was added to the normal combination valve system so that it would further reduce the rear brake line pressure and knee-point pressure when lightly loaded, but be ineffective when loaded. Many foreign manufacturers used HSPVs on smaller front-wheel-driven cars such as the VW Golf. With the introduction of ABS brakes, height-sensitive brake pressure proportioning was removed from many vehicles.

The theoretical reducer knee-point pressure p_K may be determined from a basic force analysis on the differential piston as

$$p_K = 4F_s / \pi D^2 (SL) , \text{ N/cm}^2 \text{ (psi)} \quad (5-9)$$

where D = large piston diameter, cm (in.)

F_s = spring force, N (lb)

SL = reducer slope

The theoretical reducer slope SL is expressed by the area or diameter-squared ratios as

$$SL = 1 - (d / D)^2 \quad (5-10)$$

where d = small piston diameter, cm (in.)

D = large piston diameter, cm (in.)

It must be recognized that manufacturing tolerances and frictional factors will affect the performance of the reducer valve. Furthermore, the performance characteristic during pressure increase will differ somewhat from that achieved during pressure release.

With the reducer valve characteristic indicated in Fig. 5-10, for pressures above the knee pressure the rear brake line pressure p_R is determined by

$$p_R = p_K + (p_{mc} - p_K)SL , \text{ N/cm}^2 \text{ (psi)} \quad (5-11)$$

where p_K = knee-point pressure, N/cm² (psi)

p_{mc} = master cylinder pressure, N/cm² (psi)

SL = reducer slope

In some designs, proportioning valves involving accumulators and solenoids use the ABS signal from the rear brakes to adjust the rear brake line pressure more closely to the optimum values.

5.3.3 Combination Valves

In the past, two or three different functions were combined into one valve, commonly called the combination valve. The functions included the proportioning valve, the metering valve, and the differential pressure switch, which is activated in the event of a hydraulic leak in one of the dual brake circuits.

The metering valve is used to improve front-to-rear brake balance when braking on low-friction surfaces, that is, at low brake line pressures. The metering valve prevents application of the front disc brakes for pressures up to approximately 51.7 to 93 N/cm² (75 to 135 psi). During this pressure increase, although the front brakes are not braking yet, the rear brake return spring forces are overcome so that rear brake shoes contact the drum at nearly the same time the front brake pads contact the rotor surface. Metering valves are used primarily for rear-wheel-driven vehicles, using the front disc/rear drum brake system. Front-wheel-driven vehicles in many cases do not use metering valves because the engine inertia turning on the front rotors requires brake line pressure in line with the rear brakes before brake lockup occurs on low-friction surfaces.

5.3.4 Deceleration-Sensitive Reducer Valves

With this valve design the brake line pressure at which the rear brakes receive a reduced amount of brake line pressure is a function of vehicle deceleration. The switch point is not as clearly identified as in the case of the pressure-dependent valves discussed earlier. The pressure switch point is a function of the pedal force apply rate, the basic brake system characteristics, and the amount of any residual air present in the rear brake line circuit (Ref. 5.12).

The basic designs involve a specific mass which moves due to braking inertia. In the Bendix design the mass rolls horizontally on steel balls against a preloaded spring. As soon as the spring force is overcome, the differential piston commences its pressure-reducing function. The corresponding deceleration level at the switch point is approximately 0.7 g. The inertia mass is held in place by a small spring/piston system to eliminate any "deceleration noise" prior to approximately 0.7 g.

In the Girling design, illustrated in the basic schematic of Fig. 5-13, a steel ball travels on an incline, according to the inertia force acting on the ball during braking, when the switchover deceleration point has been reached. The upward movement of the ball closes off the opening to the rear circuit. Further brake line pressure increases from the master cylinder result in the reducing function of the differential piston.

A typical brake line pressure performance chart for a deceleration-sensitive valve is shown in Fig. 5-14. The brake line pressures increase at equal amounts up to the switch point A. At this moment the ball has closed off the opening to the rear brakes, and no further brake line pressure increase occurs at the rear brakes. As the brake line pressure from the master cylinder increases at the valve inlet and against the small area of the differential piston, the differential piston begins to move away from the ball, allowing a small amount of brake

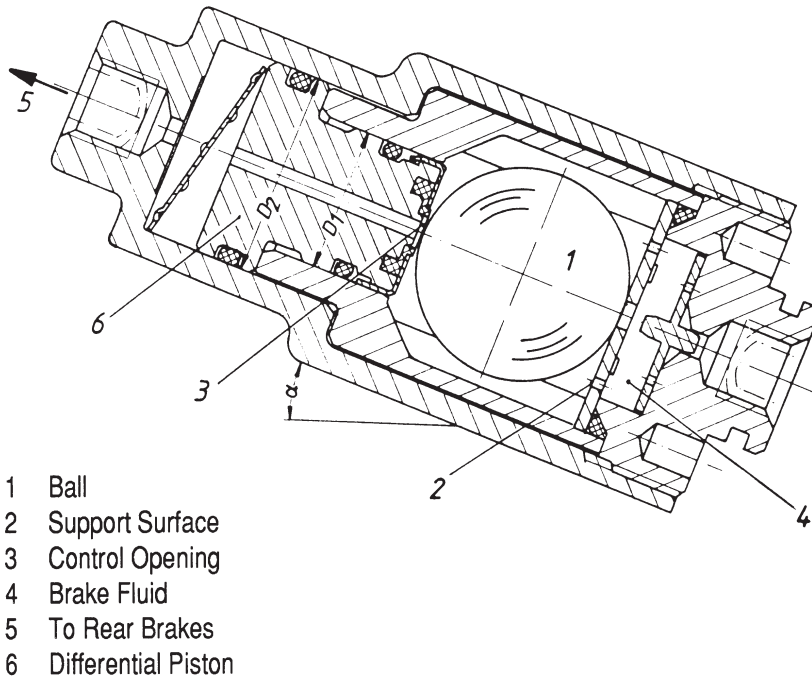


Figure 5-13. Girling G-valve.

fluid to enter the rear brake circuit and resulting in a corresponding pressure increase at the rear brakes. However, the ball again closes off the rear brake opening, and the differential piston reduces the outlet brake line pressure to the rear in relationship to the ratio of the area or diameter-squared ratios; that is,

$$\text{Reducer Slope} = (d / D)^2 \quad (5-12)$$

where d = small diameter of differential piston, cm (in.)

D = large diameter of differential piston, cm (in.)

The switch point at point A of Fig. 5-14 is reached for a deceleration, a , determined by

$$a = \tan \alpha \quad (5-13)$$

where α = installation angle relative to the horizontal baseline of the vehicle, deg

The G-valve accommodates braking on a grade. For example, when braking downhill the slope of the road causes the switch point to occur at lower decelerations.

In some designs, proportioning valves use the ABS lockup signal from the rear brakes to reduce the rear brake line pressure more closely to the optimum values. This is accomplished by means of solenoids and an accumulator incorporated into the proportioning valve.

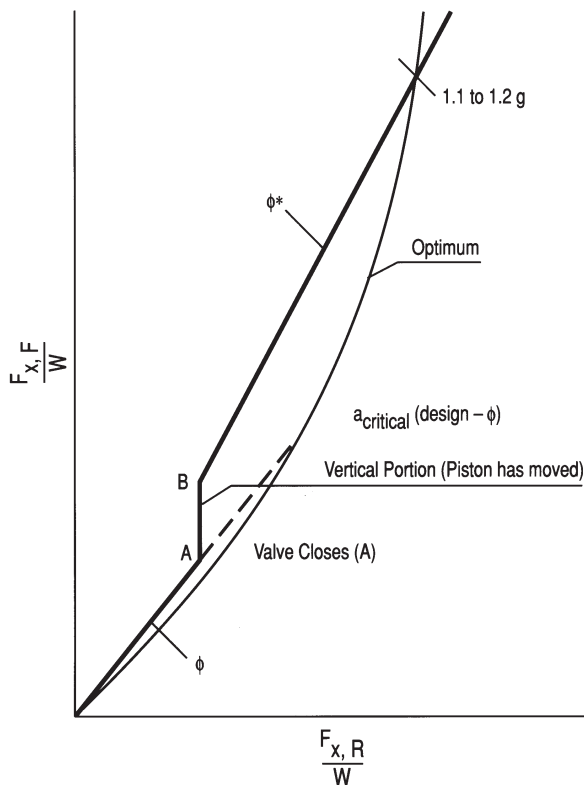


Figure 5-14. Braking forces for G-valve.

5.3.5 Step Bore Master Cylinder

The brake line pressure valves discussed earlier are installed between the master cylinder outlet and the rear brake wheel cylinders. With the standard dual or tandem master cylinder design commonly used, both pistons have the same diameter. Consequently, equal pressure levels are produced in the primary (or pushrod) piston and secondary (or floating) piston circuit. For a detailed discussion of the tandem master cylinder, see Chapter 10.

A step bore master cylinder, as shown in Fig. 5-15, operates like a normal dual cylinder, but differs in bore size between the primary and secondary sections of the master cylinder. Because both pistons are pushed with equal force, the piston with the smaller bore produces larger brake line pressures.

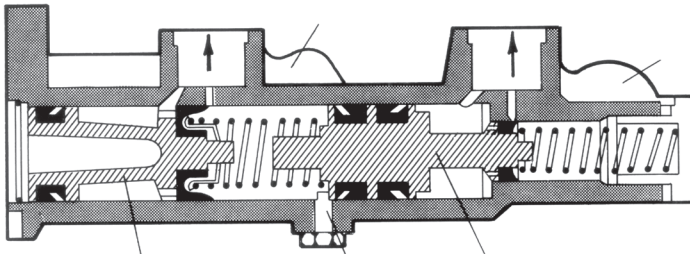


Figure 5-15. Step-bore master cylinder.

The step bore section will generally be connected to the front disc brakes of a vehicle. The step bore master cylinder can be used only in the front-to-rear dual split systems.

5.3.6 Adjustable Step Bore Master Cylinder

The adjustable master cylinder was developed from the basic step bore master cylinder (Ref. 5.13). A schematic is shown in Fig. 5-16. The master cylinder is a tandem or dual-circuit design with a third piston in addition to the pushrod and floating piston. A magnetic valve control is used to connect the space between the third piston and the floating piston, either with the brake fluid reservoir, or directly with the pressure space between the pushrod piston and the third piston. When connected to the reservoir, the third piston transmits its force directly against the floating piston. In the other case, the third piston is functionally eliminated and the force transmission occurs hydraulically.

A typical brake line pressure diagram is shown in Fig. 5-17. The two-slope brake pressure distribution provides better brake balance front to rear compared to the bilinear distribution shown in Fig. 5-10 for the reducer valves commonly used in today's passenger cars and light trucks.

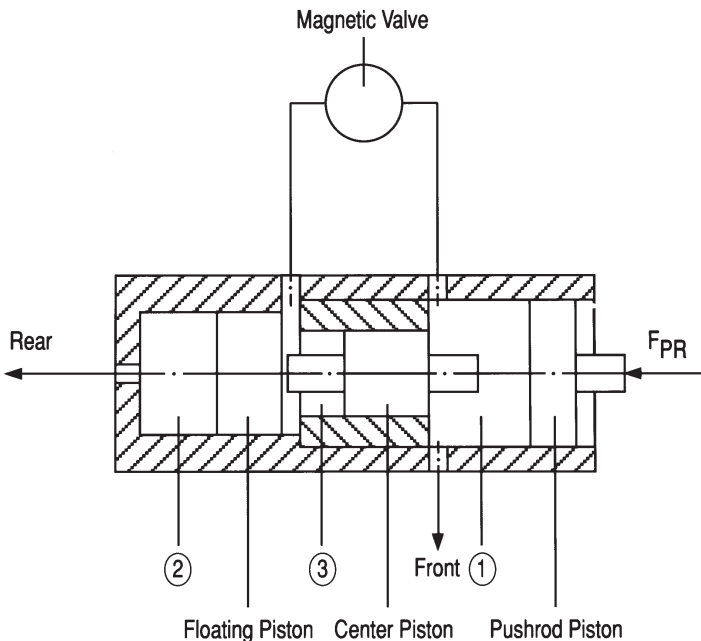


Figure 5-16. Adjustable master cylinder.

When the space 3 is not connected to the reservoir, then the pressure p_1 in the pushrod piston space 1 is given by

$$p_1 = F_{PR} / A_{mc1} , \quad \text{N/cm (psi)} \quad (5-14)$$

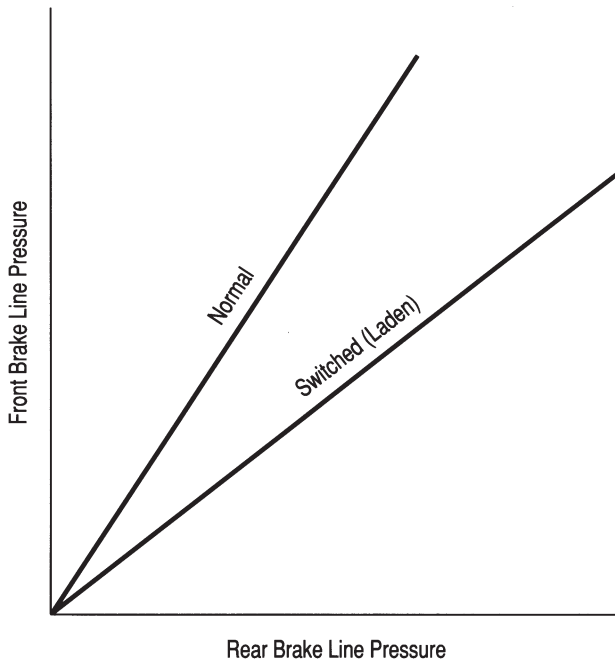


Figure 5-17. Brake line pressures for adjustable master cylinder.

where A_{mc1} = master cylinder cross-sectional area of space 1, cm^2 (in.^2)

F_{PR} = pushrod piston force, N (lb)

Furthermore, the pressure in the floating piston space 2 is the same as in the pushrod piston space 1, computed by Eq. (5-14).

In the other case, the space 3 is connected to the reservoir, resulting in atmospheric pressure in the space 3. The third piston mechanically transmits the force F_3 :

$$F_3 = p_1 A_{mc3} , \text{ N (lb)}$$

against the floating piston, producing the pressure in the floating piston space 2 determined by

$$p_{23} = F_3 / A_{mc2} = p_1 A_{mc3} / A_{mc2} , \text{ N/cm}^2 \text{ (psi)} \quad (5-15)$$

where A_{mc2} = cross-sectional area in space 2, cm^2 (in.^2)

A_{mc3} = cross-sectional area in space 3, cm^2 (in.^2)

Just as the normal step bore master cylinder, the adjustable step bore master cylinder can be used only for the basic front-to-rear dual split systems standard on many medium- and full-size rear-wheel-driven passenger vehicles.

The adjustable master cylinder is used in connection with four-wheel ABS brakes of some earlier passenger cars. When the magnetic valve is energized,

the brake force distribution to the rear brakes is increased (as if the vehicle were laden), allowing for improved rear braking efficiency. Any potential rear brake lock is prevented by ABS. In the event of an ABS brake failure, the master cylinder valve is de-energized, causing the master to switch to a steeper slope. The result is front brake lock before rear, providing a stable braking maneuver in the event brakes are locked.

5.3.7 Comparison of Brake Line Pressure Valves

As discussed in Chapter 1, an important consideration in selection of a design solution selection is system simplicity. Increased complexity will affect reliability and, to some extent, repairability. Of equal or even more importance, however, is the basic directional stability of a motor vehicle during braking with some wheels locked. For some vehicle configurations and, in particular, front-wheel-driven passenger cars, the relatively low static rear axle load may require the use of rear brake line pressure-reducing valves. If possible, and if premature rear brake lockup can be prevented under all foreseeable operating conditions, a single knee-point pressure reducer or proportioning valve should be used. If that is not sufficient, a deceleration-sensitive valve should be considered. Load-sensitive valves require linkages and levers, which with time may be out of adjustment due to spring sagging, after market suspension component installation, or simple component damage underneath the vehicle.

In the design of load-sensitive devices and adjustment linkages, care must be taken that suspension deflections caused by road roughness or crossing of railroad tracks do not alter the basic knee-point setting of the valve.

Adjustable master cylinders are an important safety contribution in combination vehicles when towing a trailer. Under these conditions, the rear brake force of the tow vehicle is increased through an electrical signal from the same light circuit that activates the magnetic control valve.

Brake engineers must not rely on ABS systems to cure the ills of the underlying basic brake system design. In the event of an ABS failure, the basic brake system must still render the vehicle directionally stable while braking at maximum effectiveness with brakes locked.

5.4 Brake Fluid Volume Analysis

5.4.1 Basic Concepts

Inspection of Eq. (5-3) reveals that vehicle deceleration will increase with brake line pressure. Inspection of Eqs. (5-1) and (5-5) reveals that brake line pressure will increase with decreasing cross-sectional area of the master cylinder. Conversely, increasing the cross-sectional areas of the wheel cylinders will also increase vehicle deceleration. However, decreasing the master cylinder cross-sectional area will reduce the amount of brake fluid volume delivered, while increasing the size of the wheel cylinders will increase the amount of brake fluid required by the wheel brakes to function properly.

In the brake fluid volume analysis, the minimum amount of brake fluid volume

that must be delivered by the master cylinder is determined so that all fluid volume-using brake system components can function properly, and the brake pedal travel does not exceed an upper safe value.

Hydraulic brakes use the principle of equal pressure throughout the brake system. The schematic of this principle is illustrated in Fig. 5-18. The piston to the left pressurizes the fluid with a given force. It represents the pedal effort input by the driver. The eight pistons to the right represent the wheel cylinder pistons. If they have the same cross-sectional area as the single piston, then each of the eight pistons carries a weight of 445 N (100 lb), or a total of 3558 N (800 lb). With a displacement of the single piston of, for example, 203 mm (8 in.), the eight pistons will move only 25.4 mm (1 in.). Of course, if the cross-sectional area of the single piston were decreased, a smaller force could produce the same pressure and, hence, lifting forces at the eight cylinders. With this change, the eight pistons would move a correspondingly shorter distance.

$$\begin{aligned} N &= 4.448 \text{ lb} \\ \text{cm} &= 2.54 \text{ in} \end{aligned}$$

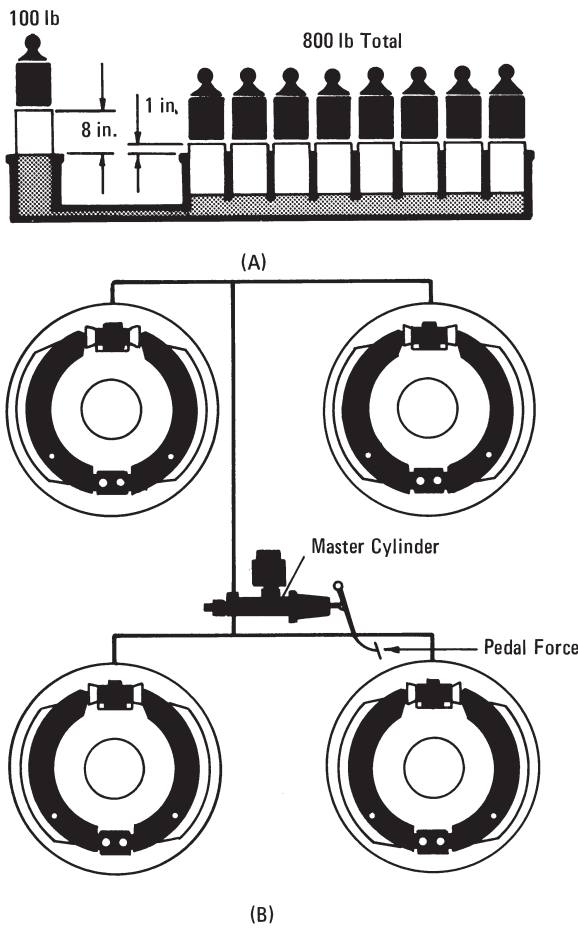


Figure 5-18. Hydraulic brake system schematic.

Consider the following application. A four-wheel disc brake vehicle has a master cylinder size of 19.05 mm bore diameter and 36 mm piston stroke (0.75 by 1.4 in.). The front disc brake wheel-cylinder diameter is 5.71 cm (2.25 in.), that of the rear 3.81 cm (1.5 in.). The master cylinder volume is computed to be 10.1 cm^3 (0.618 in.^3). The total wheel cylinder piston area pressurized by brake fluid for the four disc brakes is $4(25.6 + 11.4) = 148 \text{ cm}^2$ [$4(3.976 + 1.767) = 22.97 \text{ in.}^2$]. Consequently, the average wheel cylinder piston travel is $10.1/148 = 0.068 \text{ cm} = 0.68 \text{ mm}$ ($0.618/22.97 = 0.027 \text{ in.}$). If the wheel cylinder piston travel required to press the pads against the rotors exceeds the maximum of 0.68 mm (0.027 in.) available from the master cylinder, due to, for example, excessive axial rotor runout or air in the brake system, the pedal will go to the floor without any, or with only very little brake line pressure buildup, resulting in total loss of braking effectiveness. An important design objective for drum brakes and disc brake calipers is to minimize the distance that the wheel cylinder pistons have to travel for safe brake operation. Automatic brake adjusters are but one design solution to accomplish this design objective.

To fully understand the importance of the minimum wheel cylinder piston travel, and how it relates to other brake components, the following brake system gain analysis is presented.

For simplicity, consider a brake system with identical brakes on each wheel. With Eq. (5-2), the total brake force $F_{x,\text{total}}$ on the vehicle can be determined by

$$F_{x,\text{total}} = n_B(p_\ell - p_o)A_{wc}\eta_c BF(r / R) , \text{ N (lb)} \quad (5-16)$$

where BF = brake factor

n_B = number of brakes

p_ℓ = brake line pressure, N/cm^2 (psi)

p_o = pushout pressure, N/cm^2 (psi)

r = drum or rotor radius, mm (in.)

R = tire radius, mm (in.)

A_{wc} = wheel cylinder area, cm^2 (in.^2)

η_c = wheel cylinder efficiency

Application of Newton's second law to Eq. (5-16) yields

$$aW = n_B(p_\ell - p_o)A_{wc}\eta_c BF(r / R) , \text{ N (lb)} \quad (5-17)$$

where a = deceleration, g-units

W = vehicle weight, N (lb)

Eq. (5-17) may be rewritten in terms of pedal force rather than brake line pressure. Pushout pressures generally are small compared to normal operating pressures and are ignored in this analysis. Eq. (5-17) becomes

$$aW = n_B (F_p \ell_p \eta_p B / A_{mc}) A_{wc} \eta_c BF(r / R) , \quad N (lb) \quad (5-18)$$

where B = boost ratio

ℓ_p = pedal lever ratio

η_p = pedal lever efficiency

From a brake fluid volume analysis, it follows that the fluid displaced by the master cylinder equals the fluid absorbed by the individual wheel cylinders due to their piston travel to press the shoes against the drums. Any other brake fluid volume-absorbing components, such as brake hose expansion or caliper deformation, are ignored at this time. They will be considered in the detailed analysis presented in Section 5.4.3. Hence, the volume V_{mc} produced by the master cylinder is

$$V_{mc} = A_{mc} X = n_s A_{wc} d , \quad \text{cm (in.)}$$

or

$$A_{wc} / A_{mc} = X / n_s d \quad (5-19)$$

where A_{mc} = master cylinder cross-sectional area, cm^2 (in.^2)

d = wheel cylinder piston displacement, cm (in.)

n_s = number of brake shoes

X = master cylinder piston travel, cm (in.)

If the ratio of wheel cylinder area to master cylinder area [Eq. (5-19)] is introduced in Eq. (5-18), the following expression results

$$aW = F_p [\ell_p B \eta_p \eta_c (X / d) BF(r / R) (n_B / n_s)] , \quad N (lb) \quad (5-20)$$

where a = vehicle deceleration, g -units

F_p = pedal force, N (lb)

W = vehicle weight, N (lb)

Inspection of Eq. (5-20) reveals that vehicle braking force aW and, hence, vehicle deceleration is determined by multiplying the pedal force F_p by a total systems gain consisting of six individual dimensionless component gains, and two efficiencies. The individual gains are

pedal ratio: $\ell_p = S_F / X$; S_F = pedal travel, cm (in.)

boost ratio: B

displacement or hydraulic gain: X/d

brake factor: BF

radius ratio: r/R

shoe ratio: n_B/n_s

Each of the gains can be increased only to certain upper limits. Increasing the boost ratio creates problems in the case of a booster failure as well as in compliance with safety standards. Increasing the pedal ratio or master cylinder piston travel requires excessive pedal travels. Decreasing the minimum wheel cylinder piston travel available from the master cylinder volume requires extremely stiff brake system components and small clearance values between shoe and drum or pad and rotor. Increasing the brake factor results in brake torque variation and potential for left-to-right and front-to-rear brake imbalance. Increasing drum or rotor radius is limited by rim size. Decreasing tire radius is limited by the load-carrying capacity required by the maximum weight of the vehicle. Decreasing the number of shoes would be impractical with current design practice.

Typical values for a four-wheel disc brake vehicle system substituted for the individual gains into Eq. (5-20) may result in

$$aW = F_p [4(3)(0.8)(0.96)(36 / 0.635)(0.7)(0.35)(0.5)] = 64F_p$$

$$[aW = F_p [4(3)(0.8)(0.96)(1.42 / 0.025)(0.7)(0.35)(0.5)] = 64F_p]$$

Inspection of the numerical values reveals that the hydraulic gain equal to $36/0.635 = 56.7$ ($1.42/0.025 = 56.7$) is the most significant contribution to braking effectiveness.

Combining Eqs. (5-20) and (5-21) yields an approximate limiting empirical relationship for manual ($B = 1$) brakes in terms of pedal force F_p and maximum pedal travel S_p as:

$$F_p S_p = 0.9 aW , \text{ Ncm}$$

$$[F_p S_p = 0.35 aW , \text{ lb in.}]$$

where a = deceleration, g-units

S_p = maximum pedal travel, cm (in.)

W = vehicle weight, N (lb)

For example, for a pedal force of 580 N (130 lb) and pedal travel of 15 cm (5.9 in.), a vehicle weighing 12,251 N (2753 lb) can safely be braked at 0.8 g. If a booster were used in the braking system, then the maximum safe vehicle weight would simply be multiplied by the boost ratio B .

The approximate relationship is derived as follows.

We start with Eq. (5-3), however ignoring pushout pressures, resulting in

$$aW = p_\ell \left[(A_{wc}BF)_F + (A_{wc}BF)_R \right] \frac{2r\eta_c}{R}$$

The required fluid displacement V_{mc} produced by the master cylinder can be expressed as

$$V_{mc} = 4[(A_{wc}d)_F + (A_{wc}d)_R](1 + v)$$

where v = relative portion of V_{mc} required for hose expansion, caliper distortion, etc.

Substituting above the empirical relationship $d_{min} \approx \frac{BF}{25}$ [Eq. (5-21)] yields

$$V_{mc} = \frac{4}{25} [(A_{wc}BF)_F + (A_{wc}BF)_R](1 + v)$$

Combining the first and last equations yields

$$\frac{Wa}{2(r/R)\eta_c p_\ell} = \frac{25V_{mc}}{4(1+v)}$$

or

$$p_\ell V_{mc} = \frac{Wa(1+v)}{(12.5)(r/R)\eta_c}$$

Using typical values for $v = 0.3$, $r/R = 0.35$, $\eta_c = 0.85$ (conservative), yields

$$p_\ell V_{mc} = \frac{Wa(1.3)}{(12.5)(0.35)(0.85)} = (0.35)Wa$$

Because pedal work and master cylinder work are approximately equal, we have

$$F_p \cdot S_p = 0.35Wa$$

For example, for $W = 3000$ lb, $a = 0.7$ g, and $S_p = 5$ in., a pedal force $F_p = (0.35)(3000)(0.7)/5 = 147$ lb is required.

5.4.2 Simplified Brake Fluid Volume Analysis

Whether one uses a simplified or detailed analysis, the purpose of a brake fluid volume analysis is to determine the minimum amount of brake fluid required by the hydraulic brake system, i.e., all brake fluid-using components, and match that volume requirement with the volume delivered by the master cylinder. For the common dual brake systems, this means the proper determination of the individual travels of the primary and secondary piston.

Because the wheel cylinders are the major fluid users, past experience has provided design guidelines for the minimum piston travel required for safe operation of wheel brakes.

For a typical hydraulic brake system, the minimum safe travel d_{min} for one piston, one brake pad, or one brake shoe tip may be determined by the empirical expression

$$\begin{aligned} d_{\min} &\approx BF \quad , \quad \text{mm} \\ [d_{\min} &\approx BF / 25 \quad , \quad \text{in.}] \end{aligned} \quad (5-21)$$

where BF = brake factor

For example, for a front disc brake having a brake factor BF = 0.7, the minimum piston or pad travel is 0.7 mm (0.7/25 = 0.028 in.). If the master cylinder volume portion feeding the two front disc brakes provides a brake fluid volume sufficient to move each pad by 0.7 mm (0.028 in.) as the master cylinder bottoms out, then the brake pedal travel will not be excessive under normal operating conditions.

The floating-caliper disc brake design has only one piston. The single piston travel relative to the bore housing must be twice the safe amount or 1.4 mm (0.055 in.).

5.4.3 Detailed Brake Fluid Volume Analysis

5.4.3.1 Master Cylinder Volume Analysis

The brake fluid volume delivered by the master cylinder must be sufficiently large so that all fluid-using brake components function properly, and so that the pedal travel does not exceed approximately 8.89 cm (3.5 in.) for deceleration of 0.9 to 1 g and "cold" brakes (see Chapter 1).

The sizing of a master cylinder in terms of cross-sectional area is mostly a function of braking performance requirements with the booster failed.

The master cylinder cross-sectional area required to achieve a specified deceleration with a given pedal force is computed by combining Eqs. (5-1), (5-3), and (5-11) and ignoring pushout pressures:

$$A_{mc} = \frac{2F_p \ell_p \eta_p \eta_c [(A_{wc} BFr)_F + (A_{wc} BFr)_R SL]}{aWR - 2(A_{wc} BFr)_R p_K (1 - SL) \eta_c} \quad , \quad \text{cm}^2 \text{ (in.}^2\text{)} \quad (5-22)$$

where F_p = pedal force, N (lb)

ℓ_p = pedal lever ratio

p_K = knee point pressure, N/cm² (psi)

η_c = wheel cylinder efficiency

η_p = pedal lever efficiency

The master cylinder piston travel S_{mc} is given by

$$S_{mc} = S_p / \ell_p \quad , \quad \text{cm (in.)} \quad (5-23)$$

where S_p = maximum pedal travel available, cm (in.)

The maximum master cylinder volume $V_{mc\text{-max}}$ is obtained by combining Eqs. (5-22) and (5-23):

$$V_{mc\text{-max}} = 2F_p S_p \eta_p \eta_c \{(A_{wc} BFr)_F + (A_{wc} BFr)_R (SL)\} / \{aWR - 2(A_{wc} BFr)_R p_k (1-SL) \eta_c\}, \text{ cm}^3 (\text{in.}^3) \quad (5-24)$$

The brake fluid volume determined by Eq. (5-24), or directly from measurements of the actual master cylinder for a given vehicle, must cover all fluid volume users of the entire brake system.

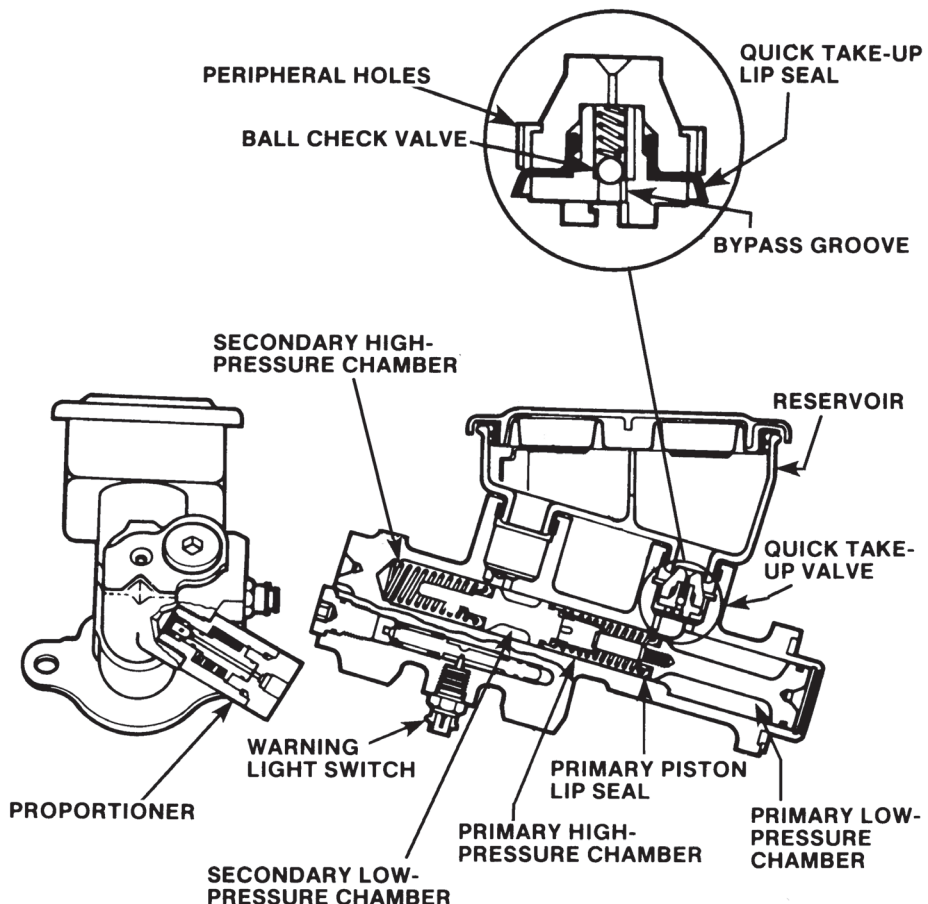
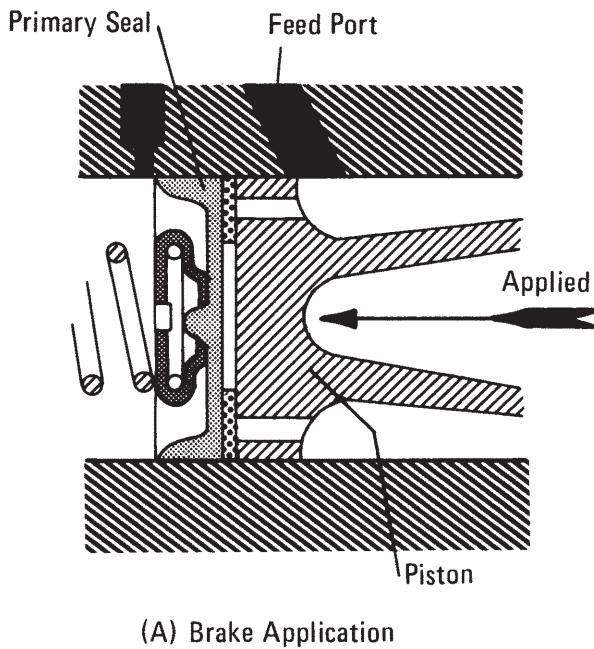
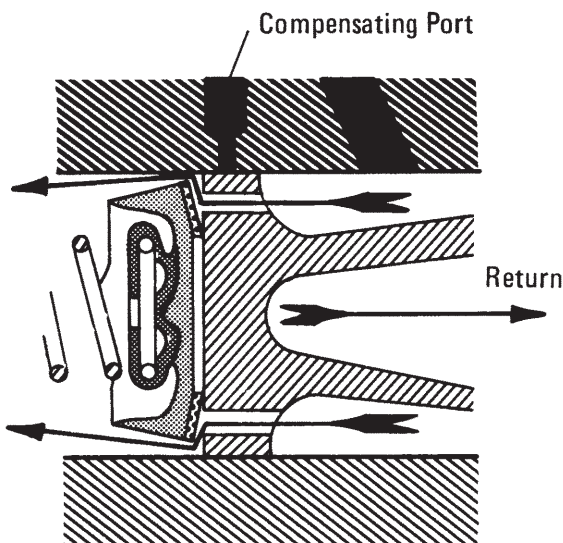


Figure 5-19. Delco-Moraine "quick-take-up" master cylinder (Bendix).



(A) Brake Application



(B) Return Stroke—Brake Fluid Flows
From Behind Piston into Pressure Chamber

Figure 5-20. Primary seal operation – pumping the brakes.

Quick take-up master cylinders as illustrated in Fig. 5-19 and used in the past in some vehicles require additional volume analysis, because the low-pressure chamber of the master cylinder provides a large amount of fluid at low pressures up to approximately 69 N/cm^2 (100 psi) to quickly apply the pads against the rotors. The area between the base of the master cylinder and the face of the primary piston is the low-pressure chamber. When the brakes are applied, the primary piston begins to move into the bore, and the volume surrounding the piston body begins to decrease, resulting in a pressure increase of the fluid behind the primary piston. As the quick take-up valve is closed to the reservoir, the fluid is pressed past the primary seal directly in front of the primary piston into the primary circuit. At a pressure of approximately 48 to 69 N/cm^2 (70 to 100 psi), the quick take-up valve opens, relieving the low-pressure chamber. For higher brake line pressures, the master cylinder operates as a normal dual or tandem master cylinder, with each circuit producing the same pressure. The quick take-up chamber usually supplies the circuit with the larger brake fluid volume, in most cases the larger brake fluid requirements of the front low-drag disc brakes.

5.4.3.2 Individual Component Fluid Requirements

The individual fluid volumes and, hence, pedal travel losses involve the factors discussed next. The individual fluid volumes associated with the various brake components are computed for a brake line pressure that will produce a deceleration of 0.9 g for the vehicle laden at GVW with a pedal travel of not more than 8.89 cm (3.5 in.).

1. Pad-Rotor Clearance

The fluid volume required to move the pads against the rotor is computed from the axial runout or clearance for the disc brake and the caliper cross-sectional area. During this portion of the pedal application, only negligible brake line pressures are produced. Disc brakes and nearly all drum brakes are self-adjusting, making the clearance a somewhat predictable minimum value.

Excessive axial runout of disc brake rotors will cause increased pad and caliper piston pushback with the brakes are released. The total clearance between the pads and the rotors may be greater than the fluid available from the master cylinder for that circuit. Proper, i.e., quick, pumping of the brakes will normally result in brake pedal rise due to fluid bypass around the primary seals from the reservoir into the brake system, as illustrated in Fig. 5-20. In some cases, excessive front-end shimmy or a severe tight turn and loose or worn suspension components may cause caliper piston pushback sufficient for the brakes to fail from excessive brake pedal travel. When the accident vehicle is examined, no excessive axial rotor runout may be observed, with the true accident causation often remaining unknown to many. See Example 5-2 for an actual case analysis where a loose front bearing caused a partial brake failure.

In the investigation of accidents involving four-wheel disc-brake vehicles with the integrated disc parking brake, using parking brake application to adjust the service brake pads, the parking brake should not be applied during the inspection because critical evidence may be destroyed.

2. *Brake Line Expansion*

The metal brake line is basically a long cylinder. When the basic equation for a pressurized cylinder is used, the volume increase V_{BL} of a brake line may be determined by

$$V_{BL} = 0.79D^3Lp_\ell/tE \quad (5-25)$$

where D = outer diameter of pipe, cm (in.)

E = elastic modulus of pipe material, N/cm² (psi)

L = length of brake line, cm (in.)

p_ℓ = brake line pressure, N/cm² (psi)

t = wall thickness of pipe, cm (in.)

For a brake line with $D = 0.475$ cm (0.187 in.), $t = 0.0686$ cm (0.027 in.), and $E = 20.6 \times 10^6$ N/cm² (30×10^6 psi), Eq. (5-25) yields the normalized brake line volume loss coefficient k_{BL} of

$$k_{BL} = V_{BL}/p_\ell L = 0.060 \times 10^{-6}, \text{ cm}^3/(\text{N/cm}^2)\text{cm} \quad (5-26)$$

[$k_{BL} = V_{BL}/p_\ell L = 0.0064 \times 10^{-6}, \text{ in.}^3/(\text{psi})\text{in.}$]

For a given vehicle with a specific brake line length L and a certain brake line pressure p_ℓ , the volume loss due to brake line expansion is determined by

$$V_{BL} = k_{BL} L p_\ell, \quad \text{cm}^3 (\text{in.}^3) \quad (5-27)$$

3. *Brake Hose Expansion*

Brake hose expansions have been measured. Typical values of brake hose expansion V_H for vehicles in use today are computed by

$$V_H = k_H L_H p_\ell, \quad \text{cm}^3 (\text{in.}^3) \quad (5-28)$$

with

$$k_H = 4.39 \times 10^{-6}, \quad \text{cm}^3/(\text{N/cm}^2)\text{cm}$$

$$[k_H = 0.47 \times 10^{-6}, \quad \text{in.}^3/(\text{psi})\text{in.}]$$

where L_H = brake hose length, cm (in.)

4. *Master Cylinder Losses*

Volume losses for master cylinders in good mechanical condition generally vary with the size of the master cylinder diameter, as indicated here (Ref. 1.3):

Diameter	K_{mc}
19.05 mm (3/4 in.)	$150 \times 10^{-6} \text{ cm}^3/\text{N/cm}^2$ ($6 \times 10^{-6} \text{ in.}^3/\text{psi}$)
23.8 mm (15/16 in.)	$190 \times 10^{-6} \text{ cm}^3/\text{N/cm}^2$ ($8 \times 10^{-6} \text{ in.}^3/\text{psi}$)
25.4 mm (1 in.)	$220 \times 10^{-6} \text{ cm}^3/\text{N/cm}^2$ ($9 \times 10^{-6} \text{ in.}^3/\text{psi}$)
38.1 mm (1.5 in.)	$450 \times 10^{-6} \text{ cm}^3/\text{N/cm}^2$ ($19 \times 10^{-6} \text{ in.}^3/\text{psi}$)

The volume loss V_{mc} is determined by

$$V_{mc} = k_{mc} p_{\ell} , \text{ cm}^3 (\text{in.}^3) \quad (5-29)$$

where k_{mc} = specific master cylinder volume loss, $\text{cm}^3/\text{N/cm}^2$ ($\text{in.}^3/\text{psi}$)

5. Caliper Deformation

Caliper deformation is difficult to measure exactly, because residual pocket air and test fluid are compressed and cause an additional small fluid loss of their own. Furthermore, different caliper designs make it impossible to state one coefficient for all applications. However, tests conducted with "steel" pads and corrected for fluid compression show that the caliper volume loss coefficient for fixed caliper designs for one caliper may be approximated by

$$V_c = k_c p_l + V_r , \text{ cm}^3 (\text{in.}^3) \quad (5-30)$$

The values for k_c are a function of the caliper piston diameter. For diameters between 38 and 60 mm (1.5 and 2.36 in.), k_c is determined by (Ref 1.3):

$$k_c = 482 \times 10^{-6} d_{wc} - 1632 \times 10^{-6} , \text{ cm}^3/(\text{N/cm}^2) \quad (5-31)$$

$$[k_c = 52 \times 10^{-6} d_{wc} - 69 \times 10^{-6} , \text{ in.}^3/\text{psi}]$$

where d_{wc} = wheel cylinder diameter, cm (in.)

$$V_c = \text{volume loss in caliper, cm}^3 (\text{in.}^3)$$

The residual air volume V_r in the caliper is approximately 0.72 cm^3 (0.044 in.^3) for a caliper diameter of 60 mm (2.36 in.), or 0.31 cm^3 (0.019 in.^3) for a 38 mm (1.5 in.) diameter caliper.

6. Brake Pad Compression

For disc brakes, pad compression is an important factor in the selection of a proper material. A certain amount of compressibility or damping is essential for disc brakes to operate without undue noise (Ref. 5.14).

For disc brake pads, the volume loss V_p due to compression is determined by (Ref. 1.3):

$$V_p = 4 \sum (A_{wc} C_s p_\ell)_i \quad , \quad \text{cm}^3 \text{ (in.}^3\text{)} \quad (5-32)$$

where A_{wc} = wheel cylinder area, cm^2 (in.^2)

C_s = brake shoe compressibility, $\text{cm}/(\text{N/cm}^2)$ ($\text{in.}/\text{psi}$)

i = identity of brake

p_ℓ = brake line pressure, N/cm^2 (psi)

For disc brake pads, a relatively well-damped pad material yields a compressibility factor $C_s = 11 \times 10^{-6}$ to $26 \times 10^{-6} \text{ cm}/(\text{N/cm}^2)$ (3×10^{-6} to $7 \times 10^{-6} \text{ in.}/\text{psi}$) at normal (cold) brake temperature, $C_s = 15 \times 10^{-6}$ to $33 \times 10^{-6} \text{ cm}/(\text{N/cm}^2)$ (4×10^{-6} to $9 \times 10^{-6} \text{ in.}/\text{psi}$) for hot brakes with a rotor temperature of approximately 672 K (750°F) with a backing plate temperature of approximately 380 K (225°F).

For example, for a passenger car with a four-wheel disc brake system with 5.71 and 3.81 cm (2.25 and 1.5 in.) wheel cylinder diameters, front and rear, hot brakes, and a brake line pressure of 620 N/cm^2 (900 psi), Eq. (5-32) yields a maximum volume loss V_p due to pad compression of

$$\begin{aligned} V_p &= 4C_s (A_{wcF} + A_{wcR}) p_\ell \\ &= 4(33)(10^{-6})(25.6 + 11.4)(620) = 3.02 \text{ cm}^2 \\ &[= 4(9)(10^{-6})(3.976 + 1.767)(900) = 0.186 \text{ in.}^3] \end{aligned}$$

With a typical master cylinder size of 2.22 by 2.54 cm ($7/8 \times 1$ in.) for a compact car, the fluid volume is approximately 11.5 cm^3 (0.7 in.^3). A pad compression loss of 3.02 cm^3 (0.186 in.^3) may account for nearly 30% of the pedal travel loss alone. In loss of pedal travel cases, the subject brake pads must be compared with original equipment pads, especially when higher brake temperatures are involved.

7. Drum Deformation

The hydraulic brake fluid volume loss V_d due to mechanical drum deformation is computed by (Ref 1.3):

$$V_d = k_d A_{wc}^2 p_\ell \quad , \quad \text{cm}^3 \text{ (in.}^3\text{)} \quad (5-33)$$

with

$$k_d = (20 \text{ to } 30) \times 10^{-6} \text{ cm/N}$$

$$[k_d = (35 \text{ to } 53) \times 10^{-6} \text{ in./lb}]$$

where A_{wc} = wheel cylinder area, cm^2 (in.^2)

8. Brake Shoe and Lining Compression in Drum Brakes

The brake fluid volume loss resulting from two brake shoes including the apply mechanism is computed by

$$V_s = \frac{k_s A_{wc}^2 p_\ell}{dw} , \text{ cm}^3 (\text{in.}^3) \quad (5-34)$$

with

$$k_s = (100 \text{ to } 150) \times 10^{-6} \text{ cm}^3/\text{N}$$

$$[k_s = (27 \text{ to } 41) \times 10^{-6} \text{ in.}^3/\text{lb}]$$

where d = drum diameter, cm (in.)

w = brake shoe width, cm (in.)

9. Thermal Drum Expansion

The brake fluid volume V_T due to the expansion of the drum due to temperature is computed by

$$V_T = \alpha_T d T_d A_{wc} , \text{ cm}^3 (\text{in.}^3) \quad (5-35)$$

where A_{wc} = wheel cylinder area, cm^2 (in.^2)

T_d = drum temperature, K (F)

α_T = thermal expansion coefficient of cast iron drum material

$$= 11 \times 10^{-6} \text{ cm/cmK} [6.55 \times 10^{-6} \text{ in./in. F}]$$

10. Air in Drum Brake Hydraulics

The brake fluid volume loss V_a due to air inclusion is approximately (Ref. 1.3):

$$V_a = 0.035 A_{wc} , \text{ cm}^3 \quad (5-36)$$

$$[V_a = 0.014 A_{wc} , \text{ in.}^3]$$

11. Brake Shoe/Drum Clearance

The inspection of an accident vehicle generally will reveal any abnormal conditions. Drum and shoe-circle diameter determine the actual lining clearance. It should be noted that some hydraulic drum brakes use a wheel cylinder piston stop, causing the piston to push against a stop in the event of excessive lining wear. When this occurs, the brake shoes are not or are only partially pressed against the drum without producing sufficient brake torque. Although the pedal may feel firm because high brake line pressures are developed, the braking effectiveness may be reduced significantly.

The brake fluid volume V_{cl} due to the clearance between shoes and drum for brakes with good automatic adjustment is

$$V_{cl} = (0.13 \text{ to } 0.15) A_{wc} , \text{ cm}^3 \quad (5-37)$$

$$[V_{cl} = (0.05 \text{ to } 0.06) A_{wc} , \text{ in.}^3]$$

12. Brake Fluid Compression

Volume losses resulting from the compression of brake fluid may have a significant effect on pedal travel as brake fluid temperatures and brake line pressures increase. Measured values of compressibility factor of different dry, gas-free fluids as a function of temperature are shown in Fig. 5-21 for regular brake fluid based on polyglycoether, mineral oil, and silicone. Inspection of Fig. 5-21 reveals that regular brake fluid will double its compressibility factor when the brake fluid temperature increases from 294 to 477 K (70 to 400°F). Silicone-based brake fluids have the highest compressibility.

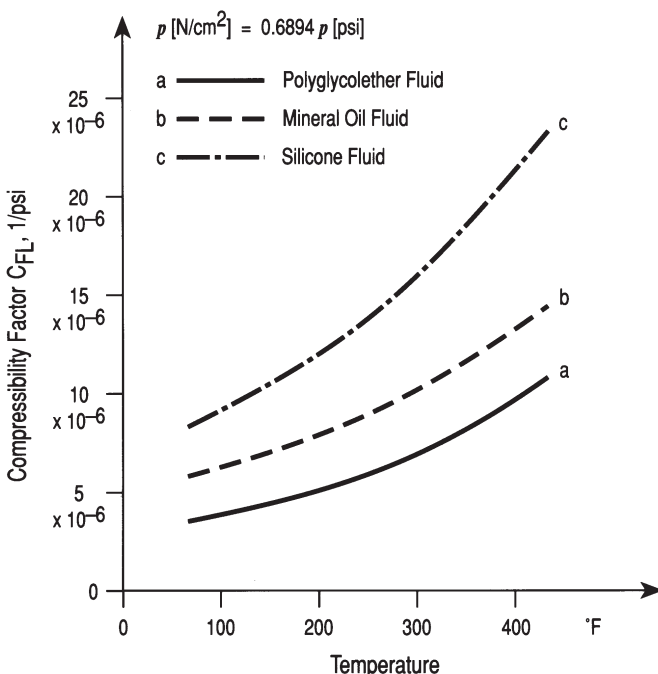


Figure 5-21. Compressibility factor C_{FL} for dry brake fluids without gas content.

The volume loss resulting from brake fluid compression is a function of the active volume V_A in the brake system pressurized during the braking process.

The active volume is determined by

$$V_A = V_o + 4 \sum^n_i (A_{wc}w)_i \quad , \quad \text{cm}^3 \text{ (in.}^3\text{)} \quad (5-38)$$

where A_{wc} = wheel cylinder area, cm^2 (in.^2)

i = brake identity

V_o = brake fluid volume with new shoes, cm^3 (in.^3)

w = wear travel of shoes, cm (in.)

The volume loss V_{FL} due to fluid compression is computed by

$$V_{FL} = V_A C_{FL} p_\ell \quad , \quad \text{cm}^3 (\text{in.}^3) \quad (5-39)$$

where C_{FL} = brake fluid compressibility factor, cm^2/N ($1/\text{psi}$)

For example, for a four-wheel disc brake vehicle with

$$A_{wcF} = 25.6 \text{ cm}^2 (3.976 \text{ in.}^2)$$

$$A_{wcR} = 11.4 \text{ cm}^2 (1.767 \text{ in.}^2)$$

$$w_F = w_R = 0.635 \text{ cm} (0.25 \text{ in.})$$

$$V_o = 164 \text{ cm}^3 (10 \text{ in.}^3)$$

$$C_{FLF} = C_{FLR} = 10 \times 10^{-6} \text{ cm}^2/\text{N} \text{ at } 422 \text{ K} (7 \times 10^{-6} \text{ 1/psi at } 300^\circ\text{F})$$

the active volume is computed by Eq. (5-38) as

$$\begin{aligned} V_A &= 164 + 4(25.6 + 11.4) \times 0.635 \\ &= 258 \text{ cm}^3 [10 + 4(3.976 + 1.767)(0.25) = 15.7 \text{ in.}^3] \end{aligned}$$

The volume loss at 620 N/cm^2 (900 psi) brake line pressure is determined from Eq. (5-39) as

$$\begin{aligned} V_{FL} &= 258 \times 10 \times 10^{-6} \times 620 \\ &= 1.6 \text{ cm}^3 (15.7 \times 7 \times 10^{-6} \times 900 = 0.099 \text{ in.}^3) \end{aligned}$$

For silicone-based fluids the volume loss would be approximately 3.6 cm^3 (0.22 in.^3); i.e., a significantly greater loss than that for normal brake fluid.

13. Air or Gas in the Brake System

Air can remain in the brake system when air pockets form which cannot be flushed out during the vacuum bleeding process at the factory. Small air bubbles will adhere to metal surfaces of springs and other parts. Due to surface tension, small-sized air bubbles will remain in the brake fluid, which can be removed only by ultrasound application. Typical residual air volumes in the entire brake system are approximately 3% of the active volume. The 3% includes the residual air in the front disc brake caliper of approximately 0.6%, and 0.4% in the rear disc brake caliper.

If one defines V_G as the volume of the enclosed air at atmospheric pressure, and assumes an isothermal or constant temperature compression based on the valid assumption that the air temperature remains equal to the temperature of the brake fluid during the compression process, then with basic thermodynamics the decrease of air volume is determined by

$$V_{GL} = V_G T / T_0 [1 - p_o / (p_\ell + p_o)] \quad , \quad \text{cm}^3 \quad (5-40)$$

where p_e = brake line pressure, N/cm² (psi)

p_o = atmospheric pressure, N/cm² (psi)

T_0 = absolute temperature at initial conditions, K (°R)

T = absolute temperature, K (°R)

V_G = enclosed gas volume at ambient temperature, cm³ (in.³)

The absolute temperature T is computed by

$$T = T_{\text{Celsius}} + 273 \quad , \quad K \quad (5-41)$$

$$[T = T_{\text{Fahrenheit}} + 460 \quad , \quad ^{\circ}\text{R}]$$

At higher pressures, p_e , the square bracket in Eq. (5-40) goes to unity, indicating that the entire enclosed air volume will be compressed and cause a corresponding drop of the pedal height toward the floor. When the brake fluid is also heated, then the temperature increase will expand the air, thus making the volume loss stemming from the air greater.

For example, for $V_G = 4.9 \text{ cm}^3$ (0.3 in.³), and ambient and operating temperature of 294 and 394 K (70 and 250°F), respectively, Eqs. (5-40) and (5-41) yield

$$T = 70 + 460 = 530^{\circ}\text{R}$$

and

$$T = 250 + 460 = 710^{\circ}\text{R}$$

and

$$V_{\text{GL}} = 4.9(394 / 294) = 6.57 \text{ cm}^3$$

$$[V_{\text{GL}} = 0.3(710 / 530) = 0.40 \text{ in.}^3]$$

14. Fluid Loss in Hydrovac

The hydraulic control of the hydrovac booster requires a small amount of brake fluid from the driver-operated master cylinder to actuate the vacuum unit. For most hydrovac used in medium trucks, the volume loss at zero brake line pressure rise is approximately 0.82 cm³ (0.05 in.³).

15. Volume Loss in Valves

Because the type of valve used in a hydraulic brake system varies with design, no specific loss coefficients can be stated. If a malfunctioning of a particular valve is suspected, special tests must be conducted with the accident and exemplar valves to clearly isolate any contribution to pedal travel loss.

16. Water Content in Brake Fluid

With time, hydraulic brake fluid will absorb water from the air through the flexible hoses. Brake fluid contaminated by water has a reduced boiling point temperature, which may lead to partial or complete brake failure at elevated brake temperatures due to brake fluid vaporization. Pedal travel will increase significantly. For diagonal split brake circuits, the entire brake system may fail (Refs. 5.15, 5.16).

17. After-market Equipment

After-market valves installed in the brake system hydraulics will have an adverse effect on pedal travel. Depending on how “limited” the master cylinder volume reserves are, they may cause critical pedal travels.

5.4.3.3 Pedal Travel Computation

With the individual volume losses determined from the appropriate sections, the total volume loss can be computed. A brake line pressure sufficient to produce a deceleration of 0.9 g of the fully laden vehicle should be used for the volume loss calculations.

The pedal travel S_p is determined by

$$S_p = [(\sum V_i / A_{mc}) + \ell_o] \ell_p, \text{ cm (in.)} \quad (5-42)$$

where A_{mc} = master cylinder cross-sectional area, cm^2 (in.^2)

ℓ_o = master cylinder pushrod travel to overcome pushrod play and compensating port, cm (in.)

ℓ_p = pedal lever ratio

V_i = volume loss for individual component, cm^3 (in.^3)

The pedal travel computed by Eq. (5-42) should not exceed 8.9 cm (3.5 in.) out of a maximum of approximately 15.2 cm (6 in.) or 60% of the maximum when the brakes are cold.

Example 5-1: For a deceleration of 0.9 g, determine the brake line pressure and pedal travel. Use the vehicle data that follow.

Weight: 16,458 N (3700 lb)

Wheel cylinder diameter, front: 5.71 cm (2.25 in.); rear: 3.81 cm (1.5 in.)

Effective rotor radius, front: 10.16 cm (4.0 in.); rear: 10.41 cm (4.1 in.)

Brake factor, front: 0.76; rear: 0.70

Tire radius: 31.75 cm (12.5 in.)

Pedal ratio: 4.2

Pedal travel: 12.7 cm (5.0 in.)

Pedal efficiency: 80%

Brake line length: 660 cm (260 in.)

Brake hose length: 152 cm (60 in.)

Wear pad travel: 0.38 cm (0.15 in.)

Initial brake system volume: 197 cm³ (12 in.³)

Residual air in brake fluid: 4.1 cm³ (0.25 in.³)

Proportioning valve: 207 N/cm² (300 psi) × 30%

Axial rotor runout front and rear: 0.00508 cm (0.002 in.)

Vacuum-boosted brakes

Solution: The master cylinder cross-sectional area is determined for the condition of booster failure. As stated in Chapter 1, a pedal force of 100 lb must produce a deceleration of 0.3 g for the vehicle laden at GVW.

By use of Eq. (5-22), the cross-sectional area A_{mc} of the master cylinder becomes

$$A_{mc} = \frac{2(445)(4.2)(0.8)[25.6(0.76)(10.16) + 11.41(0.7)(10.41)(0.3)](0.98)}{0.3(16,458)(31.75) - 2(11.4)(0.7)(10.41)(207)(1 - 0.3)(0.98)} \\ = 4.9 \text{ cm}^2$$

$$\left[A_{mc} = \frac{2(100)(4.2)(0.8)[3.976(0.76)(4) + 1.767(0.7)(4.1)(0.3)](0.98)}{0.3(3700)(12.5) - 2(1.767)(0.7)(4.1)(300)(1 - 0.3)(0.98)} \right] \\ = 0.76 \text{ in.}^2$$

A listing of master cylinder diameters usually available from the master cylinder manufacturers is shown in Table 5-1 in addition to the tolerance allowable for maximum bore diameter and minimum piston diameter. An area of 4.9 cm² (0.76 in.²) requires a master cylinder size of 25.4 mm (1 in.) diameter. The associated cross-sectional area is 5.067 cm² (0.785 in.²). The master cylinder piston travel S_{mc} available from the pedal geometry is determined by Eq. (5-23) as

$$S_{mc} = 12.7 / 4.2 = 3.02 \text{ cm}$$

$$[S_{mc} = 5.0 / 4.2 = 1.19 \text{ in.}]$$

The effective master cylinder volume is $5.067 \times 2.82 = 14.3 \text{ cm}^3$ (0.785 × 1.1 = 0.8635 in.³). The master cylinder travel actually used is approximately 2 mm (0.09 in.) less to account for pushrod play and compensating port travel. A master cylinder diameter of 25.4 mm (1 in.) ensures that, in the event of a booster failure, a pedal force of 445 N (100 lb) produces a deceleration of 0.3 g.

TABLE 5-1

Master Cylinder Sizes				
Nominal Diameter		Max. Bore Diameter	Min. Piston Diameter	Max. Allowable Tolerance
mm	in.	mm	mm	mm
12.7	1/2	12.80	12.57	0.23
14.29	9/16	14.39	14.16	0.23
15.87	5/8	15.97	15.74	0.23
17.46	11/16	17.56	17.33	0.23
19.05	3/4	19.16	18.90	0.26
20.64	13/16	20.75	20.49	0.26
22.2	7/8	22.31	22.05	0.26
23.81	15/16	23.92	23.66	0.26
25.4	1	25.51	25.25	0.26
26.99	1-1/16	27.10	26.84	0.26
27.78	1-3/32	27.89	27.63	0.26
28.57	1-1/8	28.68	28.42	0.26
31.75	1-1/4	31.84	31.58	0.26
33.0	1.2992	33.09	32.83	0.26
34.92	1-3/8	35.01	34.75	0.26
38.1	1-1/2	38.19	37.93	0.26
41.27	1-5/8	41.36	41.10	0.26
44.45	1-3/4	44.54	44.28	0.26
46.83	1-27/32	46.92	46.66	0.26
48.42	1-29/32	48.51	48.25	0.26
50.8	2	50.90	50.60	0.3
54.0	2.1260	54.10	53.80	0.3
57.15	2-1/4	57.25	56.95	0.3
65.0	2.5590	65.10	64.80	0.3
70.0	2.7559	70.10	69.80	0.3
75.0	2.9528	75.10	74.80	0.3

Brake Design and Safety

The approximate brake fluid volume required by the disc brakes is determined next. The individual wheel cylinder piston travels d_{minF} and d_{minR} are obtained from Eq. (5-21) as

$$\text{Front : } d_{minF} = BF = 0.76 \text{ mm } (0.76/25 = 0.0304 \text{ in.})$$

$$\text{Rear : } d_{minR} = BF = 0.70 \text{ mm } (0.70/25 = 0.028 \text{ in.})$$

The brake fluid volume V_F required by the disc brakes to provide sufficient pad displacement to overcome pad clearance, caliper deformation, and hose expansion is determined by

$$V_F = 4[25.65(0.076) + 11.4(0.07)] = 11 \text{ cm}^3$$

$$[V_F = 4[3.976(0.0304) + 1.76(0.028)] = 0.681 \text{ in.}^3]$$

Because the master cylinder volume of 14.7 cm^3 (0.8635 in.^3) provided by the master cylinder exceeds the volume of 11 cm^3 (0.681 in.^3) required by the brake system, the master cylinder size is properly designed, provided the pedal travel calculations carried out next yield acceptable results.

The pedal travel computation is based on the individual volume loss calculations, which in turn require the brake line pressure as an input parameter.

The brake line pressure may be obtained by combining Eqs. (5-3) and (5-11) and eliminating rear brake line pressure:

$$p_\ell = \frac{(aWR/2) - p_K(1 - SL)(A_{wc}BF\eta_c)_R}{(A_{wc}BF\eta_c)_F + (A_{wc}BF\eta_c)_R SL} , \text{ N/cm}^2 \text{ (psi)} \quad (5-43)$$

where a = deceleration, g-units

A_{wc} = wheel cylinder area, cm^2 (in.^2)

BF = brake factor

p_K = knee point pressure, N/cm^2 (psi)

p_ℓ = brake line pressure, N/cm^2 (psi)

R = tire radius, mm (in.)

SL = proportioning valve slope

W = vehicle weight, N (lb)

η_c = wheel cylinder efficiency

Substitution of the appropriate data into Eq. (5-43) yields

$$p_{\ell} = \frac{[0.9(16,458)(31.75) / 2] - 207(1-0.3)(11.4)(0.7)(10.41)(0.98)}{25.6(0.76)(10.16)(0.98) + 11.4(0.7)(10.41)(0.98)(0.3)} \\ = 1024 \text{ N/cm}^2$$

$$\left[p_{\ell} = \frac{[0.9(3700)(12.5) / 2] - 300(1-0.3)(1.767)(0.7)(4.1)(0.98)}{3.976(0.76)(4.0)(0.98) + 1.767(0.7)(4.1)(0.98)(0.3)} \right] \\ = 1482 \text{ psi}$$

A brake line pressure of 1024 N/cm² (1482 psi), required to produce the braking forces necessary to decelerate the vehicle at 0.9 g, will be used through the volume use calculations. A brake line pressure of 1482 psi can only be produced with a 1-in.-diameter master cylinder when a booster is used [see Eq. (5-5)].

The individual volume losses are computed next.

1. Pad clearance:

$$V_{pc} = 4(0.0058)(25.6 + 11.4) = 0.752 \text{ cm}^3$$

$$[V_{pc} = 4(0.002)(3.976 + 1.767) = 0.046 \text{ in.}^3]$$

2. Brake line expansion [Eq. (5-27)]:

$$V_{BL} = 0.06(10^{-6})(660)(1024) = 0.0405 \text{ cm}^3$$

$$[V_{BL} = 0.0064(10^{-6})(260)(1482) = 0.0025 \text{ in.}^3]$$

3. Brake hose expansion [Eq. (5-28)]:

$$V_H = 4.39(10^{-6})(152)(1024) = 0.68 \text{ cm}^3$$

$$[V_H = 0.47(10^{-6})(60)(1482) = 0.0417 \text{ in.}^3]$$

4. Master cylinder [Eq. (5-29)]:

$$V_{mc} = 220(10^{-6})(1024) = 0.2252 \text{ cm}^3$$

$$[V_{mc} = 9(10^{-6})(1482) = 0.0133 \text{ in.}^3]$$

5. Caliper deformation [Eq. (5-30)]:

With Eq. (5-31) we have on the front brakes

$$k_c = (482)(10^{-6})(5.71) - (1632)(10^{-6}) = 1120 \times 10^{-6} \text{ cm}^3/(\text{N/cm}^2)$$

$$\left[k_c = (52)(10^{-6})(2.25) - (69)(10^{-6}) \right]$$

$$= 48 \times 10^{-6} \text{ in.}^3/\text{psi}$$

The volume loss due to two front caliper deformations is [Eq. (5-30)]

$$V_c = (2)[(1120)(10^{-6})(1024) + 0.72] = 3.734 \text{ cm}^3$$

$$[V_c = (2)[(48)(10^{-6})(1482) + 0.044] = 0.230 \text{ in.}^3]$$

Similar computations for a rear brake line pressure of 453 N/cm^2 (655 psi) [Eq. (5-11)] for two rear calipers yields $V_c = 0.81 \text{ cm}^3$ (0.05 in.³).

6. Pad compression [Eq. (5-32)]:

$$C_s = 18.5 \times 10^{-6} \text{ cm}/(\text{N/cm}^2)$$

(5×10^{-6} in./psi was chosen.)

Front:

$$V_{PF} = 4(25.6)(18.5)(10^{-6})(1024) = 1.939 \text{ cm}^3$$

$$[V_{PF} = 4(3.976)(5)(10^{-6})(1482) = 0.1178 \text{ in.}^3]$$

Rear:

$$V_{PR} = 4(11.4)(18.5)(10^{-6})(453) = 0.382 \text{ cm}^3$$

$$[V_{PR} = 4(1.767)(5)(10^{-6})(655) = 0.0231 \text{ in.}^3]$$

7. Brake fluid compression [Eqs. (5-38) and (5-39)]:

The active brake fluid volume V_A is [Eq. (5-38)]

$$V_A = 197 + 4(25.6 + 11.4)(0.38) = 253.2 \text{ cm}^3$$

$$[V_A = 12 + 4(3.976 + 1.767)(0.15) = 15.45 \text{ in.}^3]$$

The volume loss V_F due to fluid compression is computed by Eq. (5-39) for a fluid temperature of 294 K (70°F) with $C_{FL} = 4.35 \times 10^{-6} \text{ cm}^3/(\text{N/cm}^2)$ (3×10^{-6} in.³/psi) from Fig. 5-21 as

$$V_F = (253.2)(4.35)(10^{-6})(1024) = 1.128 \text{ cm}^3$$

$$[V_F = (15.45)(3)(10^{-6})(1482) = 0.0687 \text{ in.}^3]$$

The difference in brake line pressures front and rear due to proportioning was ignored in computing fluid losses due to brake fluid compression.

8. Residual air in brake system [Eq. (5-40)]:

The residual air is 2 cm^3 (0.122 in.³). Residual air of the calipers was accounted for in point 5 above. The residual air exists at atmospheric pressure. If no temperature increase of the air occurs, then no air volume increase has to be considered. Because these calculations are done for the “cold” brakes, the residual air volume is 2 cm^3 (0.122 in.³).

With all individual volume losses established, the total column loss V_t experienced by the brake system at a brake line pressure of 1024 N/cm^2 (1482 psi) is $V_t = \Sigma V_i = 11.7 \text{ cm}^3$ (0.715 in.³).

The pedal travel S_p required to produce a brake line pressure of 1024 N/cm^2 (1482 psi) as well as to provide sufficient master cylinder piston travel to "feed" the different brake fluid users is determined from Eq. (5-42) as

$$S_p = [(11.7 / 5.067) + 0.2](4.2) = 10.54 \text{ cm}$$

$$[S_p = [(0.715 / 0.785) + 0.08](4.2) = 4.16 \text{ in.}]$$

The pedal travel falls outside of the requirements of Chapter 1, indicating that 75 to 90 mm (3 to 3.5 in.) pedal travel or approximately 60% out of a maximum of 150 mm (6 in.) should not be exceeded for cold brakes. The brake system should be redesigned with the next larger master cylinder of 26.99 mm (1-1/16 in.). The pedal travel decreases to 9.42 cm (3.71 in.) [instead of 10.54 cm (4.16 in.)].

A vacuum booster has to be used to produce a brake line pressure of 1482 psi with acceptable pedal forces. A boost ratio of five would be required based on Eq. (5-5).

Example 5-2: The vehicle of Example 5-1 has a left front wheel bearing play of 0.191 cm (0.075 in.) due to faulty repair. Compute the brake line pressure at which the piston of the front circuit master cylinder bottoms out.

The master cylinder has the following dimensions and volumes:

Diameter 25.4 mm (1 in.), front piston travel 19 mm (0.748 in.), rear piston travel 13 mm (0.512 in.). The useable brake fluid volume available from the front circuit portion of the master cylinder is 8.614 cm^3 (0.525 in.³). Only 17 mm (0.67 in.) of effective front piston travel is available due to pushrod play and the compensating port.

The volume requirements of the brake system fall into two categories, namely those components using brake fluid prior to any brake line pressure production, and those involved with producing brake line pressure.

Zero-Pressure Volumes:

Zero-pressure volume requirement of left front caliper:

$$V_{CLF} = (A_{wcF})(S_{padLF}) + V_r = (25.63)(0.191 + 0.0051) + 0.72 = 5.74 \text{ cm}^3$$

$$[(3.976)(0.075 + 0.002) + 0.044 = 0.350 \text{ in.}^3]$$

Zero-pressure volume requirement of right front caliper:

$$V_{CRF} = (25.63)(0.0051) + 0.72 = 0.85 \text{ cm}^3 [(3.976)(0.002) + 0.044 = 0.052 \text{ in.}^3]$$

Any additional residual air in the front circuit is approximately $(0.006)(253) - (2)(0.72) = 0.08 \text{ cm}^3$ $[(0.006)(15.45) - (2)(0.044) = 0.0047 \text{ in.}^3]$ (see point 13, Air or Gas in the Brake System).

The total zero pressure fluid volume required is 6.67 cm^3 (0.407 in.³). The fluid volume available for brake line pressure production on the front brakes is $8.614 - 6.67 = 1.944 \text{ cm}^3$ [0.525 - 0.407 = 0.118 in.³].

Pressurized brake fluid volumes required in the front circuit as a function of brake line pressure p_l :

1. Brake line with a brake line length of 254 cm (100 in.):

$$V_{BL} = (0.060 \times 10^{-6})(254)p_l = (15.24)(10^{-6})p_l, \text{ cm}^3$$

$$[(0.0064)(10^{-6})(100)p_l = (0.64)(10^{-6})p_l, \text{ in.}^3]$$

2. Brake hose with a hose length of 102 cm (40 in.):

$$V_{BH} = (4.39 \times 10^{-6})(102)p_l = (448)(10^{-6})p_l, \text{ cm}^3$$

$$[(0.47)(10^{-6})(40) = (18.8)(10^{-6})p_l, \text{ in.}^3]$$

3. Master cylinder (25.4 mm or 1 in. diameter):

$$V_{mc} = 220 \times 10^{-6}p_l, \text{ cm}^3; [(9)(10^{-6})p_l, \text{ in.}^3]$$

4. Elastic caliper deformation:

$$V_{calF} = (2)(482 \times 5.71 - 1632)(10^{-6})p_l = (2240)(10^{-6})p_l, \text{ cm}^3$$

$$[(2)(52 \times 2.25 - 69)(10^{-6})p_l = (96)(10^{-6})p_l, \text{ in.}^3]$$

5. Pad compression:

$$V_{pF} = (4)(25.6)(18.5)(10^{-6})p_l = 1894p_l, \text{ cm}^3$$

$$[(4)(3.976)(5)(10^{-6})p_l = (80)(10^{-6})p_l, \text{ in.}^3]$$

6. Brake fluid compression with an active volume of 164 cm³ (10 in.³) at 422 K (300°F) (Fig. 5-21):

$$V_{BFF} = (164)(8.7)(10^{-6})p_l = (1427)(10^{-6})p_l, \text{ cm}^3$$

$$[(10)(6)(10^{-6})p_l = (60)(10^{-6})p_l, \text{ in.}^3]$$

7. Valves (data may show 3 cm³ (0.2 in.³) at 829 N/cm² (1200 psi) brake line pressure for combination valve):

$$V_{prop} = (600)(10^{-6})p_l, \text{ cm}^3 [(25)(10^{-6})p_l, \text{ in.}^3]$$

The maximum brake line pressure that can be produced by the front brake circuit is limited by the volume available from the master cylinder, namely 1.944 cm³ (0.118 in.³), and the front brake system volume requirements as pressure increases. Adding all pressurized volume uses yields

$$V_{pr} = (6948)(10^{-6})p_l = 1.944 \text{ cm}^3 [(289.5)(10^{-6})p_l = 0.118 \text{ in.}^3]$$

The front circuit brake line pressure when the front master cylinder piston bottoms out is

$$p_{lf,max} = (1.944)/\{(6948)(10^{-6})\} = 280 \text{ N/cm}^2 [(0.118)/\{(289.5)(10^{-6})\}] = 407 \text{ psi}$$

The failure analysis shows that the front circuit master cylinder piston will bottom out at a brake line pressure of approximately 280 N/cm^2 (407 psi). The deceleration produced with 280 N/cm^2 (407 psi) is 0.28 g computed with Eq. (5-3). As the driver increases pedal force the rear brake line pressure will increase resulting in increased deceleration. The analysis (braking forces diagram) discussed in Chapter 7 can be used to calculate the deceleration at which the rear brakes lock for a given tire-road friction coefficient.

5.5 Dynamic Response of Hydraulic Brake Systems

5.5.1 Basic Considerations

A detailed analysis of the dynamic response of a hydraulic brake system is a complicated task. It involves the solution of several differential equations by means of computers. For valid conclusions to be reached, several input parameters must be measured for the specific brake system under consideration (Refs. 5.17, 5.18, 5.19).

Generally, the response characteristics of hydraulic brake systems are such that the time lags between input and output variables are very small and are typically less than 0.1 to 0.2 s. With the increased use of ABS brakes and electronic stability control systems (ESC), the dynamic response of hydraulic brake systems and individual brake components becomes increasingly important.

The dynamic response of a complete brake system consists of a quasi-static component and a transient component. The transient behavior is that associated with rapidly changing system variables, such as brake line pressure following a rapid pedal force input. The quasi-static behavior is associated with slowly changing variables, such as the change in coefficient of friction between lining and rotor due to a decrease in wheel speed during deceleration of the vehicle.

5.5.2 Brake Fluid Viscosity

The principal dynamic elements in a typical brake system are the brake lines and the vacuum booster. The flow of brake fluid from the master cylinder to the wheel cylinder is a function of fluid viscosity, cross-sectional flow area, and brake line length. The elements determining flow rate are the capacitance, resistance, and inertance of the section of brake line considered. The capacitance element accounts for fluid compressibility and wall compliance, while the resistance element introduces the pressure losses due to laminar or turbulent flow, i.e., frictional effects. Inertance effects result from the mass of the fluid in the brake lines. As fluid viscosity increases, the time interval between the application of force to the brake pedal and operation of the wheel brake increases. Similarly, there is an increase in brake release time.

On most vehicles, tubing length to the left front is shorter than that leading to the right front brake due to the location of the master cylinder. Because of the difference in tubing length in the front circuit, the left front brake is actuated before the right front brake. At normally low viscosity levels the difference is not perceptible. However, as viscosity increases with decreasing ambient temperatures, flow rates to each of the front brakes may become different and

a noticeable unbalance in braking left to right may exist. The level of brake unbalance is affected by the rate of pedal force application, i.e., force application to the fluid. As fluid viscosity increases, the time required for fluid to return through the tubing from the brake to the master cylinder increases due to a slower flow rate, resulting in the brakes being applied for a longer time. Slow response due to viscosity effects will affect the performance of wheel anti-lock brake systems (ABS) and ESC.

5.5.3 Brake Pedal Linkage

The dynamics of the brake pedal and linkage are of little importance to the dynamic response of a complete brake system. The weight and inertia of the foot and leg of the operator will greatly influence the dynamic behavior of the pedal.

5.5.4 Vacuum Booster

The vacuum booster contributes significantly to the response lag of the hydraulic brake system. The booster consists of several components such as pistons, valves, springs, and pushrod, all of which must be included in the mathematical expressions describing the dynamic behavior of the booster. In addition, certain assumptions must be made to simplify the thermodynamic relationships describing the pressure development in the vacuum and ambient pressure chambers (Ref. 5.20). Transient responses for the vacuum booster of a large domestic passenger car were measured and are illustrated in Fig. 5-22. Inspection of Fig. 5-22 reveals the response characteristics for a slow pedal force application to be similar to the quasi-static behavior discussed in Section 5.2.2.1 (Fig. 5-3). The response of the brake line pressure produced at the master cylinder outlet to a rapid pedal force application shows a significant

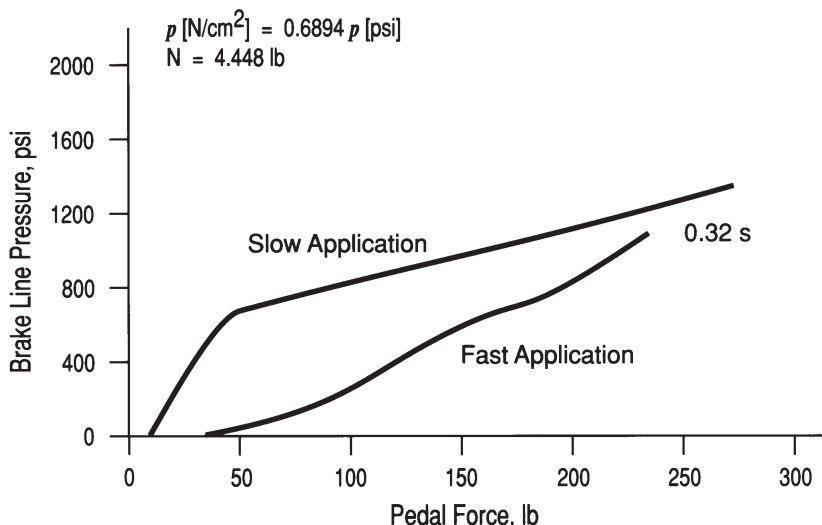


Figure 5-22. Measured steady-state and transient brake line pressure/pedal force response.

lag compared with the response associated with a slow application. Only after the rapid pedal force has attained a value in excess of 1023 N (230 lb) does the resulting brake line pressure at the master cylinder reach the same level as that associated with the slow application. Generally, the lag of booster response during rapid brake applications is felt by the driver as a hard pedal similar to the pedal response with the engine turned off, that is, no power boost.

5.5.5 Master Cylinder

The dynamics of the master cylinder are relatively insignificant in comparison with those of the complete brake system. Major reasons are the small masses of the pistons and high geometrical stiffness of the cylinder. By application of the fundamentals of mechanics, the differential equations governing the dynamics of the master cylinder may be derived. In general, the equations describe the output flow of the master cylinder chambers as a function of the input force and the brake line pressure acting on the chambers.

5.5.6 Brake Line

In the past, hydraulic brake lines have been analyzed by means of the wave equation which describes the longitudinal vibrations of the fluid in the line. For small-diameter hydraulic lines, it has been found that the viscosity of the brake fluid has a significant effect on response time. Good correlation between theoretical analysis and experiment was obtained for a model consisting of a rod representing the fluid, a spring at one end representing the stiffness of the wheel brake, and a pressure input at the other end of the rod. Analysis and test data indicate that the brake line contributes significantly to the response lag of a complete brake system.

5.5.7 Wheel Brake

The dynamic behavior of the wheel brake may be analyzed by the use of several submodels, such as thermal submodel, friction coefficient submodel, static performance submodel, and dynamic performance submodel. The static performance submodel predicts the brake torque as a function of brake line pressure and coefficient of friction between lining and rotor. The brake torque of the submodel is based on expressions similar to Eq. (5-2), however excluding tire radius. The dynamic performance submodel calculates a dynamic brake torque by treating the brake as a mass-spring-damper system. The thermal submodel considers the brake as an energy-conversion and heat-dissipation device in predicting brake temperature, as discussed in Chapter 3. The friction material submodel considers the time-varying coefficient of friction between lining and rotor. The findings on the dynamic performance of wheel brakes indicate that typical wheel brakes are highly responsive brake system components. Furthermore, noticeable differences may exist from one brake design type to the next.

5.5.8 Hydraulic Boost Systems

Hydraulic boost systems without accumulators generally exhibit somewhat quicker response characteristics than those of vacuum-assisted brakes because they are not limited by the response lag of the vacuum booster. However,

because they operate without accumulator, the operating boost pressure must be built up from zero, which contributes to response lag.

Hydraulic boost systems with accumulator have the assist pressure readily available for brake boosting. With a hydraulic booster having the boost characteristics shown in Fig. 5-8, brake response time tests were conducted for a four-wheel disc brake vehicle (Ref. 5.20). The measured brake system transients are shown in Fig. 5-23, where pedal force, master cylinder output pressure, and rear caliper wheel cylinder pressure are presented as a function of time. Inspection of the curves reveals that the pressure at the master cylinder outlet begins to rise approximately 0.06 s after pedal force begins. The average master cylinder brake line pressure lag is less than approximately 0.04 to 0.05 s for pressure up to 1034 N/cm (1500 psi). The corresponding brake line pressure at the rear brake lags the master cylinder pressure by only approximately 0.015 s.

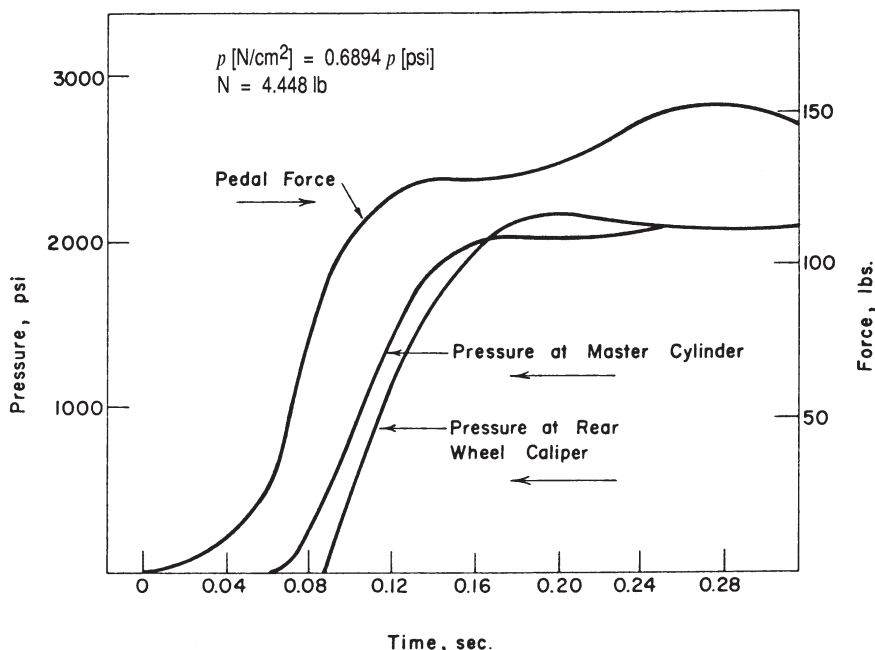


Figure 5-23. Measured brake system transients for a Fiat X1/9 equipped with ATE master cylinder and hydraulic booster.

The transient response behavior of the rear caliper brake line pressure in response to a near-instant accumulator pressure application electrically operated by a solenoid servo valve is shown in Fig. 5-24. Both the human pedal force effects and the master cylinder/booster characteristics were bypassed in the experiment. Inspection of Fig. 5-24 reveals that the rear brake pressure response is not noticeably slowed by the master cylinder/booster system. The rotating wheel (off the ground) stopped approximately 0.06 s after the brake line pressure began to rise in the rear brake caliper.

$$p \text{ [N/cm}^2\text{]} = 0.6894 p \text{ [psi]}$$

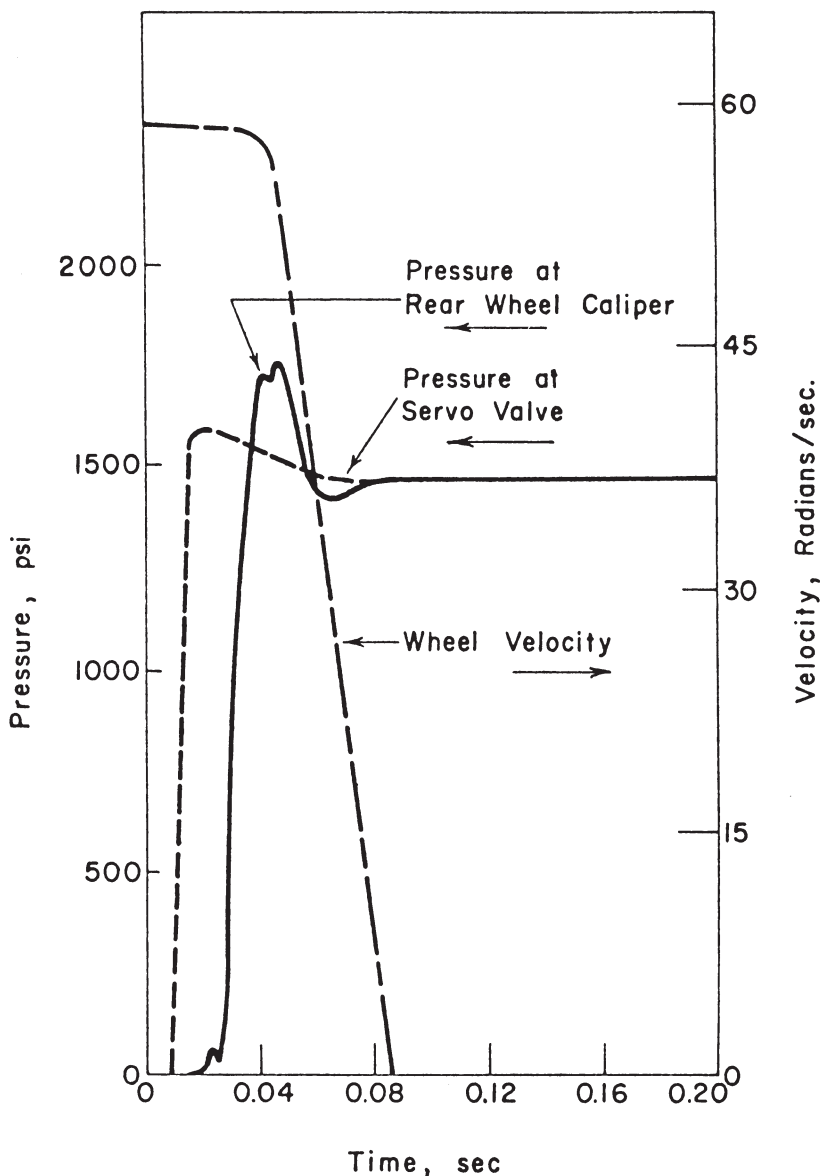


Figure 5-24. Recorded servo-activated brake system transients.

Chapter 5 References

- 5.1 Pierce, B.F., "Human Force Considerations in the Failure of Power Assisted Devices," U.S. Department of Transportation, DOT-HS-800889, July 1973.
- 5.2 Klein, H.C. and H. Strien, "Hydraulic Boosted Brakes-An Important Part of Central Hydraulic Systems," SAE Paper No. 750867, SAE International, Warrendale, PA, 1975.
- 5.3 Kurokawa, Takashi, et al., "Development of Compact Brake Booster," Sae Paper No. 2006-01-0476, SAE International, Warrendale, PA, 2006.
- 5.4 Konishi, Yasuo, et al., "Development of Hydraulic Booster Unit for Active Brake Control," SAE Paper No. 980602, SAE International, Warrendale, PA, 1998.
- 5.5 Leffler, H., et al., "A New Anti-Lock-System (ABS) Light Commercial Vehicles and Passenger Cars With Integrated Hydraulic Brake Booster," SAE Paper No. 865140, SAE International, Warrendale, PA, 1986.
- 5.6 Miller, J.W., "Hy-Power Brake Booster for FMVSS-105 Brake Requirements," SAE Paper No. 770096, SAE International, Warrendale, PA, 1977.
- 5.7 Leibner, Heinz and A. Czinczel, "ABS-Specific Brake Power-Assist Units," SAE Paper No. 845106, SAE International, Warrendale, PA, 1984.
- 5.8 Sheridan, Earl A., et al., "Trailer Vac-A New Hydraulic Trailer Brake System," SAE Paper No. 750868, SAE International, Warrendale, PA, 1975.
- 5.9 Runkle, D.E. and U. Grinbergs, "Single Power Source for Both Power Steering and Power Boosted Brakes," SAE Paper No. 720913, SAE International, Warrendale, PA, 1972.
- 5.10 Schubert, Frank R., "Full Power Hydraulic Brake System for Heavy-Duty Vehicles," SAE Paper No. 720058, SAE International, Warrendale, PA, 1972.
- 5.11 Hydraulic Valves for Motor Vehicle Brake Systems – Performance Requirements, SAE Standard J1137, SAE International, Warrendale, PA.
- 5.12 Prasad, Siva, et al., "Behavior of Deceleration Conscious Pressure Reducing Valve in Automobile Brake System," SAE Paper No. 2005-01-3140, SAE International, Warrendale, PA, 2005.
- 5.13 Nigg, R.L., et al., "The Variable Ratio Master Cylinder – Description of Its Function and Operation," SAE Paper No. 750382, SAE International, Warrendale, PA, 1975.

- 5.14 Wegmann, Enrique, "Relation between Compressibility and Viscoelastic Material Properties of a Brake Pad," SAE Paper No. 2009-01-3017, SAE International, Warrendale, PA, 2009.
- 5.15 Moisture Transmission Test Procedure – Hydraulic Brake Hose Assemblies, SAE Standard J1873, SAE International, Warrendale, PA.
- 5.16 Hunter, John E., et al., "Brake Fluid Vaporization as a Contributing Factor in Motor Vehicle Collisions," SAE Paper No. 980371, SAE International, Warrendale, PA, 1998.
- 5.17 Pang, Patrick Tinchi, "Brake System component Characterization for System Response Performance: a System Level Test Method and Associated Theoretical Correlation," SAE Paper No. 2004-01-0726, SAE International, Warrendale, PA, 2004.
- 5.18 Chao, Williams S., "Brake Hydraulic System Resonance Analysis," SAE Paper No. 975504, SAE International, Warrendale, PA, 1997.
- 5.19 Day, Andrew, et al., "Brake System Simulation to Predict Brake Pedal 'Feel' in a Passenger Car," SAE Paper No. 2009-01-3043, SAE International, Warrendale, PA, 2009.
- 5.20 Limpert, R., "Minicars RSV Brake System," 5th International Automobile Congress, 1977.

Chapter 6



Analysis of Air Brake Systems

6.1 Basic Concepts

Air brakes are power brake systems using compressed air as the energy medium. The brake pedal effort of the operator is used only to modulate the air pressure applied to the brake chambers. Brake systems must have a dual air brake system so that in the event of one circuit failure, emergency braking function is maintained. Although the energy source is compressed air, the transmission of the energy from the brake chambers to the friction surfaces involves pushrods, lever arms, cams, and rollers, or wedges. In the case of air-over-hydraulic brakes, the air pressure is converted into hydraulic pressure, which is used to press the shoes against the drums. All air brake systems have certain components in common. Differences exist between straight trucks, tractors, and trailers. Differences also exist in some design details, with respect to the number of air tanks, disc versus drum brakes, and S-cam versus wedge drum brakes. In some cases, the functions of two air tanks are combined into one larger air tank. In addition, customer preference may introduce slight changes in terms of valves used. Design details vary also between conventional and cab-over vehicles (tilt cab).

The basic tractor trailer system operates as follows: The compressor charges a wet supply reservoir from which two tractor (or truck) reservoirs are fed, namely one front and one rear circuit reservoir. The compressor also charges two reservoirs of the trailer: the trailer service reservoir and the spring brake reservoir. The dual air brake system is modulated by the driver through the dual brake application valve. When the brake application valve is released, all brake chambers exhaust through their respective quick release valves. When the front brake circuit fails, a double check valve and reservoir single check valve immediately close off the front circuit to protect the rear circuit, which continues to function normally. A similar protection is installed in the event of a rear brake circuit failure. Because of the double check valve, air is supplied to the tractor and trailer spring brakes and the trailer service brakes if the tractor rear system becomes inoperative. If both the front and rear brake systems become inoperative, spring brakes will apply automatically when the air pressure drops below approximately 40 psi.

Some vehicles are also equipped with a spring brake control valve. The valve allows the operator to modulate spring brake application by using the brake application valve should a rear circuit failure occur. This allows the rear spring brakes to operate like service brakes up to the capacity of the spring force, equivalent to approximately 60 psi brake line pressure. The spring brake control valve also eliminates the need to activate dash control valves in the case of an emergency and provides normal application and release of the spring brakes. In the event of a complete trailer breakaway, the trailer brakes are applied automatically.

6.2 Foundation Brakes

6.2.1 S-Cam Brakes

Drum brakes are the predominant foundation air brake on medium- and heavy-duty trucks, tractors, and trailers in North America. Over 90% of air brake-equipped heavy vehicles use the S-cam, or to a smaller extent, the wedge actuated foundation designs. In some cases flat-cam brakes are used, and then primarily on front axles.

The *S-cam brake* uses the leading-trailing shoe design. The shoes are applied mechanically by rotation of a cam shaped in an S-form, hence, the name S-cam brake. A typical S-cam brake design for use on a trailer axle is shown in Fig. 6-1. The main parts of this design are leading (top) and trailing (bottom) shoes, S-cam, automatic slack adjuster, and air brake chamber.

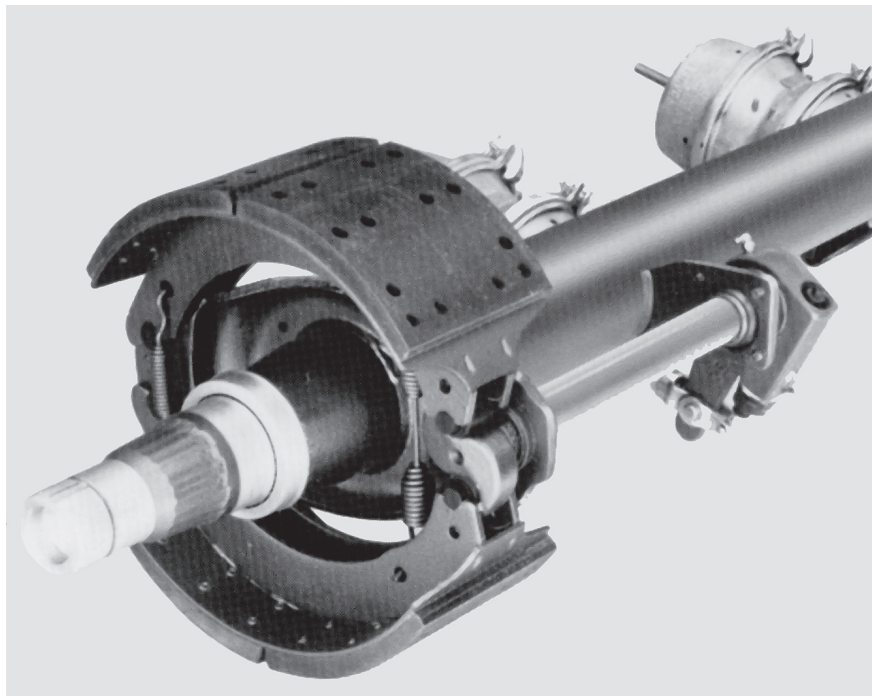


Figure 6-1. S-cam brake with automatic slack adjuster (Rockwell International).

Rotation of the cam pushes the rollers and tips of the shoes apart. Due to cam geometry, the application force against the leading shoe will have a smaller lever arm relative to the pivot anchor of the leading shoe than that of the trailing shoe, resulting in nearly uniform wear of both the leading and trailing shoe and, therefore, long lining life. As discussed in Chapter 2, this is also the reason that the standard leading-trailing shoe brake factor equations must be modified for S-cam brakes. S-cam brakes are simple and rugged. They can be inspected and maintained easily. Their major disadvantage is in stop fade, a limited brake factor, and the need for "tight" adjustment. The mechanical efficiency is approximately 65 to 70% (Refs. 6.1, 6.2, 6.3, 6.4, 6.5).

When the adjustment is at a critical level, often not detectable by the operator, thermal drum expansion and brake lining fade may cause ineffective truck braking. The thermal conditions do not have to involve excessive brake temperatures associated with extensive downhill operation of the truck. Simply exiting a freeway at 80 or 97 km/h (50 or 60 mph) may be sufficient to cause the truck to "run out of brakes" or, more specifically, out of the remaining pushrod travel. Obtaining adequate pushrod travel can be ensured by automatic slack adjusters. Automatic slack adjusters are standard equipment on all S-cam-equipped trucks and trailers. Automatic slack adjusters are required by FMVSS 121. Proper inspection and maintenance are required for safe functioning.

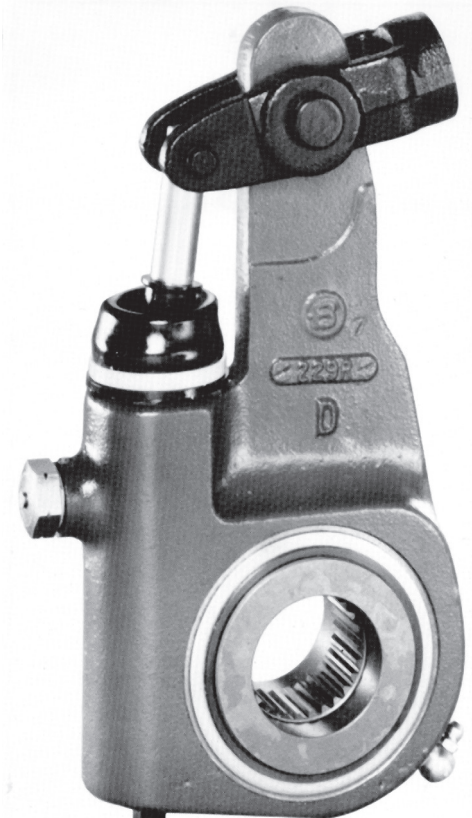


Figure 6-2. Automatic slack adjuster – stroke sensing (Rockwell International).

All automatic adjusters must have a mechanism that allows the position of the slack adjuster to change relative to the S-cam shaft, similar to manual adjustment. There are basically two types of automatic adjuster mechanisms, namely clearance and stroke sensing. With clearance sensing, a clutch stops adjusting once the shoes are firmly in contact with the drum friction surface. In the case of stroke sensing, the geometry change between adjuster rod and slack adjuster during slack rotation causes brake adjustment, as illustrated in Fig. 6-2. Automatic slack adjusters may become defective when improperly maintained (backing off manually).

6.2.2 CamLaster Drum Brake

The *CamLaster* is a new brake developed by Meritor and Freightliner during the late 1990s (Ref. 6.6). Instead of two S-cams, it uses two short pushrods that are actuated by rotation of the camshaft, which is attached to a regular slack adjuster. The effective actuator radius is 12.7 mm (0.5 in.), equaling the cam radius of the S-cam brake.

Dynamometer tests showed the CamLaster brake to produce approximately 10% more brake torque than an S-cam brake with the same lining compound, chamber size, and slack adjuster length.

6.2.3 Wedge Brake

Wedge brakes use either the leading-trailing or two-leading shoe design. A dual-chamber two-leading shoe-type foundation wedge brake is shown in Fig. 6-3. At present, approximately five percent of the air-braked trucks in North America are equipped with wedge brakes. The usage in Europe is considerably higher and increasing (Ref. 6.7). In the wedge brake, a wedge is forced between the tips of the shoes, forcing the linings against the drums. The leading-trailing shoe brake uses one brake chamber, the two-leading shoe brake two. One benefit of wedge brakes is the integral automatic adjuster which ensures optimum drum-to-lining clearance. Another advantage over S-cam brakes is the higher brake factor and, hence, more compact size and lower weight. The mechanical efficiency is approximately 90 to 95%.

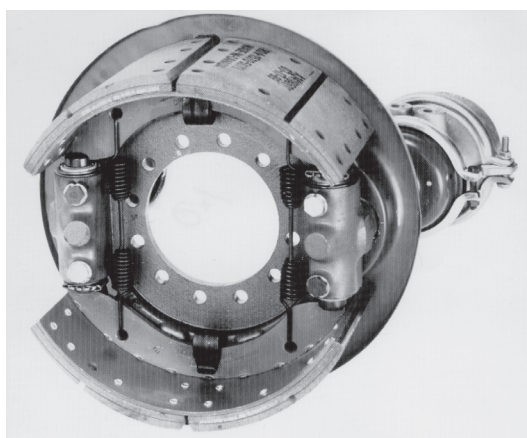


Figure 6-3. Dual-chamber wedge brake (Rockwell International).

6.2.4 Air Disc Brakes

An air disc brake using the floating caliper design is illustrated in Fig. 6-4. Shown in this figure are the ventilated rotor, sealed actuation mechanism, automatic slack adjuster, and air chamber. The rotation of the slack adjuster turns a screw or spindle, which forces the inboard and outboard pads against the disc. The swing-away caliper provides for easy pad changes. The advantages of disc brakes include linear brake factor with changes in pad friction coefficient, better fade resistance, and lighter weight. Adjustment of air disc brakes is accomplished by a regular automatic slack adjuster, if used, as illustrated in Fig. 6-4. Other air disc brake designs use lever arms or roller/ram mechanisms to produce the pressing force.

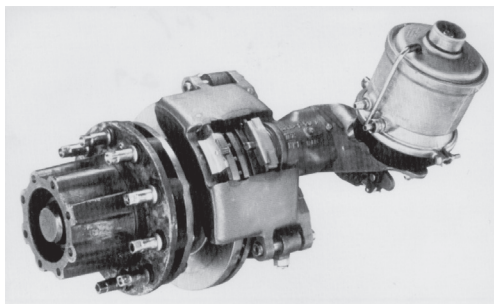


Figure 6-4. Air disc brake (Rockwell International).

6.2.5 Brake Chamber

The brake chamber converts the energy stored in the compressed air into pushrod force at the wheel brake. A combination service brake/spring parking brake is illustrated in Fig. 6-5. It is used as a service brake, an emergency brake in case of air pressure loss, and a spring-applied parking brake. The regular service brake chamber located closest to the slack adjuster applies the service brake in a normal fashion. The spring-loaded parking/emergency brake (power spring) located behind the service brake chamber moves the pushrod; i.e., it applies the brake as the spring is allowed to expand by releasing the hold-off air pressure in the spring chamber.

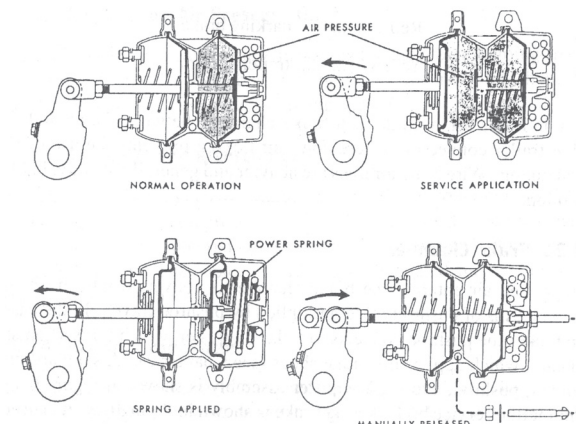


Figure 6-5. "Anchorlok" service brake/spring brake chamber.

The brake chamber illustrated in Fig. 6-5 uses a diaphragm. The size of the brake chamber is identified by the nominal area of the diaphragm. For example, a brake chamber type 30 has a nominal area of 194 cm^2 (30 in.^2) against which air pressure acts. The actual effective area involved in pushrod force production is approximately 5 to 10% smaller due to the rolling action of the diaphragm. Standard brake chamber sizes, maximum and adjustment stroke are shown in Table 6-1.

TABLE 6-1
Pushrod Adjustments

Chamber	Type	Overall Diameter		Maximum Stroke at Which Brakes Should Be Readjusted (for disc brakes, consult manufacturer)	
		in.	cm	in.	cm
Bolted Flange	A (12)	6-15/16	17.62	1-3/8	3.49
Brake Chambers	B (24)	9-3/16	23.34	1-3/4	4.45
	C (16)	8-1/16	20.48	1-3/4	4.45
	D (6)	5-1/4	13.34	1-1/4	3.18
	E (9)	6-3/16	15.72	1-3/8	3.49
	F (36)	11	27.94	2-1/4	5.72
	G (30)	9-7/8	25.1	2	5.08
Clamp Ring	9	5-1/4	13.34	1-3/8	3.49
	12	5-11/16	14.45	1-3/8	3.49
	16	6-3/8	16.19	1-3/4	4.45
	20	6-13/16	17.30	1-3/4	4.45
	24	7-1/4	18.42	1-3/4	4.45
	30	8-1/8	20.64	2	5.08
	36	9	22.86	2-1/4	5.72
Rotochambers	9	4-9/32	10.87	1-1/2	3.81
	12	4-13/32	11.19	1-1/2	3.81
	16	5-13/32	13.73	1-7/8	4.76
	20	5-15/16	15.08	1-7/8	4.76
	24	6-13/32	16.27	1-7/8	4.76
	30	7-1/16	17.94	2-1/4	5.72
	36	7-5/8	19.37	2-5/8	6.67
	50	8-7/8	22.54	3	7.62

A typical diaphragm-type brake chamber pushrod force curve as a function of pushrod travel is shown in Fig. 6-6. It shows that the pushrod force decreases for pushrod travels exceeding certain critical values, making adjustment as shown in Table 6-1 necessary.

Roto chambers use a piston-like design rather than a diaphragm to seal the chamber, resulting in a linear pushrod force output as pushrod travel increases.

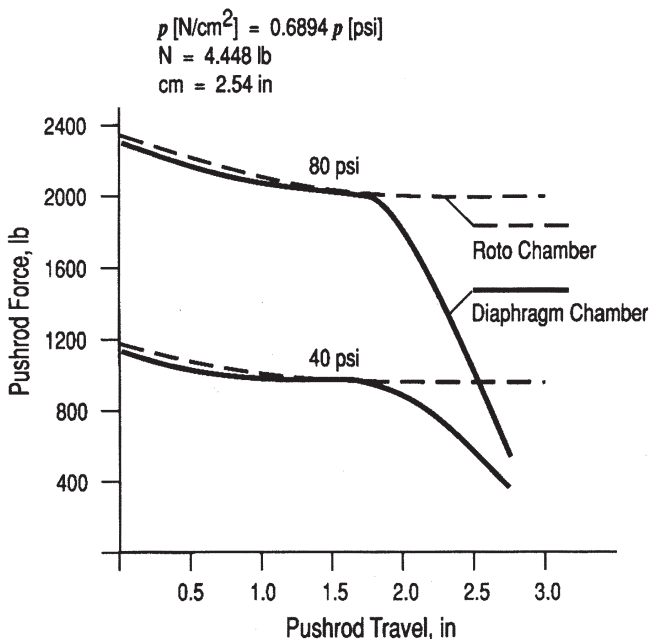


Figure 6-6. Diaphragm and roto chamber pushrod force vs. pushrod travel.

To obtain maximum brake torque, the angle formed between the pushrod and slack adjuster should be 90 degrees when one-half or less of the pushrod travel is used.

In selecting an air brake chamber the following factors must be considered:

For a diaphragm chamber:

- Advantages:
- Compact size requires less space
 - Less sensitive to dirt
 - Low wear

- Disadvantages:
- Relatively small pushrod travel, therefore high adjustment frequency
 - Decreasing pushrod force

For a roto air chamber:

- Advantages:
- Relatively long pushrod travel, therefore low adjustment frequency
 - Constant pushrod force over pushrod travel

- Disadvantages:
- Installation length longer
 - Dirt and wear sensitive
 - Frequent checking of dust boot damage to avoid entry of contaminants

6.3 Brake Torque

The brake torque T_B may be computed by:

$$T_B = (p_l - p_o) A_c B F \eta_m \rho f_a f_F r, \text{ Nm (lbft)} \quad (6-1)$$

where A_c = brake chamber area, cm^2 (in.^2)

BF = brake factor

f_a = brake adjustment reduction factor

f_F = brake temperature fade reduction factor

p_l = brake line pressure, N/cm^2 (psi)

p_o = pushout pressure, N/cm^2 (psi)

r = drum or effective rotor radius, cm (in.)

η_m = mechanical efficiency

ρ = lever ratio or gain between pushrod and brake shoe or pad application

For S-cam or CamLaster brakes, the lever ratio ρ is given by

$$\rho = \ell_s / 2\ell_c \quad (6-2)$$

where ℓ_c = effective cam radius, cm (in.) (standard S-cam and CamLaster brakes use 1.27 cm [0.5 in.] cam radius)

ℓ_s = effective slack adjuster length, cm (in.)

For wedge brakes, the lever ratio is given by

$$\rho = 1 / [2 \tan(\alpha / 2)] \quad (6-3)$$

where α = wedge angle, deg

Wedge angles vary in increments of two degrees, generally between 10 and 18 degrees.

For the Haldex disc brakes DB19, 22, and 22LT, the lever ratio $\rho = 15.8$. Consult brake manufacturers for other disc brakes.

The brake factor is discussed in Chapter 2. The brake factor of S-cam brakes is determined by Eq. (2-22). Brake factors for wedge brakes are obtained from the appropriate equation of Section 2.3.4.10. The brake factor of a typical leading-trailing type S-cam brake is approximately 1.6, indicating an average lining/drum coefficient of friction of approximately 0.35. The typical dual-chamber wedge brake factor is approximately 4 to 4.5, with an average lining friction coefficient of approximately 0.4 or higher.

For brakes in good mechanical condition, the mechanical efficiencies exhibited by S-cam and wedge brakes range from 0.65 to 0.75 and 0.8 to 0.88, respectively (Refs. 6.1, 6.2).

6.3.1 Pushrod Travel Adjustment Factor f_A for Clamp Ring Brake Chambers

Inspection of Fig. 6-6 reveals the decrease of pushrod force with increasing pushrod travel. A type 30 brake chamber will produce a maximum pushrod travel of approximately 70 mm (2.75 in.) when actuated by 69 N/cm² (100 psi). Brake chambers of size 20 and greater begin to experience an initial pushrod force decrease near a travel limit of 44 mm (1.75 in.) The pushrod force curve can be idealized by a constant portion for pushrod travels less than the critical value, followed by a linearly decreasing value for pushrod travels greater than the critical value, as illustrated in Fig. 6-7.

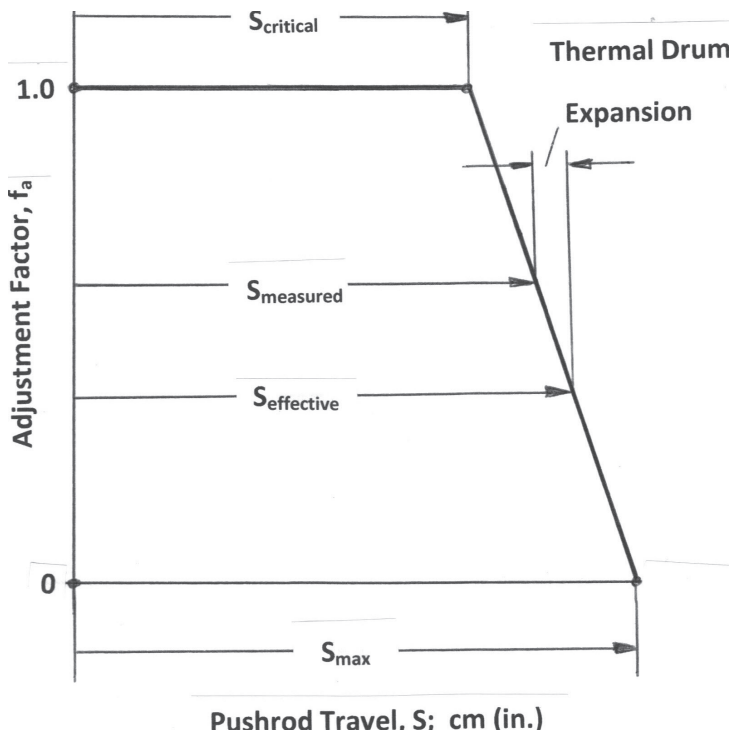


Figure 6-7. Idealized pushrod force vs. pushrod travel.

For example, a type 30 brake chamber has rated pushrod travel of 64 mm (2.50 in.), a critical travel of 51 mm (2.0 in.), and a re-adjust travel of 51 mm (2.0 in.). Limit values for other chamber sizes are shown in Table 6-2.

TABLE 6-2

Pushrod Travels and Limits

Chamber Type (in. ²)	Rated Travel (mm)	Rated Travel (in.)	Re-Adjust Travel (mm)	Re-Adjust Travel (in.)	Critical Travel (mm)	Critical Travel (in.)
9, 12	44	1.75	29	1.375	30	1.20
16, 20, 24	57	2.25	44	1.75	44	1.75
20L, 24L, 30	64	2.50	51	2.0	51	2.0
24L3, 30L3	76	3.0	64	2.5	64	2.5
36	76	3.0	57	2.25	57	2.25

For pushrod travels less than the critical value, the pushrod force is approximately 90% of the theoretical maximum force based on chamber size. The effective pushrod travel S_e for an S-cam brake is that travel that actually existed at the time of the accident or vehicle testing. For brakes operating at an elevated temperature due to prior braking, the thermal expansion of the brake drum requires an increased pushrod travel for the brake linings to contact the drum. If the brake adjustment measurements were obtained with hot brakes immediately after the accident, thermal drum expansion is included in the data collection. When pushrod travel is measured for cold brakes, thermal expansion must be considered if appropriate.

The trapezoidal idealization of the pushrod force, and hence, adjustment factor f_a , as a function of pushrod travel is shown in Fig. 6-7. All pushrod travels used in the PC-BRAKE AIR computer software are identified in Fig. 6-7. The adjustment factor f_a ranges between 0 for an ineffective brake due to excessive pushrod travel without shoe/drum contact ($S_{\text{effective}} \geq S_{\text{max}}$) to 1 for an effective pushrod travel less than the critical one ($S_{\text{effective}} \leq S_{\text{critical}}$).

6.3.2 Temperature Fade Correction Factor f_F for Drum Brakes

When the brake temperature exceeds a certain level, braking effectiveness will be reduced. More specifically, the lining to drum friction coefficient will decrease for higher brake temperatures, resulting in a reduced brake factor and, hence, brake torque. In the case of S-cam brakes, for brake temperatures greater than 589 K (600°F), the brake torque will drop significantly. In general, with the slack adjuster adjusted at 38 mm (1.5 in.) or less, the brake torque will decrease by approximately 30% of its cold value when heated to 589 K (600°F), or by 50% when adjusted to 64 mm (2.5 in.).

In-stop temperature increase will have a similar effect on brake torque. For example, a wedge brake when tested at 32.2 km/h (20 mph) and 41 N/cm² (60 psi) application pressure may produce a brake torque of approximately 13,000 Nm (115,000 lbin.) as compared with 8500 Nm (75,000 lbin.) when tested at 97

km/h (60 mph). It appears that the higher friction surface temperature causes in-stop fade, which may significantly reduce brake torque. It is important to recognize that in-stop fade is a function of the brake lining material used and the type of drum brake used. Dual-chamber wedge brakes have a steeper brake factor versus lining friction coefficient curve, and hence, will experience a greater reduction in brake factor (brake torque) than single-chamber wedge or S-cam brakes with decreasing lining friction coefficient.

The temperature fade factor f_F takes into consideration the decrease in lining-drum coefficient of friction, and hence, reduction of brake factor as brake temperature increases. It is based on brake dynamometer test data (Ref. 2.12). Brake fading of disc brakes is generally not a significant issue in single stops from highway speeds.

The fade factor f_F for S-cam brakes is computed based upon an empirical expression:

$$f_F = 1 \text{ for brake temperature } T \leq 366 \text{ K (200°F)}$$

$$f_F = 1 - 0.00058T \text{ for brake temperature } > 366 \text{ K (200°F)} \quad (6-4)$$

Eq. (6-4) can be used for any size brake chamber. It should be noted that Eq. (6-4) is based on typical dynamometer test data. When nontypical lining compounds are used, Eq. (6-4) may not apply.

6.3.3 Pushrod Travel Increase Due to Thermal Drum Expansion

The drum diameter increases due to thermal expansion as brake temperatures increase. For brakes at elevated temperatures, the pushrod travel of a type 30 chamber with a slack adjuster length of 140 mm (5.5 in.) increases by approximately 0.036 mm/K (0.0008 in./°F). For example, a brake temperature increase of 222 K (400°F) will increase the pushrod travel by 8 mm (0.32 in.) solely due to temperature. In an actual case, a new three-axle dump truck prior to ASA requirements loaded at GVW plus 13,350 N (3000 lb) had its four rear brake pushrod travels at 56 mm (2.2 in.). When exiting on a downgrade freeway off-ramp and slowing from freeway speed, the driver felt his brakes grab and then “lost” his brakes. The thermal expansion of the brake drums was sufficient to cause the brake chamber to bottom out.

6.3.4 Pushrod Travel Measurement

In the examination of accident vehicles, investigators frequently determine the brake adjustment by counting the number of turns or clicks of the adjustment nut as they tighten the shoes against the drum. This should never be done because it will destroy evidence, even if the slack adjusters are backed off by the exact amount to “restore the adjustment evidence.” The tightening of the brakes will force the shoe rollers to operate over a different (new) cam surface, thus eliminating the possibility of determining brake adjustment from a detailed cam surface/roller displacement analysis. The rule of thumb that three clicks correspond to 12.7 mm (0.5 in.) of pushrod travel may not be accurate enough. For a standard type 30 brake chamber/drum assembly, a 1 mm (0.04 in.)

clearance between lining and drum equates to approximately 7.6 mm (0.3 in.) of pushrod travel.

6.3.5 Parking Brake

The parking brake of an air-braked vehicle is applied by a compressed spring. The spring force actuation of a 30/30 type S-cam brake against the pushrod is approximately 8896 N (2000 lb) when the spring is fully compressed, and approximately 3111 N (700 lb) at 64 mm (2.5 in.) adjustment. From these data an empirical expression for F_{spring} may be determined as

$$F_{\text{spring}} = 91(98 - S) \quad , \quad \text{N} \quad (6-5)$$

$$[F_{\text{spring}} = 2000 - 520(S) \quad , \quad \text{lb}]$$

where S = brake adjustment, mm (in.)

For example, for an S-cam brake having a pushrod travel of 57 mm (2.25 in.), the spring force pushing against the slack adjuster arm will be only $91(98 - 57) = 3731$ N [2000 - (520)(2.25) = 830 lb]. For brakes in good adjustment, the maximum spring force equates to approximately 42 N/cm^2 (60 psi) of brake line pressure.

6.4 Vehicle Deceleration

For air brake vehicles, an equation similar to that for vehicles equipped with hydraulic brakes [(Eq. (5-3))] is used. Division of brake torque [Eq. (6-1)] by tire radius R yields the braking force acting on the circumference of the tire, and multiplication by two yields the braking force produced by one axle equipped with two brakes. Summation of the braking forces on all axles yields the deceleration, a , as

$$a = (2/RW) \sum [(p_i - p_o) A_c B F \eta_m \rho f_a f_F r]_i, \quad \text{g-units} \quad (6-6)$$

where i = identity of axle braked

R = tire radius, mm (in.)

W = vehicle weight, N (lb)

For example, for a three-axle truck equipped with an automatic limiting valve on the front axle, Eq. (6-6) is expressed as

$$a = (2 / RW) \{ [(p_1 - p_o) A_c B F \eta_m \rho f_a f_F r]_1 + (p_2 - p_o) r [(A_c B F \eta_m \rho f_a f_F)_2 + (A_c B F \eta_m \rho f_a f_F)_3] \} \quad , \quad \text{g-units} \quad (6-7)$$

where subscripts 1, 2, and 3 identify first (front), second, and third vehicle axle, respectively.

The summation term for each axle having a brake line pressure reducing valve is expressed separately, such as the front axle of the truck. If proportioning or limiting valves are used, expressions for the brake line pressures have to be derived for the particular axle served by the proportioning valve.

6.4.1 Automatic Front Brake Limiting Valve

The automatic front limiting valve was used in the past. Stringent FMVSS 121 requirements including ABS brakes led to its removal (Ref. 6.3).

The valve reduces the exit pressures to the front brakes in relationship to the inlet pressures. The purpose of the automatic limiting valve is to limit the level of braking done by the front brakes for low- to medium-pressure applications to ensure steerability of the vehicle on low-friction road surfaces. Because the ratios between delivery or exit port and inlet pressures are fixed by design, i.e., they cannot be selected by the driver, automatic limiting valves are also called ratio valves. In the past, variable ratio valves, allowing the driver to select a slippery road mode with low exit port pressures or a dry road mode for high exit port pressures, had been in use.

Typically, automatic limiting valves reduce the supply pressure delivered to the valve by approximately 50% as it passes through the valve for supply pressures between 0 and 28 N/cm² (0 to 40 psi). Supply pressures between 28 and 41 N/cm² (40 and 60 psi) are reduced by less than 50%, with no reduction for supply pressures above 41 N/cm² (60 psi).

The intended advantage of the automatic limiting valve is that full braking is available on the front axle with maximum pedal force while inadvertent lockup is less likely on slippery road surfaces. With the manually operated valve, inadvertent setting of the valve to the slippery road mode could result in longer stopping distances while actually braking on a dry road.

A major disadvantage of the valve is that the front brakes are not fully braked, thus allowing the rear brakes of a straight truck or tractor to lock first. Locking of the truck rear axle while the front wheels are still rolling causes directional instability, with the truck spinning out of control if it is traveling at a sufficiently high speed. For tractor-trailer combinations, locking of the tractor rear brakes before front brakes are fully braked causes jackknifing (see Chapter 8).

Use of automatic limiting valves on axles other than the front axle minimizes the potential for inadvertent lockup on that axle. For example, installing an automatic limiting valve on the tractor rear axle will improve directional stability during braking and brake pedal control, because premature rear axle locking is largely prevented. Installing automatic limiting valves on rear axles will affect brake wear balance among axles and may increase the basic response time of the brake system. Advantages and disadvantages must be evaluated carefully by means of a design solution selection table (see Chapter 1) and testing. All PC-BRAKE AIR software programs allow the front axle brakes to be modulated by a limiting pressure valve.

The use of ABS brake systems led to the elimination of automatic limiting valves. However, in the event of an ABS failure, the underlying standard brake system must render the vehicle directionally stable during a maximum effectiveness stop.

6.4.2 Proportioning Valves

The proportioning valve characteristic of air brakes is the same as for hydraulic brake systems. Up to the knee-point pressure, the output pressure of the valve is the same as the input pressure. Beyond the knee-point pressure the output pressure is reduced by the valve slope. In PC-BRAKE AIR software, all vehicle rear axle brake line pressures can be modulated by a proportioning valve. During an ABS failure the standard air brake system in terms of brake balance must render the vehicle and/or combination directionally stable, which may require a simple proportioning valve to be used.

6.5 ABS Modulating Valves

ABS systems for air brakes use concepts similar to those found in hydraulic brake systems. Major components are wheel speed sensors, usually one for each wheel on the axle; an electronic control unit, which collects the sensor information, processes it, and sends control signals to the air pressure modulation valve; and an air pressure modulation valve, which accomplishes the air pressure modulating function using electrical solenoids. The basic control process is illustrated in Fig. 6-8.

Some details associated with the analysis of the ABS control of an air brake system and, in particular, brake line pressure modulation as a function of time are reviewed in the paragraphs that follow.

The time-dependent behavior of vehicle speed V and tire circumferential speed $R\omega$ are illustrated schematically for an air brake system in Fig. 6-9(A). The

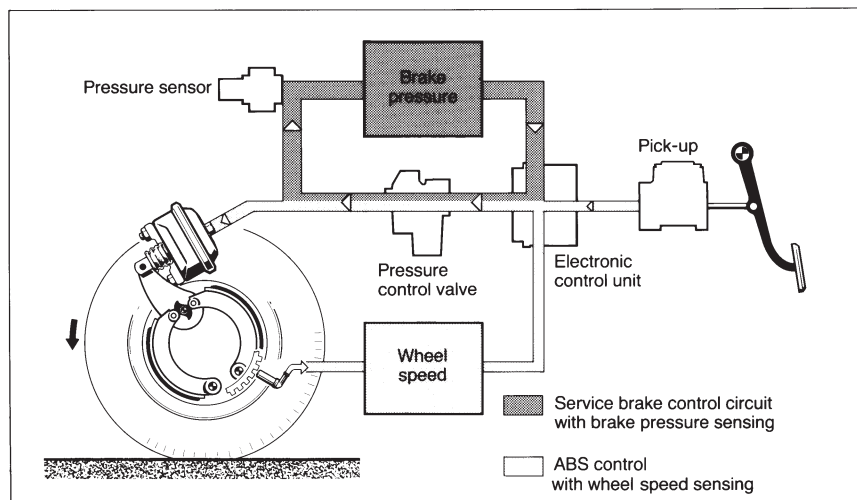


Figure 6-8. Electronically controlled commercial vehicle braking system.

angular velocity of the wheel is designated by ω , the tire radius by R measured in ft. Shown in Fig. 6-9(B) are the characteristics of brake line pressure p_e as a function of time during the ABS control operation.

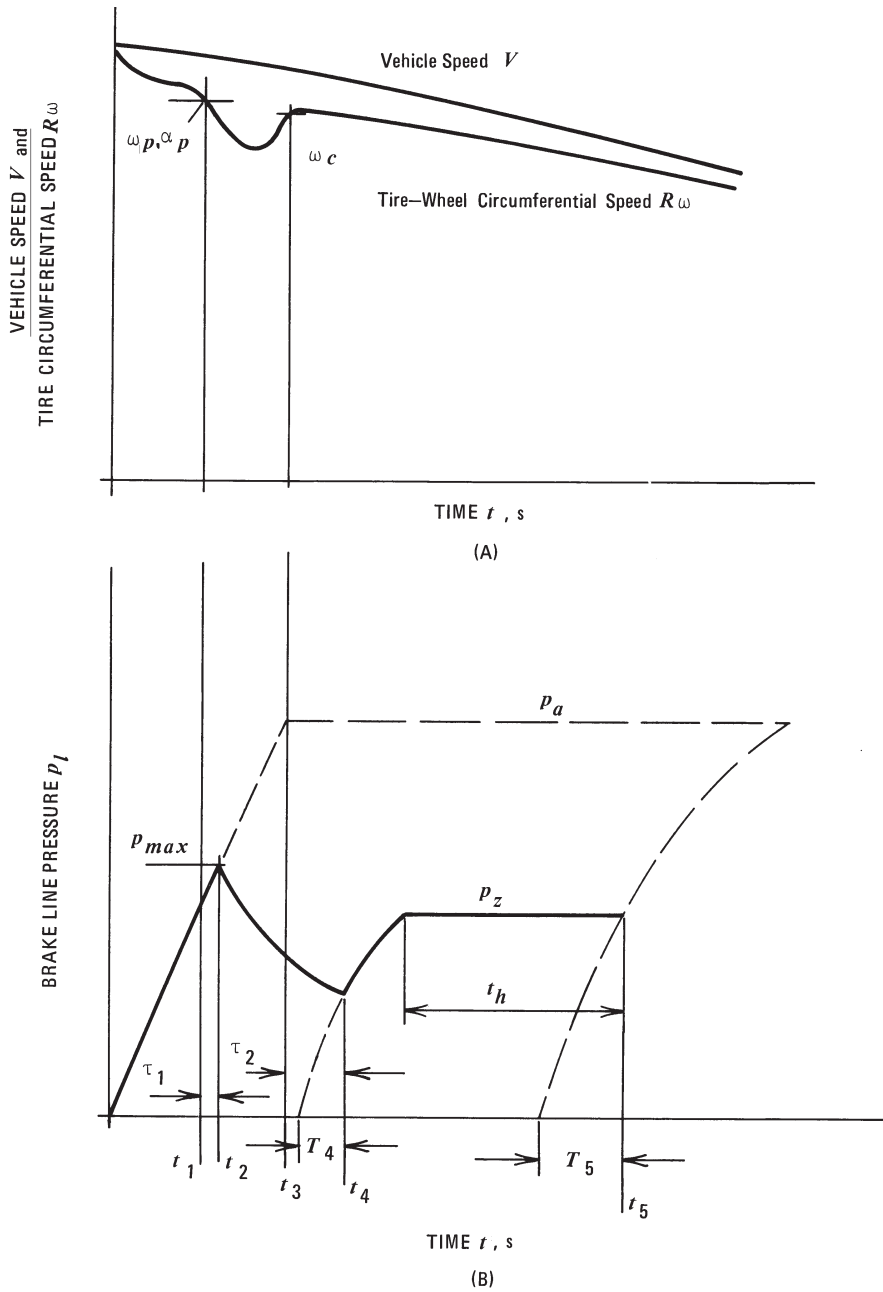


Figure 6-9. ABS control for an air brake system.

As the angular velocity and thus tire circumferential speed $R\omega$ begins to decrease more than the vehicle forward speed V , and reaches a point corresponding to the design threshold angular deceleration α_p , the brake line

pressure modulating valve receives a signal at time t_1 to reduce the pressure. After the response time τ_1 has elapsed, the pressure begins to decrease at time t_2 according to the functional relationship

$$p_\ell = p_{\max} e^{-c_1(t-t_2)} , \text{ N/cm}^2(\text{psi}) \quad (6-8)$$

where c_1 = time constant indicating pressure decrease characteristics, s^{-1}

p_{\max} = maximum brake line pressure, $\text{N/cm}^2(\text{psi})$

t = time, s

t_2 = time at which maximum brake line pressure is reached and pressure decrease begins, s

The decrease in brake line pressure causes the angular velocity of the wheel to increase again (Fig. 6-9[A]). Parallel to this process, an angular velocity ω_c is computed from a specified angular deceleration α_r and from the angular velocity ω_p of the wheel at the instant the threshold value ω_p was exceeded as

$$\omega_c = \omega_p + \alpha_r(t - t_1) , \text{ rad/s} \quad (6-9)$$

where t_1 = time at which ABS signal is received by the brake pressure modulator valve, s

α_r = specified angular deceleration, rad/s

ω_p = wheel angular velocity at peak friction value, rad/s

ω_p is a function of the ABS stop and not a function of vehicle speed, as illustrated in Fig. 6-9(A).

When the actual angular speed of the wheel has attained the computed value ω_c at time t_3 , the brake line pressure modulating valve receives the signal to increase pressure again. After the response time τ_2 has elapsed, the brake line pressure begins to increase at time t_4 according to

$$p_\ell = p_a [1 - e^{-c_2(t-t_4+T_4)}] , \text{ N/cm}^2(\text{psi}) \quad (6-10)$$

where c_2 = time constant indicating pressure increase characteristics, s^{-1}

p_a = applied pressure, $\text{N/cm}^2(\text{psi})$

t_4 = time at which pressure increase begins, s

T_4 = difference between time t_4 and time associated with pressure increase from zero pressure, s

The brake line pressure p_ℓ is increased only to a pressure p_z and always remains below the applied pressure p_a . The brake line pressure p_z is generally somewhat smaller than the pressure that causes lockup to occur. However, if the wheel/

brake tends to lock up again at a pressure equal to or lower than p_z , the previous pressure decreasing and increasing processes are repeated until a pressure p_z is produced which does not cause wheel lockup to occur. This brake line pressure is kept constant until the hold time t_h has elapsed, after which the pressure is increased again toward the applied pressure p_a to allow the ABS system to adjust the braking effort to a different tire-road friction situation that might have developed during the hold time t_h . The pressure increases toward p_a according to the approximate relationship

$$p_e = p_a [1 - e^{-c_3(t-t_5+T_5)}] , \text{ N/cm}^2(\text{psi}) \quad (6-11)$$

where c_3 = time constant indicating pressure increase characteristics, s^{-1}

t_5 = time at which pressure increase begins, s

T_5 = difference between time t_5 and time associated with a pressure increase from zero pressure, s

The use of an adjustable "hold time" t_h has the advantage that the control frequency is adjustable. This allows the prevention of control frequencies near the natural frequencies of suspension and steering components which otherwise may cause undesirable vibrations and damage to suspension components. The air consumption also may be kept low as a result of an adjustable hold time. Except for the steering axle, FMVSS 121 allows wheel lockup for up to one second.

6.6 PC-BRAKE AIR Multi-Axle Software Application

The deceleration of a truck/trailer combination can be calculated by Eq. (6-6). Not considered in the derivation of Eq. (6-6) are dynamic load transfer, tire-road coefficient of friction, and individual brake lockup, which are discussed in Chapters 7 and 8. A total of 12 axles or 24 individual brakes can be analyzed by PC-BRAKE AIR Multi-axle software.

Example 6.1: A twelve-axle coal tractor-trailer combination weighing 729,800 N (164,000 lb) had several brakes out of adjustment. The driver made a maximum effectiveness stop on a 10% down grade. Determine the probable deceleration and stopping distance of the subject combination for a speed of 109 km/h (68 mph) and compare it to the braking performance achieved by safely maintained brakes.

The subject vehicle brake data are shown in Fig. 6-10. The pushrod travel measurements for each brake are indicated. The particular PC-BRAKE AIR is run at a brake line pressure of 62 N/cm² (90 psi). The individual brake force reductions for the specific wheel brakes are shown. For example, the right-side brake of axle 7 produces 5.9% of the total braking force of the vehicle. The swept brake surface temperatures T_B calculated are achieved in a single stop from 109 km/h (68 mph) on a downgrade of 10%. For axle 7, the right swept

surface brake temperature calculated is 533 K (500°F). The input data for the brake temperature T are obtained after some trial-and-error runs.

The results show that the subject vehicle with the defective brake condition achieves a maximum deceleration of 0.218 g. The average deceleration is 0.2 g based upon the brake line pressure delay time of 0.4 s and brake torque buildup time 0.5 s. The probable stopping distance is 237 m (777 ft).

When PC-BRAKE AIR Multi-axle is run for properly adjusted brakes with $S = 25.4$ mm (1 in.) for all brakes, the maximum deceleration is 0.42 g with a stopping distance of 132 m (434 ft).

6.7 Response Time of Air Brake Systems

Air brakes have a relatively long response time and high pressure losses when compared with hydraulic brake systems. The time lag can be minimized through adequate design of the plumbing system (Refs. 6.8, 6.9).

An investigation into the dynamic behavior of air brake systems indicates that the time delay required to overcome clearance between linings and drum becomes smaller with increased brake line pressure and decreased brake chamber piston travel. The time required to build up brake torque also decreases with increasing brake line pressure, increased reservoir pressure, decreased piston travel, and decreased brake line length. For example, increasing the brake line length between the brake application valve and the brake chamber from 1.98 to 10.7 m (6.5 to 35 ft) increases the application time only a little, while the brake line pressure buildup time is nearly doubled. This is the major reason why air reservoirs are located near the brake chambers they serve. In general, brake application time is defined as the time elapsed between the instant of the first brake pedal movement and the instant the brake shoes contact the drum. The buildup time is defined as the time elapsed between the instant the brake shoes contact the drum and the instant a specified brake line pressure is obtained at the brake chambers. FMVSS 121 requires that for trucks and buses a brake line pressure of 41 N/cm^2 (60 psi) be reached at the farthest brake chamber within 0.45 s or less. The optimum result should therefore be achieved with a minimum volume, i.e., tight brake adjustment, and maximum brake line pressure.

The relay quick release valve is designed to relay the driver's foot pedal signal pressure at the reservoir location to apply the brakes to reduce brake line pressure buildup times. The relay portion of the valve acts as a remote control relay station to speed up the application and release of the brakes. The relay valve is usually located at the rear of the vehicle, closest to the brake chamber(s) it serves.

A basic schematic of a relay quick release valve is shown in Fig. 6-11. Typically, the relay valve will have a supply or reservoir port which provides reservoir pressure to the valve from a reservoir located close to the axle(s) braked, a service port which receives the signal pressure from the application valve, one or more delivery ports to permit air pressure to the brake chambers, and an

AIR BRAKE SYSTEM ANALYSIS

12 AXLE TRUCK-TRAILER COMBINATION

CASE ID.: Example 6-1; Figure 6-10

Input Data:		Note:	
Weight of Tractor, lb	$W_1 = 16000$		
Weight of Trailer, lb	$W_2 = 64000$		
Weight of Trailer, lb	$W_3 = 48000$		
Weight of Trailer, lb	$W_4 = 36000$		
Starting Brake Line Pressure, psi	$p_1 = 90$	In any of the PC-BRAKE AIR Software programs, maximum brake temperatures existing at the swept brake surface are calculated based upon a SINGLE STOP. Since thermal brake drum expansion is mainly a function of the average drum temperature, only one half of the calculated value should be used as input data. However, for accidents involving CONTINUED BRAKING (down-hill run-away trucks) often associated with poorly maintained brakes, the brake temperature input data should be obtained from Section 2.3 Continued Braking of PC-BRAKE Temperature. Since Section 2.3 uses a "lumped" temperature distribution analysis, that is, temperature is only a function of time, the calculated value must be used as input data without any modification.	
Road Slope Gradient, fraction (+/-)	$G = 0.1$		
Velocity, ft/sec	$V = 100$		
Temperature, initial °F	$T_i = 100$		
		AXLE 1	
		LEFT	RIGHT
Knee-point Pressure, psi	$p_k = 0$	0	
Valve Slope Reduction	$k = 1$	1	
Swept Brake Drum Area, ft ²	$A_s = 1.8$	1.8	2.8
Chamber Area, in ²	$A_c = 22$	22	30
Brake factor	$BF = 1.3$	1.3	1.3
Pushout Pressure, psi	$p_o = 5$	5	5
Tire Radius, in	$R = 21$	21	21
Drum or Effective Disc Radius, in	$r = 7.5$	7.5	8.25
Mechanical Efficiency	$c = 0.7$	0.7	0.7
Braking Temperature, deg	$T = 245$	493	504
Measured Stroke, in	$S = 2$	1.5	1.75
Maximum rated Stroke, in	$S_{max} = 2.25$	2.25	2.5
Critical Stroke, in	$S_c = 1.75$	1.75	2
Calculated Data			
Effective Pushrod Travel, in	$S_e = 2.12$	1.81	2.07
Adjustment Factor	$f_a = 0.27$	0.87	0.85
Fade Factor	$f_f = 0.86$	0.71	0.71
Mechanical Gain value	$D, S, \text{or } W = 5.00$	5.00	5.50
Braking Force, lb	$F_x = 699$	1890	3029
Brakeline Pressures, Braked Axles, psi	$p_1 = 90$		90
Brake Force Distribution	$BD = 0.013$	0.036	0.058
Braking Energy, BTU/hr	$q = 323288$	874723	1401500
		1397727	983906
		1397727	1574588
			1574588
Maximum Deceleration, g	$a_{max} = 0.218$		
Stopping Time, hours	$t_{st+} = 0.00395$		
Temperature, Brake, °F	$T_B = 247$	497	509
		508	387
		508	560
		560	560
Stopping Distance Equations:			
Input Data			
Brake Line Pressure Delay Time, secs	$t_a = 0.40$		
Brake Torque Build-up Time, secs	$t_b = 0.50$		
Maximum Deceleration, g	$a_{max} = 0.22$		
Vehicle Speed, ft/sec	$V = 100.0$		
Calculated Data			
Average Deceleration, g	$a_{avg} = 0.20$		
Stopping Distance, ft	$S = 777$		

Figure 6-10. PC-BRAKE AIR multi-axle input and output data.

AXLE 5		AXLE 6		AXLE 7		AXLE 8	
LEFT	RIGHT	LEFT	RIGHT	LEFT	RIGHT	LEFT	RIGHT
0	1	0	1	0	1	0	1
2.8		2.8		2.8		2.8	
30	30	30	30	30	30	30	30
1.3	1.3	1.3	1.3	1.3	1.3	1.3	1.3
5	5	5	5	5	5	5	5
21	21	21	21	21	21	21	21
8.25	8.25	8.25	8.25	8.25	8.25	8.25	8.25
0.7	0.7	0.7	0.7	0.7	0.7	0.7	0.7
435	555	100	250	506	499	385	250
1.9	1.5	2.5	2.25	1.75	1.75	2	2.25
2.5	2.5	2.5	2.5	2.5	2.5	2.5	2.5
2	2	2	2	2	2	2	2
2.17	1.86	2.50	2.37	2.07	2.07	2.23	2.37
0.66	1.00	0.00	0.26	0.85	0.86	0.54	0.26
0.75	0.68	1.00	0.86	0.71	0.71	0.78	0.86
5.50	5.50	5.50	5.50	5.50	5.50	5.50	5.50
2489	3400	0	1115	3012	3070	2119	1115
	90		90		90		90
0.048	0.065	0.000	0.021	0.058	0.059	0.041	0.021
1151854	1573242	0	515752	1393957	1420432	980289	515752

436	559	100	251	507	500	386	251
-----	-----	-----	-----	-----	-----	-----	-----

Figure 6-10. PC-BRAKE AIR multi-axle input and output data.

AXLE 9		AXLE 10		AXLE 11		AXLE 12	
LEFT	RIGHT	LEFT	RIGHT	LEFT	RIGHT	LEFT	RIGHT
0	1	0	1	0	1	0	1
2.8		2.8		2.8		2.8	
30	30	30	30	30	30	30	30
1.3	1.3	1.3	1.3	1.3	1.3	1.3	1.3
5	5	5	5	5	5	5	5
21	21	21	21	21	21	21	21
8.25	8.25	8.25	8.25	8.25	8.25	8.25	8.25
0.7	0.7	0.7	0.7	0.7	0.7	0.7	0.7
529	306	250	506	279	386	507	100
1.7	2.15	2.25	1.75	2.2	2	1.75	2.5
2.5	2.5	2.5	2.5	2.5	2.5	2.5	2.5
2	2	2	2	2	2	2	2
2.04	2.31	2.37	2.07	2.34	2.23	2.08	2.50
0.91	0.37	0.26	0.85	0.31	0.54	0.85	0.00
0.69	0.82	0.86	0.71	0.84	0.78	0.71	1.00
5.50	5.50	5.50	5.50	5.50	5.50	5.50	5.50
3175	1528	1115	3012	1318	2111	3004	0
	90		90		90		90
0.061	0.029	0.021	0.058	0.025	0.040	0.058	0.000
1469278	706837	515752	1393957	609839	976676	1390193	0

529	306	251	507	278	385	506	100
-----	-----	-----	-----	-----	-----	-----	-----

Figure 6-10. PC-BRAKE AIR multi-axle input and output data.

Brake Design and Safety

exhaust port which permits air to be exhausted directly to the atmosphere when the brakes are released.

Until the brake application cycle starts, the relay inlet valve is closed and the exhaust is open to the atmosphere. When the brakes are applied, the metered air pressure from the brake application valve forces the relay piston down and closes the exhaust port. Further movement of the piston opens the inlet valve, allowing air to pass from the reservoir to the valve, pass through the delivery

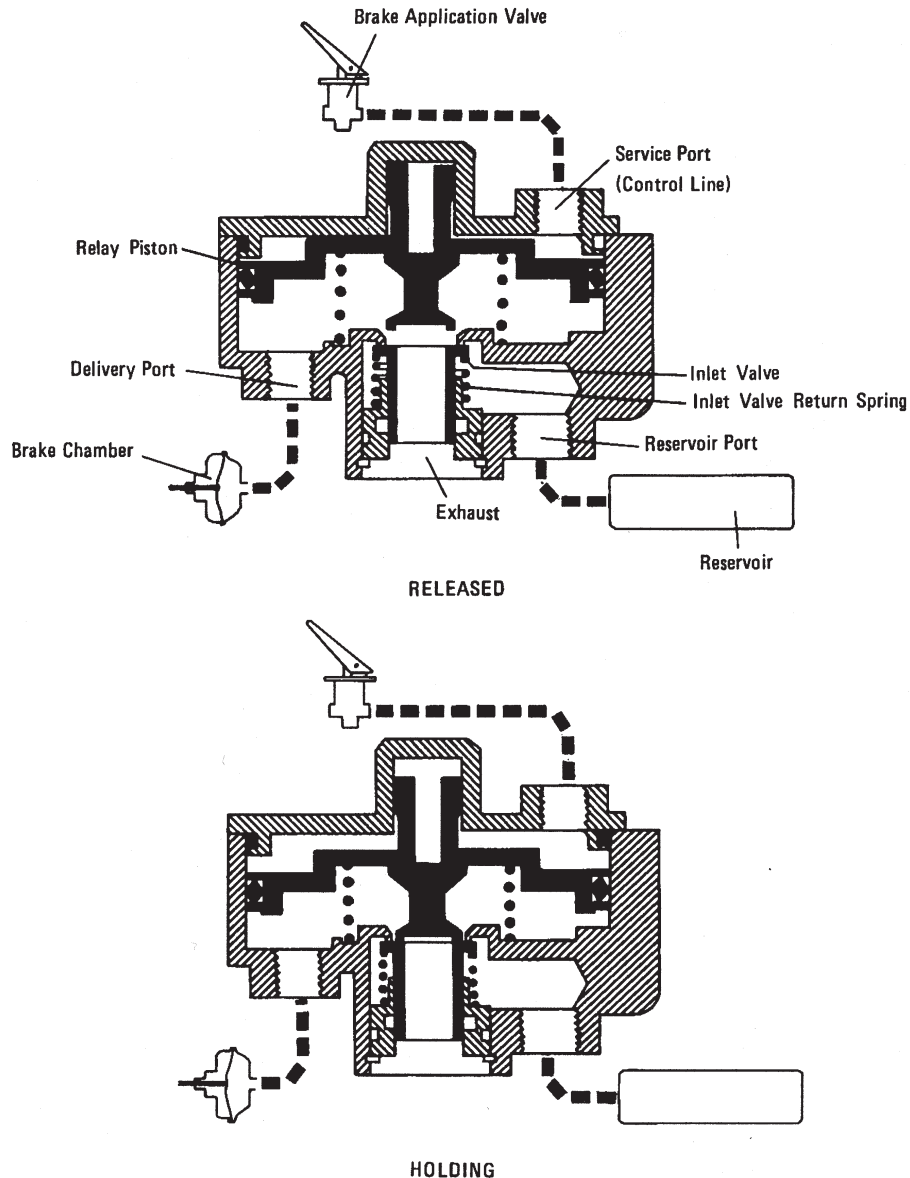


Figure 6-11. Relay quick release valve.

ports, and on to the brake chambers. As brake line pressure underneath the piston equals the controlling pressure above, the piston balances and allows the inlet valve return spring to close the inlet valve. When the brakes are released, the decrease in controlling pressure unbalances the relay piston and permits the exhaust port to open, thus releasing brake line pressure directly to the atmosphere. A simulation and testing of a relay valve is presented in Ref. 6.8.

Experiments have shown that considerable time delays are associated with the control and flow processes in the brake application valve (Ref. 6.10). The time delay of the application valve varies slightly from design to design and depends also on the volume to be pressurized. Typical time delays for application valves range from 0.05 s for a volume of $9.9 \times 10^{-4} \text{ m}^3$ (0.035 ft³) to 0.25 s for a volume of $3.54 \times 10^{-3} \text{ m}^3$ (0.125 ft³).

Brake response time tests are conducted to determine the time required by the brake chamber pressures to reach a specified value. To measure the brake pressure response time of a brake system, pressure transducers are fitted to the output port of the application valve and at the brake chambers to be measured. Typical response times measured on a tractor-semitrailer are presented in Fig. 6-12 (Ref. 6.2). Close inspection of the pressure curves reveals that approximately 0.55 to 0.6 s is required for the pressure to reach 90% of the maximum system pressure.

Inspection of the pressure rise curves of Fig. 6-12 and studies with scaled physical models representing actual pneumatic brake systems have shown that brake system response times may be composed of three parts, as illustrated in Fig. 6-13, each influenced by different factors.

In the first part, a time lag t_1 derives from the speed with which the pressure wave travels through a brake line of given length. This time delay indicates how

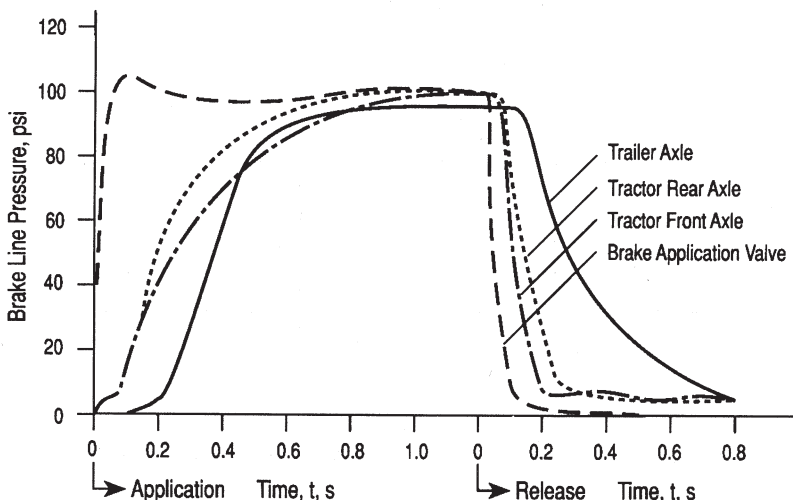


Figure 6-12. Brake response times for tractor-semitrailer combination.

long it will take for the pressure signal to travel from the brake application valve to the relay valve.

The second time lag t_2 derives from the motion of the brake chamber piston required to overcome lining-to-drum clearance. This time lag is proportional to the volume of the brake chamber displaced as the shoes move against the drum.

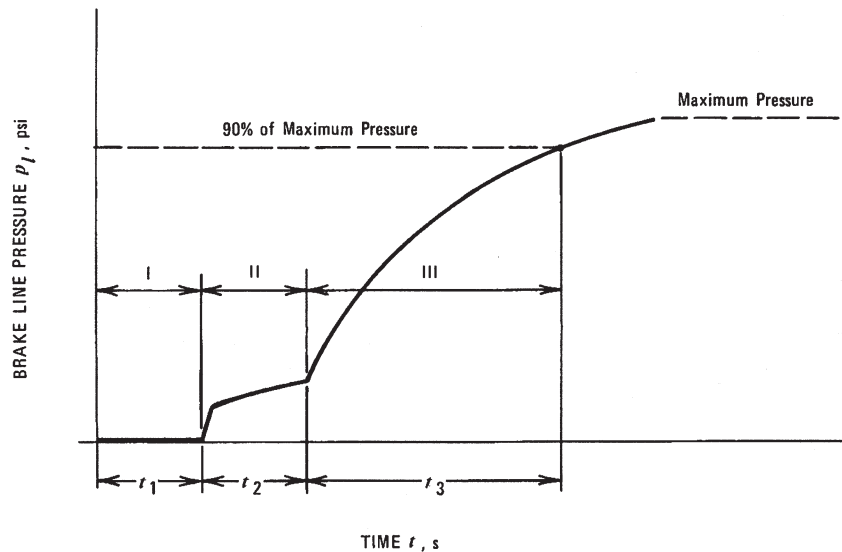


Figure 6-13. Schematic of pressure rise in air brake system.

The third time lag t_3 consists of the time required for the brake line pressure to reach a specified maximum value, typically 90% of the reservoir pressure. This lag is proportional to both the total volume and the flow resistance of the brake system.

To simplify the analysis, a basic air brake system schematic as illustrated in Fig. 6-14 is used.

The time t_1 required for the pressure wave to travel between the brake application valve and the brake chamber is determined by

$$t_1 = \ell_2 / c, \quad \text{s} \quad (6-12)$$

where c = speed of sound in air, m/s (ft/s)

ℓ_2 = length of brake line between application valve and brake chamber, m (ft)
 The speed of sound is a function of the density of the air. For atmospheric conditions, $c \approx 333$ m/s (1000 ft/s). The time is little affected by typical curves and fittings found in air brake systems. The time required by the pressure wave to travel between the application valve and the relay valve/brake chambers located the farthest away is approximately 0.02 to 0.05 s for a tractor-trailer combination.

The time lag t_2 , which is required by the brake line pressure of a typical air brake system in good mechanical condition to overcome brake chamber piston slack (pushrod travel to put shoes against drum) and shoe return

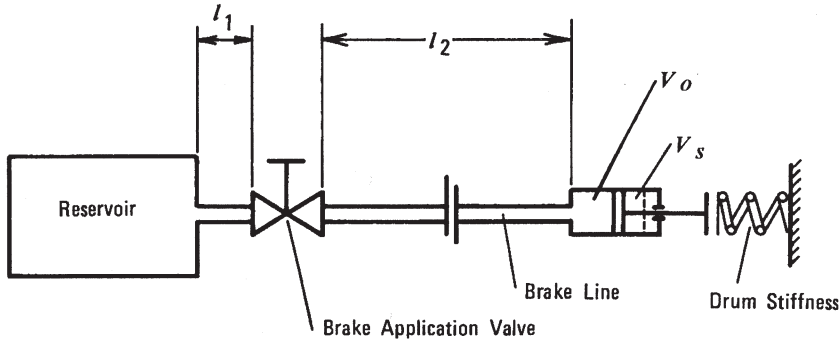


Figure 6-14. Air brake system schematic.

springs, is determined by the volume V_o to be filled before any brake chamber piston movement (pushrod travel adjustment), the volume V_s to be filled to overcome brake chamber piston slack, brake line length ℓ_1 between reservoir and application valve, and line length ℓ_2 between application valve and brake chamber(s). An approximate expression determined from experiment for a typical air brake line (Ref. 6.10) is

$$t_2 = 35.3(V_o + V_s)(0.023\ell_1 + 0.082\ell_2), \quad \text{s} \quad (6-13)$$

$$[t_2 = (V_o + V_s)(0.007\ell_1 + 0.025\ell_2), \quad \text{s}]$$

where ℓ_1 = brake line length between reservoir and brake application valve, m (ft)

ℓ_2 = brake line length between brake application valve and brake chamber, m (ft)

V_o = brake chamber volume to be filled prior to any piston displacement, m^3 (ft^3)

V_s = brake chamber volume to be filled to take up slack, m^3 (ft^3)

The time lag t_3 , which is required for the brake line pressure in the brake chambers to attain 90% of the maximum reservoir pressure, is determined by the total volume between the brake application valve and brake chamber, including the brake line, and is given by the empirical expression

$$t_3 = 4.87(\ell_1 + \ell_2)(V_s + V_o + V_2), \quad \text{s} \quad (6-14)$$

$$[t_3 = 0.042(\ell_1 + \ell_2)(V_s + V_o + V_2), \quad \text{s}]$$

where V_2 = volume of brake line connecting brake application valve and brake chamber, m^3 (ft^3).

The total time lag is increased by the time lags of the brake application valve associated with each of the three pressure phases. The valve time lag can only be determined conveniently by experiment for the particular brake application valve installed in the brake system.

The total time lag t_{total} is

$$t_{\text{total}} = t_1 + t_2 + t_3 + t_v, \quad \text{s} \quad (6-15)$$

where t_v = time lag of brake application valve, s

For example, a tractor-semitrailer combination may have the brake system data that follow:

$$\ell_1 = 3.05 \text{ m (10 ft)}$$

$$\ell_2 = 9.14 \text{ m (30 ft)}$$

$$V_2 = 0.00085 \text{ m}^3 (0.03 \text{ ft}^3)$$

$$V_s = 0.0028 \text{ m}^3 (0.10 \text{ ft}^3)$$

The total time lag computed by Eq. (6-15) is

$$t_{\text{total}} = 0.010 + 0.082 + 0.220 + 0.25 = 0.562 \text{ s}$$

In the calculations $t_1 = 0.01 \text{ s}$, $t_2 = 0.082 \text{ s}$, $t_3 = 0.220 \text{ s}$, and $t_v = 0.25 \text{ s}$ were either assumed or computed.

The time lag due to long brake line length associated with the brakes of articulated vehicles can become critical at higher speeds. Studies have shown that a time lag of one second or more between the brakes of the empty semitrailer and the tractor brakes may cause instability for speeds in excess of 97 km/h (60 mph) due to the increased horizontal forces at the kingpin of the fifth wheel, and the premature brake lockup associated with an empty combination. The relay quick release valve is important for speeding brake application as well as release.

Improvements of brake response times of pneumatic brake systems can be achieved through the use of larger cross section hoses and pipes, improved connectors and fittings, quick release valves, relay valves on tractors and trailers, and trailer brake synchronization. Larger cross section losses are not always beneficial because the increased air mass increases response times.

In articulated vehicles and truck-trailer combinations it is essential that all brakes of the vehicle combination are applied at the same time. If that is not possible, then those of the rear axle of the last trailer are applied first and then the brakes are applied progressively forward to the front axle of the tractor

to avoid too-large fifth wheel kingpin or hitch forces. The proper application of brakes is accomplished by adjusting the relay valve crack pressures so that the lowest value is associated with the relay valve located the farthest from the brake application valve. The relay valve located closest to the brake application valve has the highest crack pressure. Electrically operated solenoid valves (synchronizing valves) have been used to improve sequencing and rapid brake application. Tests have shown that brake synchronization decreases trailer brake application time by about 25% and the release time by more than 40%. The installation of a pressure reducer or proportioning valves and/or wheel anti-lock (ABS) brake systems does not seem to affect either application or release times.

Brake application sequence must not be confused with brake lockup sequence, which, for stability reasons, should always be tractor front axle first, semitrailer axle second, and tractor rear axle last (see Chapter 8).

In the United States it is common practice to define the response time of an air brake system as the time required from the instant of brake pedal movement until a pressure of 41 N/cm^2 (60 psi) is attained in the brake chambers.

Results of road tests have shown that it takes considerably more time to reach maximum brake line pressure and, hence, maximum deceleration than that required to reach 41 N/cm^2 (60 psi).

6.8 Electronic Brake Control (Braking by Wire)

Brake-by-wire control systems are making slow progress in heavy trucks and trailers. After initially being required by FMVSS 121 in 1975, it took more than 20 years for ABS brake systems to become standard equipment on air brakes of trucks and trailers. In standard air brake systems, air pressure is used to control the braking process. The air pressure at the individual wheel brakes is controlled by the operator and by valves. The brake torque is produced by friction between brake shoes and rotating drums or discs. In the electric brake system (EBS), electronic and electric components control the brake line pressure at individual brakes or brakes of one axle (Refs. 6.11, 6.12). The electrical/electronic system consists of the following components: EBS control unit, brake valve with pedal travel sensor, load sensor, trailer control valve, pressure control module per wheel including control for ABS and/or drive traction, brake pad wear sensor per wheel, wheel speed sensor per wheel, and wire cable from each brake to control unit.

The mechanical components are disc or drum brakes, air pressure producing and storage system, as well as mechanical parking brake system.

The driver communicates braking from the brake pedal and sensor electronically to the EBS unit. The EBS also receives signals from the individual brake modules (one per wheel) and the load sensing system (measuring vehicle weight and distribution). The EBS analyzes the information and sends brake pressure signals to the individual brake pressure modulators, as well as to the EBS of the trailer (if any). The pressure modulators cause the appropriate air

Brake Design and Safety

pressure to be delivered to the brakes from the air pressure reservoirs. The ABS function is improved by knowing the “intended” brake pressure on each brake. Advantages include good pedal feel; modulation of braking forces on each wheel as a function of loading and deceleration, resulting in optimum traction utilization on each wheel; and optimization of braking between tractors and trailers.

Chapter 6 References

- 6.1 Radlinski, R., S. Williams, and J. Machey, "The Importance of Maintaining Air Brake Adjustment," SAE Paper No. 821263, SAE International, Warrendale, PA, 1982.
- 6.2 Murphy, R., et al., "Bus, Truck, Tractor-Trailer Braking System Performance," US Department of Transportation Contract No. FH-11-7290, March 1972.
- 6.3 Radlinski, Richard W. and Mark A. Flick, "Benefits of Front Brakes on Heavy Trucks," SAE Paper No. 870493, SAE International, Warrendale, PA, 1987.
- 6.4 Clark, James R., "Extended Service 16.5 Inch Brake Design for Heavy Commercial Vehicles," SAE Paper No. 902250, SAE International, Warrendale, PA, 1990.
- 6.5 Williams, S. F. and R. R. Knipling, "Automatic Slack Adjusters for Heavy Vehicle Air Brake Systems," Research Report DOT HS 807724, TSA, Washington, D.C., February 1991.
- 6.6 Urban, John A., Anthony A. Moore, and Thomas J. MacMenemy, "CamLaster – A New Drum Brake for North America," SAE Paper No. 2000-013508, SAE International, Warrendale, PA, 2000.
- 6.7 Ingram, B. and R. E. Thompson, "Truck Brakes – European Style," SAE Paper No. 861964, SAE International, Warrendale, PA, 1986.
- 6.8 Natarajan, Shankar V., "Modeling The Pneumatic Relay Valve of an S-cam Air Brake System," Master of Science Thesis, Texas A&M University, May 2005.
- 6.9 Subramanian, Shankar C., "Modeling The Pneumatic Subsystem of a S-cam Brake System," Master of Science Thesis, Texas A&M University, May 2003.
- 6.10 Sido, F., "Analysis of Response Characteristics of Pneumatic Brake Systems Through Model Test," Automobiltechnische Zeitschrift, Vol. 71, No. 3, 1969.
- 6.11 Wrede, J. and Heinz Decker, "Brake By Wire for Commercial Vehicles," SAE Paper No. 922489, SAE International, Warrendale, PA, 1992.
- 6.12 Jonner, Wolf-Dieter, et al., "Electrohydraulic Brake System – The First Approach to Brake-By-Wire Technology," SAE Paper No. 960991, SAE International, Warrendale, PA, 1996.

Chapter 7



Single Vehicle Braking Dynamics

7.1 Static Axle Loads

The forces acting on a non-decelerating vehicle, either stationary or traveling at constant velocity on a straight and level roadway, are illustrated in Fig. 7-1. Due to the front-to-rear weight distribution, the front and rear axle may carry significantly different static axle loads.

The level-road static axle load distribution is defined by the ratio of static rear axle load to the total vehicle weight, designated by the Greek letter Ψ as

$$\Psi = F_{zR} / W \quad (7-1)$$

where F_{zR} = static rear axle load, N (lb)

W = vehicle weight, N (lb)

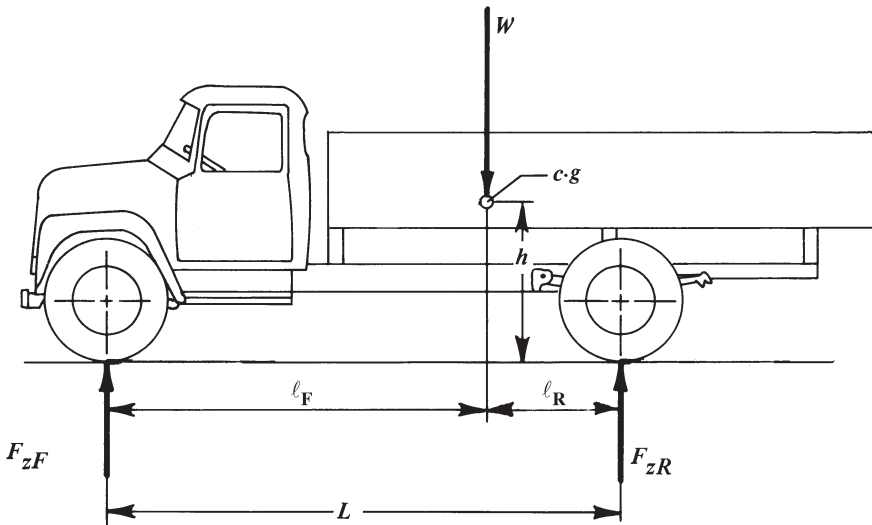


Figure 7-1. Static axle loads.

The relative static front axle load is given by

$$1 - \Psi = F_{zF} / W \quad (7-2)$$

where F_{zF} = static front axle load, N (lb)

Modern front-wheel-drive cars have Ψ -values for the empty conditions as low as 0.35, indicating that only 35% of the total weight is carried by the rear axle. This relatively low static rear axle load of a car or pickup truck when lightly loaded is one of the major reasons that a careful brake balance analysis to avoid premature rear brake lockup is required.

Application of moment balance about the front axle of the stationary vehicle shown in Fig. 7-1 yields

$$W\ell_F = F_{zR}L$$

where L = wheelbase, m (ft)

ℓ_F = horizontal distance from center of gravity to front axle, m (ft)

Solved for the horizontal distance ℓ_F between front axle and center of gravity

$$\ell_F = F_{zR}L / W = \Psi L \quad , \quad \text{m (ft)}$$

Similarly, for the horizontal distance ℓ_R between the rear axle and the center of gravity

$$\ell_R = (1 - \Psi)L \quad , \quad \text{m (ft)}$$

7.2 Dynamic Axle Loads

When the brakes are applied, the torque developed by the wheel brakes is resisted by the tire circumference where it comes in contact with the ground. Prior to lockup, the braking force is a direct function of the torque produced by the wheel brake. For hydraulic brakes, Eq. (5-2) is used for determining the actual braking forces; for air brakes an equation similar to Eq. (6-1) is used.

The forces acting on a two-axle vehicle decelerating on a straight and level road are illustrated in Fig. 7-2. Aerodynamic effects as well as engine braking are ignored.

Application of moment balance about the rear tire-to-ground contact point yields the dynamic normal force $F_{zF,dyn}$ on the front axle:

$$F_{zF,dyn} = (1 - \Psi + \chi a)W \quad , \quad \text{N (lb)} \quad (7-3a)$$

where $a = F_{x,\text{total}}/W = \text{deceleration, g-units}$

$F_{x,\text{total}}$ = total braking force, N (lb)

$F_{zR,\text{static}}$ = normal rear axle load without braking, N (lb)

W = vehicle weight, N (lb)

χ = center of gravity height (h) divided by wheelbase (L)

$\psi = F_{zR,\text{static}}/W$

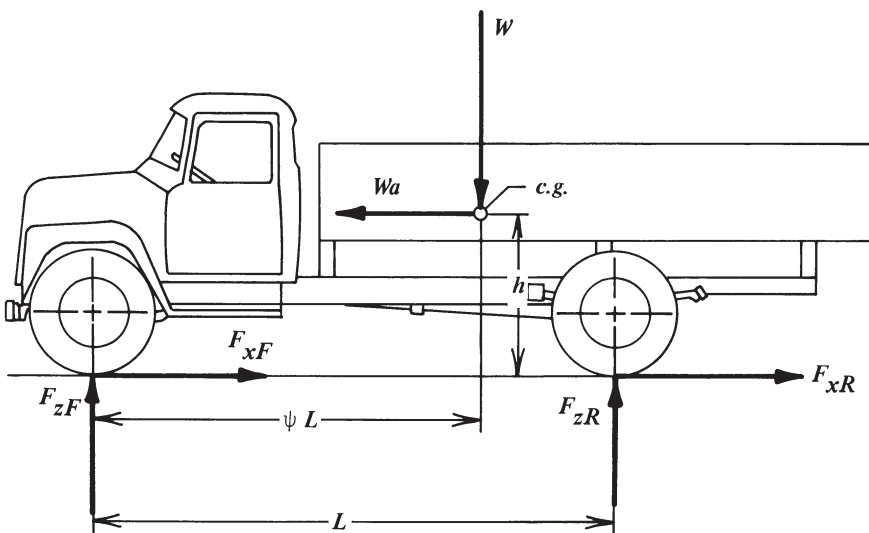


Figure 7-2. Forces acting on a decelerating vehicle.

Similarly, moment balance about the front tire-to-ground contact point yields the dynamic rear axle normal force $F_{zR,\text{dyn}}$:

$$F_{zR,\text{dyn}} = (\Psi - \chi a)W \quad , \quad \text{N (lb)} \quad (7-3b)$$

Inspection of Eqs. (7-3a) and (7-3b) reveals that the dynamic normal axle forces are linear functions of deceleration, a ; i.e., straight-line relationships. The amount of load transfer off the rear axle (and onto the front axle) is given by the term $\chi a W$ in Eqs. (7-3a) (7-3b). The normal axle loads of a typical front-wheel-drive car are illustrated in Fig. 7-3 for the driver-only and fully laden cases. Inspection of the axle loads reveals that the rear axle load is significantly less at higher decelerations than that associated with the front axle. For example, the rear axle load has decreased from a static load of 3114 N (700 lb) to only 1334 N (300 lb) for a 1 g stop, while the front axle load has increased from 5782 to 7562 N (1300 to 1700 lb).

The relative center-of-gravity height χ of a typical passenger car does not change significantly, if at all, from the driver-only to the fully laden condition.

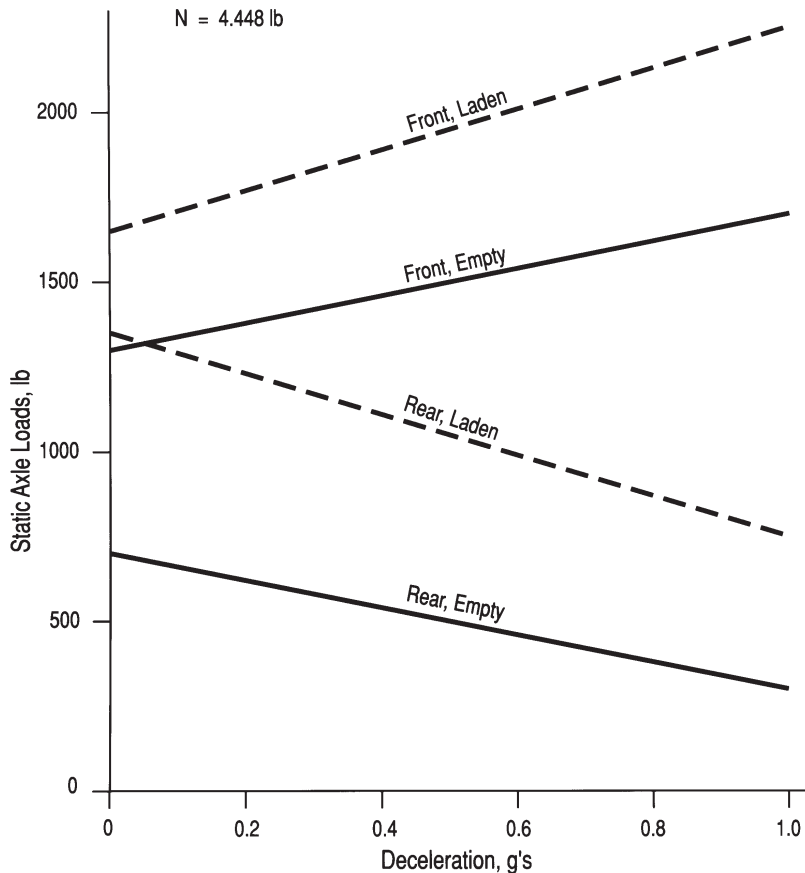


Figure 7-3. Dynamic axle loads for empty and laden vehicle (2000 and 3000 lb)

7.3 Optimum Braking Forces

7.3.1 Braking Traction Coefficient

The wheel brake torques produce braking or traction forces caused by the circumferential slip between the tire and the ground. The ratio of braking force to dynamic axle load is defined as the traction coefficient μ_{Ti} :

$$\mu_{Ti} = F_{xi} / F_{zi,dyn} \quad (7-4)$$

where F_{xi} = axle braking force, N (lb)

$F_{zi,dyn}$ = dynamic axle load, N (lb)

i = front or rear axle

The traction coefficient varies as either braking force or dynamic axle load change and, consequently, is a vehicle- and deceleration-dependent parameter. In general, the front and rear axle traction coefficients will be different. The traction coefficient must not be confused with the tire-road coefficient of friction.

Consider the following braking test. The driver applies the brake pedal such that the front brakes develop a braking force $F_{xF} = 2224 \text{ N}$ (500 lb), the rear $F_{xR} = 1334 \text{ N}$ (300 lb). The vehicle weighs $W = 13,344 \text{ N}$ (3000 lb). The deceleration is $(2224 + 1334)/13,344 = 0.27 \text{ g}$. Assuming the dynamic front axle normal force is $F_{zF,dyn} = 8896 \text{ N}$ (2000 lb), then the front axle tire traction coefficient is $\mu_{TF} = F_{xF}/F_{zF} = 2224/8896 = 0.25$ (500/2000 = 0.25). The rear axle tire traction coefficient is $\mu_{TR} = 1334/(13344 - 8896) = 0.3$. Which axle will lock up when the test is run on a roadway with a tire-road coefficient of friction of 0.8, 0.3, or 0.25?

On the dry road with $\mu = 0.8$, no brakes lock because the friction available (road torque = tire-road friction coefficient multiplied by normal force and tire radius) far exceeds the highest demand (brake torque). On the wet-slippery road (0.3), the rear brakes will just lock up because the demand equals availability ($\mu_{TR} = \mu = 0.3$). For the icy road (0.25), the front brakes lock also because braking demand equals road friction availability.

Consequently, we conclude that the brakes of a particular axle (i) will only lock or use ABS modulation when μ_{Ti} is equal to or greater than μ_{Road} . The concept of the traction coefficient will be used in brake system design, brake accident causation, directional stability, as well as the combined braking-steering analysis. The braking forces will be computed from the brake system hardware using the appropriate equations of Chapter 5 (hydraulic brakes) or Chapter 6 (air brakes). The dynamic axle loads will be computed from the appropriate equations of Chapter 7 (single vehicle) or Chapter 8 (truck-trailer combinations).

7.3.2 Dynamic Braking Forces

Solving Eq. (7-4) for the front braking force and using the dynamic normal force [Eq. (7-3a)] yields the braking force F_{xF} for the front axle:

$$F_{xF} = (1 - \Psi + \chi a)W\mu_{TF} \quad , \quad \text{N (lb)} \quad (7-5a)$$

Similarly, the braking force F_{xR} for the rear axle is:

$$F_{xR} = (\Psi - \chi a)W\mu_{TR} \quad , \quad \text{N (lb)} \quad (7-5b)$$

where μ_{TF} = front traction coefficient

μ_{TR} = rear traction coefficient

The tire-road friction coefficients μ_F or μ_R , existing at either the front or rear tires, are indicators of the ability of a road surface to allow traction to be produced for a given tire and, as such, are fixed numbers. A braked tire will continue to rotate as long as the traction coefficient computed by Eq. (7-4) is less than the tire-road friction coefficient, otherwise it will lock up or the ABS system will begin to modulate. At the moment of incipient tire lockup, the traction coefficient equals the tire-road friction coefficient.

When both axles are braked at sufficient levels so that the front and rear wheels

are operating at incipient or peak friction conditions, then the maximum traction capacity between the tire-road system is utilized; that is, $\mu_{TF} = \mu_F$ and $\mu_{TR} = \mu_R$. Under these conditions the vehicle deceleration will be a maximum, because all traction front and rear is utilized, and the traction coefficients are also equal to the vehicle deceleration measured in g-units.

7.3.3 Optimum Braking Forces

For straight-line braking on a level surface in the absence of any aerodynamic effects, optimum braking in terms of maximizing vehicle deceleration is defined by

$$\mu_F = \mu_R = a \quad (7-6)$$

where a = vehicle deceleration, g-units

μ_F = front tire-road friction coefficient

μ_R = rear tire-road friction coefficient

Frequently, the word “ideal” is used in place of the word optimum. The optimum condition expressed by Eq. (7-6) must not be confused with “ideal” conditions because there are a variety of operational conditions under which Eq. (7-6) does not yield optimum braking results. For example, for braking-in-a-turn maneuvers, not all tire-road friction can be utilized for braking because lateral tire forces must share in the total traction available with the braking forces. Furthermore, simultaneous front and rear wheel lockup produces a different vehicle response which may exhibit gentle vehicle rotation, while front wheel lockup first will not.

The optimum braking forces may be determined by setting the traction coefficients equal to vehicle deceleration in Eqs. (7-5a) and (7-5b), resulting in the optimum normalized braking force $F_{xF, \text{opt}}/W$ on the front axle

$$F_{xF, \text{opt}}/W = (1 - \Psi + \chi a)a \quad (7-7a)$$

and the optimum normalized braking force $F_{xR, \text{opt}}/W$ on the rear axle

$$F_{xR, \text{opt}}/W = (\Psi - \chi a)a \quad (7-7b)$$

It will prove convenient to use the normalized dimensionless braking forces of Eqs. (7-7a) and (7-7b); that is, the braking force per unit vehicle weight in the braking analysis of the single vehicle (Refs. 7.1, 7.2).

Inspection of Eqs. (7-7a) and (7-7b) reveals a quadratic relationship relative to deceleration, a .

Example 7-1:

The graphical representation of the optimum braking forces is a parabola as illustrated in Fig. 7-4 for a passenger car with $W = 16,013 \text{ N}$ (3600 lb), $F_{zR, \text{static}}$

$= 6672 \text{ N (1500 lb)}$, center-of-gravity height $h = 0.61 \text{ m (24 in.)}$, and wheel base $L = 2.77 \text{ m (9.09 ft)}$. The calculations underlying Fig. 7-4 were obtained from MARC 1-V module software. Consequently, the dimensionless parameters are $\psi = 1500/3600 = 0.417$ and $\chi = 2/9.09 = 0.22$. The optimum braking forces were calculated for decelerations ranging from 0.10 to 1.2 g. Anywhere on the curved optimum line, the braking forces front and rear are optimum braking forces. Consider the point marked 0.9 (g). The normalized front braking force is 0.7, the normalized rear braking force 0.2. Newton's second law is satisfied because

$$F_{xF, \text{opt}}/W + F_{xR, \text{opt}}/W = a \quad (7-8)$$

$$0.7 + 0.2 = 0.9 \text{ g}$$

Thursday, June 10, 2010
 MOTOR VEHICLE ACCIDENT RECONSTRUCTION AND CAUSE ANALYSIS
 ***** PROGRAM 'V-1' RUN FOR Example 7-1. Empty vehicle. *****
 OPTIMUM BRAKING FORCES DIAGRAM

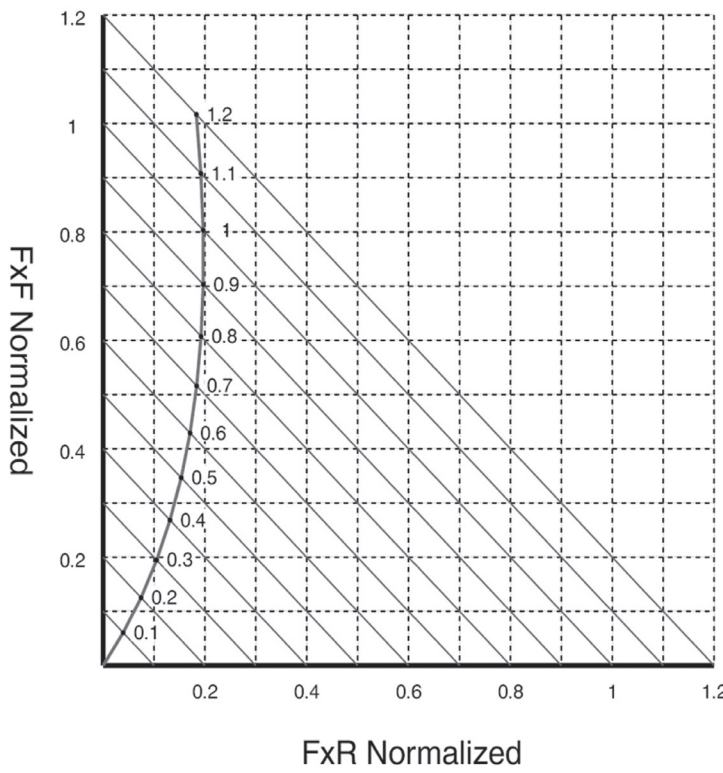


Figure 7-4. Optimum braking forces diagram.

Starting from the same optimum point $a = 0.9$, we follow the 45-degree line to the right until it reaches, let's say, $F_{xR, \text{opt}} = 0.6$. Tracing a horizontal line to the left indicates $F_{xF, \text{opt}} = 0.3$. Because $0.3 + 0.6 = 0.9$, we conclude that any point on a particular 45-degree line has the same deceleration.

Inspection of Eqs. (7-7a) and (7-7b) reveals that the optimum braking forces of a single vehicle (without trailer) are only a function of the particular vehicle geometry and weight data, i.e., Ψ and χ , and vehicle deceleration, a . They are not a function of the brake system hardware installed.

To better match actual with optimum braking forces, it becomes convenient to eliminate vehicle deceleration by solving Eq. (7-7a) for deceleration, a , and substituting into Eq. (7-8). The result is the general optimum rear braking force equation

$$(F_{xR} / W)_{opt} = \sqrt{\frac{(1-\Psi)^2}{4\chi^2} + \left(\frac{1}{\chi}\right)\left(\frac{F_{xF}}{W}\right)} - \frac{1-\Psi}{2\chi} - \frac{F_{xF}}{W} \quad (7-9)$$

Eq. (7-9) allows computation of the appropriate optimum rear braking force associated with an arbitrarily specified (optimum) front braking force.

The graphical representation of Eq. (7-9) is that of a parabola, illustrated in Fig. 7-5. The optimum curve located in the upper right quadrant represents braking, the lower left acceleration. Only the braking quadrant, and then only the section exhibiting deceleration ranges of interest, are of direct importance to brake engineers. The optimum curve shown in Fig. 7-5 represents the section of interest relative to deceleration ranges encountered frequently.

The entire optimum braking/acceleration forces diagram, however, is used to develop useful insight and design methods for matching optimum and actual braking forces for brake design purposes. In addition, the methods will also be used in the reconstruction of actual vehicle accidents involving braking and loss of directional stability due to premature rear brake lockup.

7.3.4 Lines of Constant Friction Coefficient

For increasing deceleration, assuming that the tire-road friction is high enough, the optimum braking of the rear axle begins to decrease and reaches zero where it intercepts the front braking axis. At this point, the deceleration of the vehicle is sufficiently high that the rear axle begins to lift off the ground due to excessive load transfer, sometimes observed during severe braking of motorcycles.

Similarly, in the case of increasing acceleration, the front axle begins to lift off the ground when the optimum acceleration curve intercepts the rear braking force axis. The lower left-hand portion of the diagram shown in Fig. 7-5 represents the optimum acceleration or drive thrust forces. It is used to analyze traction control dynamics.

The zero point on the rear braking force axis is determined by setting the relative front braking force equal to zero in Eq. (7-9), and solving for the relative rear braking force, resulting in

$$F_{xF}/W = 0 \Rightarrow F_{xR} / W = -(1-\Psi) / \chi$$

Similarly, setting the relative rear braking force equal to zero in Eq. (7-9) yields

$$F_{xR} / W = 0 \Rightarrow F_{xF} / W = \Psi / \chi$$

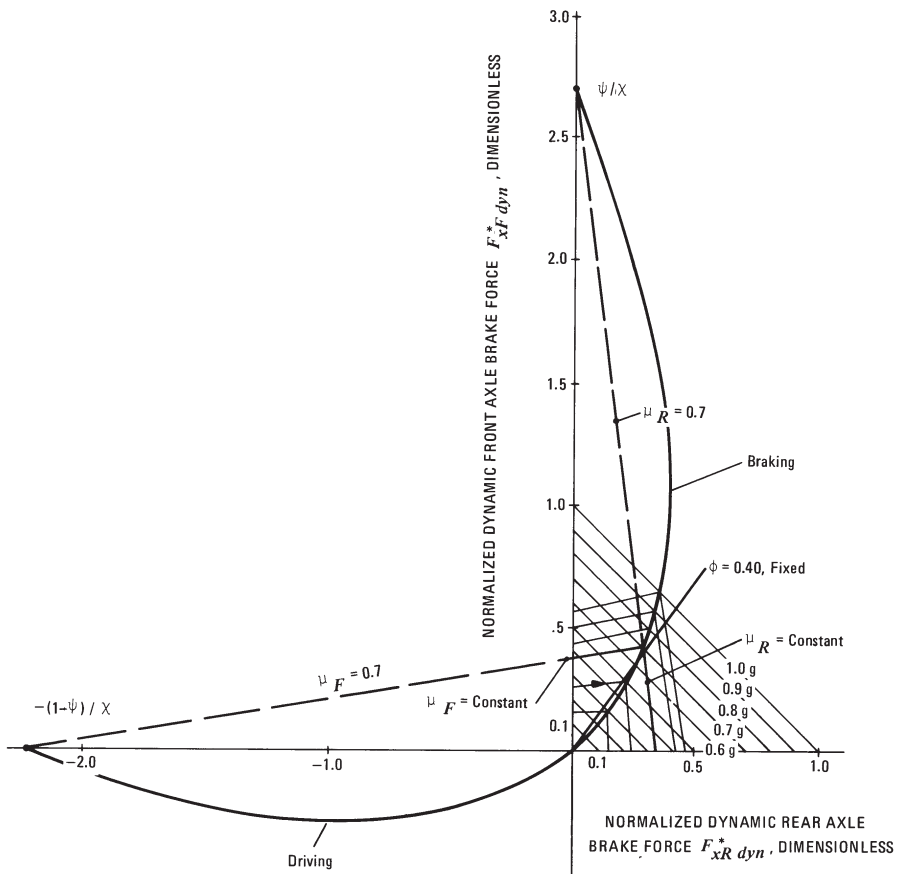


Figure 7-5. Parabola of normalized braking and driving forces.

Any point on the optimum braking forces curve represents the condition for which the front and rear tire-road friction coefficients are equal to each other as well as to the deceleration of the vehicle. Under these conditions, all available tire-road friction is utilized for vehicle deceleration. For example, at the 0.6 g optimum point, the front and rear tire-road friction coefficients are also equal to 0.6.

At the respective zero points, the tire traction forces, either braking or accelerating, are zero regardless of the level of friction coefficient existing between the tire and the ground due to the normal forces between the tire and the ground being zero.

A straight line connecting the zero point $[-(1 - \Psi)/\chi]$ and a point of the optimum force curve represents a condition of constant coefficient of friction between the front tire and ground. For example, in Fig. 7-5 connecting the zero point with the 0.7 g optimum point establishes a line of front tire friction coefficient of $\mu_F = 0.7$, constant along the entire line. Additional lines of constant friction are obtained by connecting different optimum points.

Similarly, by connecting the rear zero point (Ψ/χ) with points on the optimum curve, lines of constant rear tire friction coefficient are obtained.

Inspection of Fig. 7-5 reveals that the constant front coefficient of friction line of $\mu_F = 0.7$ intercepts the front braking force axis (y-axis) with the rear braking force equal to zero at a deceleration of approximately 0.39 g. In other words, when braking on a road surface having a tire-road friction coefficient of 0.7 with the rear brakes failed or disconnected, the front brakes are at the moment of lockup while the vehicle decelerates at approximately 0.39 g; that is, the maximum deceleration is 0.39 g.

On the other hand, when the front brakes are disconnected, the rear brakes lock up at a deceleration of approximately 0.33 g while braking on a road surface with a 0.7 coefficient of friction, as indicated by the interception of the 0.7 constant rear friction line with the rear braking force axis (x-axis).

The deceleration a_F achievable with the rear brakes disconnected is derived from Newton's Second Law and Eq. (7-5a); however, the traction coefficient is equal to the front tire-road friction coefficient because the front brakes are about to or have locked up:

$$F_{xF} = (1 - \Psi + \chi a_F) \mu_F W = a_F W$$

$$(1 - \Psi) \mu_F = a_F (1 - \chi \mu_F)$$

Solving for deceleration a_F with the rear brakes disconnected yields

$$a_F = \frac{(1 - \Psi) \mu_F}{1 - \chi \mu_F} , \text{ g-units} \quad (7-10a)$$

A similar derivation yields the deceleration a_R with the front brakes disconnected:

$$a_R = \frac{\Psi \mu_R}{1 + \chi \mu_R} , \text{ g-units} \quad (7-10b)$$

where μ_F = front tire-road friction coefficient

μ_R = rear tire-road friction coefficient

It becomes convenient to use Eqs. (7-10a) and (7-10b) along with the optimum points to draw the lines of constant friction coefficient rather than using the zero points.

Example 7-2:

Calculate the maximum deceleration for the vehicle data of Example 7-1 for a tire-road coefficient of friction of 0.8 when the rear parking brake is applied while driving. The braking forces diagram based on the data of the empty vehicle is shown in Fig. 7-6. Eq. (7-10b) applies. Substitution yields $a_R = ((0.417)(0.8)/(1 + (0.22)(0.8))) = 0.284$ g. In Fig. 7-6, drawing a straight line connecting points 0.284, 0.8 and $\psi/\chi = 0.417/0.22 = 1.9$ yields the rear line of constant

coefficient of friction $\mu_R = 0.8$. Fig. 7-6 can be used to quickly determine decelerations for any tire-road friction coefficient. For example, for $\mu = 0.5$ (wet road) the rear brakes-locked deceleration would be approximately $a_R = 0.18 \text{ g}$.

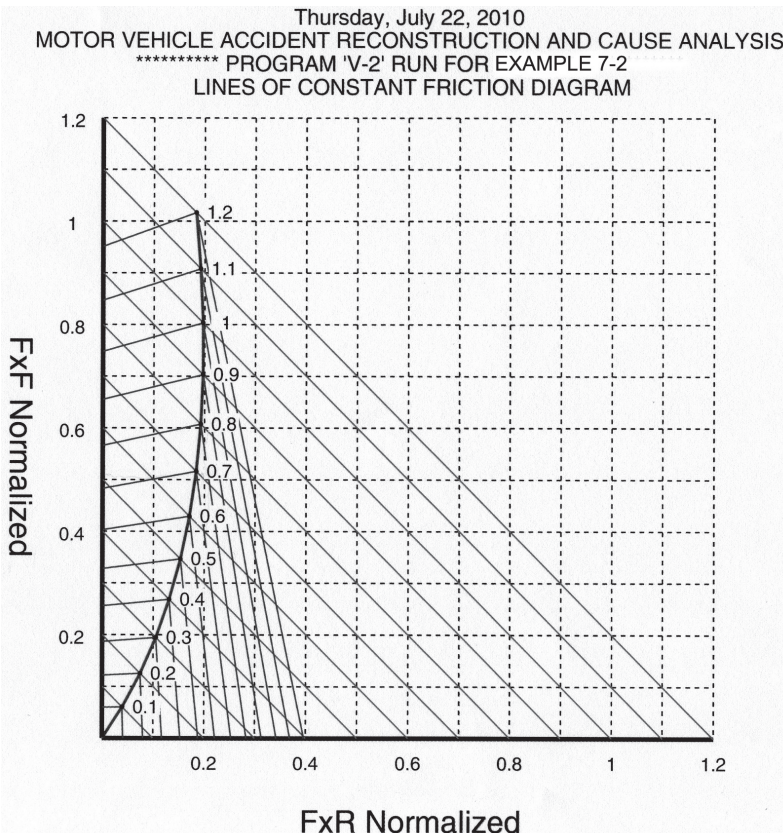


Figure 7-6. Braking forces diagram: Optimum braking forces, lines of constant friction, and lines of constant deceleration.

The algebraic expressions for the lines of constant coefficient of friction are used when the exact values for the deceleration at brake lock or ABS modulation must be computed. The equations for the lines of constant coefficient of friction front and rear can be derived from the basic equation of a straight line $y = mx + b$, where $y = F_{xF}/W$, $x = F_{xR}/W$, m = slope and b = the y-axis intercept as:

$$\text{Front: } F_{xF}/W = (\mu_F \chi)/(1 - \mu_F \chi)(F_{xR}/W) + (1 - \psi)\mu_F/(1 - \mu_F \chi) \quad (7-11a)$$

$$\text{Rear: } F_{xF}/W = -(1 + \mu_R \chi)/\mu_R \chi(F_{xR}/W) + \psi/\chi \quad (7-11b)$$

It is emphasized again that the optimum braking forces, as well as the lines of constant friction and constant deceleration, are a function of the vehicle geometrical and weight distribution only, that is y and c (driver-only and laden), and are not a function of the brake hardware installed. With the optimum curves, lines of constant deceleration, and lines of constant friction drawn into the optimum braking forces diagram, the diagram is complete and ready for

comparison or design evaluation of the braking forces actually developed by the brake system installed on the vehicle.

7.3.5 Optimum Braking Forces Parabola Analysis

In the design of braking systems using limiter or reducer valves, it is helpful to know where the slope of the optimum braking force curve becomes infinite. Taking the derivative of the rear braking force with respect to the front braking force in Eq. (7-9) and evaluating it at zero yields the maximum optimum rear braking force.

The derivative of Eq. (7-9) is

$$\frac{d(F_{xR}/W)/d(F_{xF}/W)}{d(F_{xF}/W)} = 1/(2\chi) \{(1 - \psi)^2/4\chi^2 + (1/\chi) F_{xF}/W\}^{(1/2 - 1)} - 1 = 0 \quad (7-12)$$

Setting the left-hand-side of Eq. (7-12) equal to zero yields the normalized front braking force where $(F_{xF}/W)_{\text{opt}}$ is a maximum as

$$(F_{xF} / W)_{R=\max} = (2\Psi - \Psi^2) / 4\chi \quad (7-13)$$

Substitution of Eq. (7-13) into Eq. (7-9) yields the maximum optimum rear braking force

$$(F_{xR} / W)_{\max} = \Psi^2 / 4\chi \quad (7-14)$$

The slope of the optimum braking force curve at the origin [$F_{xF}/W = 0$ in Eq. (7-12)] is computed by

$$\frac{d(F_{xR}/W)/d(F_{xF}/W)}{d(F_{xF}/W)} = 1/(1 - \psi) - 1 = \Psi/(1 - \Psi) \quad (7-15)$$

Inspection of Eq. (7-15) indicates that the slope at the origin is only a function of ψ , the relative longitudinal location of the center-of-gravity.

Evaluation of the data of Example 7-1 yields $(F_{xF}/W)_{R=\max} = \{2(0.417) - (0.4170)^2\}/\{(4)(0.22)\} = 0.75$; $(F_{xR}/W)_{\max} = (0.417)^2/\{(4)(0.22)\} = 0.2$, and the slope at the origin $0.417/(1 - 0.417) = 0.72$. Inspection of Fig. 7-4 indicates agreement between the data plotted and calculations.

The maximum optimum rear braking force expressed by Eq. (7-14) will be used in connection with the design of brake systems using proportioning valves.

7.4 Actual Braking Forces Developed by Brakes

The braking forces produced by the brake system installed on the vehicle are a function of the individual brake torques generated by the wheel brakes. For a hydraulic brake system, the braking force produced by an axle is computed by Eq. (5-2). A similar expression is used for air brake systems [Eq. (6-1)].

The brake force distribution Φ , sometimes called brake balance, is defined by the ratio of rear braking force to the total braking force, or

$$\Phi = F_{xR} / (F_{xR} + F_{xF}) \quad (7-16)$$

where F_{xF} = actual braking force produced by front brakes, N (lb)

F_{xR} = actual braking force produced by rear brakes, N (lb)

For a simple brake system without brake proportioning valves, the brake force distribution is determined from those brake components usually altered between front and rear, resulting in

$$\Phi = \frac{(A_{wc} BFr)_R}{(A_{wc} BFr)_R + (A_{wc} BFr)_F} \quad (7-17)$$

where A_{wc} = wheel cylinder area, cm^2 (in.^2)

BF = brake factor

Eq. (7-17) is used to compute the fixed brake force distribution of a braking system. When a rear brake line pressure-reducing valve is used, then the brake force distribution is fixed up to the knee-point pressure of the proportioning valve, and it changes to a different slope for higher pressures, producing less braking force on the rear (lower Φ). The brake force distribution is computed by use of Eq. (5-2) in Eq. (7-16).

7.5 Comparison of Optimum and Actual Braking Forces

When the actual braking forces equal the optimum, then all available tire-road friction is utilized for vehicle deceleration. This optimum condition of locking all brakes or ABS modulation simultaneously generally occurs only at one loading and deceleration level for a given vehicle. Of particular interest is the maximum wheels-unlocked deceleration and, hence, minimum stopping distance of a vehicle, and then either with the front or rear brakes approaching lockup first.

It should be remembered that the minimum stopping distance of a vehicle is not only a function of the maximum deceleration achieved but also of the deceleration rise time. Particularly at lower speeds the rise time will have a significant effect on the overall stopping distance (see Section 1.2.3).

For a given vehicle, the maximum wheels-unlocked deceleration can be illustrated and determined most easily from the braking force diagram shown in Fig. 7-7. The normalized optimum braking forces, front and rear, are shown. The lines of constant friction for tire-road friction coefficients of 0.6 and 0.8 are also shown. Two fixed brake force distributions are illustrated in Fig. 7-7 by two straight lines marked stable and unstable. The numerical value of the stable brake force distribution Φ_{stable} is determined by dropping a vertical line from the respective interception with an arbitrarily chosen deceleration, say 0.4 g, yielding $F_{xR}/W = 0.11$. From Newton's second law $F = \Phi(aW)$ and solving for the stable brake force distribution yields $\Phi_{\text{stable}} = 0.11/0.4 = 0.275$.

Relative to Fig. 7-7, consider a vehicle operating on a road surface having a tire-road friction coefficient of 0.6. For the vehicle having the stable brake

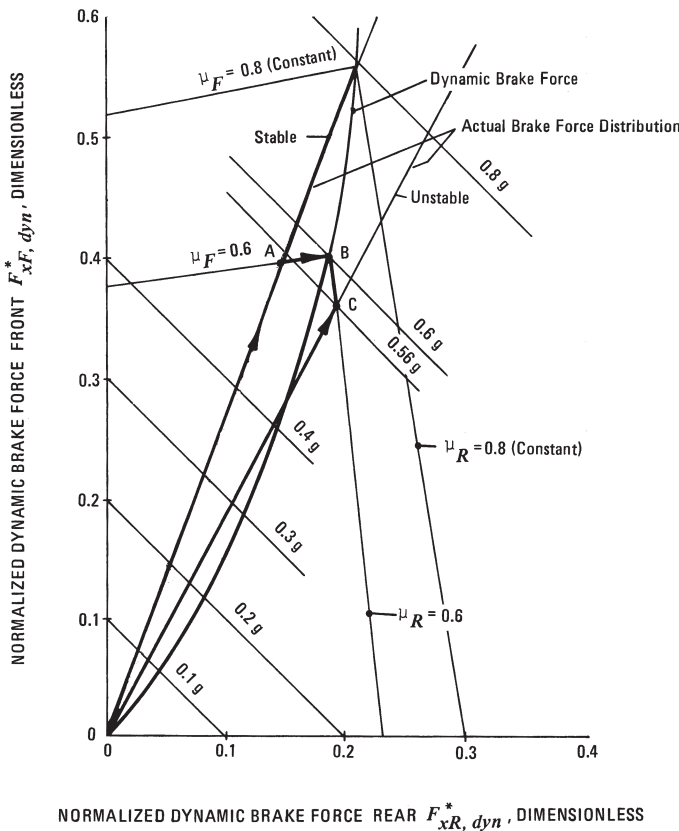


Figure 7-7. Braking forces diagram: optimum and actual braking forces.

force distribution, the actual braking forces produced, front and rear, increase along the stable line from the origin to point A. At point A, the front brake force crosses the line of constant front friction coefficient equal to $\mu_F = 0.6$. Because the tire-road friction coefficient is 0.6, the front brakes lock or ABS modulation begins at point A. If the driver does not increase pedal force, the vehicle decelerates at approximately 0.55 g with its front brakes locked or ABS modulation in a stable and straight direction. If the driver continues to increase pedal force past point A, then the actual braking forces front and rear will move from point A to point B along the line of constant front friction to point B. At point B, the rear brakes will lock and the vehicle decelerates with the brakes of both axles locked or ABS-modulated at 0.6 g. The slight increase in relative front braking force between points A and B and, hence, deceleration from 0.55 to 0.6 g, occurs due to the increased normal force on the front axle resulting from the additional load transfer caused by the increased rear braking force and associated increase in deceleration.

In most cases a graphical solution using the braking forces diagram of Fig. 7-7 is sufficient for a braking dynamics/deceleration analysis, particularly in view of the fact that the brake factors front and rear (Φ -value) and/or tire-road friction coefficients are not entirely fixed values.

The mathematical prediction of the deceleration a_A at point A is accomplished by setting the equations of the Φ_{stable} -line equal to the μ_F -constant line equal to each other and solving for the two unknown braking forces at point A, namely $(F_{xF}/W)_A$ and $(F_{xR}/W)_A$. The optimum braking curve of Fig. 7-7 was obtained for a vehicle with $\psi = 0.44$ and $\chi = 0.20$.

The first independent equation in terms of brake balance is

$$1. \quad F_{xR}/W = \Phi/(1 - \Phi) \quad (F_{xF}/W) = (0.275)/(1 - 0.275) \quad (F_{xF}/W) = 0.38(F_{xF}/W)$$

From Eq. (7-11a) the second equation is:

$$2. \quad F_{xF}/W = (0.6)(0.2)/[1 - (0.6)(0.2)](F_{xR}/W) + (1 - 0.44)(0.6)/[1 - (0.6)(0.2)] \\ = (0.136)(F_{xR}/W) + 0.382$$

Substitution of Equation (1) into (2) yields $F_{xF}/W = 0.402$ and $F_{xR}/W = 0.149$, and the deceleration at point A is $a_A = 0.402 + 0.149 = 0.551$ g. The graphical solution is equal to the mathematical solution.

For a vehicle equipped with the unstable brake force distribution, the braking forces, front and rear, increase to a level indicated by point C, corresponding to a deceleration of 0.56 g. For a maximum tire-road friction coefficient of 0.6, the rear wheels lock at the conditions marked by point C. Further increase in pedal force results in increased deceleration along line CB (line of constant friction for rear axle $\mu_R = 0.6$) until all wheels are locked at a deceleration of 0.6 g, indicated by point B. This stop is unstable because the rear brakes lock prior to the front brakes.

The unstable brake force distribution line $\Phi_{\text{unstable}} = 0.355$ crosses the optimum curve at a deceleration of approximately 0.43 g. The deceleration at which the braking process switches from stable to potentially unstable is called *critical deceleration*.

It may be computed from the optimum braking curve equation and the actual braking force equation in terms of the rear braking force:

$$(F_{xR}/W)_{\text{opt}} = (\psi - \chi a)a$$

$$(F_{xR}/W)_{\text{act}} = \Phi a$$

Solving for the critical deceleration yields

$$a_{\text{critical}} = (\psi - \Phi)/\chi = (0.44 - 0.355)/0.2 = 0.425 \text{ g}$$

For decelerations greater than 0.43 g, the rear brakes will always lock before the front because the normalized actual rear braking forces are greater than the optimum rear braking forces. For modern passenger cars, the critical deceleration should be near 1 g. Even the brake force distribution marked stable in Fig. 7-7 would not be acceptable because its critical deceleration is only 0.8 g. European safety standards require a critical deceleration of greater than 0.82 g,

generally considered too low for modern high-speed vehicles and high-traction tires. Braking safety standard FMVSS 135 prohibits locking of the rear brakes before the front brakes.

For the safe and efficient design of the front-to-rear brake balance system, it is critical that front brakes lock first, hence a safe and stable braking vehicle, and that the actual braking forces are as close as reasonably possible to the optimum braking forces, hence an efficient braking system resulting in minimum stopping distance.

In the late, '50s and early, '60s in Europe, brake force distribution was designed to optimize (minimize) stopping distance. This practice resulted in premature rear brake lockup when lightly loaded, particularly on dry high-traction roads. For skilled test drivers, acceptable results in terms of preventing loss of directional control were seen. For the average driver, however, this was not the case. The number of accidents involving vehicle spinning increased. Brake regulations such as ECE 13 and to a limited extent FMVSS 105 caused the brake force distribution to be shifted toward the front brakes. Many domestic vehicle manufacturers did not front brake bias their vehicles until the early to mid-'80s. Operational and in-use factors still result in loss of directional vehicle control due to premature rear brake lockup. In particular, after-market lining manufacturers must guard against rear brake bias by not properly matching their linings to OEM specifications.

7.6 Tire-Road Friction Utilization

Several different variations of basically the same physical concept have been used to describe how close the actual braking force is to the optimum.

The tire-road friction utilization relates the maximum wheels-unlocked deceleration to the lowest tire-road friction coefficient with which the deceleration can be achieved without locking of any brakes. In Section 7.3 the traction coefficient was introduced [Eq. (7-4)]. For a two-axle vehicle and a fixed brake force distribution the traction coefficient μ_{TR} on the rear axle is

$$\mu_{TR} = F_{xR} / F_{zR} = \Phi a W / [(\Psi - \chi a) W] = \Phi a / (\Psi - \chi a) \quad (7-18a)$$

where F_{xR} = actual rear brake force, N (lb)

F_{zR} = dynamic rear normal force, N (lb)

Similarly, on the front axle the traction coefficient μ_{TF} is

$$\mu_{TF} = (1 - \Phi) a / (1 - \Psi + \chi a) \quad (7-18b)$$

A graphical representation of Eqs. (7-18a) and (7-18b) is shown in Fig. 7-8 for the vehicle geometrical and loading data shown. The friction utilization computed by Eq. (7-18a) is illustrated by the part of the curve labeled "Rear Axle Overbrakes," and the part corresponding to Eq. (7-18b) by "Front Axle Overbrakes." The term overbraking means the same as locking up first. The optimum point for the lightly (empty) loading condition corresponds to

$a = 0.63$ g; i.e., deceleration and tire-road friction coefficient are equal. For decelerations below 0.63 g, e.g., 0.4 g, a friction coefficient between tires and road of approximately 0.44 is required for wheels-unlocked braking in the empty condition. For decelerations exceeding 0.63 g, e.g., $a = 0.9$ g, a friction coefficient of about 1.08 is required to prevent the rear brakes from locking.

In the past, European brake safety standards for commercial vehicles required that certain tire-road friction utilizations are met. If a special device was used to accomplish this, the device must be automatically acting, such as a load-sensitive brake line pressure reducer valve. In addition, a certain wheel

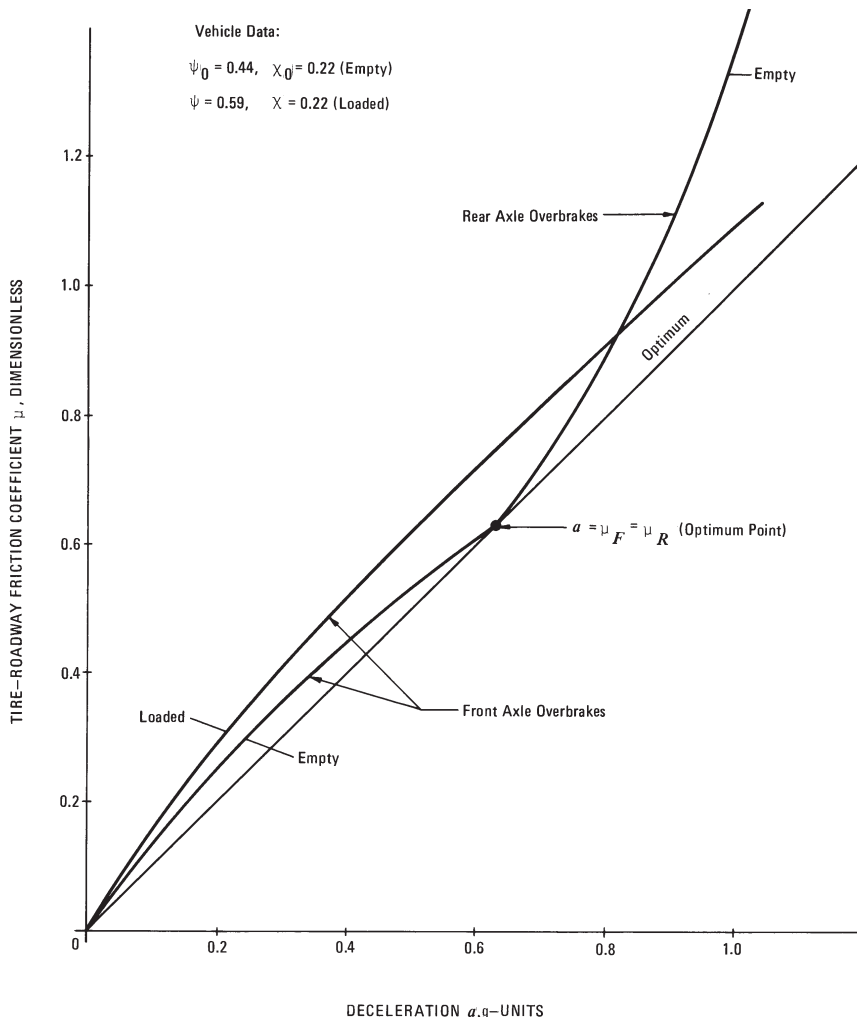


Figure 7-8. Tire-road friction utilization.

lockup sequence was required such that the tire-road friction utilization curve of the front axle lies above that of the rear axle for all loading conditions. Stated differently, for a given deceleration the friction utilization of the rear wheels is less than that of the front wheels, meaning rear wheels are last to lock. Certain options were provided for specified conditions.

For passenger cars the tire-road friction utilization on the front axle must be greater than that of the rear axle for decelerations between 0.15 and 0.30 g, and between 0.45 and 0.80 g. For decelerations between 0.30 and 0.45 g, the utilization of the rear may be greater than that of the front, provided the rear axle utilization curve does not deviate from the optimum by more than 0.05. In addition, vehicle decelerations must be greater than $0.1 + 0.85(\mu - 0.2)$. The manufacturers must provide theoretical calculations demonstrating compliance with the friction utilization requirements. The calculations involve brake system component parameters and, in particular, the brake factor. Care must be exercised in obtaining accurate input data, and in particular when using laboratory data in vehicle tests and real-world use. FMVSS 135 requires the no-lockup requirements to be demonstrated by testing.

7.7 Braking Efficiency

The concept of tire-road friction utilization may be expanded to be more generally applicable to a braking analysis. Braking efficiency is defined as the ratio of maximum wheels-unlocked vehicle deceleration to tire-road friction coefficient. The braking efficiency expresses the extent to which a given tire-road friction coefficient available to a vehicle is used for maximum wheels-unlocked deceleration.

Braking efficiency equations for rear and front axle are derived from Eqs. (7-18a) and (7-18b).

Eq. (7-18a) can be rewritten as

$$\mu_R \Psi - \mu_R \chi a = \Phi a$$

and collecting terms involving deceleration yields

$$a(\Phi + \mu_R \chi) = \mu_R \Psi$$

The braking efficiency E_R of the rear axle now becomes

$$E_R = (a / \mu)_R = \Psi / (\Phi + \mu_R \chi) \quad (7-19a)$$

Similarly, the braking efficiency E_F of the front axle becomes

$$E_F = (a - \mu)_F = (1 - \Psi) / (1 - \Phi - \mu_F \chi) \quad (7-19b)$$

Only numerical values less than unity are meaningful. If a value greater than unity is computed, e.g., for the front axle, then the corresponding braking efficiency of the rear axle will be less than unity, indicating that it is the limiting axle and will lock up first. A braking efficiency greater than unity indicates also

that the particular axle is underbraked, meaning a higher brake force could be used for lockup to occur.

Equations (7-19a) and (7-19b) are represented graphically in Fig. 7-9, in which the braking efficiency is plotted as a function of tire-road friction coefficient. Inspection of Fig. 7-9 reveals that for $\mu = 0.40$, the efficiency on the front axle is equal to approximately 0.88 for the empty driving condition. A braking efficiency of 88% indicates that 88% of the friction available is used by the braking system of the vehicle for deceleration of $0.88 \times 0.4 = 0.35 \text{ g}$ at the moment the front wheels are about to lock up.

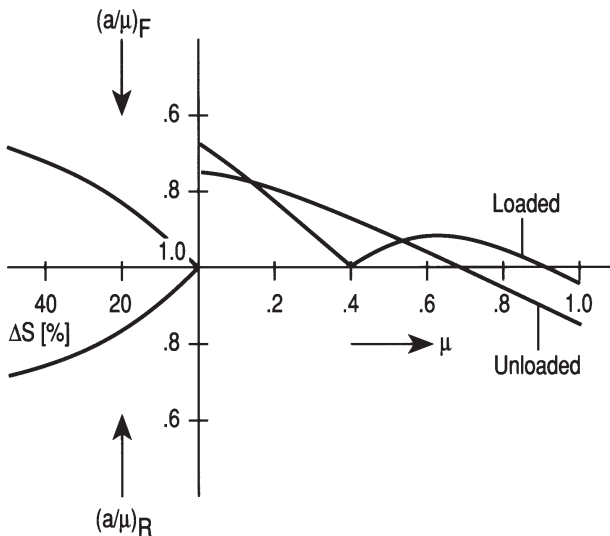


Figure 7-9. Braking efficiency diagram.

Figure 7-9 also shows the additional stopping distance over the minimum achievable with optimum braking. The ratio between stopping distance increase ΔS and minimum stopping distance S_{\min} may be derived as

$$\frac{\Delta S}{S_{\min}} = \frac{1 - (a / \mu)}{(a / \mu)} \quad (7-20)$$

The braking efficiency diagram can be expanded so that it contains tire-road friction coefficient and deceleration directly, similar to the braking force diagram shown in Fig. 7-7. The lines running under an angle are lines of constant coefficient of friction, as illustrated in Fig. 7-10 (Ref. 7.3). Data points falling in the front braking efficiency area indicate front brake lockup before rear, while data points in the rear braking efficiency area indicate premature rear brake lockup. Inspection of Fig. 7-10 reveals that for the lightly laden operating condition or the line closest to the 100% efficiency line, the critical deceleration is approximately 0.86 g, indicating stable braking for all decelerations up to 0.86 g. For the

fully laden condition, the front brakes will always lock before the rear brakes. Frequently, expanded braking efficiency diagrams are used to compare actual road test data obtained from torque hubs or platform testers to the theoretical optimum, i.e., 100% braking efficiency.

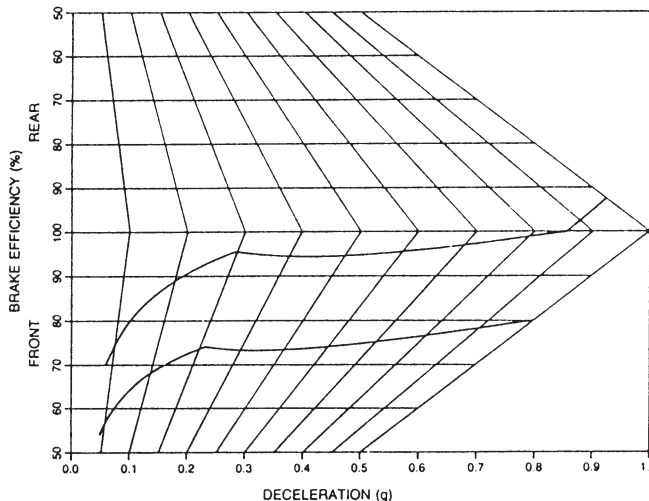


Figure 7-10. Vehicle stability analysis.

7.8 Fixed Brake Force Distribution Analysis

Before designing the braking system of a motor vehicle, the questions to be answered are: (a) can specific wheels-unlocked decelerations be achieved over a wide range of loading and roadway conditions with a fixed brake force distribution Φ , and (b) if so, what is the required brake force distribution? Additionally, a properly designed brake balance front-to-rear based on vehicle geometrical and weight data yields improved ABS braking performance.

7.8.1 Brake Force Distribution Design Selection

For a two-axle vehicle, Eqs. (7-19a) and (7-19b) may be used to develop a limiting relationship on brake force distribution Φ (Ref. 7.2)

$$(1 - \mu\chi - (1 - \Psi) / E_{\min}) \leq \Phi \leq (\Psi / E_{\min} - \mu\chi) \quad (7-21)$$

where E_{\min} = minimum braking efficiency to be achieved by the vehicle.

Application of the inequality to the limiting conditions corresponding to $0.2 \leq \mu \leq 0.8$, and the laden and empty loading conditions, defines an envelope of acceptable values of Φ . A Φ -value within this envelope may be used for design evaluation. The Φ -value finally selected for design purposes depends to some extent on the intended vehicle function. However, regardless of vehicle type, braking stability must be considered by minimizing the potential for rear brakes locking before front brakes.

7.8.2 Brakes-Unlocked Deceleration

Brakes-unlocked deceleration achievable with a given brake force distribution may easily be obtained from Eqs. (7-19a) and (7-19b).

In the case of locking the rear brakes first:

$$a = \mu \Psi / (\Phi + \mu \chi) , \text{ g-units} \quad (7-22a)$$

In the case of locking the front brakes first:

$$a = \mu (1 - \Psi) / (1 - \Phi - \mu \chi) , \text{ g-units} \quad (7-22b)$$

Often, it is of interest to know if a two-axle truck can produce certain braking efficiencies and, hence, decelerations and stopping distances, based on its geometrical loading conditions when a fixed brake force distribution is used.

Eqs. (7-22a) and (7-22b) may be used to formulate a requirement on brake force distribution Φ tailored to the braking limitations of trucks while braking on low-friction ($\mu = 0.2$) and high-friction road surfaces ($\mu = 0.8$) with specified braking efficiencies.

The greatest difficulties exist in preventing premature rear brake lockup when the empty vehicle is braking on dry road surfaces at high deceleration, or preventing front brake lockup when the loaded vehicle is braking at low deceleration on slippery road surfaces. In the first case, the static rear axle load is small because the vehicle is empty and large dynamic load transfer off the rear axle occurs due to a large deceleration. In the second case, the static front axle load is small and no significant dynamic load transfer to the front axle occurs. For these two operating conditions, the braking efficiency generally presents the minimum limit value. In the case of braking the loaded vehicle on a dry road surface, or the empty vehicle on a slippery road surface, the braking efficiencies are generally larger than those associated with the limit value.

7.8.3 Vehicle Loading-Brake Force Distribution Analysis

Based on the physical constraints resulting from lightly and fully laden, and roadway operating conditions, a requirement on the brake force distribution Φ can be developed. Although many trucks and buses are equipped with ABS brakes as required by safety standards, the underlying standard brakes must perform satisfactorily in the case of an ABS failure.

For the empty vehicle when braking on a high-friction road surface ($\mu = 0.8$) with a braking efficiency $E_R = 0.65$, Eq. (7-22a) yields

$$(0.65)(0.8) = 0.52 = 0.8 \Psi_o / (\Phi + 0.8 \chi_o) \quad (7-23)$$

where χ_o = relative center-of-gravity height

Ψ_o = static rear axle load divided by total weight

The front axle of the empty vehicle generally operates at a braking efficiency higher than the minimum value when braking on a low-friction road surface. For braking efficiency $E_F = 0.80$ and $\mu = 0.2$, Eq. (7-22b) yields

$$(0.8)(0.2) = 0.16 = \frac{(1 - \Psi_o)0.2}{1 - \Phi - 0.2 \chi_o} \quad (7-24)$$

For the loaded vehicle the rear brakes generally operates at a braking efficiency higher than the minimum value when braking on a high-friction

surface. For $E_R = 0.75$ and $\mu = 0.8$, Eq. (7-22a) yields

$$(0.75)(0.8) = 0.60 = 0.8\Psi / (\Phi + 0.8\chi_o) \quad (7-25)$$

The front axle of the loaded vehicle operates at the minimum value of braking efficiency when braking on a low-friction road surface. For $E_F = 0.65$ and $\mu = 0.2$, Eq. (7-22b) yields

$$(0.65)(0.2) = 0.13 = \frac{(1 - \Psi)0.2}{1 - \Phi - 0.2\chi} \quad (7-26)$$

The subscript "o" designates the empty operating condition. From Eqs. (7-23) through (7-26), a requirement on the brake force distribution $\Phi = f(\Psi_o, \Psi, \chi_o, \chi)$ as a function of geometric and loading parameters may be formulated. Omitting the algebra, the result from Eqs. (7-23) and (7-24) for the empty vehicle is

$$\Phi = \frac{\Psi_o(1 + 0.54\chi_o) - 0.65\chi_o}{1 - 0.19(1 - \Psi_o)} \quad (7-27)$$

and from Eqs. (7-25) and (7-26) for the loaded vehicle

$$\Phi = \frac{\Psi(1 + 0.72\chi) - 0.92\chi}{1 + 0.15(1 - \Psi)} \quad (7-28)$$

Application of Eqs. (7-27) and (7-28) generally will result in different values of Φ for the empty and laden vehicle. But if the values for Ψ , χ , Ψ_o , and χ_o are such that the brake force distributions Φ computed from Eqs. (7-27) and (7-28) are identical, a fixed brake force distribution will be adequate; i.e., the difference in center-of-gravity location between the empty and laden cases are so small that a proportioning braking system is not necessary.

Eqs. (7-27) and (7-28) may be used to mathematically eliminate Φ , and it becomes possible to derive a limiting condition on the relative static rear axle load $\Psi_o = f(\Psi, \chi, \chi_o)$ as a function of the remaining vehicle parameters. This condition must be satisfied before a fixed brake force distribution may be considered adequate for the braking process with the minimum braking efficiency specified. Omitting the algebra, the results when plotted for different values of Ψ and $\Delta\chi = \chi - \chi_o$ were found to be described by a functional relationship

$$\Psi - \Psi_o \leq \Delta\chi + 0.09 \quad (7-29)$$

The value of $\Delta\chi$ for trucks is generally small and less than 0.03 and, consequently, an approximate limiting condition on the change in relative static rear axle load is

$$\Psi - \Psi_o \leq 0.12 \quad (7-30)$$

The results indicate that vehicles equipped with fixed brake force distribution systems are capable of achieving decelerations well within the requirements for

safe braking performance, provided the vehicle experiences an increase in relative static rear axle load of not more than 12%; i.e., $\Delta\Psi = \Psi - \Psi_o \leq 0.12$. This means, also, that load-sensitive proportioning will yield little or no improvement in braking performance for trucks for which the difference in relative static rear axle load between the empty and laden case is less than 12%. On the other hand, if the difference is greater, proportioning valves may have to be used.

7.8.4 Comparison of Theoretical and Road Test Results

The limiting condition on the brake force distribution, i.e., Eq. (7-21), was applied to a variety of commercial vehicles such as light and medium trucks and school buses (Refs. 7.4, 7.5). Actual road tests were conducted to determine the maximum braking capabilities of the vehicles. The horizontal center of gravity location of the light truck with a GVW of 44,480 N (10,000 lb) remained almost unaffected by the loading, as indicated by $\Delta\Psi = \Psi - \Psi_o = 0.674 - 0.595 = 0.079$ and $\Delta\chi = \chi - \chi_o = 0.320 - 0.293 = 0.027$. The corresponding values for the medium truck were $\Delta\Psi = 0.29$ and $\Delta\chi = 0.06$, indicating a significant horizontal change in the location of the center of gravity from the laden to the empty case. The location of the center of gravity of the school bus changed little, as indicated by $\Delta\Psi = 0.105$ and $\Delta\chi = 0.001$. This result was to be expected due to the long wheelbase of the school bus.

Inspection of the $\Delta\Psi$ -values for the light truck and the school bus reveals that no difficulties exist in designing a braking system with a fixed brake force distribution for both vehicles which will yield acceptable braking performance. The $\Delta\Psi$ -value for the medium truck is, however, significantly greater than the limit value $\Delta\Psi = 0.12$ and, hence, it becomes impossible to achieve acceptable braking performance with a fixed brake force distribution on the medium truck.

Consider the light truck first. Assume a maximum and minimum value of μ equal to 0.8 and 0.2, respectively, and a minimum braking efficiency of 0.70. Applying Eq. (7-21) to the light truck results in a theoretical value of $\Phi = 0.51$, as contrasted with the actual brake force distribution of $\Phi = 0.53$. The computed distribution $\Phi = 0.51$ along with the appropriate vehicle data yields a minimum braking efficiency of 77% by use of Eq. (7-19b) for the loaded vehicle operating on a slippery road surface with $\mu = 0.2$. For all other loading and road surface conditions, the theoretical braking efficiencies are higher. For the dry road surface, the braking efficiencies computed by Eq. (8-19a) for the loaded case and Eq. (7-19b) for the empty case are 87 and 80%, respectively. These braking efficiencies would produce theoretical wheels-unlocked decelerations of 6.83 m/s^2 (22.4 ft/s^2) for the loaded vehicle and 6.28 m/s^2 (20.6 ft/s^2) for the empty vehicle on a road surface having a tire-road friction coefficient of 0.8. These theoretical values, when compared to the measured test data of 7.01 m/s^2 (23 ft/s^2) laden and 6.28 m/s^2 (20 ft/s^2) unloaded, indicate that the braking system of the light truck was designed for best braking for both loading conditions. Changes in the brake force distribution or even a proportioning braking system would yield no improvement in braking performance. However, as stated earlier, braking efficiencies should be maximized only if braking stability is ensured; i.e., front brakes lock before rear brakes over a wide range of operating conditions.

Application of Eq. (7-21) to the school bus resulted in a brake force distribution $\Phi = 0.50$ to 0.55 . The vehicle was equipped with a brake force distribution $\Phi = 0.42$. A brake force distribution of $\Phi = 0.55$ would produce theoretical braking efficiencies of 72 and 93% for the empty and laden vehicle, respectively, on slippery roadways with $\mu = 0.2$; and 92 and 96% for the empty and laden vehicle, respectively, on dry road surfaces with $\mu = 0.8$. For the empty vehicle, a theoretical deceleration of 7.22 m/s^2 (23.7 ft/s^2) may be expected on dry road surfaces. In the case of the school bus, a change in brake force distribution from 0.42 to 0.55 will improve braking performance for the vehicle on slippery road surfaces, indicated by an increase from 48 to 72% . Improvements in deceleration capability can be expected from a change in brake force distribution. However, a proportioning braking system will yield only little increase in braking performance, indicated by the small change in relative static rear axle loading of $\Delta\Psi = 0.105$.

The design of the braking system for the medium-weight truck is made difficult by a significant change in static rear axle loading indicated by $\Delta\Psi = 0.29$. The brake system of this truck was designed to meet the braking requirements for the loaded operating condition indicated by an actual brake force distribution of $\Phi = 0.74$; i.e., 74% of the total braking effort is concentrated on the rear axle. Although this design will produce desirable results for the loaded vehicle while braking on slippery or dry roads, the braking performance to be expected with the empty vehicle is unacceptable. Application of Eq. (7-21) resulted in the following inequalities for the brake force distribution of the medium-weight truck:

$$\begin{aligned} 0.27 \leq \Phi \leq 0.52 & \text{ for } \mu = 0.2, \text{ empty} \\ 0.12 \leq \Phi \leq 0.36 & \text{ for } \mu = 0.8, \text{ empty} \\ 0.58 \leq \Phi \leq 0.83 & \text{ for } \mu = 0.2, \text{ laden} \\ 0.43 \leq \Phi \leq 0.68 & \text{ for } \mu = 0.8, \text{ laden} \end{aligned}$$

These results indicate that a brake force distribution $\Phi = 0.74$ will produce acceptable braking performance only for the loaded vehicle on slippery roads. Consider the second and third inequality as a compromise; a brake force distribution of $\Phi = 0.47$ probably produces better braking performance for all road surface and loading conditions than can be expected from $\Phi = 0.74$. The theoretical braking efficiencies with $\Phi = 0.47$ are 67 and 90% for the empty and laden vehicle, respectively, on a road surface with a coefficient of friction of 0.8 . For the empty vehicle with $\Phi = 0.47$, a deceleration of approximately 5.24 m/s^2 (17.2 ft/s^2) may be expected on dry roads; a deceleration of 7.07 m/s^2 (23.2 ft/s^2) is expected for the loaded vehicle with $\Phi = 0.47$. A further increase in braking capability can be accomplished only by a proportioning brake system. This is also evident from the change in relative static rear axle loading of $\Delta\Psi = 0.29$. A load-sensitive proportioning braking system will increase the maximum wheels-unlocked decelerations to 6.1 and 7.01 m/s^2 (20 and 23 ft/s^2) for the empty and loaded conditions, respectively.

7.8.5 Effect of Drivetrain on Brake Force Distribution

The braking performance requirements of safety standards usually specify tests to be conducted with the transmission in neutral to eliminate engine drag as a

deceleration factor. Drivers, however, apply their brakes without changing gears when required to brake severely.

Engine drag and rotational mass inertias will have an effect on the base brake force distribution that should be used in a vehicle. For manual transmissions, the algebraic expressions are straightforward, but they are lengthy and involved. They are a function of gear ratios, rotational inertias, and engine speeds, as well as the basic physical expressions discussed in prior sections.

In general, for rear-wheel-drive vehicles the drivetrain effects will cause the critical deceleration (above which the rear brakes lock first) to decrease. The decrease will be greater as vehicle speed increases. For example, if the critical deceleration at low speed (or without consideration of drivetrain/speed effects) is 0.9 g at 50 m/s or 180 km/h (112 mph), the high-speed critical deceleration may only be 0.6 g. At higher speeds the rear brakes may lock up first, resulting in directional instability. For front-wheel-drive vehicles, the critical deceleration will increase as speeds increase. For example, a low-speed critical deceleration of 0.9 g will increase to approximately 0.95 to 1 g at speeds of 180 km/h (112 mph).

7.8.6 Effect of Aerodynamics on Brake Force Distribution

Aerodynamic forces affect both vehicle handling and limit braking performance. For vehicle body shapes without any special aerodynamic designs such as used in Formula 1 race cars, the normal forces on front and rear axle are decreased as a result of the aerodynamic lift. In addition, aerodynamic drag increases vehicle deceleration, and hence, axle load distribution. Equations (7-3a and b) will change by a negative aerodynamic lift term in the round bracket. The lift term increases with the speed squared. Decelerations at which the front or rear brakes lock must be computed for increasing speeds. Equations (7-22a and b) are modified by a negative lift term in the numerator. For example, Eq. (7-22b) computing front brake lockup will be:

$$a = \frac{\mu(1-\Psi) - \frac{k_{\ell F} V^2}{W}}{1 - \Phi - \mu x} , \text{ g-units}$$

where $k_{\ell F}$ = front lift coefficient, Ns^2/m^2 (lbs^2/ft^2)

V = vehicle speed, m/s (ft/s)

W = vehicle weight, N (lb)

For standard passenger cars, $k_{\ell F} = 0.125$, $k_{\ell R} = 0.25$; for spoilers front and rear $k_{\ell F} = 0.01$, $k_{\ell R} = 0.38$; for rear spoilers only $k_{\ell F} = 0.125$, $k_{\ell R} = 0.03$ (Ref. 1.3).

Brake lockup calculations including aerodynamic lift for a standard passenger car may show front brake lockup for speeds up to 180 km/h (112 mph), while the rear brakes lock first, that is, at a lower deceleration than the front brakes, at a speed of 216 km/h (134 mph).

7.9 Variable Brake Force Distribution Analysis

If for a given vehicle the brakes-unlocked decelerations achieved with a fixed brake force distribution are too low, then a variable brake force distribution must be used. The object of designing variable or proportional braking is to bring braking efficiencies closer to unity over a wide range of loading and road friction conditions, encompassing most winter and summer driving situations. Through a proportioning valve, the actual braking forces are brought closer to the optimum. As braking efficiencies are increased, front brakes should lock before the rear brakes.

7.9.1 Optimum Brake Line Pressures

In the design of the brake balance front to rear of a brake system, the optimum braking forces or the brake line pressures producing optimum forces may be used. Because electronically controlled valves modulate, or proportioning valves affect the brake line pressures reaching front and rear brakes, it is convenient to work with the optimum brake line pressures. The optimum brake line pressures may be computed from the actual braking force expression Eq. [(5-2)], however, replacing the actual braking forces with the optimum [Eqs. (7-7a) and (7-7b)]. By equating optimum and actual braking forces and solving for brake line pressure, the optimum brake line pressures for straight-line braking are

Front axle:

$$p_{\ell F, \text{opt}} = \frac{(1 - \Psi + \chi a) a W R}{2 (A_{\text{wc}} B F r \eta_c)_R} + p_{oF} \quad , \quad \text{N/cm}^2 \text{ (psi)} \quad (7-31a)$$

Rear axle:

$$p_{\ell R, \text{opt}} = \frac{(\Psi - \chi a) a W R}{2 (A_{\text{wc}} B F r \eta_c)_R} + p_{oR} \quad , \quad \text{N/cm}^2 \text{ (psi)} \quad (7-31b)$$

where a = deceleration, g-units

A_{wc} = wheel cylinder area, cm^2 (in.^2)

BF = brake factor

p_{oF} = pushout pressure, front brakes, N/cm^2 (psi)

p_{oR} = pushout pressure, rear brakes, N/cm^2 (psi)

r = effective rotor or drum radius, cm (in.)

R = effective tire radius, cm (in.)

W = vehicle weight, N (lb)

η_c = wheel cylinder efficiency

The optimum brake line pressures are a function of the basic vehicle geometry; that is, ψ and χ , driver-only and laden, and the brake system hardware installed. Electronically controlled brake systems use Eqs. (7-31a) and (7-31b) for a known (measured) deceleration to modulate the front and rear brake line pressures near their respective optimum values. The optimum brake line pressure curves are similar to the optimum braking force curves. Lines of constant deceleration are different for the empty and laden conditions.

The optimum brake line pressure diagram is shown in Fig. 7-11 for the following vehicle and brake system data: $W = 13,350 \text{ N}$ (3000 lb), $\psi = 0.4$, $\chi = 0.2$; front: $A_{wc} = 31.7 \text{ cm}^2$ (4.91 in.²), $BF = 0.71$, $r = 127 \text{ mm}$ (5 in.), $R = 356 \text{ mm}$ (14 in.), $\eta_c = 0.98$; rear: $A_{wc} = 11.42 \text{ cm}^2$ (1.77 in.²), $BF = 0.71$, $r = 140 \text{ mm}$ (5.5 in.), $R = 356 \text{ mm}$ (14 in.), $\eta_c = 0.98$. With Eq. (7-17), the brake force distribution is $\Phi = 0.97/(0.97 + 2.455) = 0.283$. With Eq. (7-18) the critical deceleration is $a_{\text{critical}} = (\psi - \Phi)/\chi = (0.4 - 0.283)/(0.2) = 0.582 \text{ g}$. A critical deceleration of 0.58 g is too low for safe braking.

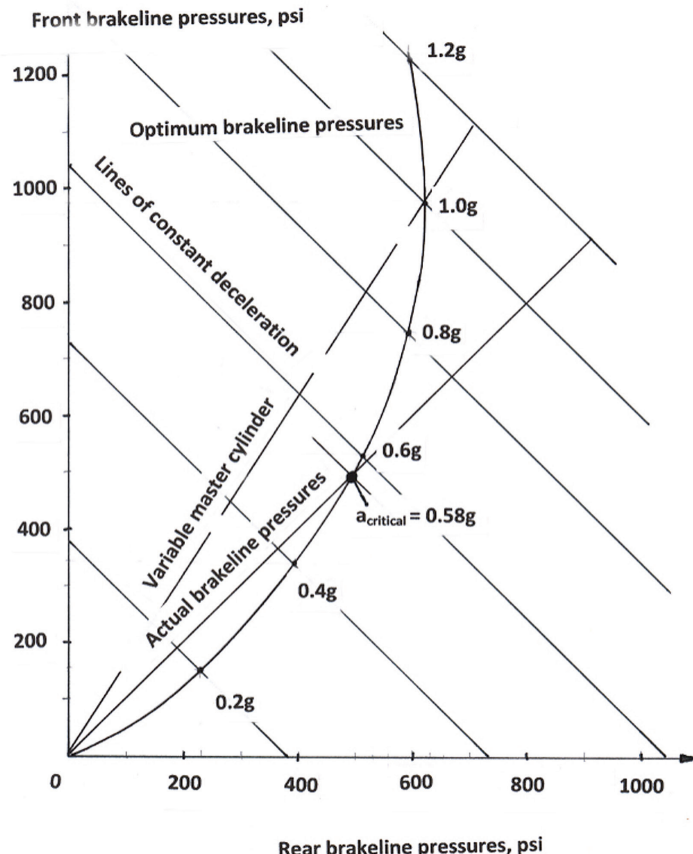


Figure 7-11. Brake line pressure diagram.

The fixed brake force distribution is indicated in Fig. 7-11 by the straight actual brake pressure line drawn under 45 degrees. An adjustable master cylinder or other valves should be incorporated in the brake system design to raise the critical deceleration to a safe level ($a_{critical} > 0.9 g$). If the actual braking system were to produce the theoretical brake line pressures front and rear for the decelerations indicated, the braking process would result in optimum braking.

The maximum optimum rear brake line pressure is determined with Eq. (7-14) as

$$\begin{aligned}
 (P_{LR, \text{opt}})_{\text{max}} &= [\psi^2/(4\chi)]W/[2A_{WC}BF\eta_c(r/R)] \\
 &= (0.4)^2/[(4)(0.2)](13,350)/\{(2)(11.42)(0.71)(0.98)(140/356)\} = 427 \text{ N/cm}^2 \\
 &= [(0.4)^2/\{(4)(0.2)\}(3000)/(0.97) = 618.6 \text{ psi}]
 \end{aligned}$$

The corresponding front brake line pressure is obtained from Eq. (7-13) as 674 N/cm² (977 psi).

For the same vehicle and brake system data, the optimum brake line pressures as a function of deceleration are shown in Fig. 7-12. For brake line pressures less than approximately 350 N/cm² (507 psi), the front brakes will lock first, for greater brake line pressures the rear brakes, potentially rendering the vehicle directionally unstable. For example, for a tire-road coefficient of friction $\mu = 0.8$, Eq. (7-22a) yields maximum wheels-unlocked deceleration = 0.727 g, requiring a brake line pressure of 440 N/cm² (637 psi) to be produced.

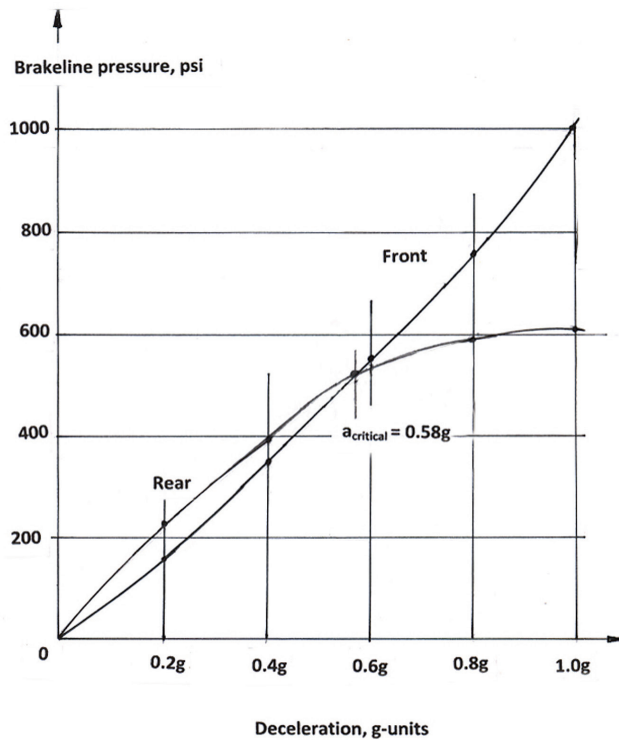


Figure 7-12. Optimum brake line pressure over deceleration.

The effects of lateral load transfer may easily be included to determine the four individual optimum brake line pressures while braking and turning. The details are discussed in Section 7.12.

7.9.2 Brake Line Pressure Limiter Valve

Pressure limiter valves discussed in Section 5.3 use a linearly increasing braking force ratio up to the critical deceleration a_{crit} and a constant rear brake force for deceleration greater than a_{crit} . A typical braking force diagram showing optimum and actual braking forces is illustrated in Fig. 7-13.

The baseline brake force distribution generally is designed so that it would intersect the empty optimum line at a deceleration of approximately 0.5 g. The baseline brake force distribution Φ_B is computed by equating optimum and

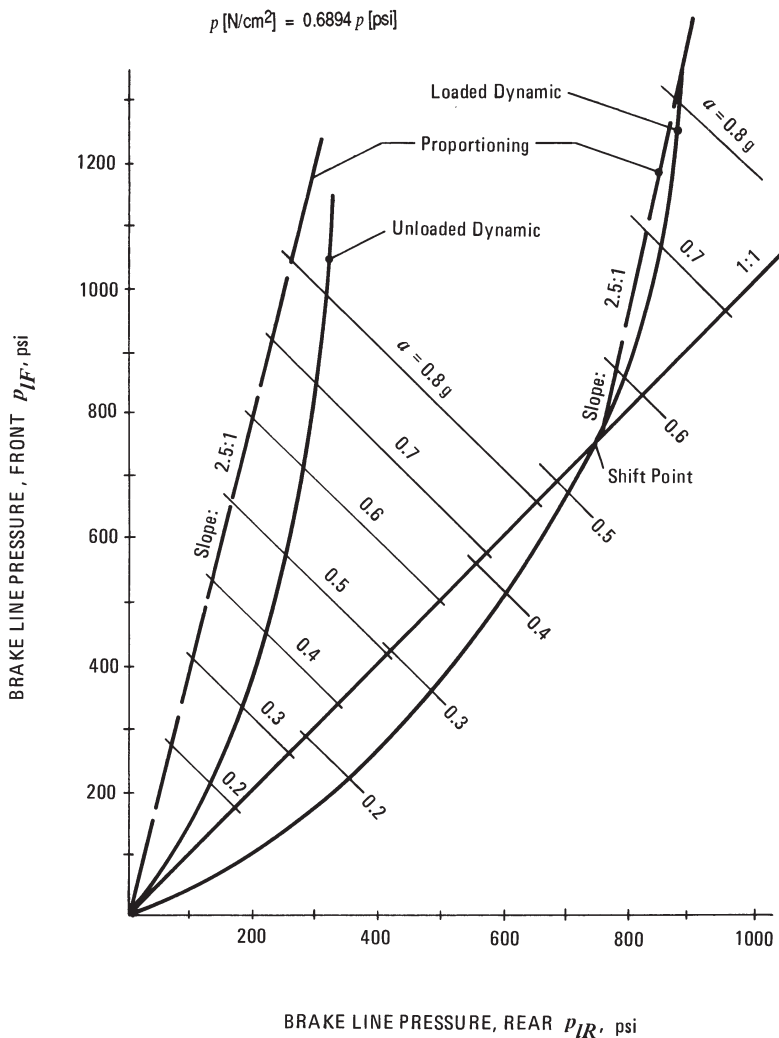


Figure 7-13. Optimum and actual brake line pressures.

actual rear braking forces for $a = 0.5 \text{ g}$, resulting in

$$\Phi_B = \Psi - a_{\text{crit}}\chi = \Psi - 0.5\chi \quad (7-32)$$

The constant vertical portion of the brake balance is designed so that the actual rear brake force is 90% of the optimum rear brake force given by Eq. (7-14):

$$(F_{xR} / W)_{\text{act}} \approx 0.9(F_{xR} / W)_{\text{max}} = 0.9(\Psi_o^2 / 4\chi_o) \quad (7-33)$$

The deceleration a_{empty} of the empty vehicle at the valve shift point is computed by applying Newton's Second Law to the rear brakes

$$\Phi_B a_{\text{empty}} = (F_{xR} / W)_{\text{act}}$$

and solving for deceleration, or

$$a_{\text{empty}} = 1 / \Phi_B (0.9)(\Psi_o^2 / 4\chi_o) \quad , \quad \text{g-units} \quad (7-34)$$

The corresponding shift point pressure p_s is given by

$$p_s = \frac{a_{\text{empty}} W_o R}{2[(A_{wc} BFr\eta_c)_F + (A_{wc} BFr\eta_c)_R]} \quad , \quad \text{N/cm}^2(\text{psi}) \quad (7-35)$$

where A_{wc} = wheel cylinder area, cm^2 (in.^2)

BF = brake factor

r = effective rotor or drum radius, cm (in.)

η_c = wheel cylinder efficiency

The deceleration $a_{s,\text{laden}}$ of the laden vehicle existing at the shift pressure is determined by the weight ratio between empty (W_o) and laden (W_ℓ) vehicle, or

$$a_{s,\text{laden}} = a_{\text{empty}} (W_o / W_\ell) \quad , \quad \text{g-units} \quad (7-36)$$

7.9.3 Brake Line Pressure Reducer Valve

The operation of reducer valves is discussed in Section 5.3. The analysis is similar to that of the limiter valve. The baseline brake force distribution is generally chosen so that it would intersect the "empty" optimum line at approximately 0.4 g, assuming no pressure reducing would occur. The baseline brake force distribution Φ_B is computed by

$$\Phi_B = \Psi - 0.4\chi_o \quad (7-37)$$

The knee-point pressure p_K of the reducer valve should be chosen so that the pressure switch occurs at 80 to 90% of the baseline critical deceleration for the empty vehicle:

$$p_K = \frac{(0.8 \text{ to } 0.9)a_{\text{crit}} W_o R}{2 \sum (A_{wc} BFr\eta_c)_{F,R}} \quad , \quad \text{N/cm}^2(\text{psi}) \quad (7-38)$$

Reducer valve slopes generally range between 0.3 and 0.5. The shift or knee-point and slope of the reducer valve should be chosen so that for the empty vehicle the reduced brake force distribution intersects the optimum braking force curve at a critical deceleration of 0.9 to 1.0 g.

When a load-sensitive reducer or proportioning valve is used, the critical deceleration for the laden vehicle should not be less than 0.9 to 1.0 g.

A load-sensitive reducer valve braking system design is illustrated in Fig. 7-13. The shift point for the fully laden case should be shifted slightly to the left to approximately 0.9 times 524 N/cm^2 (760 psi) or 472 N/cm^2 (684 psi) [(Eq. 7-38)], i.e., to lower rear brake line pressures to ensure that inadvertent brake factor increases on the rear brakes do not easily cause premature rear brake lockup. The knee-point pressure for the empty case is zero to produce stable braking for all decelerations up to about 1.0 g.

7.9.4 Deceleration-Sensitive Pressure Reducer Valve

Deceleration-sensitive reducer valves are discussed in Section 5.3. The shift point pressure is a function of the installation angle of the valve and generally ranges from 18 to 20 degrees, corresponding to a shift point deceleration $a = 0.32$ to 0.36 g .

The critical deceleration after the shift point is approximately 1.0 to 1.2 g. The brake force distribution Φ_a after the shift point is computed by

$$\Phi_a = \Psi_o - a_{\text{crit}} \chi_o \quad (7-39)$$

The baseline brake force distribution Φ_B , i.e., the brake force distribution prior to reaching the shift point, is computed by

$$\Phi_B = \frac{1}{1 + \frac{SL}{\Phi_a / (1 - \Phi_a)}} \quad (7-40)$$

where SL = reducer slope [Eq. (5-12)]

Front brake lockup below the shift point occurs at the following conditions:

$$a_{F,\text{lock}} = \frac{\mu(1 - \Psi)}{1 - \mu\chi - \Phi_B} \quad (7-41)$$

where $a_{F,\text{lock}}$ = deceleration at which front brakes lock, g-units

Above the shift point but below the piston movement the front brakes lock at:

$$a_{F,\text{lock}} = \frac{\mu(1 - \Psi)}{1 - \mu\chi - \Phi_B} , \text{ g-units} \quad (7-42)$$

Above the piston movement the front brakes lock at:

$$a_{F,\text{lock}} = \frac{\mu(1 - \Psi)}{1 - \mu\chi - \Phi_a} , \text{ g-units} \quad (7-43)$$

7.9.5 Adjustable Step Bore Master Cylinder

Performance details are discussed in Section 5.3. Using the component designation shown in Fig. 5-15, the pressure ratio rear to front after the master cylinder has switched to the “laden” condition is determined by

$$(p_R / p_F)_{\text{after}} = (p_R / p_F)_{\text{before}} (A_{mc,2} / A_{mc,3}) \quad (7-44)$$

where $A_{mc,2}$ = cross-sectional area of floating piston, cm^2 (in.^2)

$A_{mc,3}$ = cross-sectional area of step piston, cm^2 (in.^2)

$(p_R / p_F)_{\text{after}}$ = rear to front pressure ratio after switching to laden

$(p_R / p_F)_{\text{before}}$ = rear to front pressure ratio before switching to laden

Example 7-3:

Compute deceleration and braking efficiencies for a compact front-wheel-drive passenger car. Use the data that follow.

Vehicle data:

Weight, driver only: 9621 N (2,163 lb)

Laden weight: 12260 N (2,755 lb)

Driver-only rear axle load: 3656 N (822 lb); front axle: 5967 N (1,341 lb)

Laden rear axle load: 6720 N (1,510 lb); front axle: 5538 N (1,245 lb)

Wheelbase: 238.8 cm (94 in.)

Tire radius: 29.97 cm (11.8 in.)

Center-of-gravity height empty: 526 mm (20.7 in.); laden: 559 mm (22 in.)

Brake system data:

Front: Wheel cylinder diameter: 57.1 mm (2.25 in.)

Rotor radius: 9.14 cm (3.6 in.)

Brake factor: 0.68

Pushout pressure: 3.4 N/cm² (5 psi)

Rear: Wheel cylinder diameter: 19.05 mm (0.75 in.)

Drum diameter: 22.9 cm (9 in.)

Brake factor: 1.70 (LT-shoe drum brake)

Pushout pressure 55 N/cm² (80 psi)

Master cylinder diameter: 20.64 mm (0.812 in.)

Pedal ratio: 4.0 to 1; Boost ratio: 3.80 to 1

Proportioning valve: 173 N/cm² (250 psi) \times 46%

Determine if the fixed proportioning valve is sufficient for the driver-only and laden conditions or if a load-sensitive proportioning valve must be installed. Determine at which deceleration the front or rear brakes lock for a tire-road friction coefficient of 0.8.

Solution:

The brake system design evaluation begins with the computation of the optimum braking forces for the driver-only loading configuration and their comparison with the actual braking forces.

The MARC 1- V3 input and output data table of the actual braking forces is shown in Table 7-1.

With the brake system hardware as specified, a pedal force of 227 N (51 lb) is required to produce a deceleration of approximately 1 g. The results indicate pedal forces and decelerations well within the limits specified in Chapter 1.

In the next step, the optimum braking forces for the driver-only loading are compared with the actual normalized braking forces. The results are shown in the braking forces diagram of Fig. 7-14, obtained with MARC 1-V4.

The curved optimum and bilinear actual braking forces are shown. The knee point brake line pressure of 173 N/cm² (250 psi) is reached at a deceleration

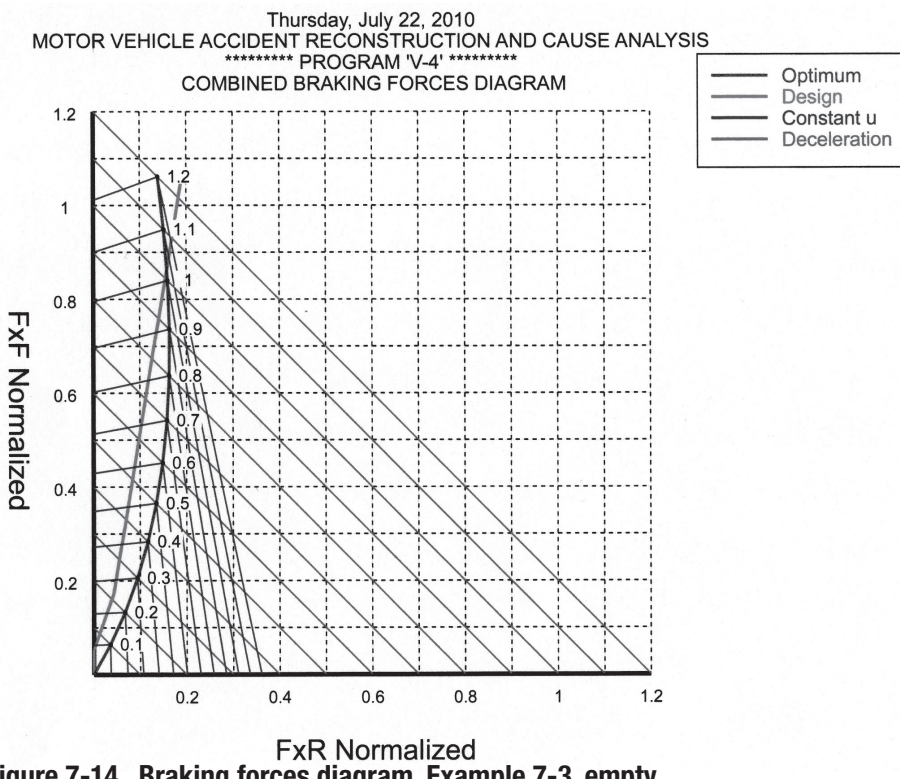


Figure 7-14. Braking forces diagram, Example 7-3, empty.

Brake Design and Safety

Thursday, July 22, 2010

MOTOR VEHICLE ACCIDENT RECONSTRUCTION AND CAUSE ANALYSIS ***** PROGRAM 'V-3' RUN FOR Example 7-3 empty ***** ACTUAL BRAKING FORCES

Data Printout for Vehicle

2012 Small Car xx

Vehicle Weight, LBS:	==> 2163.00
Knee-Point Pressure, PSI:	==> 250.00
Maximum Master Cylinder Pressure, PSI:	==> 1500.00
Proportioning Valve Slope, DIMENSIONLESS:	==> 0.46
Pedal Lever Ratio, DIMENSIONLESS:	==> 4.00
Pedal Efficiency, DIMENSIONLESS:	==> 0.80
Boost Ratio, DIMENSIONLESS:	==> 3.80
Diameter of Master Cylinder, IN:	==> 0.81

FRONT REAR

Wheel Cylinder Efficiency, D'LESS:	==> 0.98	0.96
Push Out Pressure, PSI:	==> 5.00	80.00
Brake Factor, DIMENSIONLESS:	==> 0.68	1.70
Radius of Brake Drum or Rotor, IN:	==> 3.60	4.50
Effective Tire Radius, IN:	==> 11.80	11.80
Diameter of Brake Cylinder, IN:	==> 2.25	0.75

LINE PRESSURE	FRONT FORCES/W	REAR FORCES/W	TOTAL FORCE	DECELERATION	PEDAL FORCE
80.00 PSI	0.056	0.000	121.255 LBS	0.056 g	3.41 LBS

REAR PUSH OUT PRESSURE

80.00 PSI 0.056 0.000 121.255 LBS 0.056 g 3.41 LBS

KNEE-POINT PRESSURE

250.00 PSI	0.183	0.043	489.586 LBS	0.226 g	10.65 LBS
354.17 PSI	0.261	0.055	684.353 LBS	0.316 g	15.08 LBS
458.34 PSI	0.339	0.068	879.119 LBS	0.406 g	19.52 LBS
562.51 PSI	0.417	0.080	1073.886 LBS	0.496 g	23.96 LBS
666.68 PSI	0.495	0.092	1268.652 LBS	0.587 g	28.39 LBS
770.85 PSI	0.572	0.104	1463.419 LBS	0.677 g	32.83 LBS
875.02 PSI	0.650	0.116	1658.185 LBS	0.767 g	37.26 LBS
979.19 PSI	0.728	0.128	1852.952 LBS	0.857 g	41.70 LBS
1083.36 PSI	0.806	0.141	2047.718 LBS	0.947 g	46.14 LBS
1187.53 PSI	0.884	0.153	2242.485 LBS	1.037 g	50.57 LBS
1291.70 PSI	0.962	0.165	2437.251 LBS	1.127 g	55.01 LBS
1395.87 PSI	1.040	0.177	2632.018 LBS	1.217 g	59.44 LBS

MAXIMUM MASTER CYLINDER PRESSURE

1500.00 PSI 1.117 0.189 2826.709 LBS 1.307 g 63.88 LBS

Table 7-1. MARC 1-V3. Example 7-3. Empty.

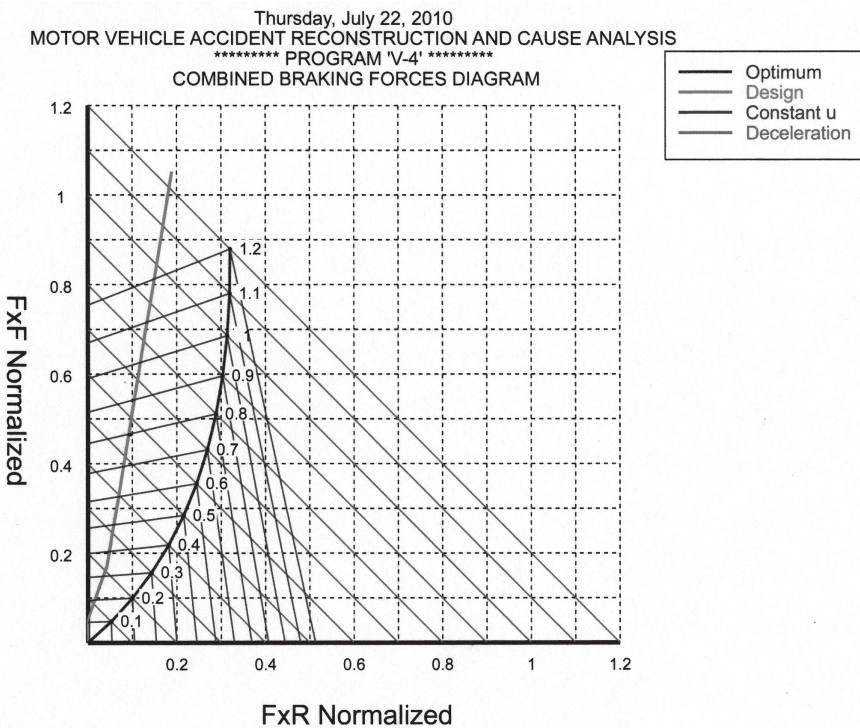


Figure 7-15. Braking forces diagram, Example 7-3, laden.

of 0.226 g. The critical deceleration is slightly greater than 1 g, indicated by the intersection of the optimum and actual braking forces. Consequently, the rear brakes will not lock before the front brakes for decelerations less than 1 g, indicating good brake balance front-to-rear for the driver-only configuration.

The front brakes will lock up at approximately 0.74 g, indicated by the intersection of the operating line of the actual braking forces with the line of constant coefficient of friction $\mu_F = 0.8$.

The exact front brake lockup deceleration can be obtained from the two equations (const μ_F and Φ_{act}). The actual braking force equation ($y = mx + b$) is obtained from the data output of MARC 1 V3 with $m = (0.884 - 0.183)/(0.153 - 0.043) = +6.373$ and $b = 0.884 - (6.373)(0.153) = -0.091$ as:

$$1. (F_{xF}/W)_{act} = 6.373 (F_{xR}/W) - 0.091$$

The equation for the line of constant front friction coefficient is given by Eq. (7-11a):

$$2. (F_{xF}/W)_{const \mu_F} = 0.214(F_{xR}/W) + 0.602$$

Solving yields $F_{xF}/W = 0.629$ and $F_{xR}/W = 0.113$ and a deceleration $a_{0.8} = 0.629 + 0.113 = 0.742$ g. The graphical and analytical values are in excellent agreement, as should be expected because the graphical representation and mathematical

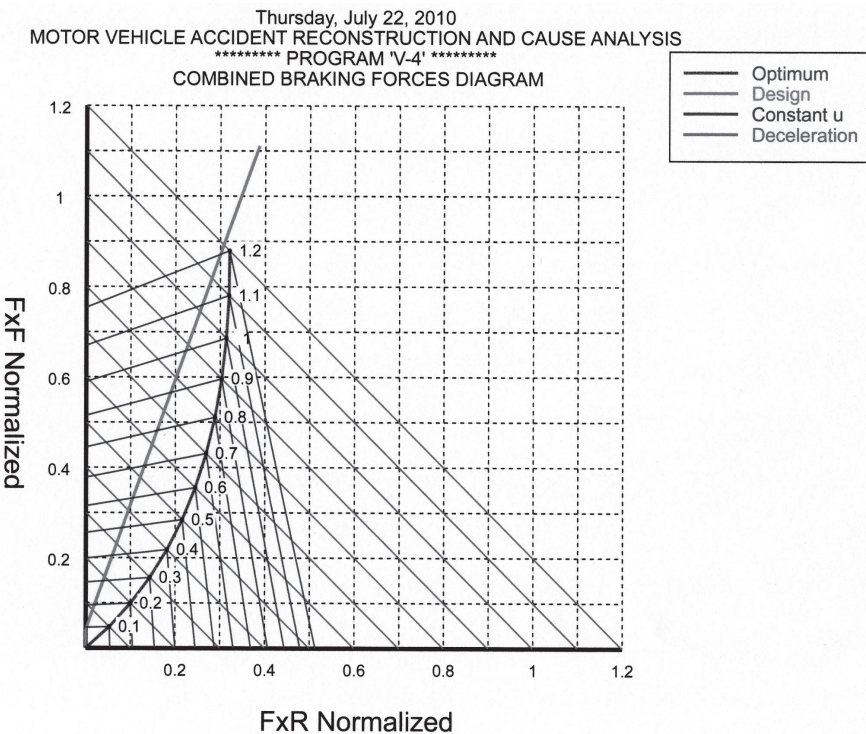


Figure 7-16. Braking forces diagram, Example 7-3, laden with LSPV.

calculations use the same data. The braking efficiency equals $0.74/0.8 = 0.925$ or 93%.

The critical deceleration can be calculated from the operating line of the actual braking forces [Eq. (1) above] and the optimum line equations front and rear. Solving the first equation above and Eqs. (7-7a) and (7-7b) simultaneously yields $a_{crit} = 1.023$ g with $(F_{xF}/W)_{opt} = 0.864$ and $(F_{xR}/W)_{opt} = 0.159$.

The next step of the brake system design analysis is the evaluation of the proportioning valve with respect to the laden operating condition. Using the laden data in the MARC 1-V module yields a pedal force of 293 N (66 lb), which is required to achieve a deceleration of 1 g. The braking forces diagram is shown in Fig. 7-15.

The actual braking force line intersects the $\mu_F = 0.8$ line at deceleration of approximately 0.55 g indicating a low braking efficiency of only 69%.

The proper design solution involves either a load-sensitive proportioning valve (LSPV) or a two-stage master cylinder, as illustrated in Fig. 7-16. The knee point pressure for the fully laden configuration moved automatically as a function of loading to 1380 N/cm 2 (2000 psi); that is, the knee point was eliminated from all expected brake line pressure ranges. The front brakes lock or the ABS system begins to modulate at a deceleration of approximately 0.64g when braking on a $\mu_F = 0.8$ roadway.

7.10 Braking Dynamics of Two-Axle Truck Equipped with Air Brakes

7.10.1 Basic Methodology

Much insight into braking dynamics of the two-axle vehicle was obtained from the mathematical analysis of the physics underlying the braking forces diagram. When dealing with the analysis and design of the brake system of heavy trucks, it becomes convenient to use a computerized method to analyze many influence factors, including push rod force variation, brake fade, loading differences for empty and laden configuration, dynamic axle loads including the effects of tandem axle suspension designs, and brake maintenance.

The general approach to the design and component selection of air brake systems involves the calculation of the traction coefficients for each brake or axle [Eq. (7-4)], and the determination of brake lock for specified tire/road friction coefficients. The braking force calculation for heavy trucks presented in Chapter 6 is expanded to compute the individual dynamic normal forces on each wheel or axle as a function of deceleration (Refs. 7.4, 7.5).

The approach consists of the following step-wise calculations: a specified brake line pressure results in certain brake forces on each axle, which produce vehicle deceleration, which causes dynamic axle loads, which is used to compute the tire-road traction coefficient μ_T required to predict wheel lockup.

Because the computations are algebraically involved, computer programs are used to facilitate the analysis. When, for a particular brake line pressure, the traction coefficient calculated for a brake or brakes of one axle exceeds the tire-road friction coefficient specified, the brake locks. The computer program goes back to the last brake line pressure before lock up and calculates the braking forces of that wheel or axle by multiplying the current normal force with the tire-road friction coefficient. A discontinuity may be created due to the brake line pressure interval chosen. PC-BRAKE Air uses 12 pressure intervals, yielding acceptable results. When 125 brake line pressure intervals are used, the discontinuities are insignificant.

7.10.2 PC-BRAKE AIR Software

The PC-BRAKE AIR software is available from website www.pcbrakeinc.com. It is used to design and analyze trucks and trailers equipped with air brakes.

The brake system design engineer will select the input data for a properly maintained brake system. Brake tests “on paper” can be run for different loading conditions, brake temperatures, brake system hardware, valve characteristics (if any), or center-of-gravity heights.

The forensic brake expert will compare the braking performance of a properly maintained brake system with the performance obtained for poorly maintained brakes, if applicable, including brakes being out of pushrod travel adjustment, oily brake shoes (lower brake factor), miss-matching of slack adjuster length, loading factors, and brake temperatures.

Example 7-4: Air Brake Design

For brake system design the following steps are suggested:

1. In Design Data all input data are provided. Set tire-road friction coefficient to artificially high $f = 3$ ($\mu_{\text{Road}} = 3$). The tire-road friction coefficient selected will not affect any calculations underlying the Design Data output.
 2. Set Starting brake line pressure = 79 N/cm^2 (115 psi); i.e., run a maximum effectiveness stop.
 3. Input initial conditions and brake system data for brakes in good mechanical condition as shown in Table 7-2.
 4. Under Calculated Data (Table 7-2) the drum/lining friction surface brake temperatures obtained for a single effective stop for each brake are shown. It is recommended to use one half of this value in the input data for single stop brake temperature (see Section 3.1.4 for more details). For a long duration braking process other brake temperature modules may be used such as repeated or continued braking discussed in Chapter 3. Brake temperature is used to compute brake fade and increased pushrod travel due to thermal drum expansion.
 5. Observe data printout for maximum deceleration, average decelerations, and stopping distance without brake lockup ($f = 3$) as $a_{\text{max}} = 0.76 \text{ g}$, $a_{\text{avg}} = 0.64 \text{ g}$ and stopping distance is 243 ft (Table 7-2).
 6. In Design Data set starting brake line pressure to 3.5 N/cm^2 (5 psi) (suggested to equal push-out pressure to start calculations with zero braking forces on each brake/axle).
 7. Observe front and rear axle utilization lines in the tire-road friction utilization diagram to determine if brake system design meets safety regulations (Refs. 7.6, 7.7, 7.8, 7.9, 7.10). In the example case, the rear axle does not exceed the requirements for decelerations less than approximately 0.75 g. When the program is run with rear brake chamber type 30 (193.5 cm^2 or 30 in.^2), rear axle will lock at decelerations slightly above 0.62 g.
 8. In Design Data, set tire road friction coefficient to actual road surface value, say $f = 0.8$. Observe in Table 7-3, Table 3 traction coefficients. For example, for rear axle left and right wheel the traction coefficient $U_{T2L} = U_{T2R} = 0.80$ for brake line pressure greater than 66 N/cm^2 (95 psi). The finding indicates that the rear axle traction coefficient calculated equals the tire-road friction coefficient at brake line pressure greater than 66 N/cm^2 (95 psi) and the rear brakes lock or ABS modulation begins.
- Note: Table 1: Braking forces are not affected by brake lockup; Table 2: Braking forces are affected by brake lockup; Table 3: Axle normal forces and traction coefficients.
- To determine rear brake lockup brake line pressure more accurately,

<u>Input Data:</u>		<u>AIR BRAKE SYSTEM ANALYSIS</u>				<u>2-AXLE STRAIGHT TRUCK</u>		<u>PLATE BRAKE</u>	
Tire-Road friction coefficient	$f = 3$								
Weight of Vehicle, lb	$W = 26000$								
Axle 1 static load, lb	$F_{z1\text{static}} = 8000$								
Axle 2 static load, lb	$F_{z2\text{static}} = 18000$								
Starting Brake Line Pressure, psi	$p_t = 115$								
Pressure Interval, psi	$D_p = 10$								
Road Slope Gradient, fraction (+/-)	$G = 0$								
Swept rotor Area of One Brake, Axle1, ft^2	$A_{s1} = 1.8$								
Swept rotor Area of One Brake, Axle 2, ft^2	$A_{s2} = 2.8$								
Knee-point Pressure, Axle 1, psi	$p_{k1} = 0$								
Valve Slope Reduction, Axle 1	$k_1 = 1$								
Height of CG, in	$h_{CG} = 70$								
Wheelbase, in	$L = 192$								
Velocity, ft/sec	$V = 100$								
Temperature, initial oF	$T_i = 100$								
Knee-point Pressure, Axle 2, psi	$p_{k2} = 0$								
Valve Slope Reduction, Axle 2	$k_2 = 1$								
<u>AXLE 1 LEFT</u>		<u>AXLE 1 RIGHT</u>		<u>AXLE 2 LEFT</u>		<u>AXLE 2 RIGHT</u>			
Chamber Area, in ²	$A_{c1L} = 24$		$A_{c1R} = 24$			$A_{c2L} = 24$		$A_{c2R} = 24$	
Brake factor	$BF_{1L} = 1.6$		$BF_{1R} = 1.6$			$BF_{2L} = 1.6$		$BF_{2R} = 1.6$	
Pushout Pressure, psi	$p_{o1L} = 5$		$p_{o1R} = 5$			$p_{o2L} = 5$		$p_{o2R} = 5$	
Tire Radius, in	$R_{1L} = 21$		$R_{1R} = 21$			$R_{2L} = 21$		$R_{2R} = 21$	
Drum or Effective Disc Radius, in	$r_{1L} = 7.5$		$r_{1R} = 7.5$			$r_{2L} = 8.25$		$r_{2R} = 8.25$	
Mechanical Efficiency	$\eta_{c1L} = 0.7$		$\eta_{c1R} = 0.7$			$\eta_{c2L} = 0.7$		$\eta_{c2R} = 0.7$	
Braking Temperature, deg	$T_{1L} = 296$		$T_{1R} = 296$			$T_{2L} = 247$		$T_{2R} = 247$	
Measured Stroke, in	$S_{1L} = 1$		$S_{1R} = 1$			$S_{2L} = 1$		$S_{2R} = 1$	
Maximum rated Stroke, in	$S_{\max1L} = 2.25$		$S_{\max1R} = 2.25$			$S_{\max2L} = 2.5$		$S_{\max2R} = 2.5$	
Critical Stroke, in	$S_{c1L} = 1.75$		$S_{c1R} = 1.75$			$S_{c2L} = 2$		$S_{c2R} = 2$	
<u>Calculated Data</u>									
Effective Pushrod Travel, in	$S_{e1L} = 1.16$		$S_{e1R} = 1.16$			$S_{e2L} = 1.12$		$S_{e2R} = 1.12$	
Adjustment Factor	$f_{a1L} = 1.00$		$f_{a1R} = 1.00$			$f_{a2L} = 1.00$		$f_{a2R} = 1.00$	
Fade Factor	$f_{F1L} = 0.83$		$f_{F1R} = 0.83$			$f_{F2L} = 0.86$		$f_{F2R} = 0.86$	
Mechanical Gain	$\rho_{D,S,\text{or } W} = 5.00$		$\rho_{D,S,\text{or } W} = 5.00$			$\rho_{D,S,\text{or } W} = 5.50$		$\rho_{D,S,\text{or } W} = 5.50$	
Braking Force, lb	$F_{x1L} = 4374$		$F_{x1R} = 4374$			$F_{x2L} = 5474$		$F_{x2R} = 5474$	
Brakeline Pressures, Braked Axles, psi	$p_t = 115$					$p_{k2} = 115$			
Relative Rear Axle Load	$\Psi = 0.69$								
Relative CG Height	$X = 0.36$								
Maximum Deceleration, g	$a_{\text{max}} = 0.76$								
Dynamic Axle Load, lb	$F_{z1} = 15180$					$F_{z2} = 10820$			
Traction Coefficient	$U_{T1L} = 0.58$		$U_{T1R} = 0.58$			$U_{T2L} = 1.01$		$U_{T2R} = 1.01$	
Braking Efficiency	$E_{1L} = 1.31$		$E_{1R} = 1.31$			$E_{2L} = 0.75$		$E_{2R} = 0.75$	
Brake Force Distribution	$BD_{1L} = 0.22$		$BD_{1R} = 0.22$			$BD_{2L} = 0.28$		$BD_{2R} = 0.28$	
Braking Energy, BTU/hr	$Q_{1L} = 2023741$		$Q_{1R} = 2023741$			$Q_{2L} = 2532744$		$Q_{2R} = 2532744$	
Stopping Time, hours	$t_{\text{stop}} = 0.00114$								
Temperature, Brake, °F	$T_{\text{brake}} = 593$		$T_{\text{brake}} = 593$			$T_{\text{brake}} = 497$		$T_{\text{brake}} = 497$	
<u>Stopping Distance Equations:</u>									
<u>Input Data</u>									
Brake Line Pressure Rise Time, secs	$t_r = 0.40$								
Brake Torque Build-up Time, secs	$t_t = 0.30$								
Maximum Deceleration, g	$a_{\text{max}} = 0.76$								
Vehicle Speed, ft/sec	$V = 100.0$								
<u>Calculated Data</u>									
Average Deceleration, g	$a_{\text{avg}} = 0.64$								
Stopping Distance, ft	$Sa_{\text{avg}} = 243$								

Table 7-2. Air Brake System Analysis, 2-Axle Straight Truck Case ID: Example 7-4.

AIR BRAKE SYSTEM ANALYSIS
2-AXLE STRAIGHT TRUCK
CASE ID.: Example 7-4.

Table 1

p_l	p_{l1}	p_{l2}	F_{X1L}	F_{X1R}	F_{X2L}	F_{X2R}
5	5	5	0	0	0	0
15	15	15	398	398	498	498
25	25	25	795	795	995	995
35	35	35	1193	1193	1493	1493
45	45	45	1590	1590	1990	1990
55	55	55	1988	1988	2488	2488
65	65	65	2386	2386	2986	2986
75	75	75	2783	2783	3483	3483
85	85	85	3181	3181	3981	3981
95	95	95	3578	3578	4478	4478
105	105	105	3976	3976	4976	4976
115	115	115	4374	4374	5474	5474

Table 2

p_l	p_{l1}	p_{l2}	F_{X1L}	F_{X1R}	F_{X2L}	F_{X2R}	$F_{X \text{ Total}}$	$a, g's$
5	5	5	0	0	0	0	0	0.00
15	15	15	398	398	498	498	1790	0.07
25	25	25	795	795	995	995	3581	0.14
35	35	35	1193	1193	1493	1493	5371	0.21
45	45	45	1590	1590	1990	1990	7162	0.28
55	55	55	1988	1988	2488	2488	8952	0.34
65	65	65	2386	2386	2986	2986	10742	0.41
75	75	75	2783	2783	3483	3483	12533	0.48
85	85	85	3181	3181	3981	3981	14323	0.55
95	95	95	3578	3578	4478	4478	16113	0.62
105	105	105	3976	3976	4976	4976	17904	0.69
115	115	115	4374	4374	5474	5474	17925	0.69

Table 3

p_l	F_{z1}	F_{z2}	U_{T1L}	U_{T1R}	U_{T2L}	U_{T2R}	U	k_L	k_H
5	8000	18000	0.00	0.00	0.00	0.00	0.00	-0.08	0.08
15	8653	17347	0.09	0.09	0.06	0.06	0.07	-0.01	0.15
25	9305	16695	0.17	0.17	0.12	0.12	0.14	0.06	0.22
35	9958	16042	0.24	0.24	0.19	0.19	0.21	0.13	0.29
45	10611	15389	0.30	0.30	0.26	0.26	0.28	0.20	0.36
55	11264	14736	0.35	0.35	0.34	0.34	0.34	0.26	0.42
65	11916	14084	0.40	0.40	0.42	0.42	0.41	0.33	0.49
75	12569	13431	0.44	0.44	0.52	0.52	0.48	0.40	0.56
85	13222	12778	0.48	0.48	0.62	0.62	0.55	0.47	0.63
95	13875	12125	0.52	0.52	0.74	0.74	0.62	0.54	0.70
105	14527	11473	0.55	0.55	0.80	0.80	0.69	0.61	0.77
115	14535	11465	0.60	0.60	0.80	0.80	0.69	0.61	0.77

Table 7-3 Example 7-4. Table data output.

in Design Data set starting brake line pressure to 95 psi and pressure interval to 1 psi. Observe in Table Data, Table 3 that the rear brakes will lock at brake line pressures between 68 and 69 N/cm² (99 and 100 psi) [0.79 < 0.80].

9. Run step 8 with tire-road friction coefficient $f = 0.3$ (snow – ice). Observe Table Data brake lockup sequence. Front brakes will lock before rear brakes at brake line pressure greater than approximately 24 N/cm² (35 psi) [exact 30 N/cm² (44 psi)] and the rear brakes at pressure greater than 31 N/cm² (45 psi) [exact 34 N/cm² (50 psi)].

Evaluating the brake design with a rear brake chamber type 30 results in nearly equal brake temperatures front and rear, less rear axle tire-road friction utilization, and rear brake lockup at 83 psi (instead of 99 psi). In the final design choice, additional factors such as brake wear, intended vehicle, availability of proven friction materials (well established brake factor BF), etc. must be considered.

Example 7-5: Forensic Brake System Analysis

Consider the truck and brake data of Example 7-4, except both front brakes are at 43.2 mm (1.70 in.) brake adjustment pushrod travel and the right rear brake was out of legal adjustment at a measured pushrod travel of 58.4 mm (2.3 in.) (Ref. 7.11). Determine the maximum deceleration and stopping distance of the truck from 110 km/h (68 mph).

The maximum brake temperatures are 570 K (566°F), 570 K (566°F), 563 K (554°F) and 407 K (273°F). The maximum deceleration is 0.56 g, the average deceleration 0.49 g, resulting in a stopping distance of 96 m (316 ft) instead of 74 m (243 ft) of the properly maintained truck. The left rear brake locks at a brake line pressure of 76 N/cm² (110 psi) (exact analysis). In the calculations, a brake pressure delay time of 0.4 s and brake torque buildup time of 0.3 s were assumed.

7.11 Three-Axle Straight Truck – Air Brakes

7.11.1 Air Springs Rear Tandem Axle

The basic analysis concepts are identical to those used for the two-axle truck except for one additional axle brake hardware, and the corresponding dynamic axle loads of the second and third axle including inter-axle load transfer. The individual traction coefficients are computed from the ratios of individual braking forces and associated dynamic normal forces or axle loads.

The basic dimensions and weights of a three-axle truck are illustrated in Fig. 7-17.

The analysis that follows applies to three-axle trucks with two independent rear air spring axles, buses with a third tag axle, and any other three-axle vehicles with rear axle designs in which axles two and three are independent of each other. Axles two and three are simply attached to the main truck frame, or chassis in the case of unitized bus body structures, without any other linkage

communication between them. Because there is no inter-axle load transfer among the rear axle, the weights of the rear axles are included in the entire weight of the vehicle; that is, no unsprung axle weights are considered in the dynamic axle load analysis.

The normal forces of the second and third axle decrease as deceleration increases.

The normal forces for the three axles are computed by:

$$F_{z1} = (1 - \psi + \chi a)W, \text{ N (lb)} \quad (7-45)$$

$$F_{z2} = (\psi - \chi a)(1 + q/(2L))W/2, \text{ N (lb)} \quad (7-46)$$

$$F_{z3} = (\psi - \chi a)(1 - q/(2L))W/2, \text{ N (lb)} \quad (7-47)$$

where

$$\psi = (F_{z2\text{stat.}} + F_{z3\text{stat.}})/W$$

$$\chi = h_{cg}/L$$

W = vehicle weight, N (lb)

h_{cg} = center-of-gravity height of entire vehicle, cm (in.)

L = wheel base, cm (in.) (distance from front axle to center of tandem axle)

7.11.2 Rear Walking Beam Tandem Axle

The unique feature of the walking beam rear suspension is the decrease of the dynamic axle load of axle 3 and the slight increase of axle 2. The sprung weight W_s and the individual unsprung weights w_2 and w_3 of the tandem axles and the dimensions required for the axle load analysis are identified in Fig. 7-17.

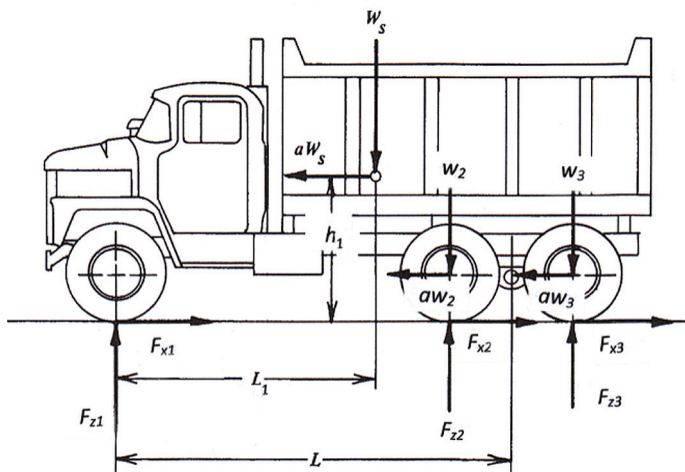


Figure 7-17. Forces acting on a three-axle truck.

The distance L_1 identifies the distance from the front axle to the center-of-gravity location of the sprung weight W_s . Consequently, L_1 is not the distance to the center-of-gravity of the entire weight (sprung weight plus unsprung axle weights). The letter h_1 identifies the vertical distance between ground and center-of-gravity of the sprung weight W_s .

The forces acting on the tandem axle suspension(s) are identified in Fig. 7-18. Although design details may vary, the dimensions for the basic geometries are shown. In order to compute inter-axle load transfer, all dimensions specified must be measured or otherwise determined.

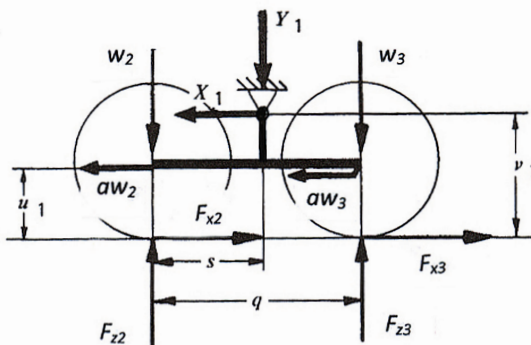
Using the free-body diagrams of Figs. 7-17 and 7-18(A), the equations computing the normal forces of axles 1, 2, and 3 are

$$F_{z1} = W_s - Y_1, N \text{ (lb)} \quad (7-48)$$

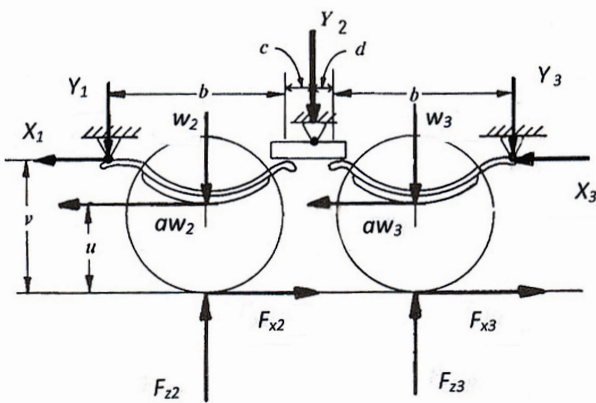
$$F_{z2} = Y_1 + w_2 + w_3 - F_{z3}, N \text{ (lb)} \quad (7-49)$$

$$F_{z3} = [Y_1 s - X_1 v_1 - (w_2 + w_3) a u_1 + w_3 q] / q, N \text{ (lb)} \quad (7-50)$$

The frame attachment forces are



(A) Walking Beam



(B) Leaf Spring

Figure 7-18. Forces acting on tandem axle suspensions.

$$X_1 = aW_s - F_{x1}, \text{ N (lb)} \quad (7-51)$$

$$Y_1 = (W_s L_1 - aW_s h_1 + X_1 v_1)/L, \text{ N (lb)} \quad (7-52)$$

where h_1 = height to center-of-gravity of sprung weight W_s , cm (in.)

L_1 = horizontal distance from front axle to center-of-gravity of sprung weight, cm (in.)

W_s = sprung weight of truck, N (lb)

w_2 = unsprung weight of axle 2, N (lb)

w_3 = unsprung weight of axle 3, N (lb)

The three axle loads for a walking beam tandem axle are illustrated in Fig. 7-19, indicating the decrease of the axle load of axle 3.

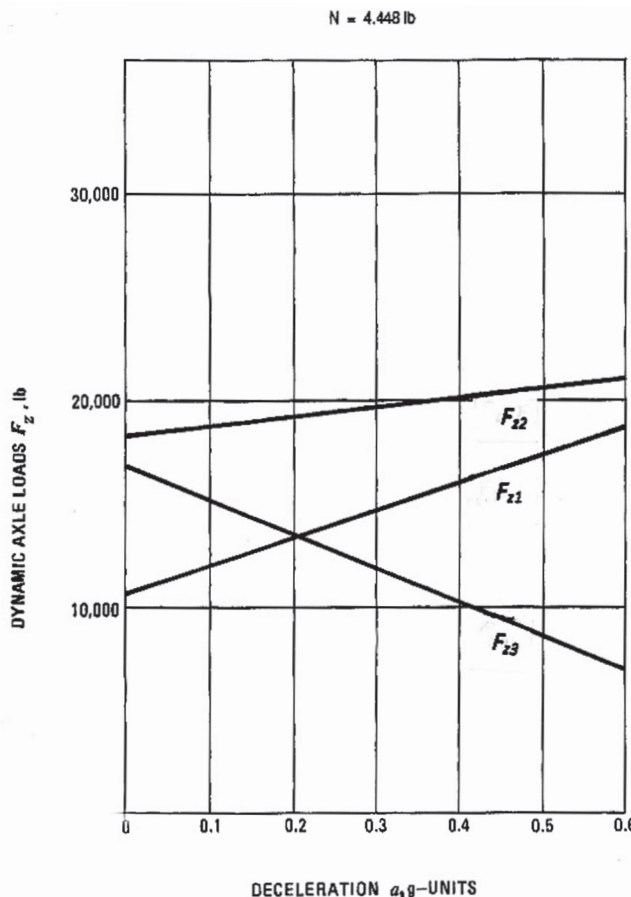


Figure 7-19. Dynamic axle loads for a three-axle truck with walking beam.

7.11.3 Rear Leaf Spring Tandem Axle

The equations for computing the dynamic normal forces of the three axles are presented in the paragraphs that follow.

$$F_{z1} = W_s - Y_1 - Y_2 - Y_3, \text{ N (lb)} \quad (7-53)$$

$$F_{z2} = Y_1 + d_1 Y_2 + w_2, \text{ N (lb)} \quad (7-54)$$

$$F_{z3} = c_1 Y_2 + Y_3 + w_3, \text{ N (lb)} \quad (7-55)$$

where

$$d_1 = d/(c + d)$$

$$R_1 = (F_{x2} - aw_2)v + (F_{x3} - aw_3)v - ahW_s + W_sL_1, \text{ Ncm (lbin.)}$$

$$R_2 = (F_{x2} - aw_2)v + aw_2u, \text{ Ncm (lbin.)}$$

$$R_3 = (F_{x3} - aw_3)v + aw_3u, \text{ Ncm (lbin.)}$$

The vertical suspension attachment forces are

$$Y_2 = [R_1 + 2R_2(L - c - b)/b - 2R_3(L + d + b)/b]/[d_1(L - c - b) + L + c_1(L + d + b)], \text{ N (lb)} \quad (7-56)$$

$$Y_1 = d_1 Y_2 - 2R_2/b, \text{ N (lb)} \quad (7-57)$$

$$Y_3 = c_1 Y_2 + 2R_3/b, \text{ N (lb)} \quad (7-58)$$

The horizontal suspension attachment forces are

$$X_1 = F_{x2} - aw_2, \text{ N (lb)} \quad (7-59)$$

$$X_3 = F_{x3} - aw_3, \text{ N (lb)} \quad (7-60)$$

A unique feature of the leaf spring suspension is the significant decrease of the dynamic normal force of the forward axle of the tandem suspension (axle #2 of a three-axle truck or axle #4 of a 3-S2 tractor trailer combination) and increase of dynamic normal force of the rear tandem axle (axle #3 of a three-axle truck or axle #4 of a 3-S2 tractor trailer combination) (Ref. 7.9). This inter-axle load transfer is caused by the equalizer arm connecting both axles. For the lightly laden operating condition and decelerations greater than 0.5 to 0.6 g, the dynamic normal force of axle #2 may become zero; that is, it will lift off the ground, as illustrated in Fig. 7-20.

The PC-BRAKE Air software for leaf spring suspensions is designed to account for axle lift-off and to change the dynamic axle load equations to those of a two-axle truck in case of a three-axle truck equipped with rear leaf suspension, or to a single-axle semitrailer in case of a 3-S2 combination equipped with leaf spring suspension on the trailer.

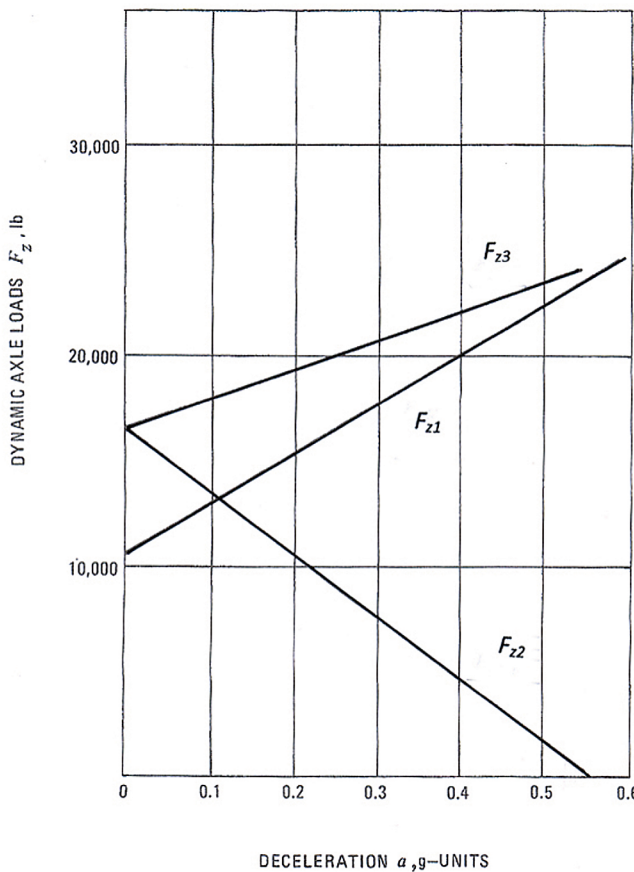


Figure 7-20. Dynamic axle loads for a three-axle truck with leaf springs.

7.12 Vehicle Stability Analysis

7.12.1 General Considerations

The response of a mechanical system to a disturbance force can be stable, unstable, or indifferent. A response is stable when, after the action of a disturbance force is removed, the system returns to its initial stable motion. A response is unstable when a relatively small disturbance force causes greater and greater deviations from the initially stable motion. In the case of an unstable response, the energy required for the unstable motion to develop is provided by the kinetic or motion energy of the system, i.e., the speed of the motor vehicle. An indifferent response occurs when a disturbance force causes a single displacement proportional to the disturbance force.

Accident and vehicle test data, as well as basic engineering analysis, indicate that locking of the rear brakes before the front brakes will result in violent vehicle instability, most frequently causing the vehicle to spin about its vertical axis. The angular spin velocity and corresponding spin angle are a function of vehicle speeds, tire-road friction coefficient, yaw moment of inertia, and vehicle dimensions. The tire marks produced by a vehicle that lost directional stability

caused by premature locking of the rear brakes is shown in Fig. 7-21. The longest tire mark was produced by the right rear tire. Close inspection reveals that the front end of the vehicle rotated clockwise to the right. The rear end did not swing out to the left into the opposite traffic lane. If the vehicle had rotated to the left, the front of the vehicle would have invaded the opposite traffic lane, potentially leading to side impact with oncoming traffic. Premature rear brake lockup is the most likely cause of rotating a vehicle sideways into the adjacent lane when traveling at highway speeds.



Figure 7-21. Tire marks caused by locking of rear brakes.

7.12.2 Simplified Braking Stability Analysis

The development of vehicle instability due to wheel lockup is illustrated in Fig. 7-22. If it is assumed that the front wheels have not yet approached sliding conditions and are still rolling, and that the rear brakes are already locked (Fig. 7-22 A), any disturbance in the lateral direction due to road grade, side wind, or left-to-right brake imbalance produces a side force F_y acting at the center of gravity of the vehicle. The resultant force F_r stemming from the longitudinal inertia force F_x induced by braking and the lateral force F_y is now acting under the vehicle slip angle α_v . The slip angle α_v is formed by the longitudinal axis of the vehicle and the direction in which the center of gravity is moving. The lateral side force F_y must be counteracted by side forces produced at the tires. Because the rear wheels are sliding, no tire side forces can be produced at the rear and, consequently, the side forces developed by the still-rotating front wheels produce a yawing moment of magnitude $F_y \Psi L$. This destabilizing moment rotates the vehicle about its vertical axis so that the initial slip angle α_v increases, resulting in vehicle spinning and directional instability.

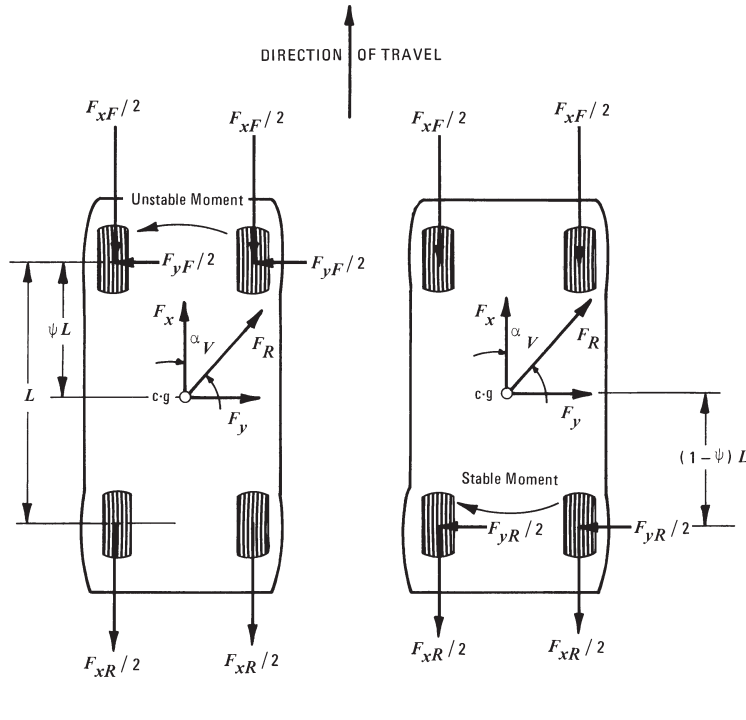


Figure 7-22. Vehicle behavior with rear or front brakes locked.

If the front brakes are locked first, an identical lateral disturbance will be reacted upon by a stabilizing moment $F_{yR}(1-\Psi)L$ produced by the rolling rear wheels. The direction of the moment is such that it rotates the longitudinal axis of the vehicle toward the direction of travel of the center of gravity of the vehicle, thus reducing the initial disturbance slip angle α_v with the vehicle remaining stable. The vehicle will travel straight with its front brakes locked. While the front brakes are locked, the vehicle will not respond to steering inputs by the driver. If a collision is unavoidable, a frontal crash typically will result in fewer injuries than a side crash due to better occupant protection.

7.12.3 Expanded Braking Stability Analysis

A simplified “bicycle” model of a braking vehicle is shown in Fig. 7-23 (Ref 1.3). Although braking, the front and rear wheels are rotating; i.e., they have not yet achieved lockup. Similar to the discussion presented in Section 7.12.3, a disturbance force produces a vehicle slip angle α_v . The lateral inertial side force F_y acting at the center of gravity is reacted upon by the tire side forces F_{yF} and F_{yR} on the front and rear axle, respectively. The tire slip angles required to produce side force, front and rear, are assumed to be both equal to each other as well as equal to the vehicle slip angle α_v . Because all tire forces are acting on their respective lever arms about the center of gravity, a moment is acting about the center of gravity of the vehicle which is reacted against by the mass moment of inertia of the vehicle, that is, the vehicle’s resistance to accelerate in rotation.

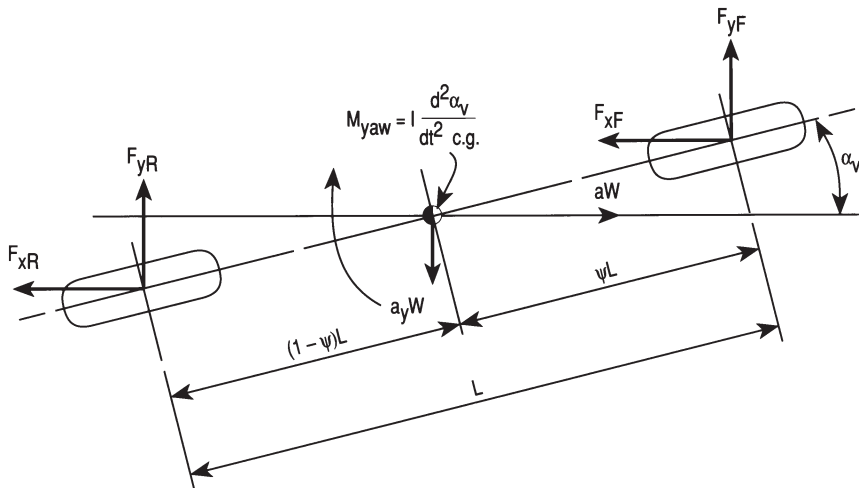


Figure 7-23. Forces and moments acting on simple vehicle model.

Application of force balance in the x- and y-directions as well as moment balance (Newton's second law in rotation $M = I\dot{\epsilon}$) about the center of gravity yields the governing dynamic equation for angular acceleration ϵ in rotation:

$$\epsilon = \frac{d^2\alpha_v}{dt^2} = \frac{L}{I} \{ \Psi F_{xF} \sin \alpha_v - (1 - \Psi) F_{xR} \sin \alpha_v + \Psi F_{yF} \cos \alpha_v - (1 - \Psi) F_{yR} \cos \alpha_v \} , \quad 1/s^2 \quad (7-61)$$

where F_{xF} = braking force on front axle in x-direction, N (lb)

F_{xR} = braking force on rear axle in x-direction, N (lb)

F_{yF} = tire side force on front axle, N (lb)

F_{yR} = tire side force on rear axle, N (lb)

I = mass moment of inertia, kgms^2 (lb ft s^2)

L = wheelbase, m (ft)

t = time, s

α_v = vehicle slip angle, deg

ϵ = angular acceleration, $1/s^2$

Ψ = static rear axle load divided by vehicle weight

Similar to linear acceleration, which expresses how quickly a vehicle changes forward speed, angular acceleration expresses how quickly a vehicle changes its rotational speed or angular velocity about its vertical axis. A positive value of angular acceleration in Eq. (7-61) indicates an increase in angular velocity and, hence, vehicle slip angle; i.e., the vehicle is directionally unstable and spins about its vertical axis. On the other hand, a negative value of angular acceleration in Eq. (7-61) indicates a decrease in angular velocity and vehicle slip angle, i.e., the vehicle returns to its initial stable course.

Consider the following cases with respect to Eq. (7-61).

- (1) The rear brakes lock with the front wheels still rotating:
 $F_{yR} = 0$; ϵ will be positive, resulting in an unstable vehicle.
- (2) The front brakes are locked with the rear brakes still rotating:
 $F_{yF} = 0$; ϵ will be negative, resulting in a stable vehicle.

Angular acceleration is a measure of the level of directional stability of the vehicle. A negative value is an indication that the vehicle is stable during braking maneuvers involving brake lockup. A positive angular acceleration means there is always a potential for vehicle instability. Typical drivers generally will not be able to control the directional path of a vehicle if the angular acceleration is greater than approximately 0.25 1/s^2 (Ref. 7.12). An angular acceleration of 0.25 1/s^2 indicates an angular velocity of approximately 14 deg/s ($57.3/4$) after one second. The associated yaw or spin angle would be approximately 7 deg one second after the instability began. For vehicles exhibiting rear brake lockup before front brake lockup, relatively small vehicle slip angles of two to five degrees generally are sufficient to generate angular accelerations in excess of the limit recoverable by the driver. If the disturbance slip angle is greater, the unstable angular acceleration and associated spin angle will increase rapidly.

A numerical evaluation of Eq. (7-61) requires computation of the braking and side forces at the front and rear tires. For the braking forces, a traction coefficient can be computed by using Eq. (7-4). The braking forces in the numerator of Eq. (7-4) may be expressed as a function of brake line pressure by using Eq. (5-2). When considering that the braking forces F_{xF} and F_{xR} are related to the braking forces developed by the brake system by the term $\cos\alpha_v$, the following expressions for the traction coefficients $\mu_{TF,x}$ and $\mu_{TR,x}$ may be derived:

Front axle:

$$\mu_{TF,x} = \frac{p_F K_F \cos \alpha_v}{W(1 - \Psi) + (p_F K_F + p_R K_R) \chi \cos \alpha_v} \quad (7-62)$$

Rear axle:

$$\mu_{TR,x} = \frac{p_R K_R \cos \alpha_v}{W\Psi - (p_F K_F + p_R K_R) \chi \cos \alpha_v} \quad (7-63)$$

where $K_{F,R}$ = axle brake gain, front or rear, cm^2 (in.^2)

p_F = front brake line pressure, N/cm^2 (psi)

p_R = rear brake line pressure, N/cm^2 (psi)

W = vehicle weight, N (lb)

χ = center of gravity height divided by wheelbase

The rear brake line pressure is computed by Eq. (5-11) when a proportioning valve is used.

The front and rear axle brake gains are computed by

$$K_{F,R} = 2[A_{wc}BF\eta_c(r/R)]_{F,R} \quad , \quad \text{cm}^2(\text{in.}^2) \quad (7-64)$$

where the following terms are evaluated for the front and rear brakes:

A_{wc} = wheel cylinder cross-sectional area, $\text{cm}^2(\text{in.}^2)$

BF = brake factor

r = effective rotor or drum radius, cm (in.)

R = tire radius, cm (in.)

η_c = wheel cylinder efficiency

The traction coefficients computed by Eqs. (7-62) and (7-63) for a specified disturbance slip angle α_v establish a specific absolute tire slip value S_b by use of basic tire data.

Because the total tire traction available has to be shared by braking and side traction, use of the absolute slip S_b and the slip angle α_v establishes values of side traction coefficient μ_y for a range of brake line pressures.

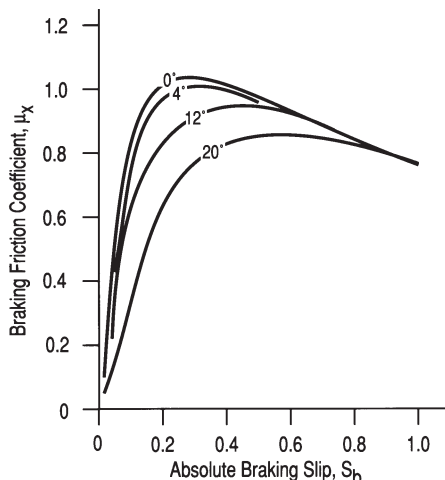


Figure 7-24. μ -slip curves as function of slip angle.

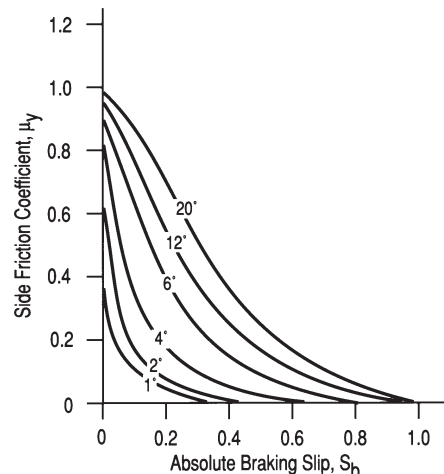


Figure 7-25. Side friction coefficient as function of braking slip and slip angle.

Similar to the braking forces [Eqs. (7-5)], the side forces front and rear F_{yF} and F_{yR} are computed for the side traction coefficient established above by the following expressions:

Front:

$$F_{yF} = \mu_y \{ W(1 - \Psi) + (p_F K_F + p_R K_R) \chi \cos \alpha_v \} \quad , \quad \text{N (lb)} \quad (7-65)$$

Rear:

$$F_{yR} = \mu_y \{ W\Psi - (p_F K_F + p_R K_R) \chi \cos \alpha_v \} \quad , \quad \text{N (lb)} \quad (7-66)$$

When the traction coefficients calculated by Eq. (7-65) or (7-66) exceeds the maximum tire-road friction coefficient, that particular axle will lock. No angular accelerations calculated beyond that point must be used. If the rear axle locks first, the vehicle will spin; if the front locks first, the vehicle will stop turning and travel at a tangent to the path curvature.

Example 7-6: Braking Stability

For the following vehicle and brake system data, determine the basic stability response. The tire braking and side force coefficients used are shown in Figs. 7-24 and 7-25.

Vehicle data loaded: $W = 13,350 \text{ N}$ (3000 lb), static rear axle load 7120 N (1600 lb), wheelbase 254 cm (100 in.), front axle brake gain $G_F = 8.92 \text{ cm}^2$ (1.383 in.²), rear axle brake gain $G_R = 2.65 \text{ cm}^2$ (0.41 in.²), pushout pressures front and rear 7 N/cm^2 (10 psi) and 55 N/cm^2 (80 psi), respectively, center-of-gravity height 53 cm (21 in.), and disturbance slip angle $\alpha = 2$ degrees.

PC-BRAKE Stability software was used for the braking stability analysis that follows.

The results are presented in a series of diagrams shown in Figs. 7-26 through 7-31. The tire-road friction coefficients for the front and rear tires are shown in Figs. 7-26 and 7-27. The tire-road friction coefficients as a function of slip shown in Figs. 7-26 and 7-27 are based upon empirical expressions published in Ref. 7.13.

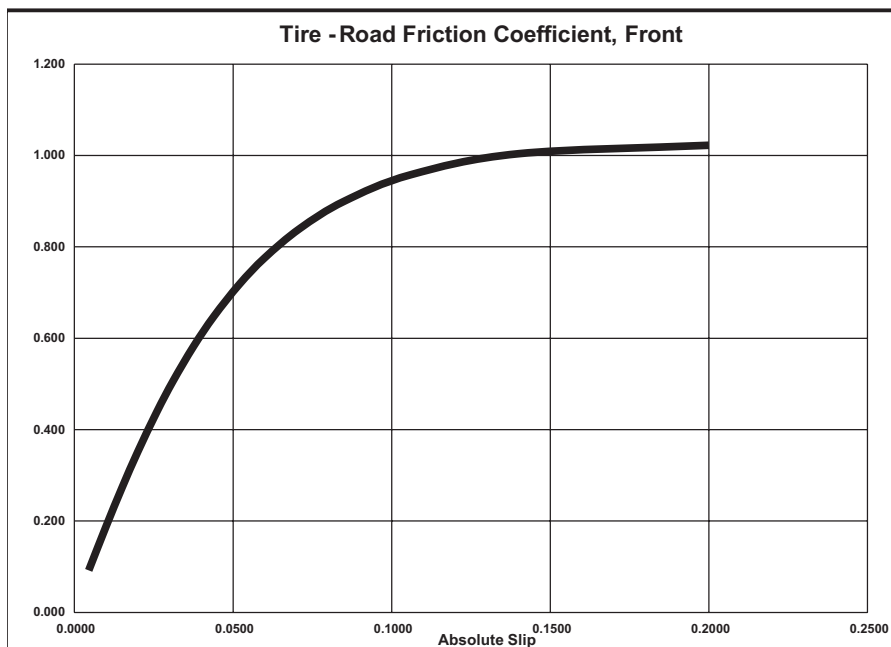


Figure 7-26. Tire-road friction coefficient, front.

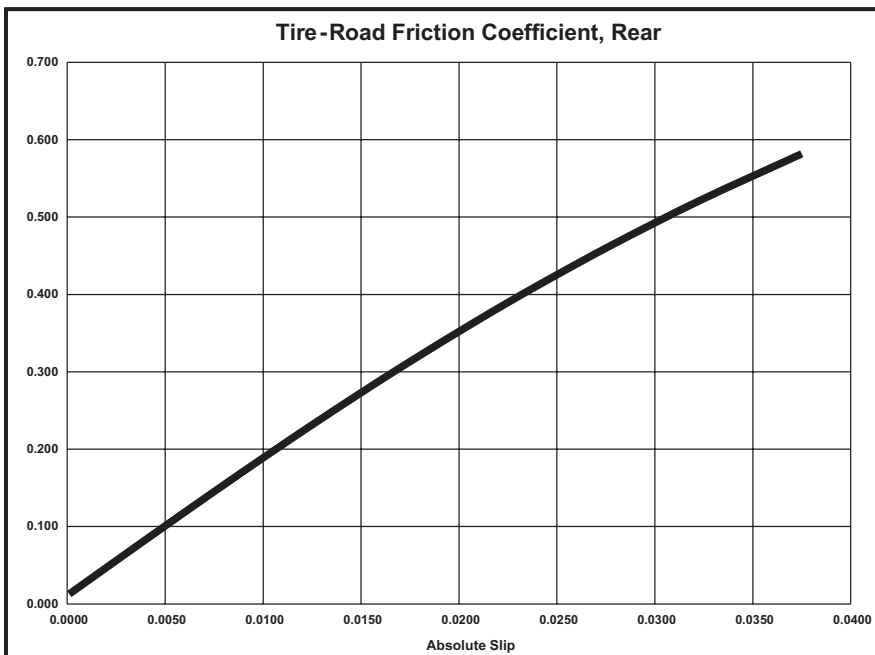


Figure 7-27. Tire-road friction coefficient, rear.

The traction coefficients computed with Eqs. (7-62) and (7-63) are shown in Fig. 7-28 as a function of brake line pressure. The front brakes will lock before the rear brakes for any brake line pressure. Inspection of Fig. 7-29 also indicates the front brakes locking before the rear brakes.

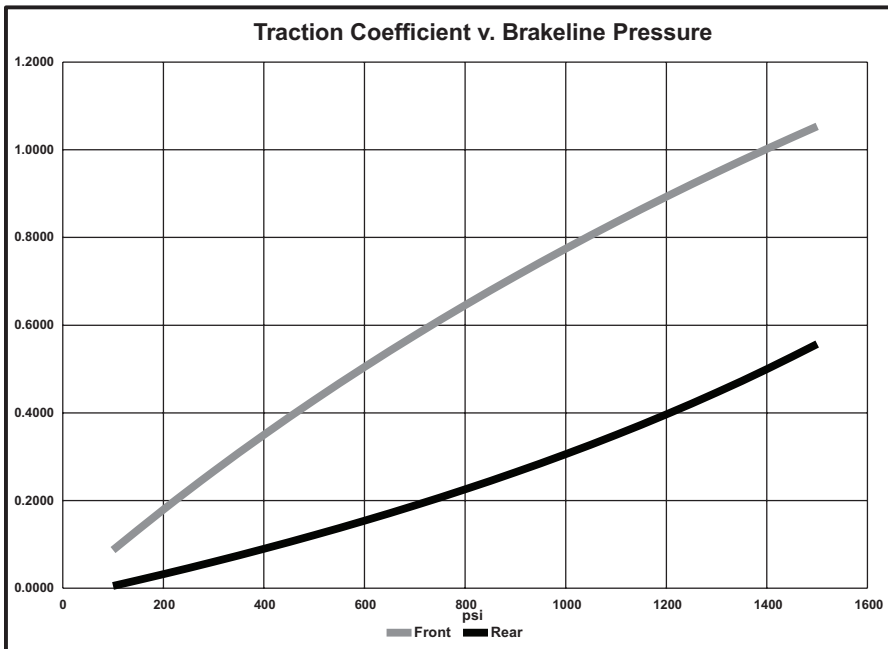


Figure 7-28. Traction coefficient vs. brake line pressure (laden).

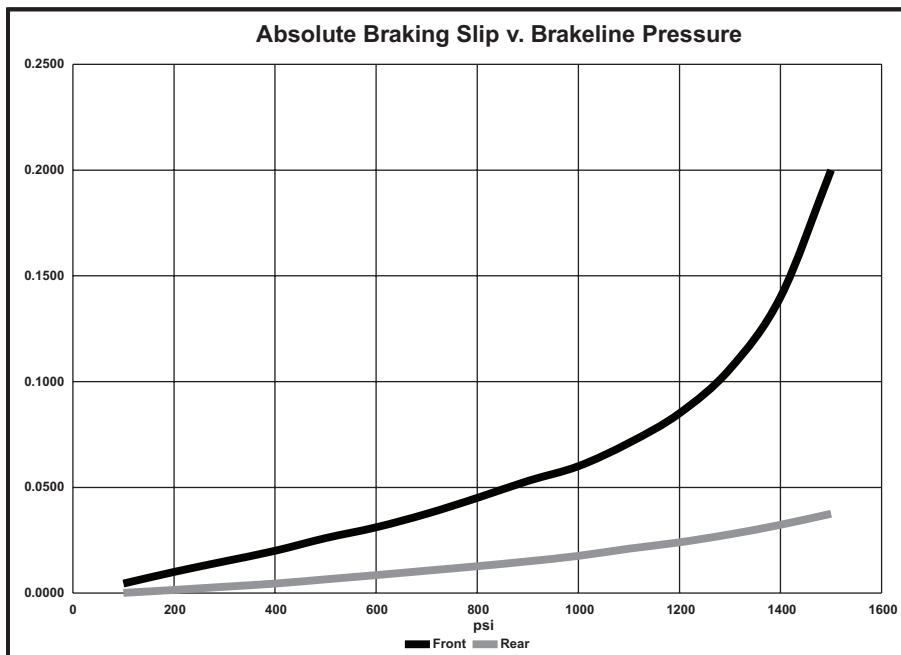


Figure 7-29. Absolute braking slip vs. brake line pressure.

The associated side traction coefficients used in Eqs. (7-48) and (7-49) are shown in Fig. 7-30. Inspection of Fig. 7-30 reveals the significant rear side traction coefficient available in comparison to the front for directional stability caused by a low rear brake balance ($\Phi = 0.23$) and relative rear axle load ($\psi = 0.53$).

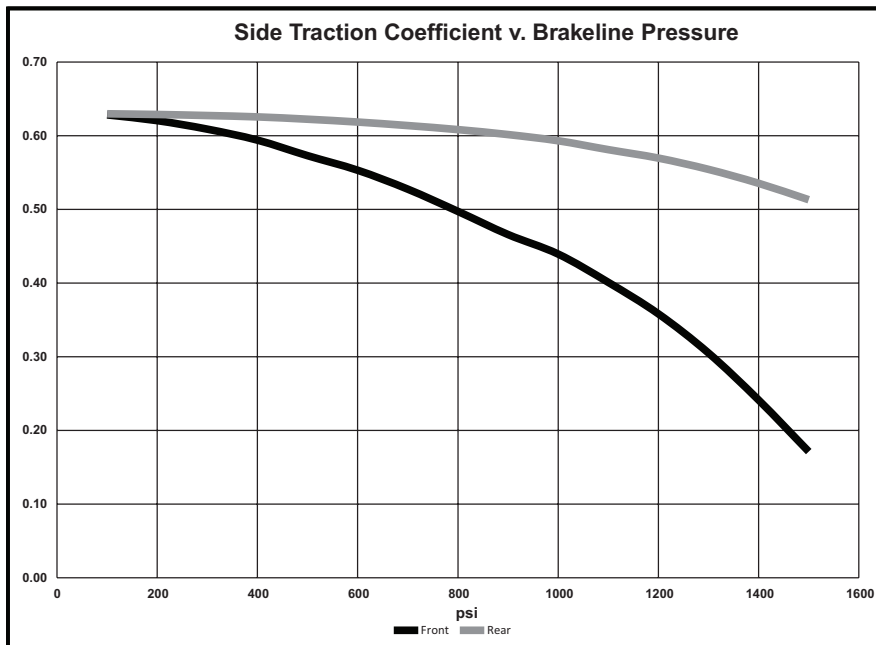


Figure 7-30. Side traction coefficient vs. brake line pressure.

Inspection of the angular acceleration as a function of brake line pressure shown in Fig. 7-31 indicates stable vehicle response for increasing brake line pressures with a negative angular acceleration for brake line pressures greater than 966 N/cm² (1400 psi). For brake line pressures greater than 966 N/cm² (1400 psi), the front brakes lock up.

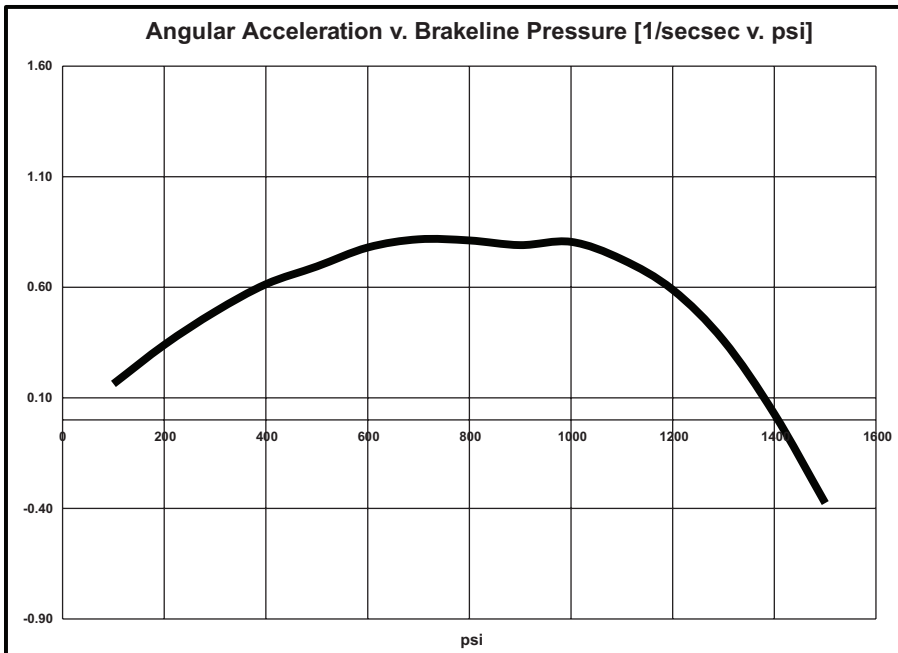


Figure 7-31. Angular acceleration vs. brake line pressure (laden).

The minor irregularity in angular acceleration curve is caused by the brake stability software and not by any vehicle dynamic factors.

7.12.4 Braking on a Split-Coefficient Road Surface

Rotation of a vehicle about its vertical axis during braking may be the result of braking on a split-coefficient road surface. In nearly all cases the angular velocity achieved by the vehicle is considerably less than that caused by premature rear-wheel lockup. Vehicles with a negative scrub radius will experience lower rotation than vehicles with positive or zero scrub radius.

The rotation of the vehicle toward the higher traction side may be analyzed by a simplified formulation assuming zero friction under the low traction side. Tire cornering stiffness values, pneumatic trail, and suspension characteristics must be considered.

7.13 Braking Dynamics While Turning

7.13.1 Basic Considerations

When braking in a turn, tires must produce longitudinal or braking forces and side forces. Vehicles that have their brake force distribution optimized for

straight-line braking do not provide optimal braking while turning. Wheels-unlocked decelerations decrease as turning severity increases.

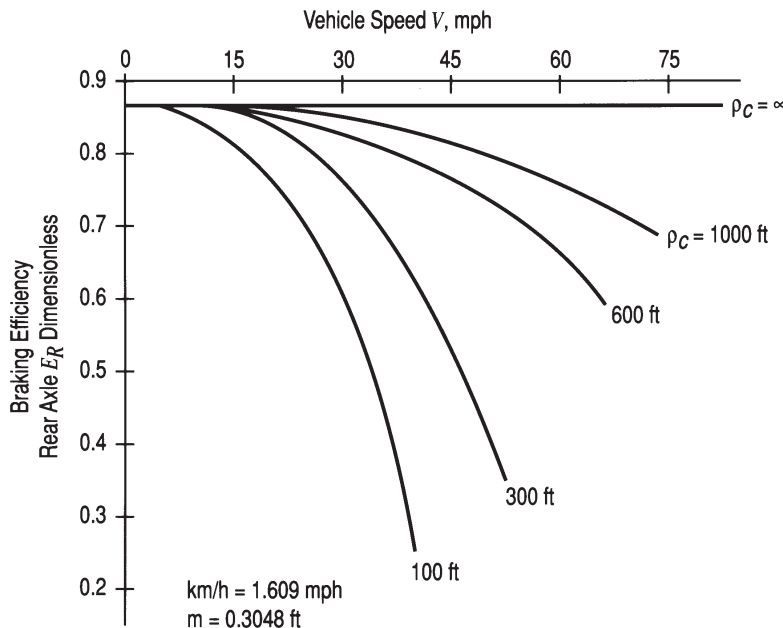


Figure 7-32. Rear braking efficiency as function of speed and road curvature for a tire-road friction coefficient of 0.6.

The rear braking efficiency as a function of speed and path radius or road curvature is illustrated in Fig. 7-32 for a tire-road friction coefficient of 0.6. Inspection of Fig. 7-32 indicates that for straight-line braking, i.e., the radius of the curve is infinite, the rear axle braking efficiency is approximately 0.86, resulting in a maximum wheels-unlocked deceleration of 0.52 g. For braking on a 300-foot radius curve from a speed of 72.4 km/h (45 mph), the braking efficiency reduces to approximately 0.45, yielding a deceleration of only 0.27 g when the inner rear wheel is near lockup. The braking dynamics used in developing Fig. 7-32 were based on a bicycle vehicle model; i.e., lateral load transfer was excluded. Critical speed calculations for braking while turning with and without lateral load transfer have been carried out (Ref. 7.14).

7.13.2 Optimum Brake Line Pressures for Braking in a Turn

The tire normal forces change due to the longitudinal deceleration of braking and the lateral acceleration or cornering force, as illustrated in Fig. 7-33. The additional longitudinal load transfer due to the centripetal force component F_{cx} acting in the direction of the longitudinal vehicle axis may be ignored for turning radii greater than 30 m (100 ft). The optimum brake line pressure analysis for straight-line braking discussed in Section 7.9.1 can be expanded to include the effects of lateral load transfer due to turning (Ref. 7.14).

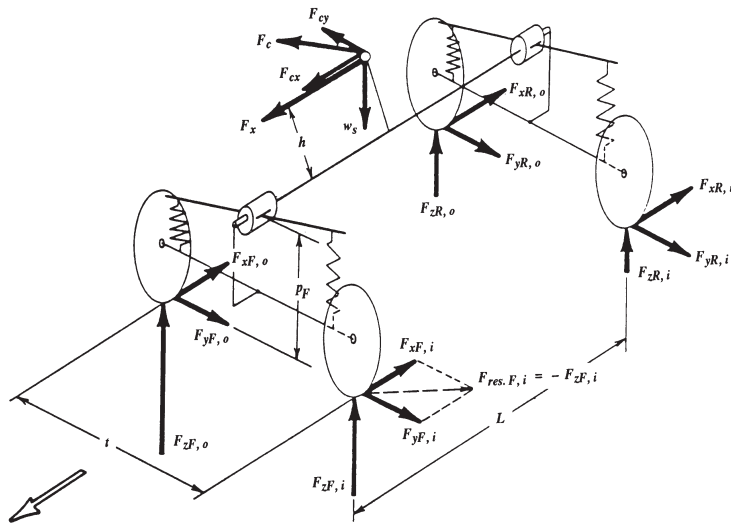


Figure 7-33. Forces acting on a braking vehicle while turning.

For a four-wheel vehicle with its center of gravity located midway between the left and right wheels, including load transfer due to the distance between roll centers and the road surface, the unsprung wheel and suspension masses, and the suspension moment due to roll stiffness, the optimum brake line pressures are:

Front, inner wheel:

$$(p_{lF_{in}})_{opt} = [a(1 - \psi + \chi a)(W/2) - a_y S_F W_S]/G_F + p_{oF}, \quad \text{N/cm}^2 (\text{psi}) \quad (7-67)$$

Front, outer wheel:

$$(p_{lF_{out}})_{opt} = [a(1 - \psi + \chi a)(W/2) + a_y S_F W_S]/G_F + p_{oF}, \quad \text{N/cm}^2 (\text{psi}) \quad (7-68)$$

Rear, inner wheel:

$$(p_{lR_{in}})_{opt} = [a(\psi - \chi a)(W/2) - a_y S_R W_S]/G_R + p_{oR}, \quad \text{N/cm}^2 (\text{psi}) \quad (7-69)$$

Rear, outer wheel:

$$(p_{lR_{out}})_{opt} = [a(\psi - \chi a)(W/2) + a_y S_R W_S]/G_R + p_{oR}, \quad \text{N/cm}^2 (\text{psi}) \quad (7-70)$$

where $G_F = 2[A_{wc} BF(r/R)\eta_c]_F, \text{ cm}^2 (\text{in.}^2)$

$$G_R = 2[A_{wc} BF(r/R)\eta_c]_R, \text{ cm}^2 (\text{in.}^2)$$

a = longitudinal deceleration, g

a_y = lateral acceleration, g

W = vehicle weight, N (lb)

W_s = sprung vehicle weight, N (lb)

The normalized roll stiffness S_F on the front suspension is (Ref. 1.4)

$$S_F = (L_R/L)(p_F/t_F) + [K_F/(K_F + K_R - W_s h_r)](h_r/t_F) + (w_F/W_s)(h_F/t_F) \quad (7-71)$$

where h_F = center of gravity height of front unsprung mass, m (ft)

h_r = perpendicular distance between center of gravity and roll axis, m (ft)

K_F = front roll stiffness, Nm/rad (ft-lb/rad)

K_R = rear roll stiffness, Nm/rad (ft-lb/rad)

L_R = horizontal distance between center of gravity and rear axle, m (ft)

p_F = front roll center-to-ground distance, m (ft)

t_F = front track width, m (ft)

w_F = front suspension unsprung weight, N (lb)

The rear normalized roll stiffness is obtained from Eq. (7-71) by replacing subscript F by R and using the appropriate vehicle data.

The optimum brake line pressure diagram with the four individual brake line pressures is shown in Fig. 7-34. The vehicle and brake system data are the following: $W = 13,350$ N (3000 lb), $\psi = 0.4$, $\chi = 0.2$; front: $A_{wc} = 31.7$ cm² (4.91 in.²), $BF = 0.71$, $r = 127$ mm (5 in.), $R = 356$ mm (14 in.), $\eta_c = 0.98$; rear: $A_{wc} = 11.4$ cm² (1.77 in.²), $BF = 0.71$, $r = 140$ mm (5.5 in.), $R = 356$ mm (14 in.), $\eta_c = 0.98$. In addition, the normalized roll stiffness values, front and rear, are $S_F = 0.25$ and $S_R = 0.15$. The sprung weight $W_s = 4060$ N (2800 lb). The optimum brake line pressures were calculated for a lateral acceleration of $a_y = 0.3$ g.

Inspection of Fig. 7-34 reveals that the range between inner and outer front brake line pressures is significantly smaller than those for the rear pressures as deceleration increases. This is to be expected because longitudinal load transfer tends to lessen the effects of lateral load transfer on the front axle, and increase them on the rear axle. The average between outer and inner brake line pressures equals the optimum brake line pressures for $a_y = 0$, as shown in Fig. 7-12.

The pressure difference between inner and outer wheel is a linear function of lateral acceleration.

During combined braking and steering maneuvers, the total traction available between tire and roadway is shared to produce longitudinal deceleration and lateral acceleration. The friction circle assumes that both longitudinal and lateral tire forces are related by the equation of a circle. A roadway having a friction coefficient of $\mu = 1.0$ is capable of producing a maximum vehicle deceleration of 1.0 g. The maximum lateral acceleration capability of the same

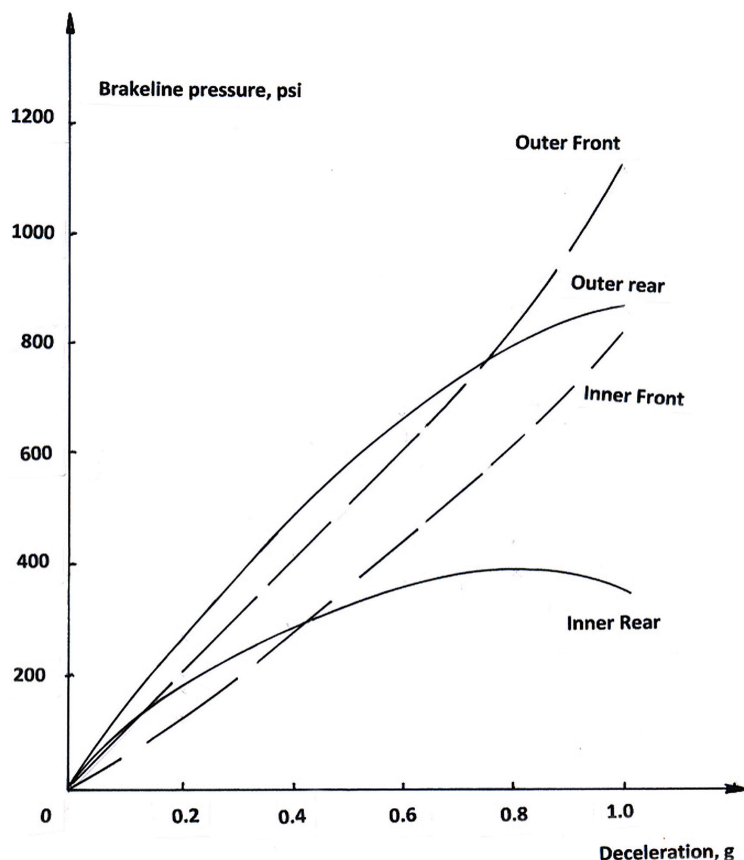


Figure 7-34. Optimum brake line pressures while turning at $a_y = 0.3$ g. (input data are the same for those of Fig. 7-12)

vehicle is usually less than 1.0 g. This is caused by differences in the mechanisms involved in producing braking and side forces. A tire-road surface having a peak braking friction coefficient of 0.9 and thus a theoretical $a_{x(\max)} = 0.9$ g tends to produce only about 0.7 to 0.75 g lateral acceleration. Tire design and suspension geometry influence maximum lateral acceleration. The friction circle concept does not accurately describe the relationship between limit braking and turning performance for a given tire-road surface condition.

Chapter 7 References

- 7.1 Limpert, R., "An Experimental Investigation of Proportional Braking," Master's Thesis, Brigham Young University, 1968.
- 7.2 Warner, C. and R. Limpert, "Proportioning Braking of Solid-Frame Vehicles," SAE Paper No. 710047, SAE International, Warrendale, PA, 1971.
- 7.3 Flaim, Thomas, "Vehicle Brake Balance Using Objective Brake Factors," SAE Paper No. 890804, SAE International, Warrendale, PA, 1989.
- 7.4 Murphy, R., et al., "Bus, Truck, Tractor-Trailer Braking System Performance," US Department of Transportation Contract No. FH-11-7290, March 1972.
- 7.5 Murphy, R., et al., "Development of Braking Requirements for Buses, Trucks and Tractor/Trailers," SAE Paper No. 710046, SAE International, Warrendale, PA, 1971.
- 7.6 Haataja, M. and T. Leiomen, "On the Distribution of Braking Force in Road Braking," SAE Paper No. 2000-01-3413, SAE International, Warrendale, PA, 2000.
- 7.7 Klug, Hans-Peter, "Nutzfahrzeug-Bremsanlagen," Vogel-Fachbuch Verlag, Germany, 1986.
- 7.8 Goering, E., et al., "Evaluation of the Brake-Force-Distribution and Its Influence on the Braking Performance of Light Commercial Vehicles," SAE Paper No. 800523, SAE International, Warrendale, PA, 1980.
- 7.9 SAE International Standard J1505, Brake Force Distribution Test Procedure—Trucks and Buses, SAE International, Warrendale, PA, April 21, 2004.
- 7.10 Limpert, R., "An Investigation of the Brake Force Distribution on Tractor-Semitrailer Combinations," SAE Paper No. 710044, SAE International, Warrendale, PA, 1971.
- 7.11 Radlinski, R., et al., "The Importance of Maintaining Air Brake Adjustment," SAE Paper No. 821263, SAE International, Warrendale, PA, 1982.
- 7.12 Burckhardt, M., "Fahrwerktechnik: Bremsdynamik und Pkw-Bremsanlagen," Vogel Buchverlag, 1991.
- 7.13 Burckhardt, M., "Fahrwerktechnik: Wheelslip Control Systems," Vogel Buchverlag, 1993.

- 7.14 Limpert, R., "An Investigation of the Brake Balance for Straight and Curved Braking," SAE Paper No. 741086, SAE International, Warrendale, PA, 1974.
- 7.15 Limpert, R., et al., "Analysis and Design of Two-Way Proportioning Valve for Improved Braking in a Turn," SAE Paper No. 760347, SAE International, Warrendale, PA, 1976.

Chapter 8



Braking Dynamics of Combination Vehicles

8.1 Tow Vehicle-Trailer Combination

The braking analysis for a combination vehicle is more complicated than for a two-axle vehicle because the summation of the axle loads of the tow vehicle is not equal to the weight of the tow vehicle. The tow vehicle axle loads are also a function of the geometry, loading and braking of the trailer(s).

8.1.1 Trailer without Brakes

For a trailer without brakes, the total braking force is produced by the braked axles of the tow vehicle. The deceleration achievable is reduced by the additional weight of the trailer. An approximate expression can be derived from Newton's Second Law with the resultant external force equal to the braking force of the tow vehicle.

For the case where the front or all tires of the tow vehicle are skidding, or the front ABS system modulates, and in the absence of any brake defects on the rear brakes, the approximate deceleration a_c is

$$a_c = W_1 \mu / (W_1 + W_2), \text{ g-units} \quad (8-1)$$

where W_1 = weight of car, lb

W_2 = weight of trailer, lb

μ = tire-road friction coefficient of tow vehicle

Equation (8-1) is approximate because the effects of tongue force on the axle loads of the tow vehicle, and the brake force distribution of the tow vehicle, and all wheel lockup are neglected.

Braking tests showed the following results for a roadway friction coefficient of about 0.76 and a car weight of 2945 lb (Refs. 8.1, 8.2).

Combination Weights	Deceleration Measured, g-units	Deceleration Eq. (8-1)
15,399 N (3462 lb)	0.63	0.65
17,401 N (3912 lb)	0.55	0.57
19,100 N (4294 lb)	0.50	0.50

8.1.2 Trailer with Brakes

8.1.2.1 Dynamic Axle Loads

The forces acting on a braking vehicle-trailer combination are illustrated in Fig. 8-1. For the non-braked trailer, the trailer braking force F_{x3} is equal to zero.

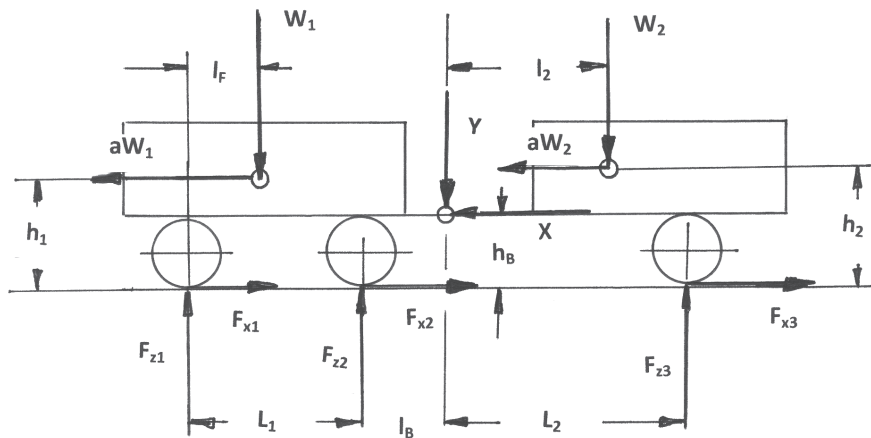


Figure 8-1. Tow-vehicle trailer combination.

The traction coefficient is determined by the ratio of braking force to dynamic axle load [(Eq. (7-4))].

The dynamic load of the front axle is:

$$F_{z1} = W_1 + (F_{z3} - W_3) - F_{z2}, \text{ N (lb)} \quad (8-2)$$

The dynamic load of the rear axle of the tow vehicle is:

$$F_{z2} = [W_1 l_F - aW_1 h_1 - (aW_2 - F_{x3})h_B + (W_2 - F_{z3})(L_1 + l_B)]/L_1, \text{ N (lb)} \quad (8-3)$$

The dynamic load of the trailer axle is:

$$F_{z3} = [W_2 l_2 - aW_2 (h_2 - h_B) - F_{x3} h_B]/L_2, \text{ N (lb)} \quad (8-4)$$

The hitch forces are: $X = aW_2 - F_{x3}, \text{ N (lb)}$ (8-5a)

$$Y = W_2 - F_{z3}, \text{ N (lb)} \quad (8-5b)$$

where a = deceleration of combination, $a = (F_{x1} + F_{x2} + F_{x3})/(W_1 + W_2)$, g-units
 h_B = vertical distance from ground to hitch ball, cm (in.)

h_1 = center-of-gravity height of tow vehicle, cm (in.)

h_2 = center-of-gravity height of trailer, cm (in.)

L_1 = wheelbase of tow vehicle, cm (in.)

L_2 = horizontal distance from hitch ball to trailer axle, cm (in.)

l_B = horizontal distance from rear axle of car to hitch ball, cm (in.)

l_F = horizontal distance from front axle to center-of-gravity of tow vehicle, cm (in.)

l_2 = horizontal distance from hitch point to center-of-gravity of trailer, cm (in.)

W_1 = weight of tow vehicle, N (lb)

W_2 = weight of trailer, N (lb)

F_{xi} = braking force of ith axle, N (lb)

8.1.2.2 Electric Trailer Brakes

For trailers with electric brakes, the brakes are actuated by an electric controller installed in the tow vehicle. The trailer brakes are applied automatically when the driver applies the service brakes of the tow vehicle and it begins to decelerate. The level of trailer braking is proportional to the deceleration of the tow vehicle. For properly maintained trailer brakes, application of maximum battery voltage (11.2 V in bench tests) to the trailer brakes yields a magnet drag force of approximately 400 N (90 lb) acting on the drum brake application lever arm. For a duo-servo brake with a brake factor $BF = 4.0$, the typical force acting on the tire circumference of one tire is approximately 6223 N (1400 lb). Decelerations achieved by four trailer brakes for a trailer loaded at GVW are approximately 0.5 to 0.55 g (Ref. 8.1).

8.1.2.3 Trailer with Surge Brakes

In a surge brake, the master cylinder located in the trailer hitch actuates the hydraulic brakes by the horizontal force produced at the hitch ball. For surge brakes, the brakes of the tow vehicle generally decelerate between 15 and 20% of the weight of the trailer. The approximate deceleration of the tow vehicle-trailer combination is determined by

$$a = \mu W_1/[W_1 + (0.15 \text{ to } 0.20)W_2], \text{ g-units} \quad (8-6)$$

When no braking skid marks are found at the scene, the tire-road friction coefficient μ is replaced by the deceleration the tow vehicle would have achieved alone.

The trailer braking force produced between the trailer tires and the ground is a function of the horizontal hitch ball force actuating the trailer master cylinder. Due to the friction in the sliding or roller mechanism of the hitch assembly, the usable actuation force is reduced.

The trailer brake gain ρ_T is expressed by the ratio of trailer braking force to actuation force between tow vehicle and trailer:

$$\rho_T = F_{x3}/X \quad (8-7)$$

where X = horizontal hitch ball force, N (lb)

F_{x3} = trailer braking force, N (lb)

The friction in the tongue reduces the actuation force against the master cylinder piston and opposes the release force. Consequently, the trailer brake gain actually usable, $\rho_{T,act}$, is given by

$$\rho_{T,act} = \rho_T(X \pm F_{HF})/X \quad (8-8)$$

where F_{HF} = friction force in hitch assembly, N (lb)

The minus sign is used for application, the plus sign for release of the brakes. The ratio of friction force to hitch ball force—an indication of the quality of a surge brake hitch—should not exceed 0.2 for roller-guided hitches. For surge brake hitches with roller systems, $\rho_{T,act} = 4$ to 6 (Ref. 1.3).

The horizontal hitch ball force X is given by

$$X = aW_2/(1 + \rho_{T,act}), \text{ N (lb)} \quad (8-9)$$

The vertical hitch ball force Y is determined by

$$Y = W_2 \{1 - F_{z3st}/W_2 + a[h_2/L_2 - (h_B/L_2)/(1 + \rho_{T,act})]\}, \text{ N (lb)} \quad (8-10)$$

In typical applications, full braking of the tow vehicle on a dry roadway produces approximately 298 to 341 N/cm² (350 to 400 psi) brake line pressure in the trailer brakes. A detailed braking analysis of car-trailer including ABS brakes is presented in Ref. 1.3.

8.2 Electronic Stability Control and Trailer Swing

A tow vehicle towing a trailer cannot become unstable as long as the hitch point moves in a straight line. Tire side forces can be produced only when the tires themselves travel under a slip angle, causing the front and rear tires to have a lateral velocity, along with the larger forward velocity (travel speed). These lateral velocities cause the hitch point to travel in a lateral direction, depending upon wheel base and hitch point overhang at the rear of the tow vehicle.

The tire side forces, and hence, slip angles are a direct function of the lateral force at the hitch point. As travel speed increases, so do the lateral velocities at the tires in order for the slip angles to remain constant. Consequently, a

tow vehicle will produce increased lateral displacements at higher speeds to counteract a lateral force at the hitch point caused by trailer swing. This observation is also a physical explanation of why tow vehicle-trailer instability becomes more critical with increasing vehicle speed (Ref. 8.3).

Electronic stability control (ESC) is required by passenger vehicles [GVW 44,500 N (10,000 lb) or less] sold in the U.S. in the 2013 model year. It has been modified (trailer stability assist – TSA) to eliminate unstable trailer swing. Auto-motor-und-sport conducted trailer stability testing with a trailer weighing 17,800 N (4000 lb) using two different tow vehicles (Ref. 8.4). Once a vehicle-trailer combination has reached its critical speed beyond which unstable trailer swing occurs, the driver may attempt to reduce the travel speed below the critical speed by a forceful brake application. Counter steering should not be attempted because driver steering inputs generally make the trailer oscillations more violent. For tow vehicles equipped with ESC, the system also checks the trailer swing. Trailer swing forces are transmitted from the trailer to the tow vehicle through the hitch. Any yaw rate and/or lateral accelerations of the tow vehicle not induced by the driver or tow vehicle must have been initiated by the trailer, causing individual brakes on the tow vehicle to be applied automatically. The brake apply methods are different among manufacturers. For example, the VW Touareg responds with a force application of all four brakes in addition to reducing engine power, resulting in a pronounced reduction of travel speed. The Mercedes S-class and M models initially attempt to stabilize the trailer through brief alternating applications of the front brakes, resulting in moments about the tow vehicle that stabilize the trailer swing. If trailer swing continues, all four brakes are fully applied.

8.3 Braking of Tractor-Trailer Combinations

For the correct design and brake balance analysis of a vehicle combination, it is essential that the optimum braking forces for each axle are known for the empty and laden cases. The optimum braking forces are a function of the dynamic axle loads. Because the equations for the axle loads are rather lengthy, the traction coefficient methodology will be used as presented in Chapter 7.

8.3.1 Tractor-Semitrailer Braking Instability

8.3.1.1 Jackknifing

Jackknifing is a term that describes the loss of directional stability of the tractor of a tractor-semitrailer combination. The articulation angle between tractor and trailer increases rapidly by spinning of the tractor about the fifth wheel. The tractor may rotate clockwise or counterclockwise depending upon left-to-right imbalance factors such as wheel alignment, left-to-right brake imbalance, lateral road friction differences, and others. If the tractor rotates counterclockwise, the left front tire of the tractor will invade the adjacent lane, frequently the opposite traffic lane of a two-lane highway, followed by continued rotation of the tractor and often causing the oncoming vehicle to crash into the passenger side of the tractor.

Jackknifing is caused by locking of the tractor rear brakes first, resulting in skidding of the rear tires (Refs. 8.5, 8.6, 8.7, 8.8, 8.9, 8.10, 8.11, 8.12). Because a locked, non-rotating tire has little or no side or lateral force (the entire friction force is directed opposite to the direction in which the tire skids), that is, there are no side forces on the rear tires of the tractor, the only available side forces of the tractor, existing at the rotating front tires, cause the front of the tractor to spin out of directional control by rotating about the fifth wheel (kingpin) of the tractor-semitrailer connection. The trailer will influence the spinning of the tractor through the horizontal forces at the kingpin (Ref. 8.12). The instability dynamics of the tractor is generally the same as that of a two-axle vehicle. For a detailed explanation of car-braking instability see Section 7.12. When operating without a trailer (bobtail configuration), special bobtail valves have been used to reduce the amount of braking on the tractor rear axle to prevent loss of stability while braking. The valve is activated when the trailer air hoses are disconnected from the tractor. ABS brakes, required by FMVSS 121 since 1997/98 in the U.S. and 71/320 in Europe since 1991, prevent premature tractor-rear brake lockup by ABS modulation below the lock-up brake line pressure of the rear brakes. FMVSS 121, considered a minimum performance standard, allows a maximum brake lockup time of one second for non-steered axles. Consequently, a vehicle traveling at 75 mph may produce solid rear tire braking skid marks of 110 ft and still comply with FMVSS 121. If an air brake ABS system were to allow a lockup of a controlled brake or axle, resulting in a tire skidding for one second, an inadequate tire-slip control air-pressure modulation algorithm rather than angular wheel deceleration threshhold might be suspected (see Chapter 9 for more details on ABS brakes).

8.3.1.2 Trailer Swing

Trailer swing is an increase of the articulation angle between tractor and trailer while the tractor remains stable. Trailer swing is not an instability in the sense that jackknifing is, because it can be controlled by the driver. Trailer swing is caused by locking of the trailer brakes first, in connection with a side force acting on the trailer. The side force could be due to road camber, lateral acceleration while traveling through a curve, wind gust, or others. Trailer swing may not be noticeable by the driver through the fifth wheel forces. Severe trailer swing may occur when the driver applies the hand-operated non-ABS trailer brakes while cornering.

8.3.1.3 Stable Braking

Locking of the tractor front brakes first renders the vehicle directionally stable; however, the operator cannot steer the tractor because locked (front) tires have no side force. Reducing brake pedal force allows the operator to regain steering control. It has been said that locking of the front brakes of a tractor-semitrailer combination first allows the driver to gain critical information about how slippery a road surface is without creating the hazards associated with jackknifing caused by premature tractor rear brakes locking.

Vehicle stability requires that the tractor front axle locks first, followed by the trailer axle, with the tractor rear axle(s) locking last. Demonstration tests

conducted by the National Highway Traffic Safety Administration with five different commercial vehicles and several drivers clearly showed the safety benefits of locking front brakes first in terms of shorter stopping distances and improved stability, even when braking on a slippery roadway while turning. In terms of apply sequence, all brakes ideally should be applied at the same moment to ensure a stretched combination, which is of particular importance when braking empty on slippery road surfaces.

8.4 Braking of 2-S1 Combination

8.4.1 General Brake Design Considerations

The insights gained from studying 2-S1 braking will prove beneficial for the analysis of combinations equipped with tandem axles. The same concepts discussed in Chapter 7 for non-articulated single vehicles apply to the foundation brake design of tractor-trailer combinations. For a two-axle vehicle, the optimum brake line pressures can easily be calculated and the foundation brakes and/or ABS system designed accordingly. For combination vehicles, the equations calculating optimum brake line pressure are algebraically involved, particularly when tandem axle suspensions must be considered. We will use the traction coefficient method where the effects of brake balance on braking effectiveness are evaluated in terms of traction coefficient as a function of brake line pressure. Much insight with respect to optimizing a brake design will be obtained by changing different valve characteristics until all axles achieve maximum tire-road friction utilization. When an ABS brake system is designed, optimum modulation requirements will benefit from knowing the brake line pressures resulting in optimum braking performance.

8.4.2 Optimum Braking Forces

A detailed discussion of optimum braking forces is presented in Section 7.3. In the optimum condition, i.e., $a = \mu$, all road friction available is used, and the braking forces are directly related to the dynamic axle loads. Optimum braking as used here involves straight-line braking on a level road. Use the terminology shown in Fig. 8-2.

The equations for force and moment equilibrium yield as the normalized optimum braking forces on each axle:

Tractor rear axle:

$$F_{x1R, \text{opt}} / W_1 = a(\Psi_1 - a\chi_1) + a(W_2 / W_1)(y - az_1)[(1 - \Psi_2 + a\chi_2) / (1 + az_2)] \quad (8-11)$$

Tractor front axle:

$$\begin{aligned} F_{x1F, \text{opt}} / W_1 &= a(1 - \Psi_1 + a\chi_1) + a(W_2 / W_1)(1 - y + az_1) \\ &[(1 - \Psi_2 + a\chi_2) / (1 + az_2)] \end{aligned} \quad (8-12)$$

Trailer axle:

$$F_{x2R, \text{opt}} / W_2 = a[\Psi_2 + a(z_2 - \chi_2) / (1 + az_2)] \quad (8-13)$$

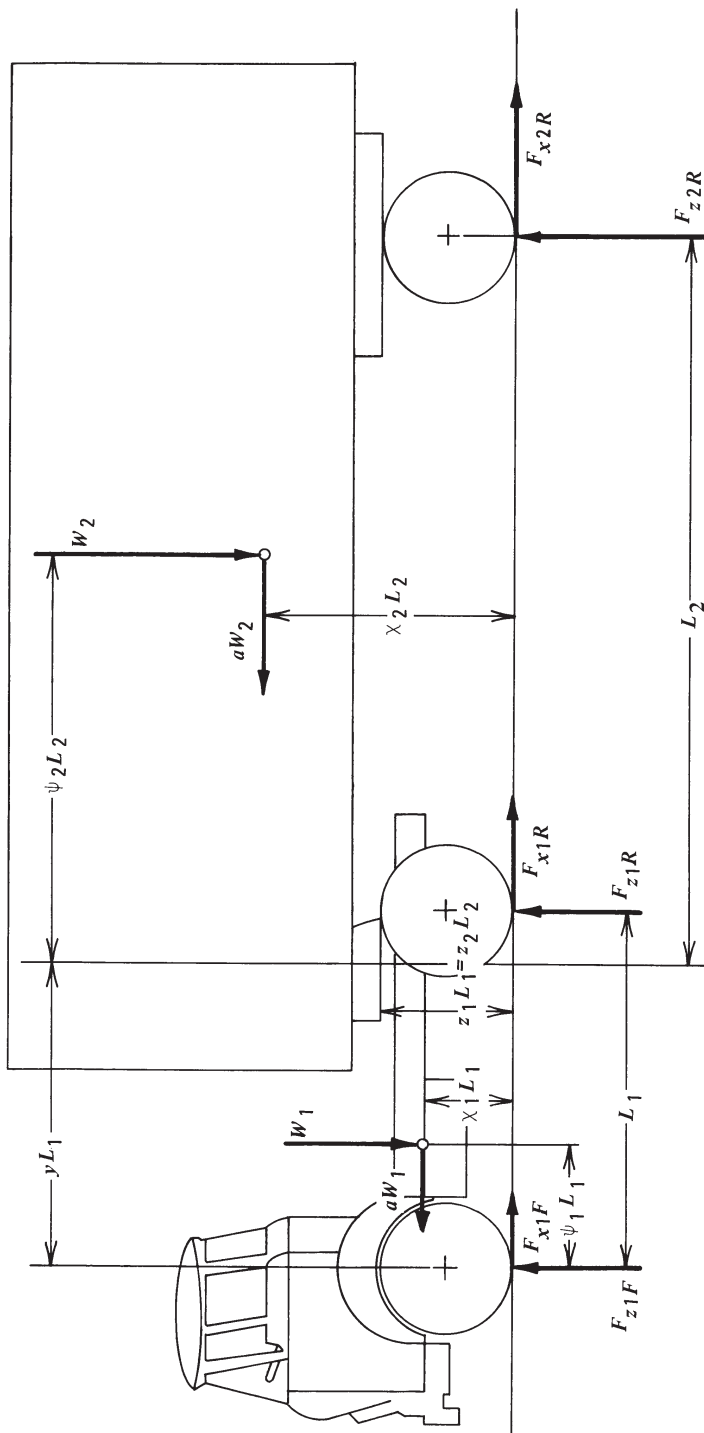


Figure 8-2. Forces acting on a decelerating 2-S1 tractor-trailer combination.

where a = deceleration, g-units

W_1 = tractor weight, N (lb)

W_2 = semitrailer weight N (lb)

y = horizontal distance between front wheels and fifth wheel divided by tractor wheelbase L_1

z_1 = fifth wheel height divided by tractor wheelbase L_1

z_2 = fifth wheel height divided by semitrailer base L_2

χ_1 = tractor center-of-gravity height divided by tractor wheelbase L_1

χ_2 = semitrailer center-of-gravity height divided by semitrailer base L_2

Ψ_1 = empty tractor rear axle load (without semitrailer) divided by tractor weight

Ψ_2 = static semitrailer axle load divided by semitrailer weight

If $W_2 = 0$, i.e., no trailer is attached to the tractor, Eqs. (8-11) and (8-12) reduce to the equations applicable to a straight truck.

The optimum (dynamic) braking forces normalized by dividing by the total combination weight ($W_1 + W_2$) are shown in Fig. 8-3. The nature of the curves shows that it will be difficult to design a fixed-brake-force distribution braking system that will produce actual braking forces on each axle that approach the optimum braking forces for the laden and empty vehicle on both slippery and dry road surfaces (low and high deceleration). Because it will be impossible to lock up all three axles simultaneously for all loading and road friction conditions or decelerations, the brake design engineer must decide how to achieve directional stability for all foreseeable operating conditions, including ABS brake system failure.

Eqs. (8-11), (8-12), and (8-13) may be rewritten to yield the optimum tractor braking forces as a function of the trailer loading condition and trailer brake force:

$$F_{x1R, \text{opt}} = aW_1 (1 - \Psi_1 + a\chi_1) + (aW_2 + F_{x2R})(y - az_1) , \text{ N (lb)} \quad (8-14)$$

$$F_{x1R, \text{opt}} = a W_1 (\Psi_1 - a\chi_1) + (aW_2 + F_{x2R})(y - az_1) , \text{ N (lb)} \quad (8-15)$$

where F_{x2R} = actual brake force of semitrailer, N (lb)

The last term in Eqs. (8-14) and (8-15) represents the influence of the trailer on the tractor. A graphical representation of Eqs. (8-14) and (8-15) is shown in Fig. 8-4 for a typical vehicle and several loading conditions. Inspection of the three curved lines for the empty, half laden, and laden operating conditions reveals that a fixed brake force distribution on the tractor will not result in optimum braking for most loading conditions and braking forces or decelerations.

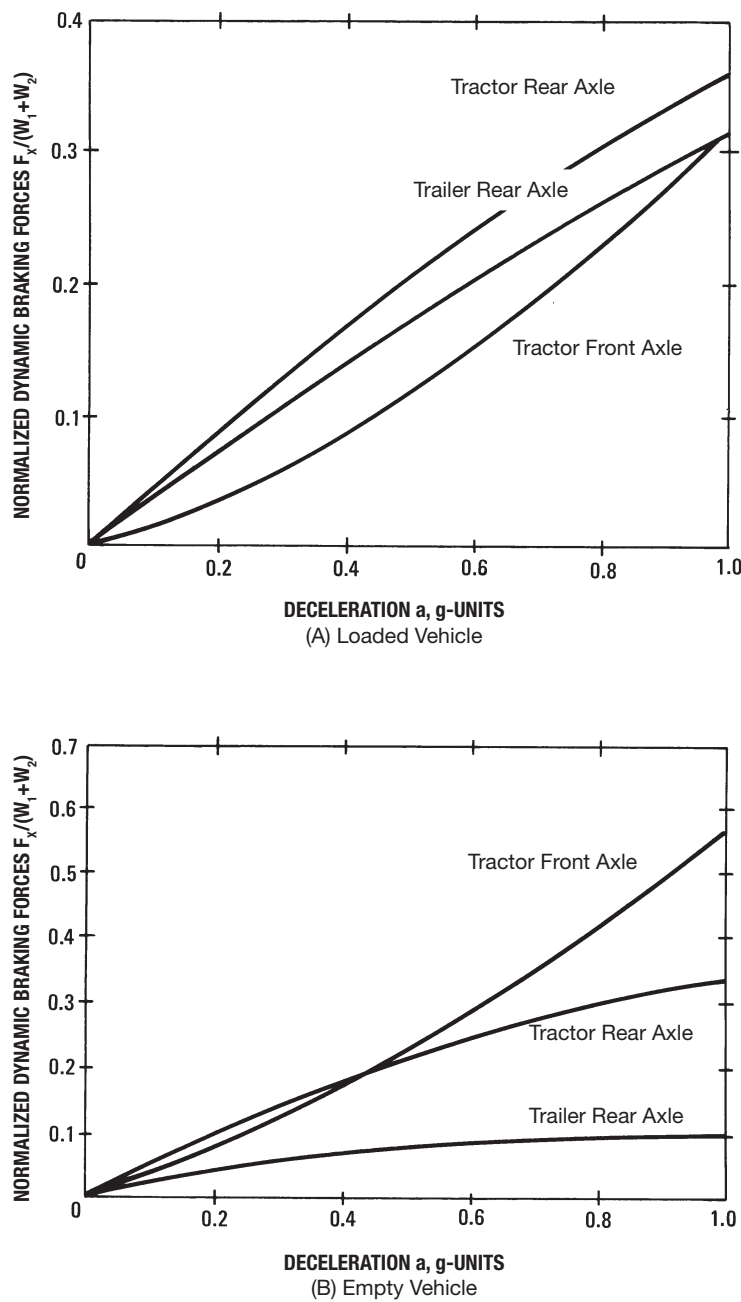


Figure 8-3. Normalized optimum (dynamic) braking forces for 2S-1 combination

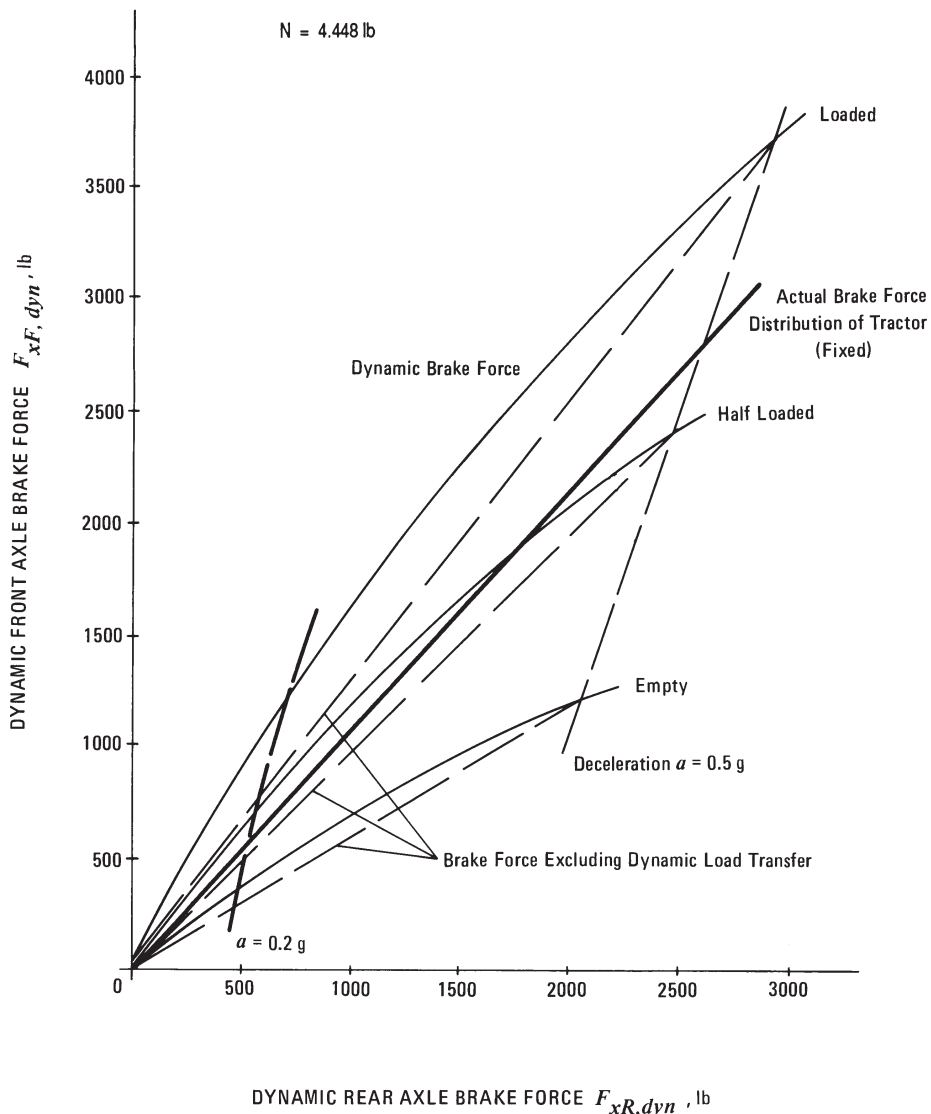


Figure 8-4. Optimum (dynamic) braking forces of the tractor of a 2-S1 combination.

The actual brake forces generated at each axle are determined by the brake line pressures supplied to the brakes, brake chamber size, mechanical gain (slack adjuster length, wedge angle), brake factor, and tire radius. For air brakes, the brake forces may be computed from Eq. (6-1), however, divided by tire radius, and for hydraulic brakes from Eq. (5-2).

A fixed brake force distribution on the tractor is presented in Fig. 8-4 as a straight line. The location or closeness of this straight line relative to the optimum braking forces determines the utilization of the given road friction by the brake system and, hence, the overall braking performance of the system combination.

8.4.3 Limiting and Proportioning Valves

For a straight truck or a car, the axle loads, either static or dynamic, are always equal to the weight of the vehicle. For a tractor-semitrailer, the axle loads of the tractor are not equal to the weight of the tractor, because part of the static trailer load is carried on the fifth wheel in addition to dynamic load transfer occurring from the trailer onto the tractor during braking, as well as the horizontal hitch forces.

The front brake line pressure-limiting valve used for straight trucks (Chapter 7) was used for combination vehicles. The brake line pressure characteristic is illustrated in Fig. 8-5.

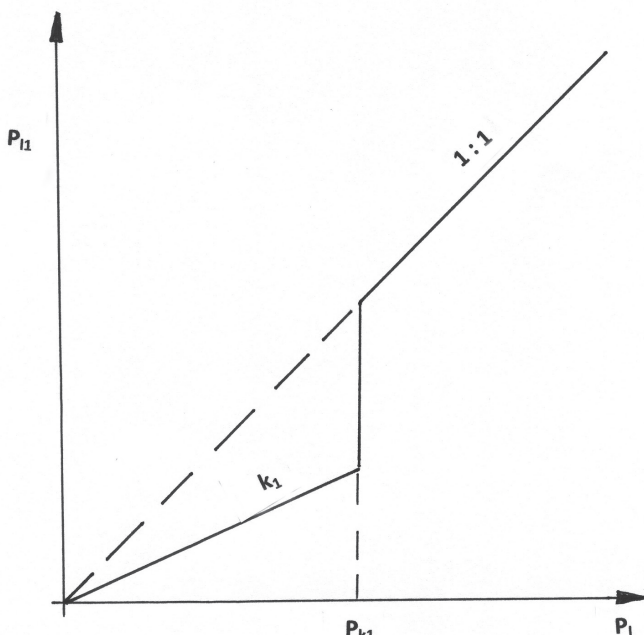


Figure 8-5. Front axle limiting pressure valve characteristics.

Up to the limit pressure P_{k1} , the front pressure is reduced by the reduction factor k_1 . For greater pressures, the front pressure equals the brake line pressure demanded by the driver's pedal effort. For any other axles, the brake line pressure follows proportioning valve characteristics illustrated in Fig. 8-6. For pressures less than the knee-point pressure, the brake line pressure to the wheel brake equals the pressure demanded by the driver's pedal effort. For greater pressures, the pressure increase is reduced by the slope factor k_2 (Refs. 7.1, 7.2).

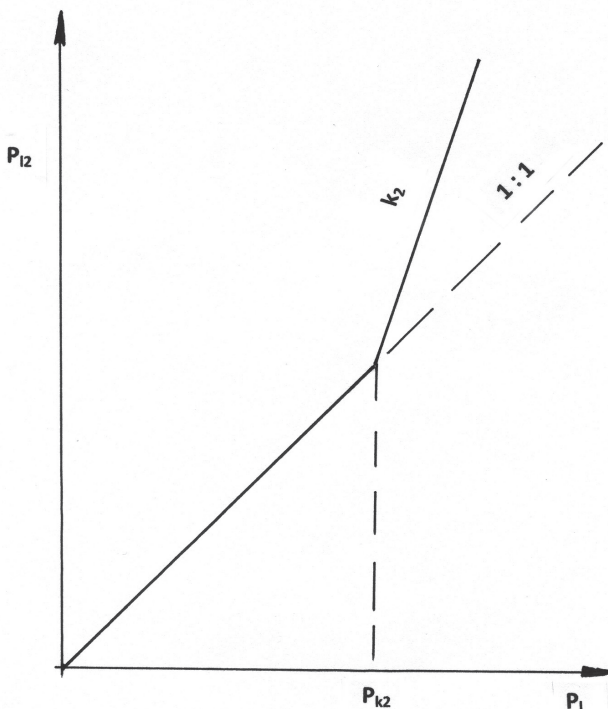


Figure 8-6. Rear axle(s) proportioning pressure valve characteristics.

8.4.4 Effects of Brake Balance on Tire-Road Friction Utilization

This analysis is presented to show the effects of optimizing the underlying standard foundation brake system by use of simple brake line pressure reducing valves. With current design practice, and in the event of an ABS failure, the typical tractor-semitrailer combination will jackknife when operating in the empty condition on slippery, wet roads. The potential for jackknifing will lessen significantly because FMVSS 121 requires high-torque brakes to be installed on the front axle. The new requirements of FMVSS 121 will yield the following performance changes.

For a speed of 96.5 km/h (60 mph), the stopping distance is reduced from 108.3 to 76.2 m (355 to 250 ft). For typical air pressure response and brake torque buildup times, the maximum sustained decelerations must increase from 0.41 to 0.61 g. This requirement most likely will lead to the installation of larger drum brakes with higher brake factors including wedge brakes or air-over-hydraulic disc brakes on the front axle.

The only warning a driver currently has against a non-functioning ABS system is a small warning light which is located among many others on the instrument panel and is required by FMVSS 121. An audible warning similar to the low air pressure buzzer will be more effective in alerting the driver about the hazardous operating conditions when the ABS system is unknowingly disabled (defective warning light bulb).

The normalized optimum braking forces of a typical tractor-semitrailer vehicle for the empty and loaded operating conditions are shown in Fig. 8-3. Optimum braking is defined by $a = \mu$ for all axles (Section 7.3.3). These curves show that the optimum braking forces are heavily influenced by the loading condition of the trailer. If the foundation brake system is designed to be near optimum for the laden vehicle, it will perform poorly for the empty case unless a proportioning brake system or ABS is provided that will vary the brake force distribution according to the loading conditions of the vehicle combination. An additional difficulty arises from the fact that a particular tractor may be used with different trailers, each having a variety of loading configurations and brake force levels.

For the optimum braking forces of the typical combination vehicle shown in Fig. 8-3, the actual brake forces for the empty and laden cases which would best approximate the optimum braking forces are illustrated by the straight broken lines in Fig. 8-7. The optimum curves indicate that for a deceleration of 0.8 g the actual brake forces, front to rear, are approximately equal to 0.22 W, 0.30 W, and 0.24 W for the laden vehicle; and 0.40 W, 0.30 W, and 0.10 W for the empty vehicle. With a laden and empty combination weight of $W = 195,712$ N (44,000 lb) and $W = 88,960$ N (20,000 lb), respectively, the brake forces for optimum braking at $a = 0.8$ g must be proportioned between 35,584 and 43,146 N (8000 and 9700 lb) on the tractor front axle; 26,688 and 58,714 N (6000 and 13,200 lb) on the tractor rear axle; and 8896 and 46,704 N (2000 and 10,500 lb) on the trailer axle to best adjust to the empty and laden conditions. The numbers indicate that, whereas the optimum brake force on the front axle varies little with change in vehicle loading, the optimum brake forces on the rear axle of the tractor and on the trailer axle are heavily influenced by the loading condition.

In our study, the front brake force of the tractor is designed to be proportional to the application valve exit pressure. The brake force at the rear axle of the tractor is determined by the load or suspension height-sensitive pressure reducing valve. Depending on the design of the pressure-reducing valve of the tractor, the brake torque on the tractor rear axle may vary, e.g., from 60 to 140% of the tractor front axle brake torque. The brake torque on the trailer axle is determined by either a pressure-reducing or -limiting valve. Depending on the design of the trailer proportioning valve characteristics, the brake torque on the trailer may vary from 20 to 100% (or more) of the front brake torque. A clear understanding of the brake line pressures yielding optimum braking will assist the brake engineer in designing an effective ABS brake system.

Road tests have shown that a proper brake force distribution among axles of a tractor-semitrailer combination has been achieved when no wheels lock below decelerations of 0.5 g with the laden combination braking on dry road surfaces. This brake force distribution generally yields acceptable braking performance with the empty combination. However, if some axle(s) lock below 0.5 g, the advantages of load-dependent brake force distribution are not fully utilized.

As a minimum, manufacturers should perform a brake design analysis to determine to what extent a bobtail valve activated following an ABS failure will prevent jackknifing of tractor-semitrailers.

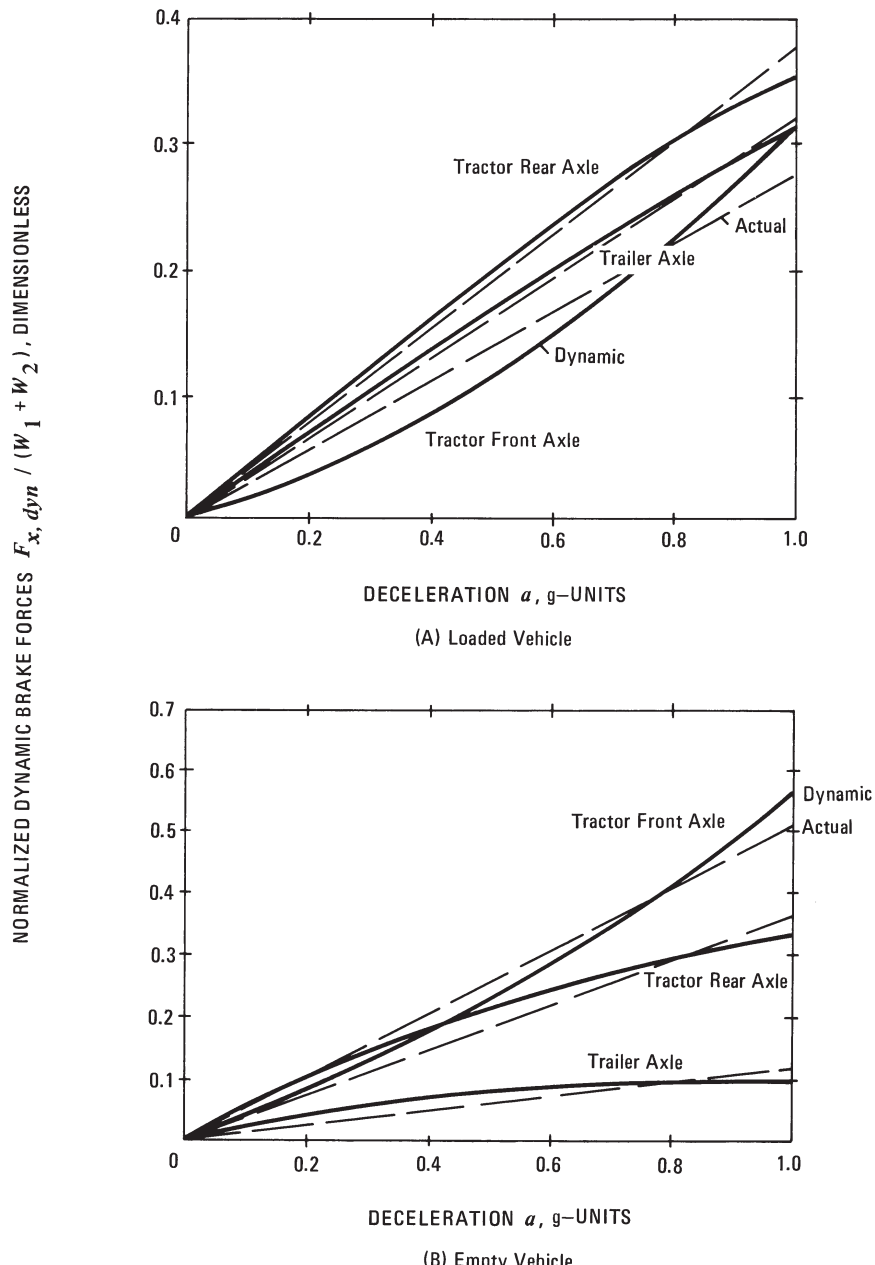


Figure 8-7. Normalized optimum (dynamic) braking forces for 2-S1 combination.

The results of the friction utilization calculations carried out for several loading and proportioning valve settings are presented for a 2-S1 tractor-semitrailer combination. The vehicle combination having the basic friction utilizations shown in Figs. 8-8 and 8-9 was analyzed relative to the effects of different brake line pressure-reducing valve characteristics.

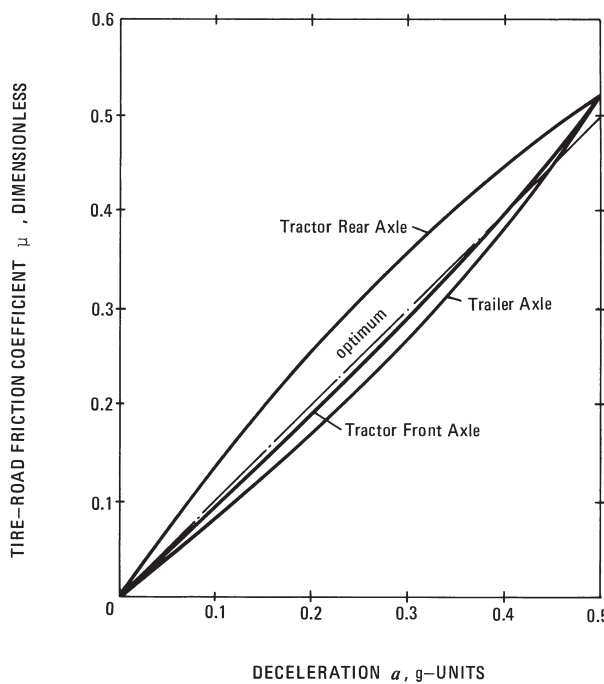


Figure 8-8. Tire-road friction utilization for loaded 2-S1 combination.

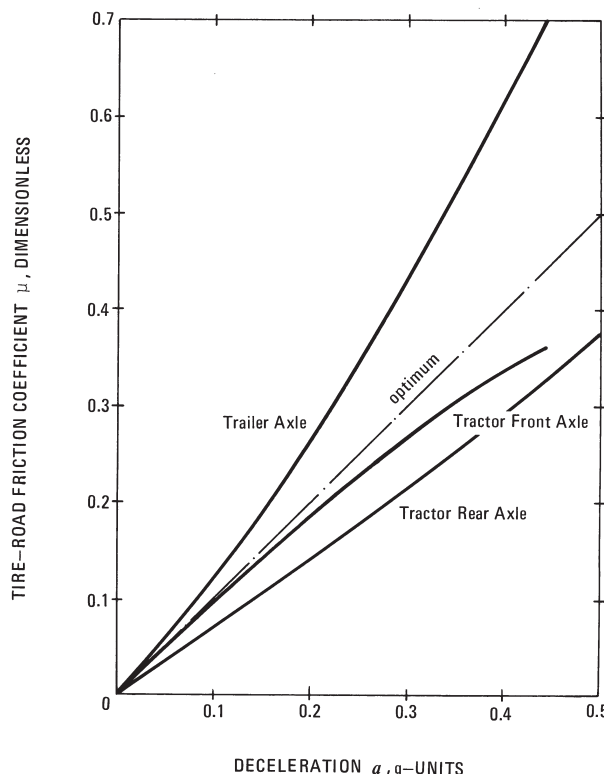


Figure 8-9. Tire-road friction utilization for empty 2-S1 combination.

1. Case 1. The vehicle combination was loaded to GVW, and the proportioning valve setting on the tractor axle and the limiting valve setting on the trailer axle are as shown in Fig. 8-10. The tire-road friction utilization diagram shown in Fig. 8-11 illustrates a near-optimum braking of the vehicle. For all deceleration levels up to approximately 0.5 g, the tractor front axle will lock first, while the tractor rear and trailer axle are close to optimum braking conditions and slightly underbraked.

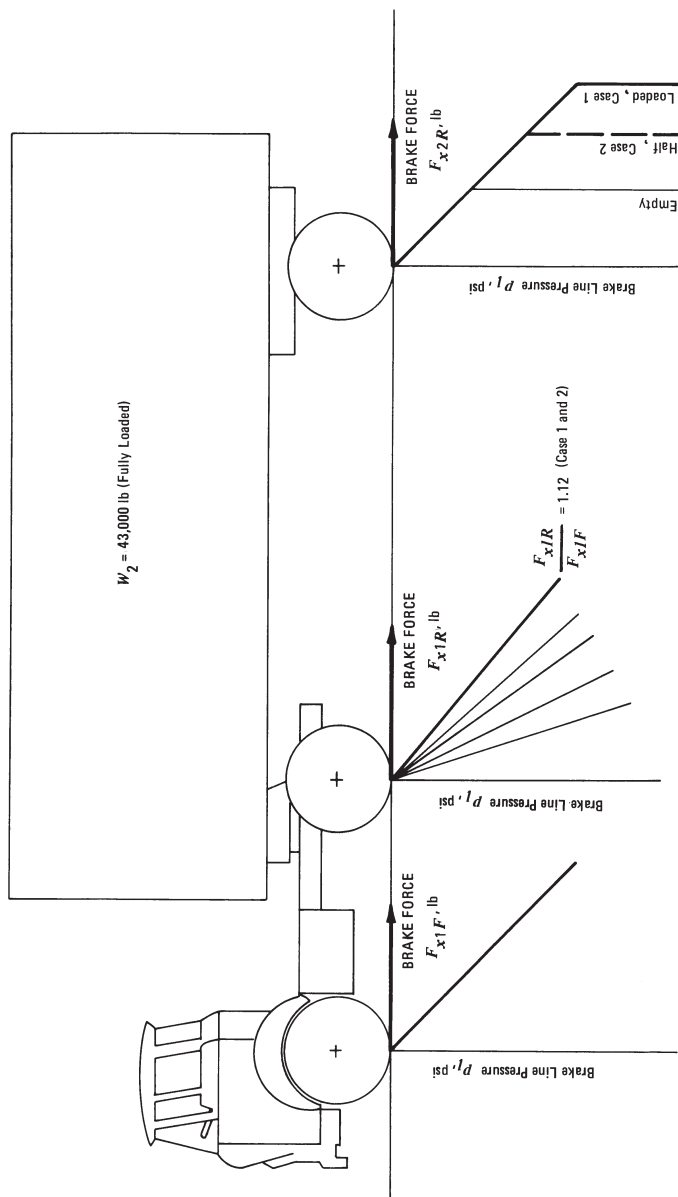


Figure 8-10. Schematic brake force distribution, Cases 1 and 2.

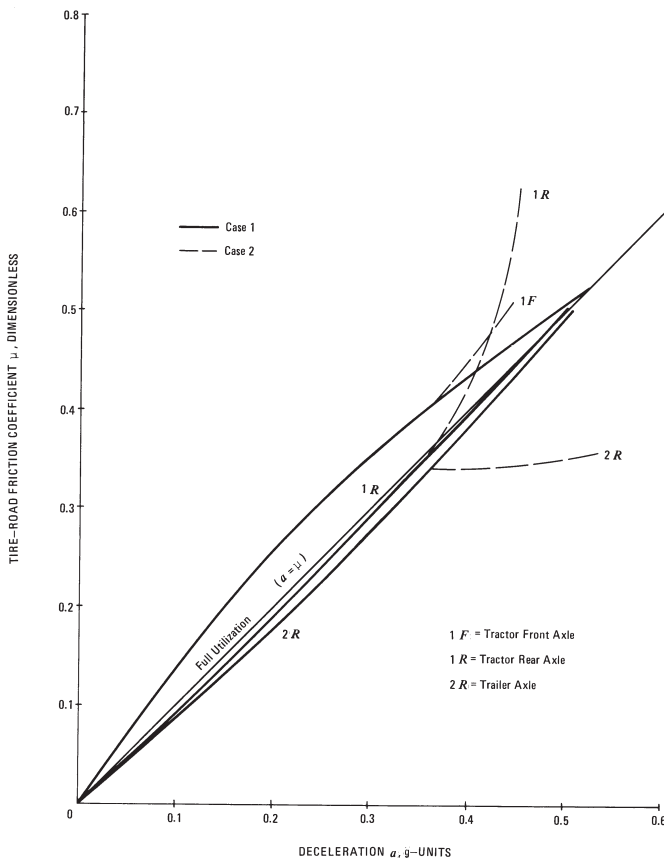


Figure 8-11. Tire-road friction utilization, Cases 1 and 2, $W_2 = 191,350 \text{ N}$ (43,000 lb).

2. Case 2. The conditions are identical to Case 1, except the trailer setting is incorrect, as indicated in Fig. 8-10 by the broken lines. Although the trailer is fully loaded, the trailer brake force is set at the lower value corresponding to the half-laden case. As an inspection of Fig. 8-11 reveals, the same tire-road friction utilization exists as in Case 1, up to a deceleration of about 0.36 g. For decelerations greater than approximately 0.42 g, the danger of locking the tractor rear axle first exists, resulting in a possible instability of the combination, most likely seen in the form of jackknifing of the tractor.
3. Case 3. The trailer is loaded to half of GVW, with the proportioning valve setting as indicated in Fig. 8-12. The trailer valve setting is for the half-laden case also. The danger of first locking the tractor rear axle exists for decelerations greater than 0.49 g, below which the front axle locks up first, as illustrated in Fig. 8-13. The trailer brakes tend to lock up for decelerations greater than about 0.32 g.

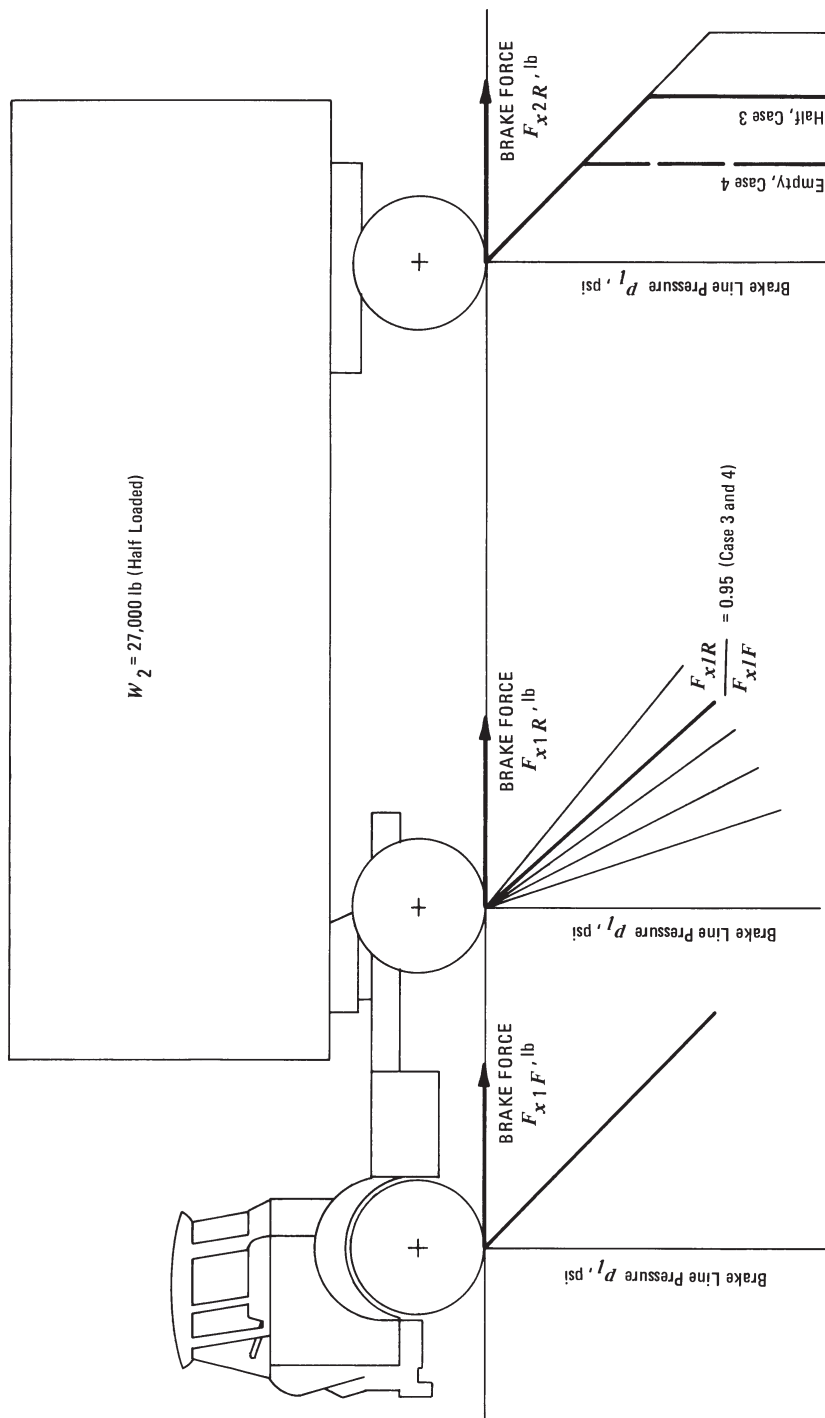


Figure 8-12. Schematic brake force distribution, Cases 3 and 4.

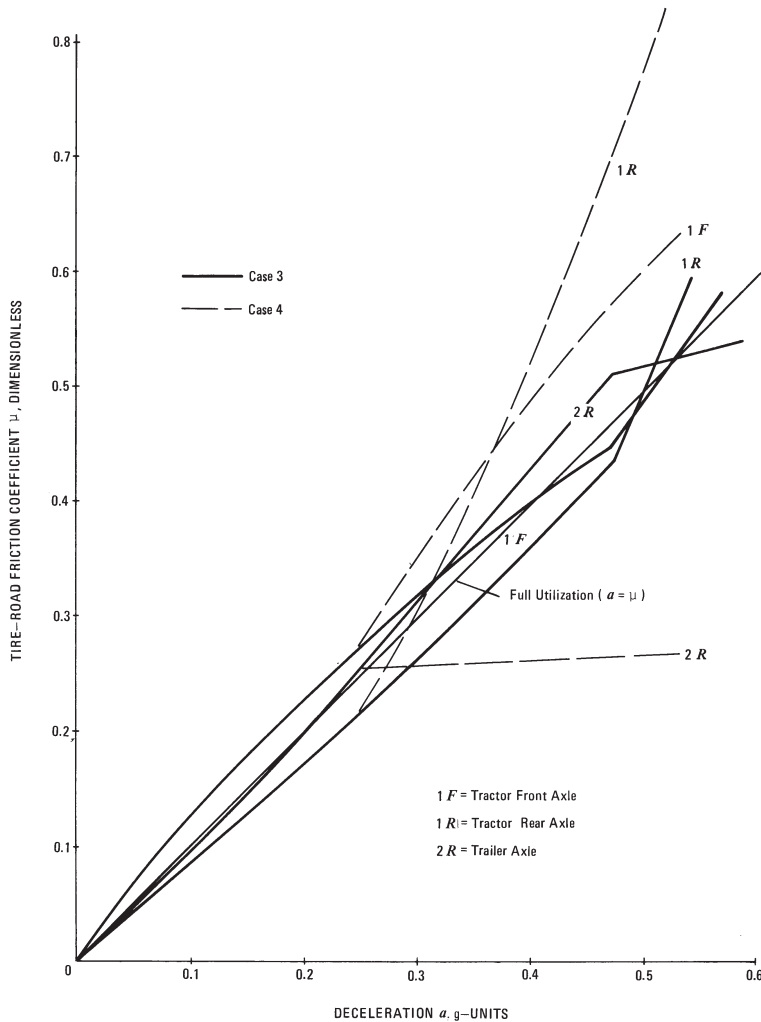


Figure 8-13. Tire-road friction utilization, Cases, 3 and 4, $W_2 = 120,150 \text{ N}$ (27,000 lb).

4. Case 4. The loading conditions are identical to Case 3, except the trailer valve is mistakenly set to the empty condition, as illustrated in Fig. 8-12. As noted from the friction utilization diagram shown in Fig. 8-13, now the tractor rear axle tends to overbrake at decelerations of 0.36 g and greater, requiring relatively high coefficients of friction between tire and road.
5. Case 5. For the empty vehicle combination, the valve settings are indicated in Fig. 8-14. The tire-road friction utilization is illustrated in Fig. 8-15. The trailer axle tends to overbrake compared to the two other axles for decelerations below 0.53 g. For decelerations above 0.53 g, the tractor rear axle begins to lock up.

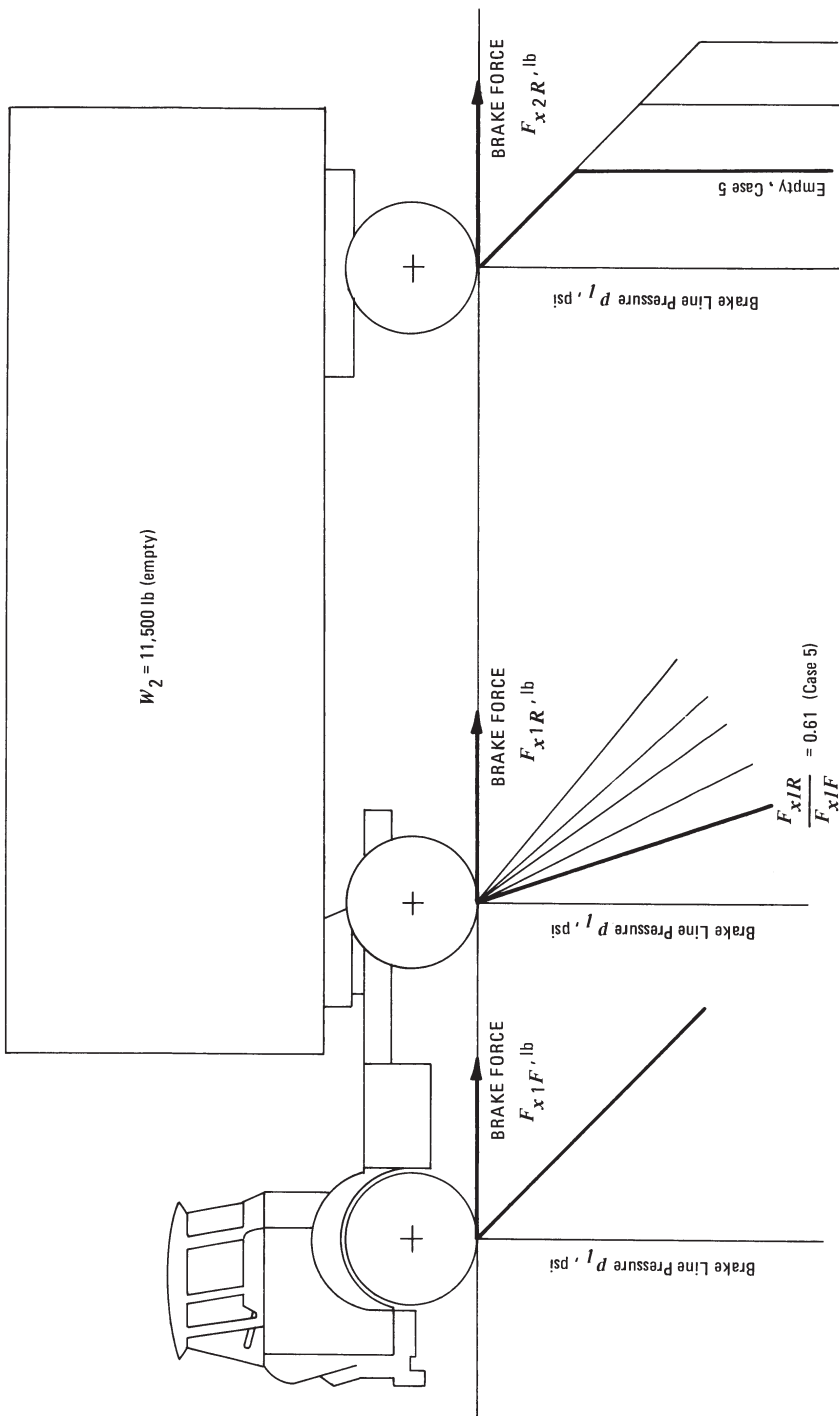


Figure 8-14. Schematic brake force distribution, Case 5.

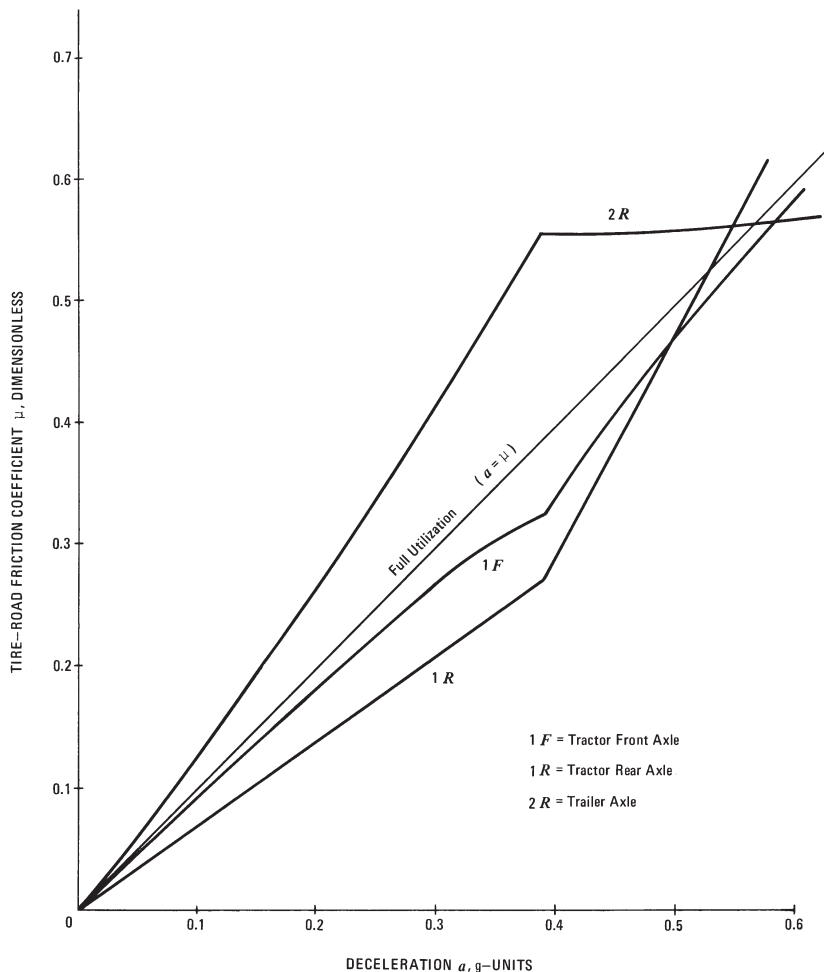


Figure 8-15. Tire-road friction utilization, Case 5, $W_2 = 45,175 \text{ N (11,500 lb)}$.

6. **Case 6.** The empty vehicle combination is braked with the valve settings as indicated in Fig. 8-16. The tractor rear axle brake force is set for the laden condition. Because domestic tractors in current use generally do not have brake line pressure-reducing valves for the rear axle, Case 6 represents operation of a tractor with ABS failure pulling an empty trailer that may be found on public highways. The trailer brake force is set for the empty condition. Examination of the friction utilization diagram shown in Fig. 8-17 reveals that a deceleration of approximately 0.4 g tends to be critical with respect to jackknifing because the tractor rear axle is always locking up first. This case illustrates the importance of automatic load-dependent and driver-independent brake torque variation (ABS or ABS failure-sensitive bobtail valve) of the tractor rear axle.

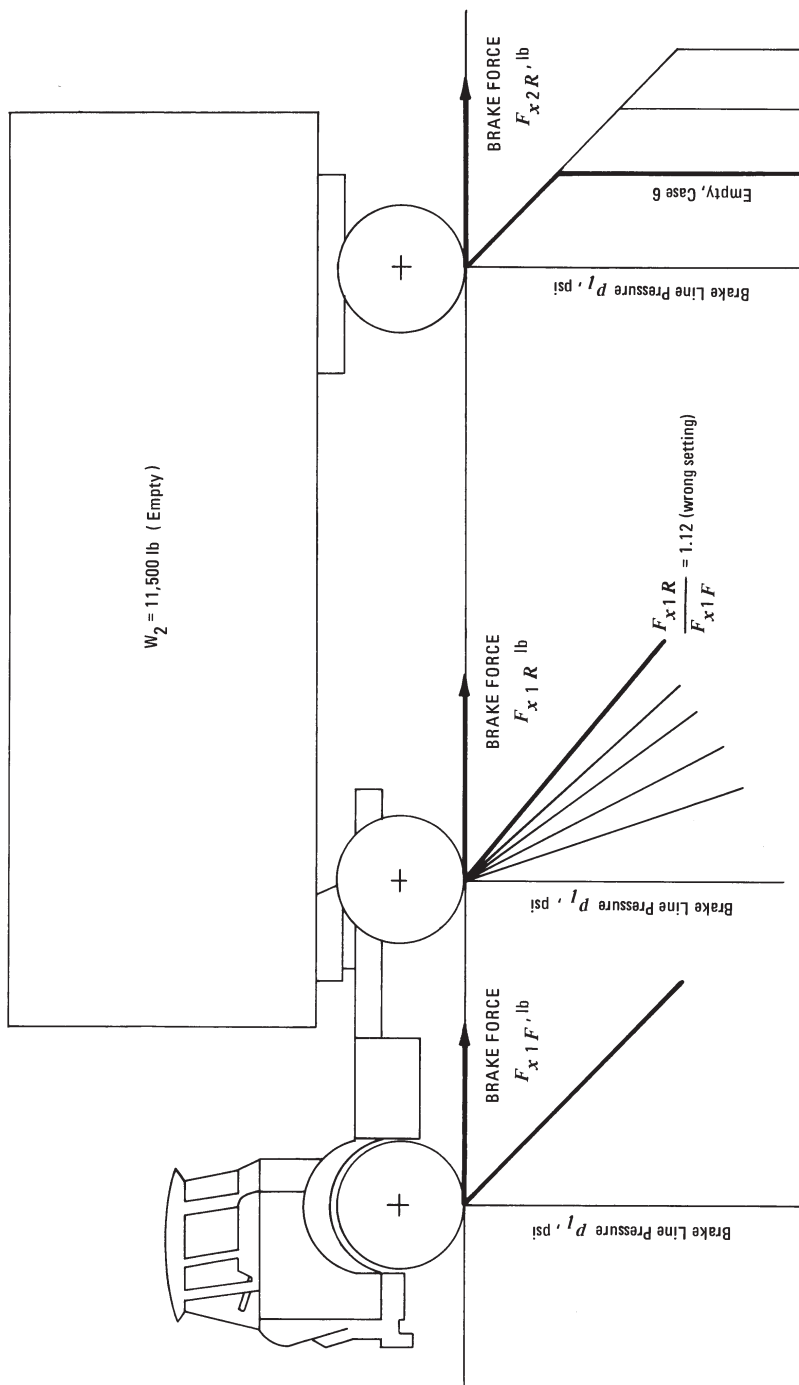


Figure 8-16. Schematic brake force distribution, Case 6.

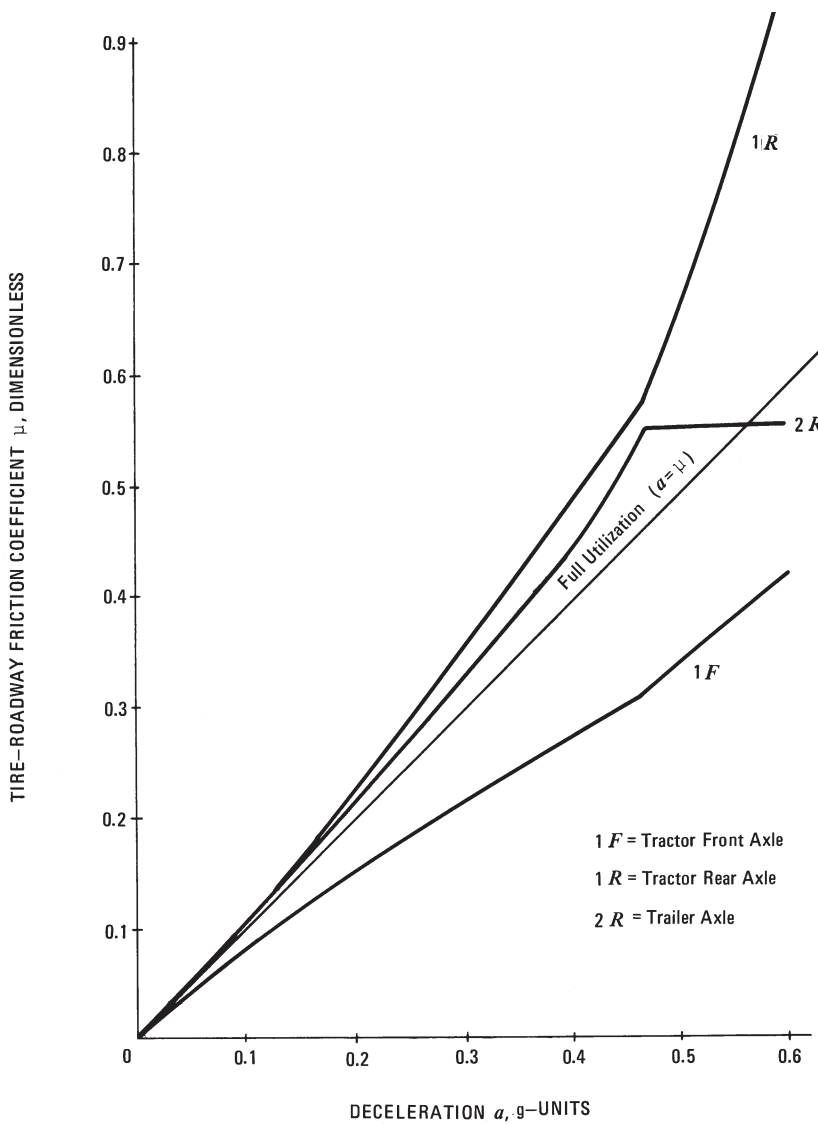


Figure 8-17. Tire-road friction utilization, Case 6, $W_2 = 51,175 \text{ N (11,500 lb)}$.

7. Case 7. The empty combination vehicle is equipped with the tractor brake pressure proportioning valve automatically set to the empty position as indicated in Fig. 8-18. The trailer brake force is no longer limited, as in the previous cases. The trailer brake force is not controlled by a valve. The results of the friction utilization calculations shown in Fig. 8-19 demonstrate an almost optimum braking, indicated by the fact that all three curves are close to the optimum or full utilization line and that the front brakes lock up first for decelerations below 0.5 g.

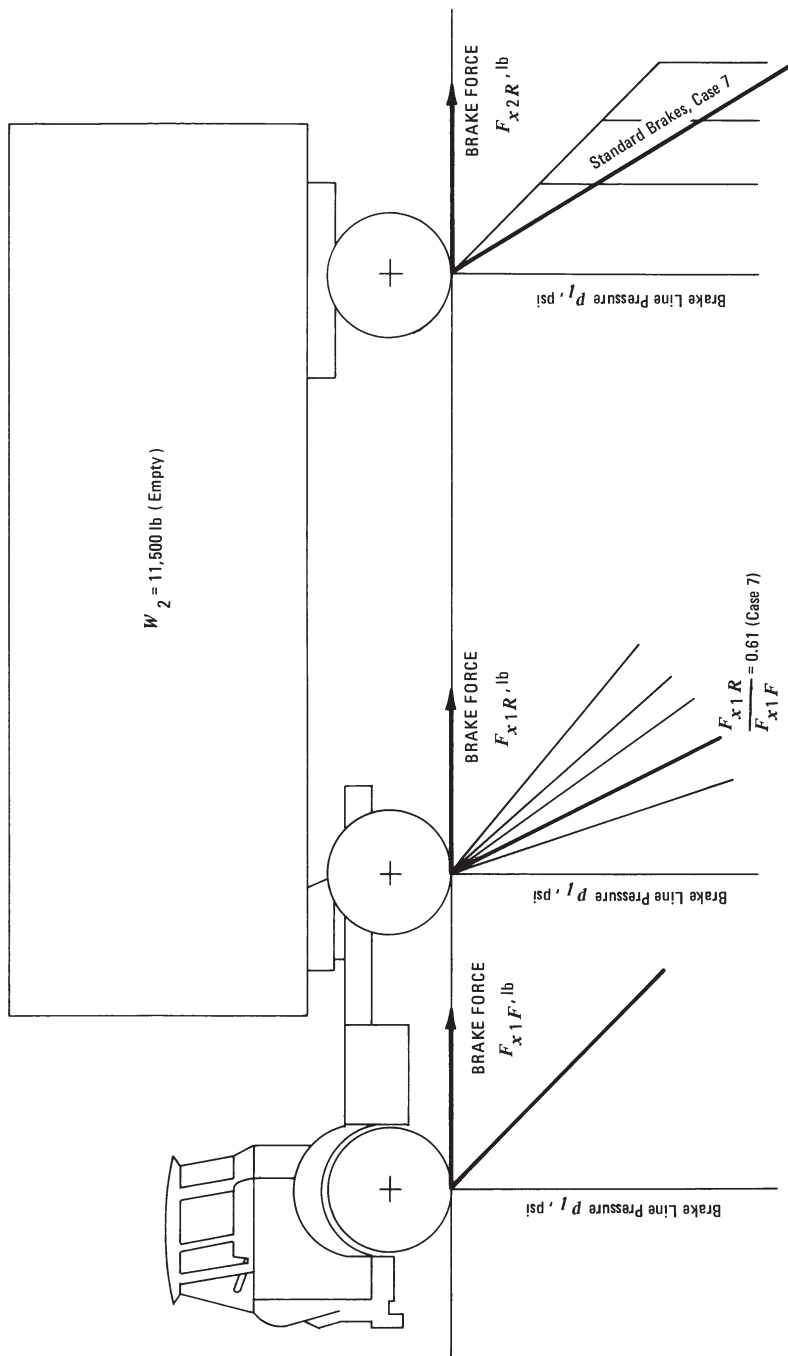


Figure 8-18. Schematic brake force distribution with proportioning valves on tractor rear and standard brakes on trailer axle, Case 7.

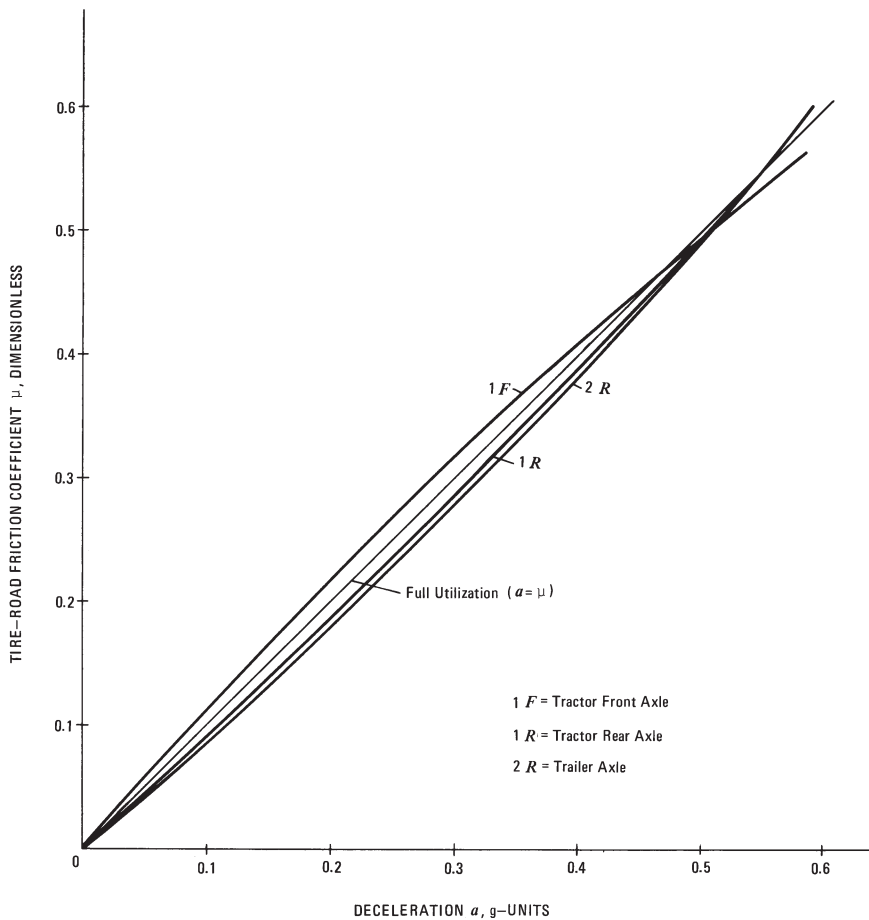


Figure 8-19. Tire-road friction utilization, Case 7, $W_2 = 51,175 \text{ N (11,500 lb)}$.

8. Case 8. The laden vehicle is braked with the tractor rear axle valve set at the laden condition. The trailer axle is not controlled and produces the brake force illustrated in Fig. 8-20, i.e., the same brake force as in the previous case. As illustrated in Fig. 8-21, the front axle tends to overbrake for decelerations below 0.43 g. Although locking of the front axle will not allow any steering wheel corrections by the driver, the combination remains stable, traveling straight ahead. Above decelerations of 0.43 g, there is a danger of overbraking of the tractor rear axle.

In the past, many tractors were equipped with a front-axle brake-line-pressure automatic limiting valve. Improvements in braking performance can be achieved by modulating the brake force of the tractor front axle if the static laden-to-empty axle ratio of the tractor front axle is greater than approximately 1.4. If the laden-to-empty ratio is less than 1.4, then only the tractor rear and trailer axle must be modulated.

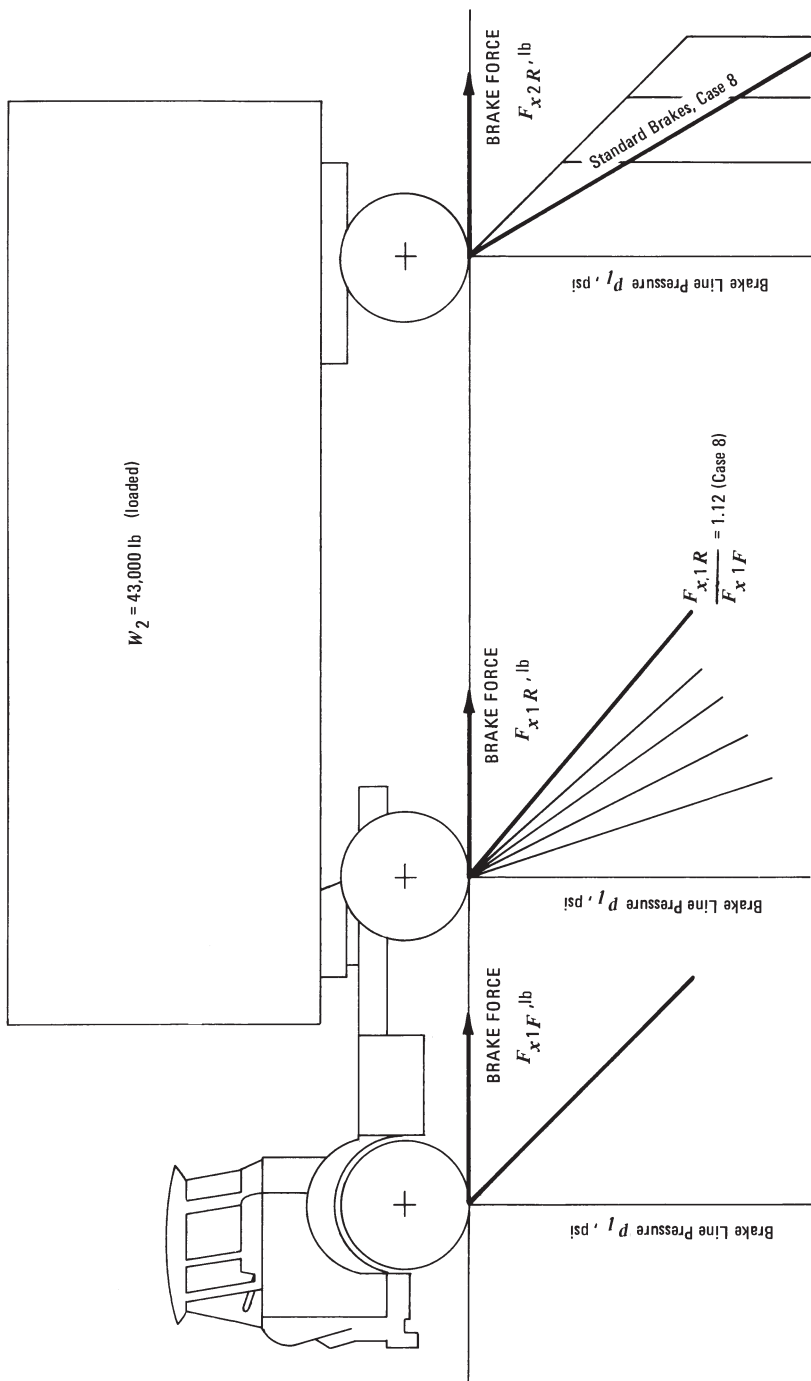


Figure 8-20. Schematic brake force distribution, Case 8.

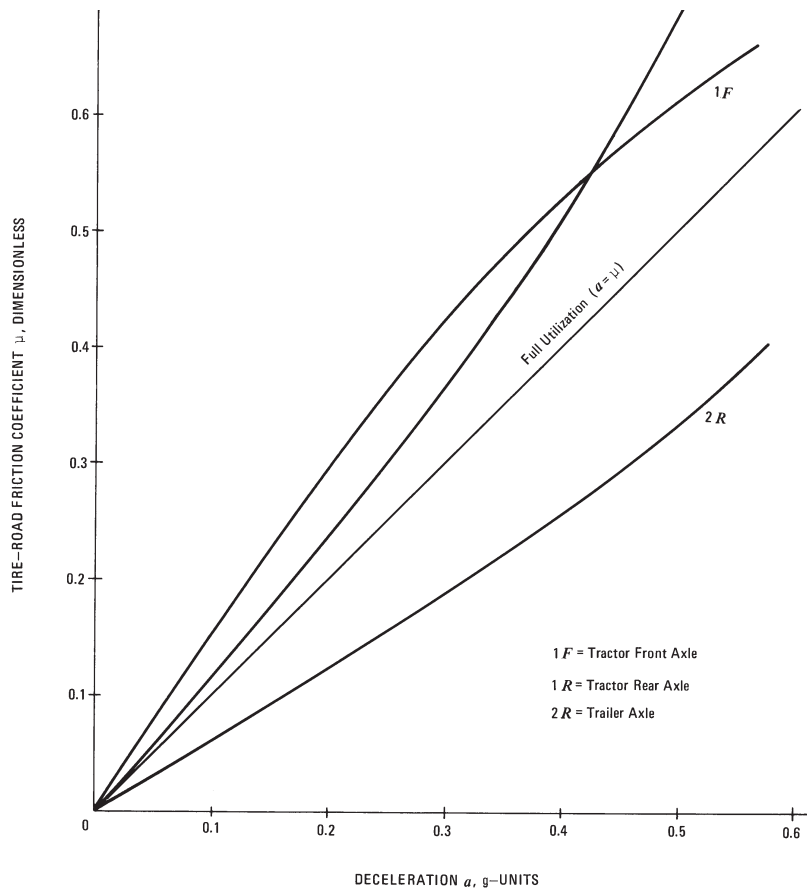


Figure 8-21. Tire-road friction utilization, Case 8, $W_2 = 51,175$ N (11,500 lb).

8.5 2-S1 Tractor-Trailer Combination – PC-BRAKE AIR Software

In the equations that follow, the subscripts of axle loads and braking forces as well as all associated parameters, such as traction coefficient, are numbered consecutively from front to rear axle.

For brake design purposes, the axle braking forces left and right are assumed to be identical. In accident reconstructions where brake failures are involved, this is often not the case, and consequently, each individual brake force (left and right brake on each axle) and traction coefficient are calculated for each axle. This formulation allows the brake engineer and accident reconstructionist to analyze different braking/skid marks at the accident scene and relate them to the mechanical condition of the brakes.

This axle front-to-rear nomenclature is used throughout PC-BRAKE AIR software. See Section 7.10.2 for PC-BRAKE AIR software applications of single vehicles.

In a 2-S1 tractor-semitrailer combination, neither the tractor nor the trailer is equipped with tandem axles. For a given tractor-semitrailer geometry, all longitudinal dimensions are specified or measured at the subject vehicle. Consequently, the following data are either measured or known: Tractor weight W_1 , trailer weight W_2 , horizontal fifth wheel location ($L_1 - l_{15}$), trailer wheelbase (L_2), tractor wheelbase (L_1), tractor (without trailer attached) longitudinal center-of-gravity location (l_1) (generally known or can be obtained from measured static axle loads of axle #1 and axle #2).

Assume the static trailer axle load $F_{z3\text{meas}}$ of the third axle of the subject tractor-semitrailer was measured. This measurement, with all other dimensions known, automatically determines the static axle loads $F_{z1\text{st}}$ and $F_{z2\text{st}}$ of the tractor.

8.5.1 Dynamic Axle Loads

The 2-S1 tractor-trailer schematic is illustrated in Fig. 8-22. Both tractor axle weights are included in the tractor weight. The trailer axle weight is included in the trailer weight. The axle normal forces of the tractor and semi-trailer are

$$F_{z1} = W_1 + Y - F_{z2}, \text{ lb} \quad (8-16)$$

$$F_{z2} = (W_1 l_1 - aW_1 h_1 - Xh_5 + Yl_5)/L_1, \text{ lb} \quad (8-17)$$

$$F_{z3} = W_2 - Y, \text{ lb} \quad (8-18)$$

The kingpin/fifth wheel forces are

$$X = F_{x1} + F_{x2} - aW_1, \text{ lb} \quad (8-19)$$

$$Y = [aW_2 h_2 + W_2 (L_2 - l_2) - Xh_5]/L_2, \text{ lb} \quad (8-20)$$

where a = deceleration, g-units $[\Sigma F_i/(W_1 + W_2)]$

F_{xi} = braking force of i th axle, lb

h_{1cg} = vertical distance ground to tractor center-of-gravity, ft

h_{2cg} = vertical distance ground to trailer center-of-gravity, ft

h_5 = vertical distance ground to fifth wheel, ft

L_1 = tractor wheelbase, ft

L_2 = trailer wheelbase, ft

l_1 = front axle to tractor cg, in.

l_5 = fifth wheel to trailer cg, in.

l_{15} = front axle to fifth wheel, in.

W_1 = tractor weight, lb

W_2 = trailer weight, lb

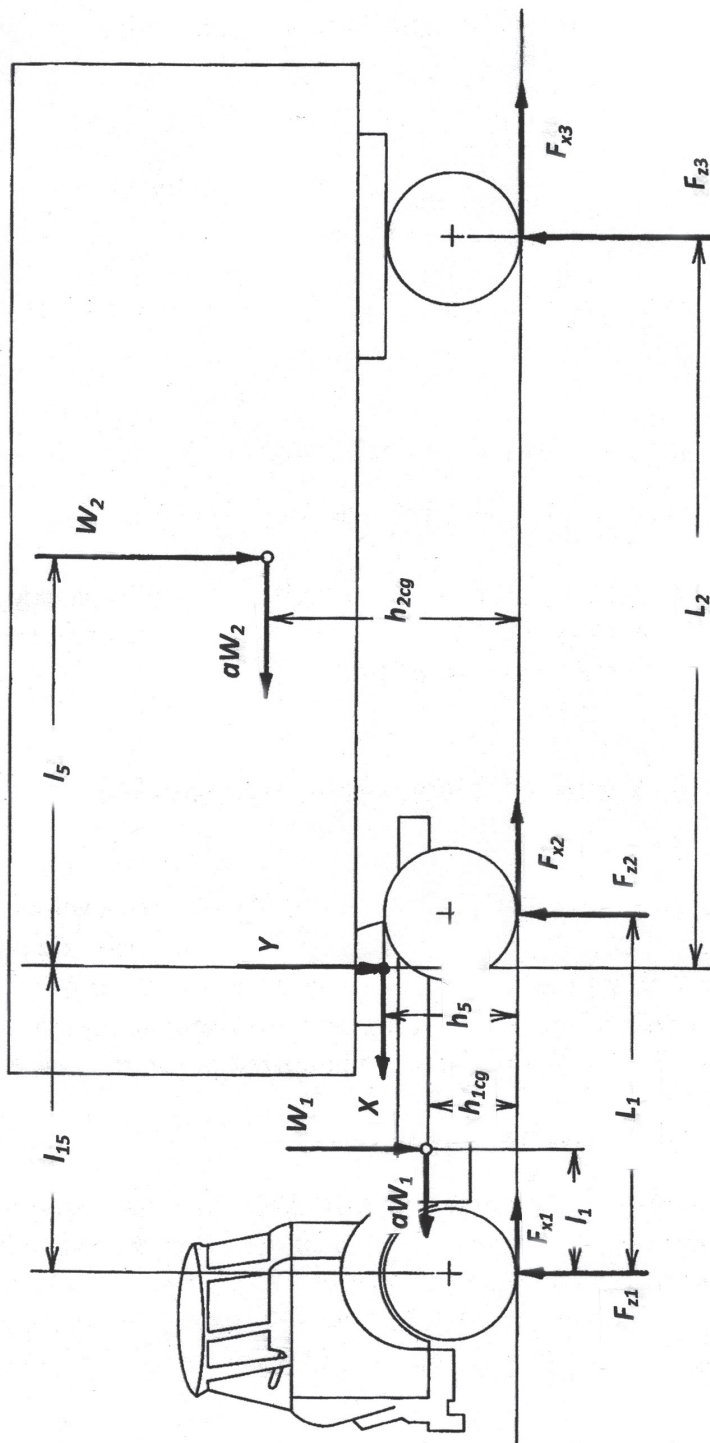


Figure 8-22. Forces acting on a 2-S1 combination.

8.5.2 2-S1 PC-BRAKE AIR Software Application

Example 8-1: Design/analyze the braking performance, brake lockup sequence of a 2-S1 combination. The brake system of an empty 2-S1 combination was optimized by using different brake factors on the trailer brakes, slack adjuster lengths on the front brakes, and brake chamber sizes, as shown in Table 8-1A, Design Data. The input and output data are shown in Tables 8-1A and 8-1B.

Solution approach:

1. In Design Data of PC-BRAKE AIR 2-S1 software with the tire-road friction coefficient high (e.g., $f = 3$), input horizontal center-of-gravity distances of trailer, and others not directly measured until static axle loads for field check are approximately equal to measured axle loads. Using the f -value artificially large eliminates brake lockup and shows the proper tire-road friction utilization diagram. Once this is done, all horizontal weight location data are correct. The starting brake line pressure must equal the push out pressure (normally 5 psi) to have zero braking forces, that is, no dynamic load transfer, as shown in Tables 8-1A and 8-1B.
2. In Design Data input, set starting brake line pressure at 45 psi for braking of empty vehicle, as shown in Tables 8-2A and 8-2B. Note: Use 115 psi for a fully laden tractor-trailer combination. Observe "Temperature, Brake" calculations and set one-half of observed brake temperature as input data in "Braking Temperature" input. PC-BRAKE AIR computes the maximum swept brake surface temperature in a single stop without any ambient cooling. The fade factor adjusts braking force accordingly.
3. In Design Data input, set Tire Road Friction Coefficient to actual value, for example, 0.7, and the starting brake line pressure at 5 psi (push out pressure). The brake line pressure interval chosen is usually 10 psi. It can be set at smaller values to make calculations for smaller pressure intervals such as 1 psi or 0.1 psi.

In Table 8-3 (Data, Table 3), observe tire-road friction utilization column and brake lockup sequence. For a tire road friction coefficient of 0.7 (Design Data input), the trailer axle locks for brake line pressures greater than 45 psi because calculated traction coefficients U_{T3L} and U_{T3R} are equal to or greater than the specified tire road friction coefficient of 0.7; the tractor rear axle locks for pressures greater than 55 psi; and the front axle locks for pressures greater than 65 psi. More exact values can be obtained by using pressure intervals of 1 psi instead of 10 psi in Design Data input.

The dynamic axle loads are shown in Fig. 8-23.

AIR BRAKE SYSTEM ANALYSIS
TRACTOR-TRAILER
2-S1 (Tractor: 2 axles; Trailer: 1 axle)
Input Data:

Tire-Road friction coefficient	$f = 3$	$L_1 = 140$
Weight of Tractor, lb	$W_1 = 12000$	$L_2 = 300$
Weight of Trailer, lb	$W_2 = 8000$	$h_s = 48$
Axle 1 Weight (meas.), lb	$F_{z1m} = 6000$	
Axle 2 Weight (meas.), lb	$F_{z2m} = 6000$	
Axle 3 Weight (meas.), lb	$F_{z3m} = 8000$	
Starting Brake Line Pressure, psi	$p_r = 5$	Velocity, ft/sec
Pressure Interval, psi	$D_p = 10$	$V = 100$
Road Slope Gradient, fraction (+/-)	$G = 0$	$T_i = 100$

CASE ID:

Example 8-1, 5 psi

<u>AXLE 1</u>	<u>LEFT</u>	<u>AXLE 1</u>	<u>RIGHT</u>	<u>AXLE 2</u>	<u>LEFT</u>	<u>AXLE 2</u>	<u>RIGHT</u>	<u>AXLE 3</u>	<u>LEFT</u>	<u>AXLE 3</u>	<u>RIGHT</u>
$A_{c1} = 1.8$		$A_{c2} = 24$		$A_{c3} = 2.8$		$A_{c4R} = 24$		$A_{c5} = 2.8$		$A_{c6R} = 22$	
$A_{c1L} = 24$		$A_{c2L} = 24$		$A_{c3L} = 24$		$BF_{1L} = 2.6$	$BF_{2L} = 1.3$	$BF_{3L} = 1.3$		$BF_{4R} = 1.3$	
Brake Factor						$p_{o1R} = 5$	$p_{o2R} = 5$	$p_{o3L} = 5$		$p_{o4R} = 5$	
Pushout Pressure, psi						$R_{1L} = 21$	$R_{2L} = 21$	$R_{3L} = 21$		$R_{4R} = 21$	
Tire Radius, in						$r_{1L} = 7.5$	$r_{2L} = 8.25$	$r_{3L} = 8.25$		$r_{4R} = 8.25$	
Drum or Effective Disc Radius, in						$\eta_{c1R} = 0.65$	$\eta_{c2R} = 0.65$	$\eta_{c3L} = 0.65$		$\eta_{c4R} = 0.65$	
Mechanical Efficiency						$T_{1L} = 240$	$T_{2L} = 200$	$T_{3L} = 200$		$T_{4R} = 200$	
Braking Temperature, deg						$S_{1L} = 1$	$S_{2L} = 1$	$S_{3L} = 1$		$S_{4R} = 1$	
Measured Stroke, in						$S_{max1R} = 2.25$	$S_{max2L} = 2.25$	$S_{max3L} = 2.25$		$S_{max4R} = 2.25$	
Critical Stroke, in						$S_{c1L} = 1.75$	$S_{c2L} = 1.75$	$S_{c3L} = 1.75$		$S_{c4R} = 1.75$	
<u>Calculated Data</u>											
Effective Pushrod Travel, in	$S_{e1L} = 1.11$	$S_{e2L} = 1.11$	$S_{e3L} = 1.08$	$S_{e4R} = 1.08$							
Adjustment Factor	$f_{a1L} = 1.00$	$f_{a2L} = 1.00$	$f_{a3L} = 1.00$	$f_{a4R} = 1.00$							
Fade Factor	$f_{F1L} = 0.86$	$f_{F2L} = 0.86$	$f_{F3L} = 1.00$	$f_{F4R} = 1.00$							

Table 8-1A. Example 8-1, empty, input and output data at 5 psi.

Mechanical Gain value	$\rho_{BS,orW} = 6.00$	$\rho_{BS,orW} = 6.00$	$\rho_{BS,orW} = 5.00$	$\rho_{BS,orW} = 5.00$	$\rho_{BS,orW} = 5.00$
Braking Force, lb	$F_{x1R} = 0$	$F_{x1R} = 0$	$F_{x2L} = 0$	$F_{x2L} = 0$	$F_{x3R} = 0$
Brakeline Pressures, Braked Axles, psi	$p_t = 5$		$p_b = 5$		$p_{bs} = 5$
Maximum Deceleration, g	$a_{max} = 0.000$				
Calculated Data					
Axle1 to 5th Wheel, in	$l_{1s} = 110$				
Axle1 to Tractor CG, in	$l_1 = 55$				
5th Wheel to Trailer CG, in	$l_t = 155$				
Height of Tractor CG, in	$h_{1CG} = 40$				
Height of Trailer CG, in	$h_{2CG} = 60$				
5th Wheel Force Horizontal, lb	$X = 0$				
5th Wheel Force Vertical, lb	$Y = 3867$				
Static Axle Load, lb	$F_{z1static} = 8114$		$F_{z2static} = 7752$		$F_{z3static} = 4133$
Dynamic Axle Load, lb	$F_{z1} = 8114$		$F_{z2} = 7752$		$F_{z3} = 4133$
Traction Coefficient	$U_{T1R} = 0.00$		$U_{T2L} = 0.00$		$U_{T3R} = 0.00$
Braking Efficiency	$E_{1L} = \#DIV/0!$		$E_{2L} = \#DIV/0!$		$E_{3L} = \#DIV/0!$
Brake Force Distribution	$BD_{1L} = \#DIV/0!$		$BD_{2L} = \#DIV/0!$		$BD_{3L} = \#DIV/0!$
Braking Energy, BTU/hr	$q_{1R} = \#DIV/0!$		$q_{2L} = \#DIV/0!$		$q_{3R} = \#DIV/0!$
Stopping Time, hours	$t_{s,t} = \#DIV/0!$		$T_{g1,z} = \#DIV/0!$		$T_{g2,z} = \#DIV/0!$
Temperature, Brake, °F	$T_{g3,z} = \#DIV/0!$		$T_{g4,z} = \#DIV/0!$		$T_{g5,z} = \#DIV/0!$
Stopping Distance Equations:					
Input Data					
Brake Line Pressure Delay Time, secs	$t_c = 0.40$				
Brake Torque Build-up Time, secs	$t_t = 0.50$				
Maximum Deceleration, g	$a_{avg} = 0.00$				
Vehicle Speed, ft/sec	$V = 100.0$				
Calculated Data					
Average Deceleration, g	$a_{avg} = 0.00$				
Stopping Distance, ft	$S_a = \#DIV/0!$				

Table 8-1B. Example 8-1, empty, input and output data at 5 psi.

AIR BRAKE SYSTEM ANALYSIS

TRACTOR-TRAILER

2-S1 (Tractor: 2 axles; Trailer: 1 axle)

CASE ID: Example 8-1, 45 psi.

Input Data:

Tire-Road friction coefficient	$f = 3$
Weight of Tractor, lb	$W_1 = 12000$
Weight of Trailer, lb	$W_2 = 8000$
Axle 1 Weight (meas.), lb	$F_{z1m} = 6000$
Axle 2 Weight (meas.), lb	$F_{z2m} = 6000$
Axle 3 Weight (meas.), lb	$F_{z3m} = 8000$

Starting Brake Line Pressure, psi

Pressure Interval, psi

Road Slope Gradient, fraction (+/-)

$$P_i = 45 \quad D_p = 10 \quad G = 0$$

Knee-point Pressure, Axle 1, psi
Valve Slope Reduction, Axle 1
Pressure Interval, psi
Road Slope Gradient, fraction (+/-)

Knee-point Pressure, Axle 1, psi	$P_{k1} = 0$
Valve Slope Reduction, Axle 1	$K_1 = 1$

AXLE 1	LEFT		RIGHT		AXLE 2		LEFT		RIGHT		AXLE 3		LEFT		RIGHT		AXLE 3		RIGHT		
	A_{s1}	A_{c1L}	A_{c1R}	B_{F1L}	B_{F1R}	P_{o1L}	P_{o1R}	R_{1L}	R_{1R}	r_{1L}	r_{1R}	η_{c1L}	η_{c1R}	T_{1L}	T_{1R}	S_{1L}	S_{1R}	S_{max1L}	S_{max1R}	S_{c1L}	S_{c1R}
Swept Brake Drum Area, ft^2	1.8	24	24	2.6	2.6	5	5	21	21	7.5	7.5	0.65	0.65	240	240	1	1	8.25	8.25	2.25	2.25
Chamber Area, in^2																					
Brake factor																					
Pushout Pressure, psi																					
Tire Radius, in																					
Drum or Effective Disc Radius, in																					
Mechanical Efficiency																					
Braking Temperature, deg																					
Measured Stroke, in																					
Maximum rated Stroke, in																					
Critical Stroke, in																					

Calculated Data:

Effective Pushrod Travel, in	$S_{e1L} = 1.11$
Adjustment Factor	$f_{a1L} = 1.00$
Fade Factor	$f_{F1R} = 0.86$

Knee-point Pressure, Axle 2, psi	$P_{k2} = 0$
Valve Slope Reduction, Axle 2	$K_2 = 1$
Knee-point Pressure, Axle 3, psi	$P_{k3} = 0$
Valve Slope Reduction, Axle 3	$K_3 = 1$

(Set brake line pressure equal to pushout pressure and all charts start at chart origin)

Table 8-2A. Example 8-1, empty, input and output data at 45 psi.

Mechanical Gain value	$\rho_{D,S,or\,W} = 6.00$	$\rho_{D,S,or\,W} = 6.00$	$\rho_{D,S,or\,W} = 5.00$	$\rho_{D,S,or\,W} = 5.00$
Braking Force, lb	$F_{x1L} = 2993$	$F_{x1R} = 2993$	$F_{x2L} = 1593$	$F_{x2R} = 1593$
Brakeline Pressures, Braked Axles, psi	$p_h = 45$		$p_{g2} = 45$	$p_{g3} = 45$
Maximum Deceleration, g	$a_{max} = 0.605$			
<u>Calculated Data</u>				
Axle1 to 5th Wheel, in	$l_{1s} = 110$			
Axle1 to Tractor CG, in	$l_i = 55$			
5th Wheel to Trailer CG, in	$l_s = 155$			
Height of Tractor CG, in	$h_{1CG} = 40$			
Height of Trailer CG, in	$h_{2CG} = 60$			
5th Wheel Force Horizontal, lb	$X = 1916$			
5th Wheel Force Vertical, lb	$Y = 4528$			
Static Axle Load, lb	$F_{z1static} = 8114$	$F_{z2static} = 7752$	$F_{z3static} = 4133$	
Dynamic Axle Load, lb	$F_{z1} = 10986$	$F_{z2} = 5542$	$F_{z3} = 3472$	
Traction Coefficient	$U_{r1L} = 0.54$	$U_{r2L} = 0.58$	$U_{r3L} = 0.84$	
Braking Efficiency	$E_{1L} = 1.11$	$E_{2L} = 1.05$	$E_{3L} = 0.00$	
Brake Force Distribution	$BD_{1L} = 0.25$	$BD_{2L} = 0.13$	$BD_{3L} = 0.12$	
Braking Energy, BTU/hr	$q_{1L} = 1384766$	$q_{2L} = 737319$	$q_{3L} = 675876$	
Stopping Time, hours	$t_{s,1} = 0.00143$			
Temperature, Brake, °F	$T_{g1,g} = 478$	$T_{g2,g} = 229$	$T_{g3,g} = 219$	$T_{g4,g} = 219$
<u>Stopping Distance Equations:</u>				
<u>Input Data</u>				
Brake Line Pressure Delay Time, secs	$t_d = 0.40$			
Brake Torque Build-up Time, secs	$t_t = 0.50$			
Maximum Deceleration, g	$a_{avg} = 0.60$			
Vehicle Speed, ft/sec	$V = 100.0$			
<u>Calculated Data</u>				
Average Deceleration, g	$a_{avg} = 0.48$			
Stopping Distance, ft	$Sa_{max} = 322$			

Table 8-2B. Example 8-1, empty, input and output data at 45 psi.

AIR BRAKE SYSTEM ANALYSIS

TRACTOR-TRAILER

2-S1 (Tractor: 2 axles; Trailer: 1 axle)

CASE ID: Example 8-1

Table 1

P_t	P_{t1}	P_{t2}	P_{t3}	F_{x1L}	F_{x1R}	F_{x2L}	F_{x2R}	F_{x3L}	F_{x3R}	BD_{1L}	BD_{1R}	BD_{2L}	BD_{2R}	BD_{3L}	BD_{3R}
5	5	5	5	0	0	0	0	0	0	#####	#####	#####	#####	#####	#####
15	15	15	15	748	748	398	398	365	365	0.25	0.25	0.13	0.13	0.12	0.12
25	25	25	25	1496	1496	797	797	730	730	0.25	0.25	0.13	0.13	0.12	0.12
35	35	35	35	2244	2244	1195	1195	1095	1095	0.25	0.25	0.13	0.13	0.12	0.12
45	45	45	45	2993	2993	1593	1593	1461	1461	0.25	0.25	0.13	0.13	0.12	0.12
55	55	55	55	3741	3741	1992	1992	1826	1826	0.27	0.27	0.14	0.14	0.09	0.09
65	65	65	65	4489	4489	2390	2390	2191	2191	0.30	0.30	0.11	0.11	0.08	0.08
75	75	75	75	5237	5237	2789	2789	2556	2556	0.30	0.30	0.11	0.11	0.09	0.09
85	85	85	85	5985	5985	3187	3187	2891	2891	0.29	0.29	0.12	0.12	0.09	0.09
95	95	95	95	6733	6733	3595	3595	3286	3286	0.29	0.29	0.12	0.12	0.09	0.09
105	105	105	105	7482	7482	3984	3984	3652	3652	0.29	0.29	0.12	0.12	0.09	0.09
115	115	115	115	8230	8230	4382	4382	4017	4017	0.29	0.29	0.12	0.12	0.09	0.09

Table 2

P_t	P_{t1}	P_{t2}	P_{t3}	F_{x1L}	F_{x1R}	F_{x2L}	F_{x2R}	F_{x3L}	F_{x3R}	F_{xtrial}	F_{xTT}	F_{xtrial} a. g's	F_{xTT}	F_{xTT}	
5	5	5	5	0	0	0	0	0	0	0.000	0	0	0	0	0
15	15	15	15	748	748	398	398	365	365	3023	0.151	1496	797	797	730
25	25	25	25	1496	1496	797	797	730	730	6047	0.302	2993	1593	1461	1461
35	35	35	35	2244	2244	1195	1195	1095	1095	9070	0.454	4489	2390	2191	2191
45	45	45	45	2993	2993	1593	1593	1461	1461	12093	0.605	5985	3187	2891	2891
55	55	55	55	3741	3741	1992	1992	1215	1215	13896	0.695	7482	3984	3652	3652
65	65	65	65	4489	4489	1672	1672	1233	1233	14788	0.700	8978	4780	4382	4382
75	75	75	75	4188	4188	1538	1538	1274	1274	14000	0.700	10474	5577	5112	5112
85	85	85	85	4094	4094	1681	1681	1226	1226	14000	0.700	11971	6374	5843	5843
95	95	95	95	4104	4104	1665	1665	1231	1231	14000	0.700	13467	7170	6573	6573
105	105	105	105	4103	4103	1667	1667	1230	1230	14000	0.700	14963	7967	7303	7303
115	115	115	115	4103	4103	1667	1667	1230	1230	14000	0.700	16459	8764	8034	8034

Table 3

X	Y	F_{z1}	F_{z2}	F_{z3}	U_{T1L}	U_{T1R}	U_{T2L}	U_{T2R}	U_{T3L}	U_{T3R}	U_{T1T}	U_{T2T}	U_{T3T}	P_t
0	3867	8114	7752	4133	0.000	0.000	0.000	0.000	0.000	0.000	0.000	0.000	0.000	5
479	4032	8832	7200	3968	0.169	0.111	0.111	0.184	0.184	0.169	0.111	0.184	0.184	15
958	4197	9850	6847	3803	0.313	0.240	0.240	0.384	0.384	0.313	0.240	0.384	0.384	25
1437	4362	10288	6094	3638	0.427	0.392	0.392	0.602	0.602	0.437	0.392	0.602	0.602	35
1916	4528	10986	5542	3472	0.545	0.575	0.575	0.700	0.700	0.545	0.575	0.841	0.841	45
3128	4478	11700	4778	3922	0.639	0.700	0.700	0.700	0.700	0.639	0.834	1.037	1.037	55
3923	4359	11965	4394	3641	0.700	0.700	0.700	0.700	0.700	0.750	1.088	1.204	1.204	65
3051	4498	11696	4803	3502	0.700	0.700	0.700	0.700	0.700	0.896	1.161	1.460	1.460	75
3149	4483	11726	4757	3517	0.700	0.700	0.700	0.700	0.700	1.021	1.340	1.661	1.661	85
3138	4485	11723	4762	3515	0.700	0.700	0.700	0.700	0.700	1.149	1.506	1.870	1.870	95
3139	4484	11723	4761	3516	0.700	0.700	0.700	0.700	0.700	1.276	1.673	2.077	2.077	105
3139	4484	11723	4762	3516	0.700	0.700	0.700	0.700	0.700	1.404	1.841	2.285	2.285	115

Table 8-3. Example 8-1, shows brake-lockup sequence.

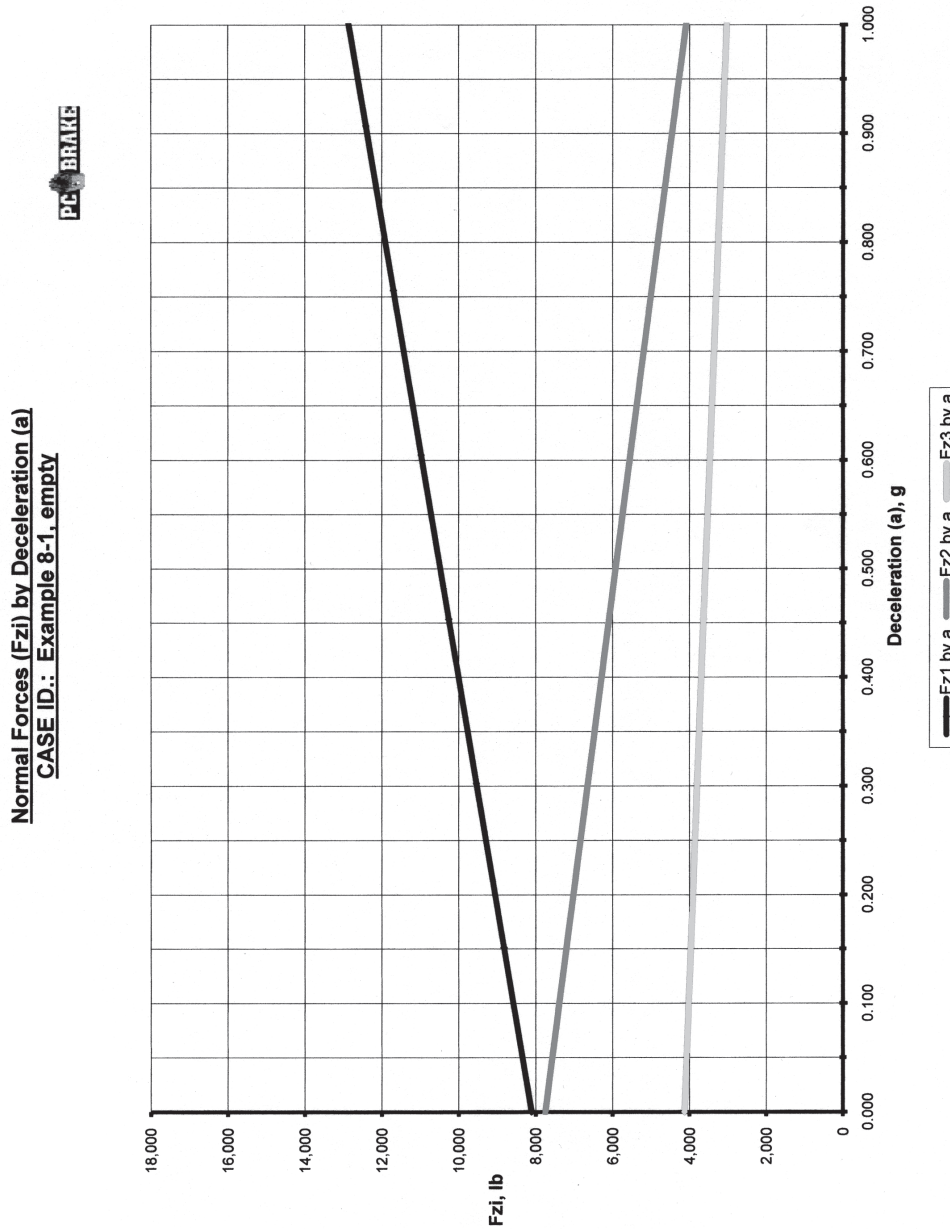


Figure 8-23. Dynamic axle loads, Example 8-1.

The tire-road friction utilization is shown in Fig. 8-24. The solid black lines shown in Fig. 8-24 represent the limit line associated with European requirements (not in the U.S.) within which the calculated friction utilization must fall. Inspection of Fig. 8-24 reveals that the trailer axle (#3) will always lock first, followed by the front axle (#1) for decelerations less than approximately 0.55 g. For deceleration greater than 0.55 g, the tractor rear axle locks before the front axle.

8.6 Braking of 3-S2 Tractor-Semitrailer Combination

Only air springs, walking beam, and leaf spring suspensions are analyzed. The tandem suspension details are the same as discussed in Chapter 7 for three-axle trucks.

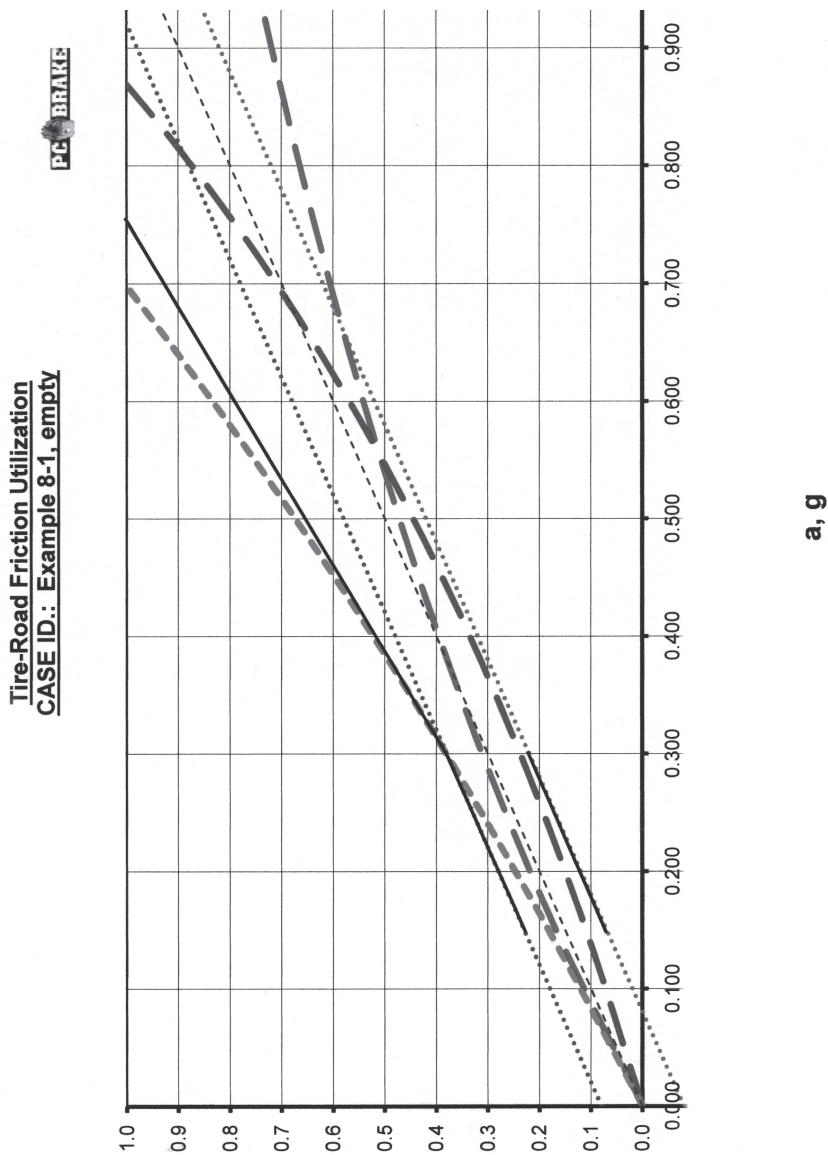


Figure 8-24. Tire-road friction utilization, example 8-1.

8.6.1 Air Springs on Tractor and Trailer Tandem Axles (3-S2-AA)

Because there is no inter-axle load transfer among the individual axles of the tandem axles, the weights of the rear axles are included in the tractor and trailer weights, respectively. The three normal forces of the three axles carrying the tractor frame are mathematically indeterminate (unless a complicated deflection relationship is used). The (reasonable) assumption was made that the normal forces of the rear axles of the trailer are distributed according to their static normal axle loads. Frequently, flat bed and other semitrailers have two rear air suspensions with an axle spread much greater than the usual 50 in. PC-BRAKE AIR 3-S2 AA (two-air spring suspension) software applies.

The axle normal forces of the tractor and semitrailer are:

$$F_{z1} = W_1 + Y - (F_{z2} + F_{z3}) \text{ , lb} \quad (8-21)$$

$$F_{z2} = [(W_1 l_1 - aW_1 h_1 - Xh_5 + Yl_5)/(L_1)][(F_{z2st})/(F_{z2st} + F_{z3st})] \text{ , lb} \quad (8-22)$$

$$F_{z3} = [(W_1 l_1 - aW_1 h_1 - Xh_5 + Yl_{15})/(L_1)][(F_{z3st})/(F_{z2st} + F_{z3st})] \text{ , lb} \quad (8-23)$$

$$F_{z4} = (W_2 - Y)(F_{z4st})/(F_{z4st} + F_{z5st}) \text{ , lb} \quad (8-24)$$

$$F_{z5} = (W_2 - Y)(F_{z5st})/(F_{z4st} + F_{z5st}) \text{ , lb} \quad (8-25)$$

where horizontal kingpin force:

$$X = F_{x1} + F_{x2} + F_{x3} - aW_1 \text{ , lb} \quad (8-26)$$

Vertical kingpin/fifth wheel force:

Y = Eq. (8-20) with X from Eq. (8-26)

a = deceleration, g-units $[\Sigma_{Fxi}/(W_1 + W_2)]$

F_{xi} = braking force of i^{th} axle, lb

F_{zist} = static axle load of i^{th} axle, N (lb)

h_{1cg} = vertical distance ground to tractor center-of-gravity, ft

h_{2cg} = vertical distance ground to trailer center-of-gravity, ft

h_5 = vertical distance ground to fifth wheel, ft

L_1 = tractor wheelbase, ft

L_2 = trailer wheelbase, ft

l_1 = horizontal distance front axle to tractor cg, in.

l_5 = horizontal distance fifth wheel to trailer cg, in.

l_{15} = horizontal distance front axle to fifth wheel, in.

W_1 = tractor weight, lb

W_2 = trailer weight, lb

8.6.2 Tractor Air Springs – Trailer Walking Beam (3-S2-AWB)

PC-BRAKE AIR 3-S2 A-WB applies.

The normal forces of the 3-S2 tractor-trailer are

$$F_{z1} = W_1 + Y - F_{z2} - F_{z3} , \text{ lb} \quad (8-27)$$

$$F_{z2} = [(W_1 l_1 - X h_5 + Y l_5 - a W_1 h_{1cg}) / (L_1)] [F_{z2st} / (F_{z2st} + F_{z3st})] , \text{ lb} \quad (8-28)$$

$$F_{z3} = [(W_1 l_1 - X h_5 + Y l_5 - a W_1 h_{1cg}) / (L_1)] [F_{z3st} / (F_{z2st} + F_{z3st})] , \text{ lb} \quad (8-29)$$

$$F_{z4} = Y_2 + w_4 + w_5 - F_{z5} , \text{ lb} \quad (8-30)$$

$$F_{z5} = (1/2) \{ [(Y_2 + 2w_5 - (X_2 v_1) / q_2 / 2) - a(w_4 + w_5) u_1 / q_2 / 2] \} , \text{ lb} \quad (8-31)$$

where kingpin forces at fifth wheel Y and X:

$$Y = [a W_{s2} (h_{s2} - v_1) + W_{s2} (L_2 - l_{s2}) - X (h_5 - v_1)] / L_2 , \text{ N (lb)} \quad (8-32)$$

$$X = F_{x1} + F_{x2} + F_{x3} , \text{ N (lb)} \quad (8-33)$$

Walking beam attachment forces to frame Y_2 and X_2 :

$$Y_2 = W_{s2} - Y , \text{ N (lb)} \quad (8-34)$$

$$X = a W_{s2} - X , \text{ N (lb)} \quad (8-35)$$

$$h_{s2} = [W_2 h_{cg2} - (w_4 + w_5) u_1] / W_{s2} , \text{ cm (in.)} \quad (8-36)$$

(sprung trailer weight cg height)

$$l_{s2} = [(F_{z4st} - w_4) (L_2 - q_2 / 2) + (F_{z5st} - w_5) (L_2 + q_2 / 2)] / W_{s2} , \text{ cm (in.)} \quad (8-37)$$

(horizontal distance fifth wheel to sprung trailer cg-location)

F_{xi} = braking force of i th axle, N (lb)

F_{zist} = static axle weight of i th axle, N (lb)

w_i = un-sprung weight of i th axle, N (lb)

W_1 = tractor weight, N (lb)

W_{s2} = sprung weight of trailer, N (lb)

q_2 = trailer walking beam axle spread
(distance between axle 4 and 5), cm (in.)

v_1 = walking beam pivot height, cm (in.)

u_1 = walking beam un-sprung weight height, cm (in.)

8.6.3 Tractor Air Springs – Trailer Leaf Springs (3-S2-ALS)

PC-BRAKE AIR 3-S2ALS applies. In a leaf spring axle, both axles of the tandem suspension are connected by an equalizer lever which transmits displacement, forces, and moments between axles #4 and #5 (Ref. 8.13).

The normal forces of the 3-S2 tractor and trailer axles are

$$F_{z1} = W_1 (1 - \psi_1 + a\chi_1) + Y(1 - y + az_1), \text{ N (lb)} \quad (8-38)$$

$$F_{z2} = [(W_1(\psi_1 - a\chi_1) + Y(y - az_1)]F_{z2st}/(F_{z2st} + F_{z3st}), \text{ N (lb)} \quad (8-39)$$

$$F_{z3} = [W_1(\psi_1 - a\chi_1) + Y(y - az_1)]F_{z3st}/(F_{z2st} + F_{z3st}), \text{ N (lb)} \quad (8-40)$$

$$F_{z4} = bdY_2/[(c + d)(b/2 + av)] + w_4 - auw_4/(b/2 + av), \text{ N (lb)} \quad (8-41)$$

$$F_{z5} = bdY_2/[(c + d)(b/2 - av)] + w_5 + auw_5/(b/2 - av), \text{ N (lb)} \quad (8-42)$$

where

Fifth wheel/kingpin vertical force:

$$\begin{aligned} Y = W_{S2} - Y_2 &\{d(b/2 - av)/[(c + d)(b/2 + av)] \\ &+ c(b/2 + av)/[(c + d)(b/2 - av)] + 1\} \\ &+ (auw_4)/(b/2 + av) - (auw_5)/(b/2 - av), \text{ N (lb)} \end{aligned} \quad (8-43)$$

Vertical force at equalizer bar attachment to trailer frame:

$$Y_2 = \{W_{S2}L_2[\psi_2 - a(\chi_2 - z_2)] + aG_1\}/H_1, \text{ N (lb)} \quad (8-44)$$

$$\begin{aligned} G_1 = uw_4/(b/2 + av) &[(z_1L_1 - v)a + L_2 - c - b] - uw_5/(b/2 - av) \\ &[(z_1L_1 - v)a + L_2 + d + b], \end{aligned} \quad (8-45)$$

Ncm (lbin.)

$$\begin{aligned} H_1 = (d/(c + d))((z_1L_1 - v)a + L_2 - c - b))((b/2 - av)/(b/2 + av)) + \\ (c/(d + c))((z_1L_1 - v)a + L_2 + d + b))((b/2 + av)/(b/2 - av)) + \\ (z_1L_1 - v)a + L_2; \text{ cm (in.)} \end{aligned} \quad (8-46)$$

$$h_{S2cg} = (W_2h_{cg2} - (w_4 + w_5)u_1)/W_{S2}; \text{ cm (in.) (sprung trailer weight)} \\ \text{cg-height, cm (in.)} \quad (8-47)$$

$$l_{S2} = [(F_{z4st} - w_4)(L_2 - q_2/2) + (F_{z5st} - w_5)(L_2 + q_2/2)]/W_{S2}, \text{ cm (in.)} \quad (8-48)$$

(horizontal distance fifth wheel to cg-location of sprung trailer weight)

F_{zist} = static axle weight of ith axle, N (lb)

W_1 = tractor weight, N (lb)

W_2 = trailer weight, N (lb)

W_{s2} = sprung weight of trailer, N (lb)

h_{lcg} = tractor center-of-gravity height, cm (in.)

h_{s2cg} = center-of-gravity height of sprung trailer weight W_{s2} , cm (in.)

$$y = l_{15}/L_1$$

$$z_1 = h_s/L_1$$

$$z_2 = h_s/L_2$$

$$\chi_1 = h_{lcg}/L_1$$

$$\chi_2 = h_{s2cg}/L_2$$

ψ_1 = static empty tractor (no trailer) rear axle loads divided by tractor weight

ψ_2 = static semitrailer axle loads divided by total semitrailer weight

The braking of a 3-S2 tractor-semitrailer loaded to 314,615 N (70,700 lb) is analyzed. The tractor is equipped with air springs, the trailer with equalizing leaf springs. PC-BRAKE AIR 3-S2-ALS applies.

Solution approach:

1. In Design Data input, set horizontal center-of-gravity distances of trailer, and others not directly measured until static axle loads for field check are approximately equal to measured axle loads. Once this is done, all horizontal weight data are correct. The starting brake line pressure must equal the push out pressure (normally 5 psi) to have zero braking forces, that is, no dynamic load transfer.
2. In Design Data input, set starting brake line pressure at 115 psi for maximum braking of loaded vehicle. Observe Temperature, Brake and set one-half of observed brake temperature as input data in Braking Temperature. PC-BRAKE AIR computes the maximum swept brake surface temperature in a single stop without any ambient cooling. The fade factor adjusts braking force accordingly. For example, for the front brakes, the maximum temperature of the swept brake surface is 631 K (676°F) while only 431 K (335°F) is used as input temperature.

The dynamic axle loads are shown in Fig. 8-25. Note the decrease of the

dynamic axle load of axle # 4 for decelerations greater than approximately 0.71 g. The geometrical and loading data of the 3-S2 combination are such that at a deceleration of 0.71 g, the normal force of axle # 4 becomes zero. For any further increase in deceleration and load transfer, the trailer becomes a single-axle trailer with the axle load of axle # 5 decreasing as Fig. 8-25 indicates.

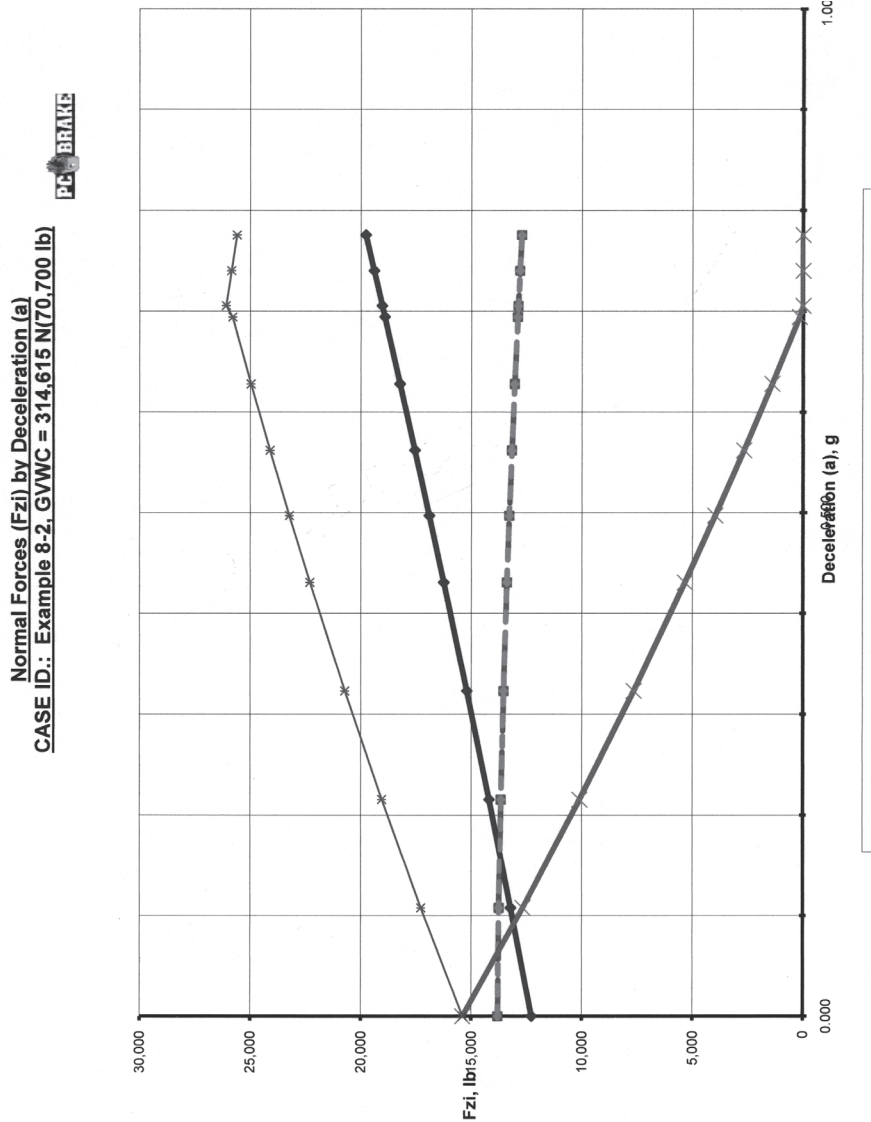


Figure 8-25. Dynamic axle loads, 3-S2A-LS, GVWC = 314,615 N.

In Design Data input, set Tire Road Friction Coefficient to actual value; for example, 0.6.

3. In Table 8-4, Data Tables 1, 2, and 3 are shown. For printing purposes, some data to the right of Table 8-4 are not shown. Data Table 1 shows the individual brake line pressures as affected by limiting or

proportioning valves (if used), and the tire-to-ground braking forces for each wheel/break location of the vehicle. The braking forces are affected by temperature fade and push rod travel. Data Table 2 shows the braking forces actually existing between tire and ground as affected by brake lockup and wheel skidding. Once lockup has occurred, the braking force between tire and ground is computed by the product of dynamic wheel load and tire-road friction coefficient. Data Table 3 shows the dynamic axle loads and tire-road friction utilization for each wheel and brake lockup sequence. Brake lockup occurs when the calculated tire-road friction utilization exceeds the existing tire-road friction coefficient.

The axle load of axle #4 is 8620 N (1937 lb) at 115 psi, as shown in Table 8-4, Data Table 3. Inspection of Table 8-4, Data Table 3 reveals that the brakes of axle #4 will have locked for brake line pressures of 35 psi, as indicated by U_{T4L} and $U_{T4R} > f = 0.6$ (tire-road coefficient of friction). The tractor rear brakes will have locked at a brake line pressure of 55 psi. The front brakes will lock for pressure greater than 105 psi. Because all brakes are locked at a brake line pressure of 105 psi, the maximum deceleration of 0.6 g is also reached for brake line pressures greater than 95 psi. Data Table 2 of Table 8-4 shows $a = 0.597$ g at 95 psi.

8.7 2-S1-2 Combination: Two-Axle Tractor, Single-Axle Semitrailer, and Double-Axle Trailer

The tongue hitch connecting trailer 1 and 2 is assumed to be horizontal; that is, force X_2 is horizontal. Consequently, there is no vertical force component ($Y_2 = 0$) at the coupling point between semitrailer and pup-trailer. PC-BRAKE 2-S1-2 applies.

The axle normal forces are

$$F_{z1} = [W_1(L_1 - l_1) + aW_1h_1 + X_1h_5 + Y_1(L_1 - l_{15})]/L_1, \text{ N (lb)} \quad (8-49)$$

$$F_{z2} = W_1 + Y_1 - F_{z1}, \text{ N (lb)} \quad (8-50)$$

$$F_{z3} = [W_2l_2 - X_2h_{23} - F_{x3}h_5 - aW_2(h_2 - h_5)]/L_2, \text{ N (lb)} \quad (8-51)$$

$$F_{z4} = [W_3(L_3 - l_3) + aW_3h_3 - X_2h_{23}]/L_3, \text{ N (lb)} \quad (8-52)$$

$$F_{z5} = W_3 - F_{z4}, \text{ N (lb)} \quad (8-53)$$

where the horizontal kingpin force is

$$X_1 = F_{x1} + F_{x2} - aW_1, \text{ N (lb)} \quad (8-54)$$

For $X_1 > 0$, the semitrailer is pushing into the tractor [not enough braking on the trailer(s)]; for $X_1 < 0$, the semitrailer is pulling on the tractor [excessive braking on the trailer(s)].

3-S2
TRACTOR AIR-TRAILER LEAF SPRINGS
CASE ID.: GWVC = 314,615 N

Table 1

P_t	P_h	P_a	P_b	P_k	P_{ls}	P_{ls}	F_{xIL}	F_{xLR}	F_{xAL}	F_{xAR}	F_{xAL}	F_{xAR}	F_{xIL}	F_{xLR}	F_{xAL}	F_{xAR}	F_{xIL}	F_{xLR}	F_{xAL}	F_{xAR}	F_{xIL}	F_{xLR}	F_{xAL}	F_{xAR}
5	5	5	5	5	5	5	0	0	0	0	0	0	0	0	0	0	0	0	0	0	0	0	0	0
15	15	15	15	15	15	15	554	554	826	826	826	826	826	826	826	826	826	826	826	826	826	826	826	826
25	25	25	25	25	25	25	1107	1653	1653	1653	1653	1653	1653	1653	1653	1653	1653	1653	1653	1653	1653	1653	1653	1653
35	35	35	35	35	35	35	1661	1661	2479	2479	2479	2479	2479	2479	2479	2479	2479	2479	2479	2479	2479	2479	2479	2479
45	45	45	45	45	45	45	2214	2214	3306	3306	3306	3306	3306	3306	3306	3306	3306	3306	3306	3306	3306	3306	3306	3306
55	55	55	55	55	55	55	2768	2768	4132	4132	4132	4132	4132	4132	4132	4132	4132	4132	4132	4132	4132	4132	4132	4132
65	65	65	65	65	65	65	3322	4959	4959	4959	4959	4959	4959	4959	4959	4959	4959	4959	4959	4959	4959	4959	4959	4959
75	75	75	75	75	75	75	3875	3875	5785	5785	5785	5785	5785	5785	5785	5785	5785	5785	5785	5785	5785	5785	5785	5785
85	85	85	85	85	85	85	4429	4429	6612	6612	6612	6612	6612	6612	6612	6612	6612	6612	6612	6612	6612	6612	6612	6612
95	95	95	95	95	95	95	4983	4983	7438	7438	7438	7438	7438	7438	7438	7438	7438	7438	7438	7438	7438	7438	7438	7438
105	105	105	105	105	105	105	5536	5536	8265	8265	8265	8265	8265	8265	8265	8265	8265	8265	8265	8265	8265	8265	8265	8265
115	115	115	115	115	115	115	6090	6090	9091	9091	9091	9091	9091	9091	9091	9091	9091	9091	9091	9091	9091	9091	9091	9091

Table 2

P_t	P_h	P_a	P_b	P_k	P_{ls}	P_{ls}	F_{xIL}	F_{xLR}	F_{xAL}	F_{xAR}	F_{xIL}	F_{xLR}													
5	5	5	5	5	5	5	0	0	0	0	0	0	0	0	0	0	0	0	0	0	0	0	0	0	
15	15	15	15	15	15	15	554	554	826	826	826	826	826	826	826	826	826	826	826	826	826	826	826	826	
25	25	25	25	25	25	25	1107	1653	1653	1653	1653	1653	1653	1653	1653	1653	1653	1653	1653	1653	1653	1653	1653	1653	
35	35	35	35	35	35	35	1661	2479	2479	2479	2479	2479	2479	2479	2479	2479	2479	2479	2479	2479	2479	2479	2479	2479	
45	45	45	45	45	45	45	2214	3306	3306	3306	3306	3306	3306	3306	3306	3306	3306	3306	3306	3306	3306	3306	3306	3306	
55	55	55	55	55	55	55	2768	3322	3986	3986	3986	3986	3986	3986	3986	3986	3986	3986	3986	3986	3986	3986	3986	3986	
65	65	65	65	65	65	65	75	3875	3987	3987	3987	3987	3987	3987	3987	3987	3987	3987	3987	3987	3987	3987	3987	3987	
75	75	75	75	75	75	75	85	4429	3969	3969	3969	3969	3969	3969	3969	3969	3969	3969	3969	3969	3969	3969	3969	3969	
85	85	85	85	85	85	85	95	4983	3951	3951	3951	3951	3951	3951	3951	3951	3951	3951	3951	3951	3951	3951	3951	3951	
95	95	95	95	95	95	95	105	5536	3933	3933	3933	3933	3933	3933	3933	3933	3933	3933	3933	3933	3933	3933	3933	3933	
105	105	105	105	105	105	105	115	5395	3931	3931	3931	3931	3931	3931	3931	3931	3931	3931	3931	3931	3931	3931	3931	3931	
115	115	115	115	115	115	115	115	115	115	115	115	115	115	115	115	115	115	115	115	115	115	115	115	115	115

Table 3

P_t	Y_2	Y	X	F_{z1}	F_{z2}	F_{z3}	F_{z4}	F_{z5}	F_{z6}	F_{z7}	F_{z8}	F_{z9}	F_{z10}	F_{z11}	F_{z12}	F_{z13}	F_{z14}	F_{z15}	F_{z16}	F_{z17}	F_{z18}	F_{z19}	F_{z20}	F_{z21}	F_{z22}	
5	14400	20900	0	12283	13808	13808	15400	0	0	0	0	0	0	0	0	0	0	0	0	0	0	0	0	0	0	
15	13612	21745	2339	13754	13754	13754	18247	17308	0	0	0	0	0	0	0	0	0	0	0	0	0	0	0	0	0	
25	12149	22556	46777	14228	13664	13664	19015	0	0	0	0	0	0	0	0	0	0	0	0	0	0	0	0	0	0	0
35	10067	23336	7016	15254	13541	13541	17566	20798	0	0	0	0	0	0	0	0	0	0	0	0	0	0	0	0	0	
45	8181	23688	9912	16024	13432	13432	15838	21974	0	0	0	0	0	0	0	0	0	0	0	0	0	0	0	0	0	
55	6261	24367	12973	16725	13321	13321	14355	22979	0	0	0	0	0	0	0	0	0	0	0	0	0	0	0	0	0	
65	5719	24491	13180	16912	13290	13290	15400	39722	0	0	0	0	0	0	0	0	0	0	0	0	0	0	0	0	0	
75	4660	24222	13579	17265	13228	13228	17307	23216	0	0	0	0	0	0	0	0	0	0	0	0	0	0	0	0	0	
85	3656	24830	14006	13170	13170	13170	17589	24142	0	0	0	0	0	0	0	0	0	0	0	0	0	0	0	0	0	
95	2589	25139	14423	17922	13109	13109	1991	24570	0	0	0	0	0	0	0	0	0	0	0	0	0	0	0	0	0	
105	2496	25157	15084	17960	13103	13103	1937	24606	0	0	0	0	0	0	0	0	0	0	0	0	0	0	0	0	0	
115	2456	25157	15094	17950	13103	13103	1937	24606	0	0	0	0	0	0	0	0	0	0	0	0	0	0	0	0	0	

Table 8-4. Brake lockup sequence, 3-S2 A-LS, GVWC = 314,615 N (70,700 lb), $f = 0.6$.

Vertical force on fifth wheel:

$$Y_1 = W_2 - F_{z3} , \text{ N (lb)} \quad (8-55)$$

Horizontal hitch force between semitrailer and pup-trailer:

$$X_2 = X_1 - F_{x3} - aW_2 , \text{ N (lb)} \quad (8-56)$$

For $X_2 > 0$, pup-trailer is pulling on semitrailer (excessive braking on pup-trailer); $X_2 < 0$, pup-trailer is pushing into semitrailer (not enough braking on pup-trailer).

F_{xi} = braking force of ith axle, N (lb)

h_1 = cg-height of tractor, cm (in.)

h_2 = cg-height of semitrailer, cm (in.)

h_3 = cg-height of pup-trailer, cm (in.)

h_{23} = vertical hitch height between semitrailer and pup-trailer, cm (in.)

L_1 = tractor wheelbase, cm (in.)

L_2 = semitrailer wheelbase, cm (in.) (horizontal distance 5th wheel to axle #3)

L_3 = pup-trailer wheelbase, cm (in.)

l_1 = horizontal distance axle #1 to tractor cg. , cm (in.)

l_{15} = horizontal distance axle #1 to fifth wheel, cm (in.)

l_2 = horizontal distance fifth wheel to semitrailer cg. , cm (in.)

l_3 = horizontal distance axle #4 to pup-trailer cg. , cm (in.)

W_1 = weight of tractor, N (lb)

W_2 = weight of semitrailer, N (lb)

W_3 = weight of two-axle trailer, N (lb)

8.8 2-S2 Tractor-Semitrailer

For a two-axle tractor attached to a two-axle semitrailer, the equations for the dynamic axle loads of the appropriate tandem axle designs can be used directly. The fifth wheel of the tractor only experiences the influence of the trailer through the horizontal (X) and vertical (Y) forces at the fifth wheel.

8.9 2-S3 Tractor-Semitrailer – Triple-Axle Trailer with Leaf Springs

The derivation of the equations for the individual normal forces of each axle follows the same concept as for other vehicle configurations. In the case of the three-leaf spring trailer suspension, the equations become extremely lengthy and algebraically involved. In the formulation that follows, a computer-based matrix solution was used.

A typical three-axle trailer leaf spring suspension with equalizer bars between axles four and five is illustrated in Fig. 8-26. The individual spring ends can slide fore and aft without transmitting any horizontal forces. Any frictional forces between spring ends and hanger support are neglected. The spring ends only transmit vertical forces. For example, Y_3 is the total vertical force of both sides of axle #3 at the leading end of the springs; Y_{34} is the vertical frame attachment force(s) of the equalizer bars on both sides between axles #3 and #4. The horizontal force X_3 exists in the tie rod(s) attached to the axle and frame bracket which hold axle #3 in place horizontally. Similar horizontal forces exist for axles # 4 and # 5.



Figure 8-26. Triple-axle trailer with leaf spring suspension.

The free-body diagrams consist of five sub-bodies; namely, the tractor, the sprung trailer, and three individual free-body diagrams for the three trailer axles.

The horizontal kingpin force and three horizontal tie rod forces X_i can easily be determined from their individual free-body diagrams for a specified brake line pressure as:

Horizontal kingpin force between tractor and trailer:

$$X_1 = F_{x1} + F_{x2} - aW_1, \text{ N (lb)} \quad (8-57)$$

Horizontal tie rod forces attaching axle #3 to frame brackets:

$$X_3 = F_{x3} - aw_3, \text{ N (lb)} \quad (8-58)$$

Horizontal tie rod forces attaching axle #4 to frame brackets:

$$X_4 = F_{x4} - aw_4, \text{ N (lb)} \quad (8-59)$$

Horizontal tie rod forces attaching axle #5 to frame brackets:

$$X_5 = F_{x5} - aw_5, \text{ N (lb)} \quad (8-60)$$

The remaining ten independent equations in terms of five dynamic axle loads and five vertical forces at the fifth wheel, and load-carrying points of the trailer springs, are:

1. $F_{z1}l_{15} - F_{z2}(L_1 - l_{15}) = -A$
2. $Y_3C_1 + Y_{34}C_2 + Y_{45}C_3 + Y_5C_4 = B$
3. $F_{z1} + F_{z2} - Y_1 = W_1$
4. $Y_1 + Y_3 + Y_{34} + Y_{45} + Y_5 = B$
5. $F_{z3} - Y_3 + Y_{34} d^* = w_3$
6. $F_{z4} - Y_{34} c^* - Y_{45} d^* = w_4$
7. $F_{z5} - Y_5 + Y_{45} c^* = w_5$
8. $-Y_3(b/2) + Y_3 4d^*(b/2) = D_1$
9. $-Y_{34}c^*(b/2) + Y_4 5 d^*(b/2) = D_2$
10. $Y_{45}c^*(b/2) + Y_5(b/2) = D_3$

The ten unknowns are in bold letters. Equations 1 through 10 are independent of each other and can be solved either through successive substitutions or by the matrix formulation method using computer software. The normal forces of the individual axles of the 2-S3 combination are given in the lengthy equations that follow.

Tractor front axle:

$$\begin{aligned} F_{z1} = W_1 - (l_{15}/L_1) \{ & K_1 + K_2 - [(-2D_3/b) - K_3] - (2D_1/b) + K_4 - K_5 \} \\ & - [A + l_{15}(W_1 + W_{2S})]/L_1, \text{ N (lb)} \end{aligned} \quad (8-61)$$

Tractor rear axle:

$$\begin{aligned} F_{z2} = (l_{15}/L_1) \{ & K_1 + K_2 + (-2D_3/b) + K_3 + (2D_1/b) + K_4 \} \\ & + [A + l_{15}(W_1 + W_{2S})]/L_1, \text{ N (lb)} \end{aligned} \quad (8-62)$$

Trailer axle #3:

$$F_{z3} = w_3 - 2D_1/b - 2d^*K_2, \text{ N (lb)} \quad (8-63)$$

Trailer axle #4:

$$F_{z4} = w_4 - d^*K_1 - c^*K_2, \text{ N (lb)} \quad (8-64)$$

Trailer axle #5:

$$F_{z5} = w_5 + 2D_3/b - 2c^*K_1, \text{ N (lb)} \quad (8-65)$$

Vertical force at the fifth wheel:

$$Y_1 = -K_3, \text{ N (lb)} \quad (8-66)$$

The vertical force at the leading portion of the springs of axle #3:

$$Y_3 = -2D_1/b - d^*K_2, \text{ N (lb)} \quad (8-67)$$

The total vertical force at the frame attachment points (left and right frame rail) of the equalizer bar between axles #3 and #4:

$$Y_{34} = -K_2, \text{ N (lb)} \quad (8-68)$$

The total vertical force at the frame attachment points (left and right frame rail) of the equalizer bar between axles #4 and #5:

$$Y_{45} = -K_1, \text{ N (lb)} \quad (8-69)$$

The total vertical force at the trailing portion of the springs of axle #5:

$$Y_5 = 2D_3/b - c^*K_1, \text{ N (lb)} \quad (8-70)$$

In the paragraphs that follow, the numerous constants are identified.

$$K_1 = [-bBc^* - 2c^*C_1D_1 - 2C_2D_2 - 2d^*C_1D_2 + 2c^*C_4D_3]/\{b[c^*C_3 + (c^*)^2C_4 + d^*C_2 + (d^*)^2C_1]\}, \text{ N (lb)}$$

$$K_2 = [-bBd^* - 2d^*C_1D_1 + 2C_3D_2 + 2c^*C_4D_2 + 2d^*C_4D_3]/\{b[c^*C_3 + (c^*)^2C_4 + d^*C_2 + (d^*)^2C_1]\}, \text{ N (lb)}$$

$$K_3 = \{bBc^* + bB(c^*)^2 + bBd^* + bB(d^*)^2 + 2c^*C_1D_1 + 2(c^*)^2C_1D_1 - 2c^*C_3D_1 - 2(c^*)^2C_4D_1 + 2d^*C_1D_1 - 2d^*C_2D_1 + 2C_2D_2 + 2c^*C_2D_2 - 2C_3D_2 - 2c^*C_4D_2 + 2c^*d^*C_1D_2 + 2d^*C_1D_2 - 2d^*C_3D_2 - 2c^*d^*C_4D_2 + 2c^*C_3D_3 - 2c^*C_4D_3 + 2d^*C_2D_3 - 2d^*C_4D_3 + 2(d^*)^2C_1D_3 - 2(d^*)^2C_4D_3 - bc^*C_3W_{2s} - b(c^*)^2C_4W_{2s} - bd^*C_2W_{2s} - b(d^*)^2C_1W_{2s}\}/\{b[c^*C_3 + (c^*)^2C_4 + d^*C_2 + (d^*)^2C_1]\}, \text{ N (lb)}$$

Brake Design and Safety

$$A = aW_1(h_5 - h_1) - W_1(l_{15} - l_1) - (F_{x1} + F_{x2})h_5, \text{ Ncm (lbin.)}$$

$$B = W_{2S}l_{2S5} - aW_{2S}(h_{2S} - h_5) - X_3(h_5 - v_3) - X_4(h_5 - v_4) - X_5(h_5 - v_5), \text{ Ncm (lbin.)}$$

$$C_1 = L_2 - 3b/2 - c - 2d, \text{ cm (in.)}$$

$$C_2 = L_2 - b/2 - d, \text{ cm (in.)}$$

$$C_3 = L_2 + b/2 + c, \text{ cm (in.)}$$

$$C_4 = L_2 + 3b/2 + c + d, \text{ cm (in.)}$$

$$D_1 = aw_3u_3 + X_3v_3, \text{ Ncm (lbin.)}$$

$$D_2 = aw_4u_4 + X_4v_4, \text{ Ncm (lbin.)}$$

$$D_3 = aw_5u_5 + X_5v_5, \text{ Ncm (lbin.)}$$

$$c^* = c/(c + d)$$

$$d^* = d/(c + d)$$

$$W_1 = \text{tractor weight, N (lb)}$$

$$W_2 = \text{trailer weight, N (lb)}$$

$$W_{S2} = \text{sprung weight of trailer, N (lb)}$$

$$w_3 = \text{weight of unsprung #3 trailer axle, N (lb)}$$

$$w_4 = \text{weight of unsprung #4 trailer axle, N (lb)}$$

$$w_5 = \text{weight of unsprung #5 trailer axle, N (lb)}$$

$$h_{1cg} = \text{tractor center-of-gravity height, cm (in.)}$$

$$h_{S2cg} = \text{center-of-gravity height of sprung trailer weight } W_{S2}, \text{ cm (in.)}$$

The leaf spring suspension dimensions for axles 3, 4, and 5 are identified in Fig. 7-18.

The dynamic axle loads of a 3-S2 tractor-trailer with a two-leaf tandem suspension are shown in Fig. 8-25. Inspection shows the significant decrease of the dynamic axle load of axle #4, the leading axle of the trailer, and the associated increase of axle #5. For a 2-S3 combination with trailer axle leaf springs, the trailer axle dynamic loads are similar. Axle #3 experiences a significant decrease, axle #4 a slight decrease, while axle #5 experiences a corresponding increase in dynamic axle load. The summation of all trailer normal forces will decrease with deceleration due to dynamic load transfer onto the fifth wheel of the tractor.

8.10 Test Results

In the early seventies, a large commercial vehicle braking research and testing study was conducted by the University of Michigan for NHTSA in preparation for FMVSS 121 rulemaking (Refs. 8.13, 8.14). Trucks, buses and tractor-trailers with a GVW greater than 44,500 N (10,000 lb) were tested to determine their existing braking effectiveness. The author was involved in the theoretical analysis of the brake designs and optimizing braking performance.

The test results of a 3-S2 with leaf spring tandem axle on the trailer are illustrated in the braking performance diagram shown in Fig. 8-27. It illustrates the relationship between pedal force, brake line pressure for the empty and laden conditions, and friction utilization. Test data show good correlation between theory and measurements. The critical element in predicting braking effectiveness is the brake factor of the brakes used. In the case of disc brakes, the brake factor data variation is less pronounced due to the linear relationship between brake factor and pad/rotor friction coefficient. The brake design engineer is again reminded that, in general, it is cost beneficial to use a brake lining compound that is well known and performance tested and to design the air brake system hardware around it.

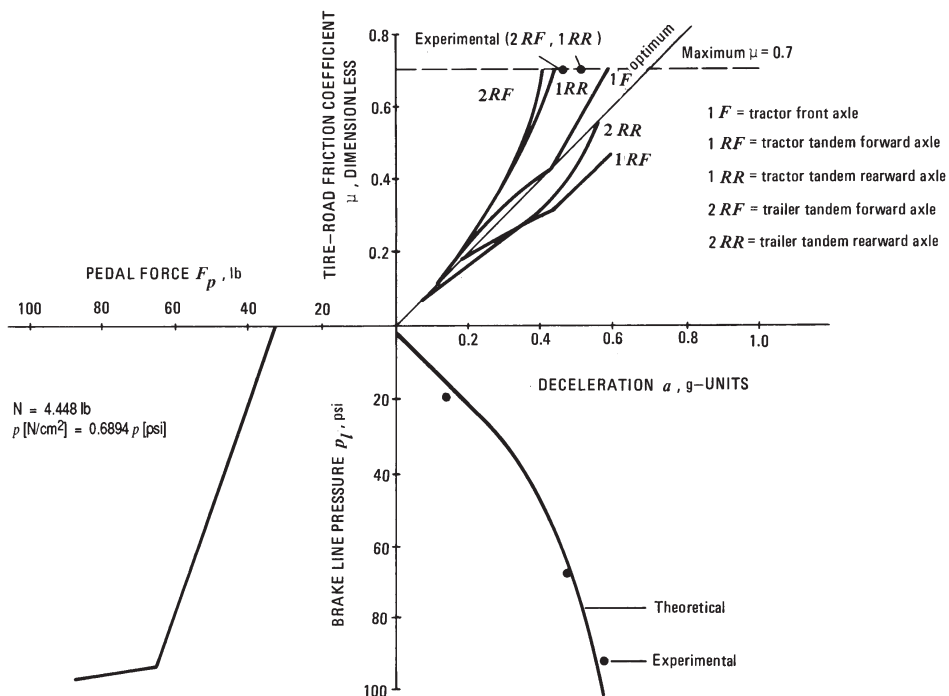


Figure 8-27. Braking performance diagram for a loaded 3-S2 combination: tractor walking beam rear axle and trailer leaf spring axle.

Chapter 8 References

- 8.1 Grandel, Juergen, "Braking of Cars Towing Unbraked Trailers of Different Weights," *Verkehrsunfall und Fahrzeugtechnik*, Oct. 1987.
- 8.2 Burckhardt, Manfred, "The Computation of Braking Deceleration of a Car Towing Unbraked Trailers," *Verkehrsunfall und Fahrzeugtechnik*, Oct. 1987.
- 8.3 Limpert, Rudolf, "Motor Vehicle Accident Reconstruction and Cause Analysis," LexisNexis, 6th edition, 2009.
- 8.4 Gespann-ESP: Anti_Koerper, http://www.auto-motor-und-sport.de/tests/technik/hxcmis_article_91458.
- 8.5 Susemihi, Enrique A., "Automatic Stabilization of Tractor Jackknifing in Tractor-Semitrailer Trucks," SAE Paper No. 740551, SAE International, Warrendale, PA, 1974.
- 8.6 Wilkins, H. A., "The Stability of Articulated Vehicles," *Journal of Automotive Engineering*, March 1971, pp. 13-17.
- 8.7 Myung-Won Suh, et al., "A Simulation Program for the Braking Characteristics of Tractor-Semitrailer Vehicle," SAE Paper No. 2000-01-3415, SAE International, Warrendale, PA, 2000.
- 8.8 Mikulcik, E. C., "The Dynamics of Tractor-Semitrailer Vehicles: The Jackknifing Problem," SAE Paper No. 710045, SAE International, Warrendale, PA, 1971.
- 8.9 Dunn, Ashley L., et al., "In-Depth Analysis of the Influence of High Torque Brakes on the Jackknife Stability of Heavy Trucks," SAE Paper No. 2003-013398, SAE International, Warrendale, PA, 2003.
- 8.10 Zagorski, Scott B., et al., "A Study of Jackknife Stability of Class VIII Vehicles with Multiple Trailers with ABS Disc/Drum," SAE Paper No. 2004-01-1741, SAE International, Warrendale, PA, 2004.
- 8.11 Dunn, Ashley L., et al., "The Effects of Foundation Brake Configuration on Class-8 Tractor Wet Stopping Performance and Stability," SAE Paper No. 2004-01-2702, SAE International, Warrendale, PA, 2004.
- 8.12 Leucht, Philip M., "The Directional Dynamics of the Commercial Tractor-Semitrailer Vehicle During Braking," SAE Paper No. 700371, SAE International, Warrendale, PA, 1970.
- 8.13 Limpert, Rudolf, "An Investigation of the Brake Force Distribution on Tractor-Semitrailer Combinations," SAE Paper 710044, SAE International, Warrendale, PA, 1971.
- 8.14 Murphy, R., et al., "Bus, Truck, Tractor-Trailer Braking System Performance," U.S. Department of Transportation Contract No. FH-11-7290, March 1972.

Chapter 9



Automatic Brake Control

9.1 Basic Considerations

Automatic brake control (ABC) systems are driver assist systems. They divide into two basic groups, namely those with driver application of the brake pedal, and those without, where some or all brakes are applied automatically for some extreme operating conditions.

ABC with pedal force application again divides into those with driver modulation ability and those without. The first group consists of brake system components that assist drivers in effectively applying the brakes within human limitations such as power brakes or brake line pressure-proportioning valves. In the second group the driver applies pedal force, and under certain conditions such as a slippery roadway, the brake line pressure is automatically modulated to prevent wheel lockup. The latter system is called an antilock brake system (ABS). Electronic brake force distribution is a refinement utilizing the rear brakes of an ABS system. A brake-assist system (BAS) reduces the stopping distance in emergency situations. The BAS comes into action when the driver applies the brake pedal quickly but not forcefully enough in critical situations. Under these conditions, BAS automatically develops maximum brake line pressure, resulting in maximum braking effectiveness.

ABC without brake pedal application by the driver divides into two groups, namely those with vehicle-internal data sensing, and those with vehicle-external data sensing. Electronic stability control (ESC) systems use vehicle-specific dynamic data to perform certain automatic braking functions. Radar controls use vehicle-exterior data obtained from roadway geometry, highway objects, or road users to automatically slow the vehicle or stop it by reducing engine power and/or brake application.

ABS brakes are standard equipment on nearly all passenger cars and light trucks currently sold in the US. In Europe, ABS brakes have been required for many years, commercial vehicles since 1991 (Directive 71/320 EEC). A significant safety development building on the ABS system is the ESC system. NHTSA has estimated that ESC for single vehicles reduces SUV crashes by 63% and

passenger car crashes by 30% (Refs. 9.1, 9.2). Federal Motor Vehicle Safety Standard 126 (FMVSS 126) requires all passenger vehicles sold in the U.S. to be equipped with ESC by 2013. In the U.S., commercial vehicles with a GVW greater than 44,500 N (10,000 lb) must be equipped with ABS brakes (FMVSS 121 and FMVSS 105).

A further development of ABS and ESC is brake control by wire. The driver's brake pedal control inputs are transmitted to a powerful computer which processes the data from the ESC about the existing dynamic driving conditions such as yaw velocity and lateral acceleration, and then calculates the optimum brake line pressures for each wheel. The individual optimum brake line pressures are then monitored electronically by a brake valve located at each wheel. Optimum brake line pressures while braking and turning are illustrated in Fig. 7-34.

9.2 Wheel-Lockup Analysis

Only a brief review of antilock brake systems and electronic stability control is presented. SAE International has published "Driving-safety systems," which includes ABS and ESC analysis (Ref. 9.3). ABS systems prevent brakes from locking during braking. Under normal braking conditions, the driver operates the brakes as usual; however, on slippery roadways or during severe braking, as the driver causes the wheels to approach lockup, the ABS brakes take over and modulate brake line pressure and, hence, braking force, independent of pedal force. Once the driver reduces pedal force sufficiently, automatic brake modulation stops and the standard brake system resumes driver-controlled braking.

The effectiveness of a brake line pressure modulating system is determined by the time available during which the control process must occur. An automatic brake control system operates safely only if it is engaged and becomes active before a safety-critical dynamic vehicle event occurs. Consequently, for both ABS and ESC systems, the time required by a tire to achieve maximum friction and to continue to lock up (100 % slip), or for the vehicle to develop directional instability, is of critical importance.

9.2.1 Tire/Wheel Braking Analysis

Tire characteristics play an important role in the braking and steering response of a motor vehicle. For ABS-equipped vehicles, the tire performance is of critical significance. All braking and steering forces must be generated by the small tire contact or tread patch connecting the vehicle to the road surface. Tire traction forces such as longitudinal or braking forces as well as side forces can only be produced when a difference exists between the speed of the tire circumference and the speed of the vehicle relative to the road surface. It is common to relate tire braking force data to tire braking slip. Braking slip is defined as the ratio of the difference of tire circumferential tread speed and absolute tire (or vehicle speed) to absolute speed. Tire side slip is defined in a similar fashion. Because tires are elastic pneumatic structures, speed differences result from elastic tire deformations and tread sliding. Only when the tire is at 100% slip is the braking

force produced by complete sliding or skidding of the tire tread patch in contact with the road.

The tire-road contact patch moves in the x-direction with the braking force acting opposite to it, as illustrated in Fig. 9-1. The angle α formed by the line of travel of the tire contact patch and the tire plane is commonly called slip angle. The tire side force acts at a right angle to the x-direction.

The absolute braking slip S_b is computed by the expression

$$S_b = (V - V_c) / V = (V - R_0 \omega) / V \quad (9-1)$$

where V = forward velocity of vehicle, m/s (ft/s)

R_0 = dynamic tire radius, m (ft)

ω = angular velocity of the wheel, rad/s

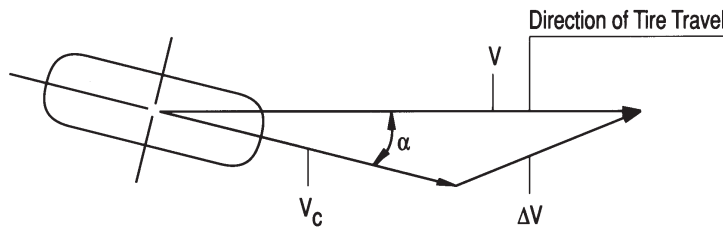


Figure 9-1. Relative velocity ΔV and tire slip for braking while turning.

Measuring vehicle velocity accurately is difficult because it would require a free-rolling wheel without any braking and/or side forces; that is, a wheel truly operating at zero slip. A fifth wheel similar to the one used for measuring velocity during vehicle testing would qualify. However, because all wheels are equipped with brakes, a so-called reference velocity has to be computed continuously. The reference velocity is slightly below the actual vehicle velocity.

Braking slip $S_{b,x}$ in the direction of vehicle travel is determined by

$$S_{b,x} = (V - V_c \cos \alpha) / V \quad (9-2)$$

where x-direction is the direction of travel of the tire

y-direction is perpendicular to x-direction

α = slip angle, deg

Similarly, side or lateral slip $S_{b,y}$ is determined by

$$S_{b,y} = V_c \sin \alpha / V \quad (9-3)$$

Typical braking friction-slip curves without any side force are shown in Fig. 9-2 (Ref. 9.4). In general, the μ -slip curve is characterized by a peak friction value obtained at the optimum slip value $S_{b, \text{opt}}$, and the sliding friction value obtained for 100% tire slip, i.e., the brake is locked. Not all tires have a pronounced peak friction value. The shape of the curve is a function of the design of the tire,

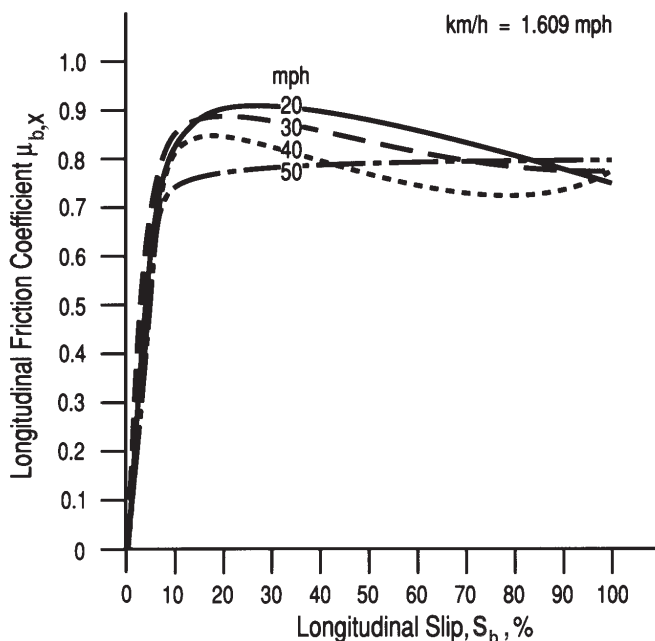


Figure 9-2. Friction-slip curve for dry concrete as function of speed.

tread design, and rubber composition, as well as the road surface and possible surface conditions such as water. The low values of tire slip are mainly related to deformation slip of the tire tread and pneumatic behavior of the tire.

An important tire parameter significant for ABS analysis is the slope of the μ -slip curve at zero-slip (Refs. 2.1, 9.4, 9.5, 9.6, 9.7). Most tires have $\Delta\mu_b/\Delta S_b$ values ranging between 20 and 30, indicating that a slip value of 1% results in a tire-road friction coefficient of $\mu_b = 0.2$ to 0.3. The zero-slip slope for most tires is nearly independent of the road surface including wet roads, again indicating that deformation slip dominates friction force production at low levels of tire slip.

An actual μ -slip curve for a particular tire is illustrated in Fig. 9-2. Inspection reveals that peak friction values exist for lower speeds but not for the 50 mph value. In order to study the basic factors influencing tire friction, we consider a friction-slip curve with a pronounced peak value. The friction curve may be idealized by two linear relationships, as shown in Fig. 9-3. The zero-slip slope is assumed to remain constant up to the point where it reaches the peak friction value. After the peak value has been reached, increased tire slip causes a straight-line reduction of tire-road friction coefficient until 100% tire slip has been obtained.

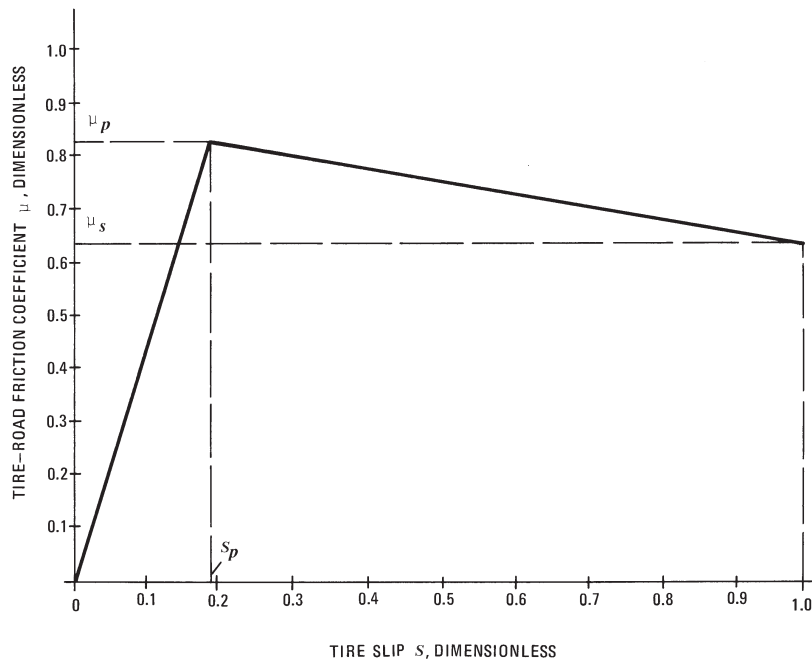


Figure 9-3. Idealized tire-road friction-slip characteristics.

For the region of $0 < S < \mu_p$, the formulation results in a differential equation of the form (Ref. 1.6):

$$\frac{d^2\beta}{dt^2} + A \frac{d\beta}{dt} = B - Ct, \quad 1/s^2 \quad (9-4)$$

where $A = (\mu_p F_z R) / (S_p I_w \omega_{0h})$, $1/s$

$B = (\mu_p F_z R) / (S_p I_w)$, $1/s^2$

$C = k/I_w$, $1/s^2$

d = differential operator

I_w = mass moment of inertia of wheel assembly, kgm^2 (lbft^2)

k = brake torque rate, Nm/s (lbft/s)

R = tire radius, m (ft)

S_p = tire slip at peak friction

t = time, s

β = wheel rotation angle, rad

μ_p = peak tire-road friction coefficient

ω_o = initial angular velocity of wheel, rad/s

Eq. (9-4) is a non-homogenous differential equation. The solution yields the time required for peak friction to be generated as

$$t_p = (S_p I_w \omega_o / \mu_p F_z R) + \mu_p F_z R / k , \quad s \quad (9-5)$$

The wheel angular deceleration ϵ_p at which maximum braking traction forces are produced, frequently called threshold angular deceleration, may be computed by

$$\epsilon_p = \omega_o k S_p / \mu_p F_z R, \text{ rad/s}^2 \quad (9-6)$$

The angular velocity of the wheel at the moment when peak friction has been achieved is given by

$$\omega_p = \omega_o \{1 + [k(S_p)^2 I_w] / [(\mu_p F_z R)^2] - (t_p)(k S_p) / (\mu_p F_z R)\}, \text{ rad/s} \quad (9-7)$$

where t_p is given in Eq. (9-5).

For the second linear (decreasing) region shown in Fig. 9-3 during which the wheel approaches lockup, the tire-road sliding friction coefficient μ_s affects the time required for the wheel to attain lockup. The time t_s required by the wheel to move from peak friction to lockup is determined from Eq. (9-4) approximately by

$$t_s = \left\{ \left[\frac{S_p I_w \omega_p}{(\mu_p - S_p \mu_s) F_z R} \right]^2 + \frac{2 \mu_p I_w \omega_p}{k(\mu_p - S_p \mu_s)} \right\}^{1/2} - \frac{S_p I_w \omega_p}{(\mu_p - S_p \mu_s) F_z R} , \quad s \quad (9-8)$$

where μ_s = sliding tire-road friction coefficient

ω_p = angular velocity of wheel at peak friction, rad/s [Eq. (9-7)]

Example 9-1:

For the data of a small car, compute all essential wheel peak and sliding friction parameters.

Tire normal force $F_z = 2776 \text{ N}$ (624 lb), wheel mass moment of inertia $I_w = 1 \text{ kgm}^2$ (0.737 lbft s^2), $R = 0.305 \text{ m}$ (1 ft), $S_p = 0.15$, $\mu_p = 1.0$, $\mu_s = 0.8$, $k = 4000 \text{ Nm/s}$ (2950 lbft/s), $V = 45 \text{ km/h}$ (66 ft/s).

Solution:

Substitution with $\omega_o = V/R = (66)/(1.0) = 66 \text{ rad/s}$ yields with Eq. (9-5):

$$t_p = [(0.15)(1)(66)] / [(1.0)(2776)(0.305)] + [(1.0)(2776)(0.305)] / (4000) \\ = 0.011 + 0.211 = 0.222 \text{ s}$$

$$\{t_p = [(0.15)(0.737)(66)]/[(1.0)(624)(1.0)] + [(1)(624)(1.0)]/(2950) \\ = 0.011 + 0.211 = 0.222 \text{ s}\}$$

Eq. (9-6) yields:

$$\varepsilon_p = [(66)(4000)(0.15)]/[(1.0)(2776)(0.305)] = 46.8 \text{ rad/s}^2$$

$$\{\varepsilon_p = [(66)(2950)(0.15)]/[(1.0)(624)(1)] = 46.8 \text{ rad/s}^2\}$$

Eq. (9-7) yields

$$\omega_p = 66\{1 + [(4000)(0.15)^2(1)]/[(1.0)(2776)(0.305)]^2 \\ - (0.222)(4000)(0.15)/[(1.0)(2776)(0.305)]\} \\ = 55.6 \text{ rad/s}$$

$$\{\omega_p = 66\{1 + [(2950)(0.15)^2(0.75)]/[(1.0)(624)(1.0)]^2 \\ - (0.222)(2950)(0.15)/[(1.0)(624)(1.0)]\} \\ = 55.6 \text{ rad/s}\}$$

Eq. (9-8) yields:

$$t_s = \{\{[(0.15)(1.0)(55.6)]/[(1.0 - 0.15 \times 0.8)(2776)(0.305)]\}^2 \\ + [(2)(1.0)(1.0)(55.6)] [(4000)(1.0 - 0.15 \times 0.8)]\}^{1/2} - [(0.15)(1.0)(55.6)] \\ /[(1.0 - 0.15 \times 0.8)(2776)(0.305)] = 0.167 \text{ s}$$

$$\{t_s = \{\{[(0.15)(0.75)(55.6)]/[(1.0 - 0.15 \times 0.8)(624)(1.0)]\}^2 \\ + [(2)(1.0)(0.75)(55.6)] [(2950)(1.0 - 0.15 \times 0.8)]\}^{1/2} - [(0.15)(0.75)(55.6)] \\ /[(1.0 - (0.15)(0.8))(624)(1.0)] = 0.167 \text{ s}\}$$

The results show that the tire will reach peak friction after 0.222 s. At that moment the angular deceleration is 46.8 rad/s², and the angular velocity has decreased from its initial value of 66 rad/s to 55.6 rad/s. The tire will go from peak friction to sliding friction in 0.167 s. The time from begin of brake torque (free rolling) until lockup is 0.222 + 0.167 = 0.389 s.

For a typical heavy vehicle brake system with $F_z = 44,480 \text{ N}$ (10,000 lb), $k = 35,254 \text{ Nm/s}$ (26,000 lbft/s), $R = 0.533 \text{ m}$ (1.75 ft), $V = 96.6 \text{ km/h}$ (88 ft/s), $\omega_o = 50 \text{ rad/s}$, $\mu_p = 0.7$, and $\mu_s = 0.6$, the results are $t_p = 0.485 \text{ s}$, $t_s = 0.243 \text{ s}$, $\varepsilon_p = 21.2 \text{ rad/s}^2$ and $\omega_p = 40 \text{ rad/s}$.

Based upon this simple analysis, the following observations are made:

1. When the wheel angular deceleration ε_p corresponding to the peak tire-road friction coefficient has been reached, the ABS brake line pressure modulator must have received the impulse for pressure isolation; that is, the brake line pressure is held constant regardless of any pressure increases caused by driver pedal force.
2. The modulator must prevent any further brake line pressure increase within the time period t_s to avoid wheel lockup.

3. Inspection of Eq. (9-6) indicates that the threshold wheel angular deceleration for a given vehicle (F_z and R) is a function of travel velocity V or ω_o , the increase of tire-road friction coefficient with braking slip (μ/S_b), the brake torque rate k directly related to the driver pedal force rate, and brake system inertia. Determining vehicle velocity accurately may be problematic.
4. The threshold angular decelerations ϵ_p will vary greatly depending upon operating parameters and may reach ratios of $\epsilon_{p\max}/\epsilon_{p\min} = 100$ or more. Consequently, while angular deceleration may be the first line of defense in preventing brake lockup, it is not sufficient. As will be discussed later, wheel rotational deceleration and tire slip control are used to provide modulated brake line pressure decrease to prevent wheel lockup.

The friction process is stable only for any point on the linearly increasing tire force including peak friction, and at the 100% slip point. For points between peak and sliding friction, the process is unstable. ABS control systems must limit the tire slip values to the stable region to prevent wheel lockup because the time required for the tire slip to move through the unstable region and achieve lockup is only a fraction of the time required to achieve peak friction.

Tires with a high peak friction point relative to the sliding friction produce dry road peak friction at approximately 20 to 30% slip. The optimum slip value decreases as tire-road friction decreases. Often, tires exhibiting a ratio of sliding to peak friction of 0.8 or so are rated highly for vehicle handling and steering response, but poorly for braking performance.

Tires showing little or no decrease in friction between peak and sliding condition produce an insignificant effect of slip on braking friction for slip values greater than approximately 30%. Their maximum friction coefficient generally is greater than the sliding friction exhibited by the former tires. These tires generally are judged better relative to their braking than handling performances.

FMVSS 121 allows complete wheel lockup during ABS modulation of up to 1 second for axles other than steering axles. For inadequate ABS systems not employing tire slip control braking skid marks in excess of 30 m (100 ft) may be produced at speeds of 112 km/h (70 mph).

To achieve a directionally stable braking maneuver, tire side forces must be considered along with the braking friction. As indicated earlier, a tire can produce a side force only if it is partially side slipping, i.e., when a slip angle exists between the actual direction of tire patch motion and the plane of the wheel. A typical tire side force friction coefficient vs. slip angle curve is illustrated in Fig. 9-4 for a free-rolling tire. The tire side force is measured at a right angle to the direction of motion of the tire contact patch. The side friction coefficient increases to a maximum value between a slip angle range of 8 to 12 degrees for most tires and decreases for higher values of slip angle. The side force production is unstable at and beyond a point where the slope is zero

$(\Delta\mu_y/\Delta\alpha = 0)$. The cornering stiffness of a tire is expressed by the slope of the curve at the origin and ranges from 0.25 to 0.4 per degree of slip angle. Consequently, a slip angle of one degree will achieve a tire side friction coefficient of 0.25 to 0.4, depending on tire construction. Operational parameters such as inflation pressure, camber angle, loading, and others will affect side force.

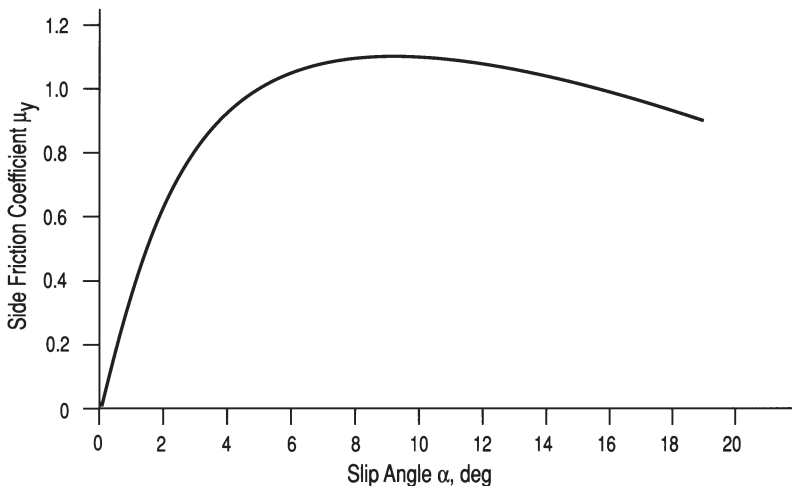


Figure 9-4. Tire side friction μ_y as a function of slip angle for free-rolling tire.

The tire side friction coefficient as a function of slip angle shown in Fig. 9-4 is only valid for a rolling, nonbraked tire. When braking is present during a steering maneuver, the tire side friction coefficient decreases with increasing values of tire slip S_b , as illustrated in Fig. 7-24. Inspection of Fig. 7-24 reveals that braking slip significantly reduces the side friction coefficient for a given slip angle. Braking slip values between 20 and 30% will reduce tire side friction coefficients by 75 to 80% of their free-rolling nonbraked levels. For example, a nonbraking side friction coefficient of 0.6 reduces to 0.15 to 0.18 in the presence of 20% braking slip.

The effects of tire slip angle on braking friction coefficient μ as a function of tire braking slip are illustrated in Fig. 7-25 for a typical passenger-car tire. The diagram shows that braking friction coefficient decreases with increasing values of slip angle. The optimum slip, at which tire peak friction occurs, increases with higher values of tire slip, indicating the “retarding” component of tire side slipping.

Although the tire characteristics discussed above are elementary, they clearly indicate the complex relationships associated with braking and side force production of a tire. For an ABS system to ensure minimum stopping distances, directional stability, and stable braking while turning, certain performance requirements must be based on the tire characteristics used.

9.2.2 Empirical Equations for Tire Braking Friction

To compute braking slip, it becomes necessary to develop empirical expressions for the μ_{x_B} -slip curves similar to the ones shown in Fig. 7-24 or 7-26. The underlying data of the curve have been measured for many different tires and roadway conditions. Although different empirical expressions have been used to describe tire friction, Burckhardt (Ref. 9.4) discusses an exponential equation that describes tire friction accurately. He uses three tire-specific constants that can be determined from three typical tire measurements, namely maximum tire friction coefficient, optimum tire slip, and tire friction coefficient at 100% tire slip. It works well for “summer” tires with a pronounced lower sliding friction coefficient as well as for “winter” tires with nearly identical peak and sliding friction coefficients.

9.2.3 Peak and Sliding Friction in the Braking Forces Diagram

The proper design of an ABS brake system relates directly to a clear understanding of the braking dynamics as revealed in the braking forces diagram. The braking forces diagram is discussed in Chapter 7. Here we will use it to analyze front and rear axle brake lockup as the traction coefficient moves from the peak to the sliding tire-road friction coefficient.

The braking forces diagram for a two-axle vehicle is shown in Fig. 9-5. The tires have a peak and sliding tire-road friction coefficient of μ_1 and μ_2 , respectively. The lines of constant friction coefficient μ_1 and μ_2 are shown in Fig. 9-5. The front tire peak friction line is marked by μ_1 , the sliding friction by μ_2 . A fixed brake force distribution is identified by the straight line marked by Φ . We consider a vehicle without ABS brakes. As the driver applies increasing pedal force, the operating point moves up on the Φ line until it reaches the μ_1 -peak friction line at point a_1 . At this point, the vehicle decelerates at a_1 with the front brakes locked. As the driver continues to apply increasing pedal force, the tire friction quickly moves from peak to sliding friction in less than 250 ms. Making the valid assumption that the rear braking force is not affected by the change in front tire friction, the operating point moves vertically down in the braking forces diagram until it reaches the μ_2 -line of constant front friction (sliding friction) at point a_2 . At this moment the vehicle decelerates at a_2 with the front tires locked. The braking force of the (rolling) rear tires is $F_{xR}/W = a_1\Phi$. As the driver continues to increase pedal force, the operating point moves along the μ_2 -constant front friction line until it reaches the rear peak friction μ_2 -line marked a_3 . At this moment, the vehicle decelerates at a_3 with the front brakes locked and the rear brakes operating at their peak friction value. A slight increase in pedal force causes the braking force between rear tires and ground to decrease, causing the operating point to reverse direction along the μ_2 -line of constant front friction until it reaches the constant rear sliding friction μ_2 at optimum point 2. The decrease in deceleration between points 3 and 4 reduces the front tire normal force with an associated decrease of braking forces of the locked front tires. At this moment, the vehicle decelerates with both axles locked at a_4 .

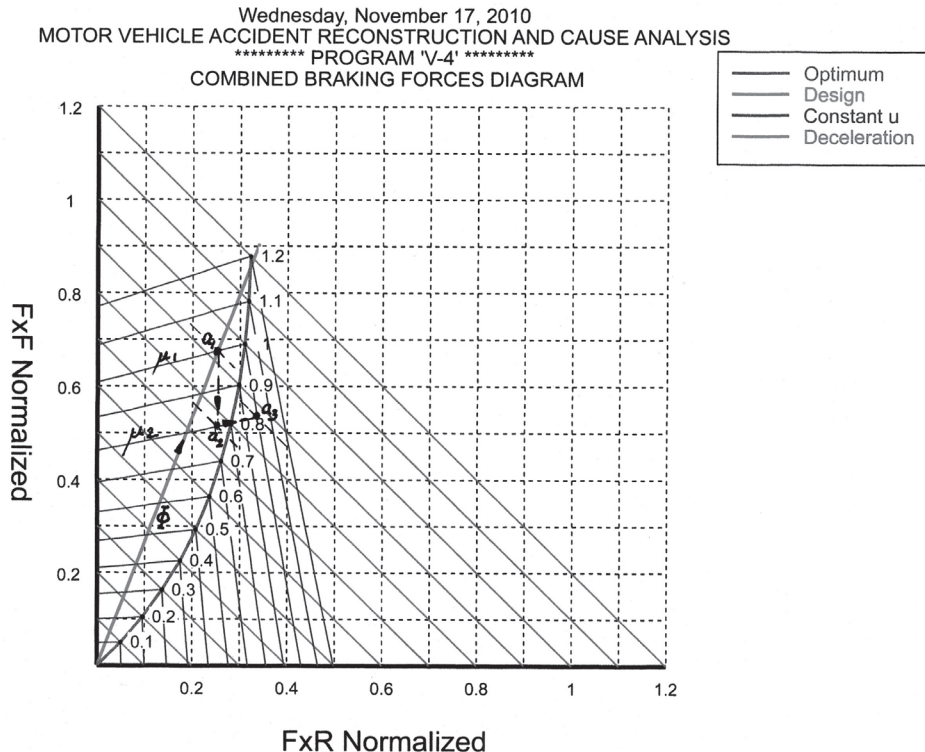


Figure 9-5. Peak and sliding tire friction in the braking forces diagram.

The deceleration at point a_1 is computed by Eq. (7-22b). The deceleration at point a_2 is determined by the intersection of $F_{xR}/W = a_1 \Phi = \text{constant}$ and the equation of the μ_2 -line of constant front friction [Eq. (7-11a)].

1. $F_{xF}/W = (\mu_{2F}\chi) / (1 - \mu_{2F}\chi) (F_{xR}/W) + (1 - \psi)\mu_{2F}/(1 - \mu_{2F}\chi)$
2. $F_{xR}/W = a_1 \Phi$
3. $F_{xF}/W + F_{xR}/W = a_2$

Although F_{xR}/W is known from Eq. (7-22b), the three equations can be solved easily by substituting (2) into (1) and then (1) into (3). The result is deceleration at a_2 :

$$a_2 = [a_1 \phi + (1 - \psi)\mu_{2F}] / (1 - \mu_{2F}\chi) \quad (9-9)$$

The deceleration at point a_3 is determined by the intersection of the lines of constant friction front locked μ_{2F} -line and the peak rear friction μ_{1R} -line [Eq. (7-11b)].

The front (1) and rear (2) constant friction lines at point a_3 are, respectively:

1. $F_{xF}/W = [(\mu_{2F}\chi)/(1 - \mu_{2F}\chi)](F_{xR}/W) + (1 - \psi)\mu_{2F}/(1 - \mu_{2F}\chi)$
2. $F_{xF}/W = -[(1 + \mu_{1R}\chi)/\mu_{1R}\chi](F_{xR}/W) + \psi/\chi$
3. $F_{xF}/W + F_{xR}/W = a_3$

Solving for deceleration a_3 and omitting the lengthy algebra yields

$$a_3 = [(1 - \psi)\mu_{2F} + \psi\mu_{1R}]/[1 + \chi(\mu_{1R} - \mu_{2F})] \quad (9-10)$$

Example 9-2:

For front and rear tires with $\mu_1 = 1.0$ and $\mu_2 = 0.80$, and vehicle data $\psi = 0.52$, $\chi = 0.21$, and $\Phi = 0.273$, compute the decelerations when the front brakes reach peak friction, the front brakes lock, and when rear brakes reach peak friction.

Solution:

Maximum deceleration is [Eq. (7-22b)] a_1 :

$$a_1 = [(1 - 0.52)(1.00)]/[(1 - 0.273) - (0.21)(1.00)] = 0.93 \text{ g}$$

Consequently, the front brakes lock at 0.93 g (or the front ABS would modulate).

At the moment the front brakes lock, the deceleration at point a_2 is

$$a_2 = [(0.93)(0.27) + (1 - 0.52)(0.80)]/[1 - (0.80)(0.21)] = 0.77 \text{ g}$$

When the rear tires reach maximum friction, the deceleration at point a_3 is

$$a_3 = [(1 - 0.52)(0.80) + (0.52)(1.00)]/[1 + (0.21)(1.00 - 0.80)] = 0.86 \text{ g}$$

When the rear tires also lock up, with the front tires already locked, the deceleration is 0.80 g.

9.2.4 Braking from High- to Low-Friction Surface

One of the critical ABS design challenges for the brake engineer exists when a vehicle traveling at high speed and severely braking on a high-friction surface suddenly enters upon a low-friction surface such as ice. The high brake torque at the front axle must be reduced quickly enough not to lock the brake when encountering the low friction coefficient. The braking forces diagram illustrating the braking process is shown in Fig. 9-6. The operating point moves from zero (origin) to the point marked a_1 at the high-friction surface μ_1 , then drops to the low-friction line μ_2 to the point marked a_2 . The deceleration analysis discussed in Section 9.2.3 applies.

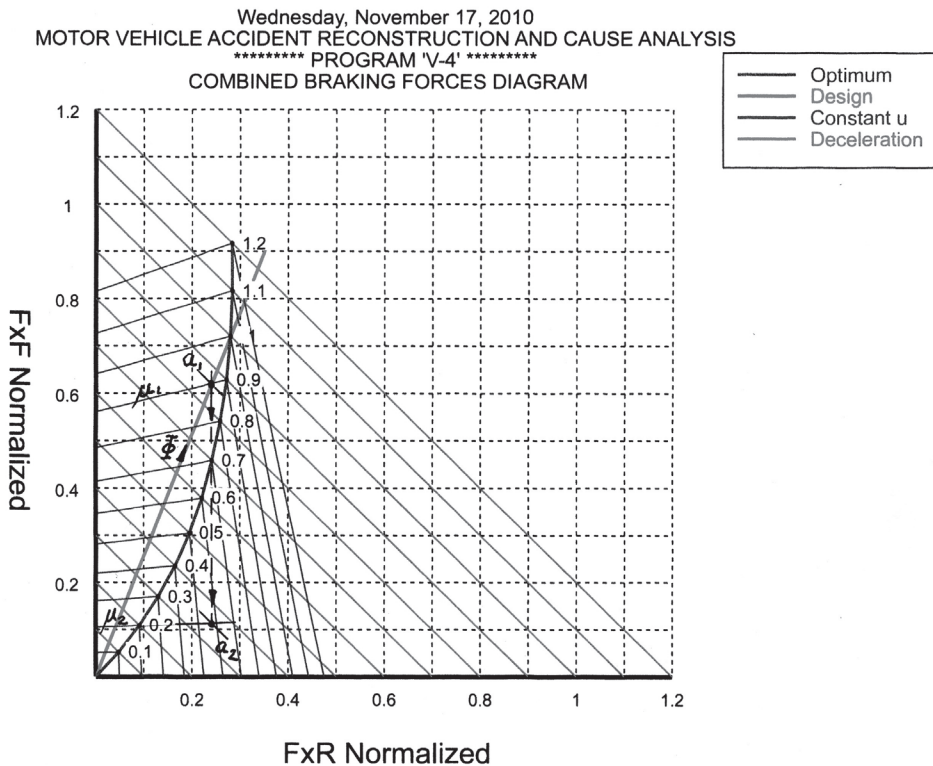


Figure 9-6. High-to-low friction in the braking forces diagram.

A simplified wheel lockup analysis is presented in the following paragraphs. Applying Newton's Second Law in rotation to a braked wheel yields

$$M_{\text{res}} = I_w (d\omega/dt), \text{ Nm (lbft)}$$

or $d\omega = [M_{\text{res}}/I_w]dt, \text{ rad/s}$

Assuming that M_{res} is not a function of time, integration yields

$$\omega_1 - \omega_t = [M_{\text{res}}/I_w]t, \text{ rad/S}$$

where ω_1 = angular wheel velocity just before entering onto slippery road surface μ_2

ω_t = angular wheel velocity as a function of time t .

The wheel stops rotating or locks up when $\omega_t = 0$. The wheel lockup time is

$$t_o = [I_w/M_{\text{res}}]\omega_1, \text{ s} \quad (9-11a)$$

With $\omega_1 = V_1/R_{\text{dyn}}$, Eq. (9-11a) becomes

$$t_o = [I_w/M_{\text{res}}]V_1/R_{\text{dyn}}, \text{ s} \quad (9-11b)$$

For a rear-wheel-drive vehicle without rotating inertias except the wheel assembly, the resulting torque is

$$M_{\text{res}} = M_b - M_r, \text{ Nm (lbft)} \quad (9-12)$$

where

M_b = brake torque of one front wheel while braking on high-friction surface, Nm (lbft)

M_r = road torque attempting to rotate wheel while on low-friction surface, Nm (lbft).

With the assumption that the hydraulic brake line pressure remains constant during the entire braking process, the brake torque of one front wheel is computed by

$$M_b = (1/2)(1 - \Phi)a_1 WR, \text{ Nm (lbft)} \quad (9-13)$$

where

a_1 = maximum deceleration on high-friction surface [Eq. (7-22b)]

$$= \mu_1(1 - \psi)/(1 - \Phi - \mu_1\chi)$$

W = vehicle weight, N (lb)

R = tire radius, m (ft)

The road torque M_r is a function of the normal force on the front wheel caused by the transitional deceleration a_2 while the front tires travel on the low-friction surface:

$$M_r = (1/2)[(1 - \psi) + a_2\chi]\mu_2 WR, \text{ Nm (lbft)} \quad (9-14a)$$

where a_2 is computed from Eq. (9-9).

Substituting Eq. (9-9) into Eq. (9-14a) after rearranging yields

$$M_r = (1/2)[(1 - \psi) + \Phi a_1 \chi - \mu_2 \chi]\mu_2 WR, \text{ Nm (lbft)} \quad (9-14b)$$

Example 9-3:

For a rear-wheel-drive car, compute the time required to lock the front brakes when traveling from a high- to a low-friction surface while braking. Use the data that follow: $W = 17,792 \text{ N}$ (4000 lb), $\psi = 0.5$, $\chi = 0.22$, $\Phi = 0.28$, $\mu_1 = 0.9$, $\mu_2 = 0.2$, $R = 0.366 \text{ m}$ (1.2 ft), $I_w = 1.76 \text{ kgm}$ (1.3 lbfts²).

Solution:

The maximum deceleration is

$$a_1 = \mu_1(1 - \psi)/(1 - \Phi - \mu_1\chi) = 0.9(1 - 0.5)/[1 - 0.28 - (0.9)(0.22)] = 0.86 \text{ g}$$

The deceleration of the vehicle with the front axle on the low-friction surface is [Eq. (9-9)]:

$$a_2 = [(0.86)(0.28) + (1 - 0.5)(0.2)]/[1 - (0.2)(0.22)] = 0.36 \text{ g.}$$

The vehicle decelerates at 0.36 g when the front wheels are on the low- and the rear wheels on the high-friction surface.

The brake torque on the high friction surface is

$$M_b = (1/2)(1 - 0.28)(0.86)(17792)(0.366) = 2016 \text{ Nm}$$

$$\{M_b = (1/2)(1 - 0.28)(0.86)(4000)(1.2) = 1486 \text{ lbft}\}$$

The road torque on the low-friction surface is

$$\begin{aligned} M_r &= (1/2)[1 - 0.5 + (0.28)(0.86)(0.22) - (0.2)(0.22)](0.2)(17792)(0.366) \\ &= 331 \text{ Nm} \end{aligned}$$

$$\begin{aligned} \{M_r &= (1/2)[1 - 0.5 + (0.28)(0.86)(0.22) - (0.2)(0.22)](0.2)(4000)(1.2) \\ &= 244 \text{ lbft}\} \end{aligned}$$

The resulting moment acting on the wheel is

$$M_{\text{res}} = 2016 - 331 = 1685 \text{ Nm}$$

$$\{M_{\text{res}} = M_b - M_r = 1486 - 244 = 1242 \text{ lbft}\}$$

The lockup time as a function of velocity is computed by Eq. (9-11b) as

$$t_o = (1.76)V_1/[(1685)(0.366)] = (0.00285)V_1, \text{ s}$$

$$\{t_o = (1.3)V_1/[(1242)(1.2)] = (0.000872)V_1, \text{ s}\}$$

For a travel velocity of 30.5 m/s (100 ft/s), $t_o = (0.00285)(30.5) = 0.087 \text{ s} = 87 \text{ ms}$. For lower velocities, the lockup time decreases (Ref. 9.8).

If the driver applied the brakes at less than maximum effectiveness, for example, $a_1 = 0.5 \text{ g}$ (instead of 0.86 g), then $M_b = 1172 \text{ Nm}$ (864 lbft) and $M_r = 317 \text{ Nm}$ (234 lbft). The lockup time becomes

$$\begin{aligned} t_o &= (1.76)V_1/[(1172 - 317)(0.366)] = 0.0056V_1, \text{ s} \\ \{1.3V_1/[(864 - 234)(1.2)] &= 0.00172V_1 \} \end{aligned}$$

At 15.2 m/s (50 ft/s), with less than maximum pedal force, the lockup time increases to 85 ms instead of 43 ms at 15.2 m/s (50 ft/s).

In the case of front-wheel-drive vehicles with manual transmission, the lockup time increases because the associated rotating masses must be decelerated by the brakes. For vehicles with automatic transmission and torque converters, the lockup times are less influenced by rotating masses.

“Panic” brake pedal application with extremely high pedal force rates is less critical in wheel lockup analysis than the situation of high-to-low friction surface braking.

The design of the hydraulic modulator determines the hydraulic brake line pressure decrease and increase performance. Extremely quick pressure reduction may cause excessive pressure drops or over shooting. Approximately 60 ms are required to reduce pressure from 80 bar to 20 bar (Refs. 9.4, 9.8).

Using the data of Example 9.3, no-lockup velocity $V_1 = 60/2.8 = 21 \text{ m/s}$ ($60/0.87 = 69 \text{ ft/s}$). Consequently, the vehicle must travel at least 21 m/s or 76 km/h (69 ft/s or 47 mph) to prevent momentary wheel lockup. See Section 5.5 for measured transients of a disc brake system. European ABS regulations allow wheel lockup of not more than 200 ms. Front- and rear-wheel-drive cars should not exceed 150 ms, mid-engine cars 120 ms (Ref. 9.4). The mass moment of inertia of a wheel affects lockup time. Changing from steel to light alloy wheels may decrease lockup time by 7%, while installation of larger, wider tires may increase lockup time by as much as 20%. Temporarily used, small run-flat tires with significantly lower mass moment of inertia will adversely affect ABS performance, particularly on slippery roadways. The mass moment of inertia of tire and wheel for a 185/65 R 15 tire is 0.816 kgm^2 (0.6 lbft^2) for a light alloy wheel and 0.869 kgm^2 (0.64 lbft^2) for a steel wheel. For a 215/65 R15 tire the inertia data are 1.173 and 1.245 kgm^2 (0.865 and 0.918 lbft^2), respectively.

9.2.5 Wheel Speed Sensor Signal Analysis

The signal from the inductive speed sensor is transmitted to the electronic control unit (ECU), where it is evaluated and angular rotational wheel deceleration is determined. The ECU sends appropriate electronic control impulses to the hydraulic pressure modulator valve which affects brake line pressure at the wheel brakes. A proper response of the modulation valve requires a valid data point within approximately 10 ms (Ref. 9.4). For a digital analysis of the speed sensor impulses, approximately 60 impulses are required for one valid data point, requiring a specific number of impulses per pulse ring rotation.

The time t_1 required for one wheel rotation is

$$t_1 = 2\pi R/V, \text{ s}$$

where R = tire radius, m (ft)

V = vehicle velocity, m/s (ft/s)

With n_1 = number of impulses per wheel rotation, the time for one impulse is

$$t_i = t_1/n_1, \text{ s}$$

The time t_{60} required to generate 60 impulses per wheel rotation is

$$t_{60} = [2\pi R/(Vn_1)](60), \text{ s}$$

Because t_{60} should be less than 0.01 s, the number of impulses n_1 per wheel rotation can be determined:

$$n_1 \geq 2\pi R(60)/(0.01V)$$

For example, for $V = 4.57 \text{ m/s}$ (15 ft/s) and $R = 0.305 \text{ m}$ (1 ft), $n_i = 2\pi(0.305)(60)/[(0.01)(4.57)] = 2516$ impulses. Consequently, at least 2516 impulses per wheel rotation must be provided. Current inductive sensor technology does not yield these results. The problem associated with the direct sensor signal is resolved with a carrier frequency signal evaluation. A special device generates large impulse frequencies. The wheel speed sensor-generated impulses are used to open and close a gate in the special device. The number of impulses generated by the device is a function of the wheel speed sensor signals generated. Normally, three wheel speed sensor impulses are averaged to eliminate manufacturing tolerances associated with the pulse ring. The carrier frequency technology provides accurate ABS data analysis for a wide range of speeds (8 to 250 km/h).

A new active sensor technology has been developed where the “Hall” effects and others are utilized in connection with a magnetic field. The designs are compact and can be installed in bearing assemblies where the common bearing seal may assume additional functions usually assigned to the pulse ring (Ref. 9.1). Doppler speed sensors may provide a better velocity sensing system independent of braked wheels (Ref. 9.9). Comparison testing and analysis for specific vehicles have been conducted to determine the accuracy of velocity sensing (Ref. 9.10).

9.3 Basic Performance Requirements of ABS Systems

The design of an ABS system begins with a complete understanding of the tire-road friction characteristics. The braking process in terms of minimum stopping distance would be optimum if the tire slip of the braked tire could always be kept at values corresponding to peak friction levels. Ideally then, a sensor would detect the magnitude of the coefficient of friction at the tire-road interface under all possible conditions, and the rest of the brake system would use this signal to modulate the brake torque in such a manner that the peak friction coefficient would be used throughout the braking process. In practice, it is not feasible to detect the tire-road friction coefficient directly because this would require a fifth wheel as employed in road friction measuring equipment or complex on-board sensors. In addition, optimum slip without side force may be 18%, while for the same tire and a slip angle of four degrees, the optimum slip may increase to 30%.

In general, the following methods have been suggested as modulating parameters for the automatic control of brake torque:

1. Angular velocity of the wheel.
2. Braking slip of the tire.
3. Velocity difference between tire and vehicle.
4. Velocity difference between the tire and the other tires of the vehicle.

Practical sensors measure wheel angular velocity from which wheel deceleration is determined by numerical differentiation. The relative tire slip

ratio is estimated by comparing a measured wheel velocity with a memory of the wheel velocity before initiation of braking. In the early stages of ABS systems, the memory consisted of a flywheel, in the case of purely mechanical ABS systems, or a capacitor, in the case of the earlier analog systems. Today, integrated circuits of microcomputer memory are used. In many ABS systems, longitudinal vehicle deceleration is measured to provide additional data input for brake line pressure modulation. In some cases, lateral acceleration is measured to improve pressure modulation. For vehicles equipped with ESC, a number of sensors are used to measure critical dynamic response parameters.

Performance requirements for wheel antilock braking systems include the following:

1. Retention of steering during ABS control for rapid pressure increases up to 1500 bar/s (21,750 psi/s).
2. Retention of vehicle stability and steering ability is generally more important than minimizing stopping distance.
3. Minimum reaction into steering wheel, especially on split-coefficient road surfaces.
4. ABS must utilize available tire-road friction optimally.
5. ABS must adapt quickly to changes in tire-road friction levels. For example, a vehicle may be braked at maximum wheels-unlocked deceleration on a $\mu = 0.8$ road surface when it suddenly enters onto a slippery $\mu = 0.2$ ice-covered section. A typical passenger car will lock its front brakes in approximately 13 ms for a speed of 5 m/s (16 ft/s) and 50 ms for 20 m/s (66 ft/s).
6. ABS must minimize the yaw moment effects when braking on a split-coefficient road surface.
7. ABS must recognize hydroplaning and maintain directional stability.
8. ABS must provide stable braking while turning.
9. When an ABS malfunctions, the standard brake system must perform safely, i.e., without loss of directional stability. ABS is not a substitute for poor brake balance.
10. ABS must perform properly with all tires specified for the vehicle.
11. ABS malfunctioning must be communicated to the driver. When a mini-spare is supplied, causing ABS failure under certain operating conditions, the driver must be properly warned.
12. Maintenance and repair skills should conform to existing or attainable repair industry practices.

9.3.1 ABS Control Concepts

The ABS system must be designed to respond within the performance characteristics set by the braked tire. The function of the ABS system is to maintain optimum braking performance of all four wheels—or more on a truck and trailer—relative to each other while braking under all foreseeable operating conditions. Two basic criteria are used to sense wheel lockup, namely circumferential or rotational wheel speed deceleration and relative wheel/tire slip (Refs. 9.11, 9.12).

The control of the different brake/wheel systems can be accomplished in several ways.

In *single-wheel control*, the wheel speed sensor of a wheel controls the adjustments made to the brake line pressure of that wheel independent of any other wheels. This control method results in maximum braking on that wheel and, hence, maximum deceleration. On split-coefficient-of-friction surfaces, the different braking forces left and right cause a yaw moment attempting to rotate the vehicle toward the higher-traction side. Single-wheel control is generally used on the front wheels of motor vehicles.

In *select-low control*, the wheel with the lower traction controls the brake line pressure for both brakes on that axle. The traction force on the higher-friction surface is not fully utilized, resulting in a lower brake torque and, hence, longer stopping distance. The advantage is higher side force traction potential and the absence of a yaw moment. Select-low control is typically used on rear wheels of passenger vehicles.

In *select-high control*, the wheel with the higher traction controls the brake line pressure of both brakes on that axle. The results are higher braking force because all traction is utilized; unbalanced brake forces left and right, which cause a yaw moment; and locking of one wheel on the low-friction surface. Vehicles having a front-to-rear dual hydraulic split system in the past have used single- or independent-wheel control on the front and select-low on the rear, with the rear wheel speed sensor located at the differential. Because both rear brakes are controlled as one unit, only one hydraulic control valve is required for the modulation of the rear brake line pressure. Electronic stability control systems require automatic brake application of any of the individual brakes, and consequently require a separate pressure modulator for each brake.

Diagonal hydraulic split systems require four wheel-speed sensors, one for each wheel, and two hydraulic control valves for the rear brakes. Although four sensor and hydraulic channels are involved, the system is only a three-channel system. The select-low control of the rear axle, controlled by the electronic module or computer, provides identical brake line pressure modulation to both rear brakes.

The basic tire characteristics important in ABS design considerations are discussed in Section 9.2. The significant physical relationships for ABS control for straight-line braking are illustrated in Fig. 9-7 (Ref. 9.1), and for braking while turning in Fig. 9-8. The critical control ranges for ABS function are cross-hatched. Inspection of Fig. 9-7 reveals that shorter stopping distances are achieved with ABS brake systems when operating on dry (1), wet (2), and icy (4) road surfaces than when all wheels are locked (100% wheel slip). When braking on snow, the snow wedge forming under the locked tire causes an additional retarding effect.

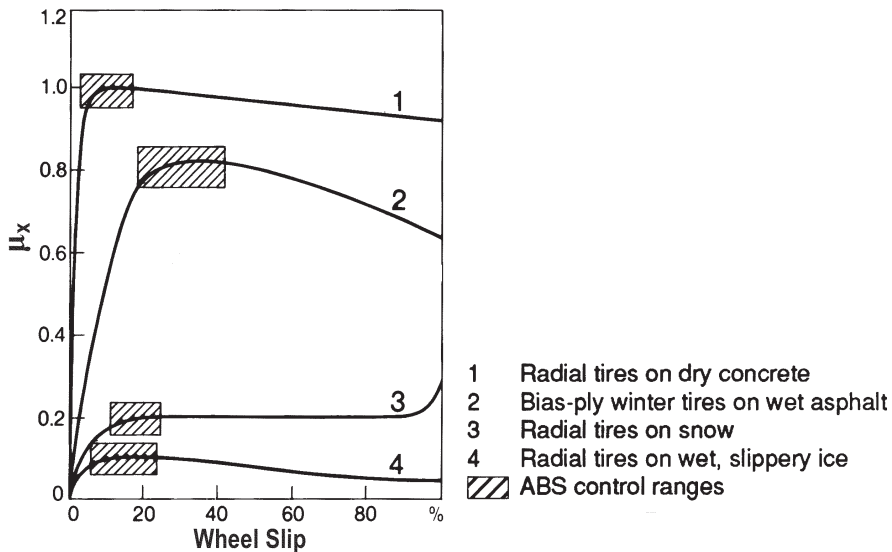


Figure 9-7. Braking coefficient μ_x with ABS control ranges for straight braking.

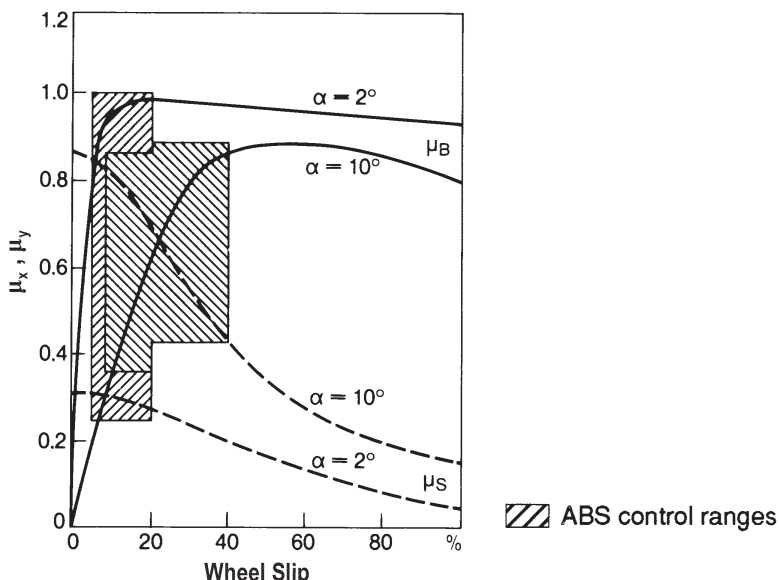


Figure 9-8. Braking μ_x and lateral friction coefficient μ_y with ABS control ranges.

Inspection of the two curves associated with low (2-degree slip angle) and high (10-degree slip angle) lateral acceleration reveals that the ABS control range must cover a wide performance spectrum. During severe braking in a turn, the ABS system should intervene early on with initially low deceleration values while the lateral acceleration is still near its maximum value permitted by the tire-road friction coefficient. As speed decreases and lateral acceleration drops, the ABS system produces increasing levels of braking slip. For optimally designed ABS systems, the stopping distance while turning is only slightly longer than that associated with a straight stop.

A typical ABS control cycle on a high-traction road surface is illustrated in Fig. 9-9. If severe braking occurs on a high-traction road surface, then the modulated brake line pressure increase must occur approximately five to ten times more slowly compared to the pressure increase prior to ABS control. The braking control characteristics reflected in Fig. 9-9 indicate such requirements.

During initial braking, the brake line pressure in the wheel cylinder and the circumferential tire speed decrease and, hence, wheel deceleration increases. At the end of phase 1, the circumferential speed wheel deceleration exceeds the

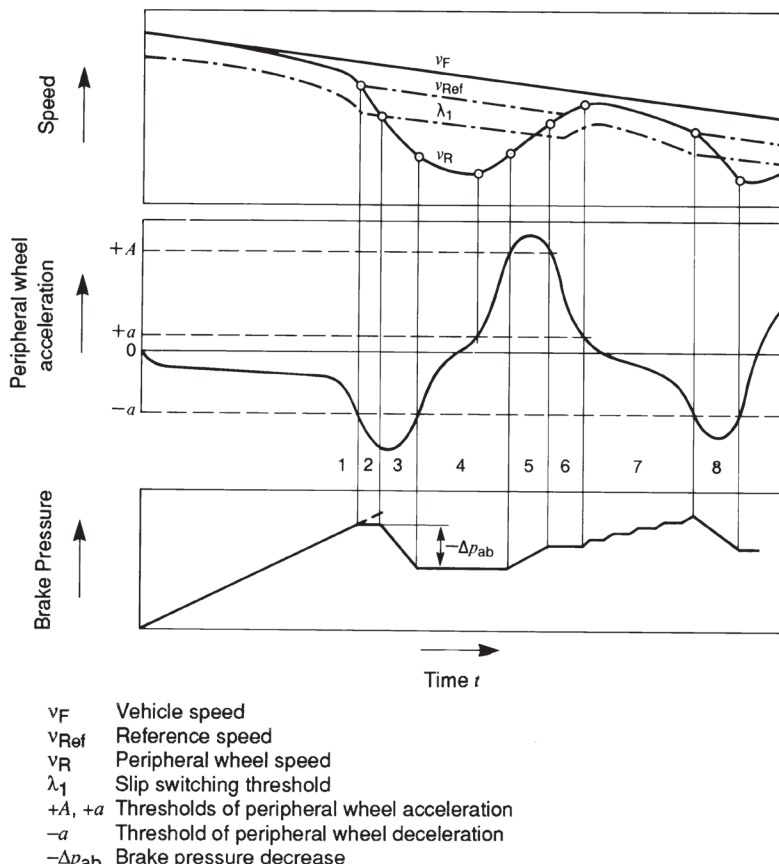


Figure 9-9. Braking control for high-friction surface (Bosch).

set threshold level ($-a$). As a result, the corresponding solenoid valve switches to the pressure-holding position. The brake line pressure is kept constant at this level because the threshold wheel deceleration level could be exceeded in the stable range of tire-road friction coefficient/brake-slip curve, thus avoiding waste of stopping distance. At the same time, the reference speed is reduced along a given ramp function. The value for the slip switching threshold λ_1 is derived from the reference speed.

At the end of the constant pressure phase 2, the wheel speed has dropped below the threshold λ_1 . The solenoid now switches to the pressure-drop position, resulting in reduced brake line pressure until the tire circumferential deceleration has exceeded the threshold value ($-a$). The speed drops below the threshold ($-a$) again at the end of phase 3, and a pressure-holding phase follows. The angular tire acceleration increases within this time period until it exceeds the threshold ($+a$). The brake line pressure still remains constant until the angular acceleration has exceeded the relatively high threshold ($+a$) at the end of phase 4. The brake line pressure then increases as long as the threshold level ($+a$) is exceeded. During phase 6, the brake line pressure is kept constant because the threshold level ($+a$) is exceeded. At the end of phase 6, the circumferential acceleration drops below the threshold ($+a$), indicating that the wheel is operating within the stable range of the friction-slip curve and is slightly underbraked.

The brake line pressure is increased in stages during phase 7 until the angular acceleration exceeds the threshold ($-a$) at the end of phase 7. Here, the brake line pressure is decreased immediately without generation of the λ_1 signal.

Braking control on a slippery low-friction road surface is illustrated in Fig. 9-10. The physical differences from braking on a dry surface are that low brake line pressures with the slippery surface may initiate ABS brake control, and significantly more time is required by the braked wheels to accelerate out of a phase of high slip levels. The logic control unit can recognize these prevailing road conditions and adapt the ABS system characteristics accordingly, as shown in Fig. 9-10. In phases 1 and 2, no difference exists between braking on dry and slippery road surfaces. Phase 3 begins with a pressure-holding phase of short duration. The wheel speed is then very briefly compared with the slip switching threshold λ_1 . Because the wheel speed is less than the value associated with that of the slip switching level, the brake line pressure is reduced for a short fixed time period. This process is followed by a short constant pressure phase. A next comparison between wheel speed and slip switching threshold λ_1 is made, leading to a pressure drop during a short fixed time period. The wheel accelerates again in the following pressure-holding phase, and its circumferential wheel acceleration exceeds the threshold value ($+a$). This condition leads to further pressure holding until the acceleration is again below the threshold value ($+a$) at the end of phase 4. In the following phase 5, step-by-step pressure increase occurs similar to the one for dry road surfaces until a pressure reduction is

initiated at the beginning of phase 6. The controller logic recognizes when the wheel operates in the range of high slip for a relatively long time. To improve driving stability and steerability, a continuous comparison is made between the wheel speed and slip switching threshold λ_1 . Based on this, brake line pressure is constantly reduced in phase 6 until the circumferential wheel acceleration exceeds the threshold value ($+a$) in phase 7. Due to the constant decrease in pressure, the wheel runs with high slip for only a short time, thereby increasing vehicle stability and steerability compared with the first control cycle.

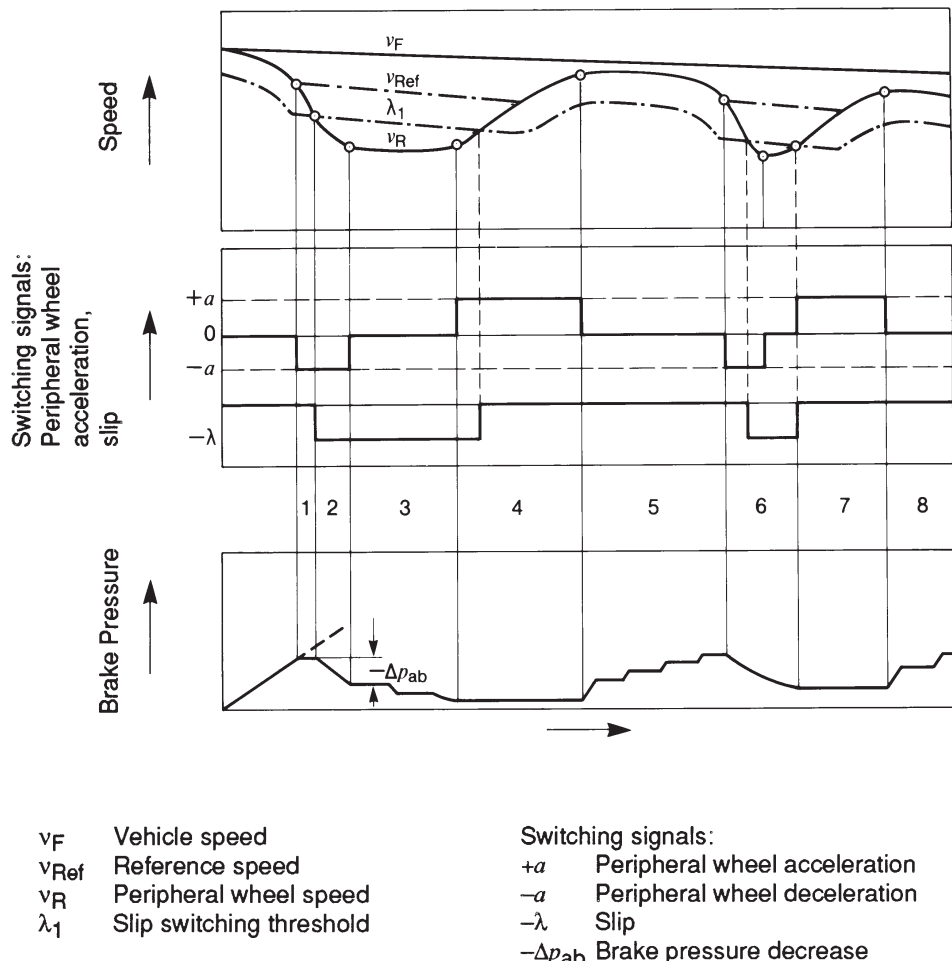


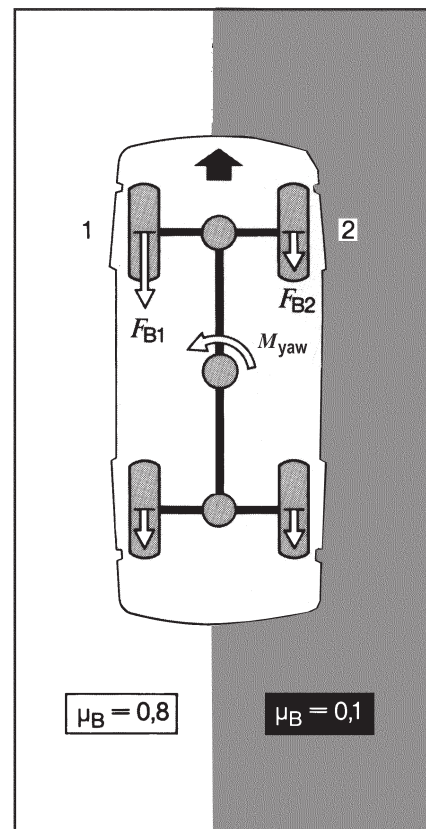
Figure 9-10. ABS control for low friction surface (Bosch)

ABS braking control with yaw moment buildup delay is used when a vehicle brakes on split-coefficient-of-friction surfaces. Extremely different braking forces left-to-right are produced on the front wheels as a result of initial braking on split-coefficient surfaces, as illustrated in Fig. 9-11.

Heavy passenger vehicles with relatively long wheelbases and large mass moments of inertia about their vertical axes develop a yaw motion relatively slowly, permitting the driver to countersteer. Smaller vehicles with lower values of mass moment of inertia require a yaw moment buildup delay system in addition to the basic ABS function of the braking system. For vehicles with low critical handling characteristics, brake line pressure is increased at the “high” wheel in stages or steps as soon as the first pressure reduction caused by wheel lockup tendencies takes place at the “low” wheel. When the pressure at the “high” wheel has reached its locking level, it is no longer influenced by the signals of the “low” wheel; that is, it is individually controlled. This feature ensures maximum braking forces at the “high” wheel while retaining steerability for the vehicle. Because the maximum pressure at the “high” wheel is reached in a relatively short time period, the increase in braking distance is small compared to a vehicle without yaw delay.

For vehicles with particularly critical handling characteristics, the ABS solenoid at the “high” wheel is controlled with a specific pressure-holding and reduction time as soon as the brake line pressure has been reduced at the “low” wheel. The pressure modulation of the “low” and “high” wheels are interrelated depending on vehicle speed. As vehicle speed and the potential for vehicle instability on split-coefficient surfaces increase, the pressure buildup times at the “high” wheel are increasingly reduced, while the pressure buildup times at the “low” wheel are increasingly extended.

The optimum yaw moment delay is a compromise between good steering response and minimized stopping distance. Differences exist between ABS manufacturers. Under extreme conditions, directional stability may be lost for ABS designs where minimum stopping distance is a major design objective.



M_{yaw}	Yaw moment
F_B	Braking force
μ_B	Braking force coefficient
1	“high” wheel
2	“low” wheel

Figure 9-11. Yaw moment control when braking on split-friction surface.

Prior to the electronic stability system, to optimize braking while turning, a lateral acceleration sensor switches off the yaw moment delay feature for lateral acceleration exceeding 0.4 g. Consequently, large braking forces are developed at the outer wheel in the curve which produces a torque directed to the outside of the curve and compensates for the torque of the lateral force. The net result is a slightly understeering vehicle easily controlled by the driver.

Vehicle specific suspension compliance must be considered when designing the wheel speed sensor attachment for an ABS system. Rotational vibrations and/or deformation effects under heavy braking must be kept at a minimum so the sensor signal is not affected. Front-wheel-drive vehicles provide little space alternatives for sensor location. Any signal disturbances must be filtered out by complicated electronic filtering.

When only wheel acceleration is used as the brake line pressure modulating parameter, several control problems arise. Rotating masses connected to the wheel, soft vs. hard brake pedal application, and high later acceleration may be critical. As shown in Section 9.2.1, for tires with a pronounced peak friction value, acceleration control may have certain advantages.

When tire slip is the only modulating parameter, the reference velocity becomes extremely critical. The reference velocity may be adversely affected by the spinning of a wheel. Under these conditions, the calculated reference velocity may be greater than the actual travel velocity of the vehicle. Under these conditions in extreme cases, reduced or no brake line pressure may be generated.

Properly designed ABS systems use both wheel angular acceleration and tire slip as brake line pressure control parameters. Any system control failure is eliminated by generating a new reference velocity for each new modulating cycle while the vehicle is braking (Ref. 9.2).

9.3.2 Electronic Traction and Stability Control Systems

The use of ABS systems has resulted in the design of advanced traction control and vehicle stability systems (Refs. 9.3, 9.13, 9.14, 9.15, 9.16).

The electronic traction system compares the speed of each wheel. If one wheel tends to spin up, then the control modulates the brake of that wheel. Without pedal force, the hydraulic unit must have its own pressure source. Traction control systems automatically apply brake(s) to prevent spinning of the wheel(s).

The advantages include improved traction, increased stability, and relatively low cost. The major disadvantages are thermal loading of brakes, and hence, limitation to lower speeds.

The disadvantages are mostly eliminated when the electronic controls also modulate the engine.

The ESC system includes lateral acceleration and yaw sensors, as well as steering wheel sensors, in most cases, to compare “driver-intended” dynamic data to

actually measured data. When the system “predicts” instability, individual wheels are braked to correct the path of the vehicle.

The electronic stability program was introduced by Mercedes on the A-model vehicle, after the so-called “Moose” test resulted in rollover in severe turning maneuvers.

The electronic stability control system is standard equipment on many new automobiles, SUVs and pickup trucks. By 2012, ESC systems are required by FMVSS 126. With increased numbers of vehicles on the road, an analysis of accident statistics indicates a drastic decrease in single-vehicle crashes and associated fatalities. The purpose of ESC is to assist drivers by preventing loss of directional stability in critical driving maneuvers by fully utilizing available tire traction. When the tire traction limits are exceeded, ESC may not prevent loss of control (Refs. 9.17, 9.18, 9.19, 9.20).

9.3.2.1 ESC Function

In one particular accident investigated by the author, an expensive 1992 sports car spun counterclockwise and entered into an out-of-control spin while traveling at 116 km/h (72 mph). With the left tires on dry pavement and the right tires off the pavement on slippery ground, the driver applied the brakes heavily. Accident scene tire mark measurements indicated that the car had rotated nearly 50 degrees while traveling approximately 10 to 12 m (35 to 405 ft) in a straight line. From being parallel with the roadway to being at 50 degrees took less than 300 ms, or approximately the time of an eye blink. Although the car was equipped with four-wheel ABS, the left-to-right brake imbalance spun the car while the driver was steering straight.

The ESC operates when a critical driving situation develops. The system requires two basic pieces of information: What the driver does, and what the vehicle does. If differences exist between the two, that is, the vehicle travels in a direction where the driver has not steered it, ESC becomes active. If the vehicle under-steers, that is, steers less into the curve than demanded by the driver, ESC automatically applies the rear brake of the inner wheel. In the case of over-steering when the car turns more into a turn than demanded by the driver, ESC automatically applies the front brake of the outer wheel (Ref. 9.1).

In the accident mentioned above, ESC would have known that the driver was steering straight while braking. Modern ABS brakes in conjunction with ESC systems would have prevented any unsafe brake imbalance (Refs. 9.21, 9.22, 9.23, 9.24, 9.25, 9.26).

9.3.2.2 Major ESC Components

Details vary among vehicle and brake manufacturers. The two basic component groups are the sensors and the actuators. The ESC control unit may be separate or directly coupled to the hydraulic modulator. The control unit consists of two computers with individual power supplies. All information is separately analyzed and compared for reliability purposes. If differences exist, the system is disabled.

The steering wheel angle sensor measures the steering wheel rotation input by the driver. The lateral acceleration is measured to determine the severity of the turning maneuver. The yaw rate or angular velocity is measured to determine to what degree a vehicle is rotating/spinning about its vertical axis. In modern systems, lateral acceleration and yaw rate data are measured by a single meter. A pressure sensor measures the actual brake line pressure, which is used by the control unit to compute individual braking forces. A hydraulic pump produces the required brake pressure. The hydraulic modulator houses the different valves for the individual wheel brakes. The valves modulate brake line pressures for pressure increase, maintaining, and pressure decrease. The wheel speed sensors measure wheel rotation, which is used to compute wheel speed. A brake pedal switch measures pedal position and brake light switch actuation. Three dash-mounted control lights are important with respect to the ESC system: ABS, hydraulic brake system, and ESC. When the ESC is operating, engine and automatic transmission controls are affected.

9.3.2.3 What Happens When ESC Is Operating?

Based upon the various data received from the different sensors, the electronic control unit recognizes a critical driving situation. In the hydraulic modulator, hydraulic pressure build-up begins for the affected brake circuit(s) (one for each wheel). The hydraulic pump begins to pump brake fluid from the reservoir into the brake circuit. Pressure accumulators are also used to eliminate pressure buildup time.

Brake line pressure is available at the wheel cylinders/calipers as well as the return pump. The return pump also operates to increase brake line pressure. Once sufficiently high brake line pressure has been achieved, it is maintained at constant level. The inlet valve closes and the return pump stops. If the sensors and computer determine no more braking is required, the outlet valve opens and pressure is released.

9.3.2.4 ESC Malfunctioning

Besides all potential mechanical defects and hydraulic leaks associated with brake systems, electrical/electronic defects can exist with respect to sensors, valves, and hydraulic modulators. Most defects, if any, are associated with wheel speed and steering angle sensors. If the ESC system is malfunctioning, the ESC warning light will illuminate permanently. ESC systems have a self-check system. This means that the system recognizes defects such as electric line failures, shorts, valve operation, or defective sensors in the control unit, hydraulic modulator, and pump.

The computer stores the failure data.

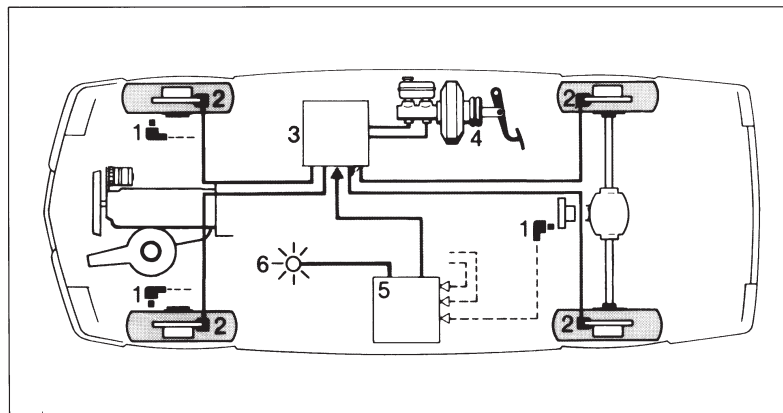
9.4 Hydraulic ABS Systems

9.4.1 Basic Considerations

A schematic of an ABS system is illustrated in Fig. 9-12. A wheel-speed sensor transmits a signal of impending wheel lockup to the logic control which, in

turn, signals a modulator to reduce brake line pressure, which causes the wheel rotational speed to increase again.

Ideally, an ABS system would modulate all four wheels independently so that maximum longitudinal as well as lateral tire forces would be produced. In the single-wheel control, the wheel speed sensor of the wheel controls the adjustments made to the brake line pressure of the wheel, independent of any other wheel. The control results in maximum braking on that wheel and, hence, deceleration. On split-coefficient-of-friction surfaces, the different braking forces left and right will cause a yaw moment, attempting to turn the vehicle toward the higher-traction side. Such a system would allow panic brake applications even while operating near or at the limit of turning speed of the vehicle. Obviously, these specifications require brake system designs with sophisticated and, hence, expensive electronic and hydraulic hardware.



- 1 Wheel speed sensor
- 2 Wheel brake cylinder
- 3 Hydraulic modulator
- 4 Master cylinder
- 5 ECU
- 6 Safety lamp

Figure 9-12. Car with ABS 2S (Bosch).

To reduce cost to a reasonable level relative to the base cost of the vehicle, certain design simplifications can be made while still achieving acceptable ABS performance.

Less expensive than the four-wheel independent system is one that uses independent front wheel modulation and select-low, rear axle control. Here, select-low refers to the fact that the rear wheel operation on the low-coefficient-of-friction road surface controls the modulation of both rear wheels. Some performance degradation from optimum braking on the rear axle occurs when operating on split-coefficient surfaces. This is because the traction force on the higher-friction surface is not fully utilized, resulting in a lower brake torque and, thus, longer stopping distance. The advantage is a high tire side force potential and the absence of a yaw moment. Braking in a turn, as well as straight-line braking performance expressed as vehicle deceleration,

approximates that of four-wheel control systems when operating on typical highways, including wet and dry surfaces.

A further decrease in costs is obtained through systems modulating only the rear axle, either each wheel independently, or the rear axle by sensing the propeller shaft angular velocity. In a panic brake application or while operating on slippery road surfaces, the front wheels can lock, thus rendering the vehicle nonsteerable. Although this provides a stable stop, the accident avoidance characteristics of a vehicle equipped with such a system are not much better than a properly engineered standard brake system when braking on a slippery road while turning. Investigations of accident studies indicate that no significant safety benefits may be expected with stable yet nonsteerable rear ABS vehicles in certain types of accidents, particularly in intersection collisions.

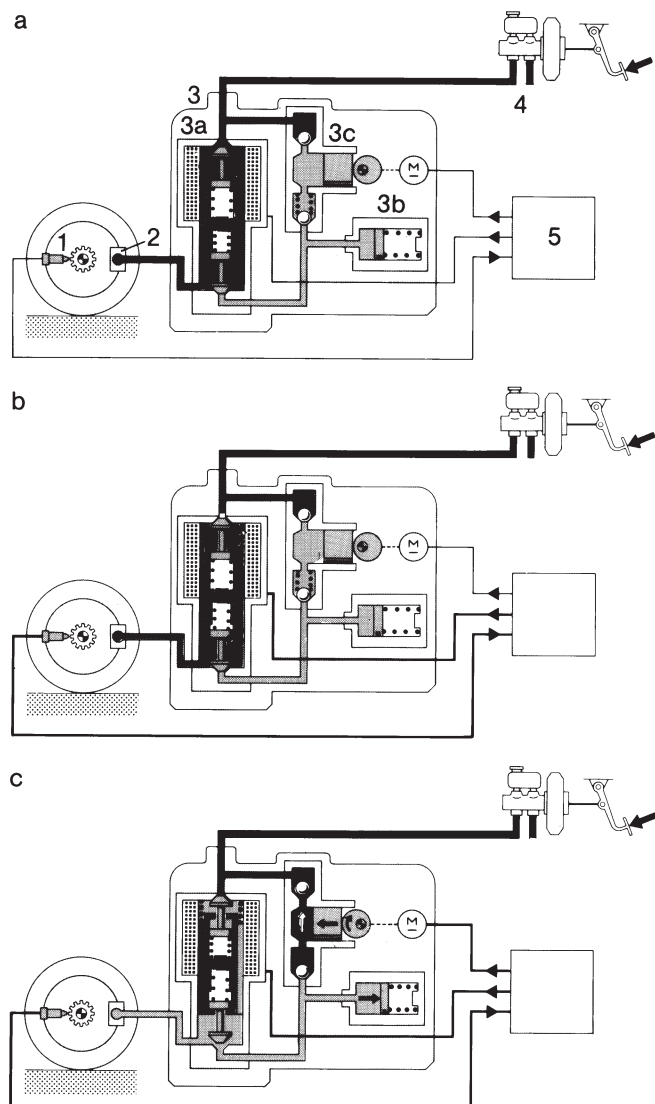
The design of the basic or standard brake system should be such that a stable stop results with the ABS system failed. Consequently, a properly engineered brake force distribution, including the use of proportioning valves, must be considered to ensure front-before-rear lockup.

9.4.2 Separate ABS Systems (Add-On)

In 1978, the separate ABS 2S design manufactured by Bosch was the first antilock brake system to go into mass production with Mercedes Benz automobiles. Other manufacturers followed in the mid-'80s. Developments in digital electronics made it possible to reliably monitor and process the complex performance requirements associated with a braked wheel. The design is very flexible, permitting the addition of the ABS components without modification to the basic hydraulic brake system, as illustrated in Fig. 9-13. It operates as follows: During driving, wheel sensors at each front wheel and at the rear axle differential (or at each rear wheel) measure wheel speed. The wheel speed signals are processed by the electronic control unit ECU, and if a wheel skid is recognized, a solenoid valve is energized in the hydraulic modulator. Each front wheel is controlled by an individual solenoid valve. At the rear axle, the wheel with the lower tire-road traction determines the hydraulic brake line pressure that modulates both rear brakes (select-low control). In the case of the standard front-to-rear split, a single solenoid valve is used for rear brake control, while two solenoid valves are required for a diagonal split. The select-low control employed on the rear axle results in slightly longer stopping distances because the maximum traction is not fully utilized by one rear wheel; however, increased directional stability is achieved.

In the separate ABS design, the modulating pressure cannot exceed the brake line pressure produced by the driver's pedal force in the master cylinder. The ECU switches the solenoid valves into three different positions, depending on the wheel speed signal processing results (Fig. 9-13).

The first de-energized condition connects the master cylinder to the wheel cylinders of the individual brakes for standard brake operation; the hydraulic brake line pressure increases as the pedal force produced by the driver increases. In the second position, the solenoid valve is excited with half the maximum



- | | | | |
|----|----------------------|----|--------------------|
| 1 | Wheel speed sensor | a) | Pressure build-up |
| 2 | Wheel brake cylinder | b) | Pressure holding |
| 3 | Hydraulic modulator | c) | Pressure reduction |
| 3a | Solenoid valve | | |
| 3b | Accumulator | | |
| 3c | Return pump | | |
| 4 | Master cylinder | | |
| 5 | ECU | | |

Figure 9-13. Brake line pressure modulation (Bosch).

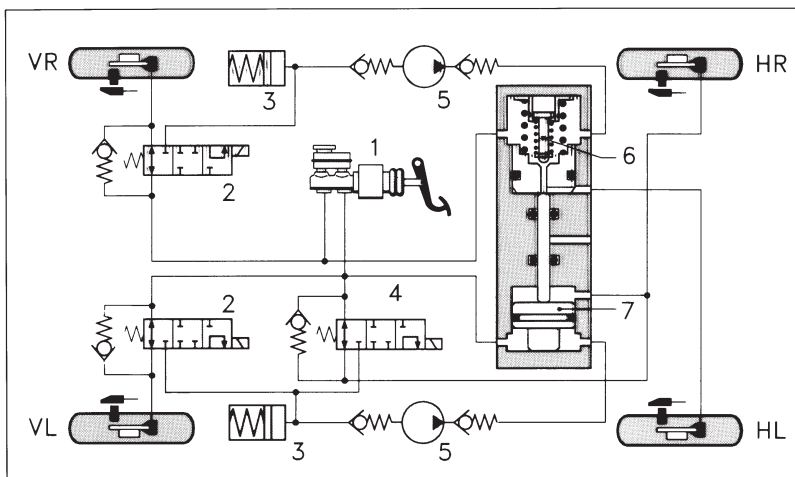
current, resulting in separation of the wheel cylinders from the master cylinder and the return line, and causing the brake line pressure to remain constant. In the third position, the solenoid valve is excited with maximum current, which isolates the master cylinder and simultaneously connects the wheel cylinders with the return line and thus accumulator. In the third position, the brake line pressure decreases, resulting in a drop of wheel brake torque. The three-position valve control permits pressure increase and decrease in stages by cyclical actuation. Depending on the traction and braking conditions, cycle rates may range from four to ten or more cycles per second.

Incorporated in the ECU are safety checks which detect any electrical failure of the ABS system. At the beginning of a trip, and each time the vehicle has stopped, the controller, safety circuits, and associated equipment are checked for proper performance. In particular, components are checked which are not active when braking without ABS and whose failure would be noticeable only when ABS braking is required. If any fault is recognized by the checking process, the entire ABS system or certain portion(s) affected are switched off, a safety lamp lights up on the dashboard, and the brake system returns to standard braking. Hydraulic leaks or other mechanical failures are not detected by the safety check.

ABS systems used for diagonal split braking designs in many cases are based on the same modular system of the front-to-rear split design. The Bosch ABS 2E diagonal split design illustrated in Fig. 9-14 operates as follows: During normal non-ABS braking, brake fluid flows through the rear-axle solenoid valve into the right rear wheel brake marked HR and through the central valve to the left rear wheel brake marked HL. In the case of ABS operation, the two left-hand solenoid valves each control one front wheel brake while the rear solenoid acts directly on the right rear wheel; the rear-axle solenoid valve acts directly on the right rear wheel. If the ECU provides the proper signal, the rear-axle solenoid switches to the pressure-holding mode.

If the pressure in the lower float-piston chamber connected directly with the brake master cylinder increases with respect to the pressure in the upper float-piston chamber connected with the rear-axle solenoid valve, an imbalance is produced which moves the float piston upward and closes the central valve. If the pressure in the right rear wheel brake (HR) is reduced, the float piston continues to move upward until a state of force equilibrium is achieved, i.e., until the brake line pressures in the rear brakes are nearly identical. This design permits the select-low control of the rear brakes by use of one solenoid valve only.

Add-on ABS system designs are reliable. No-failure performance of 15 years and 400,000 km (250,000 miles) are common (1994 Jeep Grand Cherokee of the author). They operate with vacuum or hydraulic booster, and are simply installed between the master cylinder and wheel brakes in an existing brake system. Brake force reduction is achieved through direct drainage of brake fluid from the wheel cylinder circuit to be modulated into a reservoir of limited volume. In each brake circuit, a pump driven by a common electric motor returns the brake fluid from the reservoir to the master cylinder against the



1	Brake booster	V	Front
2	Solenoid valves	H	Rear
3	Accumulator chambers	R	Right
4	Rear-axle solenoid valve	L	Left
5	Dual-circuit return pump		
6	Central valve		
7	Float piston		

Figure 9-14. Hydraulic system ABS 2E for diagonal brake circuit (Bosch).

effective actuation force of the driver's foot. This results in brake pedal pulsation during ABS operation, limits the maximum hydraulic brake line pressure based on the driver's pedal force, and necessitates the employment of central valves instead of vent ports.

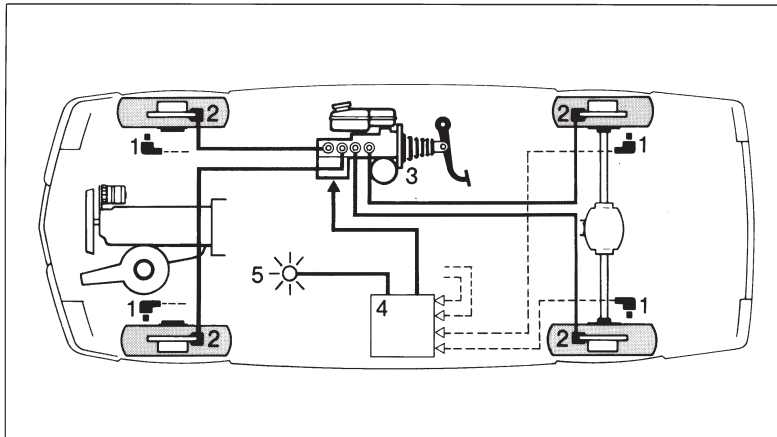
Two-channel ABS systems have been designed to reduce cost for use on diagonal split brake systems. The hydraulic modulator has only two solenoid valves, one for each circuit controlled by the front wheels. The diagonally opposite rear wheel is braked with a given delay through a standard proportioning valve. Pressure modulation always acts simultaneously on one front and one rear wheel. The disadvantage of this system still includes the rare potential for premature rear brake lockup as, for example, in the case of extreme high traction on the front wheel and reduced traction on the rear wheels caused by the use of snow tires on the front wheels and excessive tread wear on the rear tires.

9.4.3 Integrated ABS Systems

In the integrated ABS design, the hydraulic brake booster and the ABS valve block form a closed unit, as illustrated in Fig. 9-15. Advantages include a compact design requiring little space and the ability to select and optimize the performance characteristics of the booster for the particular application at hand. Unlike conventional brake boosters, the brake master cylinder pistons are decoupled from the brake pedal. This makes it possible to size the diameters of the master cylinder pistons so that, in the event of a pressure supply failure, higher brake line pressures and, hence, greater decelerations can be achieved with normal pedal forces. If a brake circuit fails, the counterpressure

at the brake pedal remains stable as a result of the decoupling process. With conventional brake boosters, a brake line failure may cause sagging of the brake pedal due to the absence of some of the resistance force against the brake pedal.

Teves, in 1985, was one of the first companies to introduce a compact integrated ABS system in 1985 on some Ford passenger vehicles. The four-wheel ABS system uses hydraulic brake fluid for the braking function of the wheel brakes and the hydraulic booster. Major system components are master cylinder, hydraulic booster, electric pump, accumulator, electronic controller, reservoir, relays, wheel speed sensors, and warning lights.



- 1 Wheel speed sensor
- 2 Wheel brake cylinders
- 3 Hydraulic modulator with master cylinder
- 4 ECU
- 5 Safety lamp

Figure 9-15. Car with ABS 3 (integrated ABS – Bosch).

The brake booster is located behind the master cylinder in basically a conventional arrangement. The booster control valve is located in a parallel bore above the master cylinder and is operated by a lever mechanism connected to the pushrod of the brake pedal.

The high-pressure electric pump runs at intervals for short periods of time to charge the high-pressure accumulator which supplies the service brakes. The accumulator is a gas-filled pressure chamber mounted to the master cylinder/booster assembly along with the electric motor and hydraulic pump.

Three solenoid valves are used to operate the ABS system. The hydraulic pump maintains pressure between 1400 and 1800 N/cm² (2030 and 2610 psi). When the brakes are applied, a scissor-lever arm activates the control valve. Hydraulic pressure, proportional to the pedal travel, enters the booster chamber. This pressure is transmitted through the normally open rear brake solenoid valve to the rear brakes. The same hydraulic pressure moves the booster piston against the master cylinder piston, which shuts off the central valve in the master cylinder. The result is brake line pressure application to the front brakes through the normally open solenoid valves.

During ABS operation, the electronic control unit causes the solenoid valves to close and open to properly modulate the respective brake line pressure to prevent wheel lock. Integrated ABS systems afford—among other things—simple installation with small space requirements by replacing the master cylinder/vacuum booster assembly. They employ external lines only leading to the wheel cylinders, provide the shortest possible response time of the hydraulic booster due to the use of high-pressure systems, and have a monofluidic design with a single-circuit pump driven by an electric motor, independent of engine speed. Neither separate nor integrated fully hydraulic ABS systems can be rated superior in all respects. However, the basic advantages of integrated ABS systems include simple mounting, free choice in the design of pedal characteristics, lower noise potential, and no sagging of pedal height in the event of a hydraulic circuit failure. Major disadvantages of integrated ABS are complex hydraulic modulation and expensive repairs.

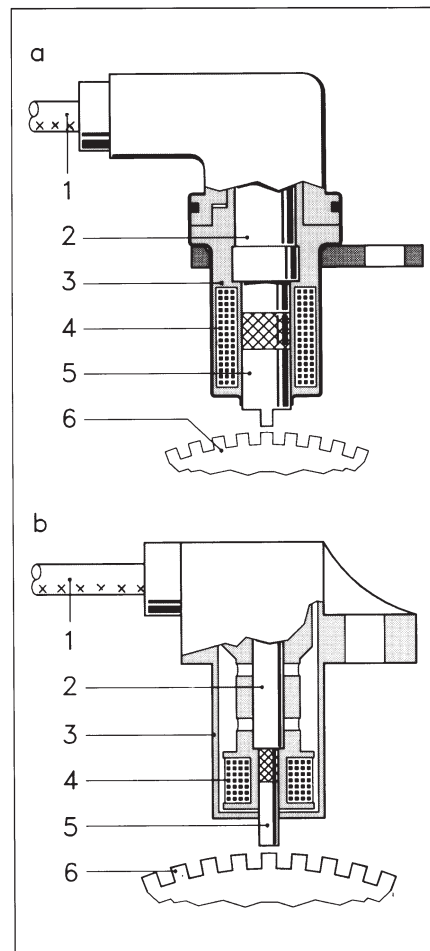
Currently, three major ABS manufacturers provide four-wheel ABS systems for the U.S. Market.

9.5 ABS System Components

9.5.1 Wheel Speed Sensors

The wheel speed sensors signal the wheel speed to the ECU. The pole pin (5) shown in Fig. 9-16 is surrounded by a winding (4) and is located directly over the sensor ring (6), a gear wheel attached to the wheel hub or differential.

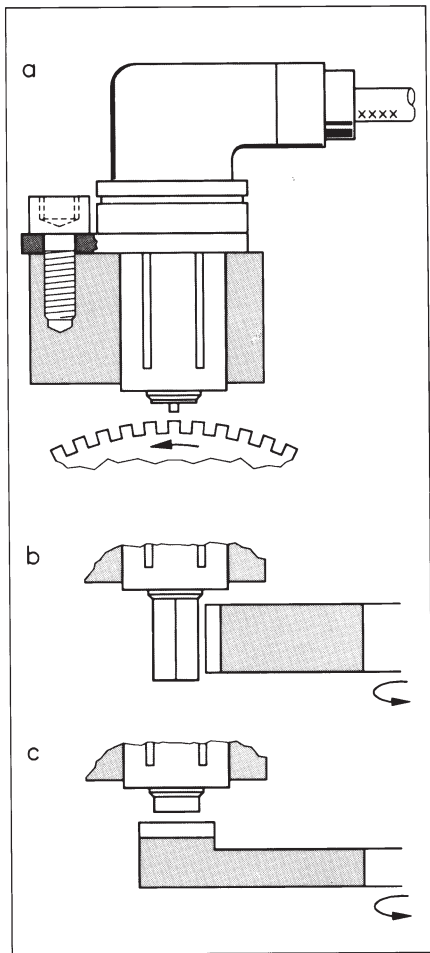
The pole is connected to a permanent magnet (2), the magnetic field of which extends into the sensor ring. When the ring rotates, the pole is faced alternately by a tooth and by a tooth gap. Consequently, the magnetic field changes repeatedly and induces an AC voltage in the winding which is tapped off at the winding ends. The frequency of the voltage serves as a signal for wheel speed. Different pole geometries are



- a) Wheel speed sensor DF2 with chisel-type pole pin
- b) Wheel speed sensor DF3 with round pole pin
- 1 Electric cable
- 2 Permanent magnet
- 3 Housing
- 4 Winding
- 5 Pole pin
- 6 Sensor wheel

Figure 9-16. Typical inductive wheel speed sensors.

illustrated in Fig. 9-17. The pole pin must be aligned to the pulse ring. To ensure a faultless signal, wheel speed sensor and sensor ring are separated from each other only by a closely controlled air gap of approximately 1 mm (0.004 in.). Vibration and deflections must be kept at a minimum. Wheel speed sensors are greased before installation to minimize adverse effects from water splash and dirt.



- a) Radial installation, radial pick-off with chisel-type pole pin
- b) Axial installation, radial pick-off with rhombus-type pole pin
- c) Radial installation, axial pick-off with round pole pin

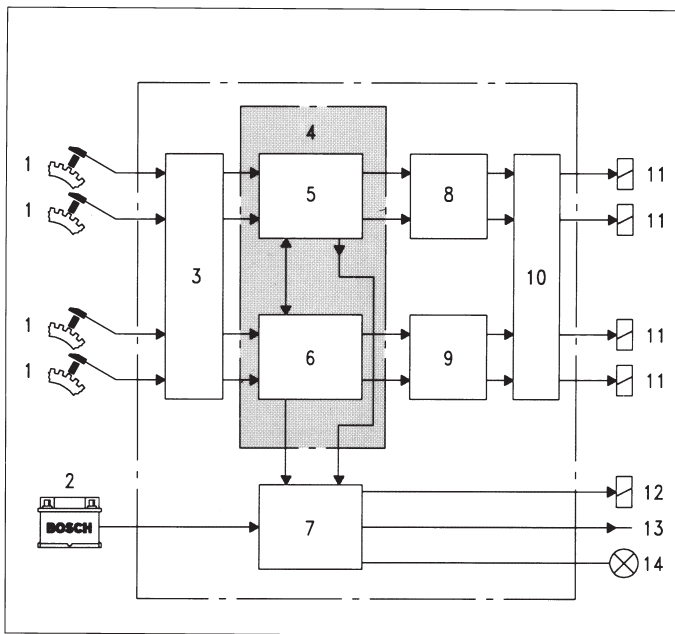
Figure 9-17. Types of installation and pole pin shapes for wheel speed sensors (Bosch).

The sensor system described is a passive or variable reluctance system. The output of the system is a function of the speed of the sensor ring. The signal amplitude is very low at low impulse ring speed; e.g., at 3 to 5 km/h (2 to 3 mph). The development of active electronic sensor components powered by the electrical system of the vehicle has greatly expanded the options for sensor design. "Zero" wheel speed is critical for other functions such as traction control, speedometer, and odometer reading.

9.5.2 Electronic Control Unit (ECU)

The ECU receives, amplifies, and filters sensor signals, as well as measures and differentiates speeds. The input data are used by the ECU to compute circumferential wheel acceleration and braking slip.

The ECU for the ABS 2S Bosch system is illustrated in Fig. 9-18. Only 60 components are installed on the 140-mm board. The digital controller, consisting of two LSI integrated circuits, combines 16,000 transistor functions on a chip area of approximately 37 mm² (0.057 in.²). Discrete semiconductor components for filtering, level adaptation, clock generation, and interference suppression, and power transistors for solenoid valve control supplement these components. The ECU should be installed in a location where high temperatures and splash water are avoided. Modern ECUs are significantly more powerful.



- | | | | |
|---|--|----|----------------------------|
| 1 | Wheel speed sensor (wheel frequencies) | 8 | Output circuit 1 |
| 2 | Battery | 9 | Output circuit 2 |
| 3 | Input circuit | 10 | Output stage |
| 4 | Digital controller | 11 | Solenoid valves |
| 5 | LSI 1 | 12 | Safety relay |
| 6 | LSI 2 | 13 | Stabilized battery voltage |
| 7 | Voltage stabilizer/fault memory | 14 | Safety lamp |

Figure 9-18. Control unit for ABS 2S (Bosch).

9.5.3 Hydraulic Modulator

The hydraulic modulator converts the ECU commands for pressure modulation in the wheel brakes by use of the solenoid valves. It acts as the hydraulic link between the master cylinder or pressure accumulator and the wheel cylinders of the individual wheel brakes.

The hydraulic modulator used for the Bosch ABS 2S is illustrated in Fig. 9-19. The return pump is used to pump the brake fluid coming from the wheel cylinders during pressure reduction to the master cylinder via the appropriate accumulators. The accumulators temporarily store the brake fluid, which is suddenly pumped back as a result of a pressure reduction. The solenoid valves modulate the pressure in the wheel brakes during ABS operation. The basic design of the solenoid valve used in the Bosch ABS 2S system is illustrated in Fig. 9-20. Special design features

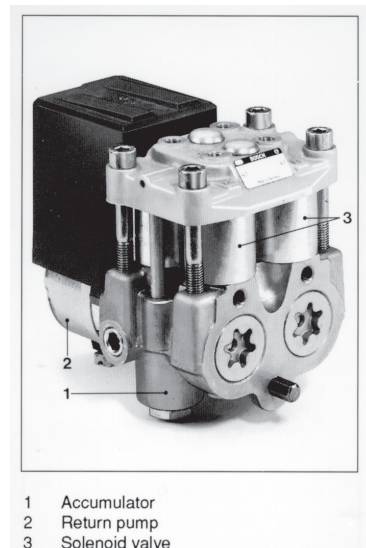
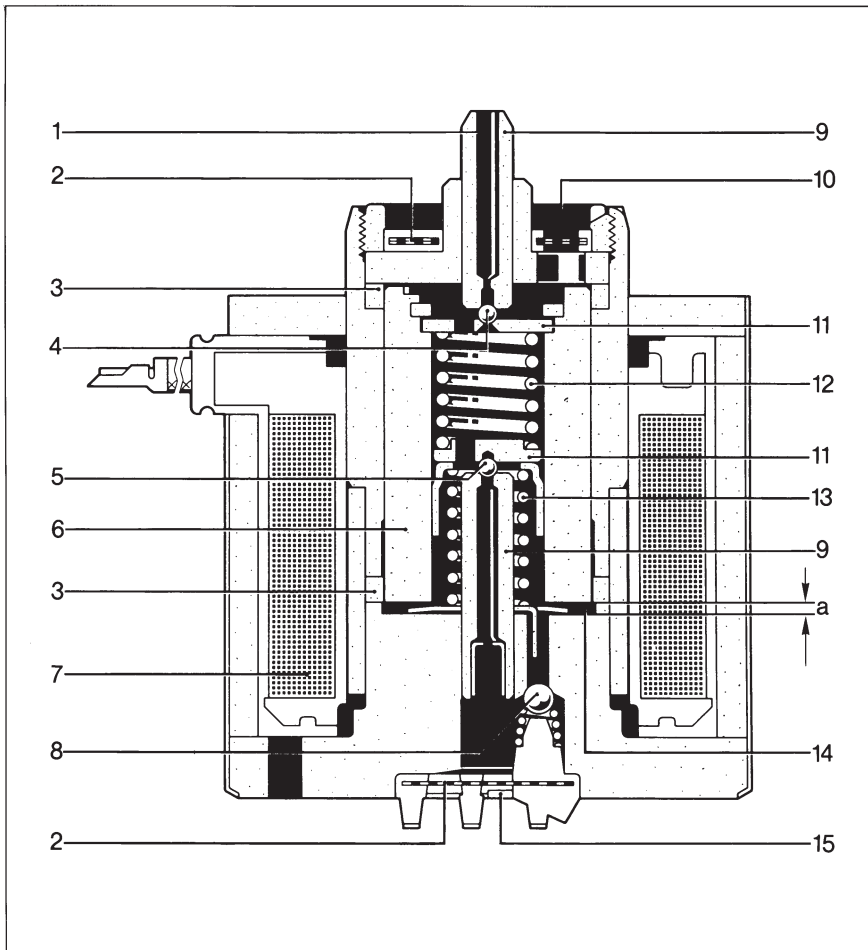


Figure 9-19. ABS 2S hydraulic modulator (Bosch).

employed to ensure high functional reliability and minimum friction involve guiding the moving armature (6) by nonmagnetic bearing rings (3). Steel balls soldered together with carrier plates (11) act as sealing elements. The steel balls are very small. Their seats are hardened and machined to extremely close tolerances to ensure proper sealing, even at pressures as high as 2068 N/cm^2 (3000 psi).



- | | | | |
|---|---------------------------|----|--------------------------------|
| 1 | To the return line | 10 | To the wheel brake cylinder |
| 2 | Filter | 11 | Carrier plate |
| 3 | Non-magnetic bearing ring | 12 | Auxiliary spring |
| 4 | Discharge valve | 13 | Main spring |
| 5 | Intake valve | 14 | Recess step |
| 6 | Armature | 15 | From the brake master cylinder |
| 7 | Winding | a | Working air gap |
| 8 | Check valve | | |
| 9 | Valve body | | |

Figure 9-20. Basic design of ABS 2S solenoid valve (Bosch).

9.5.4 Electric Circuit

The electrical connections between the individual electrically actuated components are combined in a cable harness designed and routed so that water entry is avoided. The ECU checks the voltage drop across certain critical electric lines and, when found faulty, switches the ABS system or subsystem off.

9.6 Drivetrain Influence on ABS

A free-rolling wheel provides the best prerequisites for ABS control. Any additional rotational masses will adversely affect speed sensing and data analysis. Ideally, a driver would place a manual transmission into neutral prior to braking. In emergencies, this will not be the case. Automatic transmissions with torque converters are less sensitive to vehicle inertias because they transmit only a small portion of engine drag.

Rear-wheel-drive vehicles have free-rolling front wheels providing optimum ABS control and generation of a reference speed. The additional rear drive inertias are of little consequence, except on slippery roads.

Front-wheel-drive vehicles present less favorable ABS control conditions due to the rotational inertias affecting the front wheels. Two rear-wheel speed sensors are required because the rear wheels are not connected. Rear suspension effects must be minimized through filtering of the speed signals.

Four-wheel-drive vehicles must disconnect front-to-rear coupling as well as differential locks to ensure proper ABS signal analysis and directional stability while braking. Viscous couplings may be stiff enough to adversely affect ABS performance. Provisions should be made in the gear system to automatically engage a “neutral” gear when the brake light is energized by brake pedal movement. The generation of a proper reference speed is made difficult when only one axle is driven, while the second axle is engaged only under adverse road conditions.

9.7 ABS Systems for Air Brakes

The most significant safety contribution of ABS and ESC to braking of commercial trucks and trailers is the reduction of jackknifing and loss of direction stability, particularly when lightly loaded and operating on low-friction roadways (Refs. 9.25, 9.26, 9.27).

ABS systems for air brakes use concepts similar to those found in hydraulic brake systems. Major components are wheel speed sensors, usually one for each wheel on the axle; an electronic control unit, which collects the sensor information, processes it, and sends control signals; and the air pressure modulation valve, which receives control signals from the ECU and modulates air pressure using electrical solenoids.

9.7.1 Control Analysis

A simple analysis of the ABS control of an air brake system and, in particular,

the brake line pressure modulation as a function of time is reviewed in the paragraphs that follow. Wheel acceleration is used as control parameter. As was mentioned earlier, wheel acceleration may be sufficient for tires with a pronounced peak friction value (Fig. 9-3). In general, both wheel acceleration and tire slip must be used as control parameters. Inspection of Fig. 9-21(A) indicates that no reference velocity is used. Consequently, tire slip is not a control parameter as second line of defense in preventing wheel lockup.

The time-dependent behavior of vehicle speed V and tire circumferential speed $R\omega$ are illustrated schematically for an air brake system in Fig. 9-21(A). The angular velocity of the wheel is designated by ω , and the tire radius by R measured in ft. Shown in Fig. 9-21(B) are the characteristics of brake line pressure p_ℓ as a function of time during the ABS control operation.

As the angular velocity and thus tire circumferential speed $R\omega$ begins to decrease more than the vehicle forward speed V , and reaches a point corresponding to the design threshold angular deceleration α_p , the brake line pressure-modulating valve receives a signal at time t_1 to reduce the pressure. After the response time τ_1 has elapsed, the pressure begins to decrease at time t_2 according to the functional relationship

$$p_\ell = p_{\max} e^{-c_1(t-t_2)} , \text{ N/cm}^2 (\text{psi}) \quad (9-15)$$

where c = time constant indicating pressure decrease characteristics, s^{-1}

p_{\max} = maximum brake line pressure, N/cm^2 (psi)

t = time, s

t_2 = time at which maximum brake line pressure is reached and pressure decrease begins, s

The decrease in brake line pressure causes the angular velocity of the wheel to increase again (Fig. 9-21[A]). Parallel to this process, an angular velocity ω_c is computed from a specified angular deceleration α_r and from the angular velocity ω_p of the wheel at the instant the threshold value α_p was exceeded as

$$\omega_c = \omega_p + \alpha_r(t - t_1) , \text{ rad/s} \quad (9-16)$$

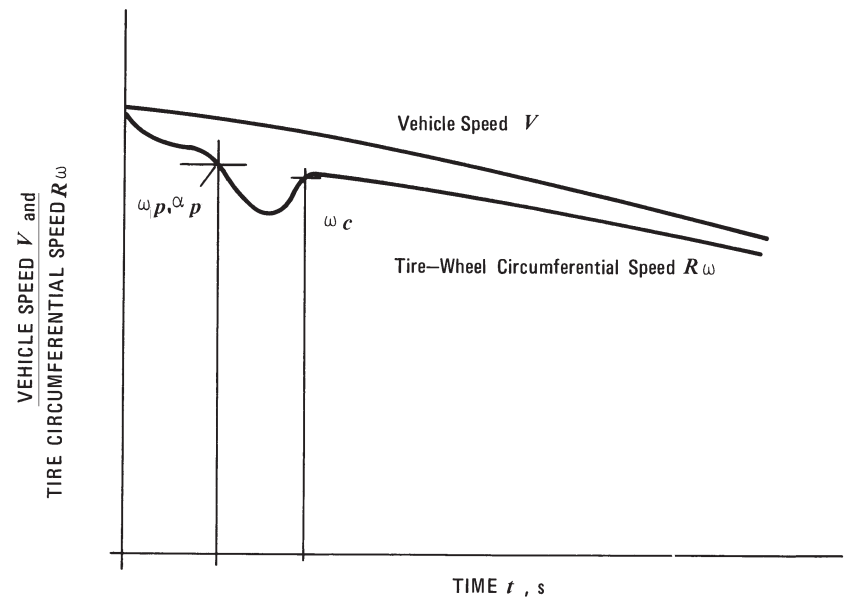
where t_1 = time at which ABS signal is received by the brake pressure modulator valve, s

α_r = specified angular deceleration, rad/s

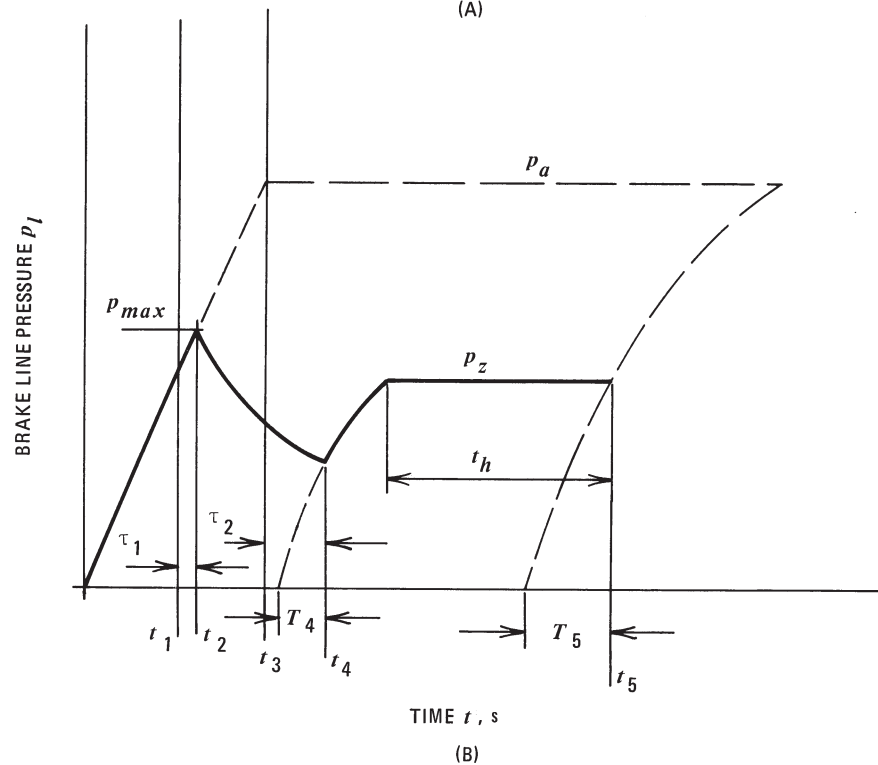
ω_p = wheel angular velocity at peak friction value, rad/s

ω_p is a function of the ABS stop and not a function of vehicle speed as illustrated in Fig. 9-21(A).

When the actual angular speed of the wheel has attained the computed value ω_c at time t_3 , the brake line pressure modulating valve receives the signal to



(A)



(B)

Figure 9-21. Wheel ABS control for an air brake system.

increase pressure again. After the response time τ_2 has elapsed, the brake line pressure begins to increase at time t_4 according to

$$p_\ell = p_a [1 - e^{-c_2(t - t_4 + T_4)}] , \text{ N/cm}^2 (\text{psi}) \quad (9-17)$$

where c_2 = time constant indicating pressure increase characteristics

p_a = applied pressure, N/cm² (psi)

t_4 = time at which pressure increase begins, s

T_4 = difference between time t_4 and time associated with pressure increase from zero pressure, s

The brake line pressure p_ℓ is increased only to a pressure p_z and always remains below the applied pressure p_a . The brake line pressure p_z is generally somewhat smaller than the pressure that causes lockup to occur. However, if the wheel speed tends to lock up again at a pressure equal to or lower than p_z , the previous pressure decreasing and increasing processes are repeated until a pressure p_z is produced which does not cause wheel lockup to occur. This brake line pressure is kept constant until the hold time t_h has elapsed, after which the pressure is increased again toward the applied pressure p_a to allow the ABS system to adjust the braking effort to a different tire-road friction situation that might have developed during the hold time t_h . The pressure increases toward p_a according to the approximate relationship

$$p_\ell = p_a [1 - e^{-c_3(t - t_5 + T_5)}] , \text{ N cm}^2 (\text{psi}) \quad (9-18)$$

where c_3 = time constant indicating pressure increase characteristics, s

t_5 = time at which pressure increase begins, s

T_5 = difference between time t_5 and time associated with a pressure increase from zero pressure, s

The use of an adjustable “hold time” t_h has the advantage that the control frequency is adjustable. This allows the prevention of control frequencies near the natural frequencies of suspension and steering components which otherwise may cause undesirable vibrations and damage to suspension components. The air consumption also may be kept low as a result of an adjustable hold time.

9.7.2 ABS Air Brake Designs

In Europe, the most commonly encountered ABS system is the four-sensor/four-channel system (4S/4C) as illustrated for a truck or tractor in Fig. 9-22. In that system, four wheels are monitored and four channels are individually controlled. The ABS part of the system consists of the wheel speed sensors, the ECU, and the pressure control valves. Pressure control valves can be designed to provide only one modulated pressure output (single-channel), or can be designed to integrate two pressure control valves into one unit (two-channel). The latter reduces cost but requires a larger space for installation.

For commercial vehicles, each wheel usually has a speed sensor. The larger rotational masses and air volume result in cycling frequencies between 2 and 3 Hz. On split-coefficient-of-friction road surfaces, and due to the larger scrub radius, large yaw moments will result. Select-low control is generally not used on commercial vehicles due to the significant increase in stopping distance. To reduce adverse effects on steering control when braking on split surfaces, most ABS systems use a modified individual control on the front axle. A pulsed increase in brake torque on the high-traction wheel results in limiting differences in air pressure left and right, which minimizes the yaw and steering moments. The advantages of stability outweigh the increase in stopping distance resulting from the high-traction wheel not operating at its maximum brake force possible.

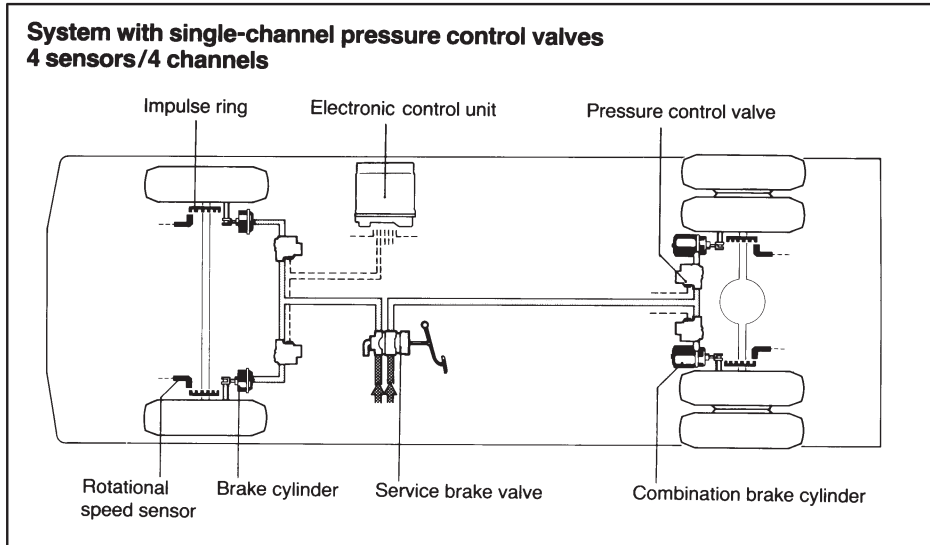


Figure 9-22. ABS for commercial vehicle.

For vehicles with tandem axles, the wheel speed sensors should be installed on the axle experiencing a decrease in dynamic axle loads during braking. When leaf spring suspensions are used, the forward tandem axle will experience a significant decrease of dynamic axle load. For maximum braking effectiveness, both axles should be equipped with speed sensors. For walking beam suspensions, the trailing tandem axle experiences a moderate decrease in dynamic axle load. It should be the wheel-speed-sensing axle.

Chapter 9 References

- 9.1 Proposed FMVSS No. 126, Electronic Stability Control Systems, Office of Regulatory Analysis and Evaluation, National Center for Statistics and Analysis, August 2006.
- 9.2 "Development of Electronic Stability Control (ESC) Performance Criteria," National Highway Traffic Safety Administration, HS 809 974.
- 9.3 *BOSCH Driving-Safety Systems*, 2nd edition, SAE International, Warrendale, PA, 1999.
- 9.4 Burckhardt, Manfred, "Fahrwerktechnik: Radschlupf-Regelsysteme," Vogel Buchverlag, 1993.
- 9.5 Ivanov, Valentin, et al., "Advancement of Vehicle Dynamics Control with Monitoring the Tire Rolling Environment," SAE Paper No. 2010-01-0108, SAE International, Warrendale, PA, 2010.
- 9.6 Salaani, M. Kamel, et al., "Measurement and Modeling of Tire Forces on a Low Coefficient Surface," SAE Paper No. 2006-01-0559, SAE International, Warrendale, PA, 2006.
- 9.7 Bian, Mingyuan, et al., "An Empirical Model for Longitudinal Tire-Road Friction Estimation," SAE Paper No. 2004-01-1082, SAE International, Warrendale, PA, 2004.
- 9.8 Qi, Xuele, et al., "Influence of Hydraulic ABS Parameters on Solenoid Valve Dynamic Response and Braking Effect," SAE Paper No. 2005-01-1590, SAE International, Warrendale, PA, 2005.
- 9.9 Ditchi, Thierry, et al., "On Board Doppler Sensor for Absolute Speed Measurement in Automotive Applications," SAE Paper No. 2002-01-1071, SAE International, Warrendale, PA, 2002.
- 9.10 Arndt, Mark W., et al., "Test Results: Ford PCM Downloads Compared to Instrumented Vehicle Response in High Slip Angle Turning and Other Dynamic Maneuvers," SAE Paper No. 2009-01-0882, SAE International, Warrendale, PA, 2009.
- 9.11 Van Zanten, A. T., "Bosch ESP Systems: 5 Years of Experience," SAE Paper No. 2000-01-1633, SAE International, Warrendale, PA, 2000.
- 9.12 Fennel, H. and E. L. Ding, "A Model-Based Failsafe System for Continental Teves Electronic-Stability-Program (ESP)," SAE Paper No. 2000-011635, SAE International, Warrendale, PA, 2000.
- 9.13 Tandy, Donald F., et al., "The Effect of Electronic Stability Control Following a Rear Tire Tread Belt Separation," SAE Paper No. 2010-01-0113, SAE International, Warrendale, PA, 2010.

- 9.14 Fowler, Graeme F., et al., "Driver Crash Avoidance Behavior: Analysis of Experimental Data Collected in NHTSA's Vehicle Antilock Brake System (ABS) Research Program," SAE Paper No. 2005-01-0423, SAE International, Warrendale, PA, 2005.
- 9.15 Tozu, Kenji, et al., "Development of Vehicle Stability Control System Based on Vehicle Side Slip Angle Estimates," SAE Paper No. 2001-01-0137, SAE International, Warrendale, PA, 2001.
- 9.16 Tang, Xinpeng and Kenichi Yoshimoto, "Research of Driver Assistance System for Recovering Vehicle Stability from Unstable States," SAE Paper No. 2001-01-1276, SAE International, Warrendale, PA, 2001.
- 9.17 Babale, Mike, et al., "Trade-offs for Vehicle Stability Control Sensor Sets," SAE Paper No. 2002-01-1587, SAE International, Warrendale, PA, 2002.
- 9.18 Durisek, Nicholas J. and Kevan J. Granat, "Industry Implementation of Automotive Electronic Stability Control (ESC) Systems," SAE Paper No. 2008-01-0593, SAE International, Warrendale, PA, 2008.
- 9.19 Kinjawadekar, Tejas, et al., "Vehicle Dynamic Modeling and Validation of the 2003 Ford Expedition with ESC Using CarSim," SAE Paper No. 2009-01-0452, SAE International, Warrendale, PA, 2009.
- 9.20 Holler, Gustav and Joseph MacNamara, "Roll Over Prevention on State-of-the-Art ABS Systems" SAE Paper No. 2001-01-2727, SAE International, Warrendale, PA, 2001.
- 9.21 Wang, Huiyi and Chunyu Xue, "Modelling and Simulation of Electric Stability Program for the Passenger Car," SAE Paper No. 2004-01-2090, SAE International, Warrendale, PA, 2004.
- 9.22 Lee, Syun K. and Nancy M. Atkinson, "Understanding the Interaction Between Passive Four Wheel Drive and Stability Control Systems," SAE Paper No. 2002-01-1047, SAE International, Warrendale, PA, 2002.
- 9.23 Kim, Dongshin, et al., "Development of Mando ESP (Electronic Stability Program)," SAE Paper No. 2003-01-0101, SAE International, Warrendale, PA, 2003.
- 9.24 Velardocchia, Mauro and Aldo Sorniotti, "A Failsafe Strategy for a Vehicle Dynamics Control (VDC) System," SAE Paper No. 2004-01-0190, SAE International, Warrendale, PA, 2004.
- 9.25 Chandrasekharan, et al., "Development of a Roll Stability Control Model for a Tractor Trailer Vehicle," SAE Paper No. 2009-01-0451, SAE International, Warrendale, PA, 2009.

- 9.26 Zagorski, Scott B., "A Study of Jackknife Stability of Class VIII Vehicles with Multiple Trailers with ABS Disc/Drum," SAE Paper No. 2004-01-1741, SAE International, Warrendale, PA, 2004.
- 9.27 Zagorski, Scott B. and Richard L. Hoover, "Comparison of ABS Configuration and Their Effects on Stopping Performance and Stability for a Class 8 Straight-Truck," SAE Paper No. 2005-01-3610, SAE International, Warrendale, PA, 2005.

Chapter 10



Analysis of Brake Failure

10.1 Basic Considerations

Brake systems for modern motor vehicles are designed to perform safely for a wide range of normal and different brake failure conditions. A review of a large number of multidisciplinary accident investigation studies as well as others reveals that brake malfunctioning was noted as an accident causation factor in slightly less than 2% of all accidents (Ref. 1.6). Brake failures involved brake lines, brake calipers, wheel cylinders, brake hoses, lining attachment, and lining mismatch. In isolated cases, owners had driven their vehicles without adequate brake maintenance so that ventilated front brake rotors had worn to the cooling vanes, or the swept surface of brake drums had separated from the hub. A review of the individual case reports showed that most brake malfunctioning was caused by faulty maintenance and repair, or lack of maintenance efforts by the owners of the vehicles. Of the 2% brake-related accidents, 89% were associated with brake malfunctioning and 11% with brake imbalance (left-to-right and front-to-rear). ABS brakes and electronic stability controls (ESC) can work effectively only when the underlying brake system is maintained properly.

Manufacturers should realize that poor maintenance must be an input parameter in the design selection process discussed in Chapter 1. Furthermore, meeting a particular safety standard does not by itself mean that the brake system is safe in all respects. For example, when FMVSS 105 became effective with the 1968 model year for passenger cars and pickup trucks, no requirements for braking on wet surfaces with low coefficients of friction were ever included. Brake design engineers, however, had to consider braking on wet and slippery roadways by using low brake torque sensitive drum brakes (leading-trailing shoe versus duo-servo or disc brakes), proper brake balance, and pedal force/deceleration gain.

For commercial vehicles equipped with air brakes, the major problems stem from S-cam brakes being out of proper adjustment, even when automatic slack adjusters are involved. This unsafe condition reveals itself frequently when a runaway truck accident occurs on a downgrade. The brake adjustment may be sufficient for many “normal” brake applications and loads not involving

excessive drum temperatures. However, under severe operating conditions, such as on a downgrade, the brake adjustment is such that no adequate brake shoe application force against the drum can be sustained. Automatic slack adjusters (ASA) required by FMVSS 121 may have become defective after mechanics had adjusted truck brakes manually after relining the brakes (Refs. 10.1, 10.2, 10.3).

10.2 Development of Brake Failure

Brake system failure generally falls into two basic categories: Brake failure caused by a component failure, and intermittent brake failure. Brake failures early in the life of a vehicle with a few miles accumulated usually indicate a manufacturing defect.

10.2.1 Component Brake Failure

In general, component failures are more easily analyzed. Frequently, a specific event indicates a brake component failure, such as a non-releasing, dragging brake indicated by a distinct smell, or disc thickness variation (DTV) revealed by a vibrating brake pedal or steering wheel. Careful inspection, documentation, and testing will reveal the particular component(s) involved in the brake failure. Inspection protocols, examination, and laboratory measurements must be carefully planned, conducted, and documented. Testing must not destroy critical evidence. See Section 10.10 for more details.

Failure of braking system components under ordinary driving conditions is likely to occur only if

1. Parts are defective.
2. Parts become severely worn.
3. Parts become degraded.
4. Parts become mechanically damaged.

Any one of the four conditions indicated can be the result of a design or manufacturing defect, operator abuse, or improper maintenance or repair. A part becomes degraded (e.g., through oil contamination) as a result of a design or manufacturing defect (e.g., leaking seal) or defective maintenance (e.g., improper repair of a seal, depositing grease on the caliper, and contaminating the pads, etc.). A part becomes severely worn through long-time use, abuse, improper installation, wrong part, or other reasons. A part is defective when it is designed, manufactured, or maintained defectively. Brake design defects could involve one component or the entire system in terms of lack of braking stability caused by premature rear brake lockup, front rotor shudder or vibration causing excessive caliper piston push back, and other reasons. Mechanical damage such as a bleeder valve fracture or brake hose leakage caused by road debris can occur suddenly and without warning. A part may become defective due to a design-induced maintenance error.

In a particular accident, the right rear drum brake was “applied” by tire tread road debris, engaging the exposed parking brake cable while the vehicle was traveling at highway speed.

Brake failures generally can be grouped into failures causing (a) insufficient brake force, i.e., stopping distance that is significantly increased over that obtained with normal brakes; (b) excessive component wear; and (c) inconvenience and control problems to the driver.

10.2.2 Intermittent Brake Failure

Intermittent brake failure occurs when the transmission of operator “apply” force to the wheel brakes is temporarily interrupted or degraded. While the driver, prior to the accident, may experience a low brake pedal with little or no pedal force, the investigating officer may find a firm pedal a short time later. Physical evidence indicating intermittent brake failure may be difficult to identify. In some cases, a careful brake system design analysis and specific component testing may be required to determine brake accident causation. If possible, a careful questioning of the driver may yield helpful information about the nature of the brake failure. More details on driver questions and brake system inspection are presented in Section 10.10.

Intermittent brake failure may be caused by a design defect, maintenance error, abuse, or operating under extreme yet foreseeable conditions. In some cases, several of these conditions combine to cause an accident. The primary intermittent brake failure usually results from inadequate force pushing the pads or shoes against the rotor or brake drum. The loss may result from fluid vaporization, or from excessive caliper piston travel required to push the pads against the rotor(s). Intermittent brake failure may affect the entire brake system or only one hydraulic circuit. Brake fluid vaporization results from excessive brake fluid temperature. Brake fluid boiling temperature is lowered when water is present in the subject brake fluid. In most cases excessive fluid temperature is caused by the heat generated between brake pad and rotor. In some isolated cases, excessive fluid temperature may be caused by heat sources other than the brake itself, such as a metal brake line contacting the exhaust after improper repairs were made. In a rare case, the metal bracket holding the rear brake line in place above the differential conducted excessive heat generated by the failing (no lubricating oil) rear differential to the brake fluid. In most cases, a spectral analysis of the subject brake fluid will reveal a threshold temperature exceeded by the fluid. Brake fluid vaporization usually involves a combination of dragging brakes and lowered fluid boiling temperatures due to water content.

Inadequate pad pushing force may result from caliper piston/pad knock back during certain severe steering maneuvers of the vehicle or motorcycle (Refs. 10.4, 10.5). Excessive lateral rotor run-out (LRO) or suspension compliance during severe turning may cause the rotor to push the pad and piston back into the piston bore. The increased piston/pad travel during brake apply may exceed the brake fluid volume available from the master cylinder. Consequently, that portion of the dual circuit master cylinder, or either hand or foot apply in case of a motorcycle, will not generate maximum brake line pressure. The caliper piston travel of a disc brake provided by the master cylinder fluid displacement is very small, normally not greater than 0.7 mm (0.028 in.) per pad. For specific details see Section 5.2.4.

Intermittent brake failure of the vacuum booster occurs only under certain operating conditions. Vacuum power brakes may be severely degraded when the engine is running at high RPMs while braking, resulting in lower than expected boost ratio. Brake systems using pressurized accumulators for brake assist do not suffer from this limitation (Toyota Prius). Diesel engine-equipped pickup trucks using a single steering pump as energy source for both brake and steering assist may adversely affect steering control during a combined braking and steering maneuver with large brake pedal forces.

10.3 Analysis of Partial Brake Failure

10.3.1 Basic Considerations

A partial brake failure exists when certain parts of a brake system fail so that the remaining system can produce only a reduced braking force. The major partial brake failures involve loss of one hydraulic circuit or the loss of power assist. Of lesser significance for passenger cars are brake failures due to excessive brake temperature, simply because they occur only under rare circumstances such as the parking brake remaining partially applied while driving or brake pads not properly returning. Insufficient pad return may be caused by increased friction on disc brake caliper guide pins, or weak or broken return springs in the case of drum brakes.

The purpose of a brake failure analysis is to determine how the intended design effectiveness or deceleration capability of the brake system, i.e., the deceleration/pedal force relationship, is altered if a partial failure should occur within the system. Both FMVSS 105 and 135 require certain braking effectiveness with partial brake failure. The diagonal brake circuits are primarily used in front-drive vehicles (small ψ) to meet federal braking requirements with one circuit failed.

10.3.2 Brake Line Failure

Any brake system contains the mechanisms for pedal force application, pedal force or brake line pressure transmission, and brake force production in the wheel brakes. The mechanism for application of pedal force F_p involves a pedal lever ratio ℓ_p such that a pedal effort $F_p \ell_p$ is applied to the master cylinder pushrod. The pedal force transmission involves a dual-circuit master cylinder and the hydraulic brake lines between the master cylinder and wheel brakes. Connected into the brake lines can be special devices such as metering, proportioning or ABS valves. The wheel brakes may be divided into those having one, two, or more actuating mechanisms (caliper pistons or wheel cylinders). The first category includes leading-trailing and duo-servo-type drum brakes, and single-caliper-type disc brakes with two opposing caliper pistons or single piston floating calipers. In the event of a circuit failure in a braking system using single actuation mechanisms, no braking action can be developed by this brake because none of the "wetted" surfaces in the failed circuit can be pressurized. Brakes involving two or more actuation mechanisms per wheel brake may be connected to separate circuits. In the case of one circuit failure, the wheel brakes produce a reduced braking force, in most cases a braking

action equal to 50% of the nonfailed system. Because the two wheel cylinders may be installed at the top and bottom of a drum brake, such a hydraulic split is sometimes referred to as a horizontal split.

The six basic possibilities for installing brake lines between a tandem or dual master cylinder and the wheel brakes to form two independent brake line circuits are shown in Fig. 10-1. System 1 shows the standard front-to-rear split used in many large rear-wheel-drive cars. Systems 2, 4, 5, and 6 develop equal braking forces for each circuit. In the case of systems 1 and 3, a failure of circuit 1 or 2 will result in different braking forces. The braking forces achievable with systems 2 and 6 are identical in the failed mode for either circuit. The effects on vehicle stability while braking under partial failure mode, i.e., a failure of circuit 1 or 2, will be different, with system 6 showing an undesirable side-to-side unbalance. Because it is obvious that a dual system of type 6 is undesirable, it is not included in any further analysis.

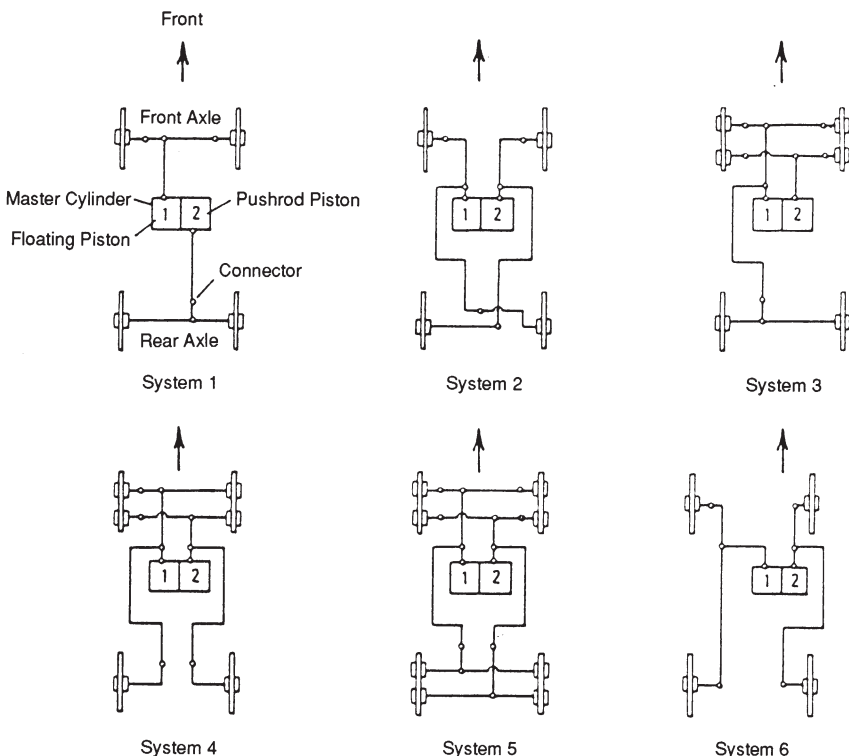


Figure 10-1. Different dual-circuit brake systems.

Three measures of partial braking performance for a dual brake system may be identified.

1. Reduced braking force of the vehicle in the partial failure mode due to a decreased brake system gain between the master cylinder exit and the wheel brakes.

2. Changes in brake force distribution front-to-rear and, hence, reduced braking efficiency, i.e., decreased wheels-unlocked deceleration, or different braking forces left-to-right and, hence, potential for lateral path deviation.
3. Increased pedal application time due to longer brake pedal travel.

All three measures will cause an increase in stopping distance.

10.3.2.1 Vehicle Deceleration

The wheels-unlocked deceleration of a vehicle with nonfailed brakes is computed by Eq. (5-3). The deceleration a , achievable with a complete brake system, may be rewritten as

$$a = (1/W) \sum_i^n [(p_\ell - p_o) A_{wc} BF \eta_c (r/R)] \text{, g-units} \quad (10-1)$$

where A_{wc} = wheel cylinder area, cm^2 (in.^2)

BF = brake factor, defined as ratio of brake drag to actuating force of one shoe

i = identifies location of wheel, i.e., front or rear, left or right

n = number of wheels braked

p_ℓ = brake line pressure, N/cm^2 (psi)

p_o = pushout pressure, N/cm^2 (psi)

r = effective drum or disc radius, cm (in.)

R = effective tire radius, cm (in.)

W = vehicle weight, N (lb)

η_c = wheel cylinder efficiency

Eq. (10-1) may be used to compute the vehicle deceleration with a partially failed system by summing only the braking forces of the wheels not affected by a system failure. In the use of Eq. (10-1) it should be remembered that the brake line pressures front and rear are generally the same in the case of a partial failure because any proportioning valve function is eliminated.

10.3.2.2 Pedal Force

The pedal force F_p is computed by Eqs. (5-1) or (5-5), solved for pedal force:

$$F_p = p_\ell A_{mc} B / \ell_p \eta_p \text{, N (lb)} \quad (10-2)$$

where A_{mc} = master cylinder area, cm^2 (in.^2)

B = power boost ratio

ℓ_p = pedal lever ratio

η_p = pedal lever efficiency

The pedal force/brake line pressure relationship is not affected by circuit failure, as indicated by Eq. (10-2). In other words, a given pedal force still produces the same brake line pressure. However, the same brake line pressure is not as effective in producing deceleration, as an inspection of Eq. (10-1) reveals. Consequently, the pedal force/deceleration relationship is affected by a circuit failure.

The power boost ratio B is affected by the performance of the vacuum booster or effectiveness of the hydro-boost. In the case of a complete power assist failure $B = 1$, and the brake system reverts to manual brakes.

10.3.2.3 Tire-Road Friction Utilization

Friction utilization is a measure of the vehicle to use a given tire-road friction coefficient for maximum deceleration prior to wheel lockup or ABS modulation (see Chapter 7). The maximum wheels-unlocked deceleration $a_{F,max}$ or $a_{R,max}$ for system 1 that can be obtained with the partially failed system on a road surface with a specified tire-road friction coefficient can be determined from Eqs. (7-17a) or (7-17b) with the front brakes failed ($\Phi = 1$), or rear brakes failed ($\Phi = 0$), respectively, and solved for vehicle deceleration. The results are

$$\text{Front failed: } a_R = \Psi \mu / (1 + \mu \chi) , \text{ g-units} \quad (10-3)$$

$$\text{Rear failed: } a_F = \frac{(1 - \Psi) \mu}{1 - \mu \chi} , \text{ g-units} \quad (10-4)$$

where a_F = deceleration with rear brakes failed, g-units

a_R = deceleration with front brakes failed, g-units

μ = tire-road friction coefficient

χ = center-of-gravity height divided by wheelbase

Ψ = static rear axle load divided by vehicle weight

Assuming sufficient brake torque can be developed at a particular axle, the maximum deceleration is only a function of the geometrical and weight data of the vehicle. Similar relationships may be derived for most of the systems indicated in Fig. 10-1.

10.3.2.4 Pedal Travel

The increased pedal travel is a significant factor when braking with one circuit failed. Reasons for this is that more time (from 0.5 to 0.7 s) is required to apply the brakes and the driver may react undesirably to the unfamiliar pedal position. It is not uncommon for drivers to totally abandon pedal application due to the longer pedal travel and reduced vehicle deceleration. For diagonal split brake systems with one circuit failed, the pedal travel will be twice as large as normal while the deceleration will be only half of its normal level. These two

factors may confuse a driver sufficiently to not continue to apply hard pedal forces. Manufacturers should properly educate and warn drivers about this feature generally unknown to the driving public.

The increase in brake system response time may be critical in accident causation when relatively low vehicle speeds are involved. In a school zone, for example, with a speed limit of 32 km/h (20 mph), the vehicle travels approximately 8.9 m/s (29 ft/s). An additional response time of 0.7 s means the vehicle will travel an extra 6 m (20 ft) before the vehicle begins to decelerate.

Because pedal travel is determined by the travel of the master cylinder pistons, the functioning of a master cylinder used in dual-circuit brake systems is discussed next for normal and failed brake system operation. A typical dual-circuit or tandem master cylinder is illustrated in Fig. 10-2. When the pushrod piston is moved toward the floating piston, hole (1) connecting chamber (2) with reservoir (3) is closed. As pedal travel continues, the resulting pressure buildup in chamber (2) is transmitted by the floating piston to chamber (4). The floating piston moves forward and hole (5) connecting chamber (6) closes. At this moment the brake fluid volume in front of each primary cup or seal is closed, and pressurization begins. If each master cylinder chamber has the same diameter, equal pressures are developed in each chamber.

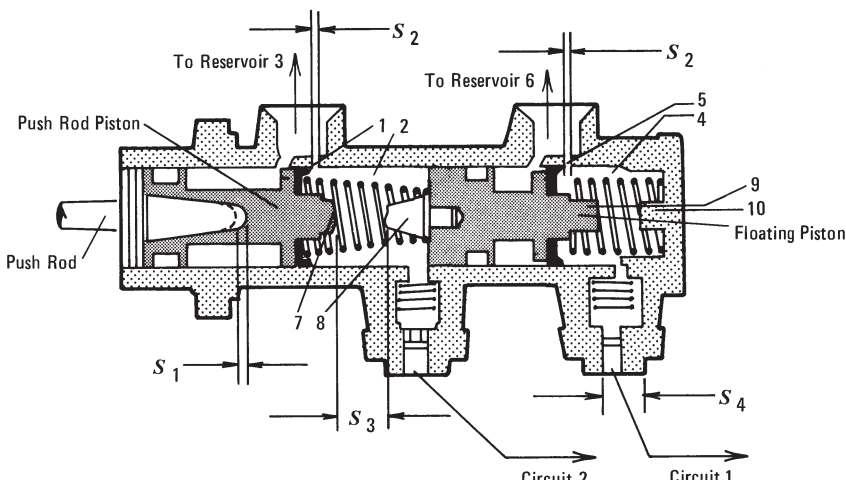


Figure 10-2. Tandem master cylinder.

If the circuit connected to chamber (2) fails through a hydraulic leak at any of its “wetted” surfaces (caliper piston, wheel cylinder, brake lines, fittings, master cylinder primary seal, etc.), no brake line pressure can be developed in chamber (2). This condition forces pin (7) of the pushrod piston to contact pin (8) of the floating piston. The pushrod force is transmitted directly to the floating piston, resulting in pressure buildup in chamber (4).

Similarly, a leak in the circuit connected to chamber (4) causes floating piston pin (9) to come in contact with stop (10). At this instant, brake line pressure can be developed in chamber (2) by the pushrod piston. The pedal travels in either

failure mode are longer than in the nonfailed condition. Longer pedal travels result in increased time before the brakes are applied and, hence, longer stopping distance. Measurements of pedal displacement indicate that a pedal travel of 127 mm (5 in.) requires approximately 0.25 s for the 90th percentile male driver.

The pedal travel is determined by the travel of the pushrod piston. Because the pushrod piston travel is affected by the travel of the floating piston, the following travels are identified and illustrated in Fig. 10-2:

1. Travel S_1 to overcome pushrod play:

$$S_1 \approx 0.02S_{av} \quad , \quad \text{mm (in.)}$$

where S_{av} = average pedal travel required for stop, mm (in.)

2. Travel S_2 to overcome hole or compensating port connecting chambers (2) or (4) with reservoir:

$$S_2 \approx 0.06S_{av} \quad , \quad \text{mm (in.)}$$

3. Possible travel S_3 of pushrod piston available for pressure buildup:

$$S_3 = kS_{av} \quad , \quad \text{mm (in.)}$$

4. Possible travel S_A of floating piston available for pressure buildup:

$$S_4 = (1 - k)S_{av} \quad , \quad \text{mm (in.)}$$

where k = ratio of pushrod piston travel S_3 to available travel of the pistons of the tandem master cylinder S_{av}

S_{av} = $S_3 + S_4$, travel of pistons associated with tandem master cylinder, available for pressure buildup, mm (in.)

The factor k generally assumes values between 0.9Φ and 1.25Φ , where Φ is the ratio of rear brake force divided by total brake force (see Section 7.4).

The maximum pedal travel $S_{p,max}$, determined by the maximum travel of the pistons of the master cylinder, the pushrod play, and the pedal lever ratio, is

$$S_{p,max} = \ell_p (S_1 + S_2 + S_3 + S_4) \quad , \quad \text{mm (in.)} \quad (10-5)$$

Eq. (10-5) can be rewritten with the previous expression for the individual travels as

$$\begin{aligned} S_{p,max} &= \ell_p S_{av} (0.02 + 0.06 + k + 1 - k) \\ &= 1.08 \ell_p S_{av} \quad , \quad \text{mm (in.)} \end{aligned} \quad (10-6)$$

where ℓ_p = pedal lever ratio

The travel of the pushrod piston and floating piston actually used in a normal braking situation is less than the maximum design value S_3 and S_4 . Let ρ be the

ratio of the actual travel used for pressure buildup by the pushrod piston and floating piston to the available travel of pushrod piston and floating piston. The brake pedal travel for normal braking for the nonfailed and failed brake system may then be represented by the following expressions:

1. Service brake not failed:

$$\begin{aligned} S_{p,nor} &= \ell_p S_{av} [0.08 + \rho k + \rho(1 - k)] \\ &= \ell_p S_{av} [0.08 + \rho] , \text{ mm (in.)} \end{aligned} \quad (10-7)$$

where ρ = ratio of actual piston travel used for pressure buildup to available piston travel

2. Circuit failure, system 1 (Fig. 10-1):

- Circuit No. 1 failed, i.e., the front brakes are failed and the rear brakes are operative, and the floating piston develops no brake line pressure

$$\begin{aligned} S_{p,rear} &= \ell_p S_{av} (0.08 + \rho k + 1 - k) \\ &= \ell_p S_{av} [1.08 - k(1 - \rho)] , \text{ mm (in.)} \end{aligned} \quad (10-8)$$

Eq. (10-8) is obtained from Eq. (10-7) by substituting the entire travel of the floating piston available into Eq. (10-7), i.e., $\ell_p S_{av} (1 - k)$ and not $\ell_p S_{av} \rho (1 - k)$ used in normal braking without brake failure.

- Circuit No. 2 failed, i.e., the rear brakes failed and the front brakes are operative, and the pushrod piston develops no brake line pressure

$$\begin{aligned} S_{p,front} &= \ell_p S_{av} [0.08 + k + \rho(1 - k)] \\ &= \ell_p S_{av} [0.08 + \rho + k(1 - \rho)] , \text{ mm (in.)} \end{aligned} \quad (10-9)$$

3. Circuit failure, system 2 (Fig. 10-1):

Any circuit failed:

$$S_{p,failed} = \ell_p S_{av} [0.58 + 0.5\rho] , \text{ mm (in.)} \quad (10-10)$$

4. Circuit failure, system 3 (Fig. 10-1):

- Circuit No. 1 failed, i.e., the floating piston develops no brake line pressure

$$S_{p,failed} = \ell_p S_{av} [1.08 - k(1 - \rho)] , \text{ mm (in.)} \quad (10-11)$$

- Circuit No. 2 failed, i.e., the pushrod piston develops no brake line pressure

$$S_{p,failed} = \ell_p S_{av} [0.08 + \rho + k(1 - \rho)] , \text{ mm (in.)} \quad (10-12)$$

5. Circuit failure, system 4 (Fig. 10-1):

Any circuit failed:

$$S_{p,failed} = \ell_p S_{av} [0.58 + 0.5\rho] , \text{ mm (in.)} \quad (10-13)$$

6. Circuit failure, system 5 (Fig. 10-1):

Any circuit failed:

$$S_{p,failed} = \ell_p S_{av} [0.58 + 0.5\rho] , \text{ mm (in.)} \quad (10-14)$$

10.3.2.5 Vehicle Stability Analysis

Dual-circuit splits producing different braking forces on the left and right wheels during a circuit failure will generate a rotating moment about the vertical axis of the vehicle. For the diagonal dual circuit, a negative scrub radius on the steered front wheels produces a steering moment during braking which automatically turns the front wheels in such a direction that a rotation of the vehicle is avoided. When properly designed, the vehicle will travel in a straight path without the driver having to turn the steering wheel.

During braking, the retarding forces between tire and ground tend to rotate the vehicle in the direction of the nonfailed front brake. For the vehicle to continue to travel straight, the side forces generated at the front and rear wheels must be of equal magnitude, but opposite direction. Because the side forces act on different lever arms, the resulting moment counteracts the moment due to braking. For side forces to be produced, both front and rear tires must generate slip angles, i.e., the vehicle will run under a small slip angle.

A stable braking maneuver will be achieved with a diagonal circuit split failure when the summation of moments due to braking, due to the side forces produced by slip angles, and due to tire realignment moment is equal to zero.

A negative scrub radius will cause the moment summation to be close to zero. If the summation is greater than zero, the driver must countersteer to maintain vehicle control.

10.3.3 Performance Calculations

The three performance measures were applied to a particular case. No attempts were made to express longer pedal travels in terms of increased application times. It may be assumed that application time increases linearly with pedal travel.

The deceleration achievable by a passenger vehicle with different circuit failures was computed and is shown in Fig. 10-3. A maximum tire-road friction coefficient of $\mu = 1.0$ was assumed for columns 1 and 4. The tire-road friction coefficient for the computations of columns 2 and 3 was assumed large enough to prevent lockup. The column identified by "Wheels Unlocked" (1) represents the maximum deceleration that can be attained by the different systems with either circuit No. 1 or No. 2 failed prior to any brake lockup or ABS modulation. The deceleration achievable with the nonfailed system is indicated also. The column identified by "No Proportioning" (2) gives the deceleration that can be achieved

with a brake system with a fixed brake force distribution and a pedal force of 489 N (110 lb) with either circuit No. 1 or No. 2 failed. The column identified by "Proportioning" (3) represents the deceleration that can be achieved by a vehicle having a brake system with proportioning valve. In this case, the proportioning valve is not affected by the failure of the front brakes, i.e., the proportioning valve is not bypassed when the front brakes are failed. The column identified by "Wheels Locked" (4) gives the maximum deceleration achievable on a $\mu = 1.0$ friction surface without regard to pedal force and lockup. Column 5 provides information on braking stability.

Inspection of Fig. 10-3 reveals that the performance of system 1 is limited to a deceleration of 0.25 g with circuit No. 1 failed, i.e., the front brakes inoperative, when a proportioning valve is installed which is not bypassed when the front brakes are failed. Proportioning valves generally are bypassed when the front circuit fails. With the proportioning valve bypassed, the deceleration achievable with a pedal force of 489 N (110 lb) is 0.5 g with the front brakes failed. Inspection of the deceleration values reveals whether the pedal force and brake system gain or tire-road friction determines the deceleration available. For example, a system with proportioning and a pedal force of 489 N (110 lb) produces a deceleration of 0.25 g for system 1 with circuit No. 1 failed. If no

	1 Wheels Unlocked		2 No Proportioning Pedal Force 110 lb		3 Proportioning Pedal Force 110 lb		4 Wheels Locked		5 Vehicle Side to- Side Stability
	1	2	1	2	1	2	1	2	
No Failure	0.80		1.23		1.23		1.00		Stable
Circuit Failed	1	2	1	2	1	2	1	2	
System 1 	0.41	0.64	0.50	0.73	0.25	0.73	0.41	0.64	Stable
System 2 	0.48	0.48	0.62	0.62	0.49	0.49	0.50	0.50	Unstable
System 3 	0.64	0.61	0.37	0.86	0.37	0.62	0.64	1.00	Stable
System 4 	0.48	0.48	0.62	0.62	0.49	0.49	0.84	0.84	Unstable
System 5 	0.80	0.80	0.62	0.62	0.49	0.49	1.00	1.00	Stable

Figure 10-3. Calculated deceleration in g-units for partial failure.

pedal force limit is set, the tire-road friction coefficient permits deceleration of 0.41 g, which indicates that either the pedal force must exceed 489 N (110 lb), or if that is undesirable, the brake system gain must be increased.

Indicated in Fig. 10-3 are also the effects of side-to-side brake unbalance on vehicle stability. Only systems 2 and 4 exhibit a measure of vehicle stability with circuit failure. The influence of an unbalance on the front and rear wheels such as experienced by system 2 (diagonal brake system split) could, to a large extent, be counteracted by a negative scrub radius.

The pedal force analysis was applied in detail to the front-to-rear split identified as system 1. Brake system data of a large automobile were used as a base for computing the pedal travels required to perform a stop under partially failed conditions. The results are shown in Fig. 10-4 in terms of pedal travel ratios. The pedal travel ratios shown in Fig. 10-4 are the pedal travel for normal nonfailed braking to maximum travels available; the pedal travel with the front brakes failed to the maximum travel available; and the pedal travel with the rear brakes failed to maximum travel available. The values were computed for $\rho = 0.5$, i.e., 50% of the available master cylinder piston travel is required for a service brake stop.

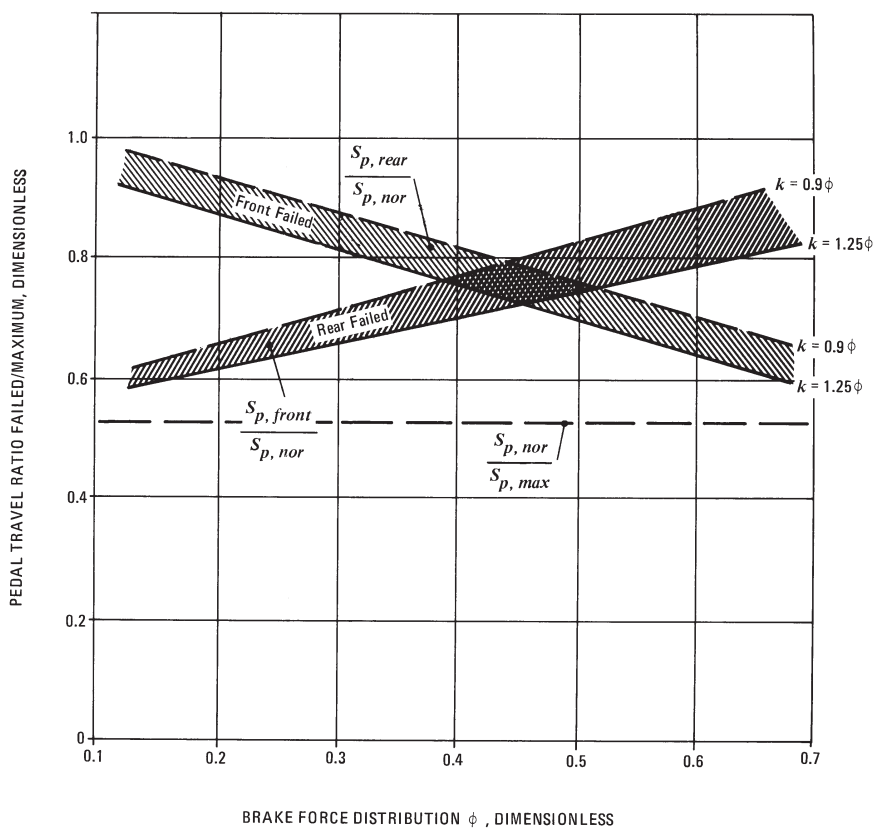


Figure 10-4. Maximum pedal travel ratios required for partial failure stops, system 1.

Inspection of Fig. 10-4 reveals that in the case of a failure of the front brakes, the ratio of pedal travel required to apply the rear brakes to maximum pedal travel is nearly twice the ratio for the nonfailed or normal brakes for brake force distributions Φ less than 0.3. In other words, for $\Phi = 0.3$ or less, the front brake fluid requirements due to a large caliper piston or wheel cylinder cross-sectional area tend to be significantly greater than those for the rear brakes, and in the case of a front brake failure, cause a significantly greater master cylinder piston travel for the front circuit and pedal travel drop toward the floor than in the case of a rear brake failure.

The ratios of pedal travel under failed conditions to those required under normal conditions (not maximum pedal travel as shown in Fig. 10-4) may be a more meaningful pedal feedback indicator to the driver. These ratios are presented in Fig. 10-5. Inspection of Fig. 10-5 clearly reveals again that the standard front-to-rear split requires significant pedal travels in the event of a front brake failure and small values of Φ . This condition exists in spite of a rather long master cylinder piston travel, as indicated by $\rho = 0.5$, used in the calculations. Front-to-rear dual brake systems are used on vehicles having front-to-rear weight distributions not requiring extremely low Φ -values to prevent premature rear wheel lockup, i.e., vehicles with relatively large Ψ -values.

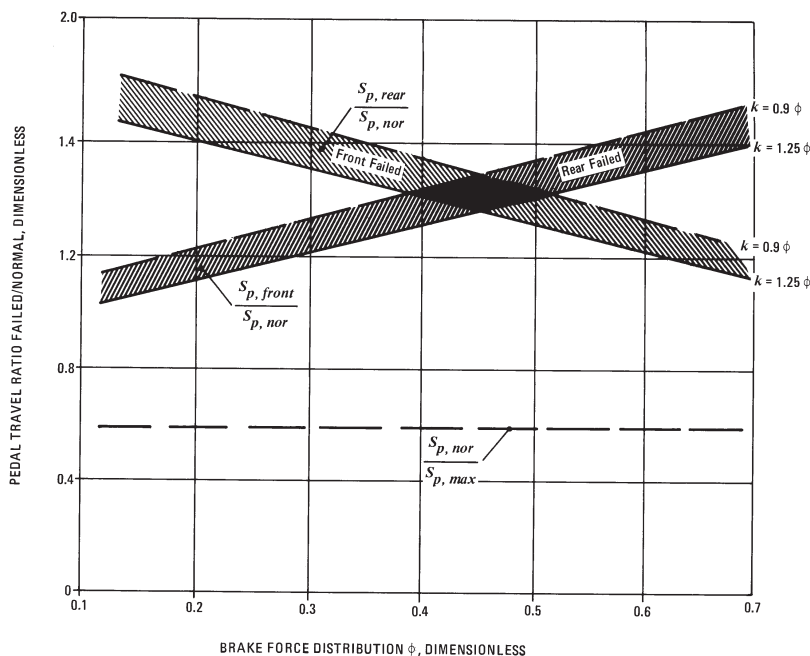


Figure 10-5. Normal pedal travel ratios required for partial failure stops, system 1.

To show the effect of a long vs. short master cylinder piston travel for the front-to-rear split dual design, the pedal travel ratios failed/normal are plotted in Fig. 10-6 as a function of ρ , i.e., vs. utilization of effective master cylinder piston travel required for a normal stop. A ratio of floating piston travel to pushrod piston travel of 74:26 and a brake force distribution $\Phi = 0.32$ were used in the

calculations. Inspection of the curve representing front brake failure reveals that long master cylinder or large pedal travel reserves, i.e., low values of ρ , result in undesirably long pedal travels in the case of front brake failure. This condition exists in spite of the highly acceptable normal-to-maximum pedal travel ratio.

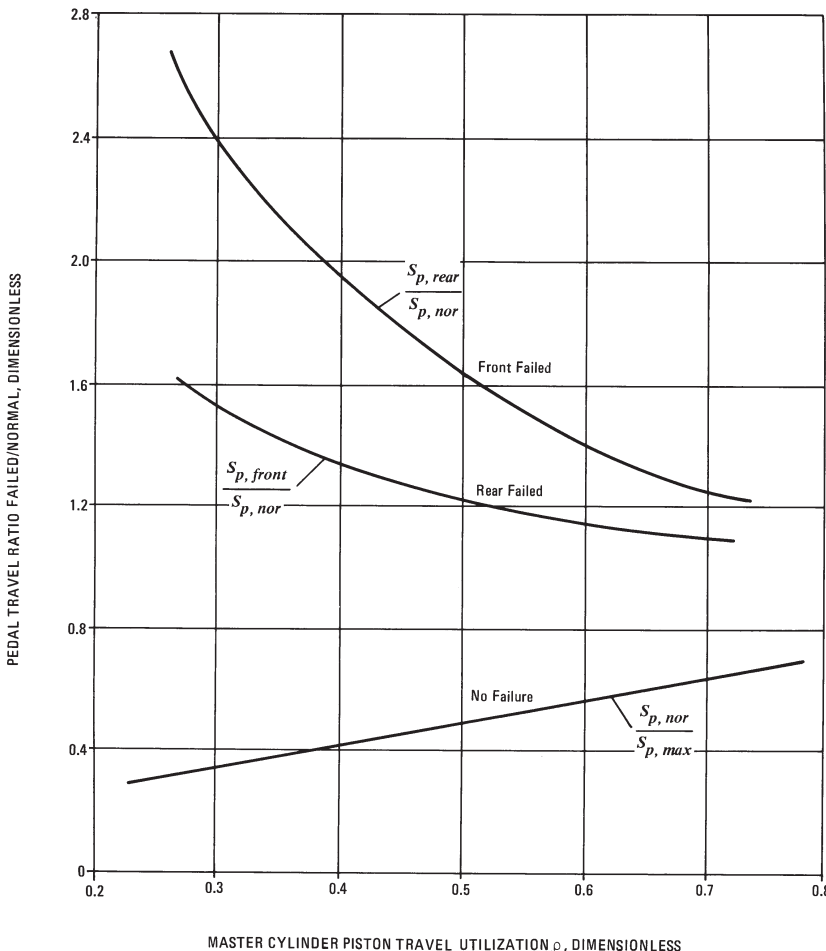


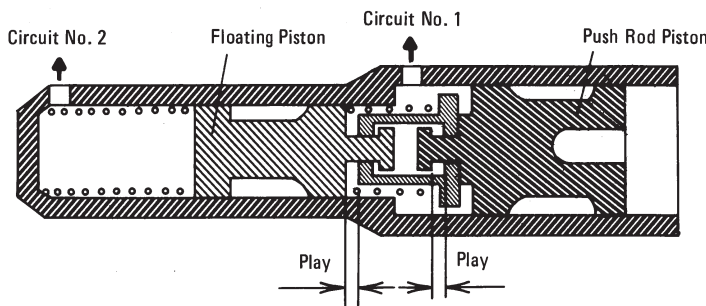
Figure 10-6. Pedal travel ratio as a function of piston travel utilization.

Braking systems using duo-servo brakes on the rear and disc brakes on the front generally have relatively small master cylinder piston travels for the rear circuit chamber. Under these conditions, a front brake failure can easily cause excessive pedal travels often “interpreted” by drivers as a complete brake failure. The reason for this undesirable characteristic stems from the high brake factor associated with duo-servo brakes, resulting in small rear wheel cylinders.

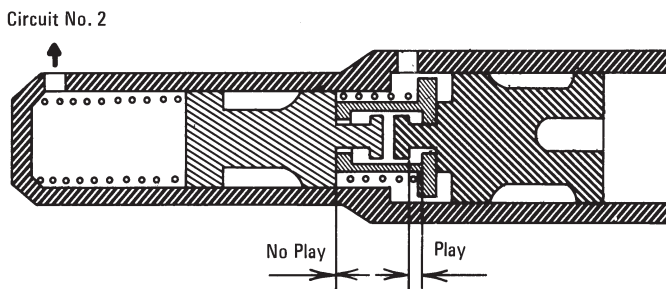
10.3.4 Improved Dual Master Cylinder Design

Significant improvements in minimizing the effects of partial failure on pedal force and pedal travel have been accomplished by means of a special stepped bore master cylinder (Ref. 10.6). The brake line pressures achieved under failed

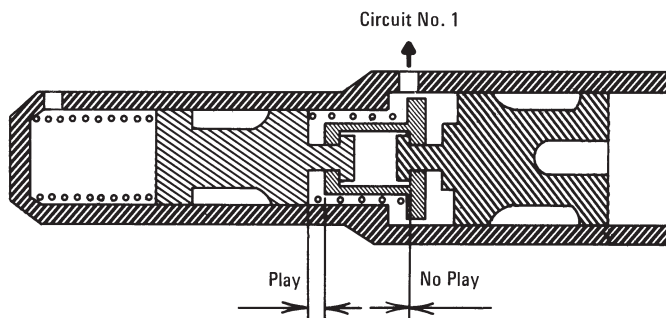
Brake Design and Safety



(A) Stepped Bore Master Cylinder, Normal Brake Application



(B) Stepped Bore Master Cylinder, Brake Application With Leakage in Circuit Number 1



(C) Stepped Bore Master Cylinder, Brake Application With Leakage in Secondary Circuit Number 2

Figure 10-7. Stepped bore tandem master cylinder.

conditions are double the pressure achieved under normal conditions. This change in effective piston area is accomplished by using a stepped bore, as illustrated in Fig. 10-7. Whereas the larger master cylinder feeds both circuits in the case of an intact brake system, the smaller-diameter master cylinder is utilized in the event of circuit No. 1 failure, and double brake line pressure is produced because the smaller piston area is one-half the area of the larger piston. If circuit No. 2 fails, the differential area between the larger and the smaller bore, i.e., one-half of the standard area, becomes the effective brake line pressure-producing area. The result is a brake line pressure under failed conditions that is twice as large as under normal conditions. Because under circuit failure conditions not all wheel brakes are actuated and normally are not locked, a nearly identical wheels-unlocked deceleration results with the same

pedal force. The pedal travel in the failed condition exceeds the pedal travel in the unfailed condition by not more than approximately 30%. Thus with this master cylinder, pedal forces and pedal travel are no longer the limiting factors in the case of partial failure braking.

Brake system splits using unequal volume distribution between circuits and significantly different cross-sectional areas for the floating and pushrod piston chambers may lead to excessively high brake line pressures in case of partial failure.

10.4 Comparison of Dual Brake Systems

A comparison of the dual brake systems represented in Fig. 10-1 indicates that a different number of connectors and flexible hoses is required for the different systems. For example, system 1 requires 17 connectors compared to 34 for system 5.

A leak is more likely to develop in a hydraulic circuit that contains more removable connections, caliper piston and wheel cylinder seals, and other devices such as valves and control elements. A comparison of the complexity of the different dual-circuit splits is shown in Fig. 10-8. All removable connections, such as T-fittings, are included in Fig. 10-8. The data indicate system 5 has a higher failure probability than the remaining systems. Difficulties also may arise in properly installing the flexible hoses near the wheels. A larger number of fittings with machined cavities will also trap a greater amount of residual air in the brake system. Not included in the number of removable connections is the third bleeder screw required for dual-caliper disc brakes if they are designed as one unit.

A hydraulic brake system may experience a temporary brake failure due to brake fluid boiling and vaporization. This condition may cause an accident, although shortly after the accident the brake pedal is found to be firm and the brake system mechanically intact. The maximum temperature of a brake should be kept below certain limits. High brake temperatures will result in: (a) brake fade (lower brake torque) and increased lining wear, (b) high tire bead temperatures, and (c) increased temperature of the brake fluid in brake calipers and wheel cylinders. Modern brake fluids boil at approximately 705 K (450°F). Consequently, prolonged downhill travel with a fully loaded vehicle may cause the brake fluid to boil, vapor to develop, and the brake system to fail. When the driver applies light pedal force, the pressurized brake fluid will boil at higher temperatures. It may be possible that the brakes worked without failure on the downhill portion, with the brake fluid just below boiling temperature, only to fail after the driver relaxed his foot off the brake pedal at the bottom of the hill, at which time the brake fluid began to boil due to the lower fluid pressure, only to fail a short distance farther at the first brake application (Ref. 5.16).

To determine excessive brake temperature for this type of intermittent brake failure, all brake components affected by high temperature must be carefully examined. It is expected that the swept surfaces of rotors and drums would

Brake System	Single-Circuit System	System No.				
		1	2	3	4	5
Wheel Cylinder	8	8	8	12	12	16
Removable Connections	17	15	16	25	26	34

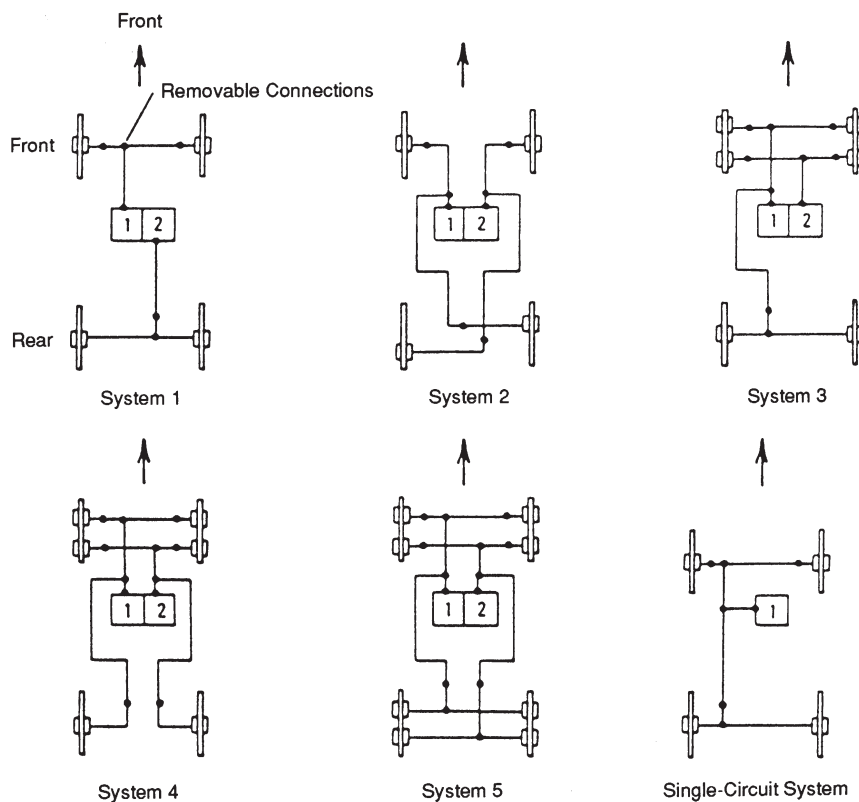


Figure 10-8. Comparison of system complexity.

show sign of discoloration (blueing); brake pads and linings may be blackened; rubber seal or dust boots may be charred from excessive heat.

One effect of brake fluid vaporization from thermal overloading on circuit failure of the different dual systems is indicated in Fig. 10-9. It is assumed that the front brakes are experiencing excessive brake temperature leading to fluid vaporization and, hence, failure of the circuits connected to the front brakes. Inspection of Fig. 10-9 reveals that only system 1, the front-to-rear split, provides a partial braking capability on the rear wheels, with the front brakes failed due to vaporization. If the rear brakes exhibit vaporization and circuit failure, all but systems 1 and 3 will fail completely.

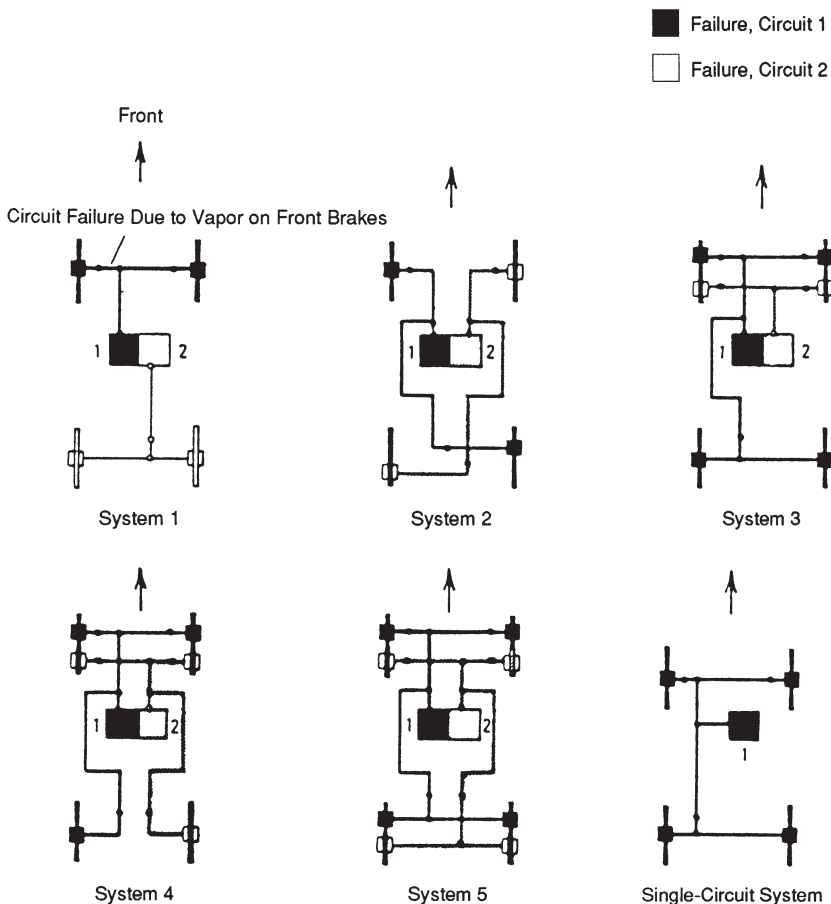


Figure 10-9. Dual systems, front brake failure due to brake fluid vaporization.

10.5 Vacuum Assist Failure

Vacuum assist or booster failure exists when the assist function of the power boost unit is degraded partially through insufficient vacuum (engine problems, vacuum pump defect, booster leaking), engine running at high RPM, or complete loss of vacuum (stalled engine, loose hose connection, check valve failure).

With the complete or partial failure of the vacuum assist unit, the reduced brake line pressure may be obtained from Eq. (10-2) with the boost ratio reduced accordingly. The lower brake line pressure may then be used in Eq. (10-1) to compute vehicle deceleration under a booster failure condition. Typical results of such an analysis are presented in Fig. 10-10 in the form of a braking performance diagram. The following observations can be made with respect to various levels of power boost failure:

1. No assist. To produce a deceleration of 0.9 g, a pedal force of 1201 N (270 lb) is required. A deceleration of only 0.32 g is produced with a pedal force of 445 N (100 lb).
2. 32% assist. The deceleration, produced by a pedal force of 445 N (100 lb), is 0.52 g. A deceleration of 0.9 g requires a pedal force of about 956 N (215 lb).
3. 60% assist. The deceleration, produced by a pedal force of 448 N (100 lb), is 0.76 g. A deceleration of 0.9 g requires a pedal force of about 667 N (150 lb).

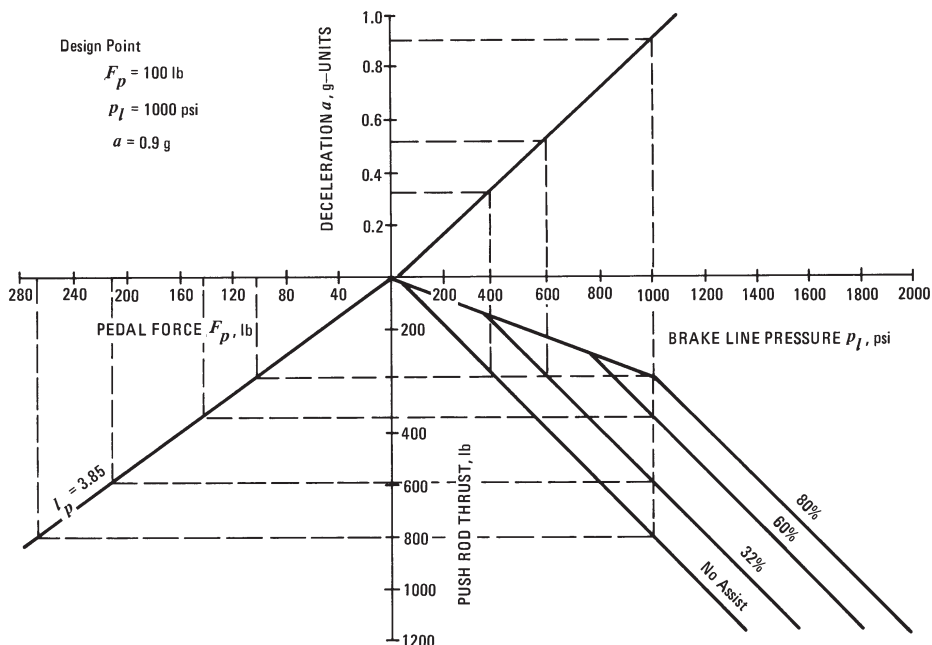


Figure 10-10. Braking performance diagram for vacuum-assisted brake system.

10.6 Full Power Brake Failure

Full-power hydraulic brake systems use a tandem master cylinder in conjunction with a pressurized accumulator or circulating pump system. Dual-circuit failure analysis is identical to that of the unassisted or vacuum power-assisted brake system. Should a power source failure occur, a sufficient level of energy is stored in the accumulator, or the emergency accumulator (spring or gas loaded) for the circulating pump system, to produce a certain number of successive emergency stops. Generally, three stops are required under complete primary energy source failure. Furthermore, most systems provide a small manual "push through" capability from the driver's pedal effort. In some designs, an electrical pump is used to generate secondary assist pressure.

10.7 Degraded Braking Due to Air Inclusion

A detailed analysis of the braking performance based on the brake fluid requirements of various brake system components is presented in Section 5.4.3. An example calculation is provided for the maximum deceleration as the front circuit piston of the dual master cylinder bottoms out due to excessive front caliper piston travel caused by improper wheel bearing play.

In connection with a particular accident investigated by the author involving a four-wheel disc brake sports car, braking tests were conducted to simulate brake fluid vaporization. Air was artificially introduced into the brake system at the master cylinder to determine partial braking performance. The results are shown in Fig. 10-11, where measured values for pedal travel, vehicle deceleration, and pedal force are plotted as a function of amount of air inclusion. Percent air identifies the percentage of brake fluid volume of the master cylinder that had been replaced by air at ambient pressure. A maximum pedal travel of 170 mm (6.7 in.) was available before the master cylinder bottomed out. Inspection of Fig. 10-11 reveals that even when 30% of the master cylinder volume has been replaced by air, a deceleration greater than 0.8 g can be achieved before the pedal contacts the floor. With 50% air, the pedal will bottom out at a deceleration of approximately 0.15 g at a pedal force of 120 N (25 lb).

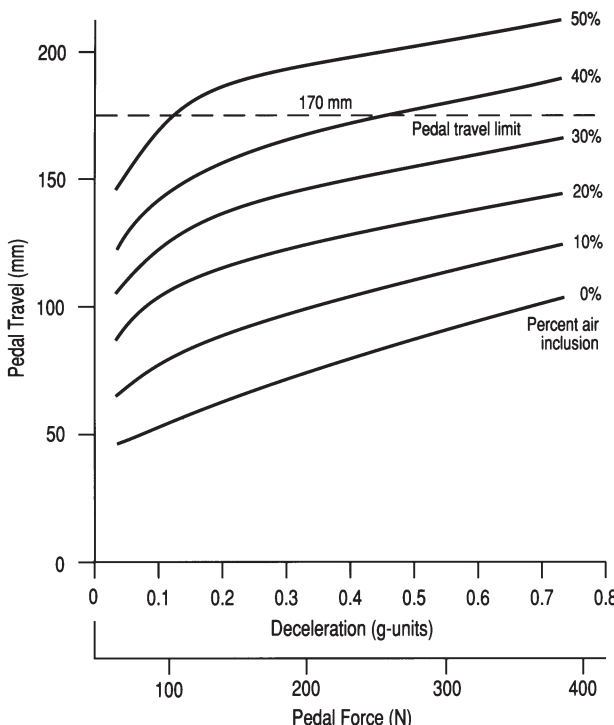


Figure 10-11. Vehicle deceleration as a function of pedal travel (1966 Porsche 911).

10.8 Brake Fluid Considerations in Design and Failure Analysis

Because the characteristics of the different types of brake fluids available are important in the design of brake systems and in the investigation and analysis of certain brake failures, some details are presented in the following sections. Brake fluid just as any other parts of a brake system is a design component whose performance characteristics must be understood by the brake design engineer.

10.8.1 Brake Fluid Properties

The most important properties of brake fluids are

1. High boiling point to avoid the development of vapor in the brake system at elevated temperatures.
2. Small amounts of water in the fluid (less than 0.2%) should not reduce the boiling point significantly.
3. Viscosity should be low when cold, or high when hot.
4. Compressibility should be low; temperature and pressure should have little effect.
5. Corrosion protection against metal parts to ensure long component life.
6. Good lubrication for long component life of moving parts.
7. Good chemical reaction with rubber parts to avoid shrinking and cause only little swelling.
8. Little or no gas production caused by turbulent-type flow processes and low pressures.
9. Rapid elimination of foam.
10. Ability to mix with property-improving additives.
11. Ability to absorb residual air during vacuum filling of the brake system at the factory.
12. Oxidation stability in foreseeable temperature ranges.
13. Low aggressivity to vehicle paint.
14. Low toxicity.
15. Proper color to avoid inadvertent use of improper fluids.

10.8.2 Different Types of Brake Fluids

In the past, three different types of fluids have been used in automotive applications. No single type satisfies all 15 requirements equally well.

The three types of brake fluids are based on

- a. Polyglycolether, the most commonly used brake fluid such as DOT 3, DOT 4, or DOT 5.1
- b. Silicone, rarely used except by U.S. military (DOT 5)

- c. Mineral oil, rarely used in automotive applications, except, for example, in the past by Rolls-Royce using fully hydraulic brake system design without master cylinder, and motorcycles.

Polyglycolether-type brake fluids are commonly used in vehicles equipped with hydraulic brake systems. Some differences exist among DOT 3, 4, and 5.1. For example, DOT 4 has better reaction ability than DOT 3 and, hence, lower sensitivity to water found in the brake fluid than DOT 3.

Silicone-based brake fluids are used less frequently. The U.S. military uses silicone fluids (Ref. 10.0). The basic element of silicone fluids is a silicium-based polymer. Advantages include non-hygroscopic characteristics; good viscosity/temperature behavior; compatible with commonly used elastomers for rubber parts; good anticorrosion properties; high boiling point. Disadvantages of silicone fluids are high compressibility (spongy brake pedal), especially under higher temperatures; high air absorption, which will be released again into the water when vibrations occur; no ability to absorb water (the flip side of being non-hygroscopic); minute amount of water may cause brake failure.

Mineral oil brake fluids are polyacrylate-based polymers. They are not compatible with commonly used seal or cup materials, SBR (styrol-butadiene-rubber) or EPDM (ethylene-propylene-diene-materials). Mineral oil fluids are used in hydro-boost hydraulic brake systems where the pedal effort is used only to control brake line pressure, i.e., in those without master cylinders. The major disadvantage is the inadvertent contamination of the mineral oil with regular brake fluid. Small amounts less than 0.2% of regular brake fluid mixed with mineral brake fluids may deteriorate rubber seals and hoses.

10.8.3 Brake Fluid Performance

The performance of brake fluids is regulated by FMVSS 116, which in most parts is based on SAE J1703. Brake fluid classifications are determined by the boiling point (dry), wet boiling point (3.0% water by weight in the fluid), and viscosity at 233 K (-40°F). An additional 12 other measures are evaluated in FMVSS 116. Based on FMVSS 116, the dry/wet boiling point temperatures are: for DOT 3, 477/413 K (400/285°F); DOT 4, 503/428 K (446/311°F); DOT 5.1, 543/464 K (518/375°F); DOT 5, 555/453 K (500/356°F). On occasion, brake fluid manufacturers market newly formulated brake fluids to improve existing ones. For example, DOT 4 Plus has higher dry and wet boiling point temperatures as well as lower cold temperature viscosity than regular DOT 4. DOT 5.1 is a brake fluid that is not compatible with regular DOT 5.

Regular brake fluids based on polyglycol-ether are hygroscopic, which means that they will absorb water from the surrounding atmosphere. More water will be found in the brake fluid with time, provided the fluid has not been changed during maintenance of the vehicle. Entry of water into the brake system through the master cylinder reservoir is generally of little significance. The small breather hole or diaphragm effectively prevents water from entering the master cylinder. In addition, there is no serious threat of overheating of brake fluid in the master cylinder—assuming proper maintenance, repair, and design—and,

hence, no brake fluid boiling occurs due to its location away from the heated friction brakes. However, water will enter the brake system through its flexible hoses by a diffusion process. The amount of diffusion water is a function of the hygroscopic properties of the fluid and the diffusion resistance of the hose material. The commonly used SBR hose material diffuses more water than EPDM materials (Ref. 10.8).

Higher levels of water contamination of brake fluid were found in the flexible brake hoses near the calipers and wheel cylinders than at the master cylinder, which generally has no flexible hoses near it. Tests have shown that the boiling point of brake fluid taken from the brake system near the brake hoses is up to 311 K (100°F) lower than that of the fluid taken from the master cylinder reservoir. In this respect, DOT 4 and 5 exhibit lower water contamination than DOT 3, which should be changed every year.

10.9 Seal and Rubber Materials

Polyglycolether and silicone-based brake fluids are compatible with SBR (styrene-butadiene-rubber) and EPDM (ethylene-propylene-diene-monomer) rubber. Mineral oil is not compatible with these elastomers and requires seal and rubber component materials such as neoprene. Most seal elastomers begin to deteriorate when exposed to temperatures above the boiling point for long periods of time. Pulsating pressure loadings as may occur at the master cylinder can only be withstood by SBR seals for temperatures less than 352 to 377 K (175 to 220°F). EPDM seal materials have temperature limits of up to 394 K (250°F). As engine compartment temperatures increase, difficulties may arise for heavy high-powered passenger cars because the cup hardness has to be maintained for minimum seal wear at the compensating ports. The change to EPDM cup material required design changes of the master cylinder because excessive wear at the compensating ports occurred. The commonly used compensating port design was replaced by central valves. DOT 4 exhibits excellent performance in connection with EPDM material in the form of slight seal swelling essential for proper operation over extended periods of vehicle life. Neoprene materials used for mineral oil have lower allowable operating temperatures than either SBR or EPDM cups (Ref. 10.9).

10.10 Data Collection in Brake System Failures

Brake failures are always of critical importance, whether or not they have caused an accident. Drivers are dependent on the proper functioning of their vehicle's brakes. Only a little less than 2% of all accidents are primarily caused by braking problems. In nearly 90% of these cases, poor and/or improper maintenance contributed to the brake failure. The nature of a brake failure can be of mechanical, hydraulic, thermal, and/or electrical (electronic) origin.

10.10.1 Driver Statement and Questioning

In an accident in which brake failure is alleged, any statement by the driver and/or passenger(s) is of critical importance to an accurate analysis. The validity of the statement depends to a large measure on the questions. Drivers

involved in an accident may never have experienced a brake failure. In some cases the driver, due to injuries or other reasons, may not be able to provide any information. Many law suits are initiated due to driver statements such as: "My brakes failed," "The pedal went to the floor," "I could not stop," "The pedal was hard," "The pedal was spongy," "The pedal vibrated," "I pumped the brakes and nothing happened," and many more. It is interesting to note that in nearly one half of all crashes, drivers do not apply the brakes at all.

Accurate information concerning pedal force and the associated pedal travel must be obtained. The person asking the questions should be familiar with the braking system. At a minimum, the brake section of the repair manual for the subject vehicle should have been reviewed. In particular, information on manufacturer's specifications on brake pedal travel under normal conditions, with partial brake failure, and booster failure should be known. With this knowledge, more helpful questions can be put to the driver.

The following questions will help in collecting accurate data from a driver involved in an accident with alleged or real brake problems.

- First, let the driver explain in his or her own words why he or she thinks the brakes failed.
- Did the brake pedal go to or hit the floor? Was the brake pedal firm? What was the brake pedal travel? Did you smell hot brakes?
- If yes, how do you know? (For example, did your shoe contact the floor? Did you have to scoot forward to push the pedal all the way? How tall are you? Did you adjust the seat before you drove the car? How do you normally adjust the seat? Was this car the one you normally drive? Was your knee bent when the pedal hit the floor?)
- Have you ever experienced brake failure before where the brake pedal went all the way to the floor, which means the pedal actually contacted the floor?
- As the brake pedal went to the floor, what was the pedal force? (If the driver cannot describe this in terms of pounds, attempt to compare it to the pedal force the driver normally uses during routine braking maneuvers such as exiting a familiar freeway or slowing at a familiar stop sign.)
- If the brake pedal felt spongy, was it firm at first and then spongy, did the pedal move without any force and then became spongy, or did it become spongy after pumping the pedal? (A spongy brake pedal could indicate air in the brake system due to improper maintenance, brake fluid vaporization due to overheating of the brakes, inadequate after-market brake pads with much higher than normal compressibility when hot, low brake fluid level allowing air to enter the master cylinder, or other defect.)
- Did you pump the brakes (to restore brake pedal height)? If so, how fast did you pump the brakes? (Slow pumping will make little difference, if any, as opposed to rapid pumping.) Could the brake pedal be pumped up?

- Did the brake warning light illuminate?
- Did a buzzer sound?
- Where is the brake warning light located?
- What color is the light?
- Was the brake pedal vibrating while the brakes were applied?
- Did the ABS/ESC warning light illuminate? What is its color and location?
- Could you feel any rim forces through the steering wheel while braking? This would indicate some front braking, possibly left-to-right brake imbalance, particularly for diagonal hydraulic split brake systems, or disc thickness variation (DTV)?
- Vehicle deceleration level could be indicated by items slipping off car seats.

The questions and areas to be explored may be expanded depending upon the particular circumstances of the accident.

10.10.2 Brake System Data Collection

In the data collection process relative to the driver, we were trying to get information on pedal force and pedal travel. Pedal force allows us to compute or estimate brake line pressure, and hence braking effectiveness or vehicle deceleration. Pedal travel allows us to determine how much brake fluid was lost, that is, not available for the production of brake line pressure. In the following list of data collection methodology, we assume that the brake system and its components were not damaged in the accident. If components were damaged, special provisions must be made.

- Prepare a meaningful and complete investigation/testing protocol.
- If any components are to be removed, obtain proper permission from all parties involved. Videotape any activity that involves the subject vehicle and/or its components.
- Photograph the subject vehicle with respect to any exterior or interior condition. Note the positions of the parking brake lever and brake pedal. Note any wedging of the brake pedal in an applied position.
- Observe any abnormalities such as fluid under the vehicle, etc.
- Raise the vehicle on a lift and inspect and photograph from underneath. The object is to discover whether any of the brake components are leaking, contaminated or defective. If so, distinguish between old and fresh brake fluid leaks. Also, distinguish between brake fluid and axle oil, or lubricating oil/grease. Make proper notation in field notes.
- Measure pad/rotor gap with feeler gage (Ref. 10.10).
- Lower the lift so that the tires do not touch the ground and open the hood. Inspect brake components such as master cylinder, brake fluid reservoir, brake fluid reservoir cover, brake lines and hoses, proportioning and ABS valves, vacuum booster, and vacuum hose connec-

tions. Note the brake fluid level through the transparent reservoir. Open the brake fluid reservoir and inspect for fluid level and any contamination in the reservoir (dirt particles, dark smudgy appearance).

- Place the transmission in neutral and rotate the wheels. Note the degree of drag, if any. Videotape the free-spinning wheels. If there is drag, measure with torque wrench.
- Check the operation of the brake warning lights on the dashboard. Before turning the ignition key, be certain that this will not affect any electronic data stored by the ABS or any other computer. Photograph the operation of warning lights. Note any defective bulbs.
- If the vehicle is equipped with ABS brakes, and after proper permission has been obtained, download ABS codes from the ABS computer. Follow the manufacturer's instructions and use proper equipment. Potential malfunctioning of ABS components will be shown. Download engine data recorder. Be familiar with certain down-load errors for Caterpillar engines (Section 10.11).
- If the vehicle is equipped with a computer module/crash recorder, and after proper permission has been obtained, download codes. Follow the manufacturer's instructions. The data may yield the delta-V sustained during the crash. For most interstate buses and tractor-trailer combinations manufactured after 1997, several key data are stored in the computer.
- Only after you are absolutely certain that there is no brake fluid leakage, while seated in the driver seat, conduct some pedal force vs. pedal travel tests. Install a pedal force gauge on the brake pedal and hook a standard tape measure at the bottom of the brake pedal while reading pedal travel with the steering wheel as a reference point. Without the engine running (no boost vacuum), read no-force travel (around one-eighth to one-quarter inch), as well as pedal force to achieve between one and two inches of pedal travel. Under normal conditions without any brake failure (no air in the system), 445 to 667 N (100 to 150 lb) of pedal force is required to produce approximately 51 mm (2 in.) of pedal travel. Refer to the manufacturer's brake specifications. Check the operation of the brake lights. Repeat the pedal force/pedal travel test with engine running. Measure pedal force for 51 mm (2 in.) pedal travel.
- While the brake system is pressurized, determine whether the wheels can be rotated. Videotape each wheel while brake pedal is applied and rotation is attempted. After the brakes are released, rotate each wheel to determine any potential brake drag. Brake dragging indicates improper return of brake pads or shoes, which may result in excessive heating of brakes and lead to failure due to brake fluid vaporization.
- In the case of disk brakes, rotate each wheel 10 to 20 times and repeat the test described above. Larger, no-pedal-force pedal travel measurements would indicate excessive lateral rotor run-out. Measure pad/rotor gap with feeler gage.

- Measure brake vacuum booster effectiveness with and without the engine running. Measure engine vacuum with the engine at idle as well as at maximum rpm.
- Measure lateral bearing play, if any, at all (four) disc brake positions with a micrometer. Before removing wheels, measure lateral rotor run-out (LRO) of brake rotors while on vehicle. When removing wheels, measure lug nut torque. Inspect and photograph the individual front and rear brakes. Remove rear brake drums, if any, and photograph. Retighten rotors with lug nuts to pre-removal nut torque. Measure rotor thickness at two locations (DTV – disk thickness variation) and measure LRO on all disk brakes. If equipped with rear drum brakes (or front brakes, in the case of a truck), measure the brake shoe diameter with a caliper and the brake drum diameter with an inside micrometer. These measurements allow computation of wheel cylinder piston travel, the amount of brake fluid required to apply the brakes, and the no-force brake pedal travel. Measure and photograph brake pad and lining thickness. If readable, note and photograph edge codes on the pads and linings. This will establish the manufacturer's identity and may be extremely critical for vehicles without (rear) ABS. After-market rear linings may have a higher lining-to-drum friction coefficient, causing premature rear brake lockup and loss of control during braking. While inspecting individual brakes, observe the movement of the disk brake pads and the free return movement of the pads after brake line pressure is released. Observe the same for drum brakes. Make certain that the piston will not travel out of the wheel cylinder to avoid spoliation of evidence by contaminating brake shoes.
- Note and photograph any abnormalities indicating excessive brake temperature, such as coloration of swept surfaces, heat deformation, charring of rubber components, and/or edge charring of pads or linings. If brake component(s) show any signs of heating, remove and properly collect and store brake fluid samples from each of the bleeding screws of each of the brakes, and from the reservoir. Videotape and photograph all activities. Properly label each container. Glass containers must be sealed tightly so that no water (or air) can be absorbed from the atmosphere. Approximately three cubic centimeters (three tablespoons) should be collected. It should be stressed that collecting, that is, removing, brake fluid from the subject brake system may affect the remaining system, and consequently requires the approval of all parties involved.

The critical elements of the brake fluid analysis are the following:

Contamination in the form of particles indicates poor maintenance or repair, and/or improper or defective manufacturing. Contamination by water indicates poor maintenance, or sometimes ineffective instructions or warnings by brake or car manufacturers to replace brake fluid in the brake system. Fluid gelling may show contamination with other fluids or substances (grease, etc.). Brake fluid is hygroscopic and, as such, absorbs water from the air. The water enters the brake system through the flexible brake hoses and not through the brake

fluid reservoir cover. Contaminated brake fluid may introduce water during maintenance work or during manufacturing (quality control).

Brake fluid samples can be tested for particle and water contamination. In addition, in a spectral analysis the temperature level that the subject brake fluid had attained can be determined. For example, the analysis may show that a particular fluid sample reached a temperature of 533 K (500°F). The analysis will also show the boiling point temperature T_{boil} of the fluid sample. If T_{boil} is less than the fluid temperature 533 K (500°F), then brake failure by vaporization has a high probability of accident causation.

- Note anything that might provide information on braking effectiveness or pedal force, such as flat spots on the tires or imprints of brake pedal rubber pads against the shoe sole. Frontal crush damage sustained during impact against the other vehicle or object may indicate a pitching motion due to braking before impact.
- Inspect individual brake components. Only after permission has been received from all parties involved can components be removed from the vehicle to be prepared for inspection. Disassembly should only be attempted after all potential component testing has been carried out. This is particularly true for master cylinders. Master cylinders may become defective due to particle contamination, excessively worn seals, or even due to air inclusion caused by improper repair. In testing the master cylinder it is important to duplicate the actual vehicle conditions as closely as possible. For example, in a simple bench test with little or no pushrod piston movement, the master may be able to develop brake line pressure, particularly if only a single and large apply force is used. However, if the master cylinder is installed in an exemplary vehicle, the master cylinder piston seals operate near their normal location within the master cylinder bore. Light pedal applications may lead to brake failure, while excessive rapid pedal forces may press the lip of the seal(s) against the bore sufficiently to close the seal, camouflaging the actual brake failure due to internal bleed-by of the master cylinder.

When any brake testing is contemplated in a brake failure investigation, careful planning and objectivity are important. Why is the test conducted? What will it show?

- Determine whether intermittent brake failures caused front-end vibrations. Sometimes, even the most detailed brake system inspection and analysis will not indicate a brake failure. One explanation, of course, is that there really was no brake failure. We are reminded again that less than 2 percent of all accidents are caused by brake failure. The other factor involved in intermittent brake failure may be front end vibration or shimmy. Under severe conditions the wobbling may be such that the pads, and hence caliper piston(s), are forced back from the rotor surfaces, resulting in an increased gap between pad and rotor. If the piston travel required to overcome this increased gap exceeds the brake

fluid capacity designed into the master cylinder, no brake line pressure can be produced in the case of diagonal hydraulic split systems, or only rear braking for front-to-rear hydraulic splits. Data collection is difficult, particularly if the front of the vehicle is damaged in the accident. Rotor run out (LRO) must be measured. Maintenance records, driver questioning with respect to front-end vibrations, and complaints by other owners or drivers of the same vehicle model involved may be of some assistance. Dynamic modeling and/or vibration testing with an exemplar vehicle may indicate that the subject vehicle has front-end sensitivity to certain imbalances, particularly if suspension components and attachment bushings show signs of wear and use.

10.10.3 Accident Scene Data Collection

10.10.3.1 Tire Markings

The accident scene may show certain tire marks from the subject vehicle before and after impact. The tire markings found at the scene must have been caused by the subject vehicle. If possible, tire markings must be classified as skid marks (from locked brake(s) due to braking) or yaw marks (from rotating tire). If possible, determine if skid marks (if any) were made by front or rear tires. Measure the length of any skid and/or tire markings with respect to the point of impact. Accident reconstruction is an important factor in any brake failure investigation.

Determine whether the tire marks are of an intermittent nature. This could primarily indicate ABS actuation, wheel hop during braking (defective shock absorber), rough and wavy road surface, or brake pedal pumping by the driver. Measure the length of each tire mark as well as each gap between tire marks. This information will prove that the ABS was operating, if the brake torque cycle rate is considered in connection with the speed of the vehicle.

In one particular case, an older pickup truck (no ABS) approached an intersection without stopping at the stop sign, causing a severe collision with another pickup truck. Approximately 15 feet of front wheel skid marks were located before impact. The driver claimed to have had an extremely hard brake pedal and that she had to generate very high pedal forces before the brakes locked. A careful data collection and accident reconstruction showed the following: The vacuum brake booster check valve had cracked just prior to the accident. The lack of any dirt accumulation in the fractured surfaces of the check valve indicated that the crack had just occurred. A failed check valve will cause the booster to lose its effectiveness, requiring the driver to apply three to six times higher pedal forces than under normal conditions to achieve the expected deceleration. In this case the female driver was only able to produce 667 to 778 N (150 to 175 lb) of pedal force after significantly longer brake pedal apply time. Also of critical importance in this case was the detailed accident reconstruction, including impact speed, travel speed before braking, and driver reaction time. It could be shown with a high degree of certainty that the driver of the pickup truck could not see the other pickup truck approaching the intersection due to view obstructions when she reacted to the brake failure.

10.10.3.2 Roadway Data

Measure all pertinent roadway data such as grade, cross slope, width, and curvature at the accident location. Measure the grade (if any) for several miles leading to the accident location. Measure points (if any and/or is known) where the driver last applied the brakes and/or stopped. Measure the last curve radius prior to the crash site. The curve radius may allow an approximate speed to be computed based on critical speed in a curve. Note any unusual dips in the road, railroad crossings, or pot holes which may cause wheel hop and loss of contact between tire and ground, resulting in momentary wheel lockup during braking and a drastic reduction of brake line pressure due to ABS modulation. Depending upon ABS computer design, the delay in brake line pressure rise may result in increased stopping distances.

Measure the tire-road friction coefficient, using either the subject vehicle (if possible) or an exemplar vehicle. Use a recognized measuring device, such as the G-Analyst. Photograph tire marks and measure their length and shape.

10.11 Failure of Air Brake Systems

Air brake systems are designed with a dual brake system split; generally the front brakes form one circuit, the rear brakes form the other. In three-axle trucks different splits may be used. Air loss in one circuit will provide full air pressure to the remaining circuit. The reduced vehicle deceleration can be computed by use of the appropriate equations of Chapter 6 [Eq. (6-7)]. Modern air brake systems are designed so that the failure of one circuit of the tractor will still provide full braking of the trailer and partial braking of the tractor.

If air loss occurs, automatic or driver-controlled brake application of the emergency/parking brakes results. The spring brakes generally provide an application force corresponding to an air pressure in the brake chamber of approximately 41 N/cm^2 (60 psi). It should be noted that when the brakes are out of adjustment, i.e., the pushrod travel is too long to effectively push the shoes against the drum, then the spring of emergency brakes will be ineffective also.

The most common brake failure found in accidents caused by air brakes results from brakes being out of adjustment or being at a critical level of adjustment so that the driver cannot easily identify how "bad" the brakes are. The mechanical condition of the brake system in terms brake adjustment, contamination (lower brake factor), brake temperature and vehicle/trailer loading are analyzed in Chapters 7 and 8. PC-BRAKE Air software may be used to analyze braking effectiveness when brakes are defective.

Obtain engine data (EDR). The velocity-time diagram when properly analyzed will show vehicle deceleration as a function of time, that is, vehicle deceleration. Any driver error or reduced braking effectiveness will be revealed (Ref. 10.10). EDR velocity-time data printouts have contained time scaling errors for Caterpillar engines (Refs. 10.11, 10.12).

Chapter 10 References

- 10.1 National Transportation Safety Board, Safety Recommendation, Manufacturers and Marketers of Automatic Slack Adjusters, In reply to H-06-8, February 15, 2006.
- 10.2 Bendix Technical Bulletin, "Automatic Slack Adjusters Not For Manual Adjustment," 5-30-2006.
- 10.3 Evans, Charles K. and J. Chris Oakwood, "Brake Caliper Fluid Displacement on Dynamometers – Is It the End for Caliper Test Stands?" SAE Paper No. 2007-01-3955, SAE International, Warrendale, PA, 2007.
- 10.4 Stringwell, Erik and Bryan Campbell, "Using the Electronic Stability Control Hydraulic Pump to Counteract Brake Pad Knock Back," SAE Paper No. 2009-01-1030, SAE International, Warrendale, PA, 2009.
- 10.5 Andres, Dennis, et al., "Brake System Analysis in Pre-Crash Accident Reconstruction," Short Paper PCB 9-2006, PC-Brake Inc., www.pcbrakeinc.com, 2006.
- 10.6 Larson, A. and L. Larson, "Stepped Bore Master Cylinder – A Way of Improving Dual Brake Systems," SAE Paper No. 750385, SAE International, Warrendale, PA, 1975.
- 10.7 Conley, James H. and Robert G. Jamison, "Army Experience with Silicone Brake Fluids," SAE Paper No. 780660, SAE International, Warrendale, PA, 1978.
- 10.8 Lee, Shuo-Jen, et al., "The Development of an Alarm Device for the Moisture Content in the Hydraulic Fluid of the Automobile Brake System," SAE Paper No. 1999-010475, SAE International, Warrendale, PA, 1999.
- 10.9 Smith, Richard F., "The Effect of Silicone Brake Fluid on Rayon Reinforced, Neoprene Tube and Cover Brake Hoses," SAE Paper No. 810802, SAE International, Warrendale, PA, 1981.
- 10.10 Limpert, Rudy, "Velocity – Time Diagram, Its Effective Use in Accident Reconstruction and Court Room Presentation," Short Paper PCB 1 – 2007, PC-Brake, Inc., www.pcbrakeinc.com.
- 10.11 Steiner, Von John, Unfalldatenspeicher fuer schwere Nutzfahrzeuge in Nordamerika, Verkehrsunfall und Fahrzeugtechnik, February 2010.
- 10.12 Drew, K., "The Reliability of Snapshot Data from Caterpillar Engines for Accident Investigation and Analysis," SAE Paper No. 2008-012708, SAE International, Warrendale, PA, 2008.

Index



- 2-S1 tractor-trailer
braking dynamics of, 281–302
effects of brake balance on tire-road friction utilization, 287–302
general design considerations, 281
limiting and proportioning valves for, 286–287
optimum braking forces, 281–302
PC-BRAKE AIR for, 302–312
- 2-S1–2 two-axle tractor, single-axle semitrailer, double-axle trailer, 318–320
- 2-S2 tractor-semitrailer, 320
- 2-S3 tractor-semitrailer, 321–324
- 3-S2 tractor-semitrailer, 312–318
with air springs on tractor and trailer tandem axles (3-S2-AA), 313
PC-BRAKE AIR for, 316–318
with tractor air springs and trailer walking beam (3-S2-AWB), 314
with tractor air springs and trailer leaf springs (3-S2-ALS), 315–318
- Accelerated testing, 12
- Add-on hydraulic ABS systems, 355–358
- Adjustable step bore master cylinder, 244–248
- Advertisement guidelines, 12
- Aerodynamics, effect on brake force distribution, 237
- Aftermarket equipment, 167
- Air brake systems
antilock brake systems for, 364–368
control analysis in, 364–367
designs for, 367–368
modulating valves for, 196–199
analysis of, 183–210
basic concepts for, 183–184
brake chamber in, 187–190
brake torque in, 190–194
braking by wire, 209–210
deceleration in, 194–196
disc, 187
drum, 186
electronic brake control, 209–210
- failure of, 403
PC-BRAKE AIR, 199–200
rear tandem axle with, 253–254
response time of, 200–209
S-cam, 184–186
in three-axle straight truck, 253–267
in two-axle truck, 249–253
wedge brake, 186
- Allowable heat flux
into brake drums, 112
into brake rotors, 112–114
- Angular acceleration, formula for, 261
- Angular velocity, formula for, 198
- Antilock brake system (ABS), 327
for air brakes, 364–368
basic performance requirements of, 343–353
components of, 360–364
control concepts for, 345–351
drivetrain influence on, 364
electric circuit, 364
electronic control unit, 361–362
- hydraulic, 353–360, 362–363
add-on, 355–358
basic considerations for, 353–355
integrated, 358–360
modulating valves for, 196–199
wheel speed sensors, 360–361
- Assembly, 12
- Automatic brake control (ABC)
for air brakes, 364–368
basic considerations, 327–328
basic performance requirements of, 343–353
control concepts for, 345–351
drivetrain influence on, 364
electronic traction and stability control systems, 351–353
hydraulic ABS, 353–360
system components, 360–364
wheel-lockup analysis, 328–343
- Automatic front brake limiting valve, 195–196
- Automatic slack adjuster (ASA), 22, 185, 374

Brake Design and Safety

- Average displacement, formula for, 121
 - Axes
 - air springs rear tandem, 253–254
 - and dynamic loads
 - for 2-S1 tractor-trailer combination, 303–304
 - for single vehicles, 214–216
 - for tow vehicle-trailer combination, 276–277
 - rear leaf spring tandem axle, 257–258
 - rear walking beam tandem axle, 254–256
 - static loads on, for single vehicles, 213–214
 - three-axle straight truck, 253–267
 - two-axle truck with air brakes, 249–253
 - Boost ratio, formula for, 128
 - Boost systems
 - analysis of, 127–141
 - comparison of boost systems, 139–141
 - full-power hydraulic brakes, 139
 - hydraulic, 136–139, 177–179
 - overview and requirements for, 127
 - vacuum-assisted, 127–135
 - dynamic response of, 176–177
 - failure of, 381–392
 - Brake-assist system (BAS), 327
 - Brake chamber, 187–190
 - clamp ring, 191–192
 - Brake control, electronic, 209–210
 - Brake factor, 27–28
 - brake wear effects on, 46
 - of drum brakes, 29–48
 - of duo-servo brakes
 - with pivot abutment, 40–44
 - with sliding abutment, 39–40
 - effects of humidity on, 46
 - effects of shoe and drum stiffness on, 47–48
 - effects of temperature on, 46
 - formula for, 27
 - importance to brake system design, 28
 - of leading-trailing shoe brakes
 - with inclined abutment, 38–39
 - with parallel sliding abutment, 36–38
 - with pivot on each shoe, 35–36
 - of S-cam brakes, 44–45
 - of two-leading shoe brakes
 - with inclined abutment, 39
 - with parallel sliding abutment, 38
 - with pivot on each shoe, 36
 - of wedge brakes, 45–46
- Brake factor sensitivity, formula for, 27
- Brake failure
 - of air brake systems, 403
 - analysis of, 373–403
 - basic considerations for, 373–374
 - brake line failure, 376–383
 - comparison of dual brake systems, 389–391
 - of components, 374–375
 - data collection in, 396–403
 - degraded braking due to air inclusion, 393
 - development of, 374–376
 - fluid considerations in, 394–396
 - full-power, 392
 - intermittent, 375–376
 - partial, 376–389
 - pedal force and pedal travel in, 18
 - performance calculations, 383–387
 - of seal and rubber materials, 396
 - of vacuum assist, 381–392
- Brake fluid
 - compression of, 164–165
 - considerations in design and failure
 - analysis, 394–396
 - mineral oil, 395
 - polyglycolether-type, 395
 - silicone-based, 395
 - viscosity of, 175–176
 - water content in, 167
 - volume analysis of, 150–179
 - basic concepts for, 150–155
 - checkpoints for, 16
 - detailed, 156–175
 - individual component fluid requirements, 159–167
 - master cylinder, 156–159
 - simplified, 155–156
- Brake force distribution
 - fixed
 - analysis of, 232–237
 - brakes-unlocked deceleration, 232–233
 - comparison of theoretical and road test results, 235–236
 - design selection, 232
 - effect of aerodynamics on, 237

- Brake force distribution
 - fixed (*Continued*)
 - effect of drivetrain on, 236–237
 - vehicle loading-brake force distribution analysis, 233–235
 - variable
 - adjustable step bore master cylinder, 244–248
 - analysis of, 238–248
 - pressure limiter valve, 241–242
 - pressure reducer valve, 242–243
 - deceleration-sensitive pressure reducer valve, 243
 - optimum brake line pressures for, 238–241
- Brake hose expansion, 160
- Brake lines
 - combination valves for, 145
 - comparison of pressure control devices for, 150
 - dynamic response of, 177
 - expansion of, 160
 - failure of, 376–384
 - optimum pressures for, 238–241
 - braking in a turn, 268–271
 - pressure limiter valve for, 142–143, 195–196, 241–242, 286–287
 - pressure reducer valve for, 143–147, 196, 242–243, 286–287
 - deceleration-sensitive, 145–147, 243
 - step bore master cylinder, 147–150
- Brake linings
 - braking power absorbed by, 70–72
 - design values, 74t
 - fluid requirements for, 162–163
 - friction and classification of, 58–59
 - horsepower into, 114
 - pressure distribution on, 29–32
 - wear in, 115
- Brake pads
 - compression of, 161–162
 - design values for, 74t
 - four-piston fixed-caliper, 55–57
 - friction and classification of, 58–59
 - “hammerhead,” 51–52, 54–55
 - horsepower into, 114
 - non-uniform pressure distribution, 52–53
 - offset piston design, 53–54
 - pad-rotor clearance, 159
- pressure and wear of, 51–57
- pulled, 54–55
- wear in, 115
- Brake pedal linkage, 176
- Brake shoes
 - fluid requirements for, 162–163
 - shoe/drum clearance, 163
 - stiffness of, effects on brake factor, 47–48
- Brake system design
 - basic considerations for, 10–11, 13
 - design and product development
 - guidelines, 11–13
 - elements of, 10–17
 - hydraulic, specific steps for, 13–15
 - PC-BRAKE AIR for, 249–253
 - selection process guidelines, 18–20
 - testing checkpoints, 15
 - Brake system failure, partial, checkpoints for, 16
- Brake systems
 - air or gas in, 165–166
 - basic safety considerations, 20
 - with booster, 17–18
 - functions of, 1–2
 - hydraulic
 - analysis of, 125–179
 - dynamic response of, 175–179
 - involvement in accidents, 20–25
 - mechanical, analysis of, 119–123
- Brake torque, 27, 190–194
 - for parking brake, 194
 - pushrod travel adjustment factor for clamp ring chambers, 191–192
 - pushrod travel increase due to thermal drum expansion, 193
 - pushrod travel measurement, 193–194
 - temperature fade correction factor for drum brakes, 192–193
- Brake wear, effects on brake factor, 46
- Brakes-unlocked deceleration, 232–233
- Braking
 - continuous, temperature analysis for, 85–88
 - degraded, due to air inclusion, 393
 - from high- to low-friction surface, 338–342
 - repeated, temperature analysis for, 82–85
 - on split-coefficient road surface, 267
 - tire/wheel analysis, 328–335

Brake Design and Safety

- Braking accident causation databases, 22–25
- Braking by wire, 209–210
- Braking dynamics
 - of combination vehicles, 275–325
 - 2-S1, 281–302
 - 2-S1–2, 318–320
 - 2-S2 tractor-semitrailer, 320
 - 2-S3 tractor-semitrailer, 321–324
 - 3-S2 tractor-semitrailer, 312–318
 - tow vehicle-trailer combination, 275–278
 - tractor-trailer, 279–281
 - trailer with brakes, 276–278
 - trailer without brakes, 275–276
 - of single vehicles, 213–271
 - actual braking forces, 224–225
 - braking efficiency, 230–232
 - comparison of optimum and actual braking forces, 225–228
 - with dynamic axle load, 214–216
 - fixed brake force distribution analysis, 232–237
 - optimum braking forces, 216–224
 - with static axle loads, 213–214
 - of three-axle straight truck, 253–267
 - tire-road friction utilization, 228–230
 - of two-axle truck with air brakes, 249–253
 - while turning, 267–271
 - variable brake force distribution analysis, 238–248
 - of three-axle straight truck, 253–267
 - of two-axle truck with air brakes, 249–253
- Braking efficiency, 230–232
 - checkpoints for, 15
- Braking energy, 66–69
 - formula for, 66
- Braking force
 - actual, 224–225
 - comparison of optimum and actual, 225–228
 - dynamic 217–218
 - ideal, 218
 - optimum
 - in 2-S1 combination, 281–286
 - braking traction coefficient for, 216–217
 - dynamic, 217–218
 - lines of constant friction coefficient for, 220–224
- parabola analysis of, 224
- peak and sliding friction in, 336–338
- for single vehicles, 216–224
- Braking power, 66–69
 - absorbed by lining and drum, 70–72
 - formula for, 66
- Braking slip, 328–330
- Braking time, formula for, 67
- Braking traction coefficient, 216–217
- Bureau of Motor Carrier Safety, parking brake regulations, 122–123
- Calipers
 - basic design considerations for, 48–51
 - deformation of, 161
 - fixed, 48, 49*f*, 55–57
 - floating, 49, 50
 - installation of, 57
- CamLaster drum brake, 186
- Clamp ring brake chambers, 191–192
- Combination valves, 145
- Combination vehicles
 - 2-S1–2 two-axle tractor, single-axle semitrailer, double-axle trailer, 318–320
 - 2-S2 tractor-semitrailer, 320
 - 2-S3 triple-axle trailer with leaf springs, 321–324
 - 3-S2 tractor-semitrailer, 312–318
 - 3-S2-AA, air springs on tractor and trailer tandem axles, 313
 - 3-S2-ALS, tractor air springs and trailer leaf springs, 315–318
 - 3-S2-AWB, air springs on tractor with trailer walking beam, 314
 - tow vehicle-trailer, braking dynamics of, 275–278
 - tractor-trailer, braking dynamics of, 279–281
- Component sizing, checkpoints for, 17
- Compression
 - of brake fluid, 164–165
 - of brake pad, 161–162
 - of brake shoe and lining, 162–163
- Compressive stress, formula for, 107
- Computer-based temperature analysis, 100–107
- Constant deceleration time, formula for, 7
- Convective cooling, 88–99
- Convective heat transfer coefficient, 88
- Crashworthiness Data System (CDS), 22

- Critical deceleration, 227
- Customer complaints and accident data, 12
- Danger, hazard, and risk, 21–22
- Deceleration
 - for air brake systems, 194–196
 - with automatic front brake limiting valve, 195–196
 - average, formula for, 10
 - and brake line failure, 378
 - brakes-unlocked, 232–233
 - critical, 227
 - formula for, 3
 - idealized, 5*f*, 6
 - measurement of, 10
 - with proportioning valves, 196
 - rise time, formula for, 6
 - and stopping distance, 2–10
- Deceleration-sensitive reducer valves, 145–147, 243
- Disc brakes, 48–61
 - adjustment of, 49–50
 - air, 187
 - caliper installation, 57
 - compared to drum brakes, 57–58
 - complete temperature analysis in a single stop, 75–82
 - design values for, 74*t*
 - pad pressure and wear in, 51–57
 - self-energizing, 60–61
 - solid, heat transfer coefficient for, 90
 - thermal stress in rotors, 107–109
 - ventilated
 - heat transfer coefficient for, 91–99
 - temperature analysis of, 104–107
- Downgrade, 2
- Driver reaction time
 - four phases of, 8
 - in emergency braking, 8–9
- Driveshaft-mounted brakes, analysis of, 122–123
- Drivetrain
 - effect on brake force distribution, 236–237
 - influence on ABS, 364
- Drum brakes
 - air in hydraulics, 163
 - brake factor of, 34–46
 - brake shoe and lining compression in, 162–163
 - braking power absorbed by drums, 70–72
 - CamLaster, 186
 - compared to disc brakes, 57–58
 - design values for, 74*t*
 - drum deformation in, 162
 - drum expansion in, 163, 193
 - heat transfer coefficient for, 89–90
 - lining pressure distribution and wear in, 29–32
 - self-energizing and self-locking, 32–34
 - temperature fade correction factor for, 192–193
 - thermal stress in, 110
- Drum expansion, thermal, 163
 - pushrod travel increase due to, 193
- Drum stiffness, effects on brake factor, 47–48
- Dual brake systems, comparison of, 389–391
- Duo-servo brakes
 - with pivot abutment, 40–44
 - with sliding abutment, 39–40
- Dynamic axle loads
 - for tow vehicle-trailer combination, 276–277
 - for 2-S1 tractor-trailer combination, 303–304
 - for single vehicles, 214–216
- Dynamic braking forces, 217–218
- Economics, 12
- Electric trailer brakes, 277
- Electronic brake control, 209–210
- Electronic control unit (ECU), 361–362
- Electronic stability control (ESC), 278–279, 327, 351–353
 - function of, 352
 - major components of, 352–353
 - malfuction of, 353
 - operation of, 353
- Electronic traction control, 351–353
- Emergency brake, *see* Parking brake
- Example problems
 - air brake design, 250–253
 - brake factor, 121–122
 - brake line pressure, 173–175
 - and pedal travel, 167–173
 - braking energy and braking power, 67–69
 - braking forces, optimum, 218–220
 - braking performance, brake lockup sequence, 305–312

Brake Design and Safety

- Example problems (*Continued*)
braking stability, 264–267
deceleration
and braking efficiencies, 244–248
maximum, 222–224
at peak friction, 338
and stopping distance, 199–200
duo-servo drum brake, 41–44
forensic brake system analysis, 253
optimum braking forces, 218–220
thermal analysis
of front disc brake, 74–75
of heavy truck brake, 87–88
of linearly decreasing heat flux, 81–82
of pickup truck brake, 78–80
of rear brake, 84–85
of tractor-semitrailer brake, 85–86
of ventilated disc brake, 93–99
time required to lock front brakes, 340–342
wheel peak and sliding friction
parameters, 332–333
- Failure analyses, 12
Fatality Analysis Reporting System (FARS), 24–25
Federal Motor Vehicle Safety Standard (FMVSS), 105, 123
FMVSS 105, 84, 120, 123
FMVSS 121, 280, 287
FMVSS 126, 328
FMVSS 135, 84, 119
Finite difference method, 100–104
temperature analysis of ventilated disc, 104–107
Fixed brake force distribution analysis, 232–237
Fixed caliper, 48, 49f
Floating caliper, 49, 50
Fourier's conduction law, 100
Friction
braking from high- to low-friction surface, 338–342
lines of constant friction coefficient, 220–224
of lining/pad, 58–59
peak and sliding, in braking forces
diagram, 336–338
tire braking, empirical equations for, 336
tire-road friction utilization
2-S1 tractor-trailer combination, 287–302
and brake line failure, 379
single-vehicle, 228–230
Friction brakes, design and analysis of, 27–61
Full-power hydraulic brakes
analysis of, 139
failure of, 392
General Estimates System (GES), 22
Heat distribution, formula for, 72
Heat flux, allowable, 112–114
Heat penetration time, formula for, 72
Heat transfer, radiative, 99–100
Heat transfer coefficient
for drum brakes, formula for, 89–90
for solid discs, formula for, 90
of ventilated disc brakes, formula for, 91–92
Horsepower, into lining or pad, 114
Humidity, effects on brake factor, 46
Hydraulic ABS systems, 353–360
Hydraulic boost systems
Hydraulic brake systems, 125–179
boost systems for, 127–141
analysis of, 136–139
dynamic response of, 177–179
vacuum, 176–177
brake fluid viscosity, 175–176
brake fluid volume analysis for, 150–179
brake line, 177
pressure control devices for, 141–150
brake pedal linkage, 176
dynamic response of, 175
manual, 125–127
master cylinder in, 177
Hydraulic modulator, 362–363
Hydrovac
analysis of, 134–135
fluid loss in, 166
Ideal braking force, 218
Inclined abutment, 38–39
Inspection and maintenance, 12
Integrated hydraulic ABS systems, 358–360
In-use factors, checkpoints for, 16–17
Jackknifing, 279–280
Leaf spring tandem axle, rear, 257–258

- Lines of constant friction coefficient, 220–224
- Loading-brake force distribution analysis, 233–235
- Manual brakes
 - hydraulic, analysis of, 125–127
 - PC-BRAKE HYDRAULIC for, 125
 - pedal force and pedal travel for, 17
- Master cylinder
 - dual, improved design, 387–389
 - dynamic response of, 177
 - fluid requirements for, 160–161
 - sizes of, 169t
 - step bore, 147–148
 - adjustable, 148–150, 244–248
 - volume analysis of, 156–159
- Mastervac, 127
- Materials selection, 12
- Mechanical brake systems
 - analysis of, 119–123
 - driveshaft-mounted brakes, 122–123
 - general observations, 119–120
 - wheel brakes, 120–122
- Mechanical gain, formula for, 120
- National Accident Statistical Sampling (NASS), 22–24
- New-versus-used, 12
- Offset piston design, 53–54
- Optimum brake line pressures, 238–241
- Optimum braking forces
 - for 2-S1 combination, 281–286
 - braking traction coefficient for, 216–217
 - dynamic, 217–218
 - lines of constant friction coefficient for, 220–224
 - parabola analysis of, 224
 - peak and sliding friction in, 336–338
 - for single vehicles, 216–224
- Packaging, labeling, and shipping, 12
- Parabola analysis of optimum braking forces, 224
- Parallel sliding abutment, 36–38
- Parking brake
 - analysis of, 120–122
 - checkpoints for, 16
 - design example, 19–20
 - dynamic response of, 177
- pedal force and pedal travel for, 18
- torque in, 194
- PC-BRAKE AIR
 - for 2-S1 tractor-trailer combination, 302–312
 - for 3-S2 tractor-semitrailer, 316–318
 - brake system design with, 249–253
 - for leaf spring suspensions, 257
 - multi-axle, 199–203
 - pushrod travels in, 191f, 192,
- PC-BRAKE FACTOR
 - for duo-servo brake with pivot support, 43
 - for LT-shoe brake with parallel sliding abutment, 37–38
 - for S-cam brake, 45
- PC-BRAKE HYDRAULIC, for manual brakes, 125
- PC-BRAKE STABILITY, 264–267
- PC-BRAKE TEMPERATURE, for continuous braking, 86
- Peak and sliding friction in braking forces diagram, 336–338
- Pedal force
 - and brake line failure, 378–379
 - idealized, 4–5
 - and pedal travel, 17–18
- Pedal travel
 - and brake line failure, 379–383
 - computation of, 167–173
 - and pedal force, 17–18
- Piston
 - four-piston caliper design, 55–57
 - offset, 53–54
- Pivot abutment, 40
- Pressure control devices, brake line, 141–150
- Pressure distribution
 - on brake lining, 29–32
 - on brake pad, 52–53
- Pressure limiter valves, 142–143, 241–242
 - for 2-S1 combination, 286–287
 - automatic, for front brake, 195
- Pressure reducer valves, 143–144, 196, 242–243
 - for 2-S1 combination, 286–287
 - deceleration-sensitive, 243
- Production approval, 12
- Production methods, 12

Brake Design and Safety

- Pulled pad design, 54–55
- Pushrods
 - adjustments for, 188
 - travel adjustment factor for clamp ring chambers, 191–192
 - travel increase due to thermal drum expansion, 193
 - travel measurement, 193–194
 - travels and limits of, 192*t*
- Radiation heat transfer coefficient, formula for, 99
- Reaction and application time, formula for, 6
- Rear leaf spring tandem axle, 257–258
- Rear walking beam tandem axle, 254–256
- Relay quick release valve, 200, 204*f*
- Reliability, 11, 20–21
- Response time
 - of air brake systems, 200–209
 - checkpoints for, 15
- Road surface, split-coefficient, braking on, 267
- Road test, comparison of theoretical and test results, 235–236
- Roll stiffness, formula for, 270
- Rotors
 - allowable heat flux into, 112–114
 - design considerations for, 115
 - thermal failure of, 110–111
 - thermal stress in, 107–109
- Rubber materials, failure of, 396
- Safety and product liability, 11
- Safety regulations, checkpoints for, 17
- Safety standards, 12
- S-cam brakes, 184–186
 - PC-BRAKE FACTOR for, 45
- Seal, failure of, 396
- Select-high control, 345
- Select-low control, 345
- Self-energizing brakes
 - disc, 60–61
 - drum, 32–34
- Self-locking drum brakes, 32–34
- Single-vehicle braking dynamics, 213–271
- Single-wheel control, 345
- Sliding abutment, 39–40
- Slowing, 1–2
- Specific design measures, checkpoints for, 16
- Speed, definition of, 3
- Stability analysis, 258–267
 - and brake line failure, 383
- braking on a split-coefficient road surface, 267
 - expanded, 260–267
 - general considerations for, 258–259
 - simplified, 259–260
- Static axle loads, 213–214
- Step bore master cylinder, 147–148
 - adjustable, 148–150, 244–248
- Stopping, 1–2
- Stopping distance
 - and deceleration, 2–10
 - expanded analysis of, 3–4
 - lightly and fully laden, checkpoints for, 15
 - simplified analysis of, 3–4
 - total, 6–7
- Strain, 29
- Stress, thermal, analysis of, 107–111
- Surface finish, 12
- Surge brakes, 277–278
- System-based design methods, 11
- Temperature
 - effects on brake factor, 46
 - surface, formula for, 73
- Temperature analysis, 65–107
 - checkpoints for, 16
 - computer-based, 100–107
 - for continuous braking, 85–88
 - disc, complete in a single stop, 75–82
 - finite difference method, 100–107
 - general considerations in, 65
 - for repeated braking, 82–85
 - simplified in a single stop, 72–75
- Temperature fade correction factor for drum brakes, 192–193
- Temperature response
 - for constant heat flux, formula for, 77
 - for time-varying heat flux, formula for, 80
- Test results, for combination vehicles, 325
- Thermal design measures, 112–115
- Thermal drum expansion, 163
 - pushrod travel increase due to, 193
- Thermal resistance, formula for, 71
- Thermal rotor failure, 110–111
- Thermal stress
 - analysis of, 107–111
 - in brake drums, 110
 - in disc brake rotors, 107–109

- Three-axle straight truck
 - air springs rear tandem axle, 253–254
 - braking dynamics of, 253–267
 - rear leaf spring tandem axle, 257–258
 - rear walking beam tandem axle, 254–256
- Threshold angular deceleration, 332
- Tire-road friction utilization
 - effects of brake balance on, 287–302
 - and brake line failure, 379
 - single-vehicle, 228–230
- Tire/wheel braking analysis, 328–335
- Total stopping distance, 6–7
- Tow vehicle-trailer combination
 - braking dynamics of, 275–278
 - trailer with brakes, 276–278
 - trailer without brakes, 275–276
- Traction coefficient for braking, 216–217
- Tractor-semitrailer braking instability, 279–281
 - jackknifing, 279–280
 - trailer swing, 280
- Tractor-trailer combinations, braking of, 279–281
 - stable, 280–281
- Trailer swing, 278–279, 280
- Trailers
 - with brakes
 - braking dynamics of, 276–278
 - dynamic axle loads, 276–277
 - electric brakes, 277
 - surge brakes, 277–278
 - without brakes, 275–276
- Transcendental equation, 77
- Trucks
 - three-axle straight, braking dynamics of, 253–267
 - two-axle, with air brakes, braking dynamics of, 249–253
- Turning
 - basic considerations, 267–268
 - braking dynamics while, 267–271
 - optimum brake line pressures for, 268–271
- Two-axle truck, with air brakes, braking dynamics of, 249–253
- Vacuum-assisted brake booster, 127–135
 - analysis of, 128–134
 - dynamic response of, 176–177
 - failure of, 381–392
- Valves
 - combination, 145
 - modulating, 196–199
 - pressure limiter, 241–242
 - for 2-S1 tractor-trailer, 286–287
 - automatic front brake, 195–196
 - for hydraulic brakes, 142–143
 - pressure reducer, 242–243
 - for 2-S1 tractor-trailer, 286–287
 - for air brakes, 196
 - for hydraulic brakes, 143–147
 - relay quick release, 200, 204f
 - volume loss in, 166
- Variable brake force distribution analysis, 238–248
- Velocity, formula for, 2–3
- Velocity-time (V-t) diagram
 - constant, 3f
 - for stopping process, 4f, 5f
- Ventilated disc brakes
 - heat transfer coefficient for, 91–99
 - temperature analysis of, 104–107
- Walking beam tandem axle, rear, 254–256
- Warnings, 12
- Wear relationship, formula for, 30–31
- Wedge brakes, 186
- Wheel brakes, see Parking brakes
- Wheel speed sensors, 360–361
 - signal analysis for, 342–343
- Wheel-lockup analysis, 328–343
 - braking from high- to low-friction surface, 338–342
 - empirical equations for tire braking friction, 336
 - peak and sliding friction in braking forces diagram, 336–338
 - tire/wheel braking analysis, 328–335
 - wheel speed sensor signal analysis, 342–343

About the Author



Dr. Rudolf Limpert is retiring from a long career as consulting engineer on motor vehicle and traffic safety. He continues to publish and teach motor vehicle accident reconstruction and design of braking systems. The author of many publications and four other books related to automotive safety, Dr. Limpert received his Ph.D. in mechanical engineering from the University of Michigan, his M.S. and B.E.S. from Brigham Young University, and his B.S. from the Engineering School of Wolfenbüttel.

Brake Design and Safety

Third Edition

Rudolf Limpert

The objectives of this third edition of an SAE classic title are to provide readers with the basic theoretical fundamentals and analytical tools necessary to design braking systems for passenger vehicles and trucks that comply with safety standards, minimize consumer complaints, and perform safely and efficiently before and while electronic brake controls become active.

This book, written for technology students, engineers, forensic experts, and brake technicians, provides readers with theoretical knowledge of braking physics, and offers numerous equations that make the information easy to understand and apply.

New to this edition are expanded chapters on thermal analysis of automotive brakes, analysis of hydraulic brake systems, and single vehicle braking dynamics.

About the Author



Dr. Rudolf Limpert enjoys retirement after a long and successful career as a consulting engineer on motor vehicle and traffic safety. He has authored many publications, along with four other automotive safety books. He continues to publish and teach motor vehicle accident reconstruction and design of braking systems. Dr. Limpert received his Ph.D. in mechanical engineering from the University of Michigan, his M.S. and B.E.S. from Brigham Young University, and his B.S. from the Engineering School of Wolfenbuettel.

SAE International®

R-398

ISBN 978-0-7680-3438-7



9 780768 034387